ADVANCES IN PRODUCTION ENGINEERING

Advanced Machining and Micromachining Processes

Edited by
Sandip Kunar,
Norfazillah Binti Talib,
and Gurudas Mandal

Scrivener Publishing

WILEY

Table of Contents

- Cover
- Table of Contents
- Series Page
- Title Page
- Copyright Page
- Preface
- 1 Overview of Advanced Machining and Micromachining Processes
  - 1.1 Introduction
  - 1.2 Electrical Machining
  - 1.3 Thermal Machining
  - 1.4 Chemical Machining
  - 1.5 Mechanical Micromachining
  - 1.6 Electrical Micromachining
  - 1.7 Thermal Micromachining
  - 1.8 Chemical Micromachining
  - 1.9 Ultrasonic Micromachining
  - 1.10 Other Micromachining Processes
  - 1.11 Future Directions and Emerging Technologies
  - 1.12 Conclusion
  - References
- 2 Abrasive Jet Machining
  - 2.1 Introduction
  - 2.2 Description of Process
  - 2.3 Equipment Description
  - 2.4 Process Parameters

2.5 Process Capabilities
2.6 Application of Abrasive Jet Machining
2.7 Benefits of Abrasive Jet Machining (AJM)
2.8 Drawbacks of Abrasive Jet Machining
2.9 Characteristics of AJM
2.10 Mechanics of Cutting in AJM
References
3 Water Jet Machining
3.1 Introduction
3.2 Description of Process
3.3 Description of Equipment
3.4 Process Parameters
3.5 Process Capability
3.6 Applications of WJM
3.7 Advantages of WJM
3.8 Disadvantages of WJM
3.9 Worked Examples
References
4 Electric Discharge Machining
4.1 Introduction
4.2 Description of Process
4.3 Basic Requirement of EDM Process
4.4 Description of Equipment
4.5 Types of Generators
4.6 Electrode Material
4.7 Choice of Dielectric Fluid
4.8 EDM Tool Design
4.9 Process Parameters

4.10 Machining Characteristics
4.11 Process Capabilities of EDM
4.12 Characteristics of Spark-Eroded Surfaces
4.13 Applications of EDM
4.14 Advantages of EDM
4.15 Disadvantages of EDM
4.16 Factors to be Considered in EDM Machine Tool Selection
References
5 Wire-Electric Discharge Machining
5.1 Introduction
5.2 Description of Process
5.3 Equipment
5.4 Process Parameters of Wire EDM
5.5 Process Capability of Wire EDM
5.6 Difference Between Wire EDM and EDM
5.7 Applications of Wire EDM
5.8 Advantages of Wire EDM
5.9 Disadvantages of Wire EDM
5.10 Process Parameters in Wire EDM
5.11 Worked Examples
References
6 Laser Beam Machining
6.1 Introduction
6.2 Lasing Action and Population Inversion
6.3 Methods to Achieve Population Inversion
6.4 Types of Lasers
6.5 Description of Process

6.6 Beam Parameters
6.7 Process Capability
6.8 Applications of LBM
6.9 Advantages of LBM
6.10 Disadvantages of LBM
6.11 Comparison Between EBM and LBM
References
7 Plasma Arc Machining
7.1 Introduction
7.2 Plasma Generation
7.3 Description of Process
7.4 Description of Equipment
7.5 Modes of Operation of DC Plasma Torches
7.6 Methods to Make Arcs More Stable
7.7 Parameters that Influence PAM Performance
7.8 Capability to Process
7.9 Applications of Plasma Arc Machining
7.10 Advantages of PAM
7.11 Disadvantages of PAM
7.12 Safety Precautions to be Taken in PAM
References
8 Ion Beam Machining
8.1 Introduction
8.2 Description of Process
8.3 Description of Equipment
8.4 Process Characteristics
8.5 Applications of IBM
8.6 Advantages of IBM

8.7 Disadvantages of IBM
References
9 Electrochemical Machining
9.1 Introduction
9.2 Electrochemical Machining Techniques
9.3 Process Parameters and Control
9.4 Material Specifications in ECM
9.5 Advancements in ECM Technology
9.6 Conclusion
References
10 Ultrasonic Machining
10.1 Introduction
10.2 Process Description
10.3 Description of Equipment
10.4 Tool Feed Mechanism
10.5 Abrasive Slurry
10.6 Liquid Media
10.7 Process Parameters
10.8 Process Capability
10.9 Applications
10.10 Advantages of USM
10.11 Disadvantages of USM
10.12 Mechanism of Material Removal in Ultrasonic Machining Operation
10.13 Recent Developments in USM
References
11 Electron Beam Machining
11.1 Introduction

11.2 Theory of EBM
11.3 Equipment
11.4 Mathematics of Electron Beam Machining
11.5 Mechanics of EBM
11.6 Process Parameter of Electron Beam Machining
11.7 Application of EBM
11.8 Advantages of EBM
11.9 Disadvantages of EBM
11.10 Worked Out Examples
References
12 Chemical Machining
12.1 Introduction
12.2 General Description of Chemical Machining Process
12.3 Five Steps of Chemical Machining
12.4 Elements of Process
12.5 Influence of Etchant Medium
12.6 Chemical Blanking
12.7 Accuracy of Chemical Blanking
12.8 Applications of Chemical Machining
12.9 Advantages of CHM
12.10 Disadvantages of CHM
12.11 Selection of Maskant
12.12 Selection of Etchants
12.13 Chemical Milling
12.14 Chemical Engraving
12.15 Photochemical Blanking
12.16 Worked Examples

References
13 Electrogrinding
13.1 Introduction
13.2 Electrochemical Grinding Operational Parameters
13.3 Process and Working Principles of Electrochemical Grinding
13.4 Components of Electrochemical Grinding Machines
13.5 Grinding Methods of ECG
13.6 Variations of Electrochemical Grinding in Research Stage
13.7 Industrial Applications of ECG
13.8 Advantages and Challenges of Electrochemical Grinding
13.9 Grinding Processes
13.10 Summary and Recommendation
References
14 Photochemical Machining
14.1 Introduction
14.2 Contextual
14.3 PCM Process
14.4 Mechanism of Etching
14.5 Steps for Experimental Designing
14.6 Process Parameters
14.7 Parametric Effect
14.8 Analysis of Machined Surfaces
14.9 Conclusion
14.10 Scope for Future Work

References
15 Abrasive-Assisted Micromachining
15.1 Introduction
15.2 Erosion Mechanism
15.3 Erosion Mechanisms in AAM Explanation
15.4 Existing Erosion Models
15.5 Development of AAM Erosion Models
15.6 Verification and Validation of AAM Erosion Models
15.7 Applications of Erosion Models
15.8 Advancements in Erosion Modeling Techniques
15.9 Concluding Remarks and Implications for AAM Erosion Modeling
References
16 Abrasive Water Jet Micromachining: Pushing the Micro-Frontier Further—A Glimpse at Recent Advancements
16.1 Introduction
16.2 The Essence of AWJMM: A Powerful Blend of Water and Grit
16.3 Some Prominent Research Works on Abrasive Water Jet Micromachining
16.4 Conclusion
16.5 A Glimpse Into the Future: What Lies Ahead for AWJMM?
References
17 Micro-Electrical Discharge Machining: State of Art
17.1 Introduction
17.2 Principles of Micro-EDM

17.3 Major Components of Micro-Electrical Discharge Machining
17.4 Process and Machining Parameters of Micro-Electrical Discharge Machining
17.5 Major Varieties of Electrical Discharge Micromachining
17.6 Hybrid Type of Electrical Discharge Micromachining
17.7 Summary
References
18 Electrochemical Micromachining
18.1 Introduction
18.2 Overview of Electrochemical Micromachining
18.3 Electrochemistry of Electrochemical Micromachining
18.4 Machining Conditions in Electrochemical Micromachining
18.5 Electrochemical Micromachining Set Up
18.6 Fabrication of Different Microtools in Electrochemical Micromachining
18.7 Process of Measurement of Microfeatures
18.8 Application of Electrochemical Micromachining
18.9 Conclusions
18.10 Future Research Opportunities
References
19 Ultrasonic Micromachining
19.1 Introduction
19.2 Principles of Ultrasonic Micromachining
19.3 Equipment for Ultrasonic Micromachining

19.4 Process Parameters in Ultrasonic Micromachining
19.5 Applications of Ultrasonic Micromachining
19.6 Advantages and Limitations of Ultrasonic Micromachining
19.7 Recent Advancements and Emerging Trends
19.8 Conclusions
Acknowledgment
References
20 Laser Surface Modification of Implant Materials: An Insight
20.1 Introduction
20.2 Fundamentals of Laser Surface Modification
20.3 Laser Surface Modification Techniques
20.4 Applications of Laser Surface Modification in Implant Materials
20.5 Characterization of Laser-Modified Surfaces
20.6 Challenges and Future Perspectives
20.7 Conclusion
References
21 Ion Beam Processing: A Brief Review
21.1 Introduction
21.2 Focused Ion Beam Process
21.3 Ion Beam Process
21.4 Developed Ion Beam Process
21.5 Combined Ion Beam Process
21.6 Conclusion
References

22 Parametric Optimization in Electrochemical Discharge Machining of Microchannel on Glass Using Multiple Tool Passes
- 22.1 Introduction
- 22.2 Methodology Adopted to Machine Microchannel
- 22.3 Experimentation
- 22.4 Multi-Response Optimization
- 22.5 Conclusions
- References

23 Abrasive Water Jet Machining
- 23.1 Introduction
- 23.2 Elements of Abrasive Water Jet Machining
- 23.3 Process Variables and Operating Factors in AWJM
- 23.4 Abrasive Water Jet Machining Applications
- 23.5 Advantages of Abrasive Water Jet Machining
- 23.6 Challenges and Limitations
- 23.7 Recent Trends and Developments in AWJM
- 23.8 Conclusion
- References

24 Effect of Ultrasonic Vibration-Assisted Micromachining on the Surface Properties of Difficult-to-Machine Materials
- Nomenclature
- 24.1 Introduction
- 24.2 The Technique of UVAMM
- 24.3 UVAMM of Difficult-To-Machine Materials
- 24.4 Conclusion
- References

25 A Significant Impact of Laser-Assisted Micromachining on Tribological Properties of High Strength Alloys
- 25.1 Introduction
- 25.2 Road Map of Laser-Assisted Micromachining
- 25.3 Micromachining
- 25.4 Lasers in Micromachining
- 25.5 Methodology of Laser-Assisted Micromachining
- 25.6 Laser-Assisted Micromachining
- 25.7 Conclusion
- Summary
- Scope for Future Work
- References

26 Abrasive Flow Finishing
- 26.1 Introduction
- 26.2 Significant Process Parameters
- 26.3 Classification of AFF Method
- 26.4 Equipment
- 26.5 Process
- 26.6 Application of Special Techniques
- 26.7 Hybrid AFF Processes
- 26.8 Monitoring of AFF Process
- 26.9 Advantages and Limitations of AFF
- 26.10 Applications of AFF
- 26.11 Summary
- 26.12 Conclusion
- References

27 Elastic Emission Machining

27.1 Introduction
27.2 Principle of EEM
27.3 Numerically Controlled Elastic Emission Machining
27.4 Conclusion
References
28 Magnetic Abrasive Finishing Process
28.1 Introduction
28.2 Primary Components of MAF
28.3 MAF Principles
28.4 Working Principle of MAF
28.5 Process Parameters in MAF
28.6 Magnetic Abrasive Preparation
28.7 MAF Tools
28.8 Types of Magnetic Abrasive Finishing Process
28.9 Advantages of Magnetic Abrasive Finishing
28.10 Disadvantages of Magnetic Abrasive Finishing
28.11 Applications of Magnetic Abrasive Finishing
28.12 Surface Finish Improvement in MAF
28.13 Challenges and Future Directions
28.14 Conclusions
References
29 Experimental Analysis of EDM Process While Machining Ti-VT20 Alloy
29.1 Introduction
29.2 Experimental Investigation
29.3 Experimental Result Analysis
29.4 Results and Discussion

29.5 Conclusion
References
30 Estimation of Machining Performance and Machining Characteristics Using Artificial Neural Network in Wire Electric Discharge Machine for Titanium & P-20 Materials
30.1 Introduction
30.2 Experimental Setup
30.3 Artificial Neural Network (ANN)
30.4 Results and Discussion
30.5 Conclusion
References
31 Chemical-Based Bulk Machining and Fabrication of Silicon Microstructures: An Overview
31.1 Silicon: Material for Integrated Circuits and MEMS
31.2 Overview of Microelectromechanical Systems
31.3 Silicon Wafers Fabrication: Procedural Stages
31.4 Silicon Microfabrication Processes
31.5 State-of-Art Application Areas and Present/Futuristic Trends
References
Index
End User License Agreement

List of Tables

Chapter 1
Table 1.1 Summarizes the mechanical micromachining operations and its applicat...

Chapter 4

Table 4.1 Comparison of dielectric fluid for brass electrode/tool steel workpi...

Table 4.2 Commercially available dielectric grade oil.

Table 4.3 Operating parameters.

Table 4.4 Size of microcracks.

Chapter 5

Table 5.1 Effect of low and high conductivity of dielectric.

Table 5.2 Wire tensions in wire EDM.

Table 5.3 Guidelines for choosing parameters for different work materials.

Table 5.4 Difference between wire EDM and EDM.

Chapter 6

Table 6.1 Details of the process of gas lasing elements.

Table 6.2 Beam parameters of commonly used lasers.

Table 6.3 Process capabilities of laser.

Table 6.4 Difference between conduction laser and penetration laser welding.

Table 6.5 Differences between EBM and LBM.

Chapter 7

Table 7.1 Comparison between non transferred arc mode and transferred arc mode...

Table 7.2 Cutting speeds of plasma arc.

Chapter 8

Table 8.1 MRR for different materials.

Chapter 11

Table 11.1 Process parameters of EBM.

Chapter 12

Table 12.1 Surface finish for different materials.

Chapter 13

Table 13.1 ECG, ECM, and EDM process comparison.

Table 13.2 Electrolytes and the corresponding materials they grind in ECG.

Table 13.3 Advantages and challenges of electrochemical grinding.

Table 13.4 Comparison of ECG with other grinding processes.

Chapter 16

Table 16.1 Uses of abrasive water jet micromachining (AWJMM) across different ...

Table 16.2 Overview of how AWJMM is applied in various industries.

Table 16.3 Research findings on abrasive water jet micromachining from selecte...

Table 16.4 Research findings on abrasive water jet micromachining from selecte...

Table 16.5 Research findings on abrasive water jet micromachining from selecte...

Table 16.6 Research findings on abrasive water jet micromachining from selecte...

Chapter 17

Table 17.1 Differentiate between macro-EDM and micro-EDM [9, 10].

Table 17.2 Variant types of electrical discharge micromachining.

Chapter 22

Table 22.1 Properties of borosilicate glass.

Table 22.2 Process parameters at three levels.

Table 22.3 Experimental plan.

Table 22.4 Experimental results.

Table 22.5 S/N ratio for the responses.

Table 22.6 Normalized values of S/N ratios.

Table 22.7 Deviation sequence, GRC, and GRG.

Table 22.8 MRPI on GRG values.

Chapter 23

Table 23.1 The process parameters of AWJM process [17].

Table 23.2 Applications of AWJM [6].

Chapter 24

Table 24.1 Characteristics of vibration-assisted micromachining.

Chapter 25

Table 25.1 Overview of laser-assisted micromachining in tribological propertie...

Chapter 29

Table 29.1 Control parameters and their levels.

Table 29.2 Control parameters and their levels.

Table 29.3 Grey relation co-efficient and grades.

Table 29.4 Validation results for improvement of grey grade.

Chapter 30

Table 30.1 The levels of different control factors.

Table 30.2 Chemical composition of titanium grade-2 material.

Table 30.3 Chemical composition of P-20 tool steel material.

Table 30.4 Standard L’16 OA.

Table 30.5 L_{16} OA assigned with factors.

Table 30.6 Measured metrics for titanium material: F-value and R-square values...

Table 30.7 Measured metrics for P-20 tool steel material: F-value and R-square...

Chapter 31

Table 31.1 Standard silicon wafer size versus thickness.

List of Illustrations

Chapter 2

Figure 2.1 Abrasive jet machining.

Figure 2.2 Illustration of abrasive jet machining (AJM).

Figure 2.3 Impact of abrasive particle density and exit gas velocity.

Figure 2.4 Effect of abrasive flow on MRR.

Figure 2.5 Relationship between gas flow rate and abrasive mass flow rate is i...

Figure 2.6 Geometry of single abrasive grit.

Chapter 3

Figure 3.1 Water jet machining process.

Figure 3.2 Mechanism of water jet shearing.

Chapter 4

Figure 4.1 EDM process.

Figure 4.2 Rotary impulse generator.

Figure 4.3 Effect of increasing current on MRR.

Figure 4.4 Effect of increasing sparking frequency.

Figure 4.5 Relationship between current on time and material removal crater si...

Chapter 5

Figure 5.1 Wire EDM setup.

Figure 5.2 Conductivities of water.

Figure 5.3 (a) Effect of frequency on surface finish. (b) Effect of overcut wi...

Figure 5.4 Effect of frequency on surface finish.

Chapter 6

Figure 6.1 Allowed energy levels.

Figure 6.2 Absorption processes in laser.

Figure 6.3 Simulated absorption in laser.

Figure 6.4 Spontaneous emission in laser.

Figure 6.5 Stimulated emission in laser.

Figure 6.6 Optical pumping methods.

Figure 6.7 Laser operation.

Figure 6.8 Solid-state laser.

Figure 6.9 CO_2 laser setup.

Chapter 7

Figure 7.1 Plasma arc machining.

Chapter 8

Figure 8.1 Low and high energy ion implantation.

Figure 8.2 Ion machining process.

Figure 8.3 Ion etching versus chemical etch.

Chapter 9

Figure 9.1 Schematic representation of the electrochemical micromachining (ECM...

Figure 9.2 Principle scheme of plasma electrolytic polishing.

Figure 9.3 Variants of electrochemical machining: (a) sinking, (b) machining w...

Figure 9.4 Schematic diagram of ECM on 304 stainless steel.

Figure 9.5 Schematic diagram of nano-electrochemical machining system.

Chapter 10

Figure 10.1 Basic principles of ultrasonic machining.

Figure 10.2 USM equipment.

Figure 10.3 Concentrator used in USM.

Figure 10.4 Geometry of the abrasive grit and dent amount.

Figure 10.5 Time period during USM.

Figure 10.6 Tool positions at various levels during machining.

Chapter 11

Figure 11.1 Electron beam machining unit.

Figure 11.2 Steps of metal removal in EBM.

Chapter 12

Figure 12.1 Chemical machining process.

Figure 12.2 (a) Flow chart for preparation of workpiece in chemical blanking....

Figure 12.2 (b) Flow chart for preparation of masters in chemical blanking.

Figure 12.2 (c) Flow chart for masking and etching in chemical blanking.

Figure 12.3 (a) Flow chart for precleaning in chemical milling.

Figure 12.3 (b) Flow chart for masking in chemical milling.

Figure 12.3 (c) Flow chart for etching in chemical milling.

Figure 12.3 (d) Flow chart for demasking in chemical milling.

Figure 12.4 Chemical milling of machined surface.

Figure 12.5 Chemical milling of aluminum.

Chapter 13

Figure 13.1 Schematic view of the working principle of ECG.

Figure 13.2 Electrochemical grinding machining (ECG) design components. Adapte...

Figure 13.3 Schematic view of wire electrochemical grinding. Reproduced with p...

Figure 13.4 Inner-jet electrochemical grinding. Reproduced with permission fro...

Figure 13.5 Ultrasonic-assisted electrochemical-drill grinding experimental co...

Figure 13.6 Image of electrochemical mill-grinding. Reproduced with permission...

Figure 13.7 Schematic principle of ICPECG. Reproduced with permission from Hel...

Chapter 14

Figure 14.1 Various steps in PCM process.

Chapter 15

Figure 15.1 The application of CMCs: (a) high-temperature parts of aero-engine...

Figure 15.2 Schematic diagram represents ultrasonic lapping device [62].

Figure 15.3 Basic tool path in the X-Y plane for cylindrical holes. The “forwa...

Figure 15.4 Schematic of the LN_2 pressurizing and dispensing equipment [77].

Chapter 17

Figure 17.1 Working principle of micro-EDM. (a) EDM gap dynamics, (b) EDM disc...

Figure 17.2 Basic components of electrical discharge micromachining [11].

Figure 17.3 Fundamental circuit configurations for (a) transistor type and (b)...

Figure 17.4 Servo feed control system overview [12].

Figure 17.5 μ-WEDM setup and experimental methodology [18].

Figure 17.6 Microscale gear fabricated using micro-EDM: (a) displays SEM image...

Figure 17.7 Various micro-EDM machining approaches: (a) wire electrical discha...

Figure 17.8 Illustration of the simultaneous micro-EDM and micro-ECM (SEDCM) p...

Figure 17.9 (a) Diagram of the hybrid micro-EDM setup with carbon nanofibers a...

Chapter 18

Figure 18.1 Schematic diagram of electrochemical machining.

Figure 18.2 Initial positions of tool and workpiece in ECM.

Figure 18.3 Final shape evolution in ECM of workpiece.

Figure 18.4 Electrical double layer.

Figure 18.5 Electrical circuit model of EMM cell.

Figure 18.6 Comparison of theoretical and experimental MRR.

Figure 18.7 Pulse wave form during EMM.

Figure 18.8 Generation of profile shape.

Figure 18.9 Shape evolution flow chart.

Figure 18.10 Shaping in EMM through mask attached to anode.

Figure 18.11 Shaping in EMM through mask attached to cathode.

Figure 18.12 Methods of microchannel generation.

Figure 18.13 Distribution of equipotential lines for conical microtool.

Figure 18.14 Schematic electrochemical micromachining set up.

Figure 18.15 Pulse shape during short circuit.

Figure 18.16 Schematic diagram for fabricating microtool.

Figure 18.17 Voltage and amplitude combinations for tool fabrication.

Figure 18.18 (a) 6.5° conical microtool. (b) Slightly reversed taper 78 µm at ...

Figure 18.19 Fabrication of disk microtool.

Figure 18.20 SEM micrograph of micro nozzle.

Figure 18.21 (a) 3D surface of channel. (b) Cross-sectional profile. (c) Rough...

Chapter 19

Figure 19.1 Schematic diagram of micro-USM setup.

Figure 19.2 Process parameters in micro-USM.

Chapter 22

Figure 22.1 Overview of the methodology adopted to optimize process parameters...

Figure 22.2 In-house ECDM experimental set-up.

Figure 22.3 Electrolyte (processing) cell arrangement.

Figure 22.4 SEM image of microchannel.

Figure 22.5 Main effects plot for means on GRA.

Chapter 23

Figure 23.1 Elements of abrasive water jet machining.

Figure 23.2 Abrasive particles (a) garnet [6], (b) silicon carbide [6], and (c...

Figure 23.3 The abrasive focusing tube and its parts [13].

Figure 23.4 Experimental set up of AWJM [16].

Figure 23.5 Abrasive blending and distribution system.

Figure 23.6 Process variables and operating factors in abrasive water jet mach...

Figure 23.7 The process variable of AWJM [17].

Figure 23.8 Machining of composite materials [21].

Figure 23.9 Multi-axis AWJM process [16].

Chapter 24

Figure 24.1 Evolution of UVAMM.

Figure 24.2 Classification VAM.

Figure 24.3 Methodology of UVAMM.

Figure 24.4 Comparison of surface roughness of conventional vs UVAMM [16, 17]....

Chapter 25

Figure 25.1 Road map of LAMM.

Figure 25.2 Classification based on geometry size.

Figure 25.3 Types of mechanical micromachining.

Figure 25.4 Lasers in machining.

Figure 25.5 Process flow of laser-assisted micromachining.

Figure 25.6 Laser-assisted micromilling [33].

Figure 25.7 Surface roughness and cutting force in LAMM [35, 40].

Figure 25.8 Laser-assisted microgrinding.

Figure 25.9 Laser-assisted microturning [46].

Chapter 26

Figure 26.1 Unidirectional AFF process.

Figure 26.2 Two-way AFF process.

Figure 26.3 Orbital AFF method.

Figure 26.4 Techniques applied for study of AFF method.

Figure 26.5 Hybrid finishing methods involving the AFF method.

Chapter 27

Figure 27.1 Schematic view for transporting and accelerating powder particles ...

Chapter 29

Figure 29.1 Schematic diagram of the electric discharge machining process.

Figure 29.2 (a) EDM machining setup. (b) Workpiece material after machining. (...

Figure 29.3 Simulink diagram.

Figure 29.4 Training performance progress for MRR.

Figure 29.5 Performance plot for MRR.

Figure 29.6 Regression plot of MRR.

Figure 29.7 Training performance progress for TWR.

Figure 29.8 Performance plot for TWR.

Figure 29.9 Regression plot of TWR.

Figure 29.10 Training performance progress for Ra.

Figure 29.11 Performance plot for Ra.

Figure 29.12 Regression plot of Ra.

Figure 29.13 Training performance progress for OC.

Figure 29.14 Performance plot for OC.

Figure 29.15 Regression plot of OC.

Figure 29.16 Plot functions for GA.

Chapter 30

Figure 30.1 Experimental set-up during machining.

Figure 30.2 AE sensor.

Figure 30.3 A sample ANN.

Figure 30.4 Variation of SR and AE_{RMS} with machining time for Pon (16 µs), Pof...

Figure 30.5 (a): Response plot on SR for titanium grade-2 material. (b): Respo...

Figure 30.6 (a): Ra v/s machining time for titanium material. (b): Ra v/s mach...

Figure 30.7 (a): AE_{SS} v/s machining time for titanium material. (b): AE_{SS} v/s ...

Figure 30.8 (a): AE_{RMS} v/s machining time for titanium material. (b): AE_{RMS} v/...

Figure 30.9 (a): EW v/s machining time for titanium material. (b): EW v/s mach...

Figure 30.10 (a): AE_{SS} v/s machining time for titanium material. (b): AE_{SS} v/s...

Figure 30.11 (a): AE_{RMS} v/s machining time for titanium material. (b): AE_{RMS} v...

Figure 30.12 Study of percentage for titanium material.

Figure 30.13 The performance plot for titanium in ANN.

Figure 30.14 Measured and predicted by ANN for SR of titanium material.

Figure 30.15 Measured and predicted by ANN for SR of P-20 tool steel material....

Figure 30.16 Measured and predicted by ANN for AE_{RMS} of titanium material.

Figure 30.17 Measured and predicted by ANN for AE_{RMS} of P-20 tool steel materi...

Figure 30.18 Measured and predicted by ANN for EW of titanium material.

Figure 30.19 Measured and predicted by ANN for EW of P-20 tool steel material....

Figure 30.20 Measured and predicted by ANN for AE_{RMS} of titanium material.

Figure 30.21 Measured and predicted by ANN for AE_{RMS} of P-20 tool steel materi...

Scrivener Publishing
100 Cummings Center, Suite 541J
Beverly, MA 01915-6106

Advances in Production Engineering

Series Editor: Dr. Sandip Kunar
(drsandipkunar@gmail.com)

"Advances in Production Engineering" addresses recent developments and research issues related to the production engineering which necessitates the development of new materials and manufacturing processes in order to produce high-quality products at lower prices and in less time. This series aims to provide a scientific platform for researchers, practitioners, professionals, and academicians to discuss the most recent technological developments in metals, polymers, ceramics, composites, biomaterials, nanomaterials, special materials, metals, micro-forming, powder metallurgy, ceramics processing, non-traditional machining, high speed machining, micro and nanomachining, and laser processing. Tribological analysis, friction behavior, modelling, and optimization techniques in materials, machining, and manufacturing are also covered in the series.

Publishers at Scrivener
Martin Scrivener (martin@scrivenerpublishing.com)
Phillip Carmical (pcarmical@scrivenerpublishing.com)

Advanced Machining and Micromachining Processes

Edited by

Sandip Kunar
Dept. of Mechanical Engineering, Aditya University, Surampalem, India

Norfazillah Binti Talib
Dept. of Manufacturing Engineering, Universiti Tun Hussein Onn Malaysia, Johor, Malaysia

and

Gurudas Mandal
Dept. of Metallurgical Engineering, Kazi Nazrul University, West Bengal, India



WILEY

This edition first published 2025 by John Wiley & Sons, Inc., 111 River Street, Hoboken, NJ 07030, USA and Scrivener Publishing LLC, 100 Cummings Center, Suite 541J, Beverly, MA 01915, USA
© 2025 Scrivener Publishing LLC
For more information about Scrivener publications please visit www.scrivenerpublishing.com.

All rights reserved. No part of this publication may be reproduced, stored in a retrieval system, or transmitted, in any form or by any means, electronic, mechanical, photocopying, recording, or otherwise, except as permitted by law. Advice on how to obtain permission to reuse material from this title is available at http://www.wiley.com/go/permissions.

Wiley Global Headquarters
111 River Street, Hoboken, NJ 07030, USA

For details of our global editorial offices, customer services, and more information about Wiley products visit us at www.wiley.com.

Limit of Liability/Disclaimer of Warranty
While the publisher and authors have used their best efforts in preparing this work, they make no representations or warranties with respect to the accuracy or completeness of the contents of this work and specifically disclaim all warranties, including without limitation any implied warranties of merchant-ability or fitness for a particular purpose. No warranty may be created or extended by sales representatives, written sales materials, or promotional statements for this work. The fact that an organization, website, or product is referred to in this work as a citation and/or potential source of further information does not mean that the publisher and authors endorse the information or services the organization, website, or product may provide or recommendations it may make. This work is sold with the understanding that the publisher is not engaged in rendering professional services. The advice and strategies contained herein may not be suitable for your situation. You should consult with a specialist where appropriate. Neither the publisher nor authors shall be liable for any loss of profit or any other commercial damages, including but not limited to special, incidental, consequential, or other damages. Further, readers should be aware that websites listed in this work may have changed or disappeared between when this work was written and when it is read.

Library of Congress Cataloging-in-Publication Data

ISBN 978-1-394-30169-0

Cover images provided by Adobe Firefly
Cover design by Russell Richardson

Preface

A key driver of a country’s socioeconomic development is its manufacturing sector. Competing on a global scale requires industries to produce goods that not only meet functional requirements but also minimize environmental impact. As a result, businesses are continually seeking innovative advanced machining and micromachining techniques that optimize efficiency while reducing environmental harm. This growing competitive pressure has spurred the development of sophisticated design and production concepts. Modern machining and micromachining methods have evolved to accommodate the use of newer materials across diverse applications, while ensuring precise machining accuracy.

The primary aim of this book is to explore and analyze various approaches in modern machining and micromachining processes, with a focus on their effectiveness and application in successful product development. Consequently, the book emphasizes an industrial engineering perspective. It is intended for a wide audience, including academics studying this expansive field, as well as researchers, industry practitioners, engineers, and research scientists.

This book covers a range of advanced machining and micromachining processes that can be utilized by the manufacturing industry to enhance productivity and contribute to socioeconomic development. Additionally, it highlights ongoing research projects in the field and provides insights into the latest advancements in advanced machining and micromachining techniques.

Chapter 1 delves into various technological domains, systematically examining techniques that exemplify precision and innovation. It provides a comprehensive overview of advanced machining and micromachining procedures, carefully uncovering the fundamental mechanics behind these methods. Chapter 2 focuses on abrasive jet machining, detailing the processes, equipment, process parameters, capabilities, applications, advantages, disadvantages, and underlying mechanisms. Chapter 3 then explores water jet machining, covering the process principles, key components, process parameters, capabilities, applications, as well as its benefits and drawbacks.

Chapter 4 details the principles of electro discharge machining, covering essential process requirements, equipment specifications, types of generators, electrode materials, selection of dielectric fluids, tool design, process parameters, machining characteristics, capabilities, advantages, disadvantages, and factors to consider when selecting machine tools. Chapter 5 focuses on wire-electro discharge machining, discussing its process principles, equipment details, parameters, machining characteristics, capabilities, applications, benefits, drawbacks, and metal removal aspects. Chapter 6 examines laser beam machining, explaining the lasing action, population inversion methods, types of lasers, process descriptions, beam parameters, capabilities, applications, advantages, and disadvantages. Chapter 7 explores plasma arc machining, describing the process, equipment, DC plasma torch operating modes, performance-influencing parameters, capabilities, applications, advantages, disadvantages, and safety precautions.

Chapter 8 explains the process, equipment details, characteristics, applications, advantages, and disadvantages of ion beam machining. Chapter 9 offers a

comprehensive introduction to electrochemical machining, discussing its fundamentals, applications, and potential future developments, emphasizing its contribution to the advancement of micromanufacturing processes across various high-tech industries. Chapter 10 details ultrasonic machining, covering the process description, equipment, tool feed mechanism, abrasive slurry, liquid media, process characteristics, capabilities, applications, advantages, disadvantages, the material removal mechanism, and recent advancements in this technique.

Chapter 11 covers the theory, mechanics, equipment, process parameters, applications, advantages, and disadvantages of electron beam machining. Chapter 12 provides an overview of chemical machining, including process details, equipment, etchant influence, maskant and etchant selection, applications, and key characteristics. Chapter 13 examines electrochemical grinding (ECG), its variations for specific applications, advantages, challenges, and compares it with other grinding methods, concluding with ECG's current state and future research recommendations.

Chapter 14 explores the photochemical machining process, covering the etching mechanism, experimental design, and parametric impacts, and identifies research gaps for future work. Chapter 15 offers insights into abrasive-assisted micromachining (AAM), summarizing key findings and its role in advancing precision manufacturing. Chapter 16 highlights advancements in abrasive materials, jet propulsion, and optimization techniques, enhancing the efficiency, precision, and sustainability of abrasive water jet micromachining (AWJM), expanding its applications and economic viability.

Chapter 17 covers the principles of electro discharge machining (EDM), focusing on material removal, key

parameters, and differences between macro-EDM and micro-EDM for precision. Chapter 18 reviews recent developments in electrochemical micromachining (EMM), detailing mass removal rates, microtool feed rate selection, and challenges in predicting shape evolution. Chapter 19 provides an overview of ultrasonic micromachining, including principles, equipment, parameters, applications, and recent advancements.

Chapter 20 discusses laser surface modification techniques, focusing on their role in improving implant surface properties. Chapter 21 reviews focused ion beam processes, including standard, developed, and combined methods. Chapter 22 examines glass workpiece micromachining using electrochemical discharge machining with a three-pass tool feed to prevent bending. Chapter 23 provides a comprehensive overview of abrasive water jet machining, from principles to applications and trends, serving both academic and practical needs in manufacturing.

Chapter 24 covers ultrasonic vibration-assisted micromachining, focusing on its applications, capabilities, and limitations for difficult-to-cut materials. Chapter 25 highlights laser micromachining's role in improving tool wear resistance, stress, and surface roughness in high-strength alloys, emphasizing key laser sources. Chapter 26 provides insights into research on the abrasive flow finishing process. Chapter 27 outlines the principles, advantages, and disadvantages of elastic emission machining. Chapter 28 offers a detailed overview of the magnetic abrasive finishing (MAF) process, including its components, mechanisms, parameters, and applications.

Chapter 29 explores the use of Genetic Algorithm (GA) for multi-objective optimization in machining, addressing conflicting performance measures. Fuzzy Grey Relation

Analysis (GRA) is applied to refine GA results, achieving an optimal parametric combination for precision machining of VT20 titanium alloy using electro discharge machining. Chapter 30 examines the machining of Titanium Grade-2 and P-20 tool steel using the L16 orthogonal array, focusing on process parameters such as current, bed speed, pulse time, voltage, and flush rate in wire electric discharge machining. Chapter 31 highlights the importance of wet bulk micromachining in MEMS fabrication, providing an overview from basic crystallography and wet anisotropic etching to advanced silicon wafer manufacturing and micro-fabrication techniques for MEMS components.

We want to thank God first and foremost. Throughout the process of compiling this book, the truth of the gift of writing for everyone became apparent. You have bestowed upon us the ability to believe in devotion, diligence, and dream-chasing. Without the confidence in you, the Almighty, this would never have been possible.

We extend our sincere gratitude to all our friends and colleagues around the world who contributed suggestions and helped shape our ideas. We are especially thankful to the quality managers whose thoughtful insights greatly influenced this work. If experts in the fields of advanced machining and micromachining processes benefit from our efforts, it will greatly please us. We are also deeply appreciative of Martin Scrivener and the team at Scrivener Publishing and all our technical reviewers for their dedication to this extensive project. Their invaluable contributions were essential in bringing this book to completion.

Finally, but most definitely not least, we want to express our gratitude to all our well-wishers for their support. Many people from all backgrounds have generously assisted us

while we produced this book. Without them, we might have given up.

The Editor
December 2024

1
Overview of Advanced Machining and Micromachining Processes

M. Abdur Rahman[1]*, Serajul Haque[1] and N. Sri Rangarajalu[2]

[1]*Department of Mechanical Engineering, B. S. Abdur Rahman Crescent Institute of Science & Technology, Chennai, India*

[2]*Department of Production Technology, MIT Campus, Anna University, Chennai, India*

Abstract

Motivated by an insatiable pursuit of precision and efficiency, the manufacturing landscape has undergone a transformative evolution driven by advanced and micromachining processes. This paradigm shift is rooted in the imperative to fabricate intricate components for diverse industries, necessitating unprecedented accuracy and intricacy. Micromachining, operating on a scale often measured in micrometers, thrives on specialized tools like laser ablation, micro-electro-discharge machining (micro-EDM), and photochemical machining, surpassing the constraints of conventional methodologies when dealing with minute features. The symbiosis between micromachining and advanced manufacturing processes catalyzes the development of micro-electromechanical systems, sensors, and biomedical devices, pushing technological boundaries. The synergy between micromachining and advanced manufacturing processes is a powerful force, paving the way for micro-electromechanical systems, sensors, and biomedical devices, pushing the frontiers of technology. This collaboration between industries striving for smaller, lighter, and more efficient products will undoubtedly shape the future of precision manufacturing. Beyond technical prowess, advanced and micromachining processes signify a philosophical shift in manufacturing, moving from mass production to tailored components that cater to specific and unique requirements. This comprehensive exploration delves into the heart of this transformative journey, analyzing the various processes that define precision and innovation. Each chapter dissects a distinct technique, revealing the underlying mechanisms propelling its capabilities and shedding light on recent research endeavors, providing a glimpse into the future of micromachining and its potential to redefine the manufacturing landscape. More than a technical treatise, this work invites readers to explore the frontiers of precision manufacturing, where human ingenuity and technological prowess converge to create possibilities once confined to the realm of imagination.

***Keywords*:** Micromachining, advanced manufacturing, precision, efficiency

1.1 Introduction

The manufacturing sector has evolved significantly, propelled by a continuous quest for precision, efficiency, and innovation. This evolution is deeply rooted in the need to meet the ever-increasing demands of diverse industries, from aerospace to medical devices, where intricate components play a pivotal role in overall system performance. At the heart of this transformation lies the unyielding pursuit of precision and efficiency. As industries demand components with tighter tolerances and enhanced performance, traditional machining methods have given way to advanced machining and micromachining processes, heralding a new era in manufacturing. The emergence of advanced machining and micromachining processes stands as a testament to human ingenuity and technological progress. These cutting-edge technologies have not only redefined the

possibilities within the manufacturing realm but have also opened doors to novel applications, pushing the boundaries of what was once deemed achievable [1].

The impact of these technologies on the manufacturing industry is revolutionary. The ability to produce components with unprecedented accuracy and intricacy has far-reaching implications, from improving the efficiency of existing systems to unlocking the potential for entirely new designs and functionalities. Micromachining and advanced manufacturing processes represent cutting-edge technologies that have revolutionized precision manufacturing on a miniature scale. In the realm of micromachining, precision is paramount as it involves the fabrication of extremely small components with dimensions typically ranging from a few micrometers to a few millimeters. This field has gained prominence due to the increasing demand for miniaturized devices in various industries such as electronics, medical, aerospace, and telecommunications [2].

At the heart of micromachining lies the ability to fabricate intricate structures with high accuracy. Traditional machining techniques often face limitations when dealing with features on a microscale. In contrast, micromachining employs specialized tools, techniques, and technologies tailored to handle the challenges posed by miniaturization. These processes include precision machining, laser ablation, micro-electro-discharge machining (micro-EDM), and photochemical machining, among others. The integration of micromachining and advanced manufacturing processes has far-reaching implications. It facilitates the development of micro-electromechanical systems (MEMS), sensors, biomedical devices, and other intricate components critical to modern technology. As industries continue to demand smaller, lighter, and more efficient products, the synergy between micromachining and advanced manufacturing will undoubtedly play a pivotal role in shaping the future of precision manufacturing. This introduction merely scratches the surface of the vast landscape of possibilities that emerge at the intersection of micromachining and advanced manufacturing processes [3, 4].

One of the hallmark features of advanced machining and micromachining processes is their ability to achieve levels of accuracy that were once considered unattainable. This newfound precision is a game-changer for industries where even the slightest deviation can have significant consequences. Intricacy in component design has reached unprecedented levels, thanks to the capabilities of these processes. Microscale features, intricate geometries, and complex structures are now achievable with a level of detail that was once inconceivable, opening avenues for innovation in product design and functionality. The advent of advanced machining and micromachining processes represents more than just a technological shift. It signifies a paradigm shift in the philosophy of manufacturing itself. The focus is no longer solely on mass production but on the ability to tailor components with precision, catering to specific and often unique requirements.

In recent years, advancements in advanced machining and micromachining processes have been instrumental in pushing the boundaries of precision manufacturing. These breakthroughs have not only enhanced the capabilities of existing technologies but have also given rise to novel methodologies, shaping the future of the manufacturing industry. For example, laser machining can achieve ultimate precision and is a promising approach for advanced materials and structures, with applications from nanometers to atomic scales [5].

Recent breakthroughs in micro-milling focus on the development of ultra-small cutting tools with enhanced durability and wear resistance. Furthermore, advancements in precision control systems enable real-time adjustments, ensuring consistent and accurate micromachining even in dynamic conditions. In laser micromachining, advancements include the integration of ultrafast laser systems, allowing for precise ablation with minimal thermal effects. The use of novel beam shaping techniques and adaptive optics

enhances the versatility of laser micromachining for a wider range of materials. Micro-EDM is a useful process for manufacturing micro components and parts in difficult-to-machine materials, but improvements in material removal rate, surface finish, tool wear, and dimensional accuracy are needed. Micro-EDM has seen improvements in electrode materials and tool design, enabling higher machining accuracy and reduced tool wear. Additionally, advancements in real-time monitoring systems provide enhanced control over the micromachining process, ensuring optimal results [6, 7].

Embarking on the exploration of advanced and micromachining processes, each subsequent chapter is dedicated to unraveling the intricacies, applications, and advancements that characterize these cutting-edge technologies. The journey through these chapters spans from foundational principles to the cutting edge of research and development, presenting a comprehensive panorama that delineates the future trajectory of manufacturing.

This book navigates diverse technological realms, systematically analyzing processes emblematic of precision and innovation. Each chapter addresses a distinct advanced or micromachining process, methodically uncovering layers to reveal the underlying mechanisms propelling these techniques. Furthermore, the book illuminates recent research endeavors within the micromachining domain, providing insights into contemporary developments in the field.

1.1.1 Classification of Advanced Machining and Micromachining Processes

Advanced machining and micromachining processes encompass a diverse array of techniques, each tailored to specific applications and materials. Classifying these processes helps provide a systematic understanding of their underlying principles and applications. The classification can be broadly categorized into two main groups: traditional advanced machining and emerging micromachining processes.

1.1.1.1 Mechanical Machining

Mechanical machining refers to the process of using mechanical tools and machines to shape, cut, or form materials into a desired shape or size. This process is commonly used in manufacturing and fabrication industries to produce precision components and parts. Mechanical machining techniques are diverse and can be applied to various materials, including metals, plastics, and composites. Here are some common mechanical machining methods:

High-speed machining (HSM): high-speed machining involves elevated cutting speeds and feeds, optimizing material removal rates [8].

Applications:

- *Aerospace components*: production of aircraft structural components and engine parts.
- *Automotive parts*: manufacturing of precision automotive components like gears and engine parts.
- *Die and mold manufacturing:* rapid and precise machining of dies and molds.

1.1.1.2 Abrasive Waterjet Machining (AWJM)

Abrasive waterjet machining (AWJM) employs a high-velocity jet of water mixed with abrasive particles for material removal [9].

Applications:

- *Composite cutting*: precision cutting of composite materials used in aerospace and automotive industries.
- *Stone and glass shaping*: sculpting and shaping of architectural stone and glass components.
- *Metal cutting*: versatile cutting method for metals in various industrial applications.

1.1.1.3 Abrasive Jet Machining (AJM)

Abrasive jet machining (AJM) uses a high-velocity stream of abrasive particles for material removal and surface finishing [10].

Applications:

- *Deburring*: removing burrs from machined components for smooth surfaces.
- *Cleaning*: precision cleaning of delicate surfaces without damaging the material.
- *Etching*: controlled material removal for artistic or functional etching applications.

1.1.1.4 Ultrasonic Machining (USM)

Ultrasonic machining (USM) utilizes ultrasonic vibrations to induce abrasive particle impact on the workpiece [11].

Applications:

- *Micro-hole drilling*: creating small and precise holes in materials like ceramics.
- *Machining brittle materials:* precision machining of materials prone to chipping or cracking.
- *Micro-electronics*: fabrication of intricate shapes in micro-electronic components.

1.1.1.5 Grinding and Superfinishing

Grinding involves abrasive particles removing material, and superfinishing provides ultrasmooth surface finishes [12].

Applications:

- *Tool and die making*: precision grinding for the production of tools and dies.
- *Automotive and aerospace components:* surface finishing for critical components.
- *Tight tolerance parts*: achieving tight tolerances in critical parts for various industries.

These mechanical machining processes play a crucial role in achieving precision and versatility across a broad spectrum of applications, contributing to the production of high-quality components in diverse industries.

1.2 Electrical Machining

Electrical machining refers to a group of manufacturing processes that use electrical energy to remove material from a workpiece. These processes are typically used for shaping or finishing hard materials that are difficult to machine with traditional methods. Electrical machining techniques are widely used in various industries, including aerospace, automotive, electronics, and tool manufacturing.

1.2.1 Electrical Discharge Machining (EDM)

Electrical discharge machining (EDM) utilizes electrical discharges to erode material from the workpiece.

Applications:

- *Dies and molds*: production of intricate dies and molds for various industries.
- *Aerospace components*: machining complex and hardened aerospace components.
- *Medical device manufacturing*: precision machining of small, intricate medical components [13].

1.2.2 Wire-Electrical Discharge Machining (Wire-EDM)

Wire-EDM employs a continuously moving wire as an electrode for precision cutting.

Applications:

- *Prototyping:* rapid prototyping of complex parts with tight tolerances.
- *Precision machining*: machining of intricate and small components for various industries.
- *Aerospace production*: production of precision components for aerospace applications [13].

1.2.3 Electrochemical Machining (ECM)

Electrochemical machining (ECM) removes material through an electrochemical reaction between the workpiece and electrode.

Applications [14]:

- *Turbine blades*: precision machining of complex shapes in turbine blades.
- *Medical components:* production of intricate medical components with high precision.
- *Aerospace parts*: machining of aerospace components from difficult-tomachine materials.

Micro-electrochemical machining (micro-ECM) has been widely used for microscale and nanoscale processing of materials. A recent work introduced a nanosecond pulse power supply for micro-electrochemical machining, utilizing an STM32F103VET6 microcomputer and a metal-oxide-semiconductor field-effect transistor. The supply achieves a continuous pulse with an 8-MHz frequency, a 50-ns pulse width, a 12-A peak current, and a 10-V maximum voltage. Compared to existing supplies, it exhibits enhanced output and improved waveforms, promising increased machining accuracy and efficiency in micro-ECM [15].

1.2.4 Electrochemical Grinding (ECG)

Electrochemical grinding (ECG) combines grinding with electrochemical machining for enhanced material removal.

Applications [16]:

- *Precision grinding*: grinding of complex shapes and hard materials with high precision.
- *Aerospace and automotive components*: surface finishing for precision components.

- *Tool and die making*: producing tools and dies with tight tolerances.

These electrical machining processes are essential for achieving intricate shapes, high precision, and efficient material removal in applications ranging from aerospace and automotive manufacturing to medical device production and beyond.

1.3 Thermal Machining

Thermal machining is a group of manufacturing processes that remove material by using heat as the primary energy source. It is also known as non-traditional machining or advanced machining. Thermal machining processes are used to machine materials that are difficult or impossible to machine using traditional machining methods, such as milling, turning, and drilling.

1.3.1 Laser Beam Machining (LBM)

Laser beam machining (LBM) utilizes a high-energy laser beam for material removal through vaporization, melting, or thermal deformation.

Applications [17]:

- *Cutting and welding*: precision cutting of metals and non-metals, as well as welding in various industries.
- *Micro-electronics*: drilling micro-sized holes and shaping intricate features in electronic components.
- *Medical device manufacturing*: precision machining of medical implants and devices.

1.3.2 Plasma Arc Machining (PAM)

Plasma arc machining (PAM) employs a high-temperature, ionized gas (plasma) to melt and remove material from the workpiece.

Applications [18]:

- *Cutting of electrically conductive materials*: precision cutting of metals like aluminum, steel, and copper.
- *Aerospace industry*: shaping and cutting components for aerospace applications.
- *Metal fabrication:* applications in metal fabrication industries for high-speed cutting.

1.3.3 Electron Beam Machining (EBM)

Electron beam machining (EBM) utilizes a focused beam of electrons for material removal through vaporization.

Applications [18]:

- *Welding*: high-precision welding of intricate components in aerospace and medical industries.
- *Precision drilling*: drilling small, precise holes in hard materials for various applications.
- *Research and development*: used in scientific research for precise material removal in controlled environments.

Thermal machining processes offer versatility and precision in various applications, making them indispensable in industries where intricate shapes, fine details, and minimal

heat-affected zones are crucial.

1.4 Chemical Machining

Chemical machining, also known as industrial etching or chemical milling, is a subtractive manufacturing process that uses chemical reactions to remove material from a workpiece to create the desired shape. It is a non-traditional machining process that is often used to produce intricate and complex shapes that would be difficult or impossible to create with traditional machining methods, such as milling, turning, and drilling.

1.4.1 Chemical Machining (CHM)

Chemical machining (CHM) involves the selective removal of material through chemical reactions, typically using etchants.

Applications [19]:

- *Aerospace industry*: production of lightweight aerospace components with intricate geometries.
- *Electronics manufacturing*: fabrication of printed circuit boards (PCBs) and semiconductor components.
- *Medical device production*: precision machining of components for medical implants.

1.4.2 Photochemical Machining (PCM)

Photochemical machining (PCM) uses photoresist coatings and light to selectively remove material through chemical etching.

Applications [20]:

- *Micro-electronics*: production of micro-electronic components with intricate patterns.
- *Precision components:* manufacturing of intricate and delicate components for various industries.
- *Automotive parts*: fabrication of precision components in the automotive sector.

Chemical machining processes are particularly valuable when intricate and detailed features are required, and traditional mechanical methods may be impractical or inefficient. They find applications in industries where precision and intricate designs are essential for the final product’s functionality and performance.

1.5 Mechanical Micromachining

1.5.1 Micro-Milling

Micro-milling is a downscaled version of traditional milling processes adapted for microscale machining, utilizing miniature cutting tools.

Applications [21]:

- *Microfabrication*: production of small and intricate components for microsystems.
- *Medical devices*: manufacturing of miniaturized components for medical devices.
- *Electronics*: precision machining of small features in electronic components.

1.5.2 Abrasive Water Jet Micromachining (AWJMM)

Abrasive water jet micromachining (AWJMM) uses a high-velocity jet of water mixed with abrasive particles for microscale material removal.

Applications [22]:

- *Micro-cutting*: precision cutting of small features in various materials.
- *Micro-drilling*: creating micro-sized holes in delicate materials.
- *Microfabrication*: Shaping microscale components for electronic and medical applications.

1.5.3 Abrasive-Assisted Machining

Abrasive-assisted machining involves the use of abrasive particles to enhance material removal in microscale machining.

Applications [23]:

- *Surface finishing*: achieving fine surface finishes in microscale components.
- *Micromachining*: enhancing precision in the fabrication of small features.
- *Tool fabrication*: production of miniature tools for micromachining processes.

1.6 Electrical Micromachining

1.6.1 Electrical Discharge Micromachining (EDMM)

Electrical discharge micromachining (EDMM) is a downscaled version of EDM adapted for microscale applications.

Applications [24]:

- *Micro-drilling*: precision drilling of micro-sized holes in various materials.
- *Micro-milling*: fabrication of intricate microscale features in small components.
- *Micro-tooling*: production of miniature tools for MEMS.

1.6.2 Electro-Chemical Discharge Machining (ECDM)

Electro-chemical discharge machining (ECDM) combines electrochemical machining with electrical discharge machining for microscale material removal.

Applications [25]:

- *Micromachining*: precision machining of small features in micro-electronic components.
- *Micro-mold making*: production of microscale molds for small parts.
- *Biomedical devices*: fabrication of microscale components for biomedical applications.

Table 1.1 shows the list of mechanical micromachining operations and its applications [21–25]. Emerging micromachining processes are critical for the fabrication of miniature components used in electronics, medical devices, and microsystems. These processes enable precision at the microscale, pushing the boundaries of what can be achieved in manufacturing small and intricate features.

Table 1.1 Summarizes the mechanical micromachining operations and its applications [21–25].

Micromachining technique	Type of operation	Applications	Products	References
Micro-milling	Mechanical cutting with miniature tools	Microfabrication, medical devices, electronics	MEMS gyroscopes, miniature surgical tools, electronic circuit components	[21]
Abrasive water jet micromachining (AWJMM)	Abrasive water jet erosion	Micro-cutting, micro-drilling, microfabrication	Microfluidic channels, precision watch components, biocompatible microstructures	[22]
Abrasive-assisted machining	Mechanical cutting with abrasive particles	Surface finishing, micromachining, tool fabrication	Micro lenses, microfluidic devices, miniature cutting tools	[23]
Electrical discharge micromachining (EDMM)	Controlled sparking for material removal	Micro-drilling, micro-milling, micro-tooling	Microfluidic injectors, biocompatible microsensors, miniature nozzles	[24]
Electro chemical discharge machining (ECDM)	Combined electrochemical and sparking removal	Micromachining, micro-mold making, biomedical devices	Microfluidic pumps, drug delivery microchips, microscale implants	[25]

1.7 Thermal Micromachining

1.7.1 Laser Beam Micromachining (LBM)

Laser beam micromachining (LBM) at the microscale utilizes a focused laser beam for precise material removal through vaporization or thermal ablation.

Applications [26]:

- *Micro-electronics*: laser ablation for microfabrication of electronic components.
- *Medical devices*: precision machining of miniature components for medical implants.
- *Micro-drilling*: creation of micro-sized holes in various materials.

1.7.2 Plasma Arc Micromachining

Plasma arc micromachining involves using a high-temperature, ionized gas (plasma) for microscale material removal.

Applications [27]:

- *Micro-cutting*: precision cutting of small features in metals and other conductive materials.
- *Micro-welding*: welding of miniature components in microsystems.
- *Aerospace components*: shaping and cutting microscale components for aerospace applications.

1.7.3 Laser-Assisted Micromachining

Laser-assisted micromachining combines traditional micromachining methods with laser assistance for improved material removal.

Applications [28]:

- *Micro-milling*: enhancing precision in milling processes at the microscale.
- *Surface modification:* laser-assisted techniques for microscale surface treatments.
- *Micro-drilling:* improved precision in creating micro-sized holes.

1.8 Chemical Micromachining

1.8.1 Chemical Micromachining (CMM)

Chemical micromachining (CMM) at the microscale utilizes chemical reactions for precise material removal.

Applications [29]:

- *Microfabrication*: etching intricate patterns in micro-electronic components.
- *MEMS production*: fabrication of micro-electromechanical systems with precise features.
- *Biomedical devices*: precision machining of microscale components for medical applications.

1.8.2 Electrochemical Micromachining (ECMM)

Electrochemical micromachining (ECMM) involves the selective dissolution of material through electrochemical reactions at the microscale.

Applications [30]:

- *Micromachining:* production of micro-sized features in various materials.
- *Microfluidics:* fabrication of microchannels for fluidic devices.
- *Microsensor manufacturing:* precision machining of sensors for microsystems.

1.8.3 Chemo-Mechanical Polishing (CMP)

Chemo-mechanical polishing (CMP) combines chemical and mechanical processes to achieve precision polishing and planarization at the microscale.

Applications [30]:

- *Semiconductor manufacturing*: polishing and planarization of semiconductor wafers.
- *Optical components*: finishing and polishing of microscale optical components.
- *MEMS devices*: surface treatment for micro-electromechanical systems.

These thermal and chemical micromachining processes enable the production of intricate and small-scale components, contributing to advancements in micro-electronics, medical devices, and various other industries requiring high precision at the microscale.

1.9 Ultrasonic Micromachining

1.9.1 Ultrasonic Micromachining (USMM)

Ultrasonic micromachining (USMM) employs ultrasonic vibrations to induce abrasive particle impact for material removal at the microscale.

Applications [31]:

- *Micro-drilling*: precision drilling of micro-sized holes in various materials.
- *Micro-milling*: shaping and machining small features with high accuracy.
- *Micro-electronics*: fabrication of microscale components for electronic devices.

1.9.2 Ultrasonic-Assisted Micromachining (UAMM)

Ultrasonic-assisted micromachining (UAMM) combines traditional micromachining techniques with ultrasonic vibrations to enhance material removal.

Applications [32]:

- *Micro-milling*: improved precision and efficiency in milling processes at the microscale.
- *Micro-grinding*: enhancing material removal rates in microscale grinding operations.
- *Micromachining of brittle materials*: reducing the likelihood of microcracks in brittle materials.

1.10 Other Micromachining Processes

1.10.1 Focused Ion Beam Machining (FIBM)

Focused ion beam machining (FIBM) uses a focused beam of ions for material removal and modification at the microscale.

Applications [33]:

- *Microfabrication*: precise milling and etching of microscale features in various materials.
- *Nanotechnology research*: creation and manipulation of nanostructures for research purposes.
- *Semiconductor industry*: ion beam milling for semiconductor device fabrication.

1.10.2 Ion Beam Micromachining (IBMM)

Ion beam micromachining (IBMM) involves the use of ions for precision material removal at the microscale.

Applications [34]:

- *Micro-Drilling*: Creating micro-sized holes with high precision.

- *Surface Modification*: Ion beam treatment for altering material properties at the microscale.
- *Microscale Texturing*: Precision texturing and patterning for microscale components.

These ultrasonic and other micromachining processes play a crucial role in the fabrication of microscale components with intricate details. They are integral to the advancement of technologies in micro-electronics, MEMS, and various industries requiring precision at the microscale.

Applications of Micromachining

The various applications of micromachining are summarized below [5, 6, 35–38]:

Category	Applications			Refere
Medical devices	Microneedles for drug delivery.	Miniature surgical tools and instruments.	Microscale components for implantable medical devices.	[35]
Electronics and semiconductors	Microfabrication of semiconductor components.	Microelectromechanical systems (MEMS) for sensors and actuators.	Microscale features on integrated circuits.	[36]
Optics and photonics	Micro-optical components for cameras and sensors.	Micromachined components for fiber optics and laser systems.	Miniaturized optical switches and modulators.	[5, 6]
Aerospace	Microscale components for satellites and aerospace applications.	Micromachining for lightweight and high-strength Materials in aerospace engineering.		[37]
Automotive	Microscale components for automotive sensors.	Micromachined parts for fuel injection systems.	Miniaturized components for advanced driver assistance systems (ADAS).	[37]
Telecommunications	Micromachined components for communication devices.	Miniaturized radio frequency (RF) components.	Microscale features for telecommunications infrastructure.	[38]
Energy	Microscale components for energy harvesting devices.	Micromachining for microelectro-mechanical energy systems.	Miniature components for sensors in energy-related applications.	[38]
Consumer electronics	Micromachined components for smartphones and wearables.	Miniaturized parts for consumer electronics devices.		[38]
Biotechnology and lab-on-a-chip	Micromachined devices for biological and chemical analysis.	Microfluidic systems for lab-on-a-chip applications.	Miniaturized components for point-of-care diagnostics.	[39]

These applications showcase the versatility of micromachining across various industries, contributing to advancements in technology, healthcare, communication, and beyond. However, it is essential to check for the latest developments in micromachining applications, as the field is dynamic and continually evolving.

1.11 Future Directions and Emerging Technologies

- Additive manufacturing integration: the integration of additive manufacturing (AM) with machining processes holds immense potential. Hybrid systems combining

additive and subtractive techniques offer the promise of manufacturing complex parts with high precision and reduced material waste. This synergy allows for the creation of near-net-shape components, which can then undergo precision machining for final refinement.

- Artificial intelligence (AI) in autonomous machining: AI and machine learning algorithms are revolutionizing machining operations. Autonomous machining systems equipped with AI-driven decision-making capabilities can optimize tool paths, predict tool wear, and dynamically adjust machining parameters in real-time. This fosters adaptive machining processes that enhance efficiency, reduce errors, and optimize resource utilization.
- Nanotechnology integration: the utilization of nanotechnology in machining processes presents exciting prospects. Nanoscale coatings and materials with enhanced properties can revolutionize tooling, reducing friction, wear, and improving tool life. Nanoscale precision in cutting tools could lead to unparalleled machining accuracy, particularly in micromachining applications.

1.11.1 Challenges and Considerations

- Process optimization: achieving optimal process parameters remains a challenge. The complexity of advanced machining processes requires a delicate balance between speed, accuracy, and material removal rates. Ongoing research focuses on developing algorithms and simulation tools to streamline process optimization.
- Environmental sustainability: as manufacturing processes evolve, sustainability becomes increasingly crucial. Efforts are directed toward reducing energy consumption, minimizing waste generation, and developing eco-friendly machining fluids. Sustainable practices are vital to minimize the environmental impact of machining operations.
- Skilled workforce: the evolving landscape demands a skilled workforce capable of operating and maintaining advanced machining technologies. Training programs and educational initiatives aimed at developing expertise in these specialized areas are essential to meet industry needs.

1.11.2 The Following are Some Additional Trends that are Likely to Shape the Future of Micromachining

Increased automation and process control:

Artificial intelligence (AI) and machine learning (ML) will play a crucial role in optimizing micromachining processes, ensuring greater precision, repeatability, and yield.

Sustainability and environmental considerations:

Development of cleaner and more environmentally friendly micromachining processes, using less hazardous materials and reducing waste generation.

Multi-scale and hierarchical manufacturing:

Integrating micromachined components with larger-scale structures and systems, creating complex hybrid devices with novel functionalities.

The future of micromachining is bright, and its potential to revolutionize various industries is undeniable. As we continue to push the boundaries of miniaturization, micromachining will be at the forefront of creating smaller, smarter, and more impactful technologies for the betterment of our world.

The future of advanced machining techniques is brimming with innovation and promise. Here is a peek into what we can expect:

1. Hyper-precision and miniaturization: Imagine machining features as tiny as a single atom! Advanced techniques like FIBM and nanodiamond tools will push the boundaries of precision, enabling the creation of micro- and nanoscale components for medical devices, electronics, and quantum technologies.
2. Multi-material and hybrid machining: Gone are the days of single-material limitations. Laser-based techniques like laser metal deposition (LMD) and laser direct metal sintering (LDMS) will enable the seamless integration of dissimilar materials within a single part, leading to components with unprecedented combinations of properties like strength, flexibility, and heat resistance.
3. Smart and autonomous machining: Machine shops will transform into intelligent factories. Sensors embedded in machines will collect real-time data, while AI algorithms will analyze it to predict and prevent failures, optimize cutting parameters, and even self-correct errors mid-process. This will lead to increased efficiency, reduced downtime, and improved part quality.
4. Sustainable and eco-friendly machining: Sustainability will be a key driver. Minimizing waste, employing recyclable materials, and using cleaner machining processes like abrasive waterjet cutting will be prioritized. This will not only reduce environmental impact but also make machining more cost-effective.
5. Democratization of advanced machining: Advanced machining will not be exclusive to large corporations anymore. User-friendly interfaces, compact machine designs, and cloud-based software will make these powerful technologies accessible to smaller workshops and individual makers, fostering a wave of innovation and entrepreneurship. The future of advanced machining is a fusion of cutting-edge technologies, driven by human ingenuity and a shared vision for a more efficient, sustainable, and miniaturized world. Buckle up because it is going to be an exciting ride!

1.12 Conclusion

In summary, the recent innovations in the manufacturing landscape reveals a notable shift driven by the constant pursuit of precision and efficiency. Throughout this chapter, we have looked into various advanced machining and micromachining processes, each contributing to the industry’s push for greater accuracy and intricacy in crafting components.

The processes we discussed, like laser ablation, micro-EDM, and photochemical machining, operate at a microscale, overcoming traditional limitations in manufacturing, especially when dealing with small features. This shift is more than just technical progress; it represents a change in manufacturing philosophy from mass production to creating components tailored to specific needs.

The collaboration between advanced and micromachining processes has played a crucial role in advancing applications such as micro-electromechanical systems, sensors, and biomedical devices. This partnership drives technological progress, resulting in smaller, lighter, and more efficient components.

This chapter systematically presented various types of advanced machining and micromachining processes and explored the mechanisms behind their enhanced capabilities. It also shed light on recent research and developments in the field, providing insights into the potential future directions of micromachining and its impact on the manufacturing landscape.

In conclusion, it is clear that advanced and micromachining processes go beyond technical advancements; they represent a significant change in manufacturing philosophy.

This shift towards customization and precision marks a new era where the focus is on creating products that meet specific needs. The convergence of human creativity and technological advancement continues to push boundaries, shaping a future where precision manufacturing not only responds to but also anticipates the evolving requirements of different industries. The transition from mass production to precision manufacturing unfolds as a story of innovation and potential, set to redefine the practical and forward-looking aspects of the manufacturing sector.

References

1. Babu, B., Dhamotharan, S., Jayaram, R., Saravanamuthukumar, P., A Summary of Recent Breakthroughs in Micro- and Nano-Machining Technologies. *Periodico*, *91*, 4, 749–765, 2022.

2. Rawal, S., Sidpara, A.M., Paul, J., A review on micro machining of polymer composites. *J. Manuf. Processes*, 77, 87–113, 2022.

3. Liu, M., Wu, X., Niu, Y., Yang, H., Zhu, Y., Wang, W., Research Progress of MEMS Inertial Switches. *Micromachines*, 13, 3, 359, 2022.

4. Mishra, R., Singh, R.P., Garg, R.K., Electrochemical Micromachining: A Review on Principles, Processes, and Applications. *International Conference on Production and Industrial Engineering*, Springer Nature Singapore, Singapore, pp. 47–58, 2023.

5. Wang, J., Fang, F., An, H., Wu, S., Qi, H., Cai, Y., Guo, G., Laser machining fundamentals: micro, nano, atomic and close-to-atomic scales. *Int. J. Extreme Manuf.*, 5, 01, 1–27, 2023.

6. S.P., U.J., H.P., G.S., Micro-electric discharge machining (Micro-EDM) of aluminium alloy and aluminium matrix composites - a review. *Adv. Mater. Process. Technol.*, 8, 1699–1714, 2022.

7. Fassi, I. and Modica, F., Editorial for the Special Issue on Micro-Electro Discharge Machining: Principles, Recent Advancements and Applications, Volume II. *Micromachines*, 14, 1, 29, 2022, https://doi.org/10.3390/mi14010029.

8. Jain, A. and Bajpai, V., *Introduction to high-speed machining (HSM)*, pp. 1–25, Academic Press, 2020, ISBN 9780128150207. https://doi.org/10.1016/b978-0-12-815020-7.00001-1.

9. Ozcan, Y., Tunc, L.T., Kopačka, J., Çetin, B., Sulitka. Modelling, M., and simulation of controlled depth abrasive water jet machining (AWJM) for roughing passes of free-form surfaces. *Int. J. Adv. Manuf. Technol.*, 114, 2, 3581–3596, 2021, https://doi.org/10.1007/s00170-021-07131-1.

10. Abrasive Jet Drilling of Glass using Normal-bed and Fluidized-bed AJM Setup. *Int. J. Eng. Innov. Technol.*, *9*, 3, 1335–1341, 2020, https://doi.org/10.35940/ijitee.b7071.019320.

11. Sabareesan, S., Vasudevan, D., Sridhar, S., Kannan, R., Sankar, V., Response analysis of ultrasonic machining process under different materials – Review. *Mater. Today: Proc.*, *45*, 02, 2340– 2342, 2020, https://doi.org/10.1016/j.matpr.2020.10.695.

12. Dyl, T.C. and Szramka, E., The effect of superfinishing conditions on surface roughness of hardened unalloyed steel. *International Conference Mechatronic Systems and Materials (MSM)*, Bialystok, Poland, pp. 1–4, 2020.

13. Kumar, D., Bajpai, V., Singh, N.K., Nano electrical discharge machining–the outlook, challenges, and opportunities. *Mater. Manuf. Process.*, 36, 10, 1099–133, 2021 Jul 27

14. Kumar, A. and Pabla, B.S., Review on optimized process parameters of electrochemical machining and its variants. *Mater. Today: Proc.*, 46, 10854–10860, 2021, https://doi.org/10.1016/J.MATPR.2021.01.807.

15. Chang, W.J., Wang, S.Y., Tang, H.H., Dong, B.L., Yang, Q., Chen, J.Y., Chen, S.H., Development of a micro-electrochemical machining nanosecond pulse power supply. *Rev. Sci. Instrum.*, 93, 2, 024707, 2022.

16. Sonia, P., Introduction of hybrid machining: Fabrication and experimental investigation of electrochemical grinding on surface roughness. *Mater. Today: Proc.*, 44, 300–304, 2021.

17. Geethapriyan, T., Raj, A.A., Kannan, T.D.B., Senkathir, S., Influence of process parameters on laser beam machining of leather for oil hydraulic system application. *Mater. Today: Proc.*, 47, 4508–4512, 2021.

18. Chien, C.-H., Zawada, A., Konarski, P., Sheu, D., Developing a desk-top electron beam micro-machining system in the low-pressure argon atmosphere. *Procedia CIRP*, 95, 950–953, 2020, https://doi.org/10.1016/J.PROCIR.2020.02.276.

19. Ibrahim, A.F., Huayier, A.F., Abdulhusein, N.A., Influence of machining parameters on material removal rate in chemical machining of silicon carbide (SIC). *J. Phys. Conf. Ser.*, IOP Publishing, 1818, 1, 212–217, 2021.

20. Saraf, A., Yadav, S., Sadaiah, M., Precision Photochemical Machining, in: *Micro and Precision Manufacturing*, pp. 41–70, Springer International Publishing, 2017, Cham, 2018, https://doi.org/10.1007/978-3-319-68801-5_3.

21. Zhang, H., Lu, S., Zhang, C., Li, G., Teng, F., Zhang, J., Sun, T., Finite Element Analysis and Experimental Investigation of Tool Chatter in Ultra-Precision Diamond Micro-Milling Process. *Appl. Sci., 12*, 23, 11968, 2022, https://doi.org/10.3390/app122311968.

22. Soori, M. and Arezoo, B., Minimization of surface roughness and residual stress in abrasive water jet cutting of titanium alloy. *Proc. Inst. Mech. Eng., Part E,* 238, 4, 1613–1625, 2024.

23. Ahmed, U. and Khan, H.F., Literature Review on Abrasive Jet Machining - Past and Present. *SJARR*, *3*, 02, 74–86, 2022, https://doi.org/10.55966/sjarr.2022.3.2.0053.

24. Singh, M., Jain, V.K., Ramkumar, J., Micro-texturing on flat and cylindrical surfaces using electric discharge micromachining. *J. Micro Nano-Manuf.*, 4, 127–137, 2020, https://doi.org/10.1177/2516598420980404.

25. Shrestha, H., Chen, Y.J., Sundaram, M., Non-contact micromachining by a dynamic feed rate controlled electrochemical discharge machining process. *Proc. Inst. Mech. Eng., Part B*, 238, 1–2, 328–334, 2022.

26. Mishra, S. and Yadava, V., Laser Beam MicroMachining (LBMM) – A review. *Opt. Lasers Eng.*, 73, 89–122, 2015, https://doi.org/10.1016/J.OPTLASENG.2015.03.017.

27. Wang, X., Huang, Y., Wang, X., Xu, B., Feng, J., Shen, B., Experimental investigation and optimization of laser induced plasma micromachining using flowing water. *Opt. Laser Technol.*, 126, 106067, 2020, https://doi.org/10.1016/j.optlastec.2020.106067.

28. Menon, V.A. and James, S., Molecular dynamics simulation study of liquid-assisted laser beam micromachining process. *J. Manuf. Mater. Process.*, 2, 3, 51, 2018.

29. Vempannan, C., Kanish, T.C., Thirumanikandan, D., Aswin, B., Electrochemical Micromachining Performance Optimization: Impact of Cathode Profile and Rotation on Machining Speed and Accuracy, in: *Advanced Manufacturing Techniques for Engineering and Engineered Materials*, pp. 20–41, 2022, https://doi.org/10.4018/978-1-7998-9574-9.ch002.

30. Honari, S., Haque, S., Lu, T., Fabrication of ultra-high Q silica microdisk using chemo-mechanical polishing. *Appl. Phys. Lett.*, 119, 3, 2021, https://doi.org/10.1063/5.0051674.

31. Vipindas, K., Kuriachen, B., Mathew, J., An insight on ultrasonic machining technology. *Int. J. Adv. Manuf. Technol.*, Elsevier, 451–478, 2021, https://doi.org/10.1016/B978-0-12-817452-4.00001-4.

32. Zhou, J., Xu, R., Jiao, H., Bao, J.D., Liu, Q.Y., Long, Y.H., Study on the mechanism of ultrasonic-assisted water confined laser micromachining of silicon. *Opt. Lasers Eng.*, *132*, 106118, 2020, https://doi.org/10.1016/j.optlaseng.2020.106118.

33. Utlaut, M., Focused ion beams for nano-machining and imaging, in: *Nanolithography*, pp. 116– 157, Woodhead Publishing, 2014, https://doi.org/10.1533/9780857098757.116.

34. Jain, V.K., Balasubramaniam, R., Mote, R.G., Das, M., Sharma, A., Kumar, A., Kamaliya, B., Micromachining: an overview (part I). *J. Micro Nano-Manuf.*, *3*, 2, 142–158, 2020, https://doi.org/10.1177/2516598419895828.

35. Gaiseanu, F., Analytical Modeling for Fabrication of Biomedical Pressure Sensors by Bulk Micromachining Technology: Silicon Capacitive Pressure Sensors, in: *Encyclopedia of Information Science and Technology*, Sixth Edition, pp. 1–19, IGI Global, 2025.

36. Singh, J., Kant, R., Nimesh, A., Katiyar, N., Bhattacharya, S., Evaluating electrochemical micromachining capabilities for industrial applications: A review. *Mater. Manuf.*, 39, 1, 1–42, 2024.

37. Kunar, S., Singh, A.K., Raviteja, D., Kibria, G., Chatterjee, P., Perveen, A., Talib, N., Overview of Hybrid Micromachining and Microfabrication Techniques, in: *Hybrid Micromachining and Microfabrication Technologies: Principles, Varieties and Applications*, pp. 1–15, 2023.

38. Singh, A.K., Kunar, S., Zubairuddin, M., Kumar, P., Marxim Rahula Bharathi, B., Elumalai, P.V., Rao, Y.K., A Review on Hybrid Micromachining Process and Technologies, in: *Hybrid Micromachining and Microfabrication Technologies: Principles, Varieties and Applications*, pp. 271–281, 2023.

39. Sharma, B. and Sharma, A., Microfluidics: Recent Advances Toward Lab-on-Chip Applications in Bioanalysis. *Adv. Eng. Mater.*, *24*, 2, 2100738, 2022.

Note

*Corresponding author: abdurrahman@crescent.education

2
Abrasive Jet Machining

Jagadeesha T.[1]* and Sandip Kunar[2]

[1]*Dept. of Mechanical Engineering, National Institute of Technology, Calicut, India*

[2]*Dept. of Mechanical Engineering, Aditya University, Surampalem, India*

Abstract

A high-velocity compressed gas jet propels abrasive particles to remove material from the workpiece surface in a non-traditional machining technique called abrasive jet machining (AJM). A few benefits of this approach are that it can create intricate shapes, handle a variety of materials, and achieve great precision with little to no heat-affected zones. Important factors that affect machining efficiency and surface quality are process parameters such abrasive type, particle size, nozzle diameter, standoff distance, and pressure. Aside from this, AJM is used in many different industries, including as aerospace, automotive, electronics, and medical, for operations like drilling, surface texturing, cleaning, and deburring. Even with its flexibility, AJM has drawbacks such the need for equipment maintenance, control over material removal rates, and the possibility of contaminating the environment with abrasive dust. To improve the potential and get over the constraints of AJM for use in the industrial future, ongoing research and development is being conducted. This chapter explores the description of process, equipment description, process parameters, process capabilities, applications, benefits, drawbacks, and mechanisms of AJM.

Keywords: AJM, mixing ratio, nozzle pressure, standoff distance, MRR

2.1 Introduction

Abrasive jet machining (AJCM) involves directing a concentrated stream of abrasive particles onto a work surface using high-pressure gas or air. The abrasive particles then erode the work material at high speeds, resulting in its removal [1].

Abrasive jet machining is primarily employed for precision cutting of complex shapes in hard and brittle materials. In AJM, the material removal is done through brittle fracture of brittle materials. Both mechanism of intergranular and transgranular brittle fracture phenomenon is observed in material removal processes. The material is also removed by impact and cavitation effects, but their rate is not so predominant compared to brittle fracture and generation of micro cracks along grain boundaries [2].

2.2 Description of Process

Material removal is predominately by jet of abrasives and carrier gas which travels with very high-velocity in the order of 300–500 m/s. The mechanics of the material is complex and combination of micro cutting, cavitation effect, and transgranular and intergranular brittle [3].

The particle size is 50 microns, the velocity is 200 m/s, the nozzle has an inner diameter of 0.5 mm, and a standoff distance of approximately 2 mm [4]. Details of AJM is shown in Figure 2.1.

2.3 Equipment Description

Figure 2.2 displays a schematic representation of AJM. Subsequently, the compressed carrier gas is passed through the mixing chamber after filtration and drying. The dust particles are removed in the filter and moisture is removed in dryer. The jet is passed through a nozzle, which improves the kinetic energy of the jet. The High velocity jet is responsible for material removal [5].

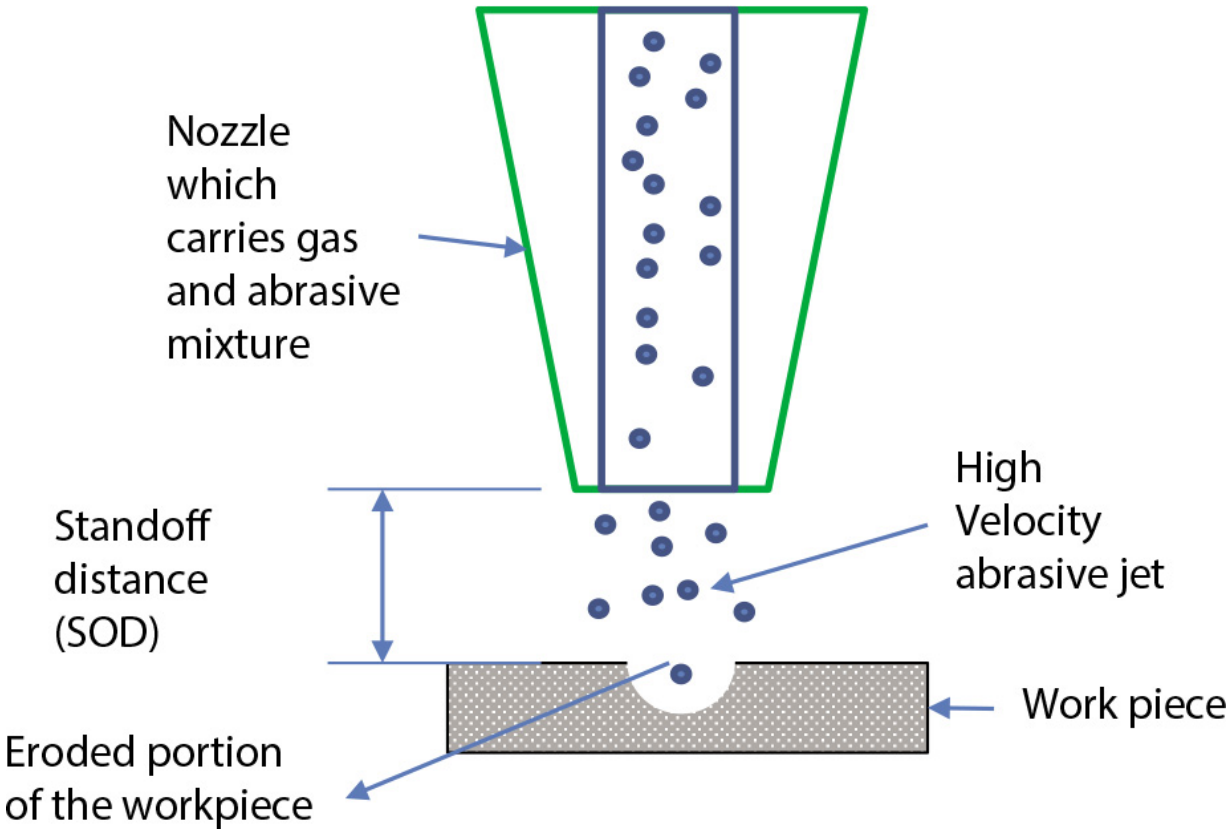


Figure 2.1 Abrasive jet machining.

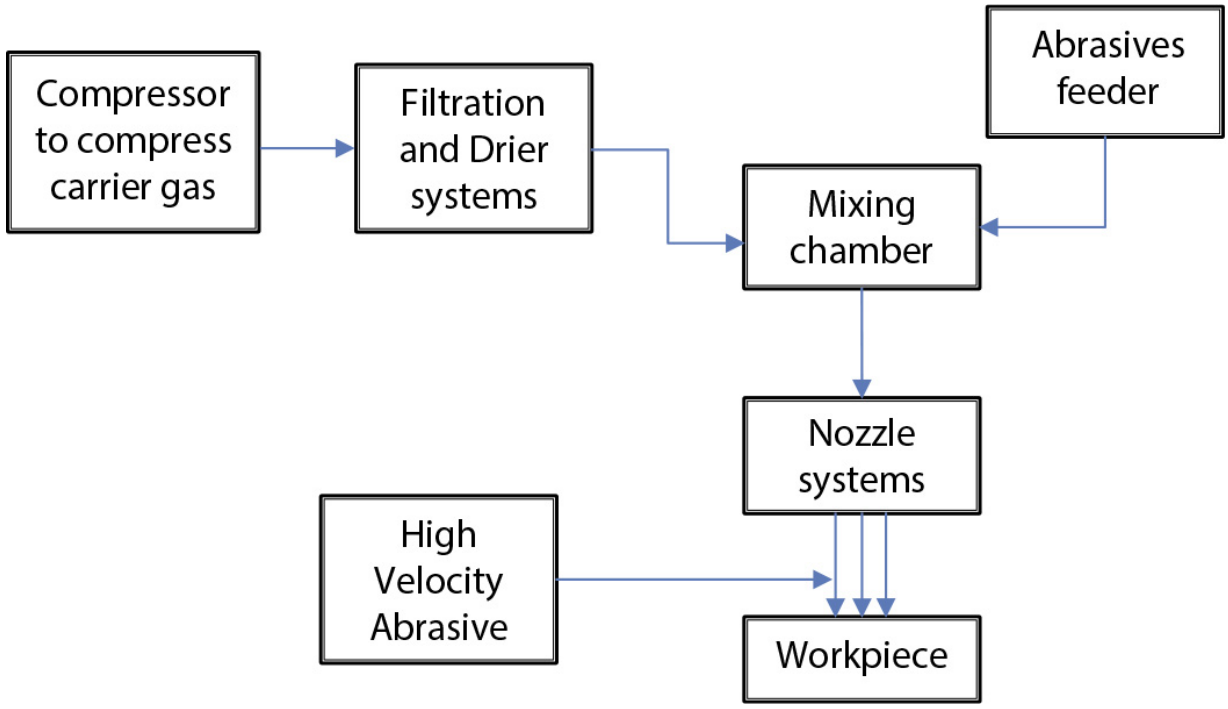


Figure 2.2 Illustration of abrasive jet machining (AJM).

The elements of AJM are:

1. Air compression unit – comprising of filtration unit and dryer.
2. Abrasive feeder
3. Mixing chamber
4. Nozzle jet
5. Abrasives particles

The selection of abrasive in AJM significantly impacts the achievable surface finish and material removal rate (MRR). Common abrasives include dolomite, aluminum oxide, glass beads, and sodium bicarbonate. Aluminum oxide and silicon carbide are offered in various grain sizes, typically ranging from 12 to 50 microns, making them suitable for cutting, deburring, and cleaning across a spectrum of materials. Glass beads, with finer grain sizes around 0.635–1.27 mm, are employed for creating a matte surface finish. Dolomite finds application in polishing and etching, while sodium bicarbonate, often available in even finer grains, proves beneficial for cleaning soft materials, deburring, and achieving a mild surface finish, particularly at temperatures below 500°C [6, 7].

2.4 Process Parameters

- **Abrasives**
    a. The materials used are glass beads, silicon carbide, aluminum oxide, and ground glass sodium bicarbonate.
    b. Uneven or even shaped.
    c. Size varies from 15 to 55 microns.

d. Mass flow ranges from 3 to 25 g/min.

- **Carrier Gas**
  a. The carrier gas is composed of air, carbon dioxide (CO_2), and nitrogen (N_2).
  b. The density of the carrier gas is 1.3 kg/m^3.
  c. The velocity ranges from 500 to 700 m/s.
  d. The pressure ranges from 2 to 10 bars.
  e. The flow rate ranges from 10 to 40 microns.
- **Abrasive Flow**
  a. The velocity ranges from 100 to 300 m/s.
  b. The mixing ratio is calculated by dividing the volume flow rate of abrasives by the volume flow rate of gas.
  c. The nozzle tip distance (SOD) ranges from 0.7 to 20 mm [8].
  d. The angle at which jet strikes should be between 60° and 90°.
- **Nozzle**
  a. The material used is tungsten carbide (WC) or sapphire.
  b. The diameter ranges from 0.3 to 0.9 mm.
  c. The life span for sapphire is 350 h and 25–35 h for tungsten carbide.

2.5 Process Capabilities

1. The rate at which material is being removed is 0.015 cm^3/min.

2. The narrow slots range from 0.15 to 0.30 mm.
3. The CLA (center line average of surface smoothness) values ranges from 0.25 to 1.25 micron.
4. It is possible to get a sharp radius of up to 0.2 mm [9].
5. The cutting capacity of this tool is up to 1.5 mm in steel and 6.3 mm in glass.
6. Machining is possible for materials that are brittle, hard, and have narrow sections.

2.6 Application of Abrasive Jet Machining

1. This method is more cost-effective than etching or grinding for brittle materials [10].
2. Removal of metallic smears from ceramics, elimination of oxides on metals, and eradication of resistive coating, among others.
3. This process is useful in wafer fabrication of semiconductors materials.
4. Parting lines of injection-molded components and forgings are trimmed and tiny castings are deflashed [11].
5. This method is utilized to engrave registration numbers onto tempered glass, which is commonly used for car windows [12].
6. Used to cut thin, brittle materials such as mica, quartz, silicon, and germanium.
7. Register treaming and micromodule manufacture for electrical contact and semiconductor processing are both highly simple and effective processes [13].

8. This tool is utilized for the purposes of etching, cutting, deburring, and polishing brittle and hard materials [14].
9. AJM can be used for heat sensitive materials [15].
10. It is suitable for doing micromachining on brittle components.
11. It is employed in aperture and fine drilling for electronic microscopes.
12. Employed for cleansing metallic molds and cavities.
13. Removing rust, paints, glues, and other impurities from surfaces, particularly those that are difficult to reach.
14. The process of removing burrs from hydraulic valve and surgical needles, nylon, Teflon, and Delrin.
15. Glass engraving is accomplished by employing rubber or iron masks.

2.7 Benefits of Abrasive Jet Machining (AJM)

1. It is possible to achieve a high surface polish based on the grain sizes.
2. The extent of damage is minimal, measuring approximately 2.5 microns in depth.
3. Heat-sensitive materials can be machined using AJM [16].
4. The absence of touch between the work piece and tool eliminates chatter and vibrations from the process.
5. AJM has a minimal capital cost and is simple to use and maintain.

6. It is possible to machine thin portions of hard, brittle materials such as mica, silicon, germanium, and ceramics.
7. It possesses the ability to create holes with complex shapes in hard and brittle materials.

2.8 Drawbacks of Abrasive Jet Machining

1. Insufficient capacity because of poor MRR. Glass has an MRR of 40 g/min.
2. Abrasives have the potential to become embedded in the work surface, particularly when working with soft materials such as elastomers or soft plastics.
3. Sometimes, this process produces taper [17].
4. Poor accuracy results from stray cutting, which is hard to prevent.
5. In order to avoid air pollution and health risks, a dust collection system is a fundamental necessity.
6. The lifespan of the nozzle is restricted.
7. Abrasive powders are not reusable due to the erosion of their sharp edges and the potential for smaller particles to block the nozzle.
8. Damage of nozzle is possible with improper standoff distance.
9. The accuracy of the procedure is diminished due to the flaring effect caused by the abrasive jet.
10. Unacceptable taper will be present in deep holes.
11. The process is polluting and not environmentally friendly.

12. The usage of AJM technique carries a risk due to the presence of airborne abrasive particles. The problem can be resolved through the utilization of abrasive water jet machining.

2.9 Characteristics of AJM

The following are the conditions for the AJM process:

1. Rate of material removal.
2. Work piece’s geometry and surface finish.
3. The rate of wear on the nozzle.

Process parameters typically have an impact on the process criteria.

The following are the characteristics of the process parameters mentioned above in relation to the process criterion.

2.9.1 The Influence of the Abrasive Flow Rate and Particle Size on the Material Removal Rate (MRR)

As abrasive flow increases, the volume of the material removed also increases. There exists a certain abrasive size of particles for which volume of the material removal is maximum. After certain size of particles reached, volume of the material removed decreases because the concentration increases of the abrasives [18–20].

2.9.2 Impact of Abrasive Particle Density and Exit Gas Velocity (Figure 2.3)

Outlet velocity of gas is high when there is little abrasive particle density. If the abrasive particles density increases,

the outlet velocity of gas decreases [19].

2.9.3 Influence of the Mixing Ratio on Material Removal Rate (MRR)

An increase in abrasive mass flow rate will cause a drop in fluid velocity, which will reduce the amount of energy available for erosion and, eventually, the MRR [20]. Using the phrase “mixing ratio” makes it easy to understand this concept. The term “mixing ratio” refers to

$$\text{Mixing ratio} = \frac{\text{Volume flow rate of abrasives per unit time}}{\text{Volume flow rate of carrier gas per unit time}}$$

Increasing the flow velocity of the abrasive can enhance the rate at which material is removed, as long as the mixing ratio remains constant [21]. The mixing ratio remains constant only when both the gas and abrasive flow rates are increased simultaneously (Figure 2.4).

An optimal mixing ratio that yields the highest MRR is determined through a process of trial and error. It might be simpler to calculate the mass ratio, α, instead of the mixing ratio. It is defined as

$$\alpha = \frac{Volume\ flow\ rate\ of\ abrasives}{Volume\ flow\ rate\ of\ carrier\ gas} = \frac{m_a}{m_a + m_g}$$

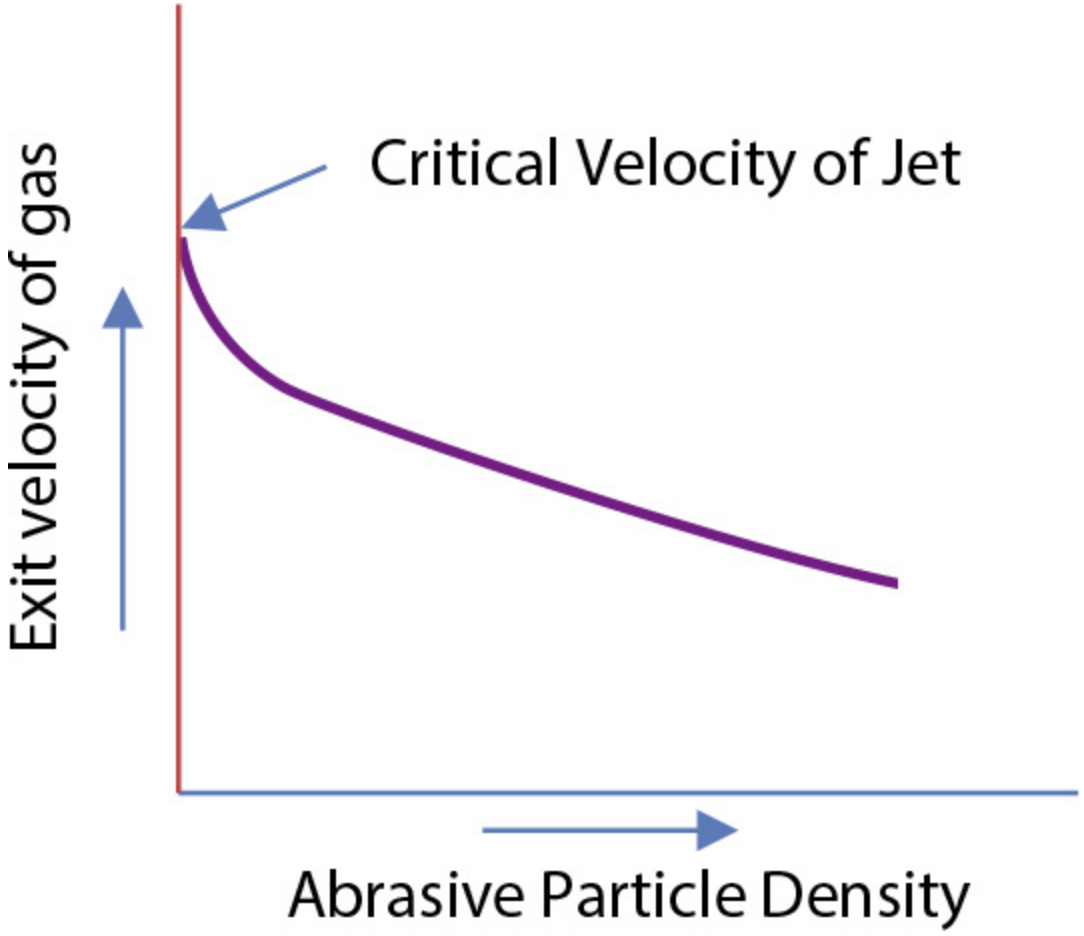


Figure 2.3 Impact of abrasive particle density and exit gas velocity.

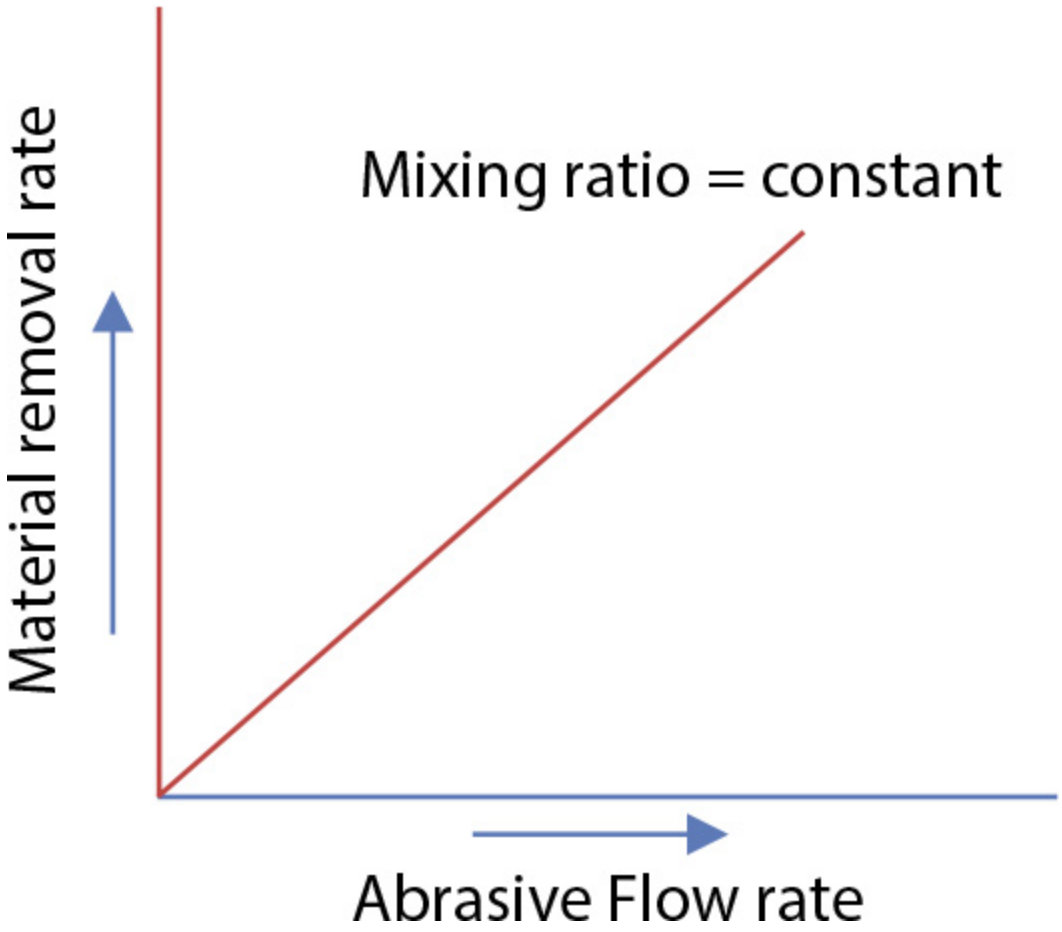


Figure 2.4 Effect of abrasive flow on MRR.

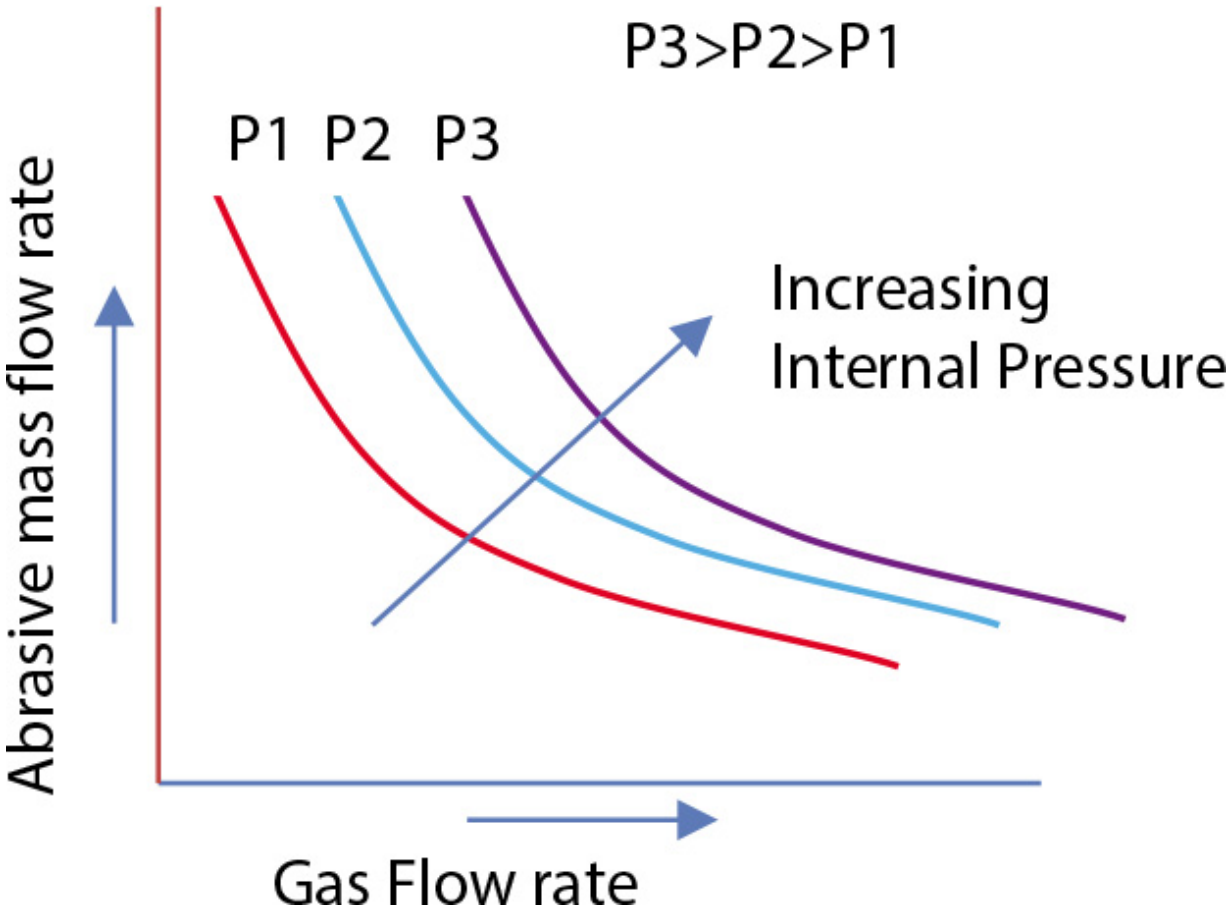


Figure 2.5 Relationship between gas flow rate and abrasive mass flow rate is investigated under varying pressure conditions.

2.9.4 Nozzle Pressure's Impact on MRR (Figure 2.5)

If the gas flow rate is increased, the abrasive flow rate can be increased. This can be done by increasing internal gas pressure [22].

As kinetic energy is increased, the volume of the material increases. Figure 2.5 shows the relationship between gas flow rate and mas flow rate of abrasives.

2.9.5 Stand-Off Distance (SOD)

The distance between the nozzle tip and top of the work surface is called standoff distance (SOD). The SOD greatly affects the accuracy of the part produced. If the SOD is small, then there will be back pressure and accuracy is reduced [23]. If the SOD is greater, then kinetic energy is reduced due to loss of energy with respect to the air around the nozzle.

2.10 Mechanics of Cutting in AJM

There are important assumptions while deriving the mechanics of cutting in AJM [24].

1. The abrasives are assumed to be spherical grit. In practice, it is not so.
2. Kinetic energy of the grit is completely used for machining using AJM.
3. The volume of the material removed is hemispherical.
4. In the case of ductile materials, the volume of material is a portion of sphere.

It is considered that abrasive particles are spherical in shape and have a specific diameter, d_g. Based on the geometry (Figure 2.6):

$$AB^2 = AC^2 + BC^2$$

$$\frac{d_g}{2} = \left(\frac{d_g}{2} - \delta\right)^2 + r^2$$

$$\frac{d_g}{2} - \left(\frac{d_g}{2} - \delta\right)^2 = r^2$$

$$r^2 = \delta^2 + d_g\delta$$

Neglecting δ^2 term

$$r^2 = d_g\delta$$

$$r = \sqrt{d_g\delta}$$

In the Case of Brittle Materials

The hemispherical crater's volume resulting from the fracture is given by:

$$\Gamma_B = \frac{1}{2}\left[\frac{4}{3}\pi r^3\right] = \frac{1}{2}\left[\frac{4}{3}\pi (r^2)^{\frac{3}{2}}\right] = \frac{1}{2}\left[\frac{4}{3}\pi (d_g \delta)^{\frac{3}{2}}\right] = \frac{2\pi}{3}(d_g \delta)^{\frac{3}{2}} \quad (2.1)$$

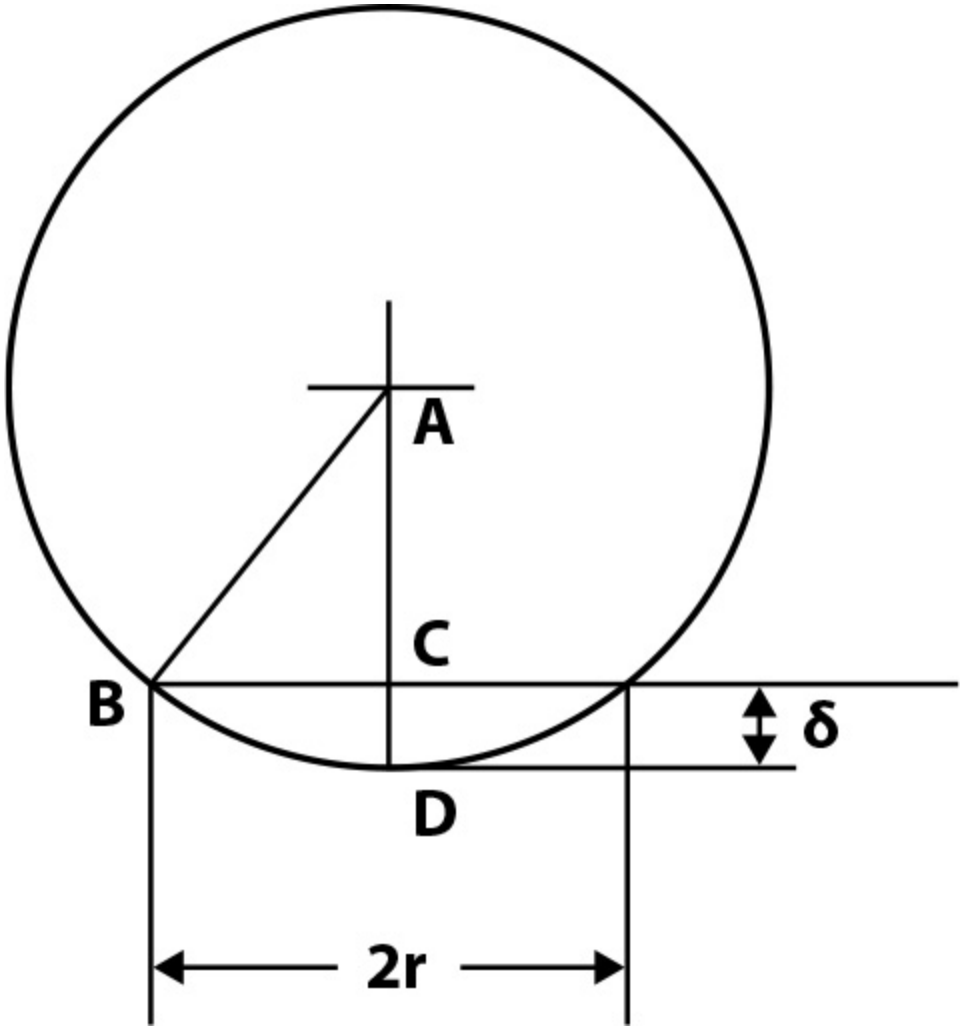


Figure 2.6 Geometry of single abrasive grit.

Assuming that grits also have a velocity (V), we can express this as follows:

$$\text{Kinetic energy} = \frac{1}{2}MV^2$$

$$volume\ of\ single\ grit = \frac{4\pi r_g^{\ 3}}{3} = \frac{4\pi\left(\frac{d_g}{2}\right)^3}{3} = \frac{\pi(d_g)^3}{6}$$

As a result, the kinetic energy of the single grit can be written as:

$$KE = \frac{1}{2}MV^2 = \frac{1}{2}\left(\frac{\pi(d_g)^3}{6}\rho_g\right)V^2 \tag{2.2}$$

Upon collision, the work material experiences a maximum force, denoted as F, resulting in the formation of an indentation, represented as δ.

The work performed during such indentation is:

$$\text{Work done by grit} = \frac{F\delta}{2} \tag{2.3}$$

We are also aware of the material's flow strength = $\sigma_w = \frac{F}{\pi r^2}$

$$F = \sigma_w \times \pi r^2 \tag{2.4}$$

$$F = \sigma_w \times \pi d_g \delta$$

Using Equation 2.4 in Equation 2.3, we get

$$\text{Work done by the grit} = \frac{F\delta}{2} = \frac{\sigma_w \times \pi d_g \delta \times \delta}{2}$$

KE of the particle = work done by the particle

$$\frac{1}{2}\left(\frac{\pi(d_g)^3}{6}\rho_g\right)V^2 = \frac{\sigma_w \times \pi d_g \delta \times \delta}{2}$$

Simplifying, we get

$$\delta = V d_g \sqrt{\frac{\rho_g}{6\sigma_w}} \tag{2.5}$$

In AJM, MRR can be written as:

$$= \{Volume\ of\ material\ removed\ per\ grit\ per\ cycle\}$$
$$\times Number\ of\ impacts\ made\ by\ abrasives\ per\ second$$

$$MRR = \Gamma_B \times \left[\frac{Mass\ flow\ rate\ of\ abrasives}{Mass\ of\ the\ abrasive\ grit}\right]$$

$$MRR = \frac{2\pi}{3}(d_g\delta)^{\frac{3}{2}} \times \left[\frac{M_a}{\frac{\pi(d_g)^3}{6}\rho_g}\right]$$

Upon simplifying, we get

$$MRR = \left[\frac{M_a(V)^{\frac{3}{2}}}{(\sigma_w)^{\frac{3}{4}}(\rho_g)^{\frac{1}{4}}}\right]$$

In the Case of Ductile Materials

The indentation volume is given by:

$$\Gamma_D = \pi\,\delta^2\left[\frac{d_g}{2} - \frac{\delta}{3}\right] = \frac{\pi\,\delta^2 d_g}{2}$$

In AJM, MRR can be written as:

$$= \{Volume\ of\ material\ removed\ per\ grit\ per\ cycle\}$$
$$\times Number\ of\ impacts\ made\ by\ abrasives\ per\ second$$

$$MRR = \Gamma_D \times \left[\frac{Mass\ flow\ rate\ of\ abrasives}{Mass\ of\ the\ abrasive\ grit} \right]$$

$$MRR = \frac{\pi\ \delta^2 d_g}{2} \times \left[\frac{M_a}{\frac{\pi (d_g)^3}{6} \rho_g} \right]$$

Substituting and simplifying, we get

$$MRR = \frac{\pi\ \delta^2 d_g}{2} \times \left[\frac{M_a V^2}{2\sigma_w} \right]$$

References

1. Springeborn, R.K., *Nontraditional machining processes*, ASTME, Michigan, 1967.
2. Sheldon, G.L. and Finnie, T., The mechanics of metal removal in erosion cutting of brittle materials. *Trans. ASME Ser. B*, 88, 393–399, 1966.
3. Lvoie, F.J., Abrasive jet machining. *Mach. Des.*, 5, 1, 23–27, 1973.
4. LaCourte, N., Abrasive jet machining – a solution for problem jobs, tooling and production, pp. 104–106, 1979.
5. Sarkar, P.K. and Pandey, P.C., Some investigation on the abrasive jet machining, Institution of India, 56, 65–74, 1975.
6. Arion, Abrasive machining, ASTME, book 6, Collected series, 1963.

7. Pandey, and Neema, M.L., Erosion of glass when acted upon by an abrasive jet. *International conference on wear of materials*, St. Louis, pp. 387–391, 1977.

8. Sapra, I.L., Studies on Abrasive jet machining, M. E. Dissertation, University of Roorkee, 1975.

9. Dombrowski, T.R., The how and why of Abrasive je machining, modern machine shop, pp. 76–77, 1983.

10. Finnie, I., The mechanism of metal removal in the erosion cutting of brittle materials. *Trans. ASME Ser. B*, 88, 393, 1966.

11. Ingulli, C.N., Abrasive jet machining. *Tool Manuf. Eng.*, 59, 28, 1967.

12. Sheldon, G.L. and Finnie, I., The mechanics of Material removal in the erosive cutting of brittle materials. *Trans. ASME Ser. B*, 88, 393, 1966.

13. Shoeyes, R., Stalens, F., Dekeyser, W., Current trends in non-conventional machining processes. *CIRP Ann.*, 35, 2, 467, 1986.

14. Venkatesh, V.C., Parametric studies on Abrasive jet machining. *CIRP Ann.*, 33, 1, 109, 1984.

15. Verma, A.P. and Lal, G.K., Basic mechanics of abrasive jet machining. *Int. J. Eng. Prod. Eng.*, 66, 74–81, 1985.

16. Verma, A.P. and Lal, G.K., An experimental study of abrasives jet machining. *Int. J. Mach. Tools Des. Res.*, 24, 1, 19–29, 1984.

17. Bitter, J.G.A., A study of erosion phenomenon, Part 1 and II. *Wear*, 5-6, 169–190, 1962.

18. Jagadeesha, T., *Unconventional machining processes*, I K International Publication House Private Limited, New Delhi, 2016.

19. Bhattacharyya, B. and Doloi, B., *Machining Processes utilizing mechanical energy*, Elsevier BV, United Kingdom, 2020.

20. Jain, N.K. and Jain, V.K., Modelling of material removal in mechanical type advanced maching processes: State of art review. *Int. J. Mach. Tools Manuf.*, 41, 11, 1573–1635, 2001.

21. Kumar, K., Zindani, D., Paulo Davim, J., *Mechanical Machining*, Springer Science and Business Media LLC, USA, 2018.

22. Madhu, M. and Balasubramanian, M., Challenges in abrasive jet machining of fiber reinforced polymeric composites- a review. *World J. Eng.*, 6, 1, 1–27, 2020.

23. Heilig, G. and May, M., Hydrodynamic ram effect driven by a hollow spherical hypervelocity projectile. *Results Eng.*, 11, 104–110, 2021.

24. Kritzinger, D., *The effect of different polishing systems on the surface roughness of a nanocomposite and a micro hybrid composite*, University of Pretoria, South Africa, 2023.

Note

*Corresponding author: jagdishsg@nitc.ac.in

3
Water Jet Machining

Jagadeesha T.[1]* and Sandip Kunar[2]

[1]*Dept. of Mechanical Engineering, National Institute of Technology, Calicut, India*

[2]*Dept. of Mechanical Engineering, Aditya University, Surampalem, India*

Abstract

Water jet machining (WJM) is a non-traditional machining process that employs a high-velocity water jet to cut and machine delicate and non-metallic materials. The process utilizes the erosive force of water to remove material, making it ideal for cutting permeable nonmetals like wood, paper, leather, and foam. Water jet machining is also used for cutting composites, stripping, deburring, and even rock excavation. The process parameters, equipment, and applications of WJM are diverse, making it a versatile and cost-effective alternative to traditional machining methods. However, the high maintenance requirement, expensive equipment, and safety considerations make it less suitable for mass production and hard, non-porous materials. Despite these challenges, WJM offers significant advantages, including the absence of heat generation, minimal burrs, and the ability to start cutting at any point without the need for pre-drilled holes. It is also environmentally sustainable and effective in addressing hazardous dust contamination and waste disposal issues. Overall, WJM is a promising technology with a wide range of applications in various industries.

***Keywords*:** Non-traditional, WJM, high velocity water jet

3.1 Introduction

Water jet machining (WJM) is a non-traditional machining process used to cut and machine delicate and non-metallic materials using mechanical energy.

Water jet machining employs high velocity (900 m/s, approximately Mach number 3) water jet. When the stream strikes a workpiece, the material is removed due to the erosive force of water. The water acts like a saw which cuts a narrow groove in the workpiece. This process is primarily used to cut and slit permeable nonmetals like wood, paper, leather and foam. It has also been used to cut composites and perform action like stripping and deburring. Pulsed water jets have been used in rock excavation and machining lead and aluminum. A variety of target material including wood, lead, leather, rubber, aluminum, copper and steel can be cut using WJM. Cutting capability reported was at pressure up to 10,000 bar [1–5].

3.2 Description of Process

In WJM, high velocity (600–1400 m/s) and high pressure (2000–8000 bar) water jet is allowed to hit a given material. The water's velocity is practically nullified upon impact with the surface, as the majority of its kinetic energy transforms into high-pressure energy. The description of the process is given in Figure 3.1. During the initial milliseconds of impact, the passing pressure exceeds several times standard pressure [6–8].

The process of water jet shearing (shown in Figure 3.2) works by wearing away the material through localized pressure that is stronger than the material itself. For certain flexible materials, it involves slicing due to the fast flow of water across the surface. In less precise cutting situations like tunnelling, other effects like cracking from

stress waves and the force of the cutting fluid filling in cracks and gaps are likely. Some scientists believe that air bubbles in the jet also help wear away the material [9–13].

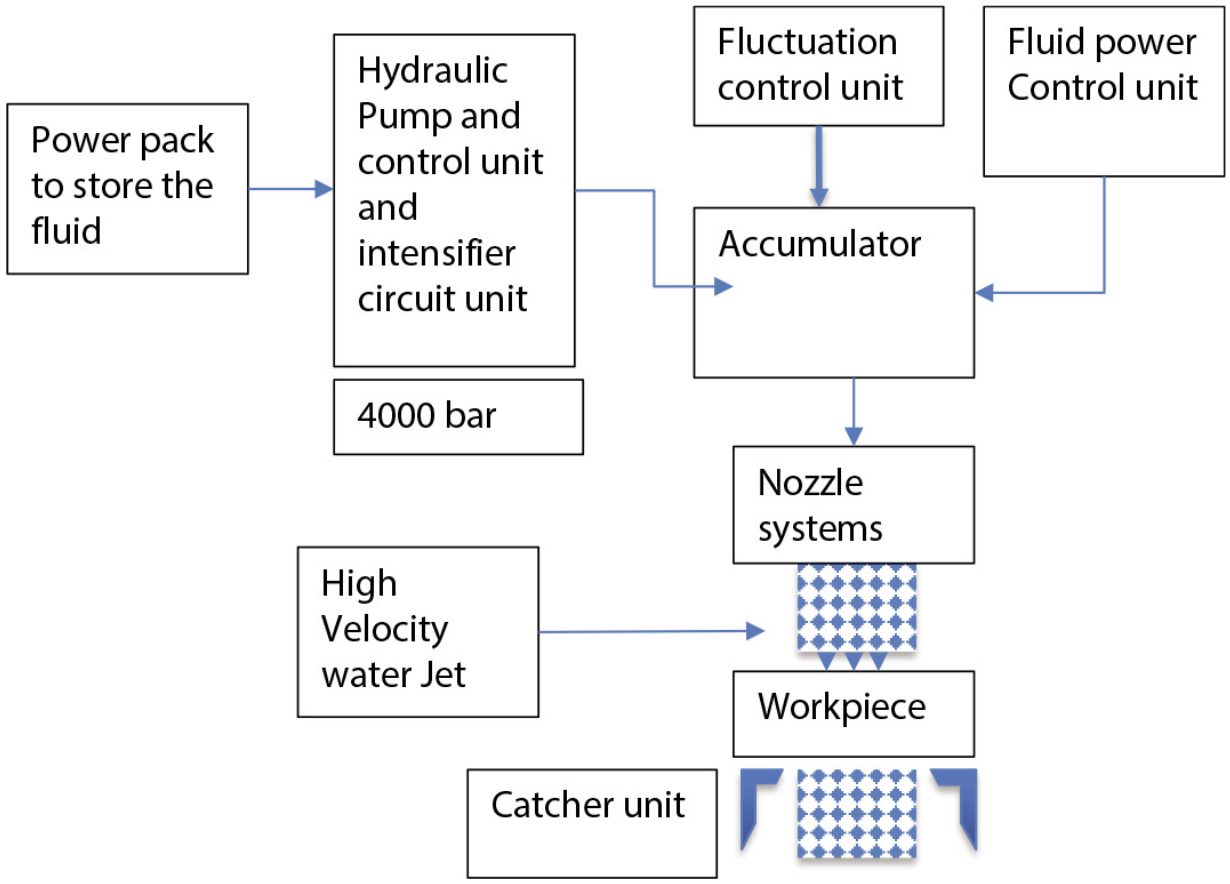
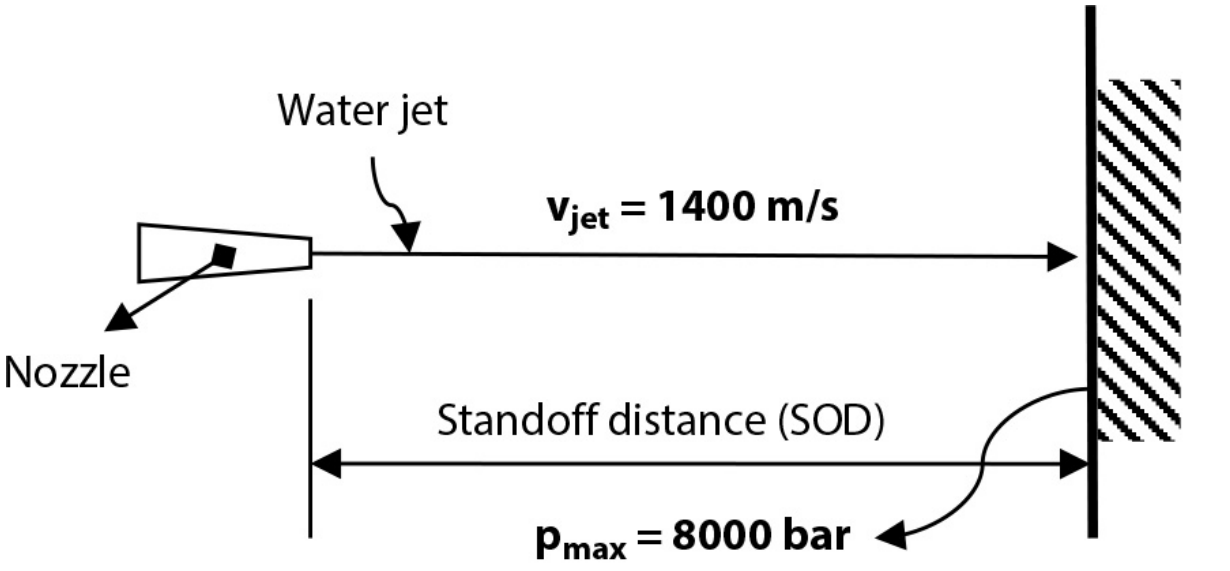


Figure 3.1 Water jet machining process.



$$stagnation\ pressure = water\ density\ (\rho)\ \frac{v_{jet}}{2} \gg \sigma_{work\ material}$$

Figure 3.2 Mechanism of water jet shearing.

In a water jet machine, water serves as the cutting tool, remaining perpetually sharp and resilient. This method produces no dust, hence minimizing risks during machining, particularly for materials like fibers and composites [14].

3.3 Description of Equipment

A schematic layout of WJM is shown in Figure 3.1. The equipment consists of 3 main units. i) High pressure is generated with intensifier along with a pump, ii) cutting unit consists of movement of nozzle and work table, and iii) a filtration system designed to eliminate particles and debris from water post-usage. The main parts are intensifier, high pressure tubing, accumulator, hydraulic pump, jet cutting nozzle and catcher.

3.3.1 Hydraulic Pump

The pump is powered by an electric motor and supplies oil at high pressures as 120 bar to drive an intensifier. The oil is drawn from the tank and is pumped to an intensifier. Low pressure oil is used by intensifier to produce high pressure water jet. The hydraulic pump provides versatile options for both water jet cutting and cleaning tasks, accommodating single or multiple cutting stations to boost machining productivity [15–16].

3.3.2 Intensifier

The function of the intensifier is to convert the energy from low pressure hydraulic fluid into ultra-high-pressure water. The intensifier takes in water at a low pressure (typically between 4 and 5 bar) and pushes it out through an accumulator at a higher-pressure range of 3800–4000 bar.

In the hydraulic system, fluid power is provided to a reciprocating piston located in the center section of the intensifier. At each end of the piston's movement, limit switches trigger the electronic controls to switch the direction control valve, reversing the piston's direction, as depicted in the Figure 3.1. The intensifier assembly generates pressure in two directions due to plungers on either side of the piston. The intensifier produces ultra-high-pressure output on one side while it is in the inlet stroke on the other. During the inlet stroke of the plunger, filtered water passes through the check valve assembly and into the high-pressure cylinder. The water compresses when the plunger changes direction and emerges at extremely high pressure.

3.3.3 Accumulator

The accumulator uses compressibility of water to maintain continuous flow of the high-pressure water when the intensifier changes its direction.

3.3.4 Nozzles

Nozzles serve to transform high-pressure liquid into a high-velocity jet. To minimize erosion, the nozzle material should possess extreme hardness. However, for achieving a smooth, contoured outcome, the material needs to be ductile and easily workable. Through careful nozzle design, the need for long-chain polymers to reduce friction in fluid flow has been eliminated. Synthetic sapphire, known for its wear resistance and machinability, is commonly used for nozzles. The presence of foreign particles like dirt in water can lead to nozzle failure due to chipping, while mineral deposits can cause constriction, also resulting in failure. Sapphire nozzles typically last between 200 and 600 hours depending on usage, but longer life can be achieved through multi-stage filtration, removing solids larger than

0.45 microns. The compact design of head allows smooth integration with motion control systems, extending from simple two-axis tables to complex multi-axis robotic setups. The internal diameter of nozzles typically falls within the range of 0.07–0.50 mm.

3.3.5 High Pressure Tubing

High-pressure tubing conveys pressurized water to the cutting head, with characteristic diameters ranging from 6 to 14 mm. This setup enables the cutting head to move flexibly, controlled either manually or via a remote-controlled valve specifically designed for this application.

3.3.6 Catcher

The catcher collects the machining debris. Water jet outside the nozzle travels at a very high speed. To reduce the exposed length of a jet, for safety and also to reduce the process noise, a catcher is used. There are two types: tube type and slot type. The tube catcher is commonly used. It is comprised of a tube ranging from 300 to 600 mm in length, connected to a drainage hose. The tube’s length ensures that the water jet disintegrates entirely before reaching the tube’s base. When it would be awkward to manipulate a catcher of this length behind a part, as with a hand-held device, a short tube catcher can be used. This uses a hard, replaceable impingement insert to break up the jet quickly. For slitting system incorporating multiple or adjustable nozzles, a slot type catcher is used. Although the slot type catcher may be most convenient in this situation, it is less effective in reducing noise levels.

3.4 Process Parameters

The process variable which controls the WJM pressure are jet nozzle parameters, jet fluid properties, workpiece

properties, material removal rate (MRR), finish of product, and rate of wear on nozzle.

3.4.1 Jet Nozzle

The standoff distance (SOD) refers to the space between the jet nozzle, typically with a diameter of 0.1–0.3 mm, and the workpiece, ranging from 2.5 to 6 mm. For materials found in printed circuit boards, this distance can be extended to as much as 20 mm. Research indicates that with a nozzle diameter of 0.12 mm and a cutting speed of 1.1 mm/s, there is a reduction in the depth of cut observed with an increased separation distance. Similarly, when cutting fiber reinforced plastics (FRP), studies have demonstrated that increasing the rate of machining and utilizing a smaller nozzle diameter lead to an expansion of the damaged layer’s width.

3.4.2 Jet Fluid

In WJM, pressures typically range from 150 to 1000 MPa, providing power between 8 and 80 kW. Increasing pressure for a specified nozzle diameter allows for more power utilization in the machining process, leading to deeper cuts. Jet velocities vary from 540 to 1400 m/s. Higher pressures enhance cutting quality by widening the jet diameter and reducing traverse speed, enabling cutting of thicker and denser materials. Additionally, higher pump pressures result in greater depth of cut. The fluid used should have low viscosity to diminish energy losses and be non-corrosive, non-toxic, readily available, and inexpensive. Water is usually employed for cutting steel alloys, while ethanol is used for meat and vegetable oil for frozen foods.

3.4.3 Target Material

Brittle materials tend to fracture during cutting, whereas ductile materials are more conducive to cutting. Material thicknesses typically vary from 0.8 to 25 mm or even greater.

3.4.4 Material Removal Rate (MRR)

Hybrid considering the loss of energy during the creation of the water jet at the orifice, the velocity of the water jet can be expressed as:

$$v = c_v \sqrt{\frac{2p}{\rho}} \tag{3.1}$$

Where

c_v *is the velocity coefficient of the orfice,*

p = *pressure and* ρ *is the density*

The volume flow rate of fluid may be expressed as:

$$q = c_c \times v \times a$$

c_c *is coefficeint of vena contracta*

v = *velocity and* a *is the area of orifice*

$$q = c_c \times v \times a \tag{3.2}$$

$$q = c_c \times v \times \frac{\pi d^2}{4}$$

$$q = c_c \times c_v \sqrt{\frac{2p}{\rho}} \times \frac{\pi d^2}{4}$$

$$q = c_d \frac{\pi d^2}{4} \sqrt{\frac{2p}{\rho}}$$

c_d *is coefficeint of discharge of the orifice*

Total power of the fluid jet can be expressed as:

$$P = p \times q \tag{3.3}$$

$$P = p \times c_d \frac{\pi d^2}{4} \sqrt{\frac{2p}{\rho}} = c_d \frac{\pi d^2}{4} \sqrt{\frac{2p^3}{\rho}}$$

In water jet machining, it is commonly assumed that the MRR is directly proportional to the power of the water jet.

$$MRR \propto Power\,(P)\ of\ the\ water\ jet$$

$$MRR = k \times Power\,(P)\ of\ the\ water\ jet$$

Where k is the constant and depends on specific energy of work material.

$$MRR = k \times c_d \frac{\pi d^2}{4} \sqrt{\frac{2p^3}{\rho}} \tag{3.4}$$

Besides these factors, the MRR is significantly affected by the SOD, which refers to the distance between the nozzle tip and the surface of the workpiece. Research indicates that the MRR tends to increase with an increase in the SOD up to a certain threshold, beyond which it stabilizes for a specific tip distance and then steadily decreases. A lower MRR at shorter SODs is attributed to the reduction in

nozzle pressure as the distance decreases. Conversely, the decrease in MRR at longer SODs is due to the reduction in jet velocity as the distance increases.

3.4.5 Geometry and Finish of Work Piece

The geometry and finish of the workpiece depend primarily on five main factors: the design of the nozzle, the jet velocity, the speed of cutting, the depth of cut (DOC), and material properties such as hardness [4].

3.4.6 Wear Rate of Nozzle

The wear rate of the nozzle is influenced by several factors, as well as the hardness of the nozzle material, the pressure of the jet, the velocity of the jet, and the design of the nozzle. Cutting is usually performed with a nozzle to workpiece standoff distance of less than 25 mm and optimally, 3 mm. Because there is a little change in the shape or diameter of the jet within 25 mm of the nozzle, the SOD can be considered a fixed parameter. Hence, only three parameters, pressure, nozzle diameter, and traverse rate, are varied, depending on the material and the thickness being cut. In general, as the power of the water stream is increased, the capacity to cut fast or to cut thicker material is also increased. This is done by increasing pressure, increasing the nozzle diameter, or decreasing the traverse rate [5–8].

3.5 Process Capability

3.5.1 Cutting and Slitting

A diverse array of materials can be cut using WJM; however, due to erosion being the primary mechanism in metal cutting, the material ideally should be porous, fibrous, granular, or soft. In this process, the cutting rate

can be exceptionally high, leading to the buildup of thickness through multilayer cutting, which may subsequently slow down the cutting rate. Alternatively, the nozzle head may be stimulated by a cam-driven actuator to manage this issue [16]. In shape cutting using WJM, pre-drilling is unnecessary since the jet can pierce the material at any location and then continue cutting in any direction. This omni-directional cutting capability enables the fabrication of complex shapes with nearly any radius easily. Thick materials can be cut using more than one passes without compromising the quality of the cut. In this approach, the first pass creates a clear slot in the material, allowing for deeper cuts in subsequent passes. Multiphases cutting requires less energy compared to a single pass with a more powerful jet. The surface finish of the cut edges is typically good, without any burrs or heat affected zone (HAZ). However, the surface finish and straightness may deteriorate when the material is very thick or when cutting speeds are excessively high. The cutting rate for various materials using WJM varies depending on the material thickness. For instance, for leather, cutting is achieved at a thickness of 2.2 mm, while for plywood, the thickness is 6 mm. The travel speed ranges from very low, such as 0.5 mm/min for vinyl chloride, to considerably higher speeds, like 200 mm/min for corrugated board.

3.5.2 Cable Stripping

Water jet cannot cut readily the metal and this principle is used in cable stripping. Thus, during cable stripping, jet easily pierces and cuts installation without harming the underlying metallic cable. Cable stripping is performed with water pressures of 70–200 MPa, much lower than WJM cutting and insulation thickness as great as 12–15 mm can be cut [5].

3.5.3 Deburring

Water jet deburring was either fan-shaped or conical-shaped jet to break or erode burrs from non-ferrous parts. Pressures up to 200 MPa drive the jet. Burrs are easily removed from areas that normally would be difficult to access, such as in narrow openings, blind holes and line-of slight internal cavities. The size of the burr that can be removed is proportional to exposure time [6–12].

3.6 Applications of WJM

Water jet machining (WJM) finds applications across a wide range of materials including metals, paper, cloth, leather, plastics, food, and ceramics. It is celebrated for its versatility and cost-effectiveness, often serving as a viable alternative to traditional machining methods. Water jet machining boasts several advantages over conventional techniques, completely eliminating HAZ, toxic fumes, layers of recast, work hardening, and stresses induced by temperature. It is also highly effective for cleaning purposes. Typically, cut surfaces exhibit a sandblast appearance and finish, with harder materials yielding a greater edge finish. Surface finish can range from 1.6 micron root mean square (RMS) to very coarse, depending on the specific application, while tolerances typically fall within the range of ± 25 microns for thin materials. Both surface roughness and tolerance are influenced by speed of machining [13].

- **Cutting:** water jet machining (WJM) finds application in cutting various materials such as fiberglass and corrugated wood. In industries like aerospace, WJM is utilized for cutting asbestos to minimize airborne dust. Additionally, it is employed for cutting fiberglass and

polyethylene automotive parts. WJM is also utilized for high-speed cutting of corrugated boxes.

- **Drilling:** precision angled and fashioned holes in diversity of material can be drilled where electro discharge machining (EDM) or electron beam machining (EBM) is expensive and time consuming.
- **Machining of plastics:** in WJM, thermal damage to materials is minimal, and the precisely pointed tool enables accurate cutting of contours. However, a primary drawback arises from the rebound of the water jet caused by fibers embedded in the matrix, which protrude after machining. The surface quality generated determines the attainable feed rate.
- **Cutting of rocks:** a 51-mm deep slot was cut in granite using two oscillating jets under a pressure of 275 MPa over 14 passes, with a feed rate of 25 mm/s. Similarly, an oscillating nozzle system operating at a feed rate of 25 mm/s and a pressure of 172 MPa was used to cut a 178-mm deep groove in sandstone. The standoff spacing was changed after each pass.
- **Deburring:** utilizing a pressure of 700 bar and a flow rate of 27 liters per minute (LPM), the method uses high pressures to remove large burrs, about 3 mm in height, from 12-mm diameter drilled holes in a hollow molybdenum chromium steel shaft in 15 s. In this approach, burrs are dislodged through the impact of water. For the removal of burrs from non-metallic materials, a higher pressure of 4000 bar and a reduced flow rate of 2.5 LPM are utilized.
- **Cutting of printed circuit boards:** utilizing a small diameter water jet positioned close to the edge of the part enables the cutting of printed circuit boards at speeds surpassing 8m/min, with an accuracy level of ±

0.13 mm. With the use of computer numerical control (CNC) technology, a variety of shaped boards that are intended for usage in cassette players and mobile radios may be easily cut.

- **Surface treatment:** this procedure is used extensively and for a variety of purposes. First of all, it eliminates deposits and residues without the use of hazardous chemicals, which reduces the need for expensive cleanup and dumping procedures. In addition, it is used for surface cleaning of castings and pipes, surface texturing, degreasing, polishing, cleaning of food utensils, ornamental finishing, and nuclear decontamination. Moreover, it offers a cost-effective method for paint removal and getting the surface ready. Lastly, before recoating or painting, it plays a crucial role in eliminating corrosion, spray leftover, salt that dissolve, chemicals, and surface degradation.
- **Wire stripping:** the procedure enables the removal of wire insulation without causing any harm to the metal or the copper wire’s liner. The hand stripping process is less efficient compared to this procedure.
- **Mining:** hydraulic coal mining is possible using WJM. In most mining applications, water pressures below 350 bar combined with large diameter nozzles have been used. A Canadian mine reported that two men produced 2250 tons of coal in one shift by hydraulic mining.
- **Tunnel boring:** Japanese railway engineers have tested percussive drills incorporating two or four nozzles, with diameters of 0.2–0.4mm, operating at 4000 bar to achieve holes 35–215 mm in diameter at drilling speeds between two to five times the normal rates. Comparable techniques have been employed in the demolition of reinforced concrete structures, the

creation of anti-skid grooves in air field runways and roadways, the construction of trenches, and the laying of cables.

3.7 Advantages of WJM

- Its cutting ability extends in multiple directions.
- Water, being inexpensive, environmentally safe, and easily disposable, is the primary medium.
- Heat generation is absent, preventing material rewelding and thermal degradation.
- Cutting can commence at any point without the need for pre-drilled holes.
- The water jet closely resembles an ideal single-point tool.
- Complex contours can be cut both horizontally and vertically.
- Deflection of the workpiece is non-existent.
- Minimal burrs are produced, and tool wear is negligible.
- The process is environmentally sustainable.
- It effectively addresses hazardous dust contamination and waste disposal issues, particularly when cutting materials like asbestos and fiber insulation.
- Multiple head processing is possible.
- Simple fixturing eliminates the need for costly and complex tooling, reducing turnaround time and costs.
- By eliminating secondary procedures like polishing and grinding, the total costs are reduced.

- The presence of narrow kerfs facilitates the compact arrangement of several components inside a singular blank.
- Optimal for the purpose of shaping material into an almost net form.
- Laser-reflective substances, such as copper and aluminum, may be effectively sliced with this method.
- Facilitates enhanced accuracy in the cutting of pliable materials.
- Capable of cutting through very thick materials, such as 383-mm titanium and Inconel 307.
- Noise reduction can be achieved by positioning generators and pumps at a distance from that cutting spot.
- Fluid can be recycled by filtering out debris.
- Requires only a small amount of fluid, typically 200–300 liters per hour.
- Workpieces remain clean and free from dust.
- Low operation and maintenance costs due to the absence of moving parts.
- Suitable for cutting soft materials like leather, rubber, and asbestos that could clog conventional saw teeth.
- Suited for use in explosive environments and cutting asbestos and glass fiber insulation.

3.8 Disadvantages of WJM

- High maintenance requirement make it unsuitable for mass production.

- Equipment are expensive and therefore hourly rates are high.
- It is not well suited for hard, non-porous materials.
- Contaminated water must be treated before disposal.
- Safety requirement is high as high pressure water jet is used.

3.9 Worked Examples

Problem 1: Estimate aqua jet velocity when the pressure is 3000 bar and allowed to impinge on the work piece. The radius of orifice is 0.15 mm and there are no losses.

Data given:

Pressure = $p = 3000\ bar = 3000 \times 10^5\ \frac{N}{m^2}$

Water density = $\rho = 1 \times 10^3\ \frac{kg}{m^3}$

Diameter of orifice = $d = 0.3\ mm$

Assuming no losses.

Solution:

Since the there is no losses, we can $c_v = 1$

$$v = c_v \sqrt{\frac{2p}{\rho}}$$

Where

c_v *is the velocity coefficeint of the orfice,*

p = *pressure and* ρ *is the density*

$$v = c_v\sqrt{\frac{2p}{\rho}} = 1\times\sqrt{\frac{2\times 3000\times 10^5}{1000}} = 774.6\, m/s$$

Problem 2: Determine the mass flow rate of water when subjected to a pressure of 3000 bar and allowed to impinge on the workpiece through an orifice with a diameter of 0.3 mm, assuming a coefficient of discharge of 0.7.

Data given:

Pressure = p = 3000 bar = $3000\times10^5\ \frac{N}{m^2}$

Water density = ρ = $1\times10^3\ \frac{kg}{m^3}$

Diameter of orifice = d = 0.3 mm

Solution:

Mass flow rate of the water jet can be given as:

$$mass\ flow\ rate = mass\ density \times volume\ flow\ rate$$

$$mass\ flow\ rate = mass\ density \times area\ of\ orifice \times velocity\ of\ jet$$

$$m = \rho \times c_d \frac{\pi d^2}{4}\sqrt{\frac{2p}{\rho}}$$

$$m = 1000\times 0.7\times \frac{\pi d(0.3\times10^{-3})^2}{4}\sqrt{\frac{2\times 3000\times 10^5}{1000}}$$

$$m = 1000\times 0.7\times \frac{\pi (0.3\times10^{-3})^2}{4}\sqrt{\frac{2\times 3000\times 10^5}{1000}}$$

$$m = 0.03832\frac{kg}{second}$$

$$m = 0.03832\times 60 = 2.3\ kg/min$$

References

1. Atkey, M., Water Jet Cutting: A Production Tool. *Mach. Prod. Eng.*, 141, 3631, 18–19, 1983.

2. Jagadeesha, T., *Unconventional Machining Processes*, I K International Publishing House Private Limited, New Delhi, 2016.

3. Farner, I.W. and Attewell, P.B., Rock Penetration by High-Velocity Water Jets. *Int. J. Rock Mech. Min. Sci.*, 2, 2, 33–41, 1965.

4. De Meis, R., Cutting with Water. *Aerosp. Am.*, 24, 3, 22–23, 1986.

5. Cooley, W.E. and Clopp, L.L., High-Pressure Water Jets for Undersea Rock Excavation. *Int. J. Eng. Ind., ASME, Ser. B*, 92, 178–185, 1970.

6. Engemann, B.K., Water Jet Cutting of Fiber Reinforced Composites. *Ind. Prod. Eng.*, 3, 162– 164, 1981.

7. Neusen, K.F. and La Brush, E.C., Material Removal by High-Pressure Liquid Jet at Ten Kilobar. *J. Eng. Ind., ASME, Ser. B*, 97, 34–45, 1975.

8. Lavoi, F., Water Jet Machining. *Mach. Des.*, 1, 6, 89–93, February 1973.

9. Price, C.N., *The Mechanics of Liquid Impact. Treatise on Material Science and Technology*, vol. 16, Academic Press, 1979.

10. Ribu, D.C., Rajesh, R., Thirumalaikumarasamy, D., Ramachandran, C.S., Investigating the Water Jet Erosion Performance of HVOF-Sprayed WC-10Co Coatings on

35CrMo Steel Utilizing Design of Experiments. *Coatings*, 1–3, 36–47, 2022.

11. Badihi, F.A., Pujiyati, S., Rahmat, A., Solikin, S., Hisyam, M., Acoustic Wave Propagation Patterns in the Ocean Column. *J. Segara*, 9, 2, 75–82, 2022.

12. Grzesik, W. and Ruszaj, A., *Hybrid Manufacturing Processes*, Springer Science and Business Media LLC, United Kingdom, 2021.

13. Neusen, K.F. and LaBrush, E.C., Material Removal by High-Pressure Liquid Jets at Ten Kilobars. *J. Eng. Ind.*, 6, 4, 19–23, 1975.

14. Youssef, Nontraditional Machine Tools and Operations, in: *Machining Technology Machine Tools and Operations*, 2008.

15. Jolodar, A.R., Abdollahi, M., Fatemi, S., Mansoubi, H., Enhancing carbon dioxide separation from natural gas in dynamic adsorption by a new type of bimetallic MOF; MIL-101(Cr-Al). *Sep. Purif. Technol.*, 1, 2, 56–63, 2024.

17. Bhattacharyya, B. and Doloi, B., *Machining processes utilizing mechanical energy*, pp. 179–201, Elsevier BV, United Kingdom, 2020. doi:10.1016/b978-0-12-812894-7.00004-9.

Note

*Corresponding author: jagdishsg@nitc.ac.in

4
Electric Discharge Machining

Jagadeesha T.[1]* and Sandip Kunar[2]

[1]*Dept. of Mechanical Engineering, National Institute of Technology, Calicut, India*

[2]*Dept. of Mechanical Engineering, Aditya University, Surampalem, India*

Abstract

The chapter provides a comprehensive overview of electric discharge machining (EDM), a vital manufacturing process that utilizes spark erosion to machine electrically conductive materials. It traces the history of EDM, outlines the process and its requirements, and delves into the equipment used, including power supply and dielectric systems. The chapter also discusses electrode materials and wear, highlighting the importance of maintaining specific conditions for effective machining. It examines the types of generators used in EDM, with a focus on the commonly used rotary impulse generator. Additionally, the chapter covers the selection of dielectric fluids, tool design considerations, and the influence of process parameters on machining characteristics. It presents the capabilities of EDM, detailing controlled parameters and their effects on outcomes like material removal rate and surface finish. The chapter also explores the surface characteristics of spark-eroded materials, the applications of EDM in various industries, and its advantages, such as the ability to machine hard materials and complex shapes. However, it also acknowledges the disadvantages, including high power consumption and difficulty in achieving sharp corners. Finally, it provides guidance on selecting EDM machine

tools based on factors like workpiece size, cavity depth, and required accuracy, underscoring EDM’s role in precision manufacturing.

***Keywords*:** Electric discharge machining (EDM), servo systems, spark erosion, HSTR alloys, pulse discharge, precision engineering

4.1 Introduction

Electric discharge machining (EDM) is widely used and has become a vital process in modern manufacturing. In EDM, material is removed using a spark between two electrically conductive materials. Basic facts of spark erosion have been known since 200 years back. Erosion of material was first reported by Joseph Priestily in 1878 [1–5].

The EDM process is similar to conventional cutting process. In EDM, the tool is an electrode and its movement are controlled precisely using servo drives. Short duration electrical pulses are used to provide cutting energy. Discharge is submerged in the dielectric medium so as to concentrate the spark energy into a smaller area. Electric discharge machining (EDM) has paved a way to machine high strength temperature resistant alloys (HSTR) and other difficult to machine conductive materials [6–8].

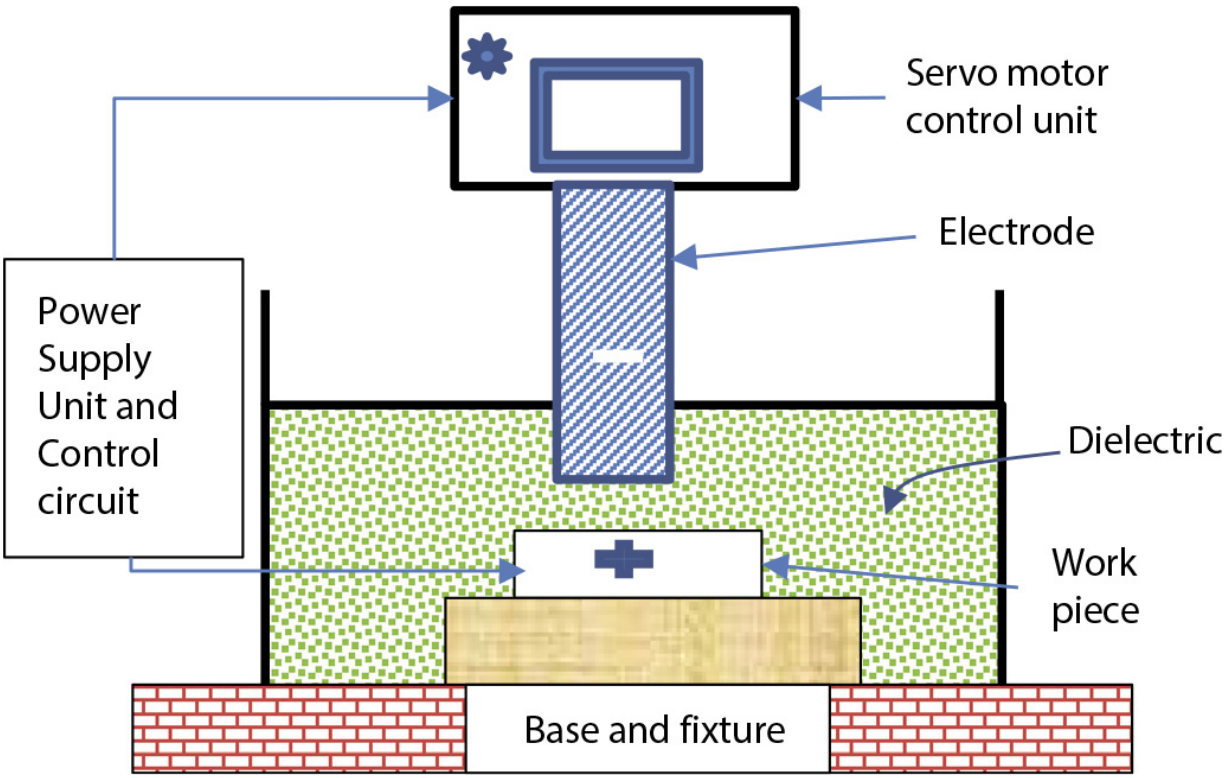


Figure 4.1 EDM process.

4.2 Description of Process

The schematic diagram of EDM is depicted in Figure 4.1. Basically, EDM is a process of removal of metals using a spark. Each spark has a thermal power concentration of $10^8\ W/mm^2$ and is capable of melting or vaporizing small amount of work material and tool is used. The machining process involves regulated removal of electrically conducting materials by initiation of swift and repeated electrical spark discharge between the tool (cathode) and work piece (anode) which are separated by a dielectric fluid medium. A suitable distance (10–500 micron), known as spark gap is kept between the tool and workpiece to cause the spark discharge [9–15].

When an appropriate voltage is applied across two electrodes separated by a dielectric, the dielectric

undergoes breakdown, creating a conductive path for spark discharge through ionization of the fluid medium, leading to the flow of current [16–20]. Each spark generates billions of electrons, initiating thousands of arcs per second, resulting in an accurate replication of the tool surface onto the workpiece.

4.3 Basic Requirement of EDM Process

1. Both the workpiece and the tool material should possess electrical conductivity.
2. The workpiece must be securely held and accurately positioned relative to the tool.
3. A precise gap of typically 0.025 mm needs to be upheld between the tool and the workpiece.
4. Dielectric fluid must flow between the tool and the workpiece, with the flow rate and pressure appropriately selected to prevent debris accumulation that could lead to short circuits [21].
5. A power supply is required to deliver pulses with specific characteristics such as pulse energy, duration, and frequency [22].
6. An effective filtration system is essential to remove debris from the electrolyte.
7. Proper safety measures must be implemented to safeguard the operator, equipment, tool, and workpiece from damage [23, 24].

4.4 Description of Equipment

A schematic layout of EDM is depicted in Figure 4.1. Electric discharge machining (EDM) has the following major modules: power supply, dielectric system, electrode and work pieces, servo systems, and frame.

(i) Power Supply

The power generator is a crucial component of the EDM system, responsible for converting alternating current (AC) into pulsed direct current (DC). This DC is essential for producing unidirectional spark discharges between the tool and workpiece gap. The EDM power supply monitors the voltage between the electrode and tool, transmitting relevant signals to the servo system to maintain the desired electrode gap [25–27].

(ii) Dielectric System

Dielectric may be fed into working area either by pressure or by vacuum suction. The dielectric has to be filtered in order to remove the metal and graphite particles. It is not necessary to use any centrifuge [28].

The commonly used fluids are paraffin oil, deionized (DI) water, transformer oil, lubricating oils, and kerosene.

(iii) Electrode and Work Piece

(a) Material for Electrode

Material used as tool electrode should have following desirable properties.

i. It should be easily maintainable
ii. It should have low wear rate
iii. Good conductor of heat and electric current

iv. Easily available and cheap

v. Easily manufacturable.

Graphite, electrolytic oxygen free copper, tellurium copper —99% cu and 0.5% tellurium, and brass are the various electrode material.

(b) Electrode Manufacture

- Conventional machining methods are widely used to make electrodes for EDM. Electroplating, metal spraying, and press forming methods are also used. Electrode dimensions must be closely controlled, particularly for flushing electrodes.
- Electrodes of materials such as copper, brass, graphite, copper tungsten, and silver tungsten are made by traditional machining such as milling, turning, drilling, and grinding. Graphite materials are widely used because of their low cost and exceptionally wear resistance. A dust collection system should be used while machining graphite and machine sideways and other precision parts should be well protected from dust. One of reducing the dust problem with graphite is to soak it with kerosene for few hours before machining [29–34].
- Electrodes are often cast from standard zinc base die casting alloys and from aluminum alloys. The electrodes can be remelted for renewed use [35–37].
- Metallic conductors are produced also by chemical etching process to remove small amount of the material, either by immersion or by local application of etching medium. Lacquer or other protection can be used for masking any portion not to be etched. After

etching the exposed surface must be neutralized [38–47].

(c) Electrode Wear

Type of wear depends on the operation, namely finishing, roughing, cavity sinking, through hole machining. For example, corner wear is an important consideration in finishing operation. Volume wear is the controlling factor in cavity sinking. Volume wear is defined as the ratio of the volume of material removed from the workpiece to the volume of material removed from the tool. Limited wear or zero wear in EDM is possible using graphite using reversed polarity (electrode is connected to positive terminal). Turbulent flow of dielectric gives higher tool wear [48–55].

(d) Electrode Holder

Different types of electrode holders are utilized in EDM to improve productivity. These holders facilitate swift and precise loading of electrodes onto the machine, incorporating mechanisms for rapid alignment of the electrode directly on the machine [56–58].

There are two types of electrode holding devices used:

i. Electromagnetic holder

ii. Quick change taper holder

(iv) Servo System

It is used to maintain a predefined gap between tool and workpiece. Too large gaps will prevent the formation of sparks. If the gap is very small, there will be short-circuit, which will damage both tool and work [59, 60].

In EDM, there is no contact between tool and work, yet sturdy machine frames for spark erosion is required because

i. Weight of the workpiece like dies, etc., is normally high.
ii. To withstand vibrations that occurs during sparking.
iii. Required for precision setting of jobs with accuracies.
iv. No misalignments after changing worn out electrode.

4.5 Types of Generators

One of the most important parts of an EDM system is power generator. The main functions of spark generator are:

i. Its primary role is to convert AC into pulsed DC.
ii. Its main function is to generate unidirectional square wave pulses to the electrode.
iii. It provides sufficient voltage to initiate and sustain discharge.
iv. It regulates the intensity of discharge current.
v. It modulates the duration of discharge.

There are four types of generators:

i. Rotary impulse generator
ii. Relaxation generator
iii. Pulse generator
iv. Hybrid generator

Rotary impulse generator is used most commonly and only this is discussed in this chapter.

Rotary Impulse Generator (Figure 4.2)

Motor generator sets were used to produce spark discharges. Now this system is not very ... widely used, because of rotating mechanical parts such as armature etc.

During one half cycle, the capacitor charges via the diode. In the subsequent half cycle, the combined voltages from the generator and the charged capacitor are applied across the gap between the work tool [61–65].

It supplies the voltage waveforms based on the principles of DC generators given by $E = \frac{ZN\varnothing}{60}\left(\frac{P}{A}\right)$, where E is the back emf (electromagnetic force). ∅ is the flux per pole. Z is the total number of armature conductors; N is the speed of armature in RPM. P is the number of poles and A is the number of parallel paths. Here, the frequency of oscillation is limited by the number of poles and the number of parallel paths. These types of generators are uneconomical and highly inaccurate and create high surface damage. These generators are not widely used [66–70].

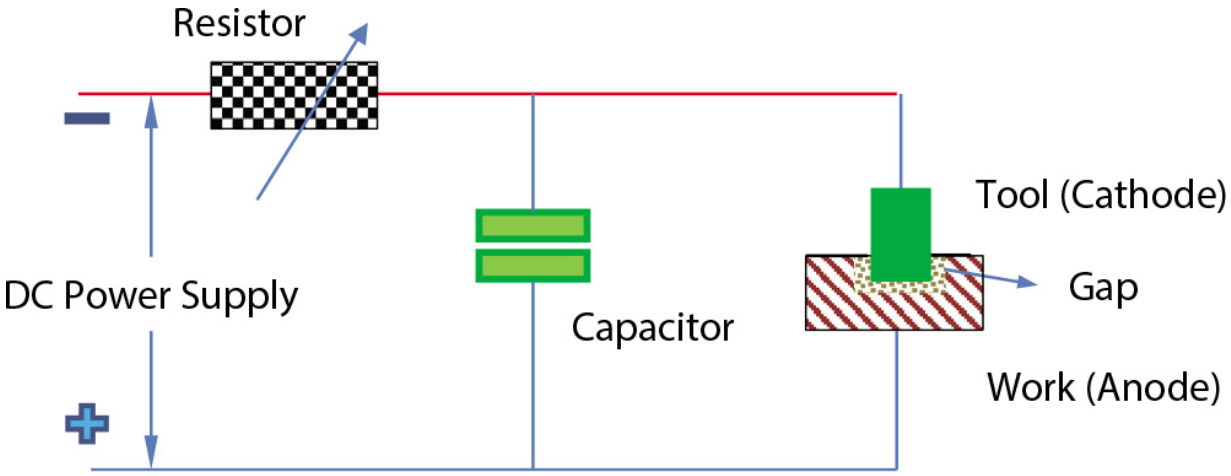


Figure 4.2 Rotary impulse generator.

4.6 Electrode Material

In the EDM process, the electrode serves as the tool responsible for shaping the hole or cavity formed on the workpiece. One of important advantages of EDM over conventional process is that a softer tool material, having a good electrical conductivity, can be used for machining of any hardness or toughness [71–74].

Desirable properties of the tool material are:

i. Tool material should have high thermal conductivity so that it dissipates the heat effectively and reduce the temperature of the surface to minimize the melting and evaporation of tool material responsible for its wear rate.
ii. It should have high electrical conductivity so that it conducts current, and spark of required quality is generated.
iii. It should have a high melting point so that the tool wear is reduced.
iv. It should be inexpensive.
v. It should be easy to manufacture.

4.7 Choice of Dielectric Fluid

The commonly used dielectric fluids include:

i. Petroleum-based hydrocarbon fluids
ii. Paraffin white spirits
iii. Transformer oil
iv. Kerosene
v. Mineral oil

vi. Polar compounds such as glycerin water (90:10) with triethylene oil as an additive.

vii. Silicone oils

Requirement of dielectric fluids are:

i. The dielectric used in the machine should have high dielectric strength.

ii. It should not chemically react with tool, workpiece, and parts of equipment such as bed, etc.

iii. It should have good wetting ability and low viscosity.

iv. It should carry away the eroded particles.

v. It should rapidly quench the spark and deionize the spark gap after the discharge.

vi. It should have a high flash point and fire point.

vii. It should not produce any toxic vapors/flumes.

viii. It should have good degree of fluidity.

ix. It should serve as effective cooling medium.

x. It should be cheap and easily available.

xi. It should be non-corrosive.

These above requirements can be met by hydrocarbon oils with a viscosity ranging from 5 to 6 Cst at 20 °C such as kerosene. Other dielectric medium are silicon oils, deionized water and polar liquids like solution of ethylene glycol. Table 4.1 shows the effect of dielectric fluid in MRR and wear ratio. Table 4.2 shows the number of dielectric available commercially. Table 4.1 gives a comparison of dielectric fluid for brass electrode and tool steel workpiece. Table 4.2 shows the commercially available dielectric oil.

Table 4.1 Comparison of dielectric fluid for brass electrode/tool steel workpiece.

Dielectric fluid	**Machining rate** $\frac{mm^3}{A}min$	**Wear ratio (volumetric)**
Hydrocarbon oil (6 Cst at 20 °C)	4	2.8
Distilled water	5.8	2.7
Tap water	6	4.1
Triethylene glycol with water 40% by volume	11	6.8
Triethylene glycol with water 40% by volume	7	11.3

Table 4.2 Commercially available dielectric grade oil.

Dielectric fluid brand	**Viscosity in cSt at 20 °C**	**Flash point, °C**
BP Dielectric	6.1	120
Castrol Honico 409	6.7	135
ESSO Mentor 20	7.5	126
ESSO Lector Number 40	7.1	134
ESSO Uniyolt Number 64	23	159
MOBIL oil Velocite Number 4	10	120
MOBIL oil Velocite Number 6	20	160
White spirit-kerosene	2	80

The selection of the dielectric relies on factors such as the size of the workpiece, shape complexity, tolerance, surface finish, and metal removal rates.

4.8 EDM Tool Design

Tool design for EDM machining falls into two main categories:

i. Cylindrical hole machining

ii. 3-D cavity machining

4.8.1 Choice of Machining Operation

In most application, it is better to use more than one machining operation to achieve required surface finish and accuracy. By choosing roughing, semi-finishing, and finishing operation, even if this implies the use of several electrodes of different dimensions, there will be considerable saving in EDM time. As a thumb rule, if the surface finish is 1.2 microns, three operations are employed.

4.8.2 Choice of Electrode Material

Usually copper, copper tungsten, and graphite are used as electrode materials. Graphite is not suitable for machining carbides and also on machines equipped with relaxation generators. When selecting electrode material, it is important to consider the cost and machining methods employed to make electrodes.

4.8.3 Machine Settings

Actual EDM tool size depends on machine settings. For all materials required, surface finish is obtained by selecting the capacitor value of the discharge circuit in the case of

relaxation generators. The machining polarity is always negative. In the case of pulse generator, more variables are required, such as machining polarity, current density level, discharge time, and pause time (during which there is no pulse: pulse off time). Manufactures of EDM supply provide these details in relation to work material, tool material and method of flushing. With the help of these data, it is possible to determine the spark gap, length of electrode, surface finish that can be achieved, the material removal rate and the percentage of electrode wear.

4.8.4 Under Sizing and Length of Electrode

Roughing electrodes must be undersized by the amount of maximum spark gap. This spark gap however does not include a safety margin to take into account possible positioning errors and differences of shapes which can occur between roughing and finishing electrodes. The additional safety under-sizing to be applied depends on the precision of the electrode. Usually, the under-sizing lies between 0.1 and 0.3 mm. The roughing electrodes are under sized by the amount of maximum spark gap plus the safety under-sizing.

The length of electrode for both roughing and finishing in the case of through hole machining is determined by multiplying the depth of hole by a factor supplied by EDM manufacturer. Roughing electrodes will be longer than the finishing electrode; to take into consideration of higher rate of wear during roughing.

4.8.5 Machining Time

Machining times are difficult to evaluate with precision and a variation of about ±5% is possible in through hole machining. In cavity machining, the variation is nearly about ±14%. The data supplied by manufactures also

includes the rate of material removal for the setting chosen. It is easy to determine the machining time for roughing, semi roughing and finishing if the method to be removed in roughing and finishing is known.

4.9 Process Parameters

The process parameters in EDM primarily pertain to waveform characteristics.

i. Open circuit voltage in volts.
ii. Working voltage in volts.
iii. Maximum current used in circuit.
iv. On time of pulse.
v. Off time of pulse.
vi. Anode and cathode working gap.
vii. Polarity used in EDM.
viii. Dielectric medium used in the machine.

Typical operating parameters and their effect on MRR and surface finish is shown in Table 4.3. Work materials used are high carbon, high chromium steel, and HRC 62 electrode material is copper.

Table 4.3 Operating parameters.

Pulse frequency	Current	Surface roughness	Crater depth		MRR
			Work	Tool	
kHz	Ampere (A)	Microns (μm)	mm	mm	mm^3/min
5	1–20	6–12	0.05–0.10	0.030	400
10	5–17	4–6	0.04–0.05	0.014	130
20	4–12	2.5–4	0.03–0.04	0.010	64
450	3–10	1.2–2	0.01–0.015	0.004	27
1000	0.5-3	0.2–0.8	0.0025	0.0008	0.15–1.5

4.10 Machining Characteristics

(i) Effect of Increasing Current

Figure 4.3 shows the effect of increasing current. With increasing current, each spark removes a larger crater of metal from the workpiece, resulting in a higher MRR. Similarly, a noticeable effect on MRR is observed with an increase in spark voltage.

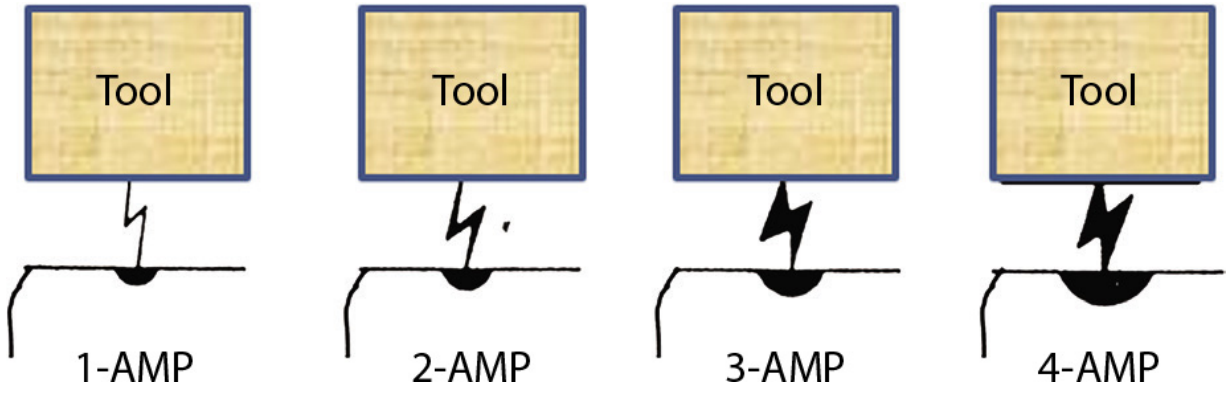


Figure 4.3 Effect of increasing current on MRR.

(ii) Effect of Increasing Sparking Frequency

Figure 4.4 shows the effect of increasing frequency. Increasing the spark frequency leads to a decrease in surface roughness. This is due to the fact that the energy allocated for material removal within a set timeframe is divided among a greater number of sparks, resulting in smaller crater sizes.

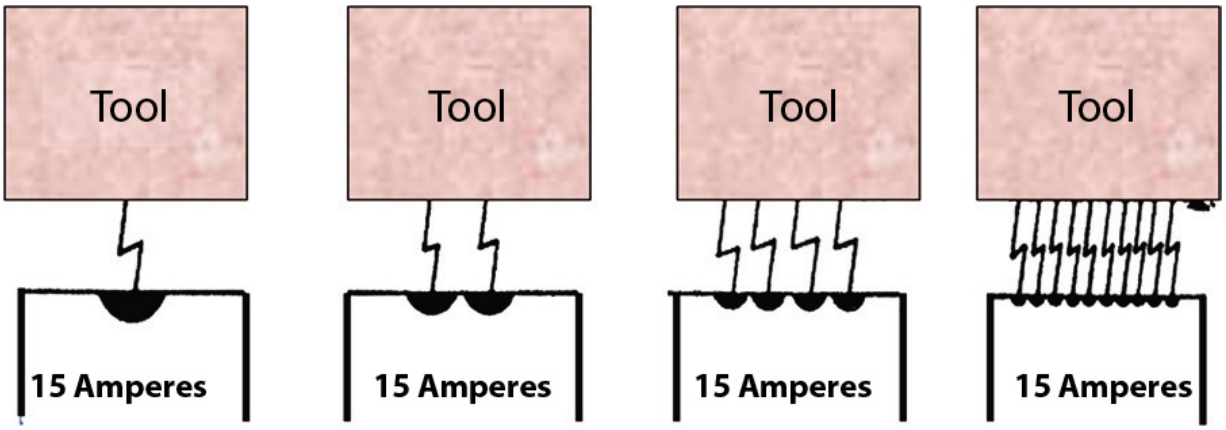


Figure 4.4 Effect of increasing sparking frequency.

(iii) Relation Between Current on Time and MRR (Figure 4.5)

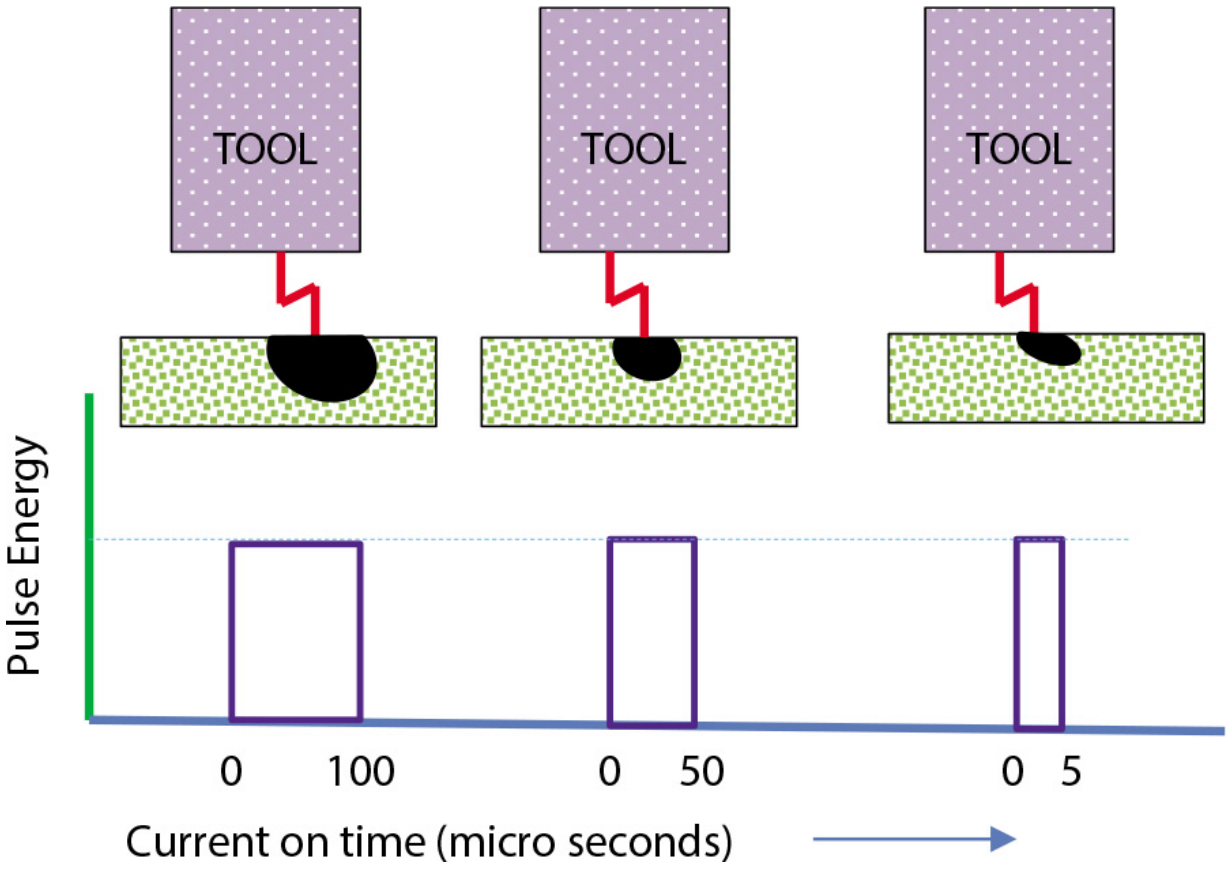


Figure 4.5 Relationship between current on time and material removal crater size decreases with decrease in current on time.

4.11 Process Capabilities of EDM

Independent controlled parameters:

i. Open circuit voltage ranges from 75 to 350 V.
ii. Frequency spans from 50 Hz to 500 kHz.
iii. Dielectric types include hydrocarbon oils, deionized water, kerosene, and gas.
iv. Dielectric flow pressure is maintained at 500 kPa.
v. Servo drive gap sensitivity control operates within the range of 0.015 to 0.15 mm.
vi. Polarity is set with the workpiece being positive and the electrode negative.

Dependent controlled parameters:

i. Average current ranges from 0.5 to 550 A.
ii. Spark gap varies between 0.015 and 0.15 mm.
iii. Overcut measures from 0.008 to 0.75 mm per side.
iv. Material removal rate spans from 0.05 to 24.5 cm^3/h.
v. Wear ratio ranges from 0.5:1 to 100:1.
vi. Surface roughness falls between 0.2 and 6.3 µm.
vii. Depth of recast layer ranges from 0.005 to 0.13 mm.
viii. Corner radius is 0.025 mm or equal to the overcut.
ix. EDM yields matte and pitted surfaces.

4.12 Characteristics of Spark-Eroded Surfaces

In EDM, MRR primarily occurs due to thermal phenomena: melting and evaporation. Temperatures can reach up to 12000°C, impacting the structure and mechanical properties of the machined surface. The significance of this effect varies depending on the work material and the conditions under which the final component is utilized.

Microscopic study of the machined surface by the EDM reveals three kinds of region.

i. Recast layer.
ii. Heat-affected zone (HAZ).
iii. Conversion zone.

Recast layer: failure to adequately flush away molten material from the workpiece results in rapid re-solidification, forming a brittle and hard recast layer.

**Heat-affected zone (HAZ): ** due to thermal expansion and thermal gradient, heating cooling of the layer creates HAZ. Thermal residual stresses developed in this region affect the performance of the product. Microcracks are observed in this zone. The size of microcracks is influenced by the material type and electrical parameters such as pulse energy and duration. Table 4.4 displays the observed sizes of microcracks during the machining of cermets.

Table 4.4 Size of microcracks.

Pulse duration (µs)	Pulse energy (Joules)	Crack depth (micron)
100	0.55	25-65
1010	0.51	90-275
100	1.1	50-125
350	4.7	90-250

Converted zone: there is a large change in grain structure from the parent material.

4.13 Applications of EDM

i. This is used to machine any hard, tough, brittle, refractory, hard carbides, hardenable steels and exotic material provided it is electrically conductive.

ii. It is used for manufacture of hardened steel die cavities and miniature holes.

iii. EDM finds utility in the cost-effective production of dies utilized in molding, casting, forging, stamping, coining, and forming processes. Additionally, it serves in various high-precision tool room applications.

iv. EDM is used to make dies/cavities for extrusion and wire drawing processes.

v. Used for making tiny holes, orifices (50 micron) and micro-sized slots.

vi. EDM is used when repetitive parts are required, they can often be produced from the easy to make male electrode.

vii. EDM is used when machining accuracy must be maintained after heat treatment of the part. EDM is

also used for metallurgical investigations.

viii. It finds application in trepanning rectangular holes in thin valve sleeves situated on curved surfaces.

4.14 Advantages of EDM

Electric discharge machining (EDM) is gaining worldwide reputation due to the following advantages:

i. EDM is applicable to all conductive metals and alloys, regardless of their physical or metallurgical properties.

ii. The majority of EDM work is dedicated to producing tool and die sets for casting, forging, stamping, and extrusion production.

iii. Complex shapes on tools can be faithfully replicated on workpieces.

iv. Elaborate shapes can be achieved by constructing tools with split sections, welded, brazed, or bonded with conductive epoxy adhesives.

v. Machining time is typically shorter than conventional methods, especially for hard materials with intricate contours.

vi. EDM is effective for machining extremely hard materials, minimizing workpiece distortion from heat treatment.

vii. Except for the blasting pressure during the plasma column’s disappearance, EDM imposes no mechanical stresses, allowing machining of delicate workpieces without distortion.

viii. It is advantageous for tool maintenance and repair, serving as a corrective means for finished, heat-treated tooling.

4.15 Disadvantages of EDM

i. Power required for machining in EDM is high compared to conventional machining.

ii. Reproduction of sharp corners is difficult in EDM. Complex contours are difficult to reproduce.

iii. Certain materials may experience surface cracking when subjected to higher energy per pulse, particularly if they tend to become ductile at room temperature.

iv. The alteration of surface microstructure by EDM can be detrimental in some cases, necessitating subsequent etching.

v. Non-conductive materials like ceramics, plastics, and glass, as they cannot conduct electricity cannot be used in EDM.

vi. EDM induces thermal distortion in some material.

vii. Electrode wear and overcutting are significant concerns in EDM operations.

viii. Many machined surfaces exhibit deeper microcracks in some cases.

ix. The volumetric metal removal rate in EDM is relatively low.

x. Achieving perfect square corners using EDM is challenging.

xi. Tool wear is a notable issue in EDM, sometimes requiring the use of two or three tools to complete an operation, thereby increasing tool costs.

xii. EDM generates a HAZ. The HAZ induces crack and unwanted stresses in the material.

xiii. Gap cleaning is very crucial in EDM.

xiv. In some materials, there is decrease in endurance limit up to 15% after EDM.

xv. In most of the jobs, batch sizes of at least 25–30 workpiece are required for economical production.

4.16 Factors to be Considered in EDM Machine Tool Selection

The following factors are to be considered in the selection of EDM tool for a particular application.

i. Size of the work piece and number of parts to be produced.

ii. Depth and orientation of cavity.

iii. Required surface finish and accuracy.

Size of the work piece: machine frame should be very rigid to machine the large-sized workpiece. Otherwise, deflection of tool/work combination or frame leads to inaccuracies. Tool size is large if the workpiece size is large. Electrode holding column must be strong and rigid enough to support the tool and able to withstand pressure of the fluid.

Depth and orientation of cavity: work table positioning enables the adjustment of the workpiece relative to the tool. Positional accuracy of the work table affects the accuracy of the workpiece. If the positional accuracy of 0.025–0.05 mm is required, then coordinate table can be used. For higher positional accuracy, CNC machine should be used.

Required surface finish and accuracy: equipment must be versatile and accurate for tool room work, where a variety of workpiece configuration needs to be machined.

The EDM machine tool design and construction is a function of the accuracy required. The required surface finish and accuracy depends on tool material, dielectric fluid, and proper choice of process variables.

References

1. Smith, G.V., *Proceedings of conference on Electrical methods of machining and forming*, p. 48, Institution of Electrical Engineering, London, 1967.

2. Livshits, A.L., *Electro erosion machining of metals*, Butler worths, London, 1960.

3. Jones, F.L., Electrode erosion by spark discharges. *Br. J. Appl. Phys.*, 1, 60–65, 1950.

4. Lazarenko, B.R. and Lazarenko, N.I., *Electrical erosion of metals*, vol. 1, Gosenergoizdat, 1994.

5. Lazarenko, B.R., *The physics of the electric spark method of machining metals*, Publication of ministry of electrical Industries, Moscow, 1946.

6. Lazarenko, B.R., *Electro spark machining of metals*, vol. 2, Consultant bureau publications, New York, 1964.

7. Lazarenko, B.R., The present state of development of electro spark machining of conductive materials abroad, in: *Electro spark machining of metals*, vol. 2, B.R. Lazarenko (Ed.).

8. Cobine, J.D., *Gaseous conductors*, Dover publications, 1958.

9. Motoki, M. and Hashiguchi, K., Energy distribution at the gap in electrical discharge machining. *Ann. CIRP*, 14, 485, 1966.

10. Rudert, D.W., Electric spark erosion as applied to metal machining engineers. *Digest*, 14, 19, 373–377, 1953.

11. Schierhott, H., Uben den abtsage vorgang bei der Funkenerosiven Bearbeitung and Regelein rich tungen der verwendeten Generatoren, Thesis T.H. Aachen, 1964.

12. Williams, W.E.M., Wood Ford, J.B., Smith, R.E., Phenomenon Accompanying Transient low voltage discharges in liquid dielectric. *AIEE Trans.*, 73, 164–169, 1953.

13. Saito, N., Mechanism of electric discharge machining. *Bull. Jpn. Soc. Proc. Eng.*, 1, 2, 95–101, 1964.

14. Heuvelman, C.J., Some aspects of research on electro erosion machining. *Ann. CIRP*, 17, 195– 199, 1969.

15. Snoeys, R. and Van Dijck, F., Investigations of electro discharge machining operations by means of thermo mathematical model. *Ann. CIRP*, 20, 35–36, 1971.

16. Opitz, H., New development in spark erosion. *Microtechnic*, 13, 147, 1959.

17. Brash, M., Electric spark machining. *Int. J. Mach. Tool Des. Res.*, 2, 281, 1962.

18. Panda, D.K., Study of thermal stresses induced surface damage under growing plasma channel in EDN. *J. Mater. Process. Technol.*, 202, 86–95, 2008.

19. Natsu, W., Shimoyamada, M., Kunieda, M., Study on expansion process of EDM arc plasma. *JSME Int. J.*, 49, 600–605, 2006.

20. Eubank, P.T., Patel, M.R., Barrufet, M.A., Bozkurt, B., Theoretical models of the electrical discharge machining

process. The variable mass, cylindrical plasma model. *J. Appl. Phys.*, 37, 7900–7909, 1993.

21. Crookall, J.R. and Heuvelman, C.J., Electro-discharge machining-the state of the art. *Ann. CIRP*, 20, 1, 113–120, 1971.

22. Dibitonto, D.D., Eubank, P.T., Patel, M.R., Barrufet, M.A., Theoretical models of the electro discharge machining process—a simple cathode erosion model. *J. Appl. Phys.*, 66, 9, 4095–4103, 1989.

23. Erden, A., Effect of materials on the mechanism of electric discharge machining. *Trans. ASME J. Eng. Mater. Technol.*, 108, 247–251, 1983.

24. Erden, A. and Bilgin, S., Role of impurities in EDM. *Proc. 21st Int. Machine tool design research conference*, Swansea, pp. 345–350, 1980.

25. Jilani, S.T. and Pandey, P.C., An analysis of surface erosion in electrical discharge machining. *Wear*, 84, 275–284, 1984.

26. Jilani, S.T. and Pandey, P.C., An Experimental investigation into the performance of water as dielectric as Dielectric in EDM. *Int. Mach. Tools Des. Res.*, 24, 1, 31–43, 1984.

27. Kruth, J.P., Stevens, L., Froyen, L., Lauwers, B., Study of white layer of a surface machined by die-sinking electro-discharge machining. *Ann. CIRP*, 44, 1, 169–172, 1995.

28. Mirnoff, N., Electro erosive metalworking—its physical fundamentals and industrial application. *Microtecnic*, xix, 3, 56–67, 1965.

29. Panda, D.K. and Bhoi, R.K., Analysis of spark eroded crater formed under growing plasma channel in electro-discharge machining. *Mach. Sci. Technol.*, 9, 2, 239–261, 2005.

30. Shankar, P., Jain, V.K., Sundarrajan, T., Analysis of spark profiles during EDM process. *Mach. Sci. Technol.*, 1, 2, 195–217, 1997.

31. Motoki, M. and Hashiguchi, K., Energy distribution at the gap in Electric discharge machining. *Ann. CIRP*, 19, 485–489, 1967.

32. Srinivasulu, K., Reddy, S.S., Varma, D.R.V.S., Mathew, K.J., Studies on electrical discharge machining of deep narrow slots in critical aero-engine components. *Proc. AIMTDR*, vol. 20, pp. 270–275, 2003.

33. Lee, T.H., Theory of electron emission in high current arcs. *J. Appl. Phys.*, 30, 2, 169–171, 1959.

34. Yadav, V., Jain, V.K., Dixit, P.M., Thermal stresses due to electrical discharge machining. *Int. J. Mach. Tools Manuf.*, 42, 1–11, 2002.

35. Descoeudres, A., Characterization of electrical discharge machining plasmas, EPFL, PhD thesis, Lausanne, 2006.

36. Kaldes, F., *Flushing in gap in EDM*, EDM digest, Germany, 1983.

37. Kurafuji, H., Development of researches and application in spark erosion and electrolytic machining in Japan. *Annals of 14th CIRP*, 1964.

38. Schumacher, B.M., After 60 years of EDM the discharge process remains still disputed. *J. Mater. Process.*

Technol., 149, 376–381, 2004.

39. Kobayashi, K., The present and future developments of EDM and ECM. *Proceedings of the 11th International Symposium for Electro Machining (ISEM-11)*, Lausanne, Switzerland, pp. 29–47, 1995.

40. Ho, K.H. and Newman, S.T., State of the art electrical discharge machining (EDM). *Int. J. Mach. Tools Manuf.*, 43, 13, 1287–1300, 2003.

41. Ho, K.H., Newman, S.T., Rahimifard, S., Allen, R.D., State of the art in wire electrical discharge machining (WEDM). *Int. J. Mach. Tools Manuf.*, 44, 12-13, 1247–1259, 2004.

42. Tani, Y., Fukuzawa, N., Mohri, N., Saito, N., Okada, M., Machining phenomena in WEDM of insulating ceramics. *J. Mater. Process. Technol.*, 149, 124–128, 2004.

43. Thija, A., Van Dijck, F., Snoeys, R., Investigation of polarity effects in EDM. paper no 73, CIRP, 1973.

44. Wälder, G., New technologies and EDM, in: *Proceedings of the 12th International Symposium for Electro Machining (ISEM-12)*, Aachen, Germany, pp. 331–340, 1998.

45. Patel, M.R., Barrufet, M.A., Eubank, P.T., DiBitonto, D.D., Theoretical models of the electrical discharge machining process. II. The anode erosion model. *J. Appl. Phys.*, 66, 9, 4104–4111, 1989.

46. Brume, M., Advances in electro erosion. *Discovery*, 20, 3, 126, 1959.

47. Williams, E.M., Woodford, J.B., Smith, R.E., Recent developments in theory and design of electrical spark

machine tools. *AIEE*, 73, 83–88, 1954.

48. Anderson, J.C., *Dielectric*, Chapman and Hall, United Kingdom, 1964.

49. Banerjee, P.P., Mishra, P.K., Bhattachraya, A., Accuracy of machining by EDM process. *17th Congress of Theoretical and Applied Mechanics*, Ranchi, 1972.

50. Chakrabarty, A.N. and Bhattacharya, A., Effect of dielectric medium on the performance of EDM process. *J. Inst. Eng.*, 51, 45–56, 1970.

51. Chaudhary, S., Das, A.K., Bhattacharya, A., Determination of critical resistance in spark erosion machining for various electrodes in a given dielectric. *Proceedings of the Second AIMTDR Conference*, 1968.

52. Davis, M.F., A synopsis of comprehensive investigations in EDM. *Creative Manufacturing Seminar, ASTME*, vol. 32.

53. Pal, M.N., Mishra, P.K., Bhattacharya, A., Optimization of circuit parameters of relaxation circuit of EDM. *International Conference on Non-Traditional Machining Processes*, Timisoara, Romania, 1971.

54. Barash, M.M., Electric machining of metals, in: *Modern Workshop Technology, Part II*, Second edition, H. Wright Baker (Ed.), pp. 5159–5168, 1960.

55. Blake, L.R., High-power spark erosion machine. *Engineer*, 199, 5159, 1955.

56. Dave, B.J., Servo controlled electrical discharge machines. *Proc. IV, AIMTDR Conference*, 1970.

57. Suzuki, K., Uematsu, Nakagawa, T., On-machine trueing dressing of metal bond grinding wheels by

electro-discharge machining. *Ann. CIRP*, 36, 1, 115–118, 1987.

58. Nalla Mohamed, M. and Sylvya Rebecca, J., Estimation of Aerosol Emission in Die Sinking EDM Process through Numerical Modelling. *Appl. Mech. Mater.*, 2, 3, 55–61, 2016.

59. Youssef, H.A., *Machining of Stainless Steels and Super Alloys*, Wiley, USA, 2015.

60. Ahsan, A., Chapter 21 Role of Heat Transfer on Process Characteristics During Electrical Discharge Machining, in: *Development in Heat Transfer*, IntechOpen, USA, 2011.

61. *Machining*, Springer Science and Business Media LLC, United Kingdom, 2008.

62. Chen, Y.-F., Chow, H.-M., Lin, Y.-C., Lin, C.-T., Surface modification using semi-sintered electrodes on electrical discharge machining. *Int. J. Adv. Manuf. Technol.*, 3, 5, 1–17, 2007.

63. Yan, M.-T., Design and experimental study of a power supply for micro-wire EDM. *Int. J. Adv. Manuf. Technol.*, 9, 1, 34–45, 2009.

64. *Advances in Materials and Mechanical Engineering*, Springer Science and Business Media LLC, United Kingdom, 2021.

65. Ghoreishi, M., *Effects of Vibration and Rotation of the Electrode in Electro-Discharge Machining*, The University of Manchester, United Kingdom, 2023.

66. Lee, S.H. and Li, X.P., Study of the effect of machining parameters on the machining characteristics in electrical

discharge machining of tungsten carbide. *J. Mater. Process. Technol.*, 1, 1, 74–87, 2001.

67. Rudorff, D.W., Principles and Applications of Spark Machining. *Proc. Inst. Mech. Eng.*, 5, 1, 63–71, 2006.

68. Puri, A., *Parametric Analysis and Robust Designing of Wire-cut Electrical Discharge Machining (WEDM) Process for Multi-criterial Yield*, Jadavpur University, India, 2020.

69. Youssef, Nontraditional Machine Tools and Operations, in: *Machining Technology Machine Tools and Operations*, 2008.

70. Bijoy, B. and Biswanath, D., *Hybrid machining technology*, Elsevier BV, United Kingdom, 2020.

71. Kaya, T., Elektroerozyon tezgahlari Ve Spesifik parcalar icin Elektrod takim Imalat metodlari, Marmara Universitesi, Turkey, 1986.

72. George, P.M., *Machinability analysis of carboncarbon composites using EDM*, Proquest, USA, 2016.

73. Manna, A., *Experimental Investigation on Machinability of Al-SiC Metal Matrix Composite*, Jadavpur University, India, 2020.

74. Jagadeesha, T., *Unconventional machining processes*, I K International Publication House Pvt. Ltd., New Delhi, 2016.

Note

*Corresponding author: jagdishsg@nitc.ac.in

5
Wire-Electric Discharge Machining

Jagadeesha T.[1]* and Sandip Kunar[2]

[1]*Dept. of Mechanical Engineering, National Institute of Technology, Calicut, India*

[2]*Dept. of Mechanical Engineering, Aditya University, Surampalem, India*

Abstract

Wire electrical discharge machining (WEDM) is a vital process in modern manufacturing, offering precise shaping of electrically conductive materials. This chapter provides an in-depth exploration of wire EDM, covering its principles, equipment, parameters, capabilities, and applications. Wire EDM operates by controlled electrical discharges between a wire electrode and a workpiece, eroding material to create intricate shapes. Critical components include power systems, dielectric systems, positioning systems, and wire electrodes. Process parameters like wire diameter and power settings significantly affect performance. Wire EDM excels in precision and complex shaping, but its high cost and limited workpiece size are drawbacks. Optimization involves selecting parameters and ensuring equipment integrity. With examples and empirical formulas, this chapter offers insights for maximizing wire EDM's potential in diverse manufacturing applications.

***Keywords*:** Wire electric discharge machining (WEDM), kerf, dielectric, overcut, wire electrode

5.1 Introduction

Electrical discharge wire cutting, often known as wire electrical discharge machining (EDM), is a method that employs electrically conductive materials to produce detailed patterns in two or three dimensions. The use of wire EDM was first recorded in 1968, and its ability to treat materials quickly led to its widespread adoption by 1975 [1].

5.2 Description of Process

Electric discharge machining (EDM) is a process of repeated sparking cycles. In wire EDM, the pulse generator system applies electrical pulses between the workpiece and the conductive wire electrode. During spark discharge, an electric current flow across the space between the conducting wire electrode and the workpiece. The energy content of a one spark discharge can be determined as product of pulse on period and peak current A single spark’s energy can eliminate a small portion of the materials in the work item. The workpiece material was electrolyzed due to a large number of these time-separated small discharges between the wire electrode and the workpiece [2].

A wire with a diameter of between 0.05 and 0.3 mm is used in wire EDM. In wire EDM, the dielectric fluid is forced to the cutting object via a nozzle. A pulsed direct current (DC) source is used to power the electrodes. Sparking produces heat, which melts the workpiece and the wire substance. At times, a portion of the substance may even evaporate, similar to traditional EDM [3]. A computer-controlled positioning device helps maintain a consistent distance between the tool and the work piece.

5.3 Equipment

A diagram of wire EDM is shown in Figure 5.1. The wire EDM equipment has the following:

1. Power systems
2. Dielectric systems
3. Locating system
4. Wire control system
5. Wire electrode
6. Workpiece
7. Flushing system

1. Power drive system: the power supply unit comprises of electric pulse generator, motor drive units for X, Y, U, V axes, and computer numerical controlled (CNC) machine. The major difference between the power supplies used for wire EDM and conventional EDM are the frequency of pulses and current used. To produce the smoother surface, pulse frequency of 1 MHz is used in wire EDM. Such a high frequency ensures that small amount of the material is removed from the work piece [4]. Normally, an iso-pulse generator is used in wire EDM, where peak current, on time, off time, and spark frequency can be controlled. The current in wire EDM is usually about 20–30 A. The potential difference of 50–60 V is used between work and tool.

2. Dielectric system: effective flushing is important in wire EDM. Flushing nozzles are placed close to the gap. Wire breakage occurs if the flushing is not proper. Flushing is difficult in wire EDM [5]. Deionized water with low viscosity is therefore utilized as a dielectric. It also uses light oil that has been properly filtered.

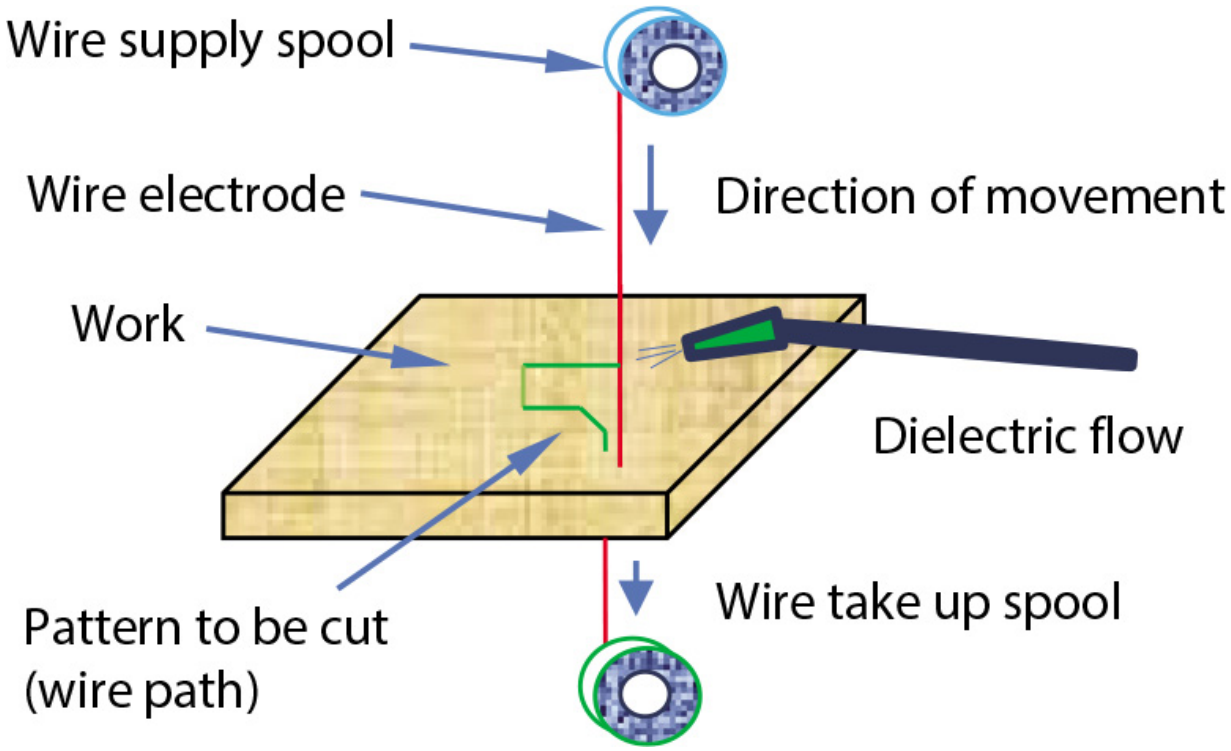


Figure 5.1 Wire EDM setup.

The low viscosity fluid is required in wire EDM to ensure the adequate flushing in small cutting gap used in wire EDM. Therefore, water is used. Water also removes heat from the cutting area more efficiently [6]. Very high metal removal rate is possible with water as dielectric but tool wear is also high. In conventional , oil is used as dielectric and poses fire hazard problems. But using water as dielectric, the fire hazard problem can be eliminated [7]. Because of the high rate of tool wear, wire cannot be reused. An efficient dielectric supply is a stream of deionized water running down the wire's axis [8]. Reusing the dielectric after filtering can lower its cost. It is recommended to do the filtering using a disposable 5-micron filter. Some of the special additives are added to deionized water to prevent rust formation [9].

Water as a Dielectric Medium

The advantages of utilizing water as a dielectric medium are as follows:

1. Water has the lowest viscosity.
2. There is no fire hazard with water and water is non-toxic.
3. High cooling rate compared to kerosene.
4. High material removal rate (MRR).
5. Better surface finish.
6. Water will not pollute the atmosphere.
7. Water is available.
8. Wide spark gap is possible which avoids short circuiting. Wide spark gap also allows higher cutting speed (high productivity).

It is important to note that the process of water ionization leads to an increase in water conductivity. In a dielectric distribution system, an ion exchange resin is utilized to keep the water's conductivity constant and prevent it from increasing. Figure 5.2 shows the details. Control of conductivity, overcut, and space between the wire electrode and work surface are important parameters. The effects of high and low conductivity are listed in Table 5.1.

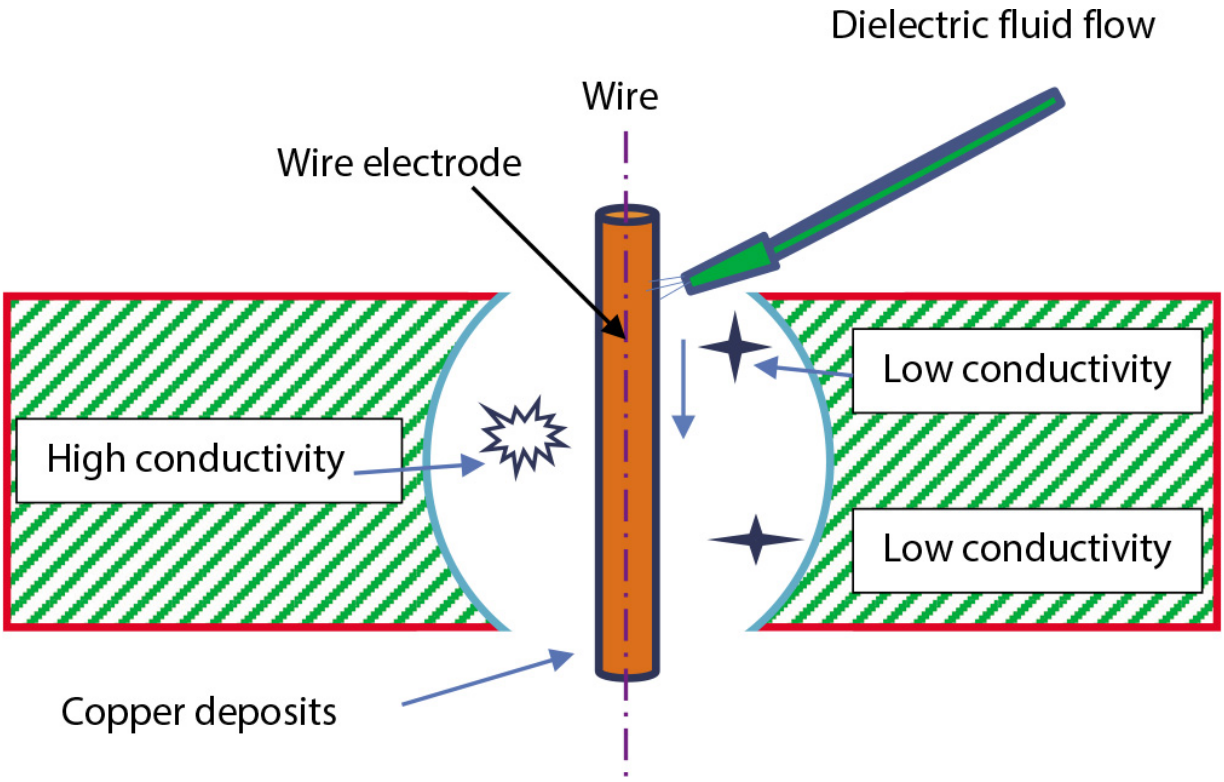


Figure 5.2 Conductivities of water.

Table 5.1 Effect of low and high conductivity of dielectric.

Low conductivity	High conductivity
Extremely low dielectric conductivity may provide a significant risk for wire metal deposition on the work piece.	Since the water dielectric has a very high dielectric conductivity, more DC current cannot build up to a suitable voltage in the gap. The machining consequently becomes unsteady.

Dielectric strength: maintaining consistent conductivity is crucial since the dielectric fluid's insulating characteristic determines overcut. The formation of metallic ions and the dissolution of surrounding gases during machining cause changes in the conductivity of dielectric water [10]. Water can be made less conductive by running it through deionizer resin.

3. Positioning system: the wire EDM machine is comprised of a CNC two-axis (XY) table, and in certain instances, it may additionally have extra multi-axis (UV) wire placement. The XY table and UV table are capable of moving in increments of 1micron using a servo motor.

By maintaining the UV table in a fixed position while the XY table moves along a specified route, a straight cut with a pre-established pattern is achieved. Taper machining requires tilting the wire electrode. This is accomplished by shifting the top wire guide along the UV axis in relation to the bottom wire guide. The appropriate taper angle is attained by the coordinated manipulation of the XY table and UV table, following established trajectories that are recorded in the controller [11]. The controller is provided with the route information of the XY table and UV table through the NC program, which includes both linear and circular components.

An adaptive control system is used to maintain a constant distance between the wire and work material. A short circuit can occur if there is contact between the wire and work by tiny material. The positioning system detects the gap and implements correction measures [12].

4. Wire drive system: the purpose of the wire drive system is to continually supply the work area with new wire. Wires must be properly tensioned to prevent breakage, vibration marks, taper, etc. Before the wire rolls into the take-up reel, it passes through a sequence of tensioning rollers under the guidance of the wire guides, which are often made of sapphire or diamond.

Regarding the wire that passes through it, the diamond wire guides have a tight tolerance. Over time, the wire guide may deteriorate or distort. A shock from the outside might potentially cause a diamond to fall out or get

damaged [13–15]. If the aperture in the wire guide's nose is not kept clean, the wire will break there.

Cutting speed in wire-cut EDM is expressed in terms of cross-sectional area cut per unit. For example, for aluminum of 150-mm thick slab, metal removal is 45,000 mm^2/h. For tool steel of 50-mm thick, metal removal is 18,000 mm^2/h. This amount to a linear cutting rate of 300–350 mm/h [16].

5. Wire electrode: the wire electrode must be homogeneous in diameter, free from twist or kink, and possess a suitable tensile strength. The substance of the electrode wire need to have:

- Brass/diffused brass/zinc coated brass.
- The deviation in diameter should fall between ±0.002 mm.
- Tensile strength should not exceed 500 N/mm^2.
- It should be wound evenly, free from breaks and kinks.

Current carrying capacity of the wire: as a general rule, a 0.2-mm brass wire can carry 0.3–0.7 A of current in air. However, under water, the same wire may carry currents of between 6 and 9 A [17]. Therefore, to prevent wire breakage during machining, wire should always be surrounded with dielectric water.

Wire tension (WT): the amount of wire that has to be stretched between the upper and lower wire guides is determined by the wire tension. The greater thickness of the work, the higher the necessary tension. Incorrect tension settings can lead to wire breaks and inaccurate work [18]. Wire tensions are shown in Table 5.2.

Wire feed: the traveling-wire electrode gets thin and brittle as a result of spark erosion. Wire feed refers to the velocity at which the wire electrode travels along the wire guide route. In general, it is optimal to set the wire feed to its maximum level. Consequently, wire breakage will be reduced, machining will become more stable, and there will be a slight improvement in cutting speed. When the wire feed is adjusted to 8 m/min, a 5-kg spool of 0.25-mm brass wire will endure for approximately 24 h of sparking [19].

Overcut: during sparking, there is a lateral space between the wire and the workpiece. The overcut is greater if:

- Machining gap potential is more
- Discharge energy is more
- Wire tension is less
- Guide span is higher
- Job is thicker
- High conductivity of dielectric water medium
- Unstable machining

Table 5.2 Wire tensions in wire EDM.

Wire tension	Tension in grams
1	300
2	420
3	540
4	660
5	780
6	900
7	1020
8	1140
9	1260
10	1380

6. Work piece material: A slightly shifted workpiece might lead to a deformed piece of work. Residual tension in the material, which might result from other procedures, should be absent. The accuracies are greatly impacted by residual tensions.

Work piece should be:

- At least electrically conducting 0.1 micro-ohm/cm
- Should be able to clamp
- Non-combustible

It should not be inert when exposed to hydrogen, oxygen, or water. The guidelines to cut various work material is presented in Table 5.3.

7. Flushing: flushing is essential to provide a stable machining condition. The cutting speed is really crucial. In the event that the nozzles (both upper and lower) are not adequately distanced from the workpiece, the cutting

performance will experience a substantial decrease. Regularly examine the nozzle for any signs of degradation. Minor damage or scratches on the contact edge have a direct influence on the cutting speed. It is necessary to replace filters according to a predetermined timetable in order to maintain the water’s cleanliness [20].

Table 5.3 Guidelines for choosing parameters for different work materials.

Work material	**Guidelines**
Carbide cutting	Carbide is sintered material where carbide particle are sintered in cobalt or nickel base. Melting point of carbide is higher compared to cobalt and nickel, so there are chances of cobalt depletion and micro cracking at cut surface if wrong parameters are set. To overcome this problem, very low conductivity and low current setting has to be used.
Aluminum	Melting point of aluminum is less. If the aluminum is cut at higher conductivity, there are chances of frequent wire breakages. If the conductivity is very high then sometimes It becomes impossible to cut aluminum. hence is it important to maintain conductivity level of 10-20 $\mu S/cm$ (usually referred as 10–20 units) while cutting aluminum.
Copper	Copper is a good conductor of electric current and also has low melting point. If high conductivity is used, then machine performance is affected. It is recommended to use 10–20 units while cutting copper. Overcut in copper is more as compared to other material.
Inconel	Use of antieleyrolysis pulse for Inconel will give good result and minimize the oxidation effect. If the wire breakage is more, then pulse off time must be increased. Cutting speed of Inconel is 40% to 50 % less compared to steel.

5.4 Process Parameters of Wire EDM

Process parameters in wire EDM are:

1. Wire

   Diameter: 0.06–0.31 mm

   Material: brass, copper, molybdenum steel

   Speed: 42 mm/s

   Tilt: ±11°
2. Dielectric

   Type: DI water

   Flow: 5–40 LPM

   Pressure: 600 KPa
3. Power supply

   Frequency: 1.1 MHz

   Current: 25–30 amps

   Voltage: 50–65 volts

   Pulse on time (example: 0–30 for normal pulse, 100–131 for equi energy pulse)

   Pulse off time (no voltage in gap)

   Spark initiation time (also called ignition delay time)

   Machining peak current

   Open gap voltage
4. Table feed

   Cutting rate: 40–110 mm/h in 25.4-mm steel

   Gap: 0.014–0.15 mm

5.5 Process Capability of Wire EDM

Process capabilities in wire EDM are:

1. It produces matte finish which increases the life of components as matte retains the lubricating oil.
2. Surface finish of 0.1 micron is possible with wire EDM.
3. Accuracy of ±8 *micron* can be achieved.
4. MRR of 45 cm^3/h can be achieved.

5.6 Difference Between Wire EDM and EDM

The material removal mechanism used in wire EDM and EDM is the same. The comparison between wire EDM and EDM is given in Table 5.4.

Table 5.4 Difference between wire EDM and EDM.

Wire EDM	EDM
Brass or molybdenum wire with a very small diameter is utilized as a tool.	Electrode made of tungsten, copper are used as tool.
The whole workpiece is not submerged in dielectric medium. Dielectric medium is supplied only to cutting zone.	Work, tool and fixtures are submerged in tank containing dielectric.
It is easy to cut complex contours. Plate thickness up to 300 mm can be cut. Also used for making punch and dies.	It is difficult to cut complex contours compared to wire EDM. It is mainly used for die sinking (volume removal applications).
In wire EDM, in addition to x and y movement of CNC table, U and v movements are possible, so taper of 20°–30° can be cut easily.	Not so easy to cut controlled taper on EDM.

5.7 Applications of Wire EDM

1. This is used to machine thick conductive material. Thickness of 200 mm or more can be machined.
2. It is used for manufacture of dies. Press stamping die machining is made simpler by punch and die
3. Punch plate and stripper can be machined from a single wire EDM–CNC program. Clearances can be controlled very accurately, hence, life of punch and die setup increases drastically.

4. Wire EDM is useful in economic manufacture of complex parts. Many hours of polishing and grinding can be saved.
5. It is used to machine medical and dental parts/prototypes.
6. It can be used to machine delicate and thin sections. There is no cutting force involved in wire EDM.
7. Hard to process materials like titanium and cast alloys with other traditional machining methods? Wire EDM can cut them.
8. Wire EDM is used for cutting hardened material such as poly crystalline diamond (PCD), cubic boron nitride (CBN), and carbides.
9. Wire EDM is used when machining accuracy must be maintained to close tolerances.
10. It is used for trepanning of holes in thin complex surfaces.

5.8 Advantages of Wire EDM

Wire EDM has the following advantages:

1. All electrically conductive metals and alloys can use this method, regardless of the work material's metallurgical, mechanical, or physical characteristics.
2. Electrode is wire. There is no tool cost, storage cost, or fabrication cost.
3. No mechanical stresses are present in the process.
4. Wire EDM is useful in economic manufacture of complex parts. Many hours of polishing and grinding can be saved.

5. Die cost is reduced by 35% to 75%. Close tolerance can be maintained between punch and die.
6. Process gives high surface finish.
7. Rejections of parts is minimum because CNC programs can be simulated before manufacturing.

5.9 Disadvantages of Wire EDM

1. High capital cost.
2. Slow cutting speeds.
3. Not appropriate for really big work pieces.
4. The same material may undergo electrolysis.

$$MRR = \frac{CI}{t_m^{1.54}}$$

Where MRR is the metal removal rate in mm^3/s and C is constant of proportionality = 664 in SI unit. I stands for discharge current, amps for amps, and t_m for work material melting temperature.

5.10 Process Parameters in Wire EDM

The discharge current and frequency are two crucial process parameters in wire EDM. The rate of metal removal rises as one of these parameters is raised. As Figure 5.3a illustrates, current and frequency have an impact on surface roughness as well. In EDM, working at high frequencies and low discharge currents yields the finest surface polish. Overcutting happens as the electrode tool goes deeper into the job. In wire electrical discharge machining (WEDM), overcut refers to the amount that the work part's machined cavity surpasses the tool's size on

both sides. It is created as a result of electrical discharges that happen to the tool's sides and front. As shown in Figure 5.3b, overcut is a function of frequency and current and can reach many hundredths of a millimeter.

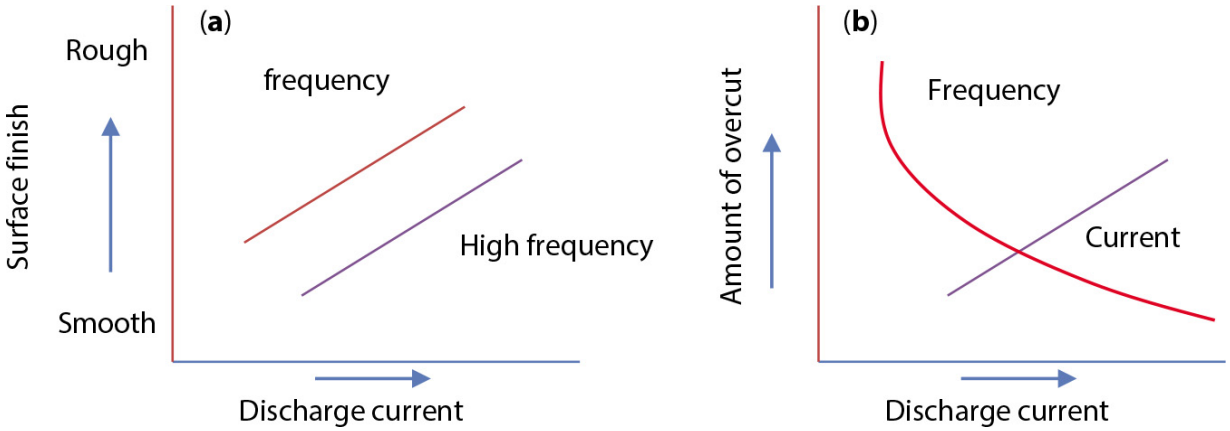


Figure 5.3 (a) Effect of frequency on surface finish. (b) Effect of overcut with respect to frequency and current.

5.11 Worked Examples

Problem 1: Based on past data, the excess material removed during a wire EDM operation on 7-mm-thick C1080 steel using a tungsten wire electrode with a diameter of 0.125 mm is expected to be 0.02 mm, resulting in a final cut width of 0.165 mm. What is the maximum feed rate that may be used in the operation when the discharge current is 10 amps?

Solution

Using the empirical formula suggested by Weller,

$$MRR = \frac{CI}{t_m^{1.54}}$$

$$t_m = 1500°C \text{ for 1080 steel.}$$

$$MRR = \frac{CI}{t_m^{1.54}} = \frac{664 \times 10}{1500^{1.23}} = 0.8233 \text{ mm}^3/\text{s}$$

Frontal area of kerf is $0.165t = 0.165 \times 7 = 1.155 \text{ mm}^2$

$$\text{Feed rate} = \frac{MRR}{\text{Frontal area of kerf}} = \frac{0.8233}{1.155} = 0.7128 \frac{\text{mm}}{\text{second}} = 42.79 \frac{\text{mm}}{\text{min}}$$

Problem 2: A wire EDM operation is to be done on a bar of 18.75-mm thick aluminum using a brass wire electrode whose diameter = 0.125mm. It is expected that over cut will be 0.025 mm. Using the current of 7 amps, what is the expected feed rate that can be used in operation? The melting temperature of aluminum is 660°.

Solution

Wire diameter = 0.125 mm

Overcut = 0.025 mm

Kerf = wire diameter +2 times overcut = 0.125 + 0.025×2 = 0.175 mm

Using the empirical formula suggested by Weller,

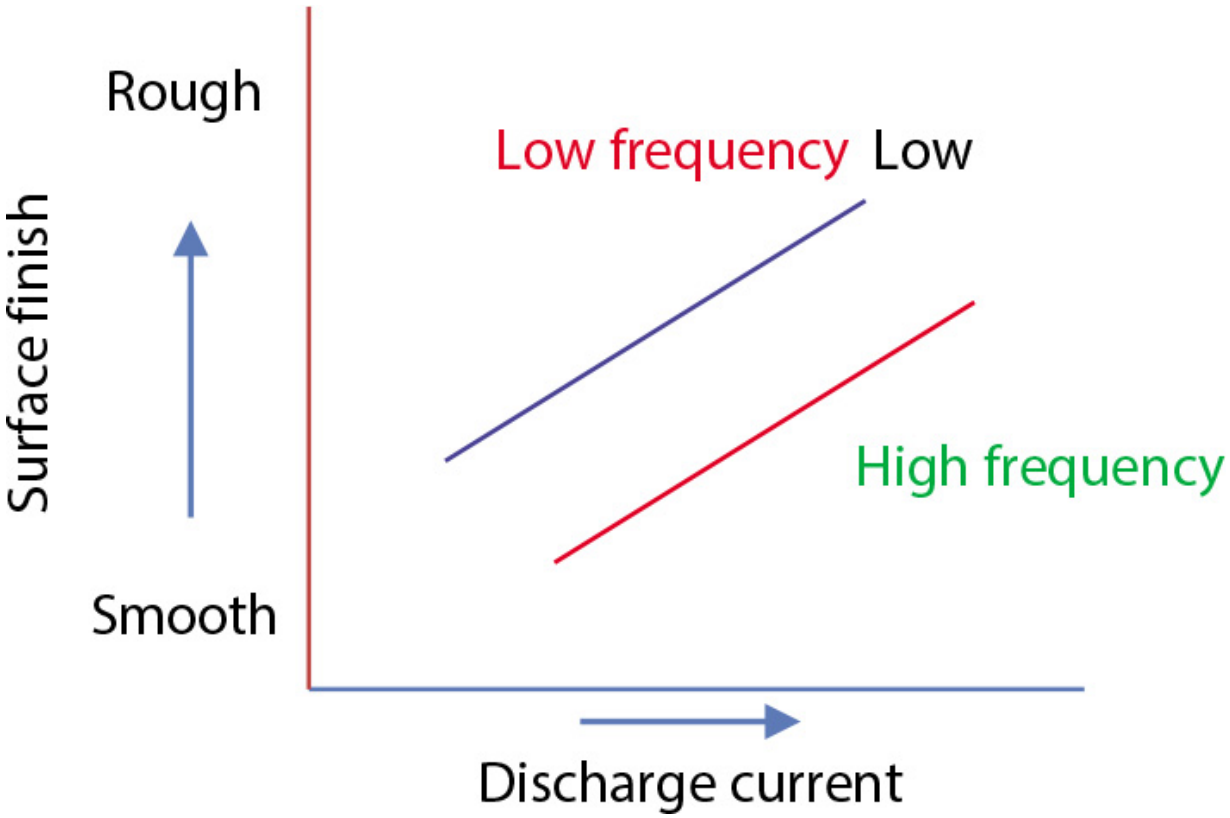


Figure 5.4 Effect of frequency on surface finish.

$$MRR = \frac{CI}{t_m^{1.54}}$$

$$t_m = 660°C \text{ for aluminium}$$

$$MRR = \frac{CI}{t_m^{1.54}} = \frac{664 \times 7}{660^{1.23}} = 1.5820 \text{ mm}^3/\text{s}$$

Frontal area of kerf is 0.175t = 0.175×18.75 = 3.28125 mm^2

Feed rate = MRR/(frontal area of kerf) = 1.5820/(3.28125) = 0.48215 mm/s = 28.93 mm/min.

Problem 3: A wire EDM operation is used to cut out punch and die components from 25-mm thick tool steel plates. However, in first cuts, the surface finish on the cut edge is poor. What changes in discharge current and frequency of

discharges should be made to improve surface finish. Explain with a schematic diagram.

Solution

As discussed earlier, surface finish in wire EDM can be increased by:

1. Increasing the frequency of discharges.
2. Reducing the discharge current.

Figure 5.4 shows the relation between discharge current and surface finish at various levels of frequency.

References

1. Benedict, G.F., *Nontraditional Machining Processes*, Marcel Dekker Inc., New York, 1987.
2. Bhattacharayya, A., *New Technology*, The Institution of Engineers India, Calcutta, 1973.
3. McGeough, J.A., *Advanced Machining Methods*, Chapman and Hall, London, 1988.
4. Pandey, P.C. and Shan, H.S., *Modern Machining Processes*, Tata McGraw Hill Publishing Co. Ltd., New Delhi, 1980.
5. Mishra, P.K., *Nonconventional Machining*, Narosa Publishing House, Calcutta, 1997.
6. Adithan, M., *Unconventional Machining Processes*, Atlantic Publishers and Distributors, New Delhi, 2009.
7. Kalpakjian, S. and Schmid, S.R., *Manufacturing Processes for Engineering Materials*, Prentice Hall, USA, 2007.

8. Black, J.T., De Garmo, E.P., Kohser, R.A., *Materials and Processes in Manufacturing*, John Wiley & Sons, United Kingdom, 2011.

9. Groover, M.P., *Fundamentals of Modern Manufacturing*, John Wiley & Sons, USA, 2010.

10. El-Hofy, H., *Advanced Machining Process*, Tata McGraw Hill, USA, 2005.

11. Brown, J.A., *Modern Manufacturing Processes*, Industrial Press, Australia, 1991.

12. Jain, V.K., *Introduction to Micromachining*, Alpha Science International Limited, India, 2010.

13. Davim, J.P., *Machining: Fundamentals and Recent Advances*, Springer, USA, 2008.

14. Grzesik, W., *Advanced Machining Process of Metallic Materials*, Elsevier, Great Britain, 2008.

15. Allesu, K., Notes on Manufacturing Science. ISTE Summer School on Modern Trends in Manufacturing Science, NIT Calicut, 2001.

16. Production Technology, *Hindustan Machine Tools (HMT)*, Tata McGraw Hill, New Delhi, 2008.

17. Nikolaev, G. and Olshansky, N., *Advanced Welding Processes*, MIR Publishers, Russia, 1977.

18. Ghosh, A. and Mallik, A.K., *Manufacturing Science*, 2nd ed., East-West Press Private Limited, New Delhi, 2010.

19. Schey, J.A., *Introduction to Manufacturing Processes*, 2nd ed., McGraw Hill Book Company, USA, 1987.

20. Jagadeesha, T., *Unconventional machining processes*, I K International Publication House Pvt. Ltd., New Delhi, 2016.

Note

*Corresponding author: jagdishsg@nitc.ac.in

6
Laser Beam Machining

Jagadeesha T.[1]* and Sandip Kunar[2]

[1]*Dept. of Mechanical Engineering, National Institute of Technology, Calicut, India*

[2]*Dept. of Mechanical Engineering, Aditya University, Surampalem, India*

Abstract

Laser beam machining (LBM) is a non-traditional machining process that uses a monochromatic laser beam to melt and evaporate materials. The laser light's characteristics, such as spectral purity, directivity, and high focused power density, make it ideal for precision tasks like cutting and welding. The lasing action, which involves transitions between atomic energy levels, and the concept of population inversion, which is necessary for laser operation, are key to understanding how lasers work. There are several methods to achieve population inversion, including optical pumping, direct electron excitation, and inelastic atom-to-atom collisions. These methods are used in different types of lasers, such as ruby, argon, and helium-neon lasers. Lasers can be broadly classified into solid-state lasers, like ruby and Nd:YAG, and gas lasers, like helium neon, argon, and CO_2. Each type has its unique construction, operation, and applications. The process capability of LBM is vast, ranging from drilling and cutting to welding. The precision and power density of lasers enable the machining of various materials, making LBM a versatile tool in industrial processes. Despite its advantages, such as no direct contact machining and the ability to work with refractory materials, LBM has its

drawbacks. These include low overall efficiency and difficulty in controlling hole size. Finally, a comparison between LBM and electron beam machining, discussing aspects like efficiency, material removal rate, and application scope is discussed. This comparison provides a broader perspective on the capabilities and limitations of these advanced machining techniques. In conclusion, the document provides a comprehensive overview of LBM, its principles, methods, and applications, and its comparison with other machining techniques.

***Keywords*:** Laser beam machining (LBM), spectral purity, directivity, lasing action, population inversion, optical pumping, direct electron excitation, refractory materials

6.1 Introduction

The term LASER stands for light amplification by stimulated emission of radiation, representing a form of electromagnetic radiation. Laser beam machining (LBM) involves the utilization of an intense, monochromatic laser beam to melt and evaporate work materials. The concentrated heat generated in the targeted area by the laser beam is capable of melting a wide range of materials, making LBM particularly effective for processing difficult-tomachine substances [1]. Laser light possesses several notable characteristics:

i. Spectral purity: laser light is highly monochromatic, allowing for the utilization of simple lenses for beam focusing, thus eliminating the need for costly color-corrected lenses [2].

ii. Directivity: laser beams exhibit high collimation, characterized by minimal divergence angles, facilitating precise control over beam directionality.

iii. High focused power density: due to its minimal beam divergence, laser energy can be efficiently concentrated onto a small area using basic optics, resulting in a high-power density. Proper focusing further enhances power density, determining the laser's suitability for various tasks such as cutting, welding, marking, and heat treatment processes [3].

6.2 Lasing Action and Population Inversion

The functioning of lasers relies on the inherent transitions between energy levels within atoms. Initially, Planck proposed that these energy levels within atoms were evenly distributed [4]. However, Einstein introduced the concept of photons, suggesting that light could be viewed as particles possessing energy. Additionally, Bohr emphasized that while atomic systems possess energy levels, they may not necessarily be uniformly spaced as Planck's oscillator.

In Figure 6.1, the horizontal lines represent the allowed energy levels. When an electron is free, its energy, being positive, can vary arbitrarily, allowing it to move at any speed. However, bound energies are constrained to discrete, specific values denoted as E_0, E_1, E_2, and so forth, as illustrated in Figure 6.1. If an atom is initially in any of these excited states, it will eventually transition to a lower energy state, emitting the excess energy as light. The frequency of the emitted light is determined by the conservation of energy principle, considering the difference in energy levels and the principles of quantum mechanics. Specifically, the transition from energy level E_2 to E_0 follows this relationship.

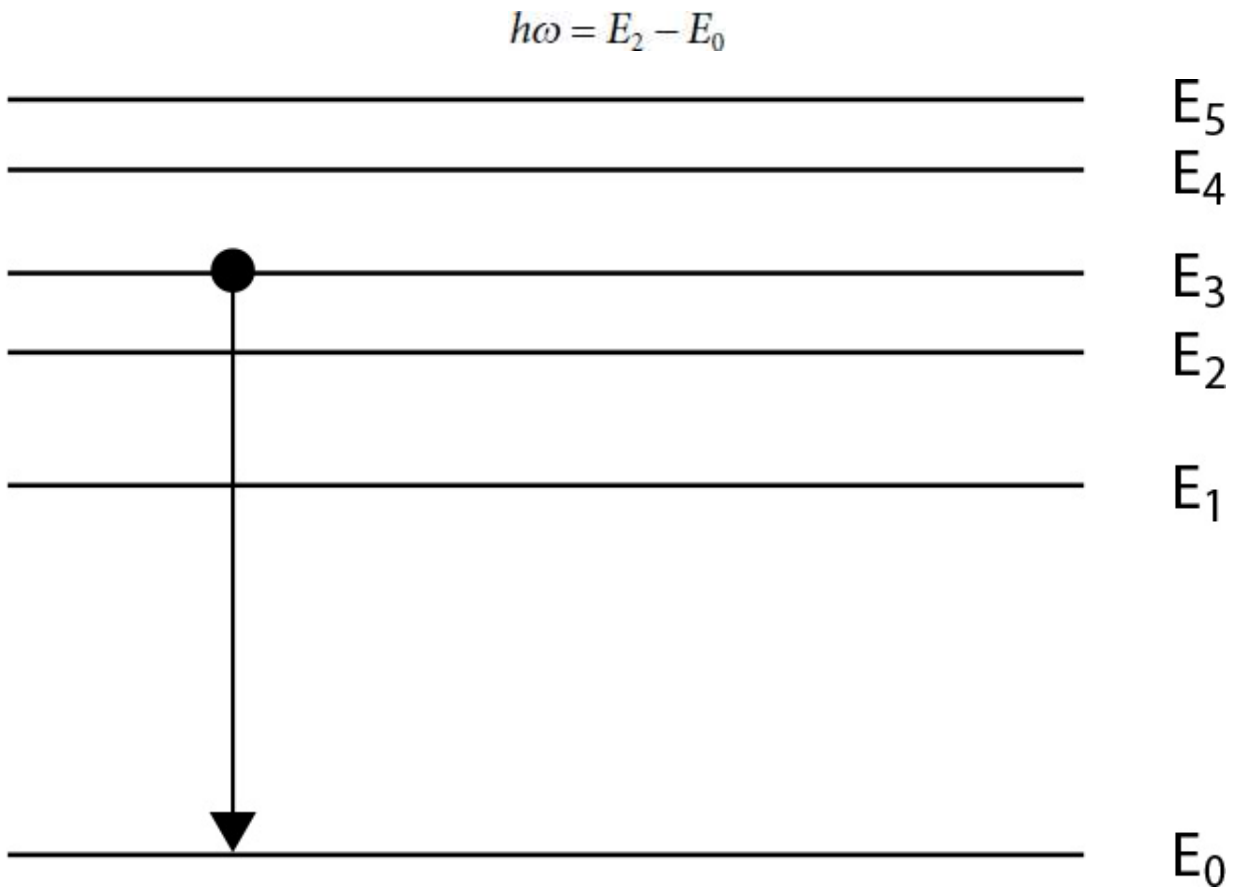


Figure 6.1 Allowed energy levels.

h = Planck's constant

ω = frequency of liberated light

E_2 , E_0 are energy levels between which transition occurs

Einstein is credited with introducing the concept of the interaction between radiation and matter. In Figure 6.2, consider any two specific energy levels of an atom, labelled as the pth and q^{th} levels. According to Einstein's proposal, when light of the appropriate frequency interacts with such an atom, it can absorb a photon of that light, facilitating a transition from state q to state p.

The likelihood of this occurrence per second is contingent upon two factors:

i. The energy disparity between the two states involved in the transition.

ii. The intensity of the light interacting with the atom.

Absorption refers to the process wherein atoms move from lower to higher energy levels. (see Figure 6.3).

Emission refers to the movement of an atom from the higher energy level (p) back to the lower energy level (q). Einstein proposed two processes through which such emission can occur:

i. Spontaneous emission: this occurs when no light is present at the higher energy level, and an atom in an excited state transitions to the lower energy level by emitting a photon [4]. Importantly, this process is independent of light intensity (refer to Figure 6.4).

ii. Stimulated or induced emission: in this process, emission is influenced by the presence of light. When light of the appropriate frequency interacts with an atom, it stimulates the emission of photons [5]. The rate of emission increases with the intensity of the light, resulting in a proportional relationship between the emission rate and the light intensity (see Figure 6.5).

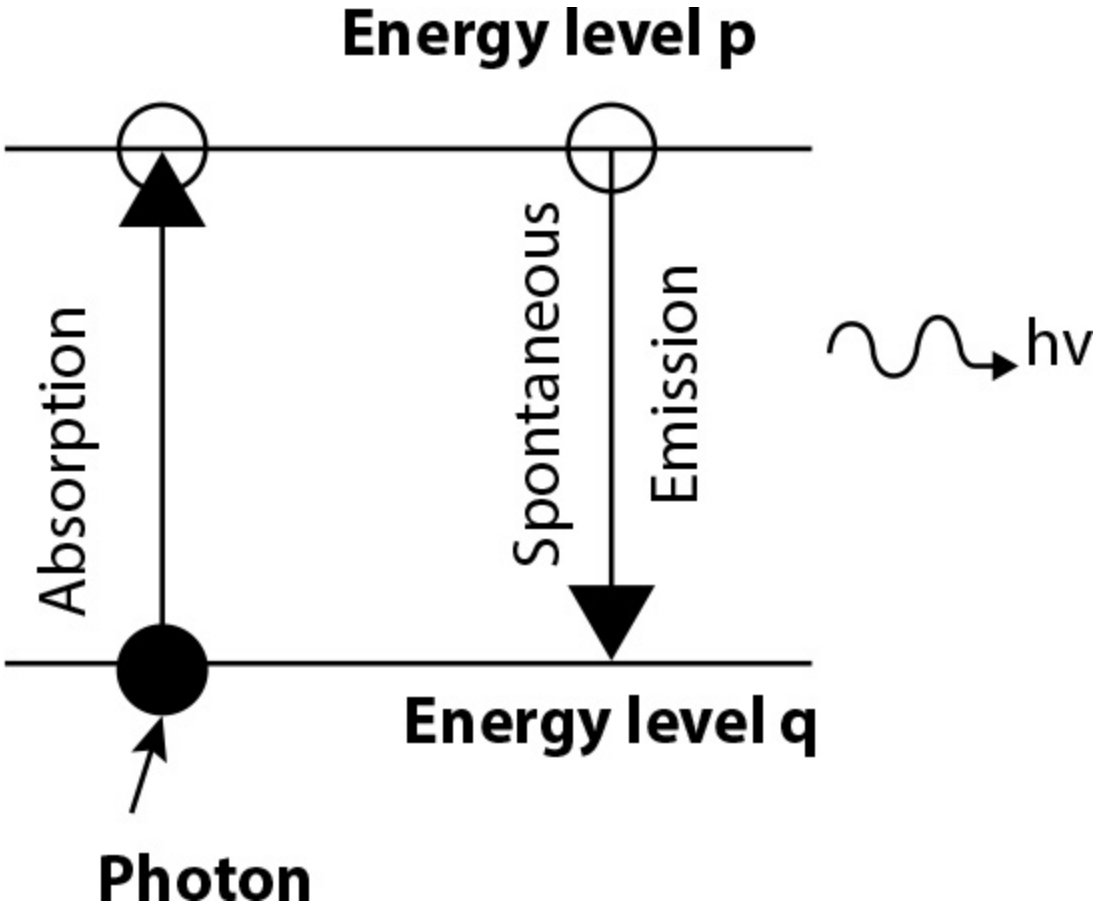


Figure 6.2 Absorption processes in laser.

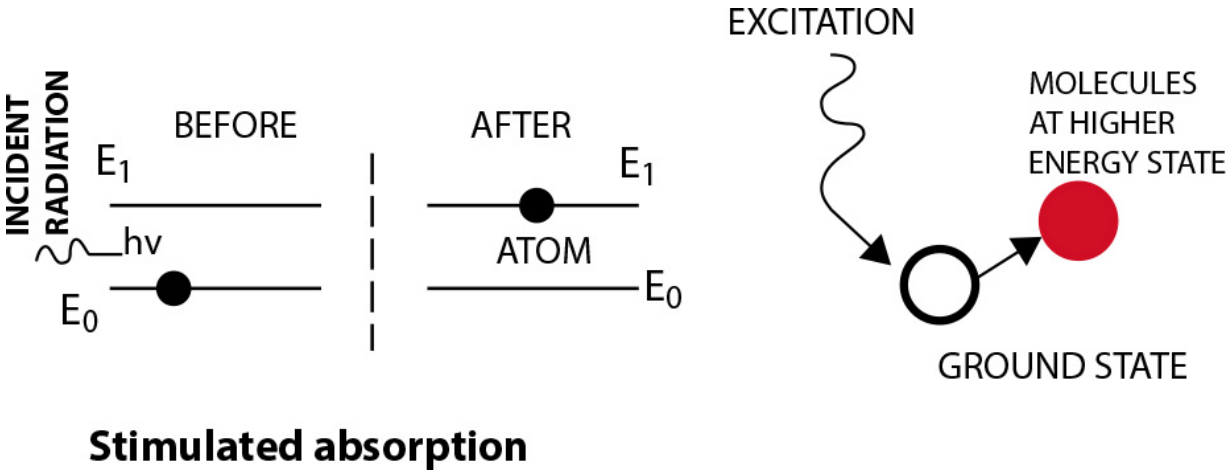


Figure 6.3 Simulated absorption in laser.

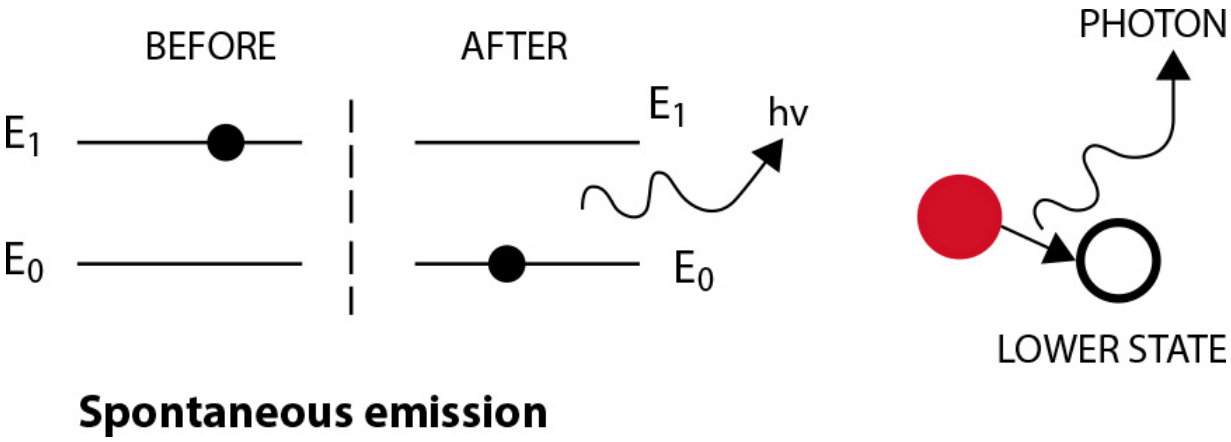


Figure 6.4 Spontaneous emission in laser.

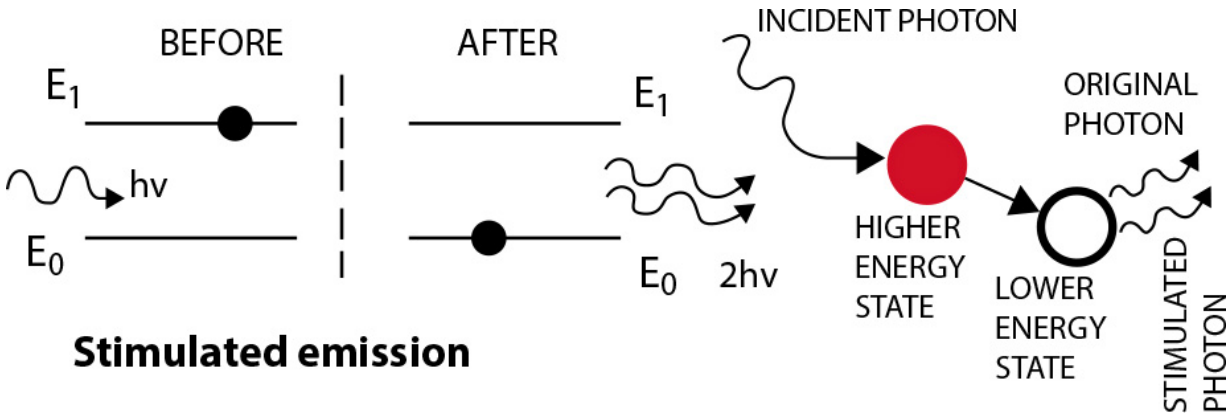


Figure 6.5 Stimulated emission in laser.

If the absorption rate for a specific energy level is known, it is possible to calculate the spontaneous emission rate and the stimulated emission rate mathematically, or any combination thereof.

When atoms in the upper energy level start emitting light of the suitable frequency, stimulated emission takes place, initiating a cascade effect where more atoms follow suit in emitting light. This cascade effect leads to a synchronized emission of photons, known as lasing action, which forms the foundation of laser operation [6].

Stimulated emission is in phase with the incident wave which is amplified but is also attenuated by absorption. From Maxwell Boltzmann relation, it is known that the

number of atoms in qth level is greater than number of the atoms in pth level, when energy $E_p > E_q$. Under these circumstances, with the shining of the light, the process of absorption will predominate. However, if the number of atoms in the pth level exceeds those in the qth level, a state of population inversion arises. Population inversion is required for stimulated emission to predominate.

6.3 Methods to Achieve Population Inversion

Different method of pumping is shown in Figure 6.6.

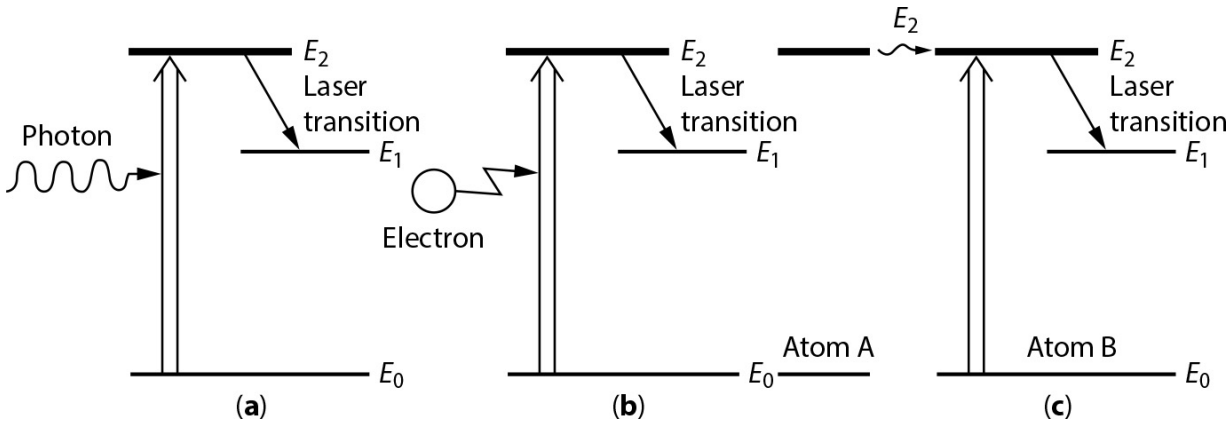


Figure 6.6 Optical pumping methods.

Population inversion can be achieved by:

i. Optical pumping (example ruby laser) (Figure 6.6a)
ii. Direct electron excitation (example argon laser) (Figure 6.6b)
iii. Inelastic atom to atom collision (example: helium neon laser) (Figure 6.6c)

(i) Optical Pumping

As shown in Figure 6.6(a), an external light source is used to produce a high population of some particular energy in

the laser medium by selective optical absorption. Optical excitation is used in solid-state lasers such as ruby laser.

(ii) Direct Electron Excitation (Argon Laser)

In gas ion lasers, such as argon lasers, electron excitation within a gaseous discharge is employed to achieve population inversion. The discharge current is carried by the laser medium itself. Under suitable pressure and current conditions, electrons within the discharge can directly stimulate active atoms, resulting in higher populations in specific energy levels compared to lower ones [7].

(iii) Inelastic Atom–Atom Collisions (Helium Neon Laser)

A combination of gases is used. Say A and B are the gases and both have some excited states A^* *and* B^*. The transfer of excitation may occur between the two atoms such that

$$A^* + B \rightarrow A + B^*.$$

If the excited state of one the atoms, say A^* is metastable, then the presence of gas B will serve as an outlet for the excitation. As a result, the excited level of atom B may become more highly populated than some lower level to which the atom B can decay by radiation. This condition arises with the helium neon laser. Excited helium atoms excite a neon atom and the laser transition then occur in the latter.

A laser's operation is depicted schematically as follows, as shown in Figure 6.7. Within a cylindrical glass vessel resides a gas known as the lasing medium. One end of the glass vessel is sealed with a mirror that reflects 100% of light, while the other end features a partially reflective mirror. Population inversion is achieved by exciting the gas

atoms or molecules using flash lamps. This process initiates stimulated emission, triggering lasing action. Stimulated emission produces photons in various directions, but the majority not aligned longitudinally are lost, generating waste heat. However, photons aligned along the longitudinal direction coalesce to form a coherent, highly directional, and intense laser beam [8, 9].

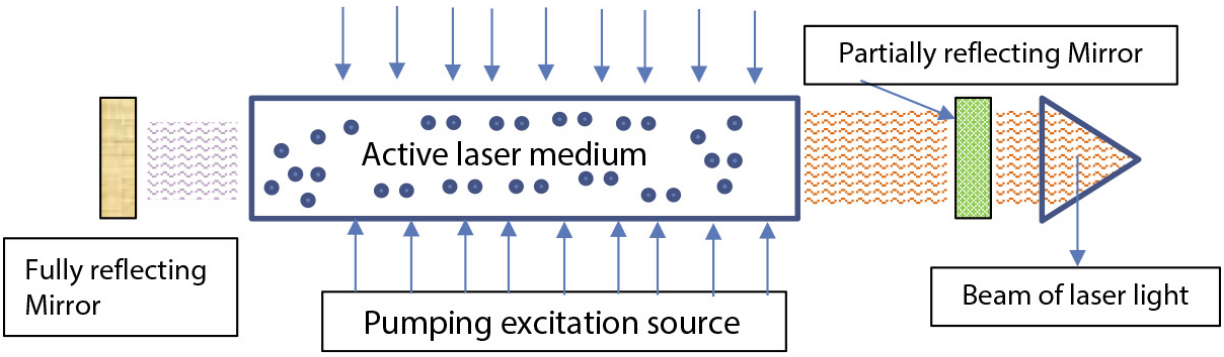


Figure 6.7 Laser operation.

6.4 Types of Lasers

Lasers can be categorized based on their lasing medium into two main types: solid-state lasers and gas lasers. Schematics of solid-state lasers are shown in Figure 6.8.

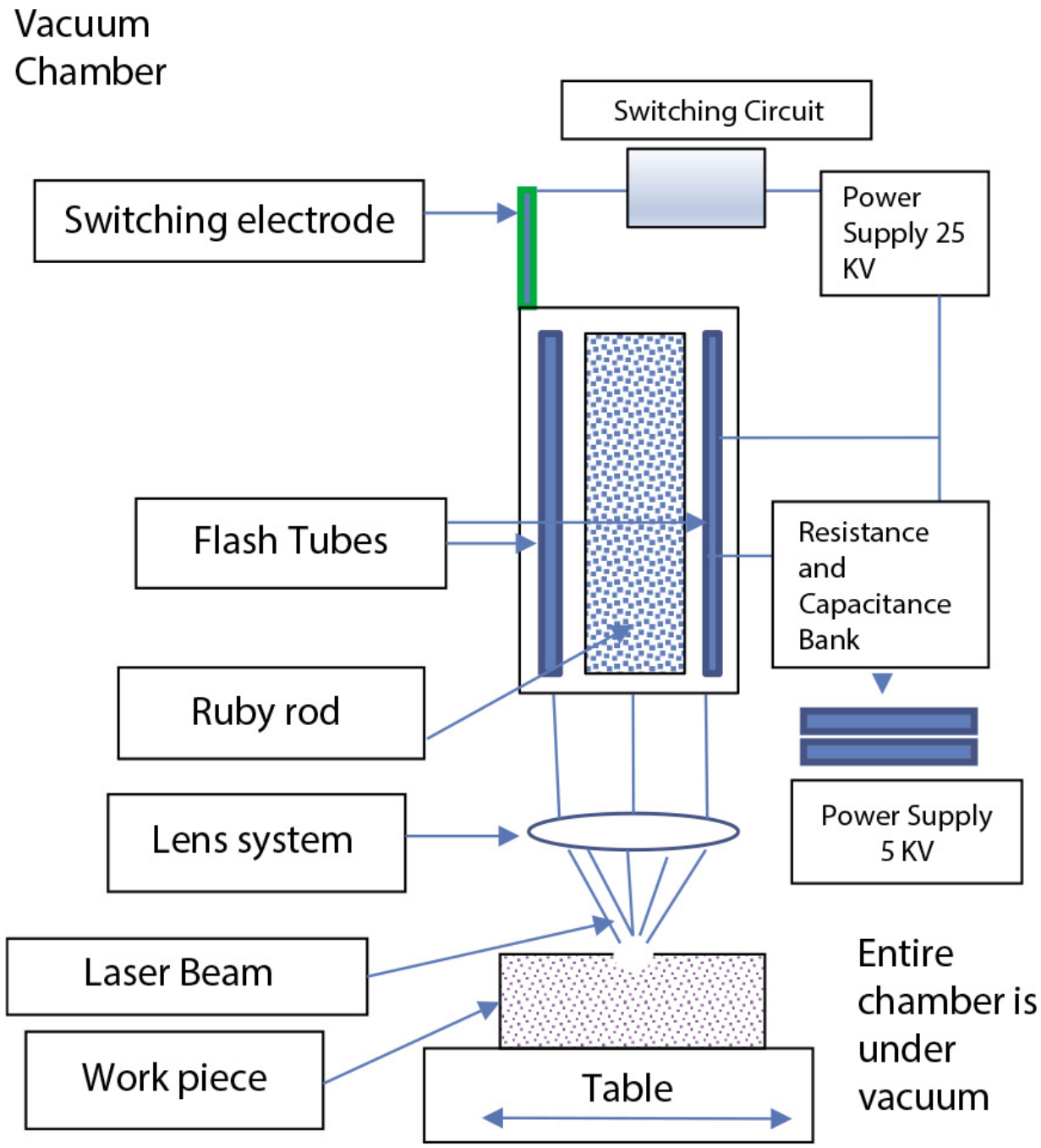


Figure 6.8 Solid-state laser.

Solid-state lasers can be subdivided into:

i. Ruby laser
ii. Neodymium: glass lasers
iii. Neodymium: YAG lasers

Gas laser can be subdivided into:

i. Helium neon lasers

ii. Argon lasers

iii. Carbon dioxide lasers

Solid-State Lasers

The laser material used in this process are ruby, Nd-glass and neodymium- yttrium aluminum garnet (YAG). Of these, neodymium-glass and Nd-YAG are widely used in machining applications. These laser materials are fabricated into rods and their ends finished to high optical tolerances. Energy is injected into the material by generating an extremely intense light flux, which is absorbed by the laser materials and subsequently converted into a collimated laser beam and light flux of high intensity is provided by xenon-filled flash lamps. The life of this flash lamp is around 10,000–100,000 pulses. Nd-glass laser operates only in a pulsed mode with a pulse duration of a few billionths of a second to a maximum of 1 millionth of a second. Neodymium-YAG lasers have the capability to generate a continuous power output by being operated either in pulsed mode or in continuous wave mode [10, 11].

Working of Solid-State Nd-YAG Laser

Solid-state lasers are comprised of several key components, including a solid, crystalline lasing medium capable of being energized to a higher state, a pumping mechanism to infuse energy into the lasing medium (typically an optical flash tube), and a resonator employing mirrors positioned at each end to reflect stimulated light through the lasing medium.

The optical flash tube functions to elevate the lasing medium to a higher energy level. Upon returning to their ground state, atoms, ions, and molecules emit photons of light in various directions. These spontaneous emissions interact with excited particles to produce laser light.

An illustration of the electrical circuit for solid-state laser operation is depicted in Figure 6.8. The flash tube operates in a pulsed manner, regulated by the charging and discharging of the capacitor. The duration of the pulse is determined by the resistance on the flash tube side, while the interval between pulses is determined by the charging resistance. Additionally, a high-voltage switching supply is utilized for pulse ignition [12–15].

CO_2 Gas Laser

A CO_2 laser system uses three gases, namely nitrogen, carbon dioxide, and helium, flowing through a glass discharge tube. Nitrogen functions as an intermediary between electrical energy and vibrational energy of CO_2 molecules. Thus, nitrogen helps to sustain the gas plasma. Helium cools the gas mixture so that it may be re-excited again. Construction of CO_2 laser is shown in Figure 6.9. The application of high voltage at both ends initiates the formation of gas plasma. The discharge energy resulting from this process induces population inversion and triggers lasing action. Positioned at the two ends of the laser system are two mirrors: one functions as a 100% reflector, redirecting photons within the gas tube, while the other serves as a partial reflector. The partial reflector permits a portion of the laser beam to be directed towards the output port, where it is utilized for material processing purposes. Laser tubes are cooled externally [16–18].

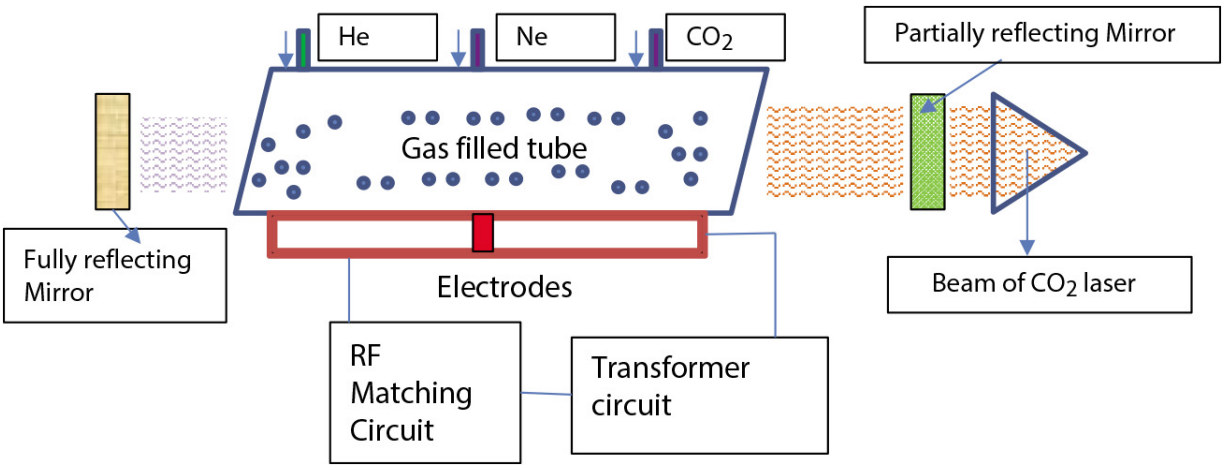


Figure 6.9 CO_2 laser setup.

Typically, the power output of a CO_2 laser is approximately 100 W/m of tube length. However, achieving high power levels necessitates an extended tube length, which is not feasible from a manufacturing standpoint. Consequently, to maximize floor space utilization, high-powered CO_2 lasers are constructed using a folded design [19–21].

The advantages of CO_2 laser over solid laser are:

i. Relatively high and continuous output
ii. High conversion efficiency—efficiency of ruby laser is around 1% whereas for YAG laser, it is around 10%
iii. CO_2 laser has few maintenance problems unlike the solid lasers which require frequent replacement of flash lamps
iv. Divergence is small and it is available in many configuration
v. It is compact
vi. High absorption of its output wave length by many materials
vii. Higher power levels

Commonly Used Gases in Laser Machining

The following gases are generally used for gas lasers as lasing medium:

i. Helium neon

ii. Argon

iii. Carbon dioxide

The detailed description of gas lasing elements are given in Table 6.1. Helium neon, argon and carbon dioxide are the commonly used gases. Out of these three, carbon dioxide is commonly used in industry due to cost benefits and production yield. Also, it is easy to maintain and the availability of carbon dioxide is not an issue in industry.

Table 6.1 Details of the process of gas lasing elements.

Helium-neon	Argon	Carbon dioxide
It is the most prevalent and cost-effective type of gas laser, is typically designed to function in the red spectrum at 632.80 nm. Additionally, it has the capability to be configured for laser emission in the green spectrum at 543.50 nm and in the infrared spectrum at 1523 nm.	It exhibits versatility by operating as a continuous gas laser across approximately 25 different wavelengths within the visible spectrum, ranging from 408.90 to 686.10 nm. However, its most notable efficiency is observed in transitions occurring at 488 nm and 514.5 nm, particularly in the green spectrum. Capable of delivering significantly higher powers compared to helium-neon gas lasers, argon lasers commonly achieve continuous power outputs ranging from 30 to 100 W through multiple transitions. The generation of such output occurs within a hot plasma and demands extremely high-power inputs, typically ranging from 9 to 12 kW, making	It demonstrates the capacity for continuous power outputs exceeding 10 kW and is also capable of operating at extremely high-power levels in pulse mode. While it showcases laser action across various infrared frequencies, it does not exhibit any in the visible spectrum. Notably, the CO_2 laser stands out as the most efficient type of laser, boasting efficiency levels surpassing 30%.

Helium-neon	Argon	Carbon dioxide
	these devices both large and costly.	

6.5 Description of Process

In a typical laser system, the output energy can reach 20 joules within a pulse duration of 0.001 seconds, resulting in a peak power of 20 kW. Such a laser system typically exhibits a beam divergence of approximately 0.002 radians. When focusing this energy with a 25-mm focal length lens, the resulting spot diameter measures around 0.05 mm². Concentrating a power of 20 kW onto this small area enables achieving power densities high enough to vaporize any known metal and even diamond. Consequently, lasers possess the capability to drill through various metals due to their ability to deliver such intense power densities [4, 22–24].

Mechanics of Material Removal

Laser machining essentially entails a rapid ablation process. The intense focus of a laser beam results in the swift evaporation of a minute portion of liquid metal, transmitting a significant impulse to the liquid. Material is ejected from the surface not only through evaporation but also in the liquid state, propelled at relatively high velocities [25].

6.6 Beam Parameters

The criteria of a process are typically impacted by the beam parameters. Beam parameters like the wavelength, output power, type is important. Except for the carbon dioxide lasers, all lasers have an efficiency of only 2–3 %

(maximum). The typical beam parameters are shown in Table 6.2.

Table 6.2 Beam parameters of commonly used lasers.

Lasing material	**Ruby**	**Nd-YAG**	**Nd-glass**	**Co_2**
Type	Solid state	Solid state	Solid state	Gas
Composition	0.03–0.07% Nd in Al_2O_3	1 % Nd doped with yttrium, aluminum and garnet	2–6 % Nd in glass	$C0_2 + He + N_2$(typically, 3:8:4)
Wavelength	0.69 micron	1.066 micron	1.064 micron	10.6 micron
Efficiency	1%	2%	2%	10–15%
Beam mode	Pulsed	Pulsed	Pulsed	Pulsed
Spot size	0.015 mm	0.015 mm	0.025mm	.075 mm
Beam output	10–100 W	10–1000 W	10–100 W	0.1–10 kW
Peak power	200 kW	400 kW	200 kW	100 kW
Beam divergence	5–7 mRad	1–5 mRad	5–7 mRad	0.1–10 mRad
Pulse rate	1–10 pps	1–300 pps	1–3 pps	CW (continuous wave)

6.7 Process Capability

Laser drilling was one of first practical application of laser technology. Some of the drilling capability of laser is given

in Table 6.3.

6.8 Applications of LBM

In addition to their common uses in communication, navigation, ranging, and metrology, lasers find a broad range of machining applications, including:

i. Material removal by drilling, trimming, and evaporating
ii. Material shaping by cutting, scribing, and controlled fracture
iii. Welding of materials
iv. The alteration of thermal and kinetic properties, such as annealing, photochemistry, regulation of grain size, diffusion, and zone melting, is vital in various processes [26].

Table 6.3 Process capabilities of laser.

Drilling diameter	0.005–1.25 mm but larger diameter can be drilled using trepanning
Drilling depth	1.7 mm
Drilling angle	15° to 90
Drilling taper	5–20% of hole diameter
Drilling L/D ratio	Up to 50:1
Drilling length	Up to 6.5 mm
Drilling tolerance	±5–20% of hole diameter
Minimum corner radius	0.25 mm

i. **Laser drilling:** micro-sized holes can be drilled using laser in difficult-to-drill materials such as ceramics and refractory materials. Because of the very nature of melting and vaporization process, high accuracy is not possible.

   A very small diameter less than 0.25 mm can be drilled using laser. Laser beam of small pulses is made to penetrate through the work material and material is removed through multiple pulses. This type of drilling is called percussion laser drilling. Larger holes are produced using computer numerically controlled (CNC) and non-circular holes are produced by laser assisted contour CNC machine. Large number of holes in turbines, nozzles, after burners can be produced using laser drilling operation [27].

   In this case, a ruby laser is used with an output of 25 joules at wave length of 1.06 micron. In this equipment, a cooling system is provided to ensure that output of the laser does not vary with temperature rise. The output of the energy can be carried by means by controls given on panel. Laser spot size vary from 0.01 mm to 1mm. Binocular microscope is provided for viewing and positioning of work. An adjustable cross wire reticule ensures accurate positioning of workpiece. Closed circuit TV (CCTV) is also provided for monitoring the process. The work table is fully enclosed for operator safety [28].

   Precisely spaced holes, 0.25–0.30 mm in diameter in 3.2-mm thick disc of 6.4-mm diameter can be done using laser. Their production by conventional machining requires diamond tipped, hardened steel drill bits. Taper is produced from 0.5mm at the entrance to 0.09-mm diameter at exit. Aspect ratio of 20:1 is achieved.

ii. **Laser cutting:** laser can be used to cut the material at the faster rate. In industry gas-assisted laser systems is used for cutting. Laser is focused by optical systems and coaxial tubes carry gases like oxygen argon and nitrogen. Oxygen gives very good cutting rate but heat affected zone (HAZ) edges are produced in oxy-cutting. Argon gives clear edges. Laser energy of 1.5×10^{2} *to* 1.5×10^{3} W/m^{2} can be used to cut thick and thin metals including plastics and ceramics [29].

Table 6.4 Difference between conduction laser and penetration laser welding.

Conduction laser welding	**Penetration laser welding**
Low intensity lasers are used	High intensity lasers are used
Amount of material removed depends on conduction of laser into work piece	High density laser vaporizes and melt the workpiece ad weld nugget is formed

iii. **Laser welding:** laser can be used to weld dissimilar materials. There are two types of laser welding:

   a. Conduction laser welding

   b. Penetration laser welding

   Detailed comparison is given in Table 6.4.

   Laser is also used for spot welding and seam welding.

iv. **Laser heat treatment:** laser can be used for heat treatment of material. Laser heat treatment can be used to carburized the material up to carburetion thickness of 2 mm. Normally, carbon dioxide layer is used for case carburization. Piston walls, turbine

blades, valve seating, piston rings are usually heat-treated using laser [30].

v. **Laser cladding:** it bears resemblance to laser heat treatment. In laser cladding, special alloying element is deposited on the part by high density lasers. The main disadvantage of cladding is selective area can be cladded depending on functional requirement [31].

vi. **Laser scribing:** laser can be utilized effectively for scribing brittle materials such as silicon wafers, glass, and ceramics. Part number of silicon wafer is done by laser marking or scribing. Silicon wafers are scribed with Q-switched YAG:Nd laser using a peak power of 300 W. Pulse rate of 400/s is used with a pulse duration of 300 ns. The beam is focused on silicon wafers with 14-mm focal length lens, which is moved at a rate of 1500 mm/min [32].

vii. **Controlled fracture:** laser energy can be used to fracture in a controlled manner. Beam is focused on small area of electronic circuits or components. It absorption creates thermal gradient in the material. Because of thermal gradient mechanical stresses are developed. These mechanical stresses cause shearing of materials over a small region. Once the crack develops, it can be propagated easily [33].

viii. **Laser trimming:** laser can be used for trimming operation. Small spot size laser is focused and material is trimmed by selective evaporation. Resistors made of chromium silicon oxide, deposited on silicon chip surfaces, have been successfully trimmed using an argon ion laser.

6.9 Advantages of LBM

i. No direct contact between the laser (tool) and work piece.
ii. Will machine and weld through optically transparent materials.
iii. Welding and machining of areas not readily accessible.
iv. Will melt and vaporize any known material.
v. Easily weld dissimilar materials.
vi. Refractory materials are easy to work with.
vii. Machining hard, brittle and non-metallic materials.
viii. Welding and machining in any desired atmospheric environment.
ix. Small heat affected zone, and negligible thermal damage or effect on adjacent regions.
x. Machining extremely small holes and precision welding of small sizes.
xi. Convenient manipulation of beam configuration and adjustment of exposed area size.
xii. Laser beams eliminate concerns regarding tool wear.
xiii. Machining of soft materials such as rubber and plastics is feasible.

6.10 Disadvantages of LBM

i. Overall efficiency is low.
ii. Pulsed mode operation (solid-state lasers).
iii. Practically limited to thin sheet plates.

iv. Machined holes may not consistently exhibit roundness or straightness.
v. Control of hole size and welding size is difficult.
vi. Repetition rate is slow.
vii. Durability and reliability are limited.
viii. Short life of flash lamp.
ix. Necessity for careful control of pulse length and power intensity to obtain a desired effect.
x. Effective safety procedure is required.
xi. High cost.

Table 6.5 Differences between EBM and LBM.

No.	Electron beam machining	Laser beam machining
1	High velocity electrons strike the work surface and its kinetic energy is converted into heat energy.	When laser beam strikes the work piece it melts and evaporates the work material.
2	Electron beam (electron gun) is a tool here.	Laser beam (lasing material) is tool here.
3	Better surface finish.	Comparatively less surface finish.
4	Metal removal rate is high.	Comparatively MRR is low.
5	Entire equipment must be maintained in vacuum.	Only laser producing unit must be in vacuum.
6	Only metal can be machined.	Any material can be machined except plastic.
7	High power is required for EBM.	Power requirement is less than EBM.
8	EBM can be used for microdrilling up to 0.002-mm diameter	LBM can be used for microdrilling up to 0.005 mm.

6.11 Comparison Between EBM and LBM

Electron beam machining (EBM) and LBM are both beam processes and use the energy in naïve form for machining purposes. Yet there is a fundamental difference between these two processes and are depicted in Table 6.5.

References

1. Kalin, N.R., Uglov, A., Kokora, A., *Laser Machining and Welding*, MIR Publishers, Moscow, 1978.

2. Schwartz, M.M., *Modern Metal Joining Techniques*, Wiley-Interscience, Hoboken, NJ, 1969.

3. *Proceedings on Laser Technology*, Indian Institute of Technology Kanpur, Short Term Course, 1981.

4. Gragliano, F.P. *et al.*, Lasers in Industry. *Proc. IEEE*, 57, 114, 1969.

5. Manufacturing Application of Laser. *Proceedings of SPIE*, vol. 621, 1986.

6. Scrase, T.E., NC Drilling with the Laser. *Metalwork. Prod.*, 114, 60–69, 1970.

7. Singh, G., Application of Lasers in Production Engineering—A Review. *J. Eng. Prod.*, 1, 1, 29–46, 1978.

8. High Power Lasers and Their Industrial Applications. *Proceedings of SPIE*, vol. 650.

9. Laser Technologies in Industries. *Proceedings of SPIE*, vol. 952, 1988.

10. *Proceedings on Laser Applications*, Indian Institute of Technology Madras, Short Term Course, 2011.

11. Application of High Power Laser. *Proceedings of SPIE*, vol. 527, 1984.

12. High Power Laser and Laser Machining. *Proceedings of SPIE*, vol. 1132, 1989.

13. Charschan, S.S., *Lasers in Industries*, Von Nostrand, New York, 1972.

14. Steen, W.M., *Laser Materials Processing*, Springer, New York, 1991.

15. Chryssolous, G., *Laser Machining*, Springer, New York, 1991.

16. Quenzer, A., Laser in Manufacturing. *Proceedings of the 3rd International Conference*, 1986.

17. Steen, W.M., Lasers in Manufacturing. *Proceedings of the 4th International Conference*, 1987.

18. Steen, W.M., Lasers in Manufacturing. *Proceedings of the 6th International Conference*, 1989.

19. Bhattacharya, A., Laser Features and Applications. *J. Met. Process.*, 45–55, 1966.

20. Bhattacharya, A., Laser for Machining Applications. *J. Inst. Eng. (India)*, 4, 56–78, 1971.

21. Bhattacharya, A. and Mullick, B.K., Machining and Welding by Laser Beam. *J. Inst. Eng. (India)*, 51, 101–113, 1971.

22. Fairbanks, R.H. and Adams, C.H., Laser Beam Fusion Welding. *Welding J.*, 43, 11–34, 1964.

23. Lawrence, T.R., Lasers. *J. Wash. Acad. Sci.*, 53, 77–91, 1963.

24. Maiman, T.H., Stimulated Optical Radiation in Ruby. *Nature*, 187, 38–45, 1960.

25. Franken, P., High Energy Laser, International Science and Technology, 1962.

26. Schawlon, L., Optical MASERS, Scientific American, 1961.

27. Schmidt, A.D., Ham, I., Hosi, T., An Evaluation of Laser Performance in Micro Welding. *Welding J.*, 44, 124–135, 1965.

28. Williams, D.A., The Laser as a Drilling Tool. *Proceedings on Laser Manufacturing*, Pennsylvania State University, 1966.

29. Kannatey-Asibu, E., *Principles of Laser Materials Processing: Developments and Applications*, Wiley, USA, 2023.

30. Dawes, C., Light and lasers, in: *Laser welding*, 1992.

31. Pereira, R., Pexinho, N., Costa, S.L., Blanco, V., Carneiro, V., Cortez, S., Parametric study of local laser heat treatment technology on multi forming of advanced-high strength steel (AHSS) part with complex shape. *Int. J. Lightweight Mater. Manuf.*, 7, 10, 439–447, 2023.

32. Saad, M.A., Allam, S.H., El-Sherbini, T.M., Laser gain calculations for soft X-ray and XUV radiation emitted from copper like ions by electron collisional pumping. *Can. J. Phys.*, 5, 3, 45–56, 2016.

33. Jagadeesha, T., *Unconventional machining processes*, I K International Publication House Pvt. Ltd., New Delhi, 2016.

Note

*Corresponding author: jagdishsg@nitc.ac.in

7
Plasma Arc Machining

Jagadeesha T.[1]* and Sandip Kunar[2]

[1]*Dept. of Mechanical Engineering, National Institute of Technology, Calicut, India*

[2]*Dept. of Mechanical Engineering, Aditya University, Surampalem, India*

Abstract

The plasma arc machining process, which was created for challenging-to-machine materials to overcome inaccuracies and failure of traditional machining methods when it comes to complex shapes and workpieces, is discussed in this chapter. Plasma generation is first discussed with detailed process used in plasma processes followed by the nature of plasma. Furthermore, description of the equipment is given with various kinds of torches used in plasma machining processes. Modes of operation of the torch processes is discussed in length with compassion between transferred type and non-transferred type. Advantages and disadvantages along with the important industrial applications are also discussed in this chapter.

***Keywords*:** Plasma arc cutting, plasma torch, plasma welding, oxygen injected plasma, transfered torch

7.1 Introduction

The technique known as plasma arc machining (PAM) involves applying an ionized gas jet at high speed onto the workpiece to remove material. Despite being relatively narrow, the plasma jet’s extremely high temperature between 11,000°C and 30,000°C—helps it melt the

workpiece material in its path. Almost any material can be processed using this method, even ones that are difficult to cut with oxy-fuel gas. Plasma consists of free electrons, positively charged ions, and neutral atoms. It can be obtained by heating a gas to a very high temperature so it is partially ionized [1–3].

Plasma arc machining operates similarly to oxy-cutting. Plasma arc machining, on the other hand, is advantageous when machining difficult-to-cut metals such as super alloys, particularly during cut-off or rough-slitting processes.

Plasma arc machining effectively cuts materials like aluminum and stainless steel by utilizing a combination of convective heat from the high-temperature plasma and direct electron bombardment. Unlike conventional methods like oxy-fuel cutting, which struggle with materials possessing high thermal conductivity, substantial heat capacity, and strong oxidation resistance, plasma arc cutting is adept at handling such challenges. This method generates a high-temperature plasma by passing gas through a narrow nozzle and applying an electric arc, reaching temperatures up to 30,000°C. The resulting intense heat allows precise cutting of these difficult-to-machine materials, overcoming their inherent properties [4].

7.2 Plasma Generation

One of the most common methods of producing plasma is to heat a gas to a high temperature to ionize it. There are two approaches to doing this.

- Applying an appropriate electric field across the gas column
- Exposing the gas column to radiation.

Heating gases to high temperatures initiates the following processes:

i. Elastic and inelastic collisions occur between the atoms.

ii. Gas ionization takes place, leading to the generation of electrons and ions.

iii. Electrons interact with atoms, increasing their thermal kinetic energy through collisions. Subsequent collisions generate more electrons and ions, forming a new state of matter known as plasma. Plasma can conduct electricity due to the presence of free charges. The temperature within a 200-A plasma column can reach exceedingly high levels, reaching temperatures as high as 28,000°C to 30,000°C [5–8].

7.3 Description of Process

In PAM, an electric arc produced between the cathode and anode nozzles bombards a stream of gas with electrons. The arc's high-speed electrons hit with gas molecules, causing diatomic molecules such as H_2, N_2, and O_2 to dissociate and ionize. When plasma-forming gas flows through the nozzle, an arc forms between the plasma arc generator's cathode electrode and the anodic nozzle (Figure 7.1). The gas flow must be controlled to steady the arc. The majority of gas heat transfer happens in the narrower nozzle region, producing a high exit gas velocity and an elevated core temperature in the plasma column [9].

The versatile nature of the plasma column enables it to be utilized for various manufacturing processes beyond cutting. Here is an expansion on its applications:

1. Welding: plasma welding employs the intense heat of the plasma column to join materials together. The high temperatures and focused energy of the plasma enable precise and efficient fusion welding, particularly for thin and delicate materials where conventional welding methods may cause distortion or damage.
2. Spraying: plasma spraying, also known as plasma spray coating, involves the deposition of a coating material onto a substrate surface using the thermal energy of the plasma column. This process is commonly used for applying protective or decorative coatings to components, enhancing their corrosion resistance, wear resistance, or thermal insulation properties [10].

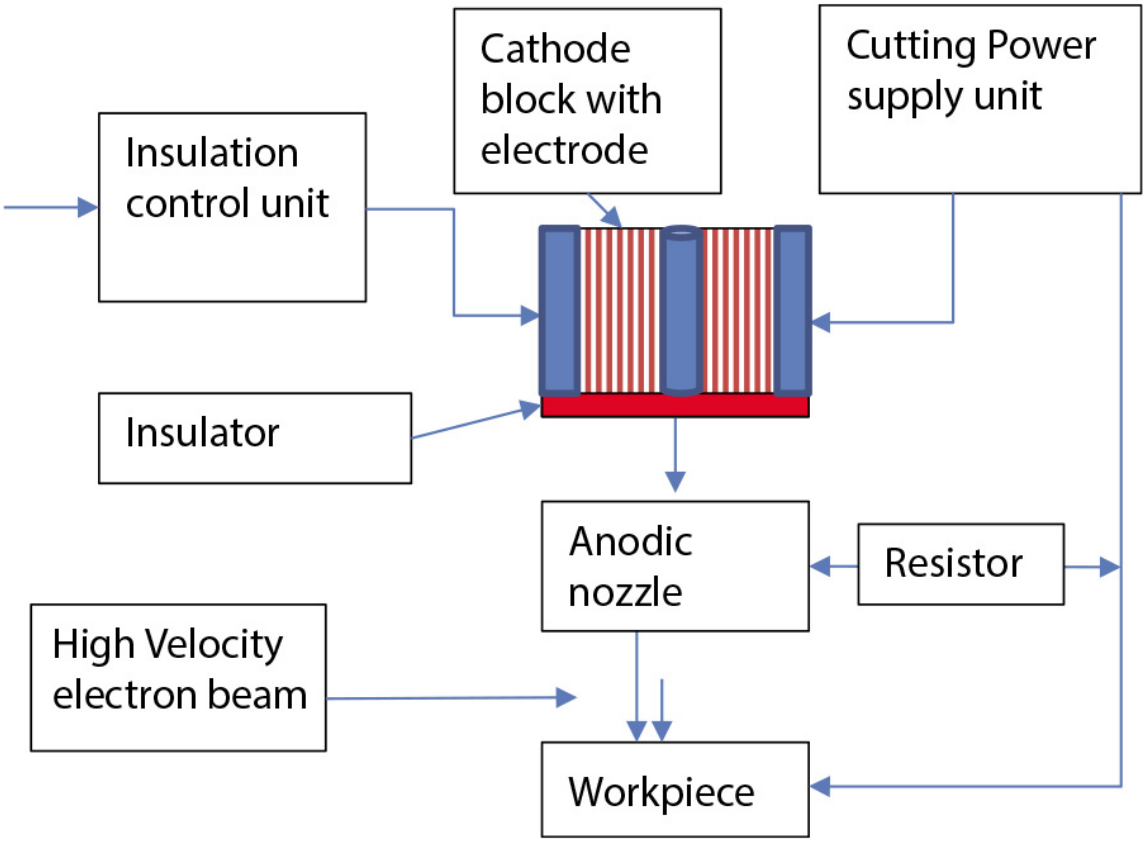


Figure 7.1 Plasma arc machining.

3. Machining: in addition to cutting, plasma can be utilized for machining operations such as drilling,

milling, and surface profiling. The intense heat and kinetic energy of the plasma enable rapid material removal, making it suitable for machining applications where high precision and productivity are required [11].

4. Preheating: plasma can serve as an effective preheating source in hot machining processes like friction stir welding. By preheating the workpiece material, plasma helps reduce thermal gradients and stresses during the machining operation, improving the overall quality and integrity of the weld or formed joint [12].

7.4 Description of Equipment

Plasma arc machining consists of

1. Power supply
2. Gas supply
3. Water cooling systems
4. Plasma control console torch

a) Power Supply

Plasma arc machining needs a direct current (DC) power source to function. At about 200 volts, the power supply has a maximum output of 1000 A. The saturation current of the power supply is the value above which the current, even in the event of a short circuit, should not increase. To maintain an arc, the voltage load must be lower than the open circuit voltage. Transformer-controlled rectifier units or DC motor-generator sets with saturable core reactors are used [13].

The current drawn in a transducer-controlled unit is directly proportional to the voltage drop across the

transducer. As the current increases, the voltage drop across the transducer rises, resulting in voltage decreases. To avoid excessive current, extra regulation is used to manage and restrict the short-circuit current.

Selenium rectifiers are preferred to silicon rectifiers because selenium rectifiers offer more surge resistance. If silicon rectifiers are used, they should be protected by an resistance capacitance (RC) network bypassing the voltage surges and by a fast-acting fuse for current surges [14].

b) Gas Supply

A plasma can flow at a velocity of several 120 m/s when the gas pressure is as high as 1.6 MPa. The momentum of the plasma jet increases with increasing gas flow rate. Moreover, a greater flow rate facilitates the removal of molten material from the melting zone.

Gas Selection

You can use any gas as long as it does not damage the workpiece or tungsten electrode. Typically, a blend of nitrogen, hydrogen, or compressed air is used to cut carbon, alloy steel, and cast iron. Combinations of nitrogen and hydrogen are used to cut non-ferrous metals such as aluminum, stainless steel, and others [15].

c) Cooling Water System

Both electrodes that are anode and cathode are water-cooled.

d) Plasma Torches

The fundamental plasma jet in PAM is produced by restricting an electric arc through a nozzle. The nozzle narrows the arc into a narrow cross-section rather than deviating into an open arc.

There are many torch designs used. They are:

1. The air plasma torch
2. Oxygen injected plasma torch
3. Water-injected plasma torch
4. Double gas plasma torch

(i) Air plasma torch: this method is employed an air plasma torch utilizes air as the ionizing gas The metallic constricting nozzle is in direct contact with the workpiece. This design allows the arc to form from the electrode to the nozzle and, subsequently, from the nozzle to the workpiece. Double arcing is an undesirable phenomenon that can occur, but it increases the risk of nozzle failure [16].

The oxygen present in air supports exothermic burning of metal and provides for very fast cuts in oxidizable materials such as steel. Other materials such as aluminum also can be cut by this torch, but cut edges are subjected to severe oxidation [17]. Tungsten electrodes are not used as electrode because they oxidize very fast due to presence of oxygen and will last for few seconds only. Since zirconium and hafnium have a strong oxidation resistance, they are used as electrodes.

(ii) Oxygen-Injected Torch

The primary heating at the workpiece involves electron energy transfer, recombination of dissociated molecules, and conductive heating from the high-temperature plasma generated by the arc. Occasionally, oxygen injection into the work area is preferred to introduce a third heating source through exothermic oxidation [18]. Upon reaching the melting point, the high-velocity gas stream efficiently removes the material.

iii) Water-Injected Plasma Torch

Water injection is employed to constrict the plasma, with approximately 10% of the water vaporizing to form steam, which aids in plasma constriction and provides insulation for the nozzle. Nitrogen, pressurized at 1 MPa, serves as the plasma gas. To prevent double arching, the lower section of the nozzle is made with ceramic [20]. Water injection not only reduces smoke but also extends the nozzle's lifespan. Additionally, it can help decrease the heat-affected zone during torch operation.

There are several advantages to this water injection:

1. It is possible to machine a square cut.
2. There is more arc stability.
3. Cutting speed can be improved.
4. Less heat-affected zone.
5. There is a reduction in smoke and fumes.
6. A longer nozzle life is achieved.

iv) Dual Gas Torch

Dual gas torch as the name indicates uses two gases. i) Plasma gas and ii) shielding gas. Plasma gas is nitrogen, and shielding gases are carbon dioxide, oxygen, water, and hydrogen. There is no problem of double arcing in dual gas torches due to use of ceramic cup. Shielding gas also cools the ceramic cups and prevents thermal damage. Sharp corners can be maintained on the top edge of workpiece using dual gas torch [21].

7.5 Modes of Operation of DC Plasma Torches

There are two modes of electrical connection in the torch:

i. Non-transferred arc mode

ii. Transferred arc mode.

Comparison between non transferred arc and transferred arc mode is given in Table 7.1.

Table 7.1 Comparison between non transferred arc mode and transferred arc mode.

Non-transferred arc mode	Transferred arc mode
The DC power supply connects the cathode tool and anode nozzle, carrying the same current.	The cathode is connected to the negative terminal of the DC source, while the work is connected to the positive terminal of the power supply through a resistor that limits the current.
This method is suitable for electrical insulators.	This method is suitable for electrical conductors.
Plasma is a flame-like state of matter, often used for spraying, ceramic work, and chemical synthesis.	Plasma, in arc form, serves welding and surface hardening purposes.
Electro thermal efficiency is about 60–70%	Electro thermal efficiency is about 85–90%
Anode dissipation is wasted on nozzle heating, resulting in inefficiency.	Anode dissipation is useful in heating of the workpiece.
Less penetration is obtained, so thin sheets can be welded.	Higher penetration is obtained, so thicker sheets can be welded.
The work piece is not part of the electrical circuit and heat is obtained from the plasma jet. Therefore, less energy is transferred to work. This is useful in cutting.	The work piece is part of the electrical circuit and heat is obtained from the anode spot and the plasma jet. Therefore, higher amount of energy is transferred to work. This is useful for welding.

7.6 Methods to Make Arcs More Stable

The electrical energy is converted into thermal energy in the form of a plasma jet by plasma torches. Stabilizing the electric arc is important because it burns in a small area and is forced by a gas or liquid. The arc column is surrounded by the vapors of the liquid stream when used.

The stabilizing medium indicates that either gas or liquid-stabilized plasma torches exist. Two approaches can be used with gas-stabilized plasma torches. I. Stabilization of the wall or sheath; and ii. Stabilization of the vortex. Also, liquid-stabilized plasma torches are available.

7.7 Parameters that Influence PAM Performance

Three categories can be used to classify the parameters that control the PAM’s performance.

1. Characteristics related to the torch’s construction and functionality.
2. Configuration parameters related to the setup’s physical setup.
3. The workspace where work is done.

7.7.1 The Parameters Related to the Design and Operation of the Torch

i) Operation Aspects

Because the arc column’s plasma is forced out of the nozzle as a high-velocity jet, the stabilized arc that emerges from

it is known as a plasma jet. The DC plasma torches operate in two different ways.

a. Non-Transferred Mode
    - Turbulent mode flame torches which uses short flame and high velocity jet of plasma. Applications include chemical synthesis, insulator working, and spraying.
    - Laminar mode flame torches which uses low velocity flames. It is used for spheroidizing and melting ceramics.
    - High power torches used for high current (2000 A or higher) applications.

b. Transferred Mode

ii) Cutting torches

- Single-flow torches
- Double-flow torches
- Multiport nozzle torch
- Oxygen-plasma cutting torch
- Welding torches
- Micro torches or needle torches.

The torches also operate on two flow modes:

1. Turbulent mode
2. Laminar mode

Turbulent mode: for material removal techniques like melt blasting or spraying, high gas flow rates that result in

turbulent jets are employed when high-velocity flames are necessary.

Laminar mode: laminar mode is used when long flames or low velocities are needed. Long nozzles are designed to produce a laminar flame by maintaining low gas flow rates.

iii) Design Aspects

The goal of the design of the plasma torch is to produce the most heat possible. Improved gas heating and decreased electrode losses, which increase the electrode's lifespan, are two additional benefits of increased efficiency. Moreover, the design guarantees the lowest possible rates of erosion.

The following design parameters affect the performance of the torch:

- Size of cathode
- Nozzle convergence
- Diameter of nozzle orifice
- Orifice length
- Gap between electrode
- Electrode cooling

The cathode: the cathode taper at the tip and the diameter of the cathode affects the drop across the cathode rod. The diameter and bluntness or sharpness of the cathode determines the erosion rate, stability of arc, and flame shape. For non-transferred applications, tapered rods with slightly blunt tips are utilized, but for cutting applications, a flat-disc sloped on the edges is used. The taper angle or sloping of disc is usually smaller or equal to convergence angle of the anode nozzle. For spraying and cutting, 10-mm diameter cathodes are used up to 500 A.

While for welding, electrodes of 6-mm diameter are used. The cathode is pressed to fit into a water cooled copper holder and brazed to it.

The anode nozzle: the anode convergence has a definite relation with the operation of the torch and is matched to the cathode taper to obtain the best performance, that is, minimum electrode erosion and electrode loss.

The nozzle orifice design is based on developing a stable plasma column. Two zones separate the plasma in a specific model. There are two types of flow regions: undeveloped and fully developed. It is preferable for the plasma flame to be fully developed and outside of the nozzle duct in order to minimize anode loss and erosion because electrode losses are higher in fully developed regions.

The nozzle diameter determines the power density in the flame. Nozzle diameters are kept small for high velocity plasma jets. In spraying, diameter of the nozzle should be variable to obtain different velocities and power densities.

General Design Considerations

1. Large current require a larger diameter cathode, orifice length, and electrode gap.
2. While operating at larger arc voltages, it is preferable to increase the angle of taper at the cathode tip.
3. While operating at transferred arc anode, flat face cathode are used due to high arc voltages.
4. Edges of constrictions are rounded off to avoid turbulence. To stabilize laminar flow modes, a large orifice has to be used.
5. In any torch, the alignment between the electrodes is very essential and any misalignment would lead to

undesirable arcing on the sides and nonuniform erosion on one side of electrode.

6. Non-transferred arc modes use long throat lengths, while for transferred arc mode, the minimum orifice length is used.
7. The cathode taper and convergence of the nozzle should be such that the arc terminates at the tip of the cathode. This means that the tip is nearest point to the anode. In some cases, the tapered sides of cathode are made parallel to the converging side of the nozzle.
8. The insulator portion should not be placed anywhere near the arc zone to avoid any damage to the insulator by radiation or convection heat.
9. The cooling provided to the cathode should be optimized for minimum uniform erosion without cracking the cathode and destroying the maximum stability. But excessive cooling in rod type electrodes at normal cooling rates is not usually obtained.
10. High quality insulation should be used in other portion of the torch as high frequency voltage is used for ignition.
11. Oxygen or compounds of oxygen in the plasma gas are detrimental to the cathode.
12. No water leakage into the plasma chamber from cooling chamber is allowed.

For successful utilization of the PAM process, it is required to analyze the following process parameters:

- **Power Supply**

  a. Type: direct current (DC)

  b. Voltage: 220 V

c. Current: 75-1050 A

d. Power: 2–250 kW

- **Primary Gas**
  a. Composition: N_2:H_2 = 95:15
  b. Pressure: 10–15 bar
  c. Flow rate: 0.6–10 m^3/h
- **Shielding Gas**
  a. Type: CO_2, H_2O, Ar, H_2
  b. Pressure: 11–15 bar
  c. Flow rate: 50–75 m^3/h
- **Nozzle**
  a. Stand off distance (SOD): 5–25 mm
  b. Diameter: 0.75–6.34 mm
  c. Life: 2.5–5.5 h
  d. Material: zirconium, hafnium
- **Cutting Parameter**
  a. Plasma jet tool
  b. Maximum velocity of the plasma jet: 500 m/s
  c. Maximum temperature: 16,000–20,000°C
  d. Material removal rate: 150 cm^3/min
  e. Maximum plate thickness: 200 mm (material dependent)
  f. Cutting speeds: 0.1–7.5 m/min

7.7.2 Parameters Associated with Physical Configuration of the Setup

Plasma arc machining is influenced by various factors such as standoff distance, angle, feed, depth of cut, and speed of work. The feed and depth of cut determine the volume of material removed.

The distance measured between the nozzle and the workpiece is called a standoff distance. Following is a list of SOD's effects.

Table 7.2 Cutting speeds of plasma arc.

Material	Thickness in mm	Arc current in A	Cutting speed (mm/min)
Stainless steel	80	850	400
	150	1050	180
Aluminum 75	80	950	780
	190	1040	190
Brass	15	430	1785
Titanium	15	500	2290

Cutting speed: the thickness of the material to be cut determines the plasma arc cutting speed. Cutting speeds must be lowered for thick material compared to thin material. The various cutting speeds of plasma arc is given in Table 7.2.

7.7.3 Parameters Related to the Setting in Which Work is Performed

A protective atmosphere has to be provided to decrease the oxidation of the exposed high-temperature machine surface. The arc's deflection should be kept to a minimum.

On the impingement area, the plasma column should spread uniformly.

7.8 Capability to Process

1. Plates thicker than 50 mm of carbon steel can be cut 10 times faster than oxy-fuel cutting.
2. Aluminum, hardened steel, and stainless steel are all cuttable materials because PAM produces cleaner, smoother cuts and is less contaminated than oxy-fuel cutting.
3. Accuracy of ±0.8 mm up to 35-mm plates, ±3 mm up to 150-mm plates.
4. The sharp radius can range from 4 mm to 38 mm in size.
5. material removal rate up to 150 cm^3/min can be obtained.
6. Cutting speed up to 7500 mm/min is achieved.
7. Kerf angle 2–7° in actual cutting condition, 1⁻2° with special arrangement.
8. In PAM, the cutting rates of 250–1700 mm/min are possible depending on type of the material and its thickness irrespective of their hardness and refractory nature.
9. It is possible to create a smoother surface than with an oxy-acetylene flame.
10. Magnesium, titanium, copper, nickel, and copper alloys can be cut using PAM.
11. It is used for profile cutting a variety of metals, including titanium, alloy steels, and mild steel.

7.9 Applications of Plasma Arc Machining

1. This method is used to replace conventional machining processes like plasma arc welding, heat treatment, metal deposition, and turning.
2. Aluminum, titanium, stainless steel, and other non-ferrous materials can process and machined using PAM.
3. Using a plasma arc, filler material is used for corroded or worn out surface to repair the surfaces or to impart new surface properties to the material such as anti-corrosion properties, anti-friction and wear resistance properties. Like laser, the surface properties can be altered for specific purposes.
4. Electrically conductive metals can be cut using PAM.
5. PAM is applicable to hole piercing.
6. Aluminum and stainless steel can be efficiently stack-cut by PAM.
7. To achieve the desired surface thickness, molten metal droplets can be sprayed using a plasma arc.

7.10 Advantages of PAM

1. Both ferrous and non-ferrous materials can be cut quickly with it. Cutting mild steel (MS) thinner than 5 mm can be done 10 times quicker than oxyfuel welding.
2. It is possible to profile-cut titanium and stainless steel.
3. No interaction between the tool and the workpiece. For this reason, complicated jigs and fixtures are not required.

4. Plasma cutting rates are high for all materials compared to other cutting methods.
5. Regardless of the material’s hardness or other characteristics, equally effective
6. Exotic metals can be machined quickly by PAM.

7.11 Disadvantages of PAM

1. This process produces burr and a secondary operation is needed to remove the burr.
2. If process parameters are not controlled effectively, taper surfaces are generated.
3. The process modifies the metallurgical surface. It creates uneven, extremely hard surfaces, which are undesirable in certain engineering applications.
4. This process generates noise and smoke. So, it is necessary to wear eye and nasal protection.
5. The process creates a heat-affected zone (HAZ) and HAZ may result in component failure before its time.

7.12 Safety Precautions to be Taken in PAM

The following are safety precautions to be taken during PAM:

1. The plasma flame emits a powerful beam that contains high levels of ultraviolet and infrared radiation. If the necessary precautions are not taken, these radiations can cause permanent damage to the eyes.
2. When using a plasma system, remember that it creates an electrical circuit between the torch and the

workpiece. Touching the torch body, workpiece, or water in a water table while the system is operating can be fatal.

3. Operator should ventilate potentially flammable atmospheres before cutting.
4. The overexposure to ultraviolet rays may lead to painful skin burns and cancer.
5. The operator should cover most of his body and eyes before starting the work.
6. It is important to use a torch in a well-ventilated area with proper exhaust due to the production of toxic gases in the atmosphere.
7. There is a lot of noise produced when using the torch. So, it is necessary to wear earplugs or muffs.
8. To operate hand torches, one should wear asbestos gloves with an inner layer of leather.
9. It is recommended to consult with medical professionals to determine how long an operator can safely remain near a plasma torch.
10. It is better to automate the torch and control it remotely when spraying and chemically synthesizing toxic powder.

References

1. Esibyan, E.M., *Plasma arc equipment*, MIR publication, Russia, 1973.
2. Artisimovich, L.A., *A physicist ABC on plasma*, MIR publications, Russia, 1985.
3. Arata, A., *Plasma, Electron and laser beam technology*, ASM publications, USA, 1985.

4. *Plasma arc machining*, US Army report, AMRACR-66-03, USA, 1981.

5. Hebble, C.M., Plasma cutting, - an exotic process into its own. *Weld. Eng.*, 58, 3–11, 1973.

6. Nachman, M., Few considerations about the designing of plasma arc torches. *Rev. Int. Hautes Temp., Refract*, 10, 2–15, 1973.

7. Kharitonov, E.P., Magnetic control of plasma arc during cutting of metals. *Weld Prod.*, 19, 12–23, 1972.

8. Budnik, N.M., Plasma spraying of protective coating from alumina on refractory materials. *Weld Prod.*, 20, 12–23, 1973.

9. Ingham, H.S. and Fabel, A.J., Comparsion of plasma flames spray gases. *Weld J.*, 54, 2–9, 1975.

10. Beider, B.D., Determination of parameters of plasma arc in a stream of Argon and nitrogen used for cutting of metals. *Weld Prod.*, 21, 6–15, 1974.

11. Larri, O. and Y., Equipment for air plasma cutting of metals. *Weld Prod.*, 21, 5–21, 1974.

12. Shapiro, I.S., The influence of parameters of the gas supply systems on the operating characteristics of plasmatrons for metal cutting. *Weld Prod.*, 23, 7–13, 1976.

13. Rao, K.N. and Gururaja, G.I., Some studies of the plasma cutting of aluminium plates. *Indian Welding J.*, 6, 3–11, 1974.

14. Trojan, J., How to apply water injected plasma cutting to CNC punching and nibbing machine, in: *Fabricator*, pp. 22–24, 2013.

15. Bijoy, B. and Biswanath, D., *Machining processes utilizing thermal energy*, Elsevier BV, United Kingdom, 2020.

16. Norrish, J., Advanced gas tungsten arc welding, in: *Advanced welding processes*, 2006.

17. Helge, I.A. and Fridtjov, I., Gravity-driven laminar film flow of power-law fluids along vertical walls. *J. Non-Newtonian Fluid Mech.*, 11, 4, 217–224, 1988.

18. Zakaria, S., Study on the Microstructure and Mechanical Properties of Submerged Arc Welded X80 Steel, in: *Proquest*, 2014.

19. Prakash, R., Non-destructive testing of composites, in: *Composites*, 2021.

20. Prasad, V., Introduction to Mechanical Engineering, in: *Springer Science and Business Media LLC*, pp. 42–73, USA, 2018.

21. Jagadeesha, T., *Unconventional machining processes*, I K International Publication House Pvt. Ltd, New Delhi, 2016.

Note

*Corresponding author: jagdishsg@nitc.ac.in

8
Ion Beam Machining

Jagadeesha T.[1]* and Sandip Kunar[2]

[1]*Dept. of Mechanical Engineering, National Institute of Technology, Calicut, India*

[2]*Dept. of Mechanical Engineering, Aditya University, Surampalem, India*

Abstract

Ion beam machining (IBM) has become a crucial technology in modern manufacturing due to its precision and versatility. This chapter provides a comprehensive overview of IBM, covering its principles, technological advancements, process characteristics, equipment configurations, applications, as well as advantages and limitations. Ion beam machining operates on the principle of ion sputtering, distinguishing it from traditional machining methods. The process involves ion bombardment of the workpiece surface within a vacuum chamber, leading to material removal through sputtering. Factors influencing material removal rates and precision include ion energy, angle of incidence, and material properties. Technological advancements in IBM have led to the development of sophisticated ion sources and vacuum chambers capable of accommodating large workpieces. These advancements enable precise control over material removal rates and surface finish enhancement. Iron beam machining finds widespread applications across industries, including precision machining of electronic components, fabrication of microstructures, thin film deposition, and polishing optical surfaces. Its advantages include universal applicability, precise machining capabilities, and residue-

free operation. However, IBM faces limitations such as relatively low efficiency, high capital costs, and potential material damage.

***Keywords*:** Ion, beam, machining, manufacturing

8.1 Introduction

In ion beam machining (IBM), material removal occurs through ion sputtering, distinguishing it as an electrothermal process. Conversely, in electron beam machining (EBM), laser beam machining (LBM), and plasma arc machining (PAM), material removal is achieved through melting and evaporation. While IBM is categorized under thermo-electric processes, it diverges from EBM and LBM by not relying on localized heating of the workpiece to its evaporation temperature. Instead, IBM is reliant on sputtering, where bombarding ions dislodge surface atoms through the kinetic transmission, akin to how a cue ball striking a packed mass of billiard balls scatters one or more away from the group. This analogy holds particularly true when envisioning the weak adhesive binding the billiard balls together, representing the inter-atomic binding energy that solid materials possess [1–3].

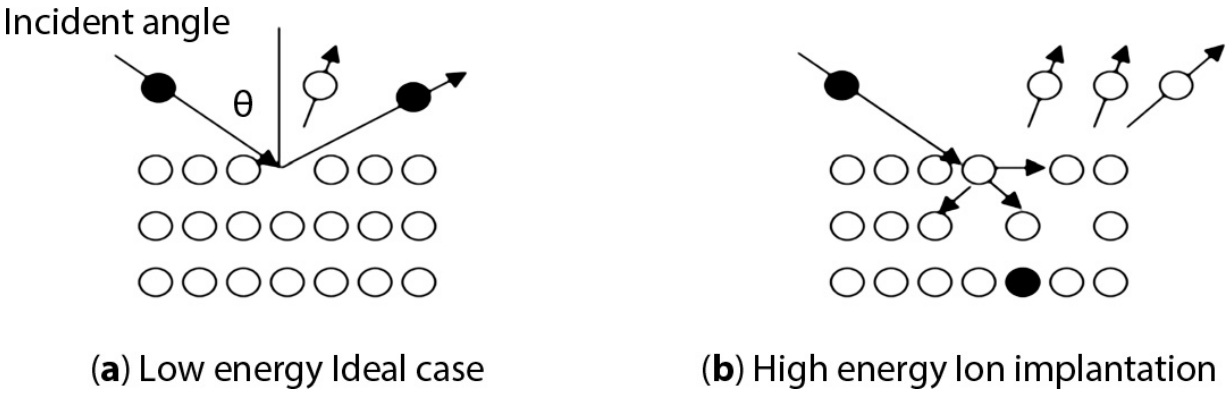


Figure 8.1 Low and high energy ion implantation.

8.2 Description of Process

In IBM, sputtering is the primary mechanism utilized for removing material from the work surface. Surface atoms are dislodged due to the impact of bombarding ions, making IBM distinct from thermo-electric processes. Ions are generated by the expulsion of electrons from atoms and subsequently accelerated within an electric field. Upon collision with the work surface, these ions dislodge atoms from the material [4].

When the ion beam strikes the surface at an angle, atom removal occurs primarily through the initial collision. The quantity of work material atoms dislodged per incident ion beam is termed the sputtering yield or sputtering coefficient. Sputtering is a probabilistic process influenced by factors such as the energy of the ion beam, angle of incidence, atomic weight of the ion, and the material being bombarded, as shown in Figure 8.1. Energies exceeding 10 to 50 eV are necessary to dislodge atoms from the workpiece. Higher incident energies result in the dislodgement of multiple atoms from the surface. Additionally, some ions become embedded within the parent material, akin to the process of ion implantation.

Metallic materials generally exhibit higher material removal rates compared to nonmetallic materials [5].

8.3 Description of Equipment

In IBM, sputtering is the primary mechanism employed to remove material from the workpiece surface. This process occurs within a vacuum chamber where charged ions, emitted from an ion source, are directed towards the workpiece using an accelerating voltage. Unlike EBM, the material removal mechanism in IBM is closely associated with the displacement of atoms from the surface by other ionized atoms, a phenomenon known as ion etching, ion milling, or ion polishing. The machining setup, depicted in Figure 8.2, features an ion source capable of generating a sufficiently intense beam with an appropriate energy distribution to effectively remove atoms from the workpiece surface upon ion impingement.

The schematic of ion machining depicted in Figure 8.2 illustrates an apparatus comprising an electron gun that emits free electrons into a vacuum chamber containing argon gas. The electrons ionize the gas, generating a stream of ions directed toward the target material.

Modern equipment can accommodate workpieces with diameters up to 600 mm, and extreme vacuum conditions are not necessary, with approximately 10^{-4} Torr being sufficient [6]. Consequently, the vacuum chamber can be rapidly pumped down. The temperature generated during IBM is minimal, preserving the characteristics of the workpiece.

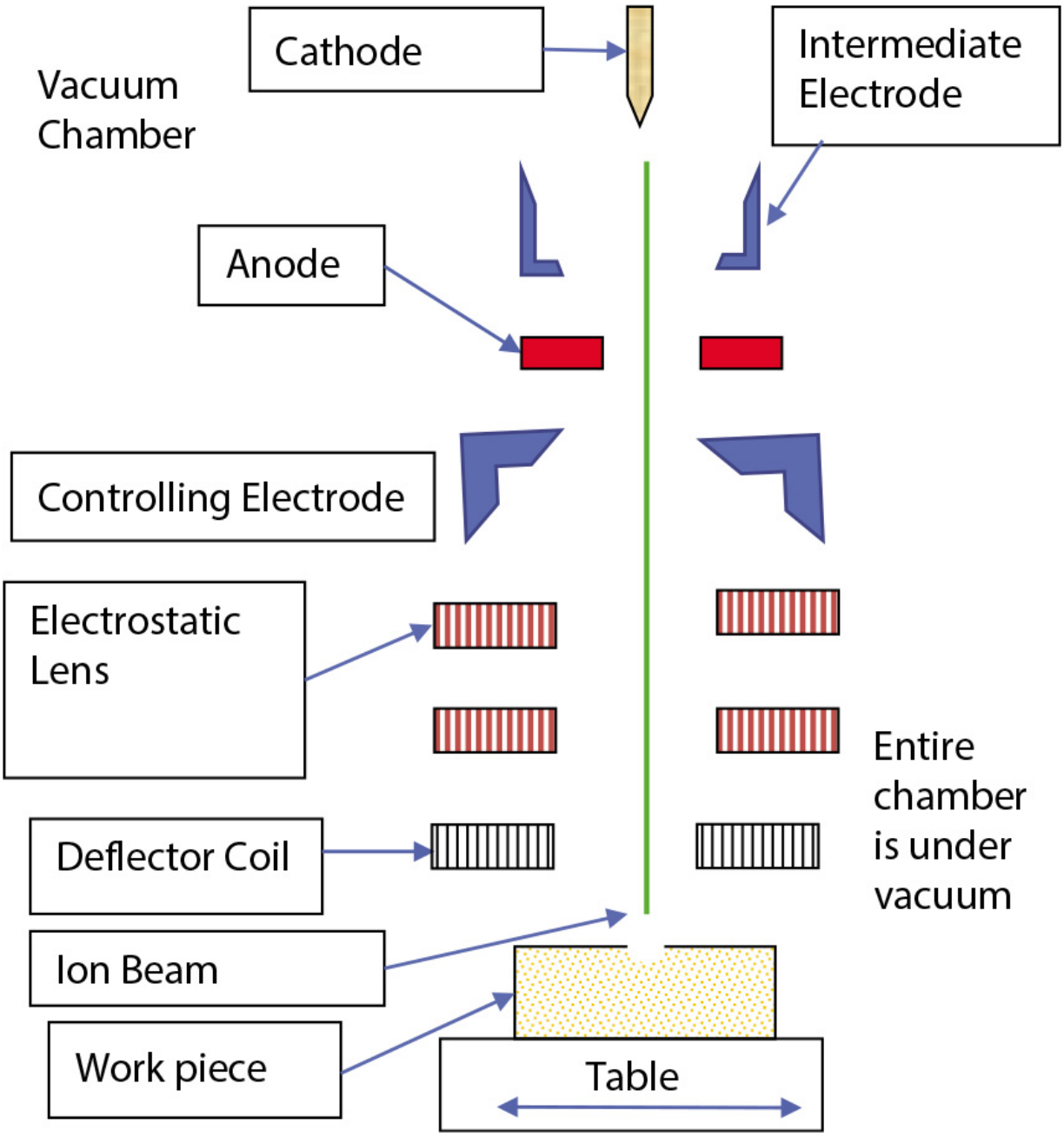


Figure 8.2 Ion machining process.

While IBM may not be a rapid process, automation enables it to operate at significant speeds, particularly for removing small amounts of material and etching thin films.

Sputter etching can be categorized based on the power source employed. Less complex and more affordable equipment utilizes direct current (DC) power, suitable for

conductive materials. For dielectric materials, radio frequency power is necessary, albeit more expensive. However, radio frequency equipment can etch any material.

8.4 Process Characteristics

Metal Removal Rate

Practical etching rates can vary significantly, reaching up to 2000 angstroms per minute (2×10^{-4} mm/min). However, it is important to note that this etching rate varies depending on the material being processed. For instance, the etching rate for tungsten is only half that of aluminum. Various factors influence the etching rate, including ion energy, ion type, incident angle, gas pressure, and the density of the target material [7–9].

An empirical equation can be employed to calculate the etch rate, taking into account these influencing factors.

$$Etch\ rate = V_r = \frac{9.6\times10^{25} Y cos\theta}{\rho_w}$$

V_r = *etch rate* = *atoms/min/cm*^{2}

ρ_w = *density of target material, atoms/cm*^{3}

Y = *yield, atoms dislodged from work by one ion*

cosθ is utilized to adjust for the diminished current densities observed at angles deviating from normal incidence. Table 8.1 illustrates the material removal rate for different materials at current density 1 mA/cm^2.

Ion beam etching, akin to chemical machining, requires masking. However, unlike chemical machining, ion beam

machining does not result in undercutting. This distinction is highlighted in Figure 8.3.

Table 8.1 MRR for different materials.

Sl no.	Material	Material removal rate nm/sec
1	Silver	2.5
2	Gold	2.45
3	Manganese	1.5
4	Aluminum	1.2
5	Chromium	0.9
6	Fe_2O_3	0.85
7	S_iO_2	0.73
8	Silicon	0.7
9	Silicon carbide	0.5
10	Carbon	0.1

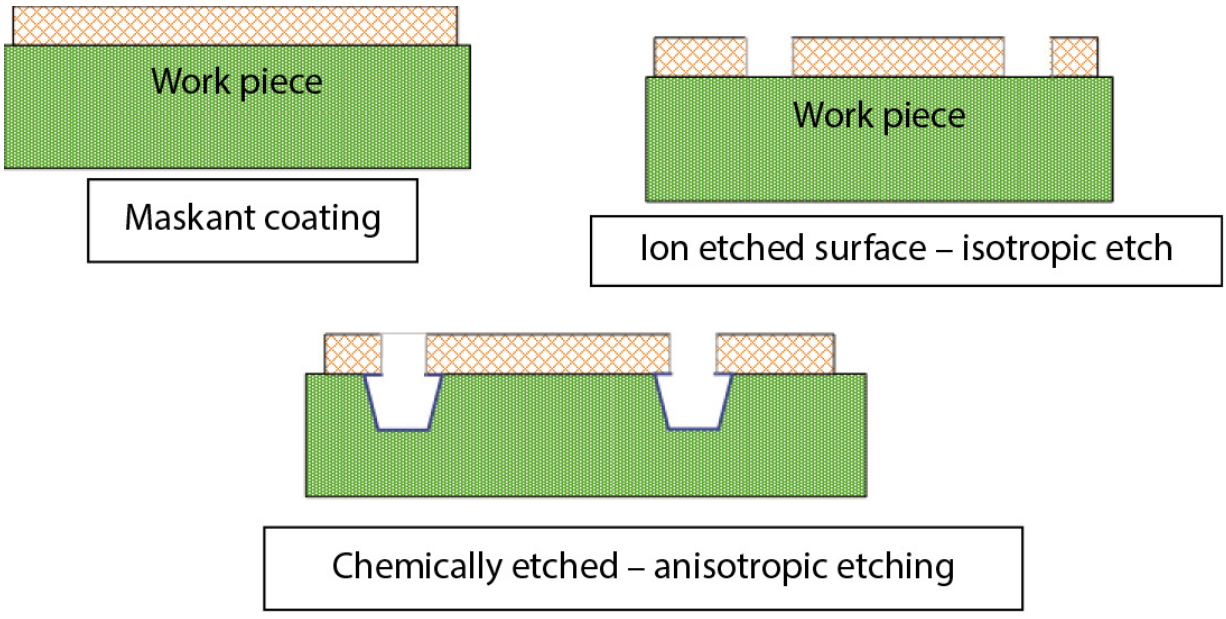


Figure 8.3 Ion etching versus chemical etch.

Accuracy

The precision of the etching process is notably high owing to the minimal amount of material removal involved. Ion beam machining (IBM) enables the attainment of very small dimensions, down to 10 nm. Despite the negligible heat generation, slight thermal effects may still occur. Materials that are thermodynamically unstable may degrade if subjected to prolonged ion bombardment. Similarly, surface-sensitive materials may suffer adverse effects from radiation exposure. This process allows for achieving tolerance levels as fine as 1%. Moreover, surface textures on the order of one micron are feasible using IBM, enabling the attainment of a surface finish of one micron [10–12].

8.5 Applications of IBM

i. Ion beam machining (IBM) finds application in the smoothing of laser mirrors and the reduction of thin film thicknesses without compromising their surface finish. It enables thinning of silicon to a thickness as low as 10 to 15 μm.

ii. IBM is utilized in the micromachining of electronic components, shaping optical surfaces, and precisely fabricating fine wire dies made from refractory materials.

iii. By employing two opposing beams, IBM can create a thin circular region on a rotating sample, producing samples suitable for transmission electron microscopy.

iv. IBM is instrumental in polishing and shaping optical surfaces through direct sputtering of preforms made from materials such as glass, silica, and diamond, utilizing patterning masks.

v. The process of IBM can generate closely packed textured cones in various materials including copper, nickel, stainless steel, silver, and gold. Additionally, sputter etching can be employed to create microscopic surface textures through the sputter deposition of a lower yield material onto the surface

vi. IBM enables the etching of metallic conductors and refractory materials, including glass, alumina, quartz crystals, silicates, agates, porcelains, cermets, and mixtures of asbestos and oxides of rare-earth metals.

vii. IBM facilitates the production of atomically clean surfaces, crucial for the adhesion of gold films to silicon and aluminum oxide substrates. Higher ion energies can be employed to remove surface oxides effectively.

viii. IBM achieves milling with a line width as narrow as 0.2 µm, essential for fabricating bubble memory devices with depth-to-width ratios of 2:1. Unlike chemical etching methods, IBM eliminates issues like undercutting since masking is solely required to shadow the beam.

ix. Ion beam etching is employed to etch specimens before studying their microstructure. IBM preserves the surface, allowing for clear observation of the material’s microstructure.

x. IBM is utilized for etching multilayered structures, such as those found in integrated circuit (IC) chips, as well as functionally graded materials.

xi. Additionally, IBM is employed in the deposition of thin films of material in electronic wafer fabrication industries. For instance, razor blades can be coated with thin films using IBM technology.

xii. IBM finds widespread application in various processes:

a. **Cleaning:** IBM is utilized for removing surface contamination, ensuring the cleanliness of substrates and materials.

b. **Polishing:** it is employed in polishing glass and preparing specimens for microstructure studies, achieving smooth and uniform surfaces.

c. **Etching:** IBM plays a crucial role in the manufacture of integrated circuits, where it is used for etching intricate patterns and features onto semiconductor substrates. It is also utilized in focused ion beam machining for precise material removal

d. **Sputter deposition:** IBM is utilized in sputter deposition processes for thin film deposition. It is instrumental in preparing specimens for microscopic study by depositing thin films onto surfaces with controlled thickness and composition.

xiii. IBM is extensively employed in micromachining within the microcircuits and semiconductor industry. It enables the machining of intricate patterns into surfaces with line widths as narrow as 0.2 μm. In ion beam setup, a master mask is illuminated by an energetic ion beam and then projected onto the substrate to be machined through an electrostatic lens. Reduction factors of 50 or more can be achieved through this process. The pattern is accurately projected onto the surface, and it is worth noting that the magnetic projection lens has no significant effect on the ion beam.

8.6 Advantages of IBM

i. Ion beam machining (IBM) is a universal process applicable across various materials and industries.
ii. Unlike chemical etching, IBM does not require any chemical agents or etchants for material removal.
iii. IBM leaves no residue behind, ensuring clean and precise machining results.
iv. IBM offers excellent resolution, limited only by the resolution of the mask used in the process.
v. Etch rates in IBM can be easily controlled and adjusted according to the specific requirements of the application.
vi. Unlike chemical etching, IBM does not result in undercutting, preserving the integrity of the machined features.

8.7 Disadvantages of IBM

i. The overall efficiency of IBM is relatively low due to the minute amount of material removed per unit of time.
ii. IBM typically involves high capital costs for equipment acquisition and setup, which can be a significant investment for businesses.
iii. Thermal or radiation damage may occur in certain materials when subjected to ion beam machining, potentially affecting the quality of the machined components.

References

1. Dugdale, R., *A Glow discharge material processing*, Mills and Boon Limited, London, 1971.

2. Taniguchi, N., Current Status in, and Future Trends of Ultra precision Machining and Ultrafine Materials Processing. *CIRP Ann. - Manuf. Technol.*, 32, 2, 573–582, 1983.

3. Allena, D.M., Shorea, P., Evansa, R.W., Fanaraa, C., O'Briena, W., Marsona, S., O'Neillc, W., Ion beam, focused ion beam, and plasma discharge machining. *CIRP Ann. - Manuf. Technol.*, 58, 2, 647–662, 2009.

4. *Ion beam machining device*, University of Tokyo, Patent No CA1217532A, Canada, 1984.

5. Volkert, C.A. and Minor, A.M., Focused Ion Beam Microscopy and Micromachining. *MRS Bull.*, 32, 389–399, 2007.

6. Giannuzzi, L.A. and Stevie, F.A., *Introduction to Focused Ion Beams: Instrumentation, Theory, Techniques, and Practice*, Springer, New York, 2005.

7. Nastasi, M., Mayer, J.W., Hirvonen, J.K., *Ion Solid Interactions: Fundamentals and Applications*, Cambridge University Press, Cambridge, UK, 1996.

8. Ziegler, J.F., Biersack, J.P., Littmark, U., *The Stopping Range of Ions in Solids*, Pergamon Press, New York, 1984, The SRIM code is available online at www.srim.org.

9. Carlslaw, H.S. and Jaeger, J.C., *Conduction of Heat in Solids*, 2nd, p. 264, Oxford University Press, Oxford, UK, 1959.

10. Dhake Harshal, G. and Samuel, G.L., Machining of axisymmetric forms and helical profiles on cylindrical workpiece using wire cut EDM, in: *Int. J. Mach. Mach. Mater*, 2012.

11. Mabena, C.M., *A Rutherford backscattering study on radiation damage and diffusion of krypton implanted into 6H-SiC*, University of Pretoria, South Africa, 2023.

12. Jagadeesha, T., *Unconventional machining processes*, I K International Publication House Pvt. Ltd, New Delhi, 2016.

Note

*Corresponding author: jagdishsg@nitc.ac.in

9
Electrochemical Machining

Thavasilingam K.[1]*, Sakthimurugan D.[1], Giridharan K.[1], Praveen Kumar A.[1] and Meenatchisundaram P.[2]

[1]Department of Mechanical Engineering, Easwari Engineering College, Chennai, India

[2]Department of Mechanical Engineering, Sethu Institute of Technology, Virudhunagar, India

Abstract

This chapter explores ECM, a specialized method at the interface of precision engineering and electrochemistry. Electrochemical machining is a very complex and adaptable technique that may be used to precisely create microstructures on a variety of conductive materials. This chapter explains the basic ideas and workings of ECM, which uses electrochemical processes to remove material at the microscale selectively. Even in complicated geometries, it achieves outstanding precision and detailed detailing by utilizing controlled disintegration by electrolysis. The chapter explains how ECM is used in a wide range of industries, including aerospace, automotive, medical devices, microelectronics, and more. It draws attention to the unmatched benefits of ECM, such as its capacity to create complex patterns, micro-cavities, and high aspect ratio structures with little to no heat-affected zones. This conversation also covers the difficulties and developments in ECM technology, looking at ways to improve accuracy and productivity through new developments in electrode design, electrolytes, and process control techniques. Basically, this chapter provides a

thorough introduction to ECM, covering its fundamentals, uses, and potential future directions. It also highlights how important it is to the advancement of micromanufacturing processes across a range of high-tech sectors.

***Keywords*:** Machining techniques, electrolyte, material specification, surface finish, nano-ECM

9.1 Introduction

Electrochemical machining (ECM) is a high-tech production process that combines the requirements of precision engineering with the concepts of electrochemistry. This technique has drawn a lot of interest since it can precisely and accurately sculpt complex microstructures on a variety of conductive materials. A significant part of improving the interfacial functional performance of machine-driven components is accomplished by surface micro texturing. Electrochemical machining is a promising solution for the production of high-quality square micropatterns [1]. A non-traditional machining technique called “electrochemical machining” uses the ideas of electrochemistry to cut material from a workpiece. In order to complete the machining process, this approach uses an electrolyte and a tool that is commonly referred to as a cathode. The electrolyte causes a chemical reaction that dissolves the material from the workpiece and gives it the required form or pattern by establishing a regulated electrical potential between the cathode and the workpiece [2]. According to Rao *et al.*, ECM has a number of benefits over traditional machining techniques. These benefits include the capacity to machine materials that are challenging to cut, the absence of tool wear, and the creation of high-quality surfaces with no residual stress [3]. Zhang *et al.* described how ECM offers the special ability to rapidly machine complicated surfaces

and hard-to-cut materials by applying the principle of electrochemical dissolution [4]. As shown in Figure 9.1, schematic representation of ECM process is illustrated. In addition, ECM has attracted a lot of interest recently in terms of research, with academics and business professionals looking into possible uses for it as well as improving operating conditions to increase efficacy and efficiency. To sum up, ECM is a flexible and efficient machining technique that has several benefits over conventional techniques [5].

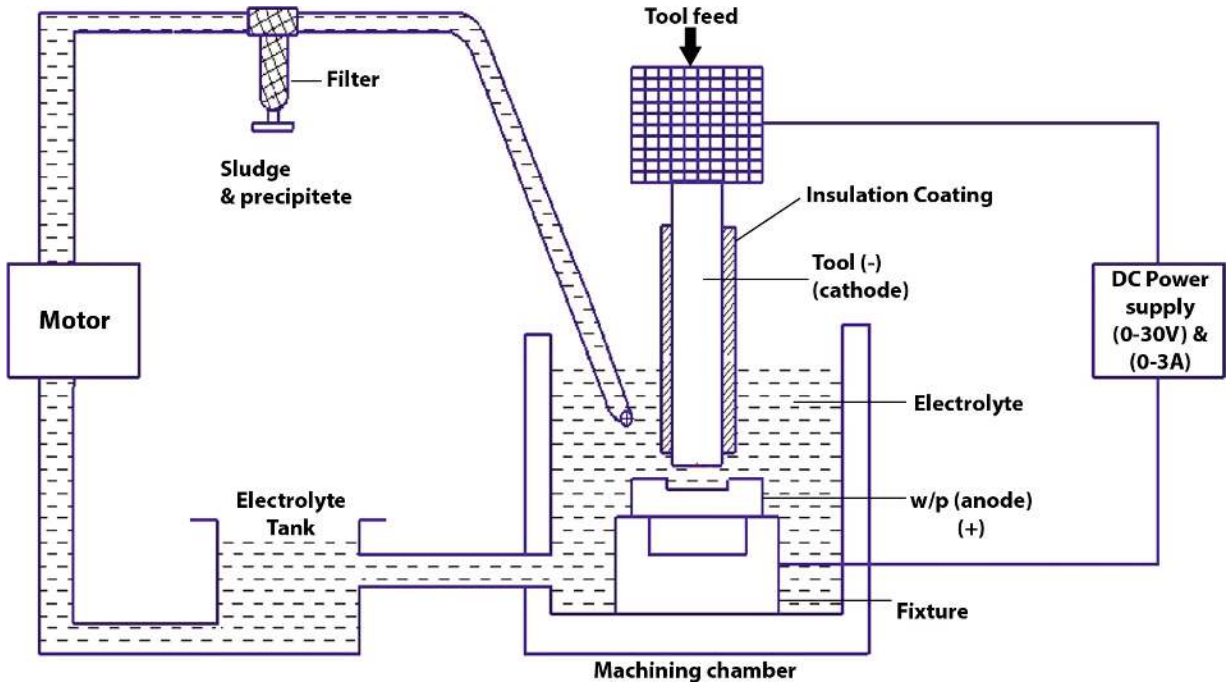


Figure 9.1 Schematic representation of the electrochemical micromachining (ECM) process.

(Source: Geethapriyan Thangamani *et al.*, 2021), [20].

9.2 Electrochemical Machining Techniques

Advanced machining processes are becoming more and more necessary in a variety of industries where microscale precision engineering is becoming increasingly important.

Of such, ECM is one of the most effective and adaptable techniques for creating complex parts and structures. In this section, deal with the basic methods that make ECM an effective tool for micromanufacturing.

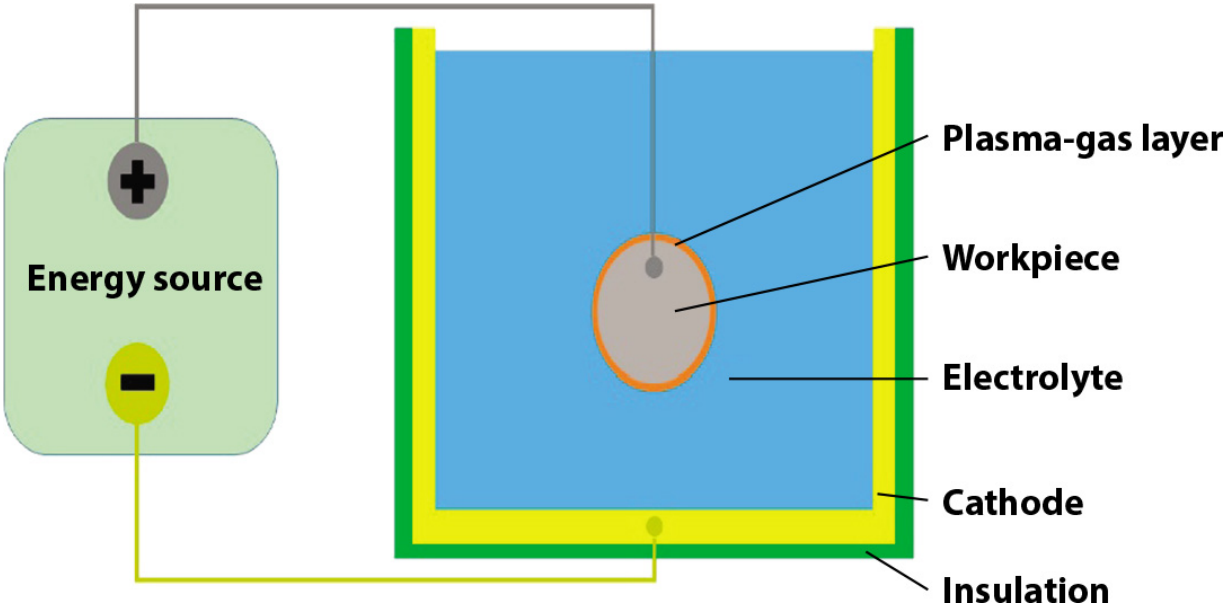


Figure 9.2 Principle scheme of plasma electrolytic polishing.

(Source: Igor Danilov *et al.*, 2019), [6].

9.2.1 Electrolytic and Electrolytic-Plasma Machining

Within ECM, there are two separate but related subfields: electrolytic and electrolytic-plasma machining. An examination of these methods, special traits, and uses shows how important they are for attaining microscale precision.

Techniques for surface treatment like plasma electrolytic polishing (PeP), a subset of ECM, are becoming more and more necessary. This study covers the scientific literature on the fundamental processes of the ionized electrolytic refining process and discusses both theoretical and empirical evidence. The simulation illustrates and explains

the polishing effect modelling approach used in the PeP process. The simulation findings suggest that PeP may be described as an electrochemical manufacturing process, and that the simulation can be used to estimate processing time and roughness, as shown in Figure 9.2 [6].

9.2.2 Tool Electrode Design

Numerous industries, including electronics, aircraft, automotive, medicinal, and optics, are using microcomponent learning. Electrochemical micromachining improves the surface quality of microcomponents. Dimensional precision and the form of the microparts that are generated are greatly influenced by the size and shape of the tool. The design and construction of a microtool for reverse ECM using a unique fixture arrangement are presented in this work. In order to increase material removal rate (MRR) and decrease overcut during machining processes, microconical tools were created using reverse polarity or reverse electrochemical micromachining aids. Because of its superior surface quality, low machining time, lack of residual stress, and lack of heat affected zone, it is more advantageous for the manufacturing of microelectrodes.

9.3 Process Parameters and Control

Understanding and improving process parameters is crucial to ECM, the goal of which is to achieve precise and controlled material removal at the microscale. This section delves into the complex realm of process parameters and their management in ECM, elucidating the ways in which voltage, current, electrolyte composition, temperature, and pH jointly impact the milling procedure.

9.3.1 Voltage, Current, and Electrolyte Composition

The foundation for attaining accuracy in ECM is the trinity of voltage, current, and electrolyte composition. This section explores the complex interrelationships between these crucial variables, revealing their significant impact on material removal rates, surface quality, and overall microscale machining precision.

The production of microtexture on surfaces is an essential technology in surface engineering that may significantly improve engineering components' load capacities, erosion resistance, frictional coefficient, part lubrication, etc. This work proposes maskless ECM, a novel electrochemical reaction-based technique for anodic dissolution. A maskless ECM setup with a tailored ECM cell and vertical crossflow electrolyte delivery system is utilized to generate tiny circular patterns on stainless steel (SUS 304). Three distinct kinds of electrolytes, including NaCl, $NaNO_3$, and NaCl + $NaNO_3$, are employed. The impacts of significant process factors, such as inter-electrode gap (IEG), rate of flow, manufacturing time, and electrolyte concentration, on mean radial overcut and mean manufacturing depth have been investigated using these electrolytes as shown in Figure 9.3 [7]. An ECM device with a pulse generator that was designed for testing was used in this investigation. The suggested operating parameters for this study are current, voltage, pulse-on-time, and electrolyte percentage. Grey relational analysis (GRA) was used for multi-response optimization, and trials were carried out utilizing Taguchi's L9 design. The optimal set of parameters identified using GRA were 12 V, 1.2 A, 15 ms for the pulse-on-time length, and 20 g/l of solution concentration. It was discovered that pulse-on-time was the most important factor. The machining process was slow due to the citric acid

functioning as the electrolyte, but the holes were cut precisely [8].

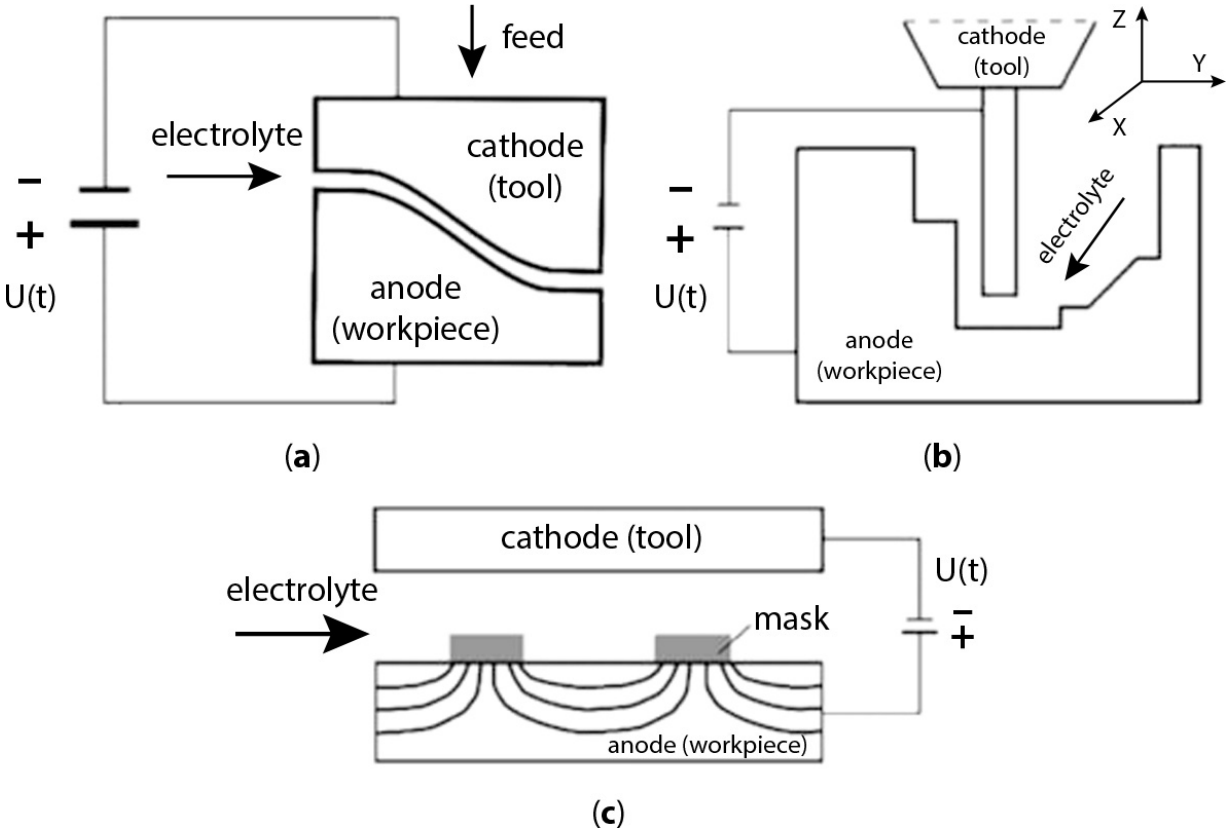


Figure 9.3 Variants of electrochemical machining: (a) sinking, (b) machining with universal electrode tool, and (c) through mask electrochemical machining.

(Source: Sebastian Skoczypiec *et al.*, 2021), [21].

9.3.2 Temperature and pH Control

Temperature and pH turn out to be important variables that can have a big impact on the machining process, influencing accuracy, rates of material removal, and overall effectiveness. This section explores the complex realm of pH and temperature regulation, revealing their functions as enablers for obtaining unmatched precision in micromachining applications.

Enhancing the ECM response rate is mostly dependent on the electrolyte temperature. In the investigations, a warmed electrode (HE) is employed. Modifications in the input variables, which involve applied voltage (V), percentage of duty cycle (%), electrolytic solution (g/l), & tool electrode temperature (°C), have an impact on the output performance, which includes the removal of material rate, conicity factor (CF), and radial overcut (ROC). The workpiece is made of aluminum 6061, with 12% of the composition consisting of powdered granulated slag from the blast furnace reinforcement and sodium nitrate acting as the electrolyte. According to the conducted research, the machining rate may be increased by 88.37% at 8 V, 90% duty cycle, 35 g/l electrolyte level, and 60°C electrode temperature [9].

9.4 Material Specifications in ECM

Electrochemical machining (ECM) is a versatile process that can handle a broad range of materials, including insulating substrates and metals and alloys. This section delves into the subtleties of material specifications in ECM, highlighting the customized methods needed for a variety of materials to get microscale precision.

9.4.1 ECM Applied in Metals and Alloys

The capacity to precisely mill metals and alloys at the microscale is essential for the advancement of current technology, as they are fundamental building components in numerous sectors. The application of ECM to metals and alloys is the main topic of this section. It covers the intricate electrochemical processes involved and presents methods for obtaining unmatched precision.

Motion control, electrolyte system, power system, machine tool, and monitoring system make up the majority of the

ECM experimental system. Due to its capacity to carry out certain shock-proof functions, the air float test equipment installed within the machine tool can effectively assure stability throughout the machining process. The machine tool is equipped with a motion controller platform that can move in three dimensions (X, Y, and Z) with positioning accuracy of up to 0.1 µm. To investigate the effect of electrode material on the electrochemical manufacturing of thin-walled job pieces made of 304 stainless steel, we conducted tests using five instrument cathodes composed of 45# metal, 304 stainless steel, aluminum alloy 6061, brass H62, and tungsten steel YK15 [10]. A unique coating material made of functionally improved fumed silica wax epoxy was created and characterized. Carnauba wax, fumed silica, and naturally produced bees were used to create the coating material. The aluminum alloy substrate was coated with the coating material, which then dried at room temperature [11]. As shown in Figure 9.4, the use of ECM to create microfeatures on surfaces by combining a pulsed potential with the appropriate technique and electrolyte for a certain metal selection. Researchers concentrate on a single metal or alloy to identify the best machining settings. In the event that a novel material was to be machined, a thorough investigation would be required to determine an adequate electrolyte as well as suitable machining parameters, such as applied voltage and pulse length. As of right now, no scientifically supported methodology exists to support the usage of a particular electrolyte solution or machining settings, particularly for the requirements of ECM technology’s micromanufacturing application [12].

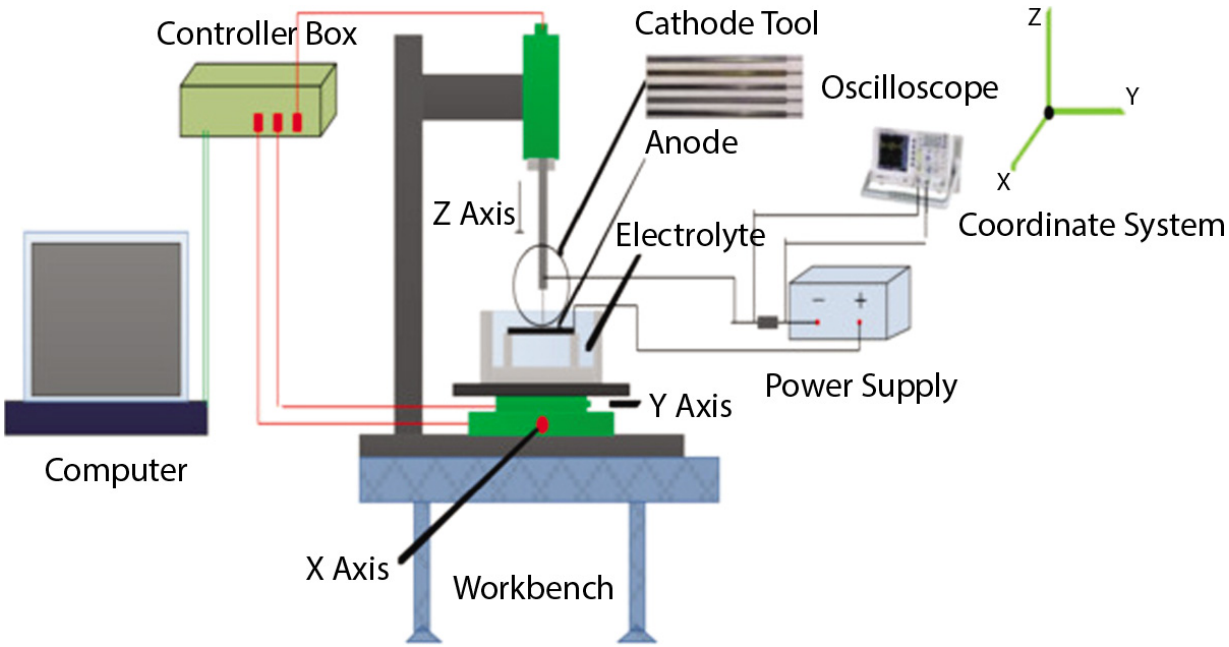


Figure 9.4 Schematic diagram of ECM on 304 stainless steel.

(Source: Jianxiao Bian *et al.* 2021), [22].

9.4.2 ECM Applied in Insulating Materials

Although most manufacturing processes include metals and alloys, the field of ECM applies its precision skills to insulating materials as well. This section delves into the unique obstacles and creative solutions associated with using ECM on insulating surfaces, highlighting the customized methods needed to get microscale accuracy in this particular field.

An electrode for an electrochemical micromachining device was insulated using hotdip aluminizing and microflame oxidation techniques. The aluminum-rich layer was converted to an aluminum oxide shielding layer by micro-arc oxidation of an electrode. This aluminum oxide shielding layer was subsequently utilized to produce an efficient layer of insulation on a stainless steel surface and attain high accuracy in ECM. The tool's resist voltage was evaluated using sodium chloride electrolysis, and its

surface and section were investigated. The ECM performance of several tools with and without an aluminum oxide shielding layer was examined by drilling on a stainless-steel workpiece. It is necessary to create an accurate and durable insulation layer. One way to improve precision is to lessen the ECM's stray effects [13].

9.4.3 Surface Finish and Microstructure

In the complex field of ECM, regulating microstructure and obtaining the best possible surface finish are critical for a wide range of applications. This section reveals techniques to craft precision at the microscale by exploring the complex interactions between ECM processes and the resulting surface finish and microstructure.

The highest deflection load was recorded in the display, and compression movement persisted when the polymer coating on the aluminum alloy underwent plastic deformation. It should be noted that the bending strength and rigidity of pure epoxy resin are 88 MPa and 86 Shore-D, respectively. The increased microhardness and lower flexural strength of epoxy resin are the causes of its highly cross-linked molecular structure [14]. Nonconventional machining techniques, like ECM, provide a superior surface finish without causing thermal or mechanical defects on the workpiece surface, in contrast to conventional machining techniques like electron beam machining (EBM), electric discharge machining (EDM), plasma arc machining (PAM), electrochemical spark machining (ECSM), and laser beam machining (LBM). High aspect ratio µ-holes, µ-channels, and various other complex microstructures on challenging-to-cut materials like titanium, copper, stainless steel, and other special alloys are well-known products of the ECM process. With the appropriate surface polish, these materials are widely used in the micro-electro-mechanical systems (MEMS), automobile, aerospace, health care, and

electronics industries. Moreover, hybrid ECM procedures make it possible to manufacture cutting-edge materials in a way that is not possible with traditional production techniques [15].

Surfaces microtexturing is the process of precisely and specifically applying a specific type of roughness arrangement on the upper surface of ceramics, metals, and polymers in order to enhance their various properties. Microscale engineering is one of the interesting and important current manufacturing technologies that aims to meet the growing need for thinner, lesser, and more precise machining. However, the manufacturing of tiny components at the micrometer scale, especially for metal micromachining, continues to be a challenge for modern industrial organizations. For micromachining, the conventional machining method is rarely used because of several difficulties, such as the creation of tools and generating heat during the cutting process [16].

9.5 Advancements in ECM Technology

Both the industrial environment and the technologies enabling microscale precision are always changing. We explore the most recent developments in ECM technology in this area, revealing novel strategies, hybrid processes, and developing patterns that together redefine the limits of precise production in the microscale age.

As a result of the unwavering quest for improved precision, effectiveness, and adaptability, the ECM field has experienced rapid advancement. The developments in ECM technology, ranging from innovative trends like nano-ECM to hybrid approaches that work in concert with other machining techniques, have the potential to completely transform how we tackle micromanufacturing problems.

9.5.1 Hybrid Approaches

Electrochemical machining (ECM) has become an important driver in the field of precision machining as the need for micromanufacturing precision grows. This section explores the cutting-edge field of hybrid approaches in ECM, where combining various machining processes produces synergies that increase accuracy and adaptability.

Although ECM has long been praised for its accuracy and material flexibility, the changing field of micromanufacturing needs even more flexibility. Combining complimentary machining processes with ECM to create hybrid techniques provides a way to handle a range of issues caused by different materials, complex geometries, and tight tolerances.

Inspired by current studies and real-world implementations, we reveal the benefits, difficulties, and game-changing potential of combining ECM with other machining techniques.

In many areas of application, ECM offers various advantages, including higher machining rate, better precision and control, and the ability to mill a wide range of materials. As such, it seems to be a very promising approach for micromachining in the future. An overview of recent advancements, industrial applications, and research in micro-ECM is provided in this publication as well as the impact of several key ECM components, including electrolyte and inter-electrode gap function, precision in machining, power supply, controlled material removal, micro-tool design and development. When it comes to high precision machining processes, ECM works well, producing an accuracy of about ±1 µm on 50 µm. In order to meet the many pressing needs of the electronics and precision industries in the field of ultra-precision microfabrication,

research and development in the ECM field will be crucial. An advanced ECM lab configuration with meticulously designed sub-components, including a power supply unit, machining unit, and electrolyte flow system was executed [17].

These days, composite materials are essential for engineering applications in the automobile, aerospace, and other industrial sectors. High specific stiffness and high strength metal matrix composites (MMC) in particular can be applied to long-range applications while weight reduction is important, like rotating shafts, robots, turbine blades, high-range machinery, and automotive engine and brake parts. Nonetheless, because of the reinforcement found in the matrix material, machining composite materials using a traditional method is still challenging [18].

9.5.2 Nano-ECM and Emerging Trends

Electrochemical machining (ECM) is at the forefront of the pursuit of precision in the ever-evolving field of micromanufacturing, as it has expanded into the nanoscale. It covers the cutting edge field of nano-ECM and other new developments that are pushing the limits of microscale accuracy and creating new opportunities for advanced manufacturing.

Engineers and scientists are now able to manipulate materials at the nanoscale with unmatched precision thanks to a paradigm change in micromanufacturing capabilities brought about by nano-ECM. In order to shed light on the fundamental ideas, practical uses, and revolutionary possibilities of nano-ECM for a variety of industries, including electronics and healthcare are developed. The goal is to present a thorough review of the current state-of-the-art in ECM while shedding light on the

new directions that were being pursued by practitioners, engineers, and researchers.

Due to the growing industrial demand for highly smooth surfaces and functional three-dimensional in form micro/nanostructures (3D-MNS) in ultra-large size integrated circuits, microelectromechanical systems, miniaturized total evaluation systems, precision optics, and other applications, micro/nanomachining (MNM) is at the very forefront of high-tech manufacturing. Electrochemical micro/nanomachining, or EC-MNM, is crucial to MNM because of its benefits over alternative methods, which include decreased tool wear, minimal surface tension, environmental friendliness, ease of usage, and cheap cost. As shown in Figure 9.5, the state of the art in EC-MNM direct writing, surface planarization and finishing, and 3D-MNS fabrications is presented in this thorough analysis. Restricting electrochemical processes to the micro/nanometer size is the fundamental idea behind EC-MNM [19].

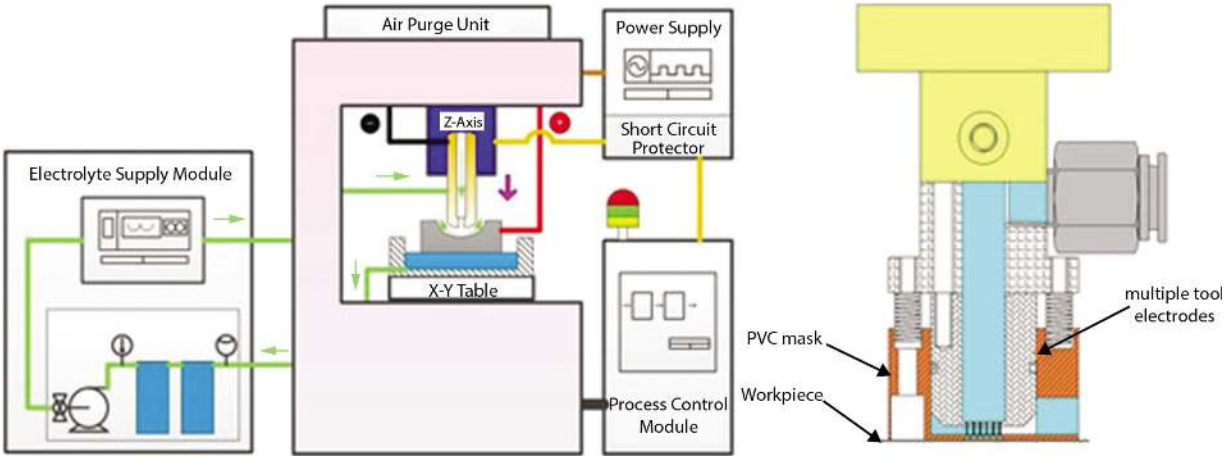


Figure 9.5 Schematic diagram of nano-electrochemical machining system.

(Source: Yanfei Lu *et al.* 2017), [23].

9.6 Conclusion

It is clear from reading through the chapters on ECM and its many aspects that ECM is more than just a machining method; rather, it is a dynamic area that is always changing to meet the ever-increasing needs of micromanufacturing precision. The significance of ECM in various sectors is highlighted by the complex interaction of process parameters, material considerations, and technological improvements.

First and foremost, it is critical to have a thorough understanding of the underlying concepts, methods, and control mechanisms. Examining the nuances of electrolytic and electrolytic-plasma machining reveals that ECM's adaptability makes perfection possible in a number of ways. As previously discussed in-depth, the three key components of electrolyte composition, voltage, and current are what make ECM successful and need to be carefully controlled for best outcomes.

Moreover, the versatility of ECM is demonstrated by the materials it can be applied to: insulating substrates, metals, and alloys. The specific methods needed for every kind of material highlight how adaptable and effective ECM is in meeting a range of manufacturing requirements.

The investigation of pH and temperature management highlights the necessity of a careful balance to preserve steady machining conditions. It is imperative for practitioners aiming to get consistent and high-precision results in ECM procedures to comprehend the influence of these aspects.

It becomes evident from the complexities of attaining the ideal surface finish and managing microstructure that ECM is more than simply material removal—it also entails precisely constructing surfaces. The talks about metals, alloys, and insulating materials highlight the necessity of

using a sophisticated approach to accommodate the special qualities.

The chapter on developments in ECM technology presents a changing picture of the industry, where new trends and hybrid methods are redefining the limits of precision in micromanufacturing. The utilization of hybrid approaches that combine ECM with other machining processes offers an insight into the manufacturing of the future, when flexibility and adaptability will be critical.

Ultimately, the investigation of nano-ECM and new developments propel us to the forefront of microscale accuracy. The field's dedication to pushing the boundaries of what is possible in micromanufacturing is demonstrated by the integration of ECM into the nanoscale and the ongoing search for cutting-edge technologies.

Electrochemical machining is revealed to be a dynamic and ever-evolving field at the forefront of micromanufacturing, in addition to a machining technique. The exploration of its many facets reveals the complex dance of parameters, the flexibility to work with a variety of materials, and the unwavering quest of accuracy, all of which lead to the conclusion that ECM will play a significant role in determining the direction of microscale advanced manufacturing in the future. With the rapid advancement of technology, ECM is well-positioned to be a key player in creating the complex structures that characterize the upcoming generation of precision-engineered components.

References

1. Kunar, S., Kumar, R., Reddy, M., Generation of square micropattern using Electrochemical Machining. *Mater. Today: Proc.*, *49*, 1210–1214, 2022, https://doi.org/10.1016/j.matpr.2021.06.290.

2. Pawar, P.S., Kumar, A., Ballav, R., Analysis of Machined Depth and Hole Diameter on Sodalime Glass Using Electrochemical Discharge Machining Process. *J. Eng. Sci.*, 6, F1-F7, 2019, https://doi.org/10.21272/jes.2019.6(2).f1.

3. Rao, P.S., Jain, P., Dwivedi, D.K., Study and Effect of Process Parameters on External Cylindrical Surfaces of Titanium Alloys by Electro Chemical Honing (ECH) Process, in: *Annals of DAAAM for. . & Proceedings of the. . International DAAAM Symposium*, 2016, https://doi.org/10.2507/26th.daaam.proceedings.078.

4. Zhang, H., Liu, S., Yue, W., Xiao, H., Zhang, P., Experimental Study of Surface Characteristic in Electrochemical Machining of 35CrMo Steel. *Metals*, 1–20, 2018, https://doi.org/10.3390/met8070509.

5. Bian, J., Ma, B., Ai, H., Qi, L., Experimental Study on the Inner Wall Ring Groove of 1J116 Soft Magnetic Alloy Based on Electrochemical Machining. *Atlantis Highlights in Engineering*, 5, 1–15, 2019, https://doi.org/10.2991/pntim-19.2019.9.

6. Danilov, I., Hackert-Oschätzchen, M., Zinecker, M., Meichsner, G., Edelmann, J., Schubert, A., Process Understanding of Plasma Electrolytic Polishing through Multiphysics Simulation and Inline Metrology. *Micromachines*, *10*, 3, 214, 2019, https://doi.org/10.3390/mi10030214.

7. Kunar, S., Mahata, S., Bhattacharyya, B., Influence of electrolytes on surface texture characteristics generated by Electrochemical Machining. *J. Micromanuf.*, *1*, 2, 124–133, 2018, https://doi.org/10.1177/2516598418765355.

8. Subburam, V., Ramesh, S., Freitas, L., II, Optimization and Effect Analysis of Sustainable Micro Electrochemical Machining Using Organic Electrolyte, in: *Materials Forming, Machining and Tribology*, pp. 33–46, 2021, https://doi.org/10.1007/978-3-030-70009-6_4.

9. Maniraj, S. and Thanigaivelan, R., Effect of electrode heating on performance of Electrochemical Machining. *Mater. Manuf. Processes*, *34*, 13, 1494–1501, 2019, https://doi.org/10.1080/10426914.2019.1655153.

10. Bian, J., Ma, B., Ai, H., Qi, L., Experimental Study on the Influence of Tool Electrode Material on Electrochemical Machining of 304 Stainless Steel. *Materials*, *14*, 9, 2311, 2021, https://doi.org/10.3390/ma14092311.

11. Thavasilingam, K., Kumar, A.S., Khan, M.A., Devanand, S., Giridharan, K., Effect of fumed silica in rice bran wax-epoxy coating on aluminum substrate: mechanical, thermal, and water absorption properties. *Biomass Convers. Biorefin.*, *13*, 5, 4229–4240, 2021, https://doi.org/10.1007/s13399-021-01889-w.

12. Leese, R.J. and Ivanov, A., Electrochemical Machining: An introduction. *Adv. Mech. Eng.*, *8*, 1, 168781401562686, 2016, https://doi.org/10.1177/1687814015626860.

13. Hung, J.C., Liu, Y.R., Tsui, H.P., Fan, Z.W., Electrode insulation layer for electrochemical machining fabricated through hot-dip aluminizing and microarc oxidation on a stainless-steel substrate. *Surf. Coat. Technol.*, *378*, 124995, 2019, https://doi.org/10.1016/j.surfcoat.2019.124995.

14. Thavasilingam, K., Senthil Kumar, A., Sakthimurugan, D., Meenatchisundaram, P., Synthesis and characterization of fumed silica dispersed bees/carnauba wax-epoxy biocomposite coating: a comparative study. *Biomass Convers. Biorefin.*, *13*, 8, 7375–7383, 2023, https://doi.org/10.1007/s13399-023-04112-0.

15. Singh, J., Kant, R., Nimesh, A., Katiyar, N., Bhattacharya, S., Evaluating Electrochemical Machining capabilities for industrial applications: A review. *Mater. Manuf. Processes*, *39*, 1, 1–42, 2023, https://doi.org/10.1080/10426914.2023.2219304.

16. Maharana, H., Kumar, R., Narayana Murty, S., Ramkumar, J., Mondal, K., Surface microtexturing of dual phase steel and copper by combining laser machining and electrochemical dissolution. *J. Mater. Process. Technol.*, *273*, 116260, 2019, https://doi.org/10.1016/j.jmatprotec.2019.116260.

17. Bhattacharyya, B., Munda, J., Malapati, M., Advancement in electrochemical micromachining. *Int. J. Mach. Tools Manuf.*, *44*, 15, 1577–1589, 2004, https://doi.org/10.1016/j.ijmachtools.2004.06.006.

18. Maniraj, S., Thanigaivelan, R., Gunasekaran, K., Saravanan, K.G., Optimization of Process Parameters in Electrochemical Machining of AMCs by Using Different Techniques of Weight Evaluation. *Adv. Mater. Sci. Eng.*, *2023*, 1–9, 2023, https://doi.org/10.1155/2023/1366857.

19. Zhan, D., Han, L., Zhang, J., He, Q., Tian, Z.W., Tian, Z.Q., Electrochemical micro/nanomachining: principles and practices. *Chem. Soc. Rev.*, *46*, 5, 1526–1544, 2017, https://doi.org/10.1039/c6cs00735j.

20. Thangamani, G., Thangaraj, M., Moiduddin, K., Mian, S.H., Alkhalefah, H., Umer, U., Performance Analysis of Electrochemical Micro Machining of Titanium (Ti-6Al-4V) Alloy under Different Electrolytes Concentrations. *Metals*, 11, 2, 247, 2021, https://doi.org/10.3390/met11020247.

21. Skoczypiec, S., Lipiec, P., Bizoń, W., Wyszyński, D., Selected Aspects of Electrochemical Micromachining Technology Development. *Materials*, 14, 9, 2248, 2021, https://doi.org/10.3390/ma14092248.

22. Bian, J., Ma, B., Ai, H., Qi, L., Experimental Study on the Influence of Tool Electrode Material on Electrochemical Micromachining of 304 Stainless Steel. *Materials*, 14, 9, 2311, 2021, https://doi.org/10.3390/ma14092311.

23. Lu, Y., Rajora, M., Zou, P., Liang, S., Physics-Embedded Machine Learning: Case Study with Electrochemical Micro-Machining. *Machines*, 5, 1, 4, 2017, https://doi.org/10.3390/machines5010004.

Note

**Corresponding author*: thavasi.k.89@gmail.com

10
Ultrasonic Machining

Jagadeesha T.[1]* and Sandip Kunar[2]

[1]*Dept. of Mechanical Engineering, National Institute of Technology, Calicut, India*

[2]*Dept. of Mechanical Engineering, Aditya University, Surampalem, India*

Abstract

Ultrasonic machining (USM) stands out as a pivotal unconventional mechanical abrasive process, leveraging the amalgamation of ultrasonic vibration and abrasive particles to remove material efficiently. The tool is subjected to mechanical vibrations at ultrasonic frequencies and the necessary amplitude, which causes hammering effects that remove material. Brittle fracture is the method used to remove the material. This non-thermal method preserves structural integrity and works well with complex and delicate materials. Here, the study explores the particulars of USM, including a description of the process and its underlying concepts. A discussion of the various USM equipment components and tool feed mechanisms provides insights into its wide range of industrial applications. Additionally explained are new breakthroughs, advancements in USM technology, and mechanisms of material removal.

***Keywords*:** Ultrasonic machining, abrasive, material removal

10.1 Introduction

Ultrasonic machining (USM) is a one of the most important unconventional mechanical abrasive processes in which combination of ultrasonic vibration and multiple cutting point tool like abrasive is made used. Basic principle of ultrasonic machine is shown in Figure 10.1. Abrasives with liquid is mixed to form an abrasive slurry and it is introduced between the work and tool by a special pumping mechanism using slurry motor and control mechanism. Tool is given mechanical oscillations by the sine generator power unit coupled with the power amplifier circuit to give an amplitude of 50 micron with high frequencies in the order of 25–50 kHz. Slurry consisting of abrasive particle and carrier fluid is flown in between the gap of the tool and work pie which removes the material removal by trans granular and intergranular brittle fracture of the work piece material [1–3].

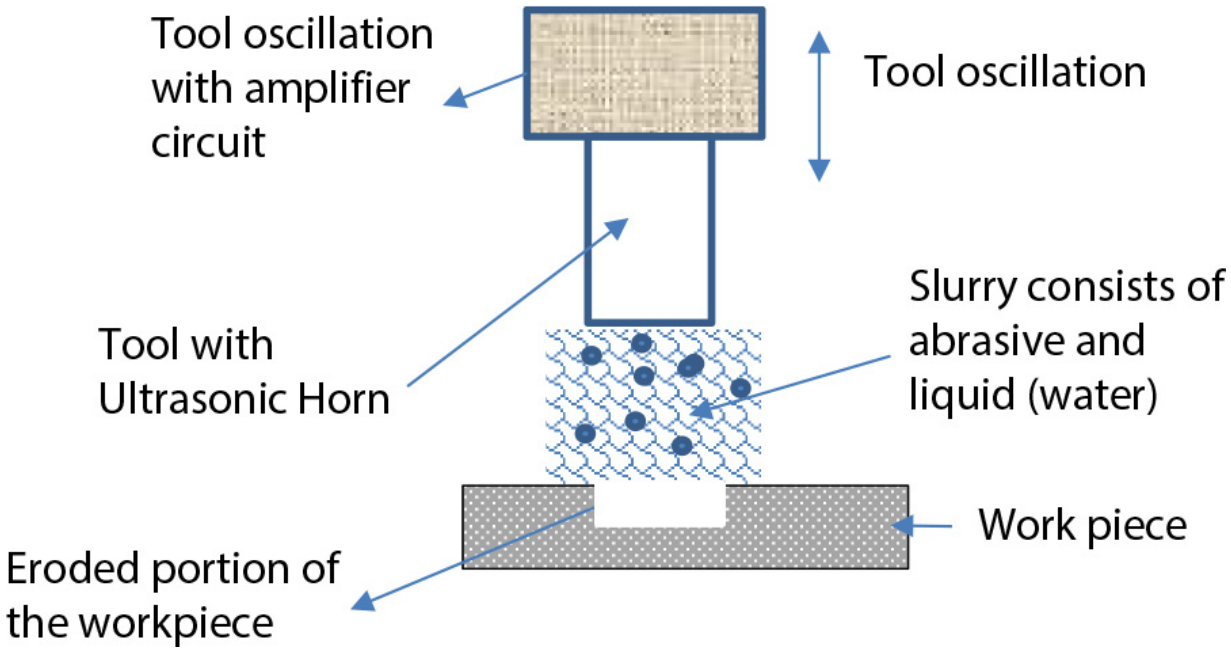


Figure 10.1 Basic principles of ultrasonic machining.

10.2 Process Description

Ultrasonic machining a semi-mechanical, non-conventional manufacturing process and tool is given amplification using the transducer and power circuit. This process can be used for brittle material, both conductive and non-conductive materials [4].

The tool is given both high amplitude and high frequency oscillations. The axial load is given by the system to the ultrasonic tool to have a hammering effect of the abrasives grits over the workpiece.

Since the frequency is in the ultrasonic range, it is optically called USM. High frequency up to 50 kHz is used in some cases. High noise is generated during the process and operator safety is important [5].

10.3 Description of Equipment

The various parts of the ultrasonic machine equipment is shown in the Figure 10.2.

The USM unit mainly consists of:

i. Power generation unit
ii. Magneto-strictive unit
iii. Unit to hold ultrasonic tool
iv. Ultrasonic tool

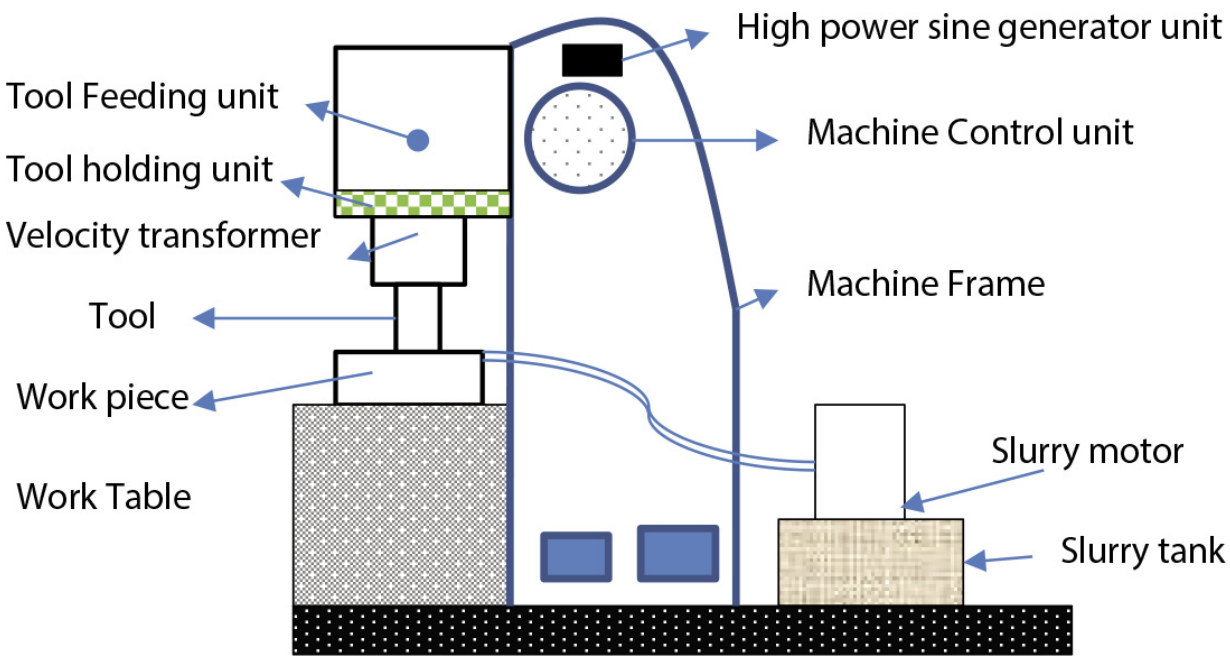


Figure 10.2 USM equipment.

(i) Power Generation Unit

This unit uses normal current of 50 Hz and using the power circuit unit low frequency is converted into high frequency sine wave of the order 25–50 kHz. Sine waves are generated from this unit with high frequency and high amplitude [6].

(ii) Conversion Unit

Unit commonly known as transducer is used in a USM unit to convert one form of energy to other. Electrical transmission signals received from controller has to converted into mechanical vibration of the velocity transformer. High frequency waves and high amplitude waves for 100 microns is obtained using the combination of power unit and transducer unit [7–9].

There are mainly two types of transducer:

i. Piezo electric current transducer

ii. Magneto-striction type of transducer.

(iii) Concentrators (Acoustic Horn)

This is also called velocity transformer. The power and transducer unit produce a low amplitude vibration. This low amplitude of vibration gives less material removal rate. In order to enhance the volume of the material removed, the amplitude of vibration is increased by concentrators, or horn or velocity transformer. Figure 10.3 shows the shape of such a horn.

(iv) Tool

Most of the tools are made of ductile materials and tool should be able to withstand severe oscillations without undergoing appreciable plastic deformation. The tool wear should be minimum to avoid the distortion and to enhance volume of the work material removal. Certain combination of the tools gives the best results which depends on type of abrasives used, what proportion they are mixed, slurry content and also work and tool combination [10–12].

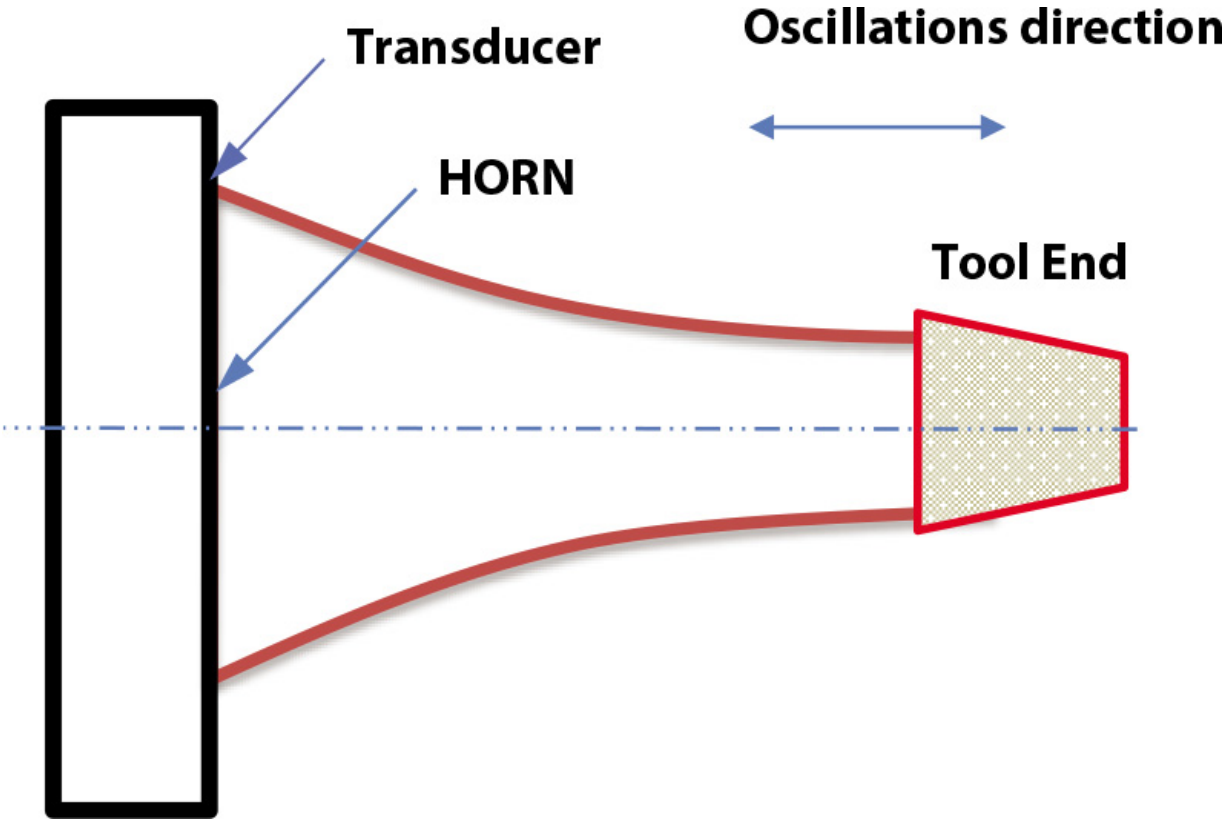


Figure 10.3 Concentrator used in USM.

10.4 Tool Feed Mechanism

Tool is the feed to work piece area with proper control unit. Rapid movement of the tool and sudden stoppage of the tool causes the breaking and frequent change of tool, which increase the overall cost of the machining processes. The axial force is applied to the tool to keep the contact between abrasive slurry and tool/work combinations. Tool should be able to sustain both static and impact stress which arises due to movement of the tool and jerk [13–15].

The commonly used feed mechanisms in USM are:

i. Gravity tool feeding unit
ii. Spring-driven tool feeding unit
iii. Fluid flow tool feeding unit

iv. Motor-driven tool feeding unit

(i) Gravity Feeding Unit

In this mechanism, usually, the mechanical type of counterbalancing is used. Rope and pulley arrangement are used. The proper choice of the bearings is needed to ensure the smooth movement of the tool. Acceleration and jerk cause tool breakage which is expensive to replace and also time consuming. Smooth and very accurate control is not possible with gravity feed mechanism [16].

(ii) Spring-Driven Feeding Unit

In this mechanism, spring is used to control the feed. Combination of springs with variety of spring constants is used for easy and precise control.

(iii) Fluid Flow Feed Mechanism

This mechanism uses either hydraulic oil or air and has a working medium to control the tool feed mechanism. Hydraulic mechanism is used for high precision movement due to high bulk modulus of the liquid and incompressibility of the fluid make it more compatible with high load application. Gas feed controls are used where accurate movement is not needed. Direction, pressure, and flow of fluid can be controlled precisely using direction control values, pressure control values such as pressure relief values, pressure reducing values and both meter in and meter out flow control valves. Pneumatic controls are usually binary control and in-between controls are difficult to achieve in pneumatics compared to hydraulic control [17–20].

(iv) Motor-Controlled Feed Mechanism

Precise control of the tool feed movement can be achieved by motor mechanism.

10.5 Abrasive Slurry

Large varieties of abrasive slurries are used in USM. Some of them are boron carbide, silicon carbide, aluminum oxide, and diamond dust.

It is important to select abrasive particle properly and the choice of the abrasive git has to be done carefully by considering the following factors:

i. Shape and size of the particles
ii. Mechanical strength of the particles such as toughness, etc.
iii. Cost of abrasives
iv. Durability of abrasives over a long time.

While choosing the abrasive slurry and mass mixing or loading factor, one has to consider the individual concentration and ability to extract the heat. Undesirable cavitation effect is caused by boiling in the gap [21].

10.6 Liquid Media

In the liquid medium, about 35–65% of the abrasive by volume are suspended in the USM process [22].

For liquid medium, the functions are:

i. The liquid medium serves as a connecting bridge between anode and cathode.
ii. It transports the abrasive material to gap between the tool and work.
iii. This medium serves as a coolant and transports waste abrasives and other swarf.

iv. Ultrasonic energy of the tool is transformed into mechanical vibration through the liquid medium.

v. It is important that they do not cause corrosion to the anode, cathode, and ultrasonic equipment [23].

Water is commonly utilized as the primary liquid medium because it fulfills the majority of the specified requirements. Additionally, a corrosion inhibitor is introduced into the water [24].

10.7 Process Parameters

i. Transducer final amplitude (20–60 microns)

ii. Horn vibration (20–40 kHz)

iii. Axial force (F) applied to tool to get hammering mode

iv. Feed force on the tool

v. Grit size

vi. Abrasive material used such as Al_2O_3, SiC, B_4C, boron silicarbide, and diamond

vii. Yield stress of the anode and cathode material

viii. Contact area of the work with tool to calculate the number of impacts

ix. Slurry concentration ratio of abrasive in water

x. Tool combination

xi. Work material combination

xii. Slurry ratio used in the USM

10.8 Process Capability

i. The machining process can effectively work on materials with a hardness ranging from 50 Rockwell hardness (HRC) to 75 HRC (such as tungsten carbides, glass, tungsten, and ceramics), surpassing the capabilities of traditional methods. However, it is important to note that the USM process is not suitable for softer and more ductile materials like copper, lead, ductile steel, and plastics, as these materials takes away energy through deformation and are not compatible with this technique [25].

ii. Tolerance can range from 10 microns to 30 microns.

iii. Drilling holes as small as 75 microns is possible, with a maximum depth of 50 mm attainable without difficulty. Utilizing special flushing techniques enables achieving hole depths of up to 150 mm.

iv. Ratio of diameter to length up to 60:1 can be obtained using this processes.

v. Removal rate of linear material is from –0.03 to 30 mm/min.

vi. Finish of surface varies from –0.2 micron to 0.8 micron.

vii. Compared to conventional grinding, non-directional surface texture is possible.

viii. Radial overcut may range from 1.8 to 4.5 times mean of the abrasive grit particles.

10.9 Applications

i. Manufacturing cavities in ceramics that are generally electrically non-conductive.

ii. This can be utilized for machining delicate components where the scrap rate would otherwise be high.

iii. Utilized in multi-stage processes to manufacture turbine blades made of silicon nitride (Si_3N4).

iv. A study by Benedict in 1973 reported a significant quantity of small-diameter holes, specifically 950 holes measuring 0.30 mm, created using hypodermic needles.

v. Utilized in the material removal from hard and brittle substances including semiconductors, glass, sapphire, carbides, and its derivatives.

vi. Utilized in machining holes and surface impressions of various shapes, including round, square, and irregular.

10.10 Advantages of USM

i. It is suitable for material removal from easily fracturable and breakable materials.

ii. There is no heat generation, resulting in negligible alterations to the physical structure of the workpiece material.

iii. Materials that are non-conductive due to high electrical resistance, which is not possible by electro discharge machining (EDM) and electrochemical machining (ECM), can be effectively machined using USM.

iv. USM is a process that produces no burrs or distortions.

v. It can be integrated with other advanced technologies such as EDM, electro chemical grinding (ECG), and ECM [26].

vi. USM enables high accuracy and excellent surface finish to be achieved.

10.11 Disadvantages of USM

i. High volume of the material cannot be removed by this process.

ii. Deep hole drilling becomes challenging due to restricted slurry movement.

iii. The wear rate of cutting tools increases on front and side surfaces due to complex interactions between anode, cathode and abrasive particles. It is a multi-physics problem with stress field, flow, and fracture involved along with thermal field.

iv. Tools made of brass, tungsten carbide, mild steel (MS), or tool steel will experience wear from abrasive grit at ratios ranging from 1:1 to 200:1.

v. Ultrasonic machining (USM) is suitable for workpieces with a hardness exceeding 45 HRC.

vi. Abrasive may get into the work piece which are not sufficiently hard.

10.12 Mechanism of Material Removal in Ultrasonic Machining Operation

Based on the theoretical analysis and experimental findings (*i.e.*, the actual results), USM is a kind of material removal that takes place by abrasion in the form of small grains. The process involves mainly four mechanism for the material removal.

i. Abrasives grit particles are thrown away due to lower size of particles.

ii. Abrasive particles may get hammered between the tool and work.

iii. Vapor pressure of the carrier fluid may affect the volume of the material removed.

iv. High impact of the sharp abrasive particles may erode the material away.

Material removal due to throwing and hammering is considered significant and material removal due to cavitations and chemical erosion can be ignored [27].

It is assumed abrasive grit used in the process are spherical and diameter of the abrasive grit used is d_g, movement of the abrasive particles under the action of vibration tool which vibrates at a frequency in the range of 25–50 kHz is responsible for volume of the material removal.

Numerous researchers have contributed to the development of diverse mechanisms for material removal processes. The theory formulated by M.C. Shaw is given below. The following are the assumption made in the subsequent derivation for the volume material removal rate.

i. The shape of each grit is assumed to be spherical.

ii. Each abrasive is same and capable of removing the same amount of material.

iii. The metal removal rate depends on amount of workpiece in one hit.

iv. The volume of the material removal depends on number of grits impact per cycle.

v. The rate at which material is removed is directly proportional frequency.

When abrasive particle hits the work, a piece lets it makes δ amount of dent in the work pieces, as shown in Figure

10.4.

Using Pythagoras,

$$AB^2 = AC^2 + BC^2$$

$$\frac{d_g}{2} = \left(\frac{d_g}{2} - \delta\right)^2 + r^2$$

$$\frac{d_g}{2} - \left(\frac{d_g}{2} - \delta\right)^2 = r^2$$

$$r^2 = \delta^2 + d_g\delta$$

Neglecting the δ^2 term, it can be written as,

$$r^2 = d_g \delta$$

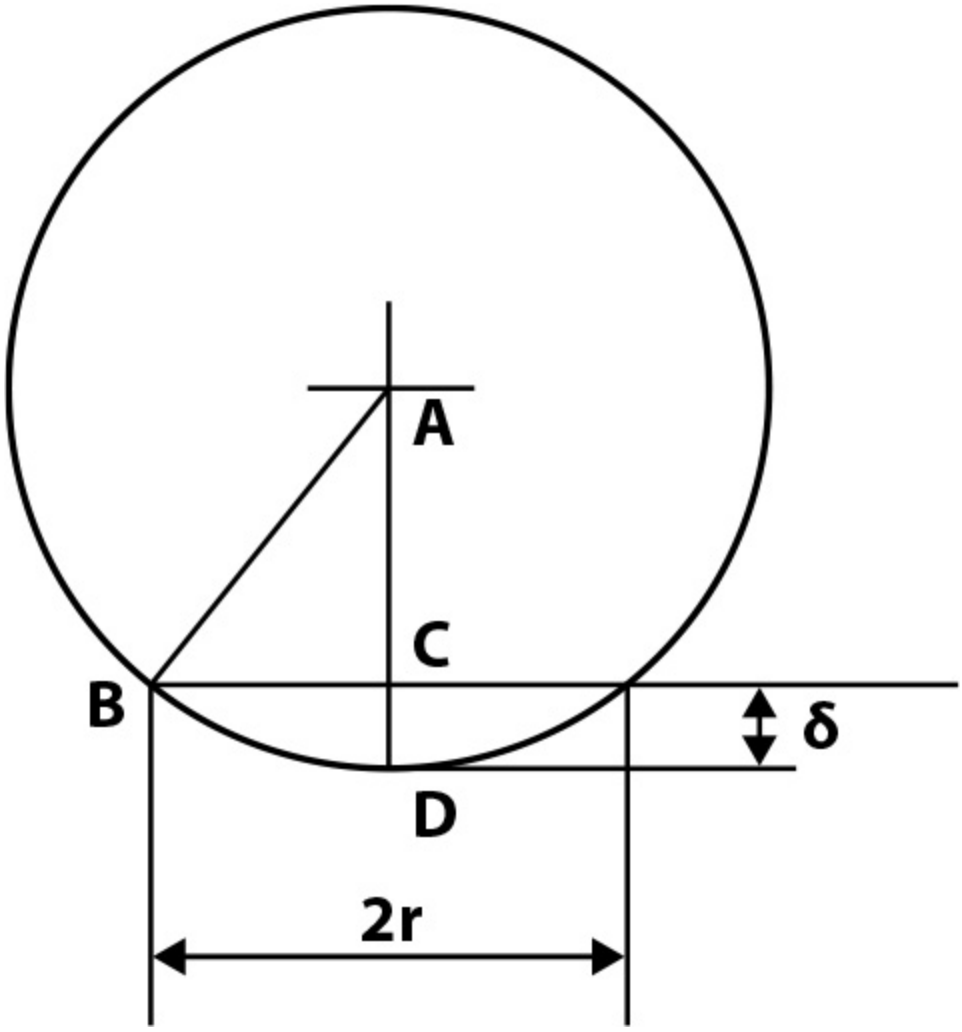


Figure 10.4 Geometry of the abrasive grit and dent amount.

Which gives the radius as,

$$r = \sqrt{d_g \delta}$$

Volume of the material removal = volume of the hemispherical crater produced. For that, the volume of the material removal from the workpieces is given by,

$$\Gamma = \frac{1}{2}\left[\frac{4}{3}\pi r^3\right] = \frac{1}{2}\left[\frac{4}{3}\pi (r^2)^{\frac{3}{2}}\right] = \frac{1}{2}\left[\frac{4}{3}\pi (d_g\delta)^{\frac{3}{2}}\right] = K_1 (d_g\delta)^{\frac{3}{2}} \quad (10.1)$$

Where the term K_1 is constant.

The number of impacts (N) is related using the following Equation 10.2.

$$N = \frac{K_2}{{d_g}^2} \quad (10.2)$$

Where K_2 is constant.

It is important to note that all the particles under tool and work piece will participate in the material removal. Some may get thrown away due to high kinetic energy and may not remove the material. In addition, there are other phenomenon such as cavitation, dulling of abrasives, etc., which may affect the material removal due to process parameters chosen while machining a particular material with work-tool combinations.

Material removal in USM processes is given as:

Material removal

$$= \{Volume\ of\ material\ removed\ per\ grit\ per\ cycle\}$$
$$\times\ Number\ of\ impacts\ made\ by\ abrasives\ per\ second$$
$$\times\ Number\ of\ impact\ per\ cylce$$
$$\times\ Probability\ of\ abrasive\ particle\ under\ tool\ being\ effective$$

$$MRR = \Gamma f \frac{K_2}{d_g^{\,2}} K_3 \qquad (10.3)$$

$$MRR = \left[K_1 \left(d_g \delta \right)^{\frac{3}{2}} \right] f \frac{K_2}{d_g^{\,2}} K_3$$

$$MRR = \left[K_1 K_2 K_3 f \sqrt{\frac{(\delta)^3}{d_g}} \right]$$

Equation 10.3 is the specific equation for a particular work and tool combination.

Model 1: Grain Throwing Model

Let us consider that the tool strikes and throws a particle onto the work surface. Suppose that there is a sinusoidal vibration and that the tool's displacement (y) is specified in terms of the oscillation's amplitude (a/2) and time period (t).

The sinusoidal function can be given as,

$$X = \frac{a}{2} \sin(2\pi ft)$$

Differentiating on both sides with respect to t, we get velocity,

$$\text{Velocity, } V = \frac{a}{2} 2\pi f \cos(2\pi ft)$$

From here, we get the maximum velocity, $V_{max} = \pi af$

Let us assume the grits also has the velocity V_{max}, so kinetic energy can be written as:

$$KE = \frac{1}{2} M V_{max}^{\ 2} = \frac{1}{2}\left(\frac{\pi \left(d_g\right)^3}{6} \rho_g \right)(\pi af)^2 \tag{10.4}$$

Note: since we are calculating the kinetic energy of the grit in this instance, the diameter of the grit must be taken into account while calculating mass.

δ gives the depth of penetration made by grit into the workpiece. The work done by the grit can be calculated by:

$$\text{Work done by the grit, } W = \frac{F\delta}{2} \tag{10.5}$$

Also, the flow strength of material can be written as, $\sigma_w = \frac{F}{\pi r^2}$

$$F = \sigma_w \times \pi r^2 \tag{10.6}$$

Substituting Equation 10.6 in Equation 10.5, we get,

$$\textit{i.e.}, \text{ work done by the grit, } W = \frac{F\delta}{2} = \frac{\sigma_w \times \pi d_g \delta \times \delta}{2} \tag{10.7}$$

We know, work done by the grit and the kinetic energy of the particle should be equal. That gives,

$$\frac{\sigma_w \times \pi d_g \delta \times \delta}{2} = \frac{1}{2}\left(\frac{\pi \left(d_g\right)^3}{6} \rho_g \right)(\pi af)^2$$

On simplifying, we get,

$$\delta = \pi\ A\ f\ d_g \sqrt{\frac{\rho_g}{6\sigma_w}} \tag{10.8}$$

Substituting Equation 10.8 in the general Equation 10.3, we get the volumetric material removal rate due to throwing mechanism.

Volumetric material removal rate is given by,

$$MRR = \left[K_1 K_2 K_3 d_g f^{\frac{5}{2}} \left[\frac{\rho_g (\pi a)^2}{6\sigma_w} \right]^{\frac{3}{4}} \right] \tag{10.9}$$

Model 2: Grain Hammering Model

This model works very well when the gap between the tool and work piece is less compared to the size of the abrasive grit or almost equal to the size of the abrasive grit particle. T is the total time and during the entire T material is not removed. Only during ΔT during grain comes in contact with the tool and work and material is removed by hammering mode. It is important to maintain the correct force so that grains are not crushed but participate in volume of the material removal. Time period of one cycle is shown in Figure 10.5 and tool position at various levels during USM is shown in Figure 10.6.

The mean value of the force (F_{avg}) experienced on the grit can be given by,

$$F_{avg} = \frac{1}{T} \int_0^T F(t) dt \tag{10.10}$$

We can express the momentum equation as:

$$\frac{1}{T}\int_0^T F(t)dt = \left[\frac{F}{2}\right]\Delta T \qquad (10.11)$$

The total penetration resulting from the hammering can be determined by,

$$\delta = \delta_w + \delta_t$$

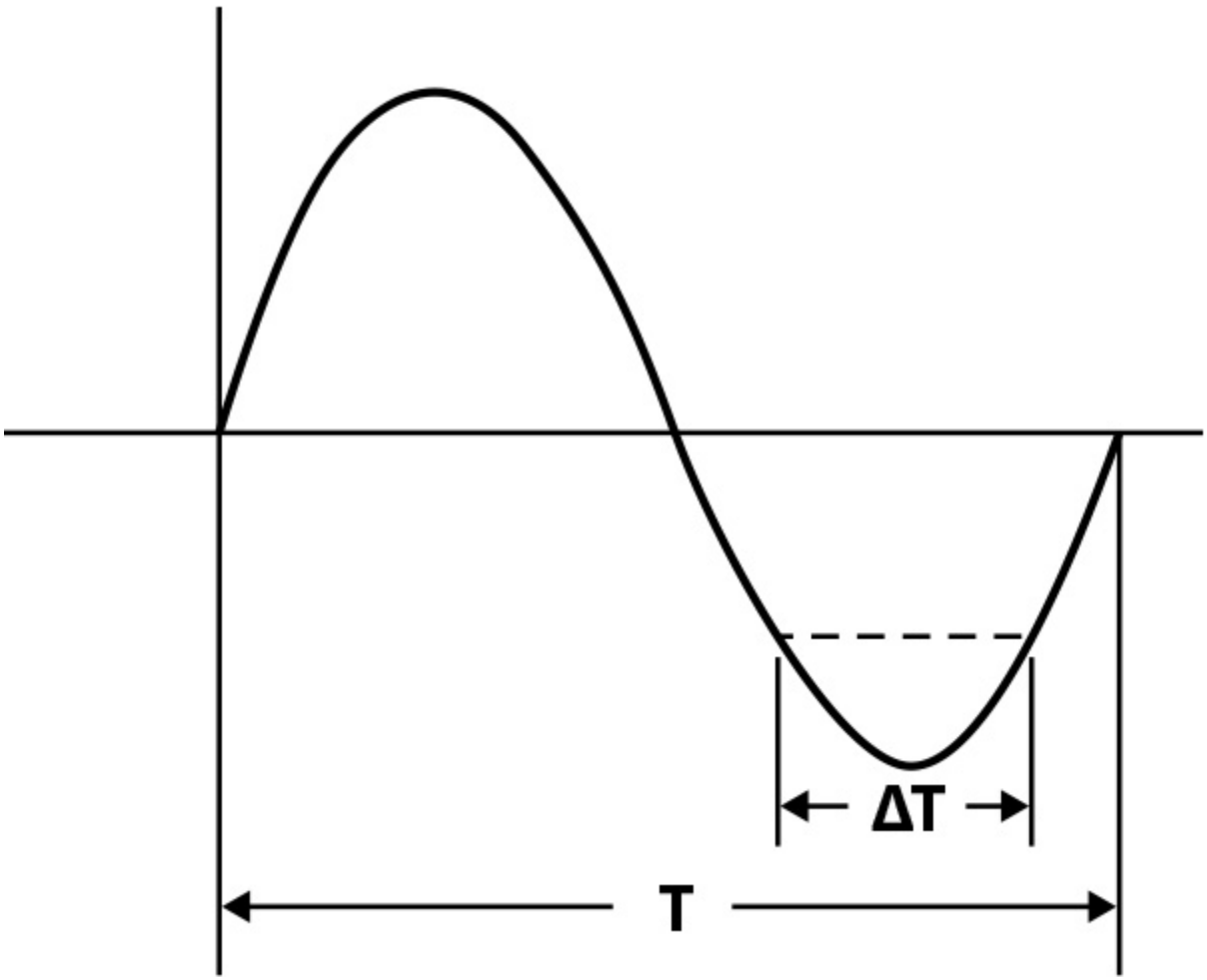


Figure 10.5 Time period during USM.

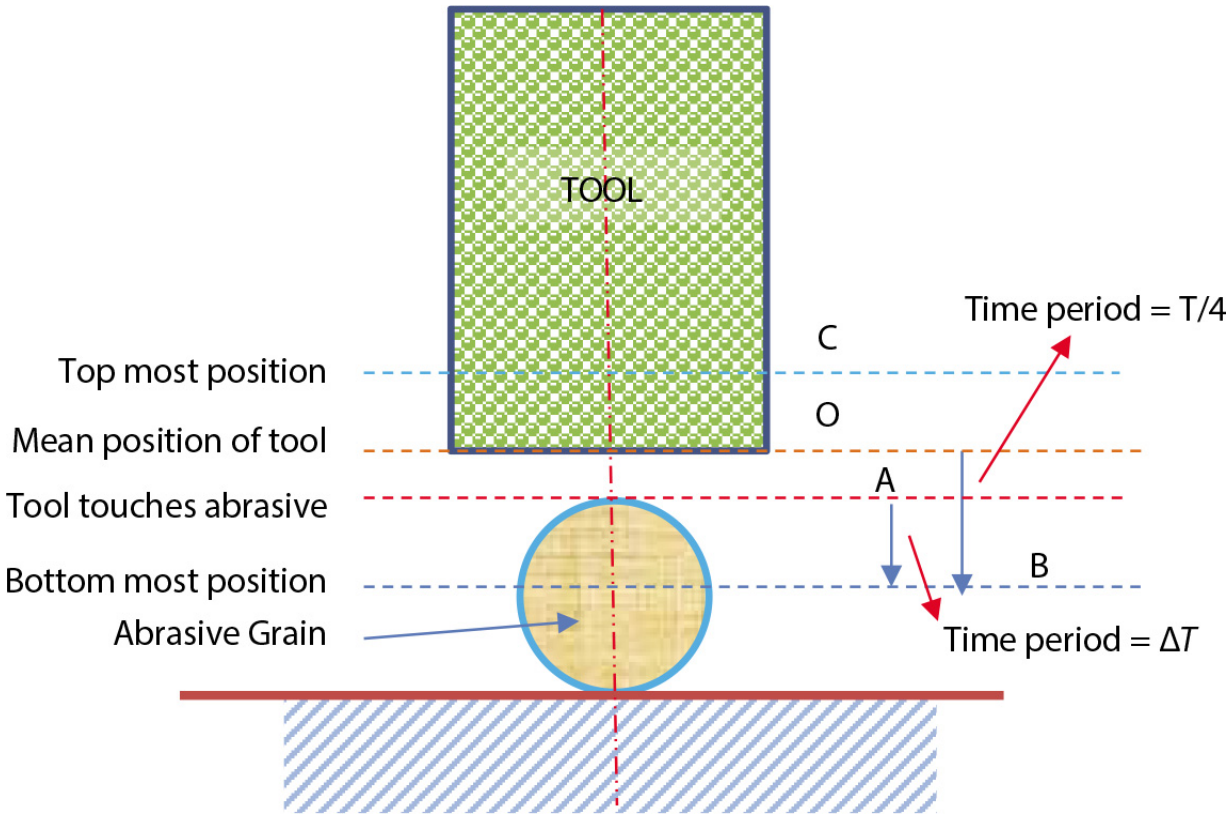


Figure 10.6 Tool positions at various levels during machining.

Let us take the amplitude of the oscillation of the tool as a/2. So, the value $(a/2)/(T/4)$ gives the mean velocity of the tool during the quarter cycle. Hence, the duration (ΔT) required to travel from position A to position B can be found using the following expression.

$$\Delta T = \frac{\delta T}{2a} \qquad (10.12)$$

Using Equation 10.12 in Equation 10.11,

$$F_{avg} = \frac{F\Delta T}{2T} = \frac{F\delta T}{2T \times 2a} = \frac{F\delta}{4a}$$

On rewriting,

$$F = F_{avg}\left[\frac{4a}{\delta}\right] \tag{10.13}$$

$$\sigma_w = \frac{F}{N(\pi d_g d_w)} \tag{10.14}$$

$$\sigma_t = \frac{F}{N(\pi d_g d_t)} \tag{10.15}$$

From Equations 10.14 and 10.15, it can be written,

$$\frac{\sigma_w}{\sigma_t} = \frac{\delta_t}{\delta_w}$$

Also, from Equations 10.2, 10.13, and 10.14, we get

$$\sigma_w = \frac{F}{N(\pi d_g d_w)} = \frac{F_{avg}\,4ad_g^2}{\delta(\pi d_g d_w)K_2} = \frac{F_{avg}\,4ad_g}{K_2\pi d_g {\delta_w}^2\left[\frac{\delta_t}{\delta_w}+1\right]}$$

Taking $\frac{\delta_t}{\delta_w} = \lambda$, and rearranging we get

$$\delta_w = \sqrt{\frac{F_{avg}\,4ad_g}{\sigma_w \pi K_2(\lambda+1)}}$$

Equation 10.3 given below can be used to calculate the volumetric material removal rate from the work piece caused by the hammering mechanism:

$$MRR = \left[K_1 K_2 K_3 \, f \sqrt{\left[\frac{(\delta_w)^3}{d_g} \right]} \right] \tag{10.16}$$

$$V_{hammering} = K_1 K_2 K_3 \, f \, d_g \left[\frac{F_{avg} \, 4a}{\sigma_w \pi K_2 (\lambda + 1)} \right]^{\frac{3}{4}}$$

10.13 Recent Developments in USM

Ultrasonic machining is now commonly used across various sectors. The most recent progress are given below.

i. Contouring using USM
ii. Rotary USM
iii. US-assisted ECM

(i) Contouring Using USM

Contouring using USM has been designed to address challenges involved in the production of intricate 3D cavities. The computer numerically controlled (CNC) machine is used together with the conventional USM technique. The CNC tool can be directed along a predetermined tool path, which is generated by the software based on the shape of the workpiece. This approach has the capability to achieve greater sinking depth and create larger cavities.

(ii) Rotary USM

This technology is employed for the purpose of machining non-metallic and composite materials. In this procedure, the tool is rotated at a high speed about 50,000 revolutions per minute (RPM). This technique results in reduced machining time. Major benefits of rotary USM include:

i. Better mechanical properties.

ii. The high material removal rate as a result of the high speed.

iii. Low tool pressure available for fragile and delicate parts.

(iii) Ultrasonic-Assisted ECM

This hybrid machining process is a combination of two machining methods, bringing together the benefits of both USM and ECM. This combination results in a metal removal method that incorporates both mechanical abrasion from USM and anodic dissolution.

References

1. Rozenbery, L.D., Chapter 1 and 2, in: *Physical principles of ultrasonic Technology*, vol. 1, Penum press, New York, 1973.

2. Neppiras, E.A., and Foskett, R.D., Ultrasonic machining. *Philips Technical Review*, 18, 11, 325–368, 1956–57.

3. Neppiras, E.A., and Foskett, R.D., Ultrasonic machining, operating conditions and performance of ultrasonic drills. *Philips Technical Review*, 18, 12, 368, 1959.

4. Nishimura, G., Yanagishima, K., Shima, T., Ultrasonic mechanical machining, part IX. *J. Fac. Eng.*, 26, 2, 129, 1959.

5. Goetze, D., The effect of Vibration amplitude, Frequency and composition of the abrasive slurry on the rate of ultrasonic machining in SAM1095 Tool steel. *J. Acoust. Soc. Am.*, 28, 6, 1032, 1956.

6. Goetze, D., The effect of pressure between tool tip and workpiece on the rate of ultrasonic machining SAE 1095 Tool steel. *J. Acoust. Soc. Am.*, 29, 4, 426, 1957.

7. Nishimura., G. and Kawa., SS., Ultrasonic mechanical machining, part IV. *J. Fac. Eng.*, 25, 4, 213, 1958.

8. Shaw, M.C., Ultrasonic Grinding, International Institution for production engineering research. *Microtonic*, X, n6, 257, 1956.

9. Pentaland, H. and Extermanis, J.A., Improving ultrasonic machining rates, some feasibility studies. *Tran. ASME*, 2, 1, 25–37, 1965.

10. Markov, A.I., *Ultrasonic machining of intractable materials*, Illiffe books limited, London, 1966.

11. Kennedy, D.K. and Grieve, R.J., Ultrasonic machining, A review. *Prod. Eng.*, 54, 13–19, 1975.

12. Balmuth, L., Method of abrading. British patent, 602, 801, 1948.

13. Neppiras, E.A., Report on Ultrasonic machining: What is ultrasonic machining. *Met. Work, Product*, 100, 27, 1283, 1956.

14. Dikushin, V.I., and Barke, V.N., *Ultrasonic erosion and its dependence on vibrational characteristics of tool*, p. 10, Stanki instruments, India, 1958.

15. Taniguchi, N., Analysis of machining force of ultrasonic machining. *Rep. Fac. Engg.*, 9, 131– 146, 1958.

16. Neppiras, E.A., Ultrasonic machining and Forming. *Ultrasonics*, 2, 167–173, 1964.

17. Kennedy, D.C., Ultrasonics machining: review, in: *The production engineer*, p. 7, 1975.

18. Theo, T.B., Aspinwall., D.K., Wise, M.L.H., A review on ultrasonics. *Int. J. Mach. Tools Manuf.*, 38, 4, 219–255, 1998.

19. Kazantsev, V.F., Improving the output and accuracy of ultrasonic machining. *Machines and Tooling*, 37, 4, 33–39, 1966.

20. Legge, P., Machining without abrasive slurry. *Ultrasonics*, 4, 157–162, 1966.

21. Takeyama, H., Burrless Drilling by means of ultrasonic vibration. *Ann. CIRP*, 40, 83–86, 1991.

22. Chandra, N. and Rahman, M., Effect of machining parameter in ultrasonic vibration cutting. *Int. J. Mach. Tools Manuf.*, 48, 9, 965–974, 2007.

23. Kainath, G.S., Nandy, Singh., K., On the mechanics of material removal in ultrasonic machining. *Int. J. Mach. Tool Des. Res.*, 19, 33–41, 1979.

24. Soundrarajan, V. and Radhakrishnan, V., An experimental investigation on basic mechanism involved in ultrasonic matching. *Int. J. Mach. Tool Des. Res.*, 26, 3, 307–332, 1986.

25. Miller, G.E., Special theory of ultrasonic machining. *J. Appl. Phys.*, 28, 2, 149, 1957.

26. Singh, R. and Khamba, J.S., Ultrasonic machining of titanium and its alloys: A review. *J. Mater. Process. Technol.*, 173, 125–135, 2006.

27. Jagadeesha, T., *Unconventional machining processes*, I K International Publication House Pvt. Ltd, New Delhi,

2016.

Note

*Corresponding author: jagdishsg@nitc.ac.in

11
Electron Beam Machining

Jagadeesha T.[1]* and Sandip Kunar[2]

[1]*Dept. of Mechanical Engineering, National Institute of Technology, Calicut, India*

[2]*Dept. of Mechanical Engineering, Aditya University, Surampalem, India*

Abstract

Electron beam machining (EBM) is a precision material removal technique using focused electron beams. Originating in 1958, EBM has found widespread applications in micro-cutting due to its ability to melt and vaporize materials without tool wear. Conducted in a vacuum chamber to prevent electron scattering, EBM employs components like the electron gun and focusing units to control beam parameters. The mechanics of material removal involve the dissipation of kinetic energy of electron beam as heat upon interaction with work piece material. Process parameters such as beam current and pulse duration significantly influence material removal rates. Electron beam machining's applications span diverse industries, from drilling micro-holes in semiconductors to slicing silicon wafers. However, EBM entails challenges like high equipment costs, limited suitability for thick materials, and the need for skilled operators and meticulous maintenance due to the vacuum environment. Despite these drawbacks, EBM remains a vital technique for achieving high precision in micromachining operations.

***Keywords*:** Electron beam machining, micromachining, metal vaporization, thermionic emission, material removal rate

11.1 Introduction

In 1958, a German engineer, Steigerwald, designed a prototype electron beam equipment for welding application. Later on, this technology spread in other industrial applications. The process in which high velocity focused electron beam is used achieve material removal is called electron beam machining (EBM). These electrons travel with the 50–80% of velocity of light (1.6×10^8 m/s) and heats, melts and vaporizes the work material at the point of bombardment. Since the electrons would be scattered by collision with gas molecules and should be prevented, the process takes place vacuum chamber [1].

Electron beam machining can be used to economically for microcutting of materials. Electron beam machining removes the material by the process of melting and vaporization. The beam power determines the area of evaporation. The EBM is widely used in making precision holes of diameter ranging from 0.05 mm to 1 mm [2].

11.2 Theory of EBM

In EBM, the work piece is stricken with high velocity pulsating stream (2000 Hz) of free electrons (accelerated using very high voltage of 120–150 kV). As the beam interacts with the work piece, heat energy is generated as the kinetic energy of beam gets converted to heat energy. This concentrated heat increases the work piece temperature so that it melts and vaporizes the work piece material in small amounts.

Minimum diameter of electron beam concentration area is 0.0127 mm. The process is usually done in vacuum to avoid collisions of electrons with surrounding air molecules which would scatter or diffuse the electron beam. Also, lead

shielding is required to protect the machine operator from radiations. Electron beam machining is used for drilling small hole and creating narrow slots or contour in thin work pieces to close tolerance. There is no tool wear of pressure on the work. The material removal rate is faster [3, 4].

11.2.1 Mechanics of Material Removal in EBM

The fast-moving electron beam, when impinged on a surface, penetrates through one layer undisturbed. This layer is called the transparent layer. After that, it starts colliding with molecules and comes to rest ultimately. The collisions dissipate the kinetic energy and generates heat. Thus, the heat is developed inside the material below the transparent layer [5]. The depth of penetration of electrons depends on the kinetic energy, as established in the equation shown below.

$$Penetration\ depth = \delta(mm) = 2.6\times10^{-17}\frac{V^2(volts)}{\rho(\frac{kg}{mm^3})}$$

11.3 Equipment

Figure 11.1 shows the simplified arrangement of EBM. The major components are worktable, focusing lens, deflector coil, and electron beam gun.

a) Electron Beam Generation by Electron Gun

The electron beam is produced by raising the temperature of tungsten or tantalum filament to about 2000 °C. At these conditions, the electron cloud is emitted from the filament.

Electron gun consists of:

i. **Tungsten filament:** it acts as the cathode and is connected to negative terminal of the direct current (DC) power source. Filament is also made of tantalum and function is to emit electrons.

ii. **Grid cup:** this is negative-biased with respect to the filament. This is also called bias cup or Wehnelt electrode. It acts as gird that controls the beam current to 1–80 mA. This is achieved by regulating the count of electrons. Beam current is turned ON/OFF by using the bias cup.

iii. **Anode:** this is connected to the positive terminal of the DC power supply. The perforated anode is kept at high positive potential of about 150 kV.

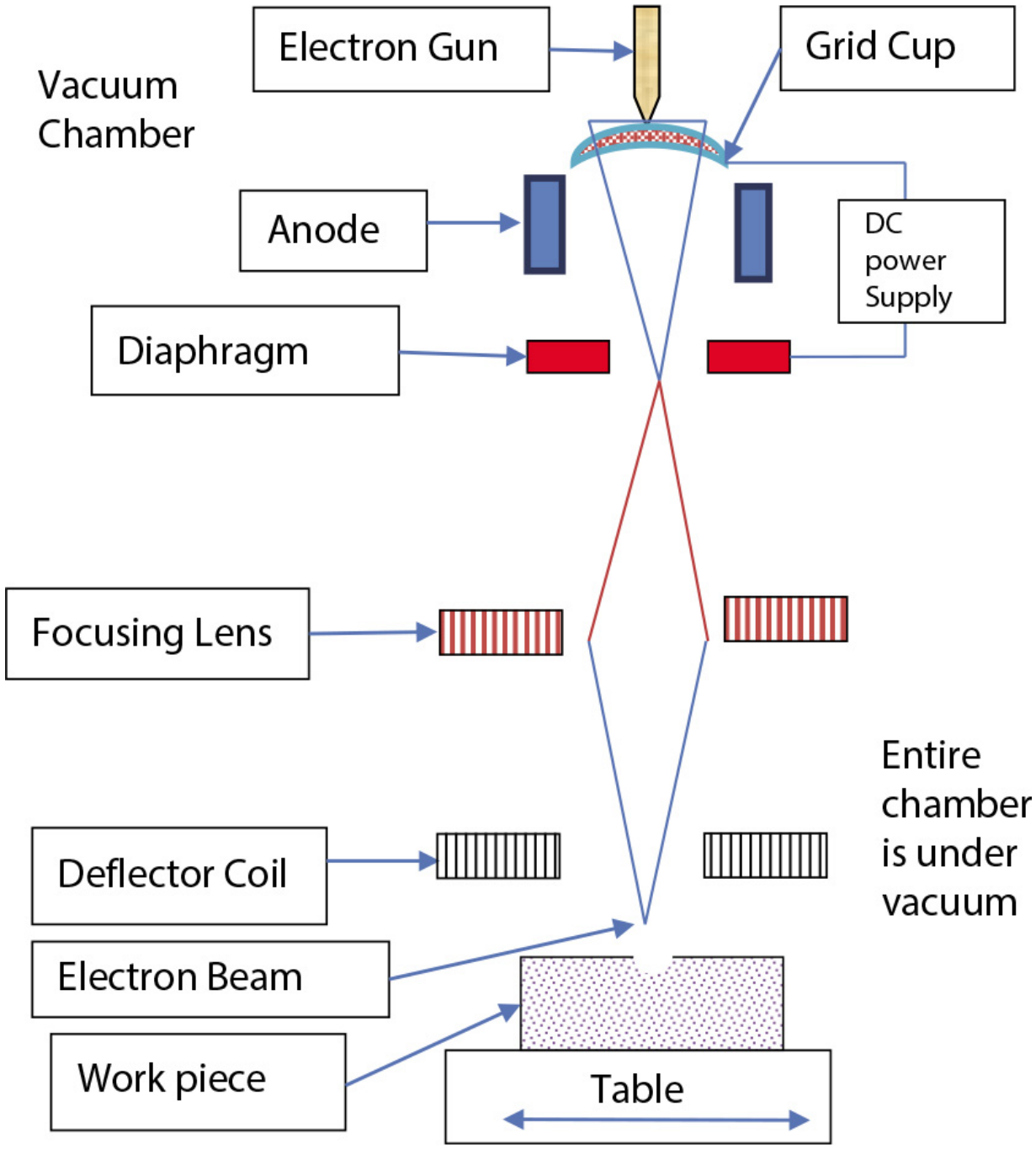


Figure 11.1 Electron beam machining unit.

Due to the high potential difference between the anode and the cathode, electron beam is emitted from the hot cathode tip to the anode. The electrons are accelerated, and their velocity increased to a very high value (about the 50–80%

of speed of light) as it passes through the perforated anode [6].

High accelerating voltages (120–150 kV) are given to the anode to get high energy intensities which in turn permit high depth-to-width ratio of the holes machined.

b) Vacuum System

The collision of electron beam with air molecules necessitates vacuum conditions.

High vacuum is needed due to following reasons:

i. If there is no vacuum, then emitter would oxidize in the presence of air when the temperature is about 2000°C.
ii. Electrons would lose the energy by collision with air molecules and this passage of the electrons would be retarded.
iii. If vacuum is not maintained, contamination of metal vapor with debris occurs. Therefore, the entire setup is maintained in vacuum. It is usually maintained at a vacuum of 10^{-4} *to* 10^{-5} Torr.

c) Focusing Units

Focusing of electron beam is done electromagnetically or electrostatistically. The function of electrostatic lens is to condense the divergent beam of electrons into a narrow converging beam up to a diameter of 1 micron. In electromagnetic focusing, deflecting coil is used to have a range of movement of 12 mm. The electron beam can be controlled very accurately. For drilling holes in complex shapes, a highly developed multi-axis deflector is required [7–9].

Working: when a high velocity DC source is applied to the electron gun, tungsten or tantalum filament wire

temperature rises to around 2000°C. Due to high temperature, there will be thermionic emission of electrons from the cathode. These clouds of electrons are channelled by the grid cup to reach the anode. By applying 100 kV to 200 kV at the anode, the electrons arriving the anode are accelerated to speeds as high half the velocity of light [10, 11].

Such high velocities of the electron beam are kept until they strike the work piece because electron beams travel in vacuum without any collision. In order to focus the electron beam in the desired spot on the work piece, focusing lens are employed [9]. An optical graduated viewing system is also provided in order to allow the operator to see the work and in order to position the beam precisely upon a particular spot on job.

The electron beam travelling at high velocity when impinges on the work piece surface generates heat as the kinetic energy is dissipated and this high intensity heat melts and vaporizes the work material at the area of focus.

Due to the high power intensity, the material vaporization happens within few microseconds of electron beam impingement. This process is carried out in repeated pulses of short duration [12–15]. With pulse frequency ranging from 16,000 to 25,000 Hz and pulse duration ranging from 4 to 65,000 µs, the process is performed in repeated pulses. Steps of metal removal are shown in Figure 11.2.

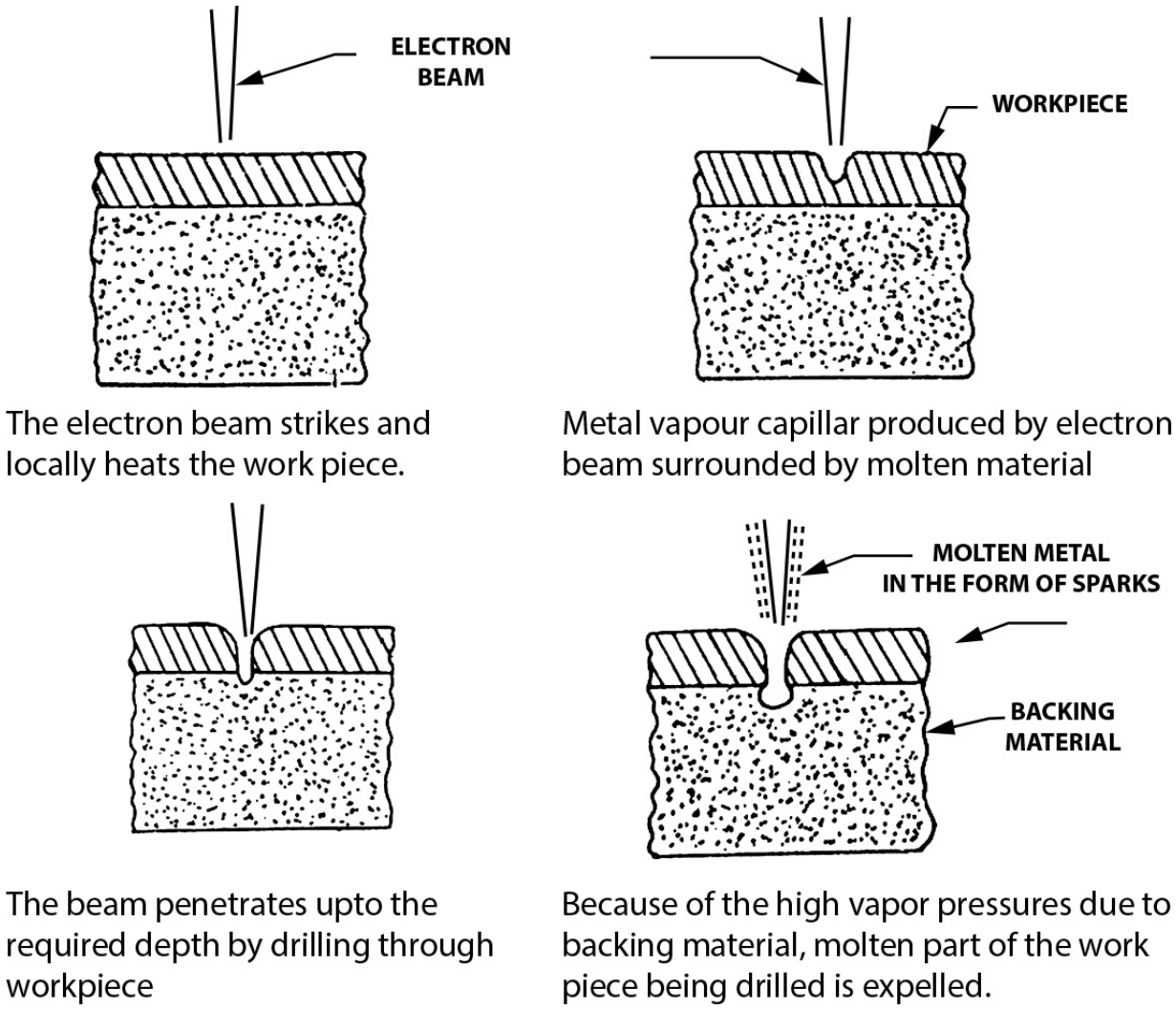


Figure 11.2 Steps of metal removal in EBM.

Pulse assisted electrochemical machining (PECM) offers an inexpensive and efficient technique for machining of advanced materials to generate intricate profiles, *i.e.*, microcavities, die, molds, etc. PECM improves the precision and machined quality because of a pulsed voltage with greater current density compared to electrochemical machining.

11.4 Mathematics of Electron Beam Machining

Free electrons are accelerated greatly due to effect of magnetic or electric field. Even with relatively small potential difference, electron velocity can be that of speed of light.

Consider an electron that moves in electric and magnetic field. The electron is subjected to Lorenz force of:

$$F_L = \vec{F}_e + \vec{F}_m \tag{11.1}$$

$F_L = Lorenz\ force$

$\vec{F}_e = force\ due\ to\ electric\ field$

$\vec{F}_m = force\ due\ to\ magnetic\ field$

Also,

$\vec{F}_e = force\ due\ to\ electric\ field = -eE_s$

$\vec{F}_m = force\ due\ to\ magnetic\ field = -e\mu V_s H$

where

$e = charge\ of\ the\ electron,$

$E_s = electrostatic\ field$

$V_s = speed\ of\ the\ electron$

$\mu = magenetic\ permeability$

$H = strength\ of\ magnetic\ field$

The magnetic field is always at right angles to the direction of electron movement. Hence, it does no work, but can only change the direction of electron movement. Thus, the kinetic energy of the electron is not affected by the

magnetic field having no component acting in the direction of the electron movement [16].

In a given electric field, the addition of kinetic and potential energies of electrons is constant, when

$$\frac{1}{2}m_e V_s^2 - eE_s = C_o \tag{11.2}$$

At the terminal conditions $V_s = 0$, $E_s = 0$, $C_o = 0$, thus,

$$\frac{1}{2}m_e V_s^2 = eE_s$$

From which the speed of the electron is given by

$$V_s = \sqrt{\frac{2eE_s}{m_e}}\frac{m}{s} \tag{11.3}$$

where

e = charge of the electron in Coulomb

E_s *= electrostatic field in volts*

V_s *= speed of the electron in m/s*

The static mass of electron is $m_e = 9.1\times10^{-28}$ *gm* and *e* = 1.6×10^{-19} *Coulomb*

$$V_s = \sqrt{\frac{2eE_s}{m_e}} = \sqrt{\frac{2\times1.6\times10^{19}\times E_s}{9.1\times10^{-28}}} = 600\sqrt{E_s} \tag{11.4}$$

Thus, the variation of the speed of the electron is a function of the potential difference of the electric field. The order of this velocity can be calculated with velocity of the light, when

$$\frac{V_s}{C_L} = \frac{600\sqrt{E_s}}{930 \times 10^3} \tag{11.5}$$

Where C_L is the velocity of light in km/sec.

If the applied voltage lies in the range of 10^6 *to* 10^8 V, the order of electron velocity would lie in the range of the velocity of the light, thus imparting a very high amount of kinetic energy to the electrons [17–20].

This, electrons moving in the electric field, can accumulate considerable energy when the electron reach anode surface, a rapid change in momentum takes place through the collisions with the atoms of the work material when the kinetic energy of the impinging electrons are transferred to the atoms of the work material under bombardment [21]. The various technological processes like microwelding, melting, and cutting, and making thin films can be carried out by controlling the concentrated thermal energy obtained through electron bombardment.

11.5 Mechanics of EBM

The smallest elementary particle that is stable is the electron. It has a mass of 9.1×10^{-28} *gm* with charge of -1.6×10^{-19} *columbs*. The electron velocity, when it is assumed that the starting velocity is negligible, is given by

$$V_s = \sqrt{\frac{2eE_s}{m_e}} = \sqrt{\frac{2 \times 1.6 \times 10^{19} \times E_s}{9.1 \times 10^{-28}}} = 600\sqrt{E_s}\,\frac{\text{km}}{\text{sec}}.$$

The electron beam power is given by

$P_b = E_s e n_e I_b$

$n_e I_b$ = number of electrons per second

n_e = number of electrons per second per amp

$$n_e = 6.3\times10^{-18}\ \frac{\text{electron}}{\text{sec}}\text{amp}$$

$$en_e = 1.6\times10^{-19}\times 6.3\times 10^{-18}\ \frac{\text{electron}}{\text{sec}}\text{amp} = 1$$

Therefore, power is given by

$$P_b = E_s I_b \tag{11.6}$$

$$I_b = \text{beam current in amps}$$

The pressure from the electron beam and reaction of vapors from the evaporating material cause the stable condition of cone penetration and movement of the material from its leading wall in the zone of crystallization [22].

The force of the electron beam on the molten material is given by

$$F_b = n_e m_e V_s \tag{11.7}$$

Combining Equations 11.3 and 11.7,

$$F_b = \frac{I_b}{e} m_e \sqrt{\frac{2eE_s}{m_e}} \tag{11.8}$$

$$F_b = \frac{I_b\sqrt{E_s}}{e}\sqrt{\frac{2m_e}{e}}\ \text{Newton}$$

In centimeter gram second system (CGS) unit,

$$F_b = \frac{I_b\sqrt{E_s}}{e}\sqrt{\frac{2m_e}{\mathrm{e}}}$$

$$F_b = \frac{I_b\sqrt{E_s}}{e}\sqrt{\frac{2\times 9.1\times 10^{-28}}{1.6\times 10^{-19}\times 10^{3}}}\times 10^{5} = 0.34 I_b\sqrt{E_s} \quad dynes.$$

if I_b is expressed in current per cm^2, Equation 11.8 would give the pressure due to electron bombardment per cm^2.

The force on the fused metal arising out of the evaporation of metal from the surface can be determined by equating the velocity of atoms due to thermal energy acquired by the work material due to electron bombardment with the mean velocity of atoms of metal evaporating from the surface of the material.

According to the classical kinetic theory of heat, each atom of a crystalline solid acquires energy, on an average of $k\theta$:

$$\frac{1}{2}\mathrm{m_a V_a^2} = k\theta$$

$\mathrm{m_a}$ = atomic mass of workpiece material, kg

$\mathrm{V_a}$ = *thermal velocity accquired, m/sec*

θ = *temperature raised through electron bombardment, k*

k = *Boltszmann's constant* = 1.38×10^{-23} *J/k/atom*

Thus, the thermal velocity is given by

$$\mathrm{V_a} = \sqrt{\frac{2k\theta}{\mathrm{m_a}}} \qquad (11.9)$$

where

the mean velocity of evaporation is evaluated from the total force of reaction, when

$$F_n = n_a m_a V_e \tag{11.10}$$

n_a = number of electrons in the beam

m_a = mass of electron in the state of rest, kg

V_e = mean velocity of evaporation, m/s

From Equation 11.10,

$$V_e = \frac{F_n}{n_a m_a} \tag{11.11}$$

From Equations 11.9 and 11.11, we get

$$\frac{F_n}{n_a m_a} = \sqrt{\frac{2k\theta}{\mathrm{m_a}}}$$

From which we get

$$F_n = n_a \sqrt{2k\theta \mathrm{m_a}} \tag{11.12}$$

Calculations indicate that F_n determined from Equation 11.12 is considerably greater than F_b calculated from Equation 11.8. Thus, the pressure caused by evaporating reaction is much greater than the force caused by direct bombardment of electrons.

Thus, if the beam is moved, the metal on the leading wall of the fused zone will be subjected to simultaneous action of electron beam pressure and evaporating metal reaction while the rear wall of the fused zone does not undergo this pressure.

11.6 Process Parameter of Electron Beam Machining

The main important process parameters are beam current, pulse duration, lens current, beam deflection, and spot

diameter.

Beam current is continuously alterable between 100 µA and 1 A. Energy per pulse increases as the beam current increases.

The electron emission by the heated tungsten filament is determined by its capacity of thermionic emission. It is given by the Richardson-Dushman equation,

$$J = AT^2 e^{\left(-\frac{WE}{KT}\right)}$$

J = *current density of the emitted current* $(\frac{amp}{cm^2})$

W = *work function of the material of the filament* (*volts*)

T = *absolute temperature of the filament* (k)

E = *electronic charge* (*Coulomb*)

k = *Boltzmann constant* = $1.3\times10^{-23}\ j/k$)

A = *constant* = $120\ \frac{amp}{cm^2}/degree^2$

The validity of the above equation holds only when the filament is held in free space. The presence of electric field around filament contributes to the alteration of current density significantly.

The beam current is regulated by varying the grid bias voltage. As the grid becomes more negative in polarity with respect to the cathode, the electron emission is increasingly restricted.

Pulse duration affects both diameter and depth of hole. The diameter and depth of hole created is directly proportional length of pulse duration. It also determines amount of recast layer and heat affected zone (HAZ). Typical pulse duration ranges from 50 µs to 100 ms.

Lens current parameters determine the working distance, *i.e.,* the distance between the electron beam gun and the focal point. It also determines the dimensions of area of concentration of electron beam which further determines the dimension of the hole created in the work piece material. The beam power must be sufficient to cause melting and vaporization of work material.

Beam deflection signal is used to control the beam deflection coil. In order to move the beam in the pattern to cut out the required shape at the hole's outer edge, the signal can be programmed accordingly. This method is only applicable when the dimension of the shape required is less than 6 mm. Typical process parameters and capabilities of EBM is given in Table 11.1.

Table 11.1 Process parameters of EBM.

Accelerating voltage	50 to 200 kV
Beam current	100 to 1000 µA
Beam power	0.5 to 50 kW
Pulse time	4-64000 µs
Pulse frequency	0.1 to 16000 Hz
Electron velocity	1.6×10^{8} m/s
Spot size	0.013 to 0.025 mm
Range of deflection	6.4 mm^2
Intensity of beam	1.55 x 10^6 to 1.55 x 10^9 W/cm^2
Power density	6500 billon W/mm^2
Medium	Vacuum 10–5 to 10^{-6} Torr
Work piece material	Almost all materials can be machined
Depth of cut	Up to 6.5 mm
Hole taper	1° to 2°
Metal removal rate	up to 50 mm^3/s
Specific power consumption	0.5 to 50 kW
Tolerance	Up to 10% of depth
Surface roughness	1 micron Ra value

Spot diameter depends on various factors. They are beam current, magnetic lens, accelerating voltage, and distance between gun and work piece. The three factors that contributes most significantly to the change in the dimension of the spot are given below.

i) Effect of thermal velocities: the spot size will be spread out as different electrons converge at different

points along the longitudinal axis of beam. The minimum dimension of spot diameter is given by

$$\delta D_t = \frac{2r_c x}{r_i}\sqrt{\frac{KT}{eV}}$$

δD_t = *minimum spot diameter*

r_c = *cathode spot radius*

r_i = *radius of beam at magnetic lens*

x = *distance between gun and work piece*

e = *electron charge*

V = *anode voltage*

Boltszmann's constant = $1.38\times10^{-23}\ J/k/atom$

T = *absolute temperature of cathode*

ii) Spherical deviation of the focusing lens: this deviation results in the crossing of marginal rays at different positions in the axis from that of the rays. So, instead of an ideal point image, a disc is formed with diameter given by

$$\delta D_s = 2.5 r_i^3 \left\{\frac{x}{f(S+D)^2}\right\}$$

S = *lens pole piece separation of the magnetic lens*

D = *bore diameter of the magnetic lens*

f = *focal length of the magnetic lens*

iii) Space charge spreading of target: the minimum spot size is limited when the electrons converging in a conical beam to a point as the target is subjected to mutual repulsion and the equation is given as,

$$\delta D_c = 11.8 \times 10^4 x^{\frac{5}{2}} I^{\frac{5}{4}} V^{\frac{-15}{8}} r_i^{\frac{-3}{2}}$$

The reduced formula obtained by combined effect of these three gives

$$\delta D = \sqrt{\delta D_i^2 + \delta D_s^2 + \delta D_c^2}$$

iv) Control of focal distance of magnetic lens:

$$\frac{\mathrm{f}}{(\mathrm{S}+\mathrm{D})} = \frac{25\mathrm{V}}{(\mathrm{NT})^2}$$

V = electron accelerating voltage

NT = ampere turns of the lens winding

11.7 Application of EBM

i. EBM is primarily used on thin materials for micromachining operations. These operations include cutting, drilling, perforating, slotting, scribing, and milling.

ii. EBM can be used for producing metering holes either of round shapes or profiled holes. These metering holes are required on sleeve valves, rocket fuel injectors, and injector nozzles of diesel engines.

iii. It is used to drill holes in the pressure differential devices that are used in nuclear power plants, aircraft engines, etc.

iv. EBM can be used for slicing of silicon chips in the semiconductor industry.

v. EBM can be used for making precise holes in wire drawing dies, fine orifices, and spinnerets for production of synthetic fibers.

vi. It is an effective method to remove broken taps in holes.

vii. Used in manufacture of components of electron beam microscope and to conduct microdrilling operations up to 0.002 mm in dies used for wire drawing where the orifices are thin.

viii. EBM can be used for mass perforation of holes in sheet metal and in polythene sheets.

ix. EBM can be used to make holes in gas orifices used in air crafts, nuclear reactors, and for drilling fine holes in rotor and stator blades for supersonic aircraft engines.

x. This technique is used in the manufacture of computer memories, emission cathodes, and integrated circuits via electron beam lithography.

xi. This method is particularly advantageous for machining materials having high melting point and low thermal conductivities.

xii. It is used for drilling synthetic jewels in the watch industry.

xiii. Used for drilling holes through thin sheet metal, which are further used for making filters and screens in the food processing industry.

11.8 Advantages of EBM

i. Holes of different shapes and sizes can be machined using EBM. Very accurate and precise holes down to 30 microns can be drilled.

ii. High rate of drilling of fine holes (4000 holes/s) is possible with EBM.

iii. Capable to machine any material irrespective of its properties.

iv. Thin, fragile, and brittle material can be machined as this method does not involve any mechanical or thermal distortion during the process.

v. The absence of mechanical contact between tool and work make it an excellent technique for micromachining operations.

vi. Harder material can be machined quickly compared to conventional machining.

vii. High aspect ratio (150:1 to 200:1) can be drilled using EBM.

viii. Due to small beam diameter, close tolerances on the hole diameter can be obtained. Electron beam machining can drill holes and cut slots in work piece that cannot be done using conventional methods.

ix. The process can be automated easily. In certain cases, work piece remains stationary, while the beam is programmed to move in a predetermined path. Positioning and indexing can be done automatically.

x. Metallurgical and physical damage to the work piece is less.

xi. Extremely close tolerances of the order ±1 *to* 5 µm are possible using this process.

xii. Narrow slots of 25 microns can be easily machined using EBM.

xiii. Jobs can be positioned precisely within tolerance of ±10 µm.

xiv. Cutting pressure and tool wear is absent in this process.

xv. Input energy can be controlled precisely. Therefore, the distortion can be reduced to minimum when machining thin sections.

xvi. There is no physical or metallurgical damage to the surface. Depth of surface layer affected due to machining is reduced to minimum. The HAZ is minimal.

11.9 Disadvantages of EBM

i. Highly skilled operator is required to operate the machine as well as to do computer numerically controlled (CNC) programming. Equipment cost is also high.

ii. The machining is carried out in vacuum, pumping down time for creating vacuum is non-productive and time consuming. Maintaining high degree of vacuum is expensive.

iii. Also, considerable time is required in evacuating the chamber after a batch of jobs have been processed.

iv. The process is generally not applicable to very thick material. Usually, part thickness is about 10 mm.

v. EBM is a thermal machining process, recast layer of about 0.025 mm will present after machining. Heat affected zone is also present due to EBM.

vi. Metal removal rate is very small. Therefore, this is economical only for small cuts.

vii. This method is not suited for work pieces having large dimensions.

viii. High specific energy consumption.

ix. Straight sinking deep holes are difficult to make. Taper (about 5°) is inevitable.

x. All EBM operations are done in vacuum and this restricts the maximum size of the work piece to the vacuum chamber size.

xi. Small amount of recast and metal splash occur in the spot where the electron beam is focused and this has to be removed by abrasive cleaning.

xii. Perfect cylindrical hole cannot be produced by using this process as a small crater is created as the beam impinges on the work.

xiii. Large cycle time is required to set up the work piece.

xiv. X-rays are produced by the interaction of work piece surface and the impinging beam. Therefore, the equipment should be used by a highly skilled operator.

xv. Maintenance cost is high for EBM.

11.10 Worked Out Examples

1. During the drilling of holes in steel work piece by EBM, an accelerating voltage of 160 kV is used. Determine the electron range.

   Solution

$$\text{Density of steel is } 7.8\frac{g}{cc} = \frac{7.8}{1000 \times 1000} = 7.8 \times 10^{-6}\ kg/mm^3$$

$$Penetration\ depth = \delta(mm) = 2.6\times10^{-17}\frac{V^2\ (volts)}{\rho(\frac{kg}{mm^3})}$$

$$\delta(mm) = 2.6\times10^{-17}\frac{160000^2(volts)}{7.8\times10^{-6}\left(\frac{kg}{mm^3}\right)} = 0.0853\ mm = 85.33\ micron$$

2. Calculate the velocity of electron impingement in electric field having strength of 2.5×10^5 V. if the beam current is 2×10^{-5} A, calculate the power of the electron beam.

   Solution

$$V_s = \sqrt{\frac{2eE_s}{m_e}} = 600\sqrt{E_s}\frac{km}{sec} = 600\sqrt{2.5\times10^6} = 3\times10^5\frac{km}{sec}$$

$$P_b = E_s I_b = 2.5\times10^5\times2\times10^{-5} = 5\ W$$

3. Calculate the electron beam pressure if the current density is 2×10^{-3} A/cm^2 and the voltage is 4×10^6 V.

   Solution

$$F_b = \frac{I_b\sqrt{E_s}}{e}\sqrt{\frac{2\times9.1\times10^{-28}}{1.6\times10^{-19}\times10^3}}\times10^5 = 0.34I_b\sqrt{E_s}\quad dynes$$

   if I_b is expressed in current per cm^2, Equation 11.8 would give the pressure due to electron bombardment per cm^2:

$$F_b = 0.34I_b\sqrt{E_s}\quad dynes = 0.34\times2\times10^{-3}\times\sqrt{4\times10^6} = 1.36\ dynes/cm^2$$

References

1. Melaka, A.H., *Electron beam welding: principles and practice*, McGraw Hill, London, 1971.

2. Dupak, J. and Vlcek, I., Electron gun for welding in instrumentation, in: *Sixth International Conference on Electron Beam Technologies EBT'2000*, Varna, Bulgaria, 4–7 June, p. 45, 2000.

3. Leonard, L.H., Electron beam welding at atmospheric pressure, in: *Fifth electron beam symposium*, March, 1963.

4. Metal Hand book, *Volume 1, Properties and selection of Metals*, ASME Publications, USA, 1961.

5. Burton, G. and Matchett, R.I., Welding, drilling and machining by Electron beam, in: *American machinist*, Feb, 1959.

6. Bakish, R. and White, S.S., *Hand book of electron Beam welding*, John Wiley Publication, USA, 1964.

7. Steigerwald, K.H., State of art of electron beam technology for metal removal, welding and heat treatment process, in: *IMTDR conference*, 1980.

8. Arata, A., *Plasma, Electron and laser beam technology*, ASM Publications, USA, 1985.

9. Christy, R.W., Formation of thin polymer films by electron bombardment. *J. Appl. Phys.*, 31, 45–56, 1960.

10. Anon, Some elementary consideration in design of electron beam for welding and heating, in: *Proc. 3rd symposium on electron beam technology*, Boston, 1962.

11. Yoshida, S., Radioactive isotope study of the dissociation of barium wide under electron bombardment. *J. Appl. Phys.*, 27, 1180–1191, 1956.

12. Anon, Electron beam processing. *Aircr. Prod.*, 22, 8–15, 1960.

13. Lamba, S., Application of Electron beam for evaporations and machining of materials, in: *Proc. 4th symposium on electron beam technology*, Boston, 1962.

14. Duhamel, R.F., *Practical Electron Beam cutting and milling applications*, ASTME, Creative manufacturing seminars, 1962.

15. Kuper, G.I., Electron beam device for removal of dielectric and metallic materials. *VDIZ*, 116, pp. 5–17, 1974.

16. Miyazaki, T., Characteristics of electron beam drilling of metals. *Bull. Jpn. Soc. Precis. Engg.*, 10, 2–18, 1976.

17. Bellows, G. and Kohls, J.B., Drilling without drills, special Report, 743, in: *American Mechinist*, 173–188, 1982.

18. Liang, S. and Shih, A.J., *Analysis of Machining and Machine Tool*, Springer Science and Business Media LLC, United Kingdom, 2015.

19. Bhattacharyya, B. and Doloi, B., *Machining processes utilizing thermal energy*, Elsevier BV, USA, 2020.

20. Edwards-Smith, W., *Modern Fabrication Techniques*, Elsevier BV, 1973.

21. Yuan, C.G., Pramanik, A., Basak, A.K., Prakash, C., Shankar, S., Drilling of titanium alloy (Ti6Al4V) – a

review, in: *Machining Science and Technology*, United Kingdom, 2021.

22. Youssef, H,.A., Nontraditional Machining Processes - an Overview, in: *Machining of Stainless Steels and Super Alloys*, 2016.

Note

*Corresponding author: jagdishsg@nitc.ac.in

12
Chemical Machining

Jagadeesha T.[1]* and Sandip Kunar[2]

[1]*Dept. of Mechanical Engineering, National Institute of Technology, Calicut, India*

[2]*Dept. of Mechanical Engineering, Aditya University, Surampalem, India*

Abstract

Chemical machining, a precise manufacturing process, involves controlled material removal using chemical reactions with acids or alkalis. This method is commonly used on thin sheets and foils, with photoresist masking determining the areas for material removal. The process includes preparing the workpiece by cleaning and applying photoresist, preparing masters for chemical blanking, masking with photoresists using techniques like doping or spraying, and etching for blanking by immersing the workpiece in an etchant bath. Achieving tolerances as tight as ±0.01 mm is possible with optimal control of time, temperature, and solution. The original artwork is typically made larger than the actual size and then reduced photographically to create multiple image masters. Chemical machining offers high precision and can produce intricate shapes with accuracies suitable for various applications in industries like aerospace and electronics.

***Keywords*:** Chemical machining, chemical blanking, chemical milling, photochemical blanking, chemical engraving

12.1 Introduction

The use of chemicals to remove material is an old art. In 2300 BC, a solution made from citric acid was used by the Egyptians to decoratively etch copper jewelry. The use of chemical processes was prevalent for decorative etching until the 19th century. However, with the advent of photography, a new dimension was added to chemical machining. In chemical machining, material is removed from the workpiece by controlled dissolution using strong chemical reagent known as etchant [1, 2].

The same process can be suitably applied to a variety of operations which includes milling, engraving and blanking. The chemical processes are:

i. Chemical milling
ii. Chemical engraving
iii. Chemical blanking

There are two methods of metal removal by chemical means. They are:

1. Non-selective metal removal
2. Selective metal removal

In non-selective metal removal, metal is removed from the entire exposed surface of a part. It is advantageous in removing burr/metal from casting, forging, extrusions. We can remove the material by immersing workpiece in the etchant.

In selective metal removal, work is covered with chemically resistant layer and thereby preventing chemical action on these areas. Area where metal removal is required is left unprotected. The work is then placed in etchant solution

and metal is removed from the unprotected area. Thus, this is selective metal removal process using chemicals [3].

12.2 General Description of Chemical Machining Process

Figure 12.1 shows a schematic diagram of a chemical machining process. Here, an etchant solution is used to remove the desired metal in the chemical machining processes. The workpiece can either be dipped into the etchant solution or the etchant can be sprayed on to the metal to be removed from workpiece.

Chemical reactions will gradually transform the metal into a metallic salt. The metal removal rate can be controlled by controlling concentration, composition, and operating conditions of the etchant solution [4].

In the case of selective metal removal process, an etchant resistant material known as maskant or resist can be used to protect the unmachined portion of the workpiece. The process is shown in Figure 12.1.

The workpiece is first coated with the maskant material. Depending on the type of the maskant used, the surfaces to be etched are then located by scribing the maskant by using photographic techniques or by screen printing technique.

12.3 Five Steps of Chemical Machining

For producing machine parts using chemical machining process, the following steps are followed.

1. **Preparation of workpiece:** the workpiece material must be cleaned to remove dirt, oil, grease, dust or rust. Good cleaning produces good adhesion between the work material and maskant. Ultrasonic and chemical cleaning is commonly used.

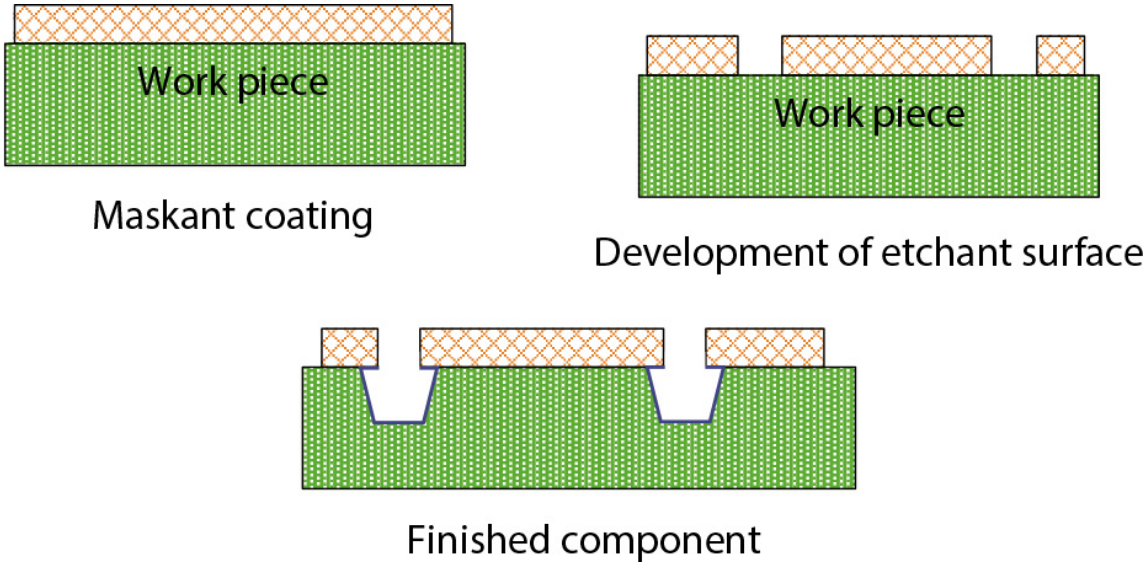


Figure 12.1 Chemical machining process.

2. **Coating with the masking material:** the proper choice of masking material is essential. Mask should be readily strippable, chemically impregnable and it should adhere well and able to withstand chemical abrasion during etching.
3. **Scribing of the mask:** is done to expose the areas that receives chemical machining process and are guided by templates.
4. **Etching:** this is an important stage required to produce the required component from the sheet metal.
5. **Cleaning the masking material:** in the final step, masking material is removed from the etched part then the dimensions and surface quality are inspected before shipment.

12.4 Elements of Process

The characteristics of the chemical process are usually governed by the following two important process parameters, also known as elements of process.

1. Etchant resistant material: type, thickness of the resists
2. Etchant solution: composition, concentration, and operating conditions
3. Etching medium
4. Etching time.

Etchant resistant material: etchant material used in practice can be classified as:

a. Cut and peel maskant
b. Photoresist maskant
c. Screen print resists.

a) Cut and Peel Maskant

The process steps for cut and peel maskant is given below.

i. The entire workpiece is coated with maskant either by spraying maskant or by dipping the workpiece or flow coating.
ii. After scribing unwanted portion of the maskant peeled away, exposing the area to be chemically etched.
iii. Material is removed from the area where chemicals are exposed and material is not removed from the area where mask is present. Mask offers high resistance offered to the etchant. Depending upon the thickness of the maskant, etching depth of 10 mm or more is possible with cut and peel maskant.

iv. Step etching is possible using these maskant.

Typical cut and peel maskant are vinyl, neoprene rubber, and butyl-based materials, like bee wax and burgundy pitch [5].

Advantages of Cut and Peel Maskant

i. This can be used to machine parts which have many irregularities.
ii. We can machine large parts.
iii. It is a quick method. Most rapid and economical for simple geometry.
iv. Etching depth of 7 mm or more from one side is possible [6].
v. It can be used to produce multisteps on the work surface.

Disadvantages of the Cut and Peel Maskant

i. They are not suitable for thin parts because of the possibility of distortion by the scribing and peeling operation.
ii. Very high accuracy is not possible using this maskant.
iii. Skilled personnel is required.
iv. It is an expensive and time-consuming process.
v. Repeatability of the process is less due to the possibility of human error.

b) Photoresist Maskant

This type of masking is also known as photochemical machining and is used to produce intricate and precise

shapes by using a photographic image to selectively cure the photo resist mask on a workpiece.

First step in this technique is preparation of photo master: the profile to be produced on the workpiece is hand drawn or generated using the computer. Usually, the profile is drawn to a large scale (around 20 to 50 times the original dimension). This computer-generated profile is photographed and the photo master is prepared. If the application requires many identical parts to be blanked out of one sheet of material, a precision step and repeat camera is used to provide duplicate images on a single photo master [7].

The second step in this technique is parts preparation: after the photo master is created, all the dirt and oxides from the part needs to cleaned. A thin layer of light activated etchant resist material is coated over the part after cleaning is done and then baked dry.

The third step is to expose the part to strong ultraviolet (UV) light source. A strong ultra violet light source is used to selectively expose the photo resist while the photo master and work piece are held together.

After exposure, the photo resist is developed to remove the coating from all areas where etching is desired. After the photo resist has been developed, the parts are chemically etched, stripped of residual photoresist, and inspected.

Advantages of Photo Resist Maskant

i. This can be used to machine thin parts up to 0.005-mm thick.

ii. Highest and most consistent details can be obtained.

iii. Only photographic negative is needed and no printing equipment are needed.

iv. Changes can be incorporated easily in photo master.

Disadvantages of the Photo Resist Maskant

i. They are used to etch depth up to a thickness of 2 mm.
ii. Good clean room facility is required.
iii. Skilled operator is required to perform job.
iv. Processing cost is higher compared to others.
v. Etchant if not adhered, causes more undercutting.

c) Screen Print Maskant

Screen resists are material which can be applied to work piece through normal silk-screening technique. That material is applied through a silk or stainless-steel mesh which has a photographically made stencil placed on it. Stencils avoid deposition of resists in areas that will be subsequently etched away [8].

The stencils are generally made photographically. Printing accuracy is lower than the photo resist maskant but better than cut and peel method. Coating thickness deposited by screen printing is intermediate between the photographic resists and cut and peel maskant. Therefore, the chemical resistance is substantially higher than the photographic resists but lower than cut and peel maskant [9].

The etch depth and accuracy in screen printing is restricted to 2 mm and ± 0.1 mm, respectively.

Advantages of Screen Print Maskant

i. It is an extremely rapid method of producing a large number of parts to moderate accuracies. It is high volume production process.
ii. Accuracy is higher than the cut and peel maskant [10].

iii. Set up cost is low.

iv. Wide variety of etchants is available for different material.

v. Lower production cost.

Disadvantages of the Screen Print Maskant

i. They are used to for parts having only flat surfaces or very moderate contours. They cannot be used for complex contours.

ii. The printing accuracy is less than the photographic printing [11].

iii. Changes are difficult to incorporate when compared to photo printing.

Process Steps Involved

1. Cleaning the material to remove dirt and oil films.
2. Applying resist by screen printing.
3. Drying the image either by air or baking cycle.
4. Etching of part.

12.5 Influence of Etchant Medium

Etching medium has an important role to play in metal removal rate (MRR) in chemical machining. Etchants are added with additives and inhibitors to get good surface quality and to get uniform MRR. The etching medium should not result in diffusion of atomic hydrogen in titanium and steel. In the case of aluminum alloys, intercrystalline corrosion can be avoided using additives and inhibitors [12–14].

Copper, aluminum, and magnesium usually show higher MRR compared to steel and titanium. Quality of etched surface depends on chemical solubility of work material and its grain size. If the surface is metallurgically homogenous, uniform erosion is possible.

12.6 Chemical Blanking

The process steps involved in chemical blanking are:

1. Preparation of workpiece
2. Preparation of masters
3. Masking with photo resists
4. Etching for blanking

1. Preparation of the workpiece: Figure 12.2(a) shows the flow chart for the preparation of the workpiece.

2. Preparation of the masters: the flow chart for the preparation of the masters is shown in Figure 12.2(b). Masters are the tools for chemical blanking. It consists of art work and negative used to produce acid resistant image. Individual size can vary from microdimensions to a maximum of 350 by 350 mm. This is then reduced photographically and multiple image masters are made.

3. Masking with photo resists: the flow chart for masking with photo resists is shown in Figure 12.2(c).

i. Doping, whirl coating, or spraying can be used to apply the photoresists to the workpiece.

ii. Exposure to UV light partially polymerizes the light-sensitive resins in conventional photoresist, enhancing its resistance to organic solvents used as developers.

iii. Development involves immersing the workpiece in an appropriate organic solvent. Then, the work piece is rinsed with running water in order to remove developers and dissolved polymer from the non-image areas.

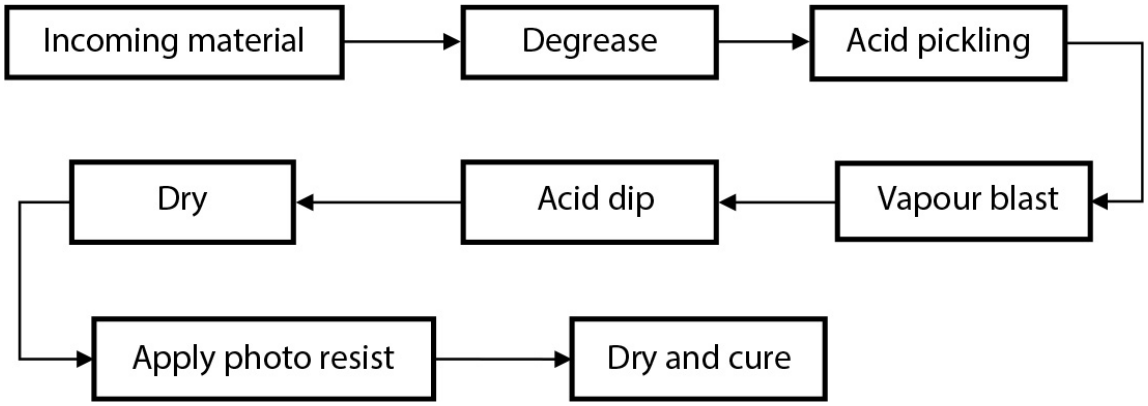


Figure 12.2 (a) Flow chart for preparation of workpiece in chemical blanking.



Figure 12.2 (b) Flow chart for preparation of masters in chemical blanking.

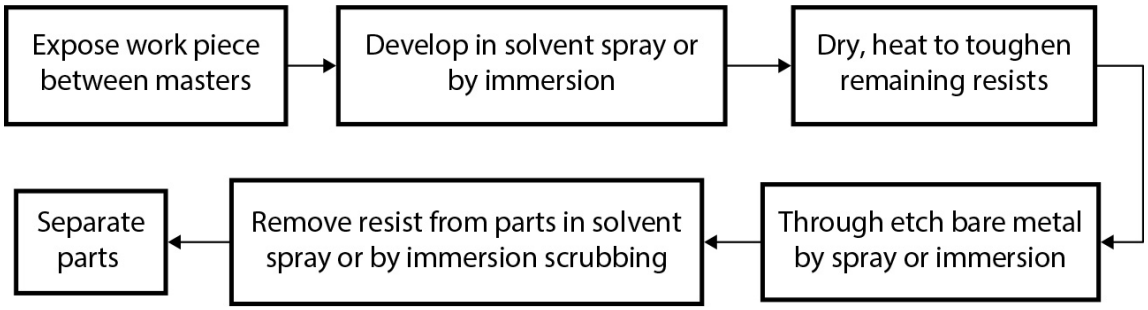


Figure 12.2 (c) Flow chart for masking and etching in chemical blanking.

iv. Drying: after the development, photoresist is dried at room temperature and baked again at 110 °C for 15

min. This process increases hardness and chemical resistance of the photoresist.

4. Etching for blanking: removal of material by etching is done by immersing the work piece in a bath containing etchant. The bath is agitated by air or mechanical means. Specially designed spray etching machines are used where component size is large.

12.7 Accuracy of Chemical Blanking

The chief disadvantage of the chemical blanking is undercutting. During etching operations, the material is eroded in a downward direction as well as the lateral direction. Material removal in downward direction is known as depth of cut. Removal of material in the lateral direction is referred to as undercut. Factors like strength of the etchant, work piece material and the depth of cut affects the extent of undercut. The compensation must be made during selective masking to ensure the proper final size and is given an etch factor. The ratio of depth of cut to the undercut is defined as the etch factor.

$$Etch\ factor = \frac{depth\ of\ cut}{undercut}$$

12.8 Applications of Chemical Machining

1. This is used for aluminum aircraft wing skin.
2. Used for helicopter vent screen.
3. Used for instrument panels such as front panel of oscilloscope, where high detail engraving is required.

4. Engraving of any metal piece.
5. Used for producing stepped webs.

12.9 Advantages of CHM

1. Burr-free machining is possible with chemical machining (CHM). Also, it gives good surface finish.
2. CHM has low scrap rate, around 3%.
3. No stress is induced during the process; therefore, it is suitable for thin and delicate sections.
4. A reduction in weight on complex contours which is difficult to machine using conventional methods can be achieved.
5. Low tooling and capital costs are involved.
6. Thin sections of hard brittle materials can be machined without distortion.
7. The hardness of the metal to be machined has no significant effect on the process.
8. Brittle materials can be machined with ease.

12.10 Disadvantages of CHM

1. Surfaces must be metallurgically homogenous.
2. Sharp corners are difficult to make using this process.
3. Etchant vapors are corrosive in nature. Hence, the process equipment must be kept safe from the etching and other operating equipment.
4. The maximum working metal thickness is small.
5. The parts finished by the chemical machining have undercutting which is further increased with the

increase in metal removal thickness.

6. Productivity is relatively low in this process. Optimum productivity is determined by the part size, metal thickness to be machined, and quantity of the parts required.
7. Scribing accuracy is very limited. Dimensional accuracy is less.
8. Porous casting often yield uneven etched surfaces.

12.11 Selection of Maskant

The factors which greatly influences the selection of the maskant are:

1. The chemical resistance offered by the maskant to the etchants.
2. Ease of removal of maskant at the end of operation.
3. Shape and size of parts.
4. Economic involved in the process.
5. Rate of production of parts.

In order to increase the resistance of the etchant, multiple coating of the maskant is utilized. When thicker and rougher dip or spray coating are used the exposure time increases significantly. For example, the maskant material used in aluminum alloys are polymer, butyl rubber, and neoprene. In iron-based alloys, we use polymer, polyvinyl chloride, and polyethylene butyl rubber. In nickel, neoprene is used, and in magnesium, copper (and its alloys), titanium, and silicon, we use polymer maskant material.

Desirable Properties of Maskant

1. It should adhere itself properly to the workpiece.
2. It should be easy to scribe.
3. It should not react easily with the etchant.
4. It should not lose its properties at high temperature.
5. It should be easy to remove.

12.12 Selection of Etchants

The function of etchants is to dissolve and thus remove the metal from the working zone by converting it into metallic salts.

The selection of etchant is governed by following factors:

1. Type of the material to be etched.
2. Type of maskant or resists employed.
3. The metal removal rate desired.
4. The operating conditions.
5. The requirements of surface finish.
6. The economics involved in material removal.

Ideal Properties of the Etchant

1. A high etch rate.
2. Generate satisfactory surface finish.
3. Yield minimum undercut.
4. It should be a compatible maskant.
5. It should be cheap.
6. Process parameters should be controlled easily.

7. It should be safe to use.

12.13 Chemical Milling

Chemical contour milling or etching is utilized predominantly in relatively large surface areas to fabricate three dimensional shapes by selective or overall removal of.

12.13.1 Process Steps for Chemical Milling

Chemical milling is the unique invention of the aircraft industries. Chemical milling is the process used to produce parts with exact tolerance by chemical removal of metal using etchant. The chemical milling consists of five main steps.

Precleaning (Figure 12.3a): thorough cleaning is required to ensure the good adhesion of maskant and uniform dissolution of the metals. Different cleaning methods are used. Refractory materials like tungsten are cleaned by wiping with solvent only. It is difficult to clean porous materials because the cleaning solvents get trapped. Generally, cleaning involves: vapor degreasing, alkaline cleaning, and deoxidizing. After cleaning, parts must be allowed to dry.

Masking (Figure 12.3b): the mask is usually applied by dip method, flow coat, or airless spray methods. The type of mask and number of coats depend on size and configuration and material of the part. Aluminum and magnesium are usually given two coats whereas steel is given four or more coats. After the coat is applied, the part is cured for 3–24 h, depending on the size of the part. Suitable curing temperature must be used to get a good masking.

Scribing: the patterns are placed on maskant and scribed using a fine knife. Usually, chemical milling templates are

made of epoxy-impregnated fiberglass, aluminum, or steel. After the part is scribed, the mask is hand stripped. Areas to be milled are exposed to etchant.

Etching (Figure 12.3c): etching for chemical contouring is done by immersion. Sometimes spraying is used. Step etching is done by repeated cycles of scribing and peeling off unwanted mask areas followed by etching. Taper machining is done by immersing or withdrawing the work piece from the etching bath at a controlled slow rate. The positioning of the work piece in the tanks should be such as to prevent the trapping of gases which prevent the chemical attaching by etchant and also reduce the heat dissipation. Etchant used in chemical contouring are similar to those described under chemical blanking. Large quantities of etchants are generally required because of large areas to be machined. Therefore, other factors such as cost of the chemicals, ease of control of regeneration and waste disposal, safety precautions, ventilations and materials for the construction of tanking, and piping are to be considered carefully.

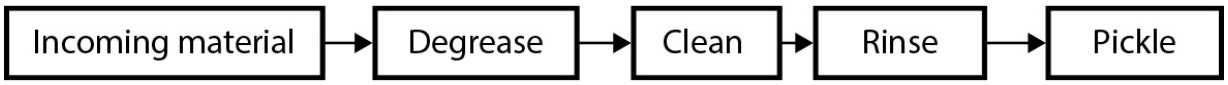


Figure 12.3 (a) Flow chart for precleaning in chemical milling.

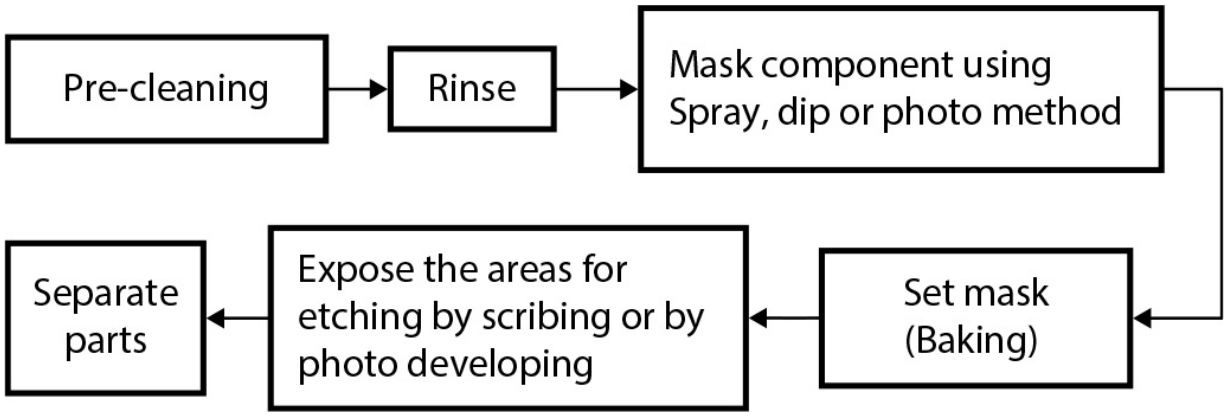


Figure 12.3 (b) Flow chart for masking in chemical milling.

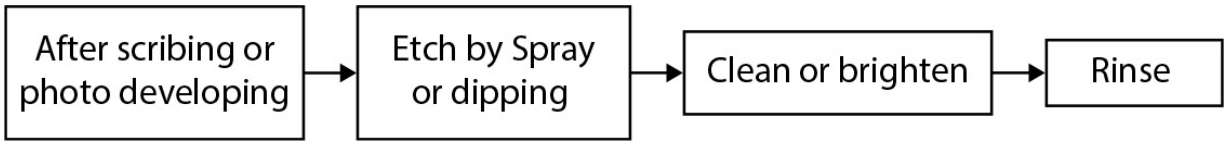


Figure 12.3 (c) Flow chart for etching in chemical milling.

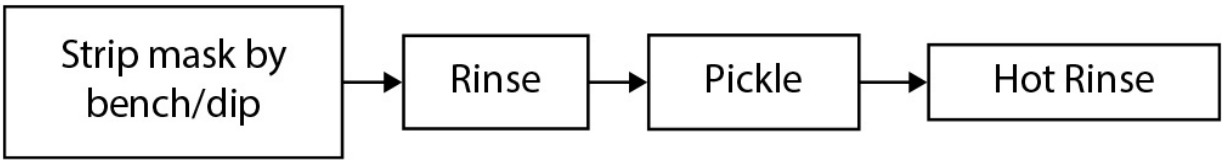


Figure 12.3 (d) Flow chart for demasking in chemical milling.

Demasking (**Figure 12.3d**)**:** mask removal is accomplished by hand stripping or by immersing the masked part in a suitable demasking solution. After the part is demasked, it is cleaned and then inspected.

12.13.2 Process Characteristics

The important process characteristics are:

1. Metal removal rate
2. Accuracy
3. Hydrogen embrittlement

i) Metal removal rate: the rate of material removal is decided by what type of etchant is utilized in the process. Using an etchant with rapid material removal capabilities can have their own side effects.

ii) Accuracy: the undercutting in chemical milling is the same as in a chemical blanking operation. In chemical contouring, the etch factor is defined as the undercut divided by the depth of cut, where depth of cut is approximately equal to undercut per edge.

iii) Surface finish: the surface waviness and defects are smoothened to a certain extent but not greatly modified in its initial state when contouring most metals.

iv) Hydrogen embrittlement: hydrogen embrittlement can occur due to the absorption of hydrogen in chemical machining in certain metals.

12.13.3 Process Parameters of Chemical Milling

1. Depth of cut: cuts up to 50 mm is possible with chemical milling. However, following maximum depths are possible.

   Sheet and plate = 12.5-mm maximum depth/surface

   Extrusions = 3.2-mm maximum depth/surface

   Forgings = 6.3-mm maximum depth/surface

   Usually, depth of cut tolerance is around 0.025 to 0.05 mm.
2. Minimum land width (width of cut): the minimum land width is usually two times the depth of cut.

3. Grain direction: grid pattern should be placed at 45° to grain direction.
4. Surface finish: it depends on the material, heat treatment condition, and depth of cut (Table 12.1).

Stepped sections: stepped sections may be made by progressively unmasking a part. The part may be etched from one side or both sides.

Table 12.1 Surface finish for different materials.

Aluminum	70 to 150 microns
Magnesium	30 to 70 microns
Steel	30 to 250 microns
Titanium	15 to 50 microns

Trim area: while designing, the excess material surrounding the actual part must be integrated into the design.

12.13.4 Applications of Chemical Milling

1. Utilized in the removal of material from parts produced with irregular geometry in processes such as forging, casting, extrusions, or forming.
2. To reduce the web thickness in part, which is difficult to do with conventional machining.
3. Tater sheets and pre-formed shapes.
4. Produce stepped webs.
5. The following parts are manufactured by chemical milling:
    i. Air craft doors and access panels.
    ii. Shells for missiles.

iii. Helicopter blades.

iv. Architectural trim panels.

12.13.5 Advantages of Chemical Milling

1. Parts can be milled from both sides simultaneously. This reduces the warpage, distortion of formed surface, and residual stress.
2. Large pieces can be milled.
3. Overall machining can be reduced by first chemically milling to oversize and then reduce it by conventional methods, as shown in Figure 12.4.
4. Weight of extrusions, forgings, and casting can be reduced significantly using chemical milling.
5. Complicated parts can be milled and it reduces the use of riveting, welding, metal bonding, or additional stiffening.
6. Warpage can be reduced if parts are formed and heat treated before chemical milling.
7. No mechanical work is done on the job surface which offer higher fatigue strength.
8. No burrs are produced in this process.

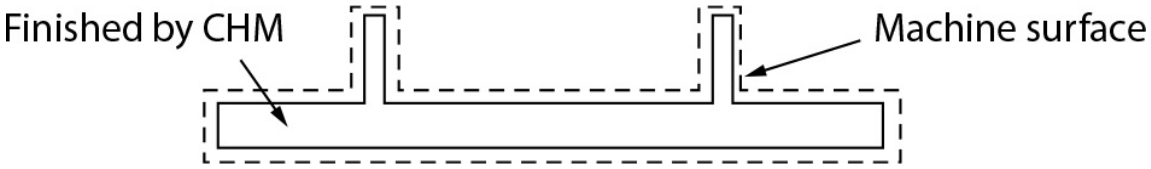


Figure 12.4 Chemical milling of machined surface.

9. Tooling cost is less.
10. Tolerances of 0.075 mm are obtainable in 12-mm depth of cut.

11. Up-supported sections as thin as 0.375 mm can be machined.
12. Parts manufactured by chemical milling do not need subsequent treatment.

12.13.6 Disadvantages of Chemical Milling

1. Fillet radius produced by chemical machining is determined by depth of cut, alloy, etchant, maskant, etc. Sharp cuts are not possible.
2. Porous and heterogeneous material like aluminum are normally difficult to chemically mill.
3. Welded area if milled by chance results in pits and other defects.
4. Some reproduction of surface irregularities, dents, and scratches.
5. Deep and narrow cuts are difficult to make using chemical milling.
6. Larger space area is required for large work pieces.
7. Process is slow and consumes considerable time for removal of large quantities of material.
8. Not suitable for etching holes.
9. Manufacturing cost is high. Depth of cut is limited.
10. Sharp inside radii cannot be generated.
11. Etchant vapors are corrosive.
12. Work material of homogeneous composition and structure are needed.

12.14 Chemical Engraving

Chemical engraving is the use of chemical material removal process to produce parts such as name plates, front panels, and other parts. A sequence of steps involved in chemical engraving is as follows:

1. Image is placed on metal using an acid resistant material which can be screen printed or photographically printed.
2. The part is then etched to the desired depth, rinsed, and dried.
3. Layer of filling material is then placed over the top of resist, either by roller coating spraying, dipping, or flow coating.
4. The resist can be removed by dipping the entire plate in a stripping solution after the filling enamel has dried. Although the filling material is not removed.

Tooling: the tooling required for chemical engraving is either a photographic positive image desired or silk screens with the inverse image of the desired pattern. Silk screens are cheaper.

Tolerances: mechanical tolerances are not tight and easy to control by initial artwork and proper etching time.

Surface finish: an ideal surface finish required is of the order of 500 microns**.**

Applications

1. Chemical engraving is used when a large amount of nomenclature is to be inscribed such as instrument front panels, motor name plates, etc.

2. It is used to engrave hard-to-work material such as stainless steel.
3. Used for engraving highly intricate details and to produce printed circuit boards.

12.15 Photochemical Blanking

A modification of chemical milling, photo chemical blanking applies a resistant mask to the workpiece using photographic technique.

12.15.1 Photo Chemical Blanking Process

It is similar to chemical milling as they both use an etchant.

1. Material is cleaned by degassing, pumice scrubbing, electro cleaning, or chemical cleaning.
2. The cleaned metal is coated with photographic material. The various methods used for coating are dipping, spraying, flow coating, roller coating, or laminating.
3. After coating with resist, it is generally necessary to bake the panel prior to exposing it. This is called prebake. The purpose of prebake is to drive off solvents in simple drying operations.
4. The work is placed between both negatives after it has cooled. Then it is exposed to UV rays in a vacuum.
5. When exposed to UV light, coating becomes hard in unexposed area and soft in exposed area.
6. Developer is used to remove only the soft part of the bake/photoresist.
7. Art work is photographically reduced to expose the photographic resists.

8. The next step is etching which removes the unwanted metal unprotected by the photoresist. Etchant is applied to the workpiece by spraying.
9. Following etching, work is generally washed and dried.

12.15.2 Applications of Photo Chemical Machining (PCM)

1. They are used extensively for thin materials. Thin parts, which are difficult to handle, and die accuracies are difficult to get by conventional mechanical methods.
2. Difficult to punch, hard and brittle materials, can be machined. Such as the material used for springs.
3. Chemical milling is used where absolutely burr-free part is required.
4. It is used in production of extremely complex parts.
5. Products like printed circuit boards, fine screens, and flat springs.
6. Materials such as aluminum, copper, zinc, steels, lead, nickel, and titanium, are processed using PCM.

12.15.3 Advantages of PCM

1. Especially useful for machining thin sheets and materials.
2. Hard and brittle materials can be processed.
3. There is no burr produced in the process.
4. Set up and tooling cost is less. Tool (mask) is made by photographic technique, can be stored easily, and reused many times.
5. The physical characteristics of the materials are not changed.

6. The process allows greater design flexibility.
7. Accuracy and etch rate is more in conventional chemical milling.

12.15.4 Disadvantages of PCM

1. Release of corrosive etchant vapors.
2. Skilled laborers are required.
3. A good photographic facility is essential for developing and printing to achieve part accuracy.
4. Process is relatively slow.
5. Tolerance increases with increase in metal thickness.
6. Sharp radii cannot be produced.

12.16 Worked Examples

1. Chemical milling is used in machining a part made of an aluminum alloy. The thickness is 20 mm. Dimensions 200 mm by 400 mm to be etched. Corner radius maintained to be 15 mm. Etchant used is NaOH. The feed rate is 0.024 mm/min and the etch factor is 1.75. Determine a) the metal removal rate in mm^3/min, b) time of machining, and c) required dimensions of the opening in the cut and peel maskant to get pocket dimension.

Solution

Refer to Figure 12.5.

Initial area would be less than given dimensions of 200 mm by 400 mm.

$$\text{Area} = 200 \times 400 - (30 \times 30 - \pi 15^2) = 80000 - 193 = 79807\ mm^2$$

$$\text{Metal removal rate} = 0.024 \frac{mm}{min} \times 79807\ mm^2 = 1915.4\ mm^3/min$$

$$\text{Time to machine} = \frac{Thickness}{feed\ rate} = \frac{12}{0.024} = 500 min = 8.33\ hour$$

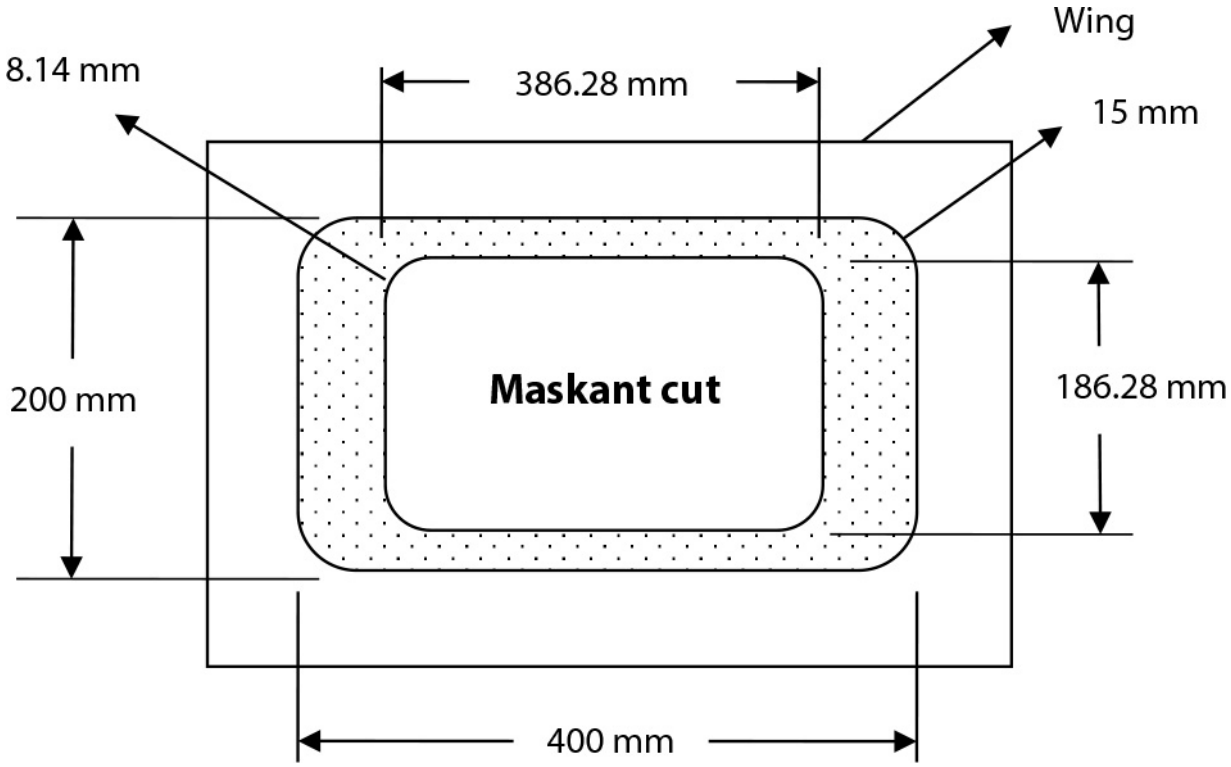


Figure 12.5 Chemical milling of aluminum.

Etch factor =1.75.

$$1.75 = \frac{depth\ of\ cut}{under\ cut}$$

$$under\ cut = \frac{depth\ of\ cut}{etch\ factor} = \frac{12}{1.75} = 6.86\ mm$$

Therefore, maskant opening length = $L - 2u = 400 - 2\times2.86 = 386.28\ mm$

Maskant opening width = $W - 2u = 200 - 2\times6.86 = 186.28\ mm$

Radius on corners = $R - u = 15 - 6.86 = 8.14\ mm$.

References

1. Barr, A.E. and Oliver, D.A., *Electrochemical Machining*, McDonald and Company, USA, 1975.
2. Gunter, D., Photochemical Machining. *Engineering*, 24, 2, I–IV, 1984, London.
3. Snoeys, R., Staelens, F., Dekeyser, W., Current Trends in Non-Conventional Material Removal Processes. *CIRP Ann.*, 35, 2, 467–480, 1986.
4. Taniguchi, N., Current Status in, and Future Trends of, Ultraprecision Machining and Ultrafine Materials Processing. *CIRP Ann.*, 32, 2, 573–582, 1983.
5. Bellows, G., *Chemical Machining*, Machining Data Centre, Metcut Research Associates Inc, USA, 1982.
6. Harris, W.T., *Chemical Milling*, Oxford University press, United Kingdom, 1976.
7. Bisshart, W.C., *Printed Circuit boards – Design and Technology*, Tata McGraw hill publishing house, India,

1988.

8. Jagadeesha, T., *Unconventional machining processes*, I K International Publication House Pvt. Ltd, New Delhi, 2016.

9. Mahamood, R.M. and Akinlabi, E.T., *Advanced non-contact cutting and joining technologies*, Springer Nature, Switzerland, 2018.

10. Bhattacharyya, B. and Doloi, B., *Machining processes utilizing chemical and electrochemical energy*, Elsevier BV, USA, 2020.

11. Youssef, Non-traditional Machine Tools and operations, in: *Machining Technology machine tools and operations*, USA, 2008.

12. Helmi, A., *Machining of Stainless steels and super alloys*, John Wiley, USA, 2015.

13. Gaderer, M., Kunde, R., Brandt, C., *Measurement of Particle Properties, Concentration, size and Distribution and Density*, Wiley, USA, 2010.

14. *Non-Traditional Micro machining Processes*, Springer Nature, USA, 2017.

Note

*Corresponding author: jagdishsg@nitc.ac.in

13
Electrogrinding

Chika Oliver Ujah[1]*, Nebechi Kate Obiora[2] and Daramy V.V. Kallon[1]
[1]*Department of Mechanical and Industrial Engineering Technology, University of Johannesburg, Johannesburg, South Africa*
[2]*Africa Centre of Excellence for Sustainable Power and Energy Development (ACE-SPED), University of Nigeria, Nsukka, Nigeria*

Abstract

Electrochemical grinding (ECG) is a process that combines electrochemical removal with mechanical abrasion to machine various work pieces. This chapter explains the working principles, including electrochemical processes, rotating grinding wheels, and material removal mechanisms. It also discusses operational parameters such as voltage, electrolyte concentration, duty cycle feed rate, electrode temperature, current, and material removal rate. This chapter discusses the various variations of (ECG) that are tailored for specific applications. Electrochemical grinding is used in various industries and has the potential to be used in different applications, which are also discussed in this chapter. The advantages and challenges of this grinding method are outlined, and a comparison is made with other grinding processes. The chapter concludes with a summary of ECG's current state and recommendations for future research.

***Keywords*:** Electrochemical grinding, operational parameters, variations of electrochemical grinding, advantages, challenges

13.1 Introduction

The two production processes, electrochemical machining (ECM) as well as electrical discharge machining (EDM), among the ever-expanding family of new 'non-conventional' machining techniques, have gained greater industrial application in recent years. Electrochemical grinding (ECG) and ECM often have more intricate, challenging, and unpredictable properties than EDM. Therefore, it is not surprising that the technology has not yet reached its ultimate state of development. However, for a significant range of machining processes, both ECM and EDM have established themselves as superior to conventional methods [1]. Electrochemical grinding (ECG) and electrochemical deep grinding (ECDG) are not exactly the same. The anode workpiece undergoes both the ECM process and mechanical grinding at the same time during the ECDG process. The high-speed ECM method helps to considerably enhance the cut-depth without causing any workpiece damage. Scraping the insoluble components and electrolyte product further improves the feed rate and stability of the machining process [2]. Compared to traditional ECG, this dual-action enables deeper material removal in a single pass which is the primary emphasis of ECDG.

13.1.1 Overview of Electrochemical Grinding (ECG)

In the United States, ECG was first employed commercially in 1953 to grind tungsten carbide cutting blades. The aim of this method is to increase the speed of the grinding process and extend the life of the diamond tool, so diamond wheels are required [3]. The machining procedure, ECG uses mechanical abrasive action and simultaneous electrochemical reaction for workpiece material's removal. Large depths of cut reduce generated stress, and increased wheel life are some benefits of this technique over traditional grinding [4]. The essence of applying a hybrid process is to leverage the

advantages that can be enhanced or integrated, and simultaneously prevent some of the negative impacts of applying the different procedures separately [5]. It is used to machine heat-sensitive parts and alloys that are challenging to machine. The ECG procedure can only employ materials that are electrically conductive. Soft materials are not suitable for this technique. For the ECG procedure to be effective, both the part and the abrasive disk must have good conductivity [6]. It follows that ECG cannot be used to machine non-conductive materials efficiently. While the method can remove material up to 10 times faster than traditional grinding for appropriate conductive materials, it is not cost-effective for non-conductive or soft materials [7]. Electrochemical grinding operates at micro- and macro-levels. One of the key categories of operations for the miniaturization of mechanical systems is tool-based micromachining.

13.1.2 Evolution of ECG for Machining

The ECG process was introduced in the USA in the early 1950s. It uses both mechanical and electrochemical action to remove material [1]. Since its introduction in the early 1950s, ECG for machining has evolved, following advances in electrochemical discharge machining (EDM) in the USSR. The cathode was not a tool per se but served as an abrasive electrically conducting grinding wheel [7]. Electrochemical grinding's capacity to generate excellent surface finishes and precise tolerances has made it useful for different industries, aircraft and medical devices' manufacturing [8]. To better understand the process and increase its efficiency, experiments have been carried out on ECG setups by altering the grinding wheel speed, electrolyte concentration, applied voltage, and current (machining parameters) [6]. Hybrid techniques that combine the effects of tool rotation and electrolyte stirring have been introduced recently in ECM, leading to better surface polish and material removal [9].

13.1.3 Comparison Between ECG and Electrochemical Machining (ECM)

There are some similarities among non-conventional machining methods including ECG, EDM, and ECM, but there are also significant differences between them.

These hybrid processes—ECG, EDM, and ECM—offer a number of benefits over traditional machining procedures by combining ECM with other machining techniques. Table 13.1 shows comparative analysis of electrochemical grinding (ECG), electrochemical machining (ECM) and electrical discharge machining. Numerous applications can benefit from these procedures due to their increased material removal rates, longer tool life, and capacity to machine tough and challenging materials. The need for conductive work pieces and tooling materials in ECG, the narrow range of materials available in EDM, and the lower accuracy in ECM as compared to conventional grinding are some of the drawbacks and restrictions for each technique.

Table 13.1 ECG, ECM, and EDM process comparison.

Processes	ECG	ECM	EDM
Material removal	Electrochemical and mechanical reactions	Electrochemical processes	Thermal energy based machining
Tooling	Rotating abrasive wheel	Tool shaped inversely to the desired geometry	Electrolyte and workpiece
Process parameters	– Supply voltage – Flow rate – Concentration of electrolyte	– Speed of feeding of the drill – Concentration of the electrolyte – Voltage for working – Speed of flow of the electrolyte	– Machining voltage – The electrolyte concentration – The speed of advance of the electrode tip- the electrolyte temperature

13.2 Electrochemical Grinding Operational Parameters

Chemistry and electricity are two intriguing fields that come together in electrochemical technologies for different applications to generate tailored results like water purification, waste water treatment, and other environmental sanitation related processes [10]. These fields inform the parameters on which the entire procedure lies. The entire ECG is influenced by chemistry and electricity which synergize to achieve the mechanical process of grinding. Some of these parameters are discussed below.

13.2.1 Machining Voltage

Voltage is a critical factor in ECG that influences the material removal rate and overall process efficiency. Although it usually ranges from 7–12 volts, the voltage utilized in ECGs can range from 1 to 20 volts [11]. An increased voltage tends to lessen the abrasive action and emphasize the electrochemical component more. On the other hand, lower voltages can make the process more abrasive. Arcing can occur from excessive voltage, which can be harmful to the machining process [12]. The ideal voltage is determined by the particular material and process specifications. For example, one investigation showed that when the application voltage was raised from 6 volts to 30 volts, the ablation speed and peak achievable flow rate significantly enhanced, rising from 25.8 mg/min to 85.8 mg/min and from 0.7 mm/min to 6.5 mm/min, depending on the application [13]. For this reason, ECG carefully monitors and modifies the machining voltage in order to maximize material removal rate, preserve process stability, and guarantee the required surface finish.

13.2.2 Electrolyte Concentration

Electrolyte concentration is a crucial element in ECG since it impacts material removal rate (MRR) and overall process efficiency. The electrolyte concentration determines how much electrochemical activity is present in relation to abrasive action during the process [14]. An elevated concentration of electrolytes results in a rise in MRR [15]. Research revealed that when the electrolyte's NaCl content rises, the material removal rate does as well [16]. The ideal electrolyte concentration, however, varies depending on the particular material and process needs.

13.2.3 Duty Cycle

Duty cycle is a term used to describe the proportion of the pulse-on to pulse-off time duration during the ECG process. Lower electrical energy consumption during material removal leads to less electrochemical action and more abrasive action during the operation; a shorter duty cycle reflects this concept [17]. The duty cycle is closely correlated with the quantity of workpiece material removed during the process. Nevertheless, the ideal duty cycle is contingent upon the particular material and process requirements. A duty cycle of 70% produced the highest material removal rate, according to research on electrochemical milling [18]. By adjusting the duty cycle, the ECG process can achieve maximum energy efficiency, which could result in energy savings and increased process sustainability.

The duty cycle, which shows the percentage of the entire cycle duration that is completed on time, is an important quantity in ECG. It is defined mathematically as [19]:

$$Duty\ cycle = \left(\frac{On\ time}{Off - time + On\ time} \times On\ time \right) \times 100\%$$

13.2.4 Tool Feed Rate

In ECG, tool feed rate is a crucial process variable that influences both machining efficiency and MRR. The MRR and machining efficiency can be greatly increased by using appropriate high electrode advance rates [13]. The ideal tool feed rate is determined by the particular material and process requirements. According to one study, aluminum work pieces had the maximum MRR when cutting speed was 0.15 mm/min [6]. Applied voltage, electrolyte temperature, and duty cycle could also affect the optimal feed rate.

13.2.5 Temperature of the Electrode

The electrode temperature is an essential process variable in ECG. The electrode's temperature influences electrochemistry speed; this has an effect on the material abrasion rate and the polishing of the surface. A number of factors, such as flow rate, and electrolyte concentration affect the temperature of the electrode, voltage, and current density. Elevated electrode temperatures may result from high current densities and low electrolyte concentrations, thereby causing heat damage to the workpiece and decreasing process efficiency. For the ECG to function at its best and prevent thermal damage, it is crucial to monitor and regulate the electrode temperature [20, 21].

13.2.6 Current

Electrochemical grinding relies on current as an operating parameter to influence machining efficiency and MRR. The ideal current depends on the material and process requirements, with a study that shows that increasing the level of power densification will result in a greater MRR [20]. The surface roughness of the part is determined by the electrical discharge. Variations in surface polish may result with higher current densities because of factors like gas dispersion and the Joule heat generated during the ECG process [22].

13.2.7 Material Removal Rate (MRR)

As a vital part of electrochemistry, Faraday's second law of electrolysis applies to ECG procedure. It states that the amount of electricity flowing through the electrolyte is directly proportional to the mass of ions deposited at the electrodes. This law is important when it comes to ECG since it controls the rate at which material is removed. So, the amount of material removed is proportional to current that is passed.

13.2.7.1 Mathematical Correlations of Material Removal Rate Due to Abrasive Process in ECG

The whole volumetric material abrasion will be accomplished because ECG combines traditional machining with electrochemical operations. This is because it is expected that the mechanical and electrochemical removal processes will happen independently in ECG.

i. The total material removed is given as [19]:

$$m = m_m + m_{ec}$$

Where, m_m is material removed from the conventional mechanical machining and m_{ec} is material removed from the electrochemical process. A greater percentage of material removal occurs through the electrochemical actions that occur on anode/cathode. There are various factors that influence the material abrasion efficiency in ECG, like density (which is directly correlated to the amount of material ablated), current (which is linearly dependent on the material ablation speed), applied voltage, feed rate, and electrolyte type.

ii. MRR is defined as [23]:

$$MRR = \frac{GI}{\rho F}$$

Where G is the electrochemical equivalent, I is current, ρ is density of workpiece, F is Faraday constant (96,500 A/s), electrochemical equivalent (G) stands as the proportionality constant and can be mathematically expressed by the second Faraday's law as:

$$\mathrm{G} = \frac{Atomic\ weight}{Anode\ material\ Valency}$$

These parameters require optimization to increase effectiveness and performance of this machining process.

iii. Electrochemical disintegration versus ablation speed: the material ablation speed as a function of dissolution can be expressed in g/min as [24]:

$$Mec = \frac{M_a^{\bullet}}{nF} \times I \times 60$$

Where, M_a is anodic materials atomic weight, n is valency of anodic material, I is current, η is efficiency of the current, F is Faraday constant (96,500 A/s).

iv. The volumetric ablation rate, Vm (mm_3/min), may therefore be calculated as follows:

$$\mathrm{Vm} = \frac{M_a I 60 \eta}{nF\rho}$$

It should be noted that $\rho = g/mm^3$.

v. When the over potential at the electrodes, which includes the activation and concentration over potentials is ΔV and the supplied potential is V (volts), the electric current passing through the distance separating the electrodes can be described by the equation shown below:

$$I = \frac{V - \Delta V}{R}$$

The ECG working gap resistivity is denoted by R which is comprised of two components such as the electrolyte layer's ohmic resistance amid electrode spacing (R_e) and resistivity of the anode coating on the electrode plate (R_p).

$$R = R_p + R_e$$

vi. The electrolytic resistance can then be expressed as:

$$R_e = \frac{rh}{A} = \frac{h}{\sigma_e A}$$

Where A is the working range (mm^2), σ_e is the electrolyte conductivity, r is electrolytes-specific resistance (Ω-mm), h is inter-electrode effective cutting distance (mm).

vii. Current per machining unit area that goes through the cutting distance (I/A) is the current density expressed as:

$$J = \frac{(V - \Delta V)\sigma_e}{K_p h}$$

Where K_p is the coefficient that indicates how much of the process takes place in the absence of the polarization phenomenon. The reduction of the working gap voltage reduces the electrochemical decomposition speed due to the perturbation caused by the polarization of the electrode; therefore, this coefficient can also be considered as an energy loss.

viii. Under steady-state grinding conditions, the velocity or rate, in VT (mm/min), of the anode's galvanic corrosion current towards the catalyst can be estimated as follows:

$$v_t = \frac{60 M_a (V - \Delta V)\sigma_e \eta}{nF\rho K_p h}$$

The rate at which metal is removed by ECG relies on different factors like the supply voltage, steady state gap, workpiece material, electrolyte, set depth of cut, wheel grain size, and velocity of wheel rotation. The optimal ranges are 800–1600 rpm, 5–7 min^{-1}, and 0.09–0.15 mm/min for the grinding wheel's rotation, the feed speed of the electrode or the feed speed of the mold [13]. As the current supplied rises, the MRR rises, wheel rotation speed, electrolyte feed rate, or workpiece feed rate decreases with a decrease in these parameters [25]. More electrochemical activity and less abrasive force are produced by a slower feed, whereas more abrasive action is produced by a faster feed.

ix. Material removal rate in relation to mechanical grinding: the amount of metal removed by mechanical grinding is directly correlated with the material's penetration velocity and machining area, M_m (g/min); the MRR, could be written as [24]:

$$M_m = \rho f B d_s$$

Where ρ is material density (g/mm^3), d_s is depth of cut, f is feed speed (mm/min), B is cut width.

x. Feed rate in ECG caused by mechanical action is calculated by:

$$f = Z_t t_z$$

Where Z_t is the quantity of grains that are subjected to abrasion, and t_z is the thickness of the layer that is abraded during the operation. It has been established that ECG is specially designed for hard and difficult to machine metals and alloys. High entropy alloys like titanium-based alloys, which perfectly fit into this description [26], have been studied with recourse to the application of ECG. Owing to titanium's low electrical conductivity, alloying elements (metals with better electrical conductivity) are electrically removed using ECG, while titanium is mechanically removed through the same process [27]. This study clearly reveals the combination of mechanical and electrochemical procedures involved in ECG. Since mechanical abrasion and electrochemical dissolution are two methods of material removal used in ECG, the overall material removal rate of the ECG procedure equals the sum of their respective MRRs.

13.3 Process and Working Principles of Electrochemical Grinding

The diagram of basic operation principles of ECG is shown in Figure 13.1 [28].

Combining the efficiency of electrolysis with a conventional grinding wheel is the principle that drives the hybrid process of ECG [28].

13.3.1 Electrochemical Processes

To complete the electrical circuit and facilitate the electrochemical processes that occur throughout the process, the workpiece in addition to the grinding wheel are immersed into an electrolyte fluid, usually sodium chloride or sodium nitrate [29]. When the electrolyte solution is connected to an electric current, electrochemical oxidation and reduction take place on the surface of the electrode [30]. The electrochemical process precisely shapes and finishes the workpiece by combining anodic material disintegration with mild abrasive action [12].

Dissolution in ECG must be strictly limited to the places that need to be machined. Consequently, it has been discovered that pulse current, as opposed to continuous current, enhances the ECG procedure. Anode dissolution that is more localized minimizes dissolution at nearby locations. In addition, maintaining equilibrium between mechanical and electrochemical processes in a traditional ECG is crucial, if challenging. Since pulse ECG offers a wide range of duty cycle and pulse on-time options, it can adjust the ratio of electrochemical to mechanical movements more easily than a conventional ECG. Surface polish is improved and overcut is decreased by increasing the duty cycle and pulse off-time [31, 32].

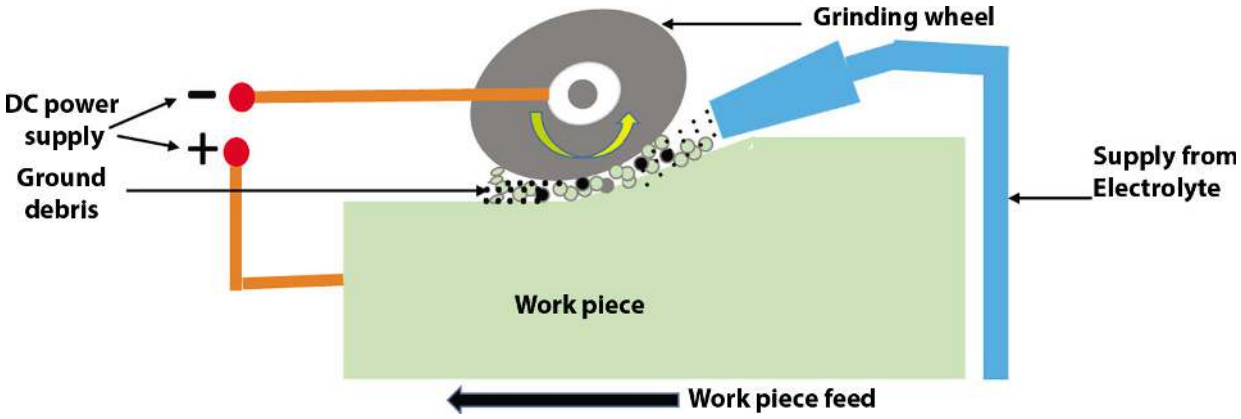


Figure 13.1 Schematic view of the working principle of ECG.

13.3.2 Rotating Grinding Wheel

The bonding material used in the production of ECG wheels is nickel, brass, copper, or copper-impregnated resin. Electrochemical decorated anodic dissolution is used on metal-bonded wheels, in which the wheel serves as the anode and the scrap metal as the cathode. Abrasive particles are used as cutting instruments, and mechanical abrasion is used in order to get rid of the coating of oxide on the workpiece [20]. Oxide layers can be removed from the workpiece's surface by the grinding wheel's abrasive action since it is coated in materials that are abrasive, like aluminum oxide or diamond [25]. The problem of corrosion due to ECG usually arise from grinding issues between grinding wheel and the material to be ground. During fabrication of parts in ECG set up, for example, metals like aluminum or its oxides, their corrosion properties can be improved using carbon nanotubes [33].

13.3.3 Material Removal

Through the grinding wheel's electrochemical reaction with abrasive and the workpiece, material is removed using electrical energy in the ECG procedure. As a result of its great efficiency and affordability, ECG is especially well-suited for challenging-to-machine materials like GH4169 alloy [34]. Electrochemical grinding entails the anode workpiece being dissolved quickly by ECM and a significant amount of electrolytic products adhering to the machined surface [2]. When a higher current is supplied, a higher current density causes more energy to reach the electrode surface in an equivalent period of time. The removal of the substance proceeds more quickly as a result. This is beneficial since the machining times are reduced. Conversely, an excessively high current density could impede the surface's quality [35]. It is crucial to plan the ECG operation such that the region where the wheel and the workpiece is will be as big as feasible in order to optimize the rate of material removal for a certain current density. The electrolyte's overheating serves as a constraint on this area. The average contact-arc length ranges from 19 to 25 mm, depending on the kind of electrolyte utilized [3].

13.4 Components of Electrochemical Grinding Machines

Figure 13.2 shows the various components that ECG machining is comprised of. The major components include: the electrolytic tank, power supply, grinding wheel (cathode), work piece fixing table, workpiece (anode), and collection tank [37].

13.4.1 Conductive Grinding Wheel

This negatively charged wheel removes material from a conductive workpiece by working with an electrolyte. Copper, bronze, or brass are examples of materials that can be used to make the conductive binder that makes up the grinding wheel. Non-conductive abrasive grit particles, like diamond or alumina, are present in this binder. The electrochemical process, which is produced by the combination of the conductive wheel and the electrolyte, is useful for cutting materials that are generally challenging to cut with traditional techniques [8, 14, 36].

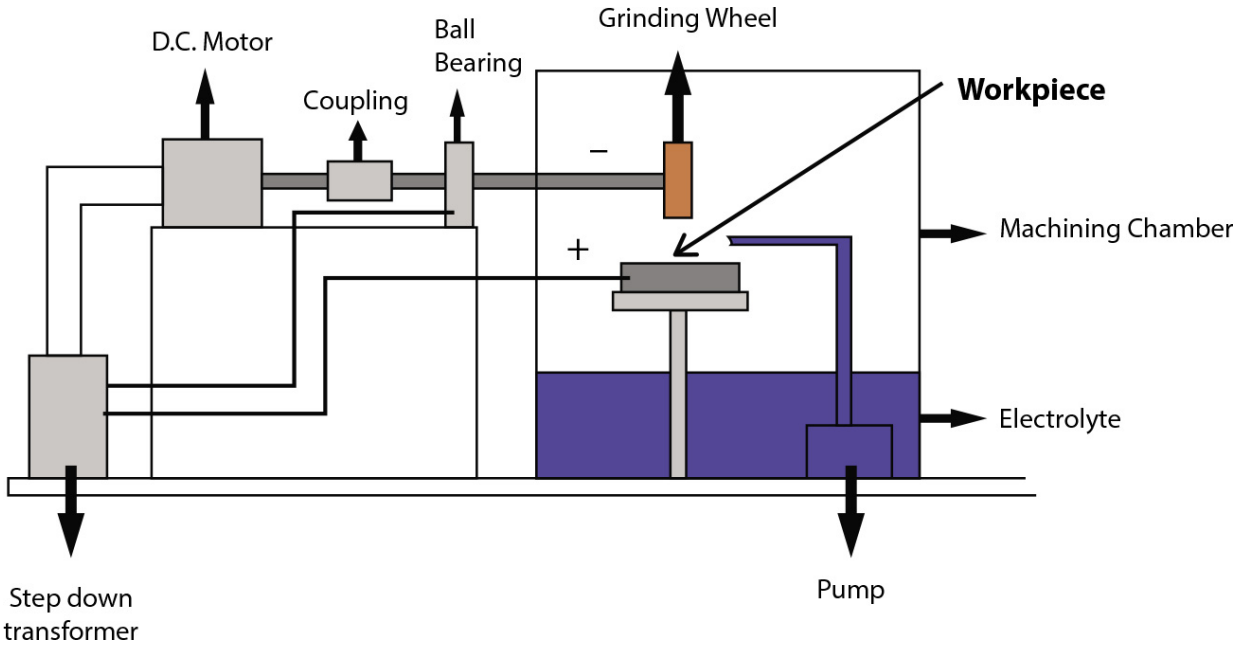


Figure 13.2 Electrochemical grinding machining (ECG) design components. Adapted with permission from Elsevier, 2020 [6].

The conductive workpiece serves as the anode and the electrically conducting abrasive grinding wheel as the cathode. This component is what differentiates the ECG from other ECMs where it serves as an actual working tool rather than an electrode specially designed for a unique purpose [37]. The effectiveness and efficacy of ECG operations are greatly influenced by the conducting element inside the grinding wheel as well as other wheel parameters [38].

13.4.2 Electrolyte Fluid

Between the revolving workpiece and the grinding wheel's abrasive, an electrolyte is introduced into the small space. Through abrasion and electrochemical attack, metal is extracted from the electrically conducting workpiece [36]. Similar to its effects in ECM, pulsating electrolyte flow in ECG may have an impact on the surface profile, heat transfer, and material removal rate [39]. Considering the amount of charged ions required for electrochemical processes, increased electrolyte flow rates result in higher MRR. Turbulence from wheel/ workpiece rotations can affect machined component's accuracy and MRR. Conversely, low flow rates can decrease shear pressures at wheel/workpiece interfaces, negatively impacting MRR and hydroxide reaction product elimination. Therefore, balancing MRR and turbulence effects requires careful consideration of electrolyte flow rate impacts [40]. Table 13.2 shows the type of electrolytes used by different workpieces.

In order to mill ferrous, nickel, and cobalt alloys, NaCl is a useful electrolyte, but its aggressive anodic dissolution and corrosion make it unsuitable for certain applications. To address these issues, tungsten carbide and other alloys use $NaNO_3$ (sodium nitrate), supplemented with additives like chelating agents and rust inhibitors to create bonds with individual metal ions [20].

13.4.3 DC Power Supply

The required electrical energy for the ECG procedure is provided by a direct current (DC) power supply. A crucial factor in influencing the efficiency of the ECG process and the pace of material removal is the voltage that the workpiece and the grinding wheel need to receive from the DC power source in order for them to undergo an electrochemical reaction [13]. Electrochemical reactions can take place on the workpiece's metal surface since the DC power source gives the setup low voltage and high current. The strong current encourages quicker material removal while the low voltage prevents excessive heat development and ensures safety. An electrolytic cell is created by connecting the negative-charge grinding wheel and the positive-charge workpiece to the DC power supply [41]. The phenomena of electrochemical overcut can be efficiently controlled in ECG by using a DC pulse power supply [42]. Overcut is the term for inadvertent material removal or deviance from the intended machining profile brought on by electrochemical activity in ECG. Every input parameter in an ECG, including feed rate, depth of cut, wheel characteristics, input voltage, current density, and electrolyte properties, affects overcut. The goal of almost all ECM tool design methods is to reduce overcut in the process [19].

Table 13.2 Electrolytes and the corresponding materials they grind in ECG.

Source: Reference [19].

Electrolyte type	Appropriate materials for grinding
Sodium chloride (NaCl)	Ferrous alloys Cobalt alloys Nickel alloys
Sodium nitrate ($NaNO_3$)	Titanium alloys Nickel alloys
Sodium carbonate (Na_2CO_3)	Brass Bronze Magnesium alloys
Sodium sulfate (Na_2SO_4)	Low carbon steel Cast iron
Potassium hydroxide (KOH)	Tool steels High strength steels
Sodium hydroxide (NaOH)	Copper Aluminum alloys Molybdenum
10% HF + 10% HCl +10% HNO_3	Titanium alloys

13.4.4 Pump and Filter

The complexity and design of filters utilized in ECG systems can differ. Depending on the precise impurities that must be eliminated and the required level of electrolyte purity, they can range from straightforward mesh filters to more sophisticated systems like cyclonic separators or magnetic filters. Electrochemical machining involves the supply and purification of an electrolyte between the workpiece and tool. The pump and filter system supply and purify this conductive fluid, aiding in the material's electrochemical

dissolution. The pump distributes the electrolyte at high pressure and flow rate for effective material removal and cooling. The filter out contaminants to prevent clogging and contamination, influencing the precision and quality of the machining process [43]. The circulation and filtration of the electrolyte fluid are essential to process control because they maintain the proper composition and quality of the electrolyte, which influences the precision and efficiency of the material removal process in ECG [8]. The pump and filter systems ensure that its stability and efficiency are in place.

13.4.5 Pressure Gauge

The pressure gauge helps to ensure that the electrolyte is supplied at an appropriate pressure. It works together with other components like the pump to keep the ECG process optimized [44]. The size and type of the workpiece, the separation between the workpiece and the wheel, and electrolyte concentration all affect the ideal pressure and flow rate [45]. Although pressure gauges might not be a typical part of every ECG setup, they can be useful for monitoring and managing several parts of the machining process. Pressure gauges can help to increase the effectiveness, reliability, and caliber of ECG processes by giving real-time data on variables such electrolyte flow, workpiece clamping, electrode wear, and coolant pressure.

13.4.6 Flow Meter

The flow meter monitors the electrolyte flow in the ECG system. It has various components that affect its performance. Specifications of the centrifugal pump, such as voltage and rotating speed (rpm), are important factors that affect the electrolyte's flow rate and pressure [46]. An essential component of the ECG process's effectiveness is the electrolyte flow. On the one hand, a lot of charged ions are accessible for electrochemical reactions at high electrolyte flow rates, which raises MRR [31]. There are however no specific flow meters for ECG process as it is an innovative field. The choice of flow meter will depend on intended use. For instance, if the electrolytes flow rate is needed, the flow meter that will be suitable for conductive electrolytes could be considered; if the abrasive slurry should be measured, meters unaffected by debris could be preferred. The ability to precisely control and monitor the electrolyte flow rate enhances the effectiveness and caliber of the process, making flow meter a crucial component of ECG.

13.5 Grinding Methods of ECG

Electrochemical grinding is very useful for machining challenging materials, including tungsten carbide, Inconel, Monel, Hastelloy, and stainless steel. The method is well-known for producing exact cuts devoid of heat, stress, burrs, and mechanical distortions, which makes it appropriate for items that need to be highly precise and have a consistent surface, such as those that are delicate or sensitive to heat [47].

13.5.1 Internal Grinding

Electrochemical grinding, or internal grinding, is the technique of utilizing ECG to precisely machine the inside surfaces or bores of a workpiece. The workpiece (the anode) in this particular application is positioned inside an abrasive grinding wheel (the cathode). The area that remains amidst the workpiece and the grinding wheel is infused with a solution of electrolytes. With the use of an electric current, the process combines the mechanical grinding action with electrochemical dissolution to remove material accurately from inside surfaces [23]. Numerous industries, like the automotive, aerospace, and medical device sectors, use internal grinding within ECG. It is especially helpful in the production of parts where internal features and surface quality are crucial, like turbine blades, engine parts, medical implants, and precision molds.

13.5.2 Cylindrical Grinding

In ECG, the term “cylinder grinding” describes the application of ECG techniques to cylindrical workpieces or components. It involves shaping the external diameter of a cylindrical workpiece. In this procedure, the cylindrical surface of the workpiece is cleaned of electrically conductive material using an abrasive grinding wheel equipped with a negatively charged electrode. Precise material removal is made possible by the grinding wheel’s rotation and passage along the cylindrical component’s length.

Electrochemical grinding has an edge in cylindrical grinding because it can create intricate cylindrical test specimens from new high-temperature materials [21]. With this procedure, you can achieve higher precision and efficiency by combining aspects of electrochemical metalworking. Internal cylindrical plunge electrochemical grinding (ICPECG) can be challenging in terms of calculating the MRR because of its complex structure [42]. Notwithstanding the difficulties, the combination of cylindrical ECG’s mechanical and electrochemical operations provides creative ways to machine complex cylindrical components.

Other grinding processes possible with ECG include: face grinding: where the workpiece’s flat surface is polished smooth by using a grinding wheel to remove material, form grinding: where the workpiece is shaped into a desired shape or form using a grinding wheel, and surface grinding.

13.6 Variations of Electrochemical Grinding in Research Stage

Different variations of ECG are being proposed and modified to meet different requirements and address the limitations of existing ECG procedures.

13.6.1 Wire Electrochemical Grinding

Wire electrochemical grinding (WECG) (Figure 13.3) is a novel technique that uses bipolar current and neutral electrolyte to machine tungsten micro rods. With this technology, the tool electrode can be a flowing wire, which eliminates the unavoidable problem of bipolar current-induced tool wear [48]. In contrast to traditional ECG, which employs an abrasive grinding wheel as the cathode, WECG provides a special method for producing intricate and accurate forms in tiny parts. High-precision machining is made possible by the use of wire as the cathode, which makes it ideal for applications needing tight tolerances and excellent surface finishes. This technique has demonstrated potential in the manufacturing of high-precision parts for a variety of sectors, especially in the machining of microscale components.

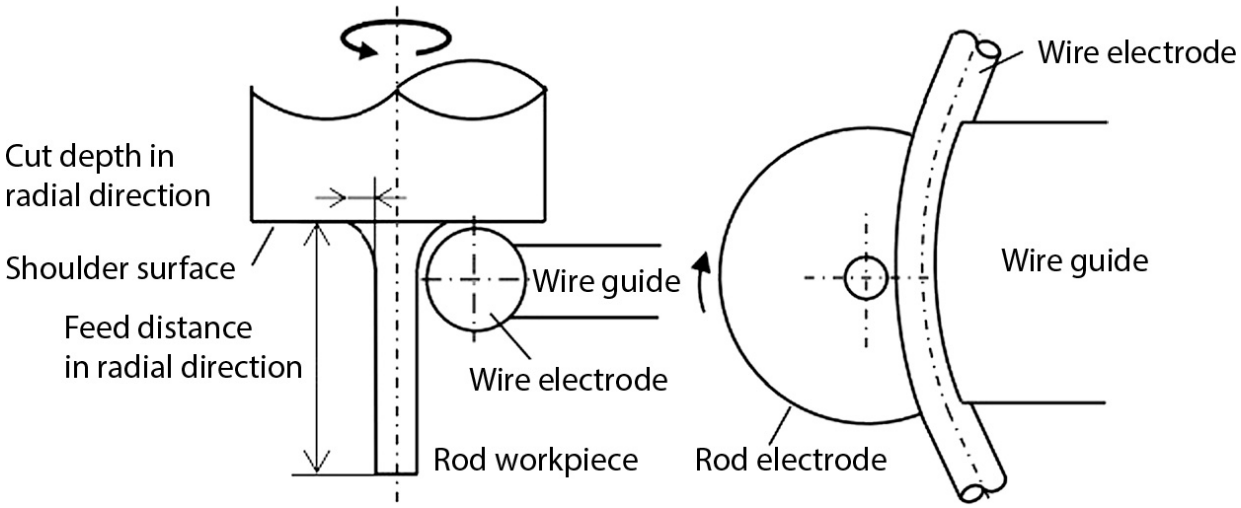


Figure 13.3 Schematic view of wire electrochemical grinding. Reproduced with permission from Elsevier 2018 [48].

13.6.2 Inner-Jet Electrochemical Grinding

Inner-jet electrochemical grinding (IECG) (Figure 13.4) has been researched for use in machining materials that are challenging to work on. Utilizing an abrasive tool flow channel structure predicated on electrolyte exit holes in the sidewall of a dead-end tube, IECG aims to increase machining stability and efficiency while achieving high material removal rates. The technique has been researched for use in the machining of materials like GH4169 alloy SUS420J2 stainless steel, and it has demonstrated a promising result in producing excellent surface finishes and accurate cuts [49, 50]. The technique has received special attention due of its potentials for producing precise parts required in different industries, including the fabrication of medical devices, automobiles, and aircraft components.

13.6.3 Ultrasonic-Assisted Electrochemical-Drill Grinding

Excellent microscopic holes on superalloys are created using a technology that combines electrochemical drilling, ultrasonic vibration, and mechanical grinding, as shown in Figure 13.5. The high-speed spinning electrode in ECG benefits greatly from the application of ultrasonic vibration in relations to machining stability, efficiency, and surface quality [51]. The tool cathode is a ball-end electrode filled with abrasive diamond particles. It rotates quickly and vibrates ultrasonically along its axis. As a result of metal passivation in the passive electrolyte, a gentle passive oxide coating is formed on the material's surface. This negative layer is removed by the diamond abrasives, revealing new metal materials for the electrochemical processes that follow. Materials are removed by this method, which blends grinding with electrochemical processes [52].

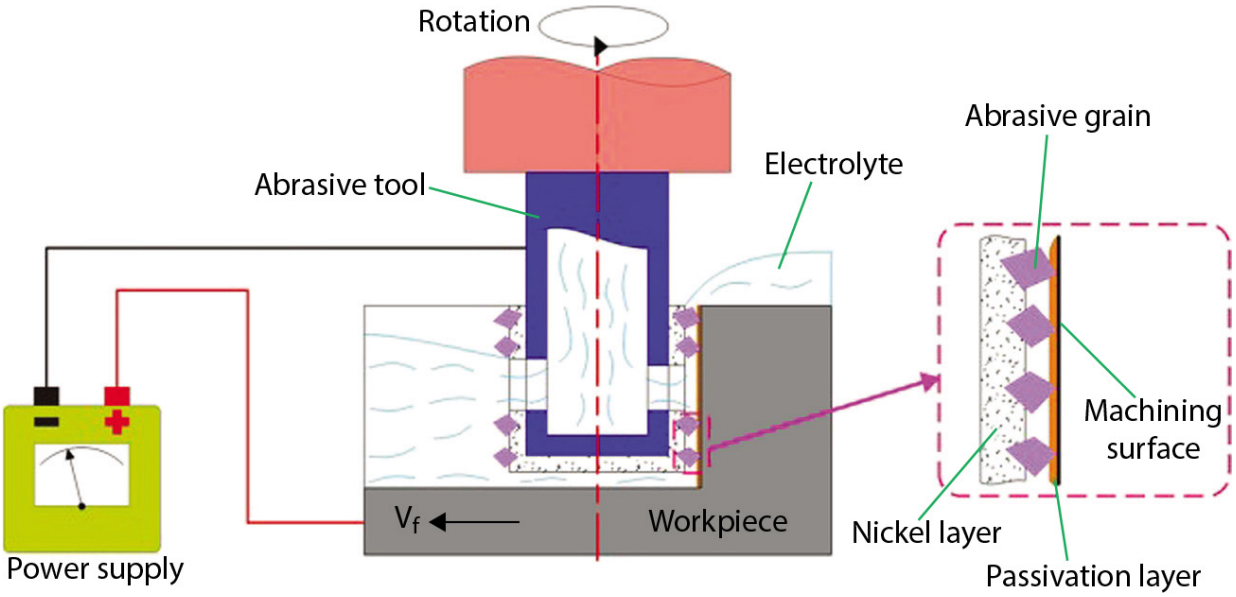


Figure 13.4 Inner-jet electrochemical grinding. Reproduced with permission from Springer Nature 2017 [34].

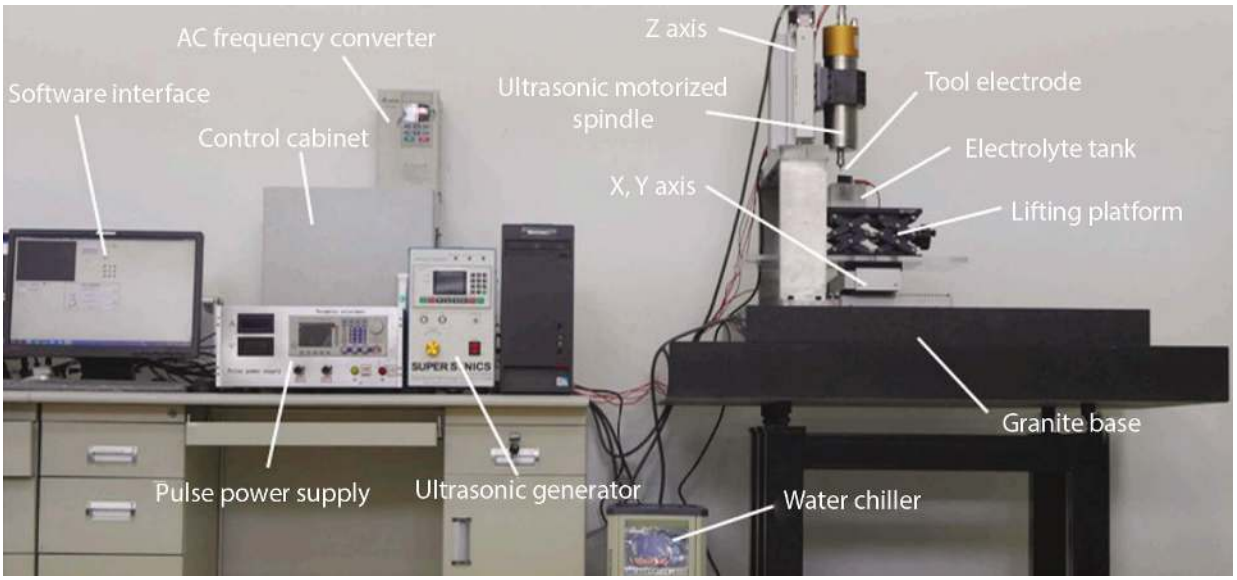


Figure 13.5 Ultrasonic-assisted electrochemical-drill grinding experimental configuration. Reproduced with permission from MDPI, 2020 [51].

13.6.4 Pulsed Electrochemical Grinding

Pulsed electrochemical grinding (PECG) is a unique machining technique that blends elements of traditional grinding and electrochemical machining. When a workpiece material interacts with an electrolyte in PECG, it dissolves electrochemically, which causes the metal removal process to occur. This method is very useful for complex geometries and sophisticated materials because it precisely removes material using intermittent electrical pulses. Pulsed electrochemical grinding has a number of benefits, such as the capacity to machine materials that are difficult to cut and attain high precision with less heat-affected zone [11, 53]. There are two cuts in the process: a high voltage, low feed rate roughing cut (highly abrasive removal and low electrochemical

dissolution), and a low voltage, very quick feed rate finish cut (strong electrochemical action and negligible mechanical contribution) [32]. It was proposed as a solution to the issue of the ECG's inability to be precisely controlled because of the degree of material degradation in the process.

13.6.5 Abrasive Electrochemical Grinding (AECG)

Metal or graphite wheel electrodes, which are utilized in ECG, are sometimes substituted by a grinding wheel with metal bonding in AECG. When this happens, the electrochemical breakdown and mechanical abrasion are coupled [5]. Abrasive electrochemical grinding (AECG) involves submerging a conductive workpiece (cathode) in an electrolytic solution and a conductive grinding wheel (anode). Workpiece dissolution is aided by electrochemical processes that take place at the interface between the workpiece and the grinding wheel when an electric current passes through the system. While this is going on, the workpiece is being worn down by the abrasive particles embedded in the grinding wheel, which removes materials from both mechanical and ECG action [31].

13.6.6 Electrochemical Mill-Grinding (ECMG)

It is possible to manufacture alloys that are challenging to produce by using ECMG, a processing method that merges ECG and electrochemical milling [54]. A simulated ECMG is shown in Figure 13.6. An electrolytic solution is used in ECMG to immerse a stationary workpiece (cathode) and a revolving electrode (anode). Through an electrochemical dissolution process, material is selectively dissolved from the workpiece while an electric current is transferred between the electrode and the workpiece. The combination of the spinning electrode's motion, the electrode and workpiece in relation to one another produces the milling action.

13.6.7 Internal Cylindrical Plunge Electrochemical Grinding (ICPECG)

Internal cylindrical plunge electrochemical grinding (ICPECG) is a method of machining that is used for internal grinding of cylindrical components. The plunge grinding method, which involves advancing the grinding tool radially into the internal cylindrical workpiece, is what distinguishes ICPECG [56]. This method uses an electrochemical procedure to remove material from the inside surfaces of cylindrical workpieces [34]. The principle of operation is presented in Figure 13.7. A conductive grinding wheel is put into the workpiece and an electrolyte is exchanged between it and the workpiece during the process [34]. As a result, the material can dissolve more easily by electrochemistry, removing the material precisely and effectively.

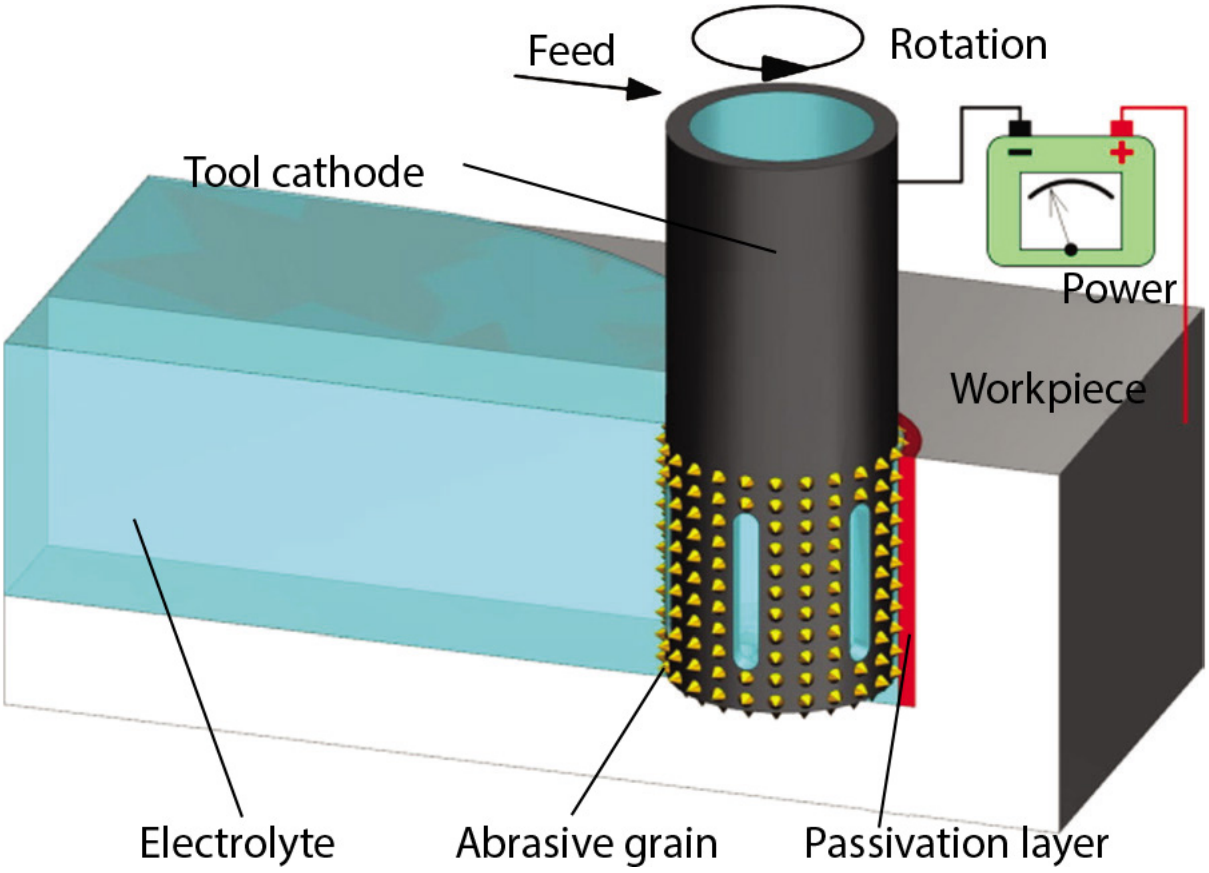


Figure 13.6 Image of electrochemical mill-grinding. Reproduced with permission from Elsevier, 2023 [55].

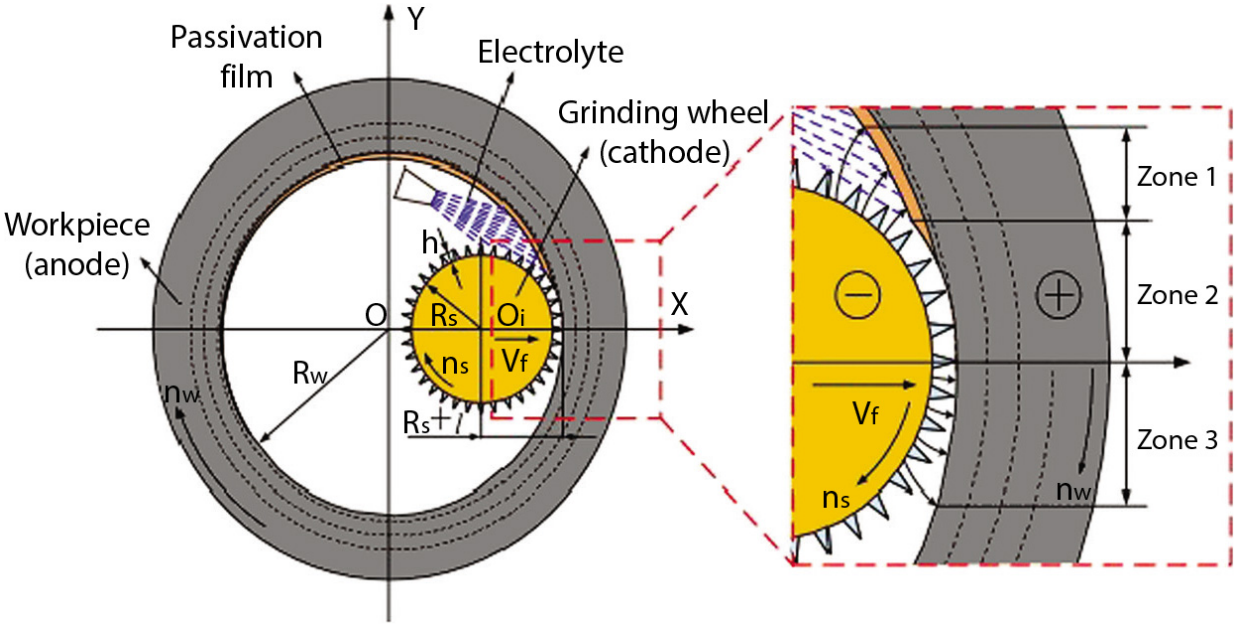


Figure 13.7 Schematic principle of ICPECG. Reproduced with permission from Heliyon 2023 [56].

13.6.8 Electrochemical Face Grinding (ECFG)

Through the operation of an electrochemical action between the wheel's face and the workpiece surface, material can be removed in electrochemical face grinding (ECFG), a variation of ECG, where the tool's disc-shaped axis is perpendicular to the workpiece area [57]. When it comes to creating thin-walled objects that are challenging to cut, ECFG is a prospective machining technique. However, in the inter-electrode gap the field pattern of the current may alter and the electrochemical levelling effect of the multiple surfaces may be jeopardized during ECFG. The recommendation of superimposing linear and circular translational movements was made for improving the efficiency of electrochemical polishing on several surfaces of the ring [58].

13.7 Industrial Applications of ECG

13.7.1 Grinding High-Powered Blades

Aero engines' blades are crucial parts of the aero engines. During operation, the leading and trailing edges separate and combine airflow, making them essential functional zones. A tiny profile error can have a big effect on the engine's efficiency and aerodynamic performance [59]. Electrochemical grinding as a kind of ECM can be used to finish blades which can be manufactured by the process of ECM. This process is preferred due to its excellent material removal rates and the fact that it leaves no damage from thermal and mechanical processes [60]. Materials that are challenging to machine, like titanium alloys and super-alloys based on nickel are used to make aerospace blades [61], and hence, the ECG process is a best fit to achieve both good finishing and dimensional accuracy of the blades. In a US patent, ECG was proposed to be used for super-alloyed turbine blades [62]. This could also apply to every other blade which could find use in high-power industrial applications.

13.7.2 Sharpening Hypodermic Needles

Precision items, like tiny medical tools and parts for medical devices, are made in the medical industries using ECG. Moreover, it is used in the production and upkeep of high-precision medical devices and instruments, giving producers a micromachining choice with more precise adjustment. These hypodermic needles are soft and fragile and ECGs' gentle approach is suitable for this application while leaving it burr free [63]. A novel kind of ECG called electrochemical jet-assisted grinding was proposed for silicon carbides which find its application in semiconductors. It operates with soft abrasion [64] which lowers the risk of overheating and potential damage to the needle. Extremely accurate material removal from the needle tip is made possible by ECG. This accuracy guarantees that the sharpened needle keeps its geometry and structural integrity intact, and these are essential for its operation. The sharpened needle might have a smooth, polished surface as a result of the ECG procedure. In order to minimize tissue stress during injections and guarantee patient comfort, a smooth finish is crucial. A variety of materials, including specialty alloys and stainless steel, are used to make hypodermic needles. Needles composed of these materials can be sharpened by ECG, guaranteeing uniformity in quality and sharpness amongst various kinds of medical needles.

13.7.3 Grinding Tungsten and Carbide Tool Bits

Electrical and electronic engineering depend heavily on ceramic metal tungsten parts because of their stable surface layers and special features. Electrical contacts, temperature compensators, voltage controllers, washers, heaters, rocket engine fuel fittings, and spacecraft descent modules are among the devices that use them. In industry-produced specific units and equipment, ceramic metal-tungsten is finding

increasing use [65]. It can be difficult to handle this kind of material due to its unfavorable physical properties as well as the very high standards imposed by the environments in which products are employed [66]. Electrochemical grinding provides better surface finishes that conventional machining processes cannot handle due to its hardness, brittleness and shape complexity.

13.7.4 Grinding of Cutting Tools

For cutting tools, ECG has various benefits in comparison with traditional grinding methods. Electrochemical grinding is frequently used on hard materials, like stainless steel and certain exotic metals, where traditional machining is challenging. Drills and end mills can be made and re-sharpened using ECG, enabling accurate geometries and longer tool life. In order to ensure constant performance and quality, the technology can also be utilized to produce and recondition inserts used in turning, milling, and other machining operations. Electrochemical grinding can be used to produce unique profiles or specialized cutting tools with intricate geometry to meet a variety of industries' machining needs.

13.7.5 Production of Thin-Walled Tube

Electrochemical grinding is also used in the production of thin-walled tubes [31]. One kind of ECG that shows promise for producing thin-walled parts that are challenging to cut is electrochemical face grinding technique [58]. Electrochemical grinding is a highly beneficial method for manufacturing thin-walled tubes due to its low heat generation, precise results, burr-free finishing, and versatility in handling intricate geometries. Electrochemical grinding is projected to be used more frequently in the manufacturing of thin-walled tubes across various sectors due to its distinct advantages and capabilities.

13.7.6 Aerospace

Electrochemical grinding is frequently used in the aerospace sector to cut materials that are challenging to manufacture, like stainless steel, exotic metals, and high-temperature alloys [29]. Turbine blades are components of an aircraft and ECG is advantageous in its finishing. Other components that require high precision are landing gears, wing assemblies, fuel nozzles, etc. Furthermore, in order to remove surface imperfections, ECG is used in the re-profiling of locomotive gears, the elimination of fatigue fractures in submerged steel constructions, and other locations where significant material loss and residual stress are unwanted [14]. Electrochemical grinding's material removal method is highly efficient and reduces waste, which is in line with the aerospace industry's emphasis on resource optimization and sustainability. Electrochemical grinding shows itself to be a practical and beneficial machining technology in the aerospace industry, where performance, precision, and durability are indisputable requirements. Aerospace producers can achieve strict quality standards and ensure durability, efficiency, and safety in aerospace components by utilizing ECG's capabilities to make its devices.

13.7.7 Bearing Raceways

Electrochemical grinding has been effectively used for internal grinding of bearing raceways when combined with plunge machining [56]. The method offers a practical means of resolving the inability of the traditional grinding method to satisfy raceway's requirements, like precision and excellent surface condition, besides optimal efficiency. High carbon chromium (GCr15) bearing steel is a common material used for bearing ring forging. It has a high contact fatigue performance, isotropic high hardness, low alloy content, and good wear resistance following tempering and quenching [67]. Electrochemical grinding helps to machine this hard, difficult to machine material.

13.7.8 Energy Sector

Energy-related components like solar panels, wind turbine parts, and fuel cells frequently need to have specific materials machined to a high degree of accuracy. Electrochemical grinding is a good option for the energy sector since it can machine these materials without causing heat damage or stress. Battery electrodes can be precisely machined and refined using ECG, which guarantees even thickness, ideal surface characteristics, and improved electrochemical performance. The method can also be used to create capacitor plates with intricate features and complex geometries, which will enable quick charge-discharge cycles and effective energy storage. Energy storage device current collectors and connectors can be made with ECG, which guarantees stable electrical connections, low resistance, and long-term durability.

Table 13.3 Advantages and challenges of electrochemical grinding.

Advantages	Challenges	Reference
Electrolyte serve as coolants for friction between grinding wheels and workpiece.	Environmental toxicity of electrolytes and fumes.	[27]
Efficient material removal.	Material removal rate is low (15 mm/s).	[43, 68]
Low-induced stress.	Requires precise control of voltage and electrolyte temperature.	[4]
No metallurgical damage to workpiece.	Corrosion of workpiece and grinding wheels due to electrolytic fluid.	[69]
Low cost of maintenance in comparison with traditional grinding processes.	Requires frequent changing of electrolyte.	[70]
Low-heat generation.	Limited to surface parts.	[14]
Stress-free process of machining.	Large setup space requirement.	[8]

13.8 Advantages and Challenges of Electrochemical Grinding

Electrochemical grinding is a key technology in the field of advanced manufacturing processes. It combines the advantages of ECM with conventional grinding techniques. There are, however, exigencies related to ECG process optimization, highlighting the need for careful parameter calibration, particularly in applications requiring strict performance attributes. Table 13.3 summarizes the advantages and limitations of ECG.

13.9 Grinding Processes

Other grinding techniques besides ECG are employed in a variety of applications. Several of these procedures are:

Table 13.4 Comparison of ECG with other grinding processes.

Source: Reference [24].

Characteristics	Electrochemical grinding (ECG)	Conventional grinding	Abrasive flow machining (AFM)	Water-jet machining
Material removal mechanism	Mechanical abrasion and electrolytic dissolution	Abrasive grains causing mechanical abrasion	Flowing abrasive slurry causing mechanical abrasion	High-pressure water jet with or without abrasives
Suitable materials	Conductive materials (metals and alloys)	All materials	Hard and brittle materials, slurry compatible materials	All materials, limited by surface quality and pressure
Advantages	– Precise material removal – Low heat generation – Burr-free finish – Good for complex geometries – Can handle brittle materials	– Simple and versatile – No conductive requirements – Large variety of materials	– Good surface finish – Low environmental impact – Suitable for fragile materials	– No tool wear – Reaches inaccessible areas – Low heat generation
Disadvantages	– Limited to conductive materials – Requires electrolyte handling – Slower material removal rates – Higher initial setup cost	– High heat generation – Tool wear and dressing required – Rougher surface finish	– Restricted control over geometry – High slurry consumption – Potential for environmental hazards	– High capital cost – Complex setup and process control – Rougher surface finish on some materials
Applications	– High-precision parts – Medical devices	– General machining – Deburring – Finishing – Gear shaping	– Finishing of brittle materials – Micromachining – Glass shaping – Biocompatible device creation	– Composite cutting – Delicate material removal

Characteristics	Electrochemical grinding (ECG)	Conventional grinding	Abrasive flow machining (AFM)	Water-jet machining
	– Aerospace components – Bearing railways – Cutting tool sharpening	– Mold and die making		– Sign cutting – Food processing

13.9.1 Conventional Grinding

This method is frequently used to polish and grind a large variety of materials, from metals to ceramics to composites. Material is ground off the surface of the workpiece using a rotating grinding wheel.

13.9.2 Abrasive Flow Machining (AFM)

For this method, material is being abraded away from the component face using a fluidized bed of abrasive particles. It is suitable for large workpieces and can handle a wide range of materials.

13.9.3 Water-Jet Machining

With this non-contact technique, material is removed off the workpiece's surface using a high-pressure water stream. It can produce accurate cuts without producing heat or causing mechanical deformation, making it appropriate for fragile materials.

13.9.4 Laser Grinding

In this technique, material is ground from the workpiece's surface using a laser beam. It has great precision and adaptability, making it possible to machine intricate forms and sizes. Electrochemical grinding is compared with other grinding processes in Table 13.4.

13.10 Summary and Recommendation

We reviewed the intricacy of contemporary machining techniques in this chapter, focusing on ECG. Electrochemical grinding is a cutting-edge machining technique that merges electrochemical processes with traditional grinding. A DC voltage is applied between a non-conductive workpiece and a conductive grinding wheel in this process. Compared to traditional grinding techniques, this approach produces a smoother surface finish by removing material via anodic dissolution. Reduced mechanical stresses, a small heat-affected zone, faster material removal rates, and the capacity to machine hard materials and complex geometries are just a few benefits that come with using ECG. Due to its accuracy and efficiency, the method is widely employed in various industries, including aerospace, electronics, automotive, and medical.

Electrochemical grinding has a clear advantage over many conventional machining and grinding methods because it can machine electrically conductive materials more precisely, especially for components with complex geometry and intricate structures. With the least amount of tool wear and heat damage due to its special feature, ECG can accomplish exact tolerances, smooth surface finishes, and effective MRR. Additionally, ECG can be very helpful when processing hard and challenging-to-machine materials, like heat-treated steels and superalloys, where traditional machining techniques could be less

efficient or not feasible. As a result of its greater adaptability, accuracy, and efficiency, ECG is therefore a strong competitor for applications in advanced manufacturing.

References

1. Furtak, T.E., Electrochemical surface science. *Surf. Sci.*, 299–300, C, 945–955, 1994, doi: 10.1016/0039-6028(94)90708-0.
2. Ge, Y., Zhu, Z., Wang, D., Zhu, D., Study on material removal mechanism of electrochemical deep grinding. *J. Mater. Process. Tech.*, 271, April, 510–519, 2019, doi: 10.1016/j. jmatprotec.2019.04.033.
3. Brooks, A.J., Electrochemical grinding of ceramic form tooling. *J. Mater. Process. Tech.*, 55, 70–75, 1995.
4. Qu, N.S., Zhang, Q.L., Fang, X.L., Ye, E.K., Zhu, D., Experimental Investigation on Electrochemical Grinding of Inconel 718. *Procedia CIRP*, 35, 16–19, 2015, doi: 10.1016/j. procir.2015.08.055.
5. Kozak, J. and Skrabalak, G., Analysis of abrasive electrochemical grinding process (AECG). *Lect. Notes Eng. Comput. Sci.*, 2, 1147–1152, 2014.
6. Bhuyan, B.K., Garg, C., Gupta, L., Design and development of tabletop electrochemical grinding setup. *Mater. Today Proc.*, 21, 1479–1482, 2020, doi: 10.1016/j.matpr.2019.11.058.
7. Thorat, S., *Electrochemical Grinding - Diagram, Working, Advantages and Applications*, 2022, [Online]. Available: https://learnmech.com/electrochemical-grinding-ecg-advantages-and-disadvantages/.
8. *Electrochemical Grinding- Components, Working, Advantages, Uses*, Testbook Edu Solutions Pvt. Ltd, India, 2023, [Online]. Available: https://testbook.com/mechanical-engineering/electrochemical-grinding.
9. Singh, G., Sudhakar Rao, P., Singh, R., Electrochemical Machining Process Using Different Electrolytes for Improved Process Efficiency. *E3S Web Conf.*, 391, 1–10, 2023, doi: 10.1051/ e3sconf/202339101168.
10. Sodokin, R.N.D., Ujah, C.O., Von Kallon, D.V., Production of Cooking Gas through Electrochemical Decomposition of Organic Matter. *IJHEHAR* 2, 2, 95–120, 2023.
11. Kirk, A., *Manufacturing Gears With Pulsed Electrochemical Machining (PECM)*, Voxel Pixel Perfect Machining, USA, 2021, [Online]. Available: https://www.voxelinnovations.com/post/machining-gears-with-pecm.
12. J.J., *The Complexities of Electrochemical Grinding - Metal Cutting Corporation*, Metal Cutting Corporation, New Jersey, 2021, [Online]. Available: https://metalcutting.com/knowledge-center/complexities-electrochemical-grinding/.
13. Qu, N.S., Zhang, Q.L., Fang, X.L., Ye, E.K., Zhu, D., Experimental Investigation on Electrochemical Grinding of Inconel 718. *Procedia CIRP*, 35, December, 16–19, Metal Cutting Corporation, New Jersey, 2015. 10.1016/j.procir.2015.08.055.
14. *Electrochemical grinding - Wikipedia*, California, 2019, [Online]. Available: https://en.wikipedia.org/wiki/Electrochemical_grinding.
15. Yehia, H.M., Hakim, M., El-assal, A., Effect of the Al2O3 powder addition on the metal removal rate and the surface roughness of the electrochemical grinding machining.

Proc. Inst. Mech. Eng., Part B, 234, 12, 1538–1548, 2020. 10.1177/0954405420921721.

16. Sankar, M., Gnanavelbabu, A., Rajkumar, K., Thushal, N.A., Electrolytic Concentration Effect on the Abrasive Assisted-Electrochemical Machining of Aluminium-Boron Carbide Composite. *Mater. Manuf. Processes*, 32, 6, 687–692, 2016.

17. Luo, H., Zou, H., Liu, B., Yue, X., Electrochemistry Communications Fabrication of micro rotary structures by wire electrochemical grinding. *Electrochem. Commun.*, 116, 106745, 2020, April, doi: 10.1016/j.elecom.2020.106745.

18. He, Y., Xu, B., Guo, H., Zhou, X., Numerical simulation and experimental study on electrochemical milling of cemented carbide. *Adv. Mech. Eng.*,, 15, 9, 1–11, 2023, doi: 10.1177/16878132231196490.

19. Patel, D.S., Jain, V.K., Ramkumar, J., Electrochemical grinding. *Nanofinishing Sci. Technol. Basic Adv. Finish. Polishing Process.*, 321–352, 675, 2016, doi: 10.1201/9781315404103.

20. R., D.N., Amarnath, N.A.S., Akash, S., Anand Shankar, M., Kumar, A., Working of Electrochemical Grinding and Honing. *J. Eng. Res. Appl.*, 9, 1, 24–29, 2019, doi: 10.9790/9622.

21. Barrow, R.B., Electrochemical Grinding of Cylindrical Test Specimens. 1090–1092, 2017. asmedigitalcollection.asme.org

22. Qu, N.S., Fang, X.L., Zhang, Y.D., Zhu, D., Enhancement of surface roughness in electrochemical machining of Ti6Al4V by pulsating electrolyte. *Int. J. Adv. Manuf. Technol.*, 69, 9–12, 2703– 2709, 2013, doi: 10.1007/s00170-013-5238-9.

23. Phillips, R.E., *What Is Electrochemical Grinding and How Does It Work*, Mechanical Booster, New York, pp. 65–70, 1986, [Online]. Available: https://www.mechanicalbooster.com/2018/09/electrochemical-grinding.html.

24. Bhattacharyya, B. and Doloi, B., *Hybrid Machining Technol.*, 2020, doi: 10.1016/B978-0-12-812894-7.00006-2.

25. *Electrochemical Grinding Process Overview*, California, 2022, Wikipedia, [Online]. Available: https://en.wikipedia.org/wiki/Electrochemical_grinding.

26. Ujah, C.O., Popoola, A.P., II, Popoola, O.M., Afolabi, A.E., Uyor, U.O., Mechanical and Oxidation Characteristics Developed via Spark Plasma Sintering for High-Temperature/Strength Applications. *J. Mater. Eng. Perform.*, 32, 1, 18–28, 2022, doi: 10.1007/s11665-022-07066-y.

27. Przystupa, K. and Litak, G., Electrochemical Grinding Of Titanium-Containing Materials. *Adv. Sci. Technol. Res. J.*, 11, 4, 183–188, 2017, doi: 10.12913/22998624/78167.

28. Sonia, P., Introduction of hybrid machining: Fabrication and experimental investigation of electrochemical grinding on surface roughness. *Mater. Today Proc.*, 44, 300–304, 2021, doi: 10.1016/j.matpr.2020.09.470.

29. *Electrochemical Grinding Services Explained_ Advantages and Applications - HyTech Spring and Machine Corp*, Today's Medical Development, Germany, 2023, [Online]. Available: https://hytechspring.com/electrochemical-grinding-services-explained-advantages-and-applications/.

30. *What is Electrochemical Grinding Equipment_ - Today's Medical Developments*, 2023, [Online]. Available: https://www.todaysmedicaldevelopments.com/article/what-is-electrochemical–grinding-equipment-/.

31. Rajurkar, A. D. S. K.P., Zhu, D., McGeough, J.A., Kozak, J., New Developments in Electro-Chemical Machining. *CIRP Annals*, 48, 2, 567–579, 1999.

32. Tehrani, A.F. and Atkinson, J., Overcut in pulsed electrochemical grinding. *Proceedings of the Institution of Mechanical Engineers, Part B: Journal of Engineering Manufacture*, vol. 214, no. 4, pp. 259–269, July 1999.

33. Ujah, C.O., Popoola, A.P., II, Popoola, O.M., Aigbodion, V.S., Influence of CNTs addition on the mechanical, microstructural, and corrosion properties of Al alloy using spark plasma sintering technique. *Int. J. Adv. Manuf. Tech.,* 106, 2961–2969, 2020.

34. Li, H., Niu, S., Zhang, Q., Fu, S., Qu, N., Investigation of material removal in inner-jet electrochemical grinding of GH4169 alloy. *Sci. Rep.*, 7, 1, 1–11, 2017, doi: 10.1038/s41598-017-03770-1.

35. Rao, P.S. and Dwivedi, D.K., Electro Chemical Honing (ECH) of external cylindrical surfaces of titanium alloys. *Procedia Eng.*, 100, 936–945, 2015, January, doi: 10.1016/j.proeng.2015.01.452.

36. *Electrochemical Grinding (ECG) _ OpenLearn - Open University*, 2017.

37. Patel, P.R. and Thanki, S.J., Electrochemical grinding process, current state and future direction: A systematic literature review. *Int. J. Appl. Eng. Res.*, 9, 6, 637–644, 2014.

38. Geddam, A. and Noble, C.F., An assessment of the influence of some wheel variables in peripheral electrochemical grinding. *Int. J. Mach. Tool Des. Res.*, 11, 1, 1–12, 1971, doi: 10.1016/0020-7357(71)90043-6.

39. Fang, X., Qu, N., Zhang, Y., Xu, Z., Zhu, D., Effects of pulsating electrolyte flow in electrochemical machining. *J. Mater. Process. Technol.*, 214, 1, 36–43, 2014, doi: 10.1016/j. jmatprotec.2013.07.012.

40. Sapre, P., Mall, A., Joshi, S.S., Analysis of electrolytic flow effects in micro-electrochemical grinding. *J. Manuf. Sci. Eng.*, 135, 1, 1–10, 2013, doi: 10.1115/1.4023266.

41. Kumar, E.A., Electrochemical Grinding: Definition, Parts or Construction, Working Principle, Application, Advantages, and Disadvantages. *Mech. Eng.*, The Mechanical Engineering.com, India, 1–8, 2021. [Online]. Available: https://themechanicalengineering.com/electrochemical-grinding/.

42. Ma, X. *et al.*, Modeling of the material removal rate in internal cylindrical plunge electrochemical grinding. *J. Manuf. Process.*, 92, January, 89–106, 2023, doi: 10.1016/j.jmapro.2023.02.024.

43. M, S., *Electrochemical Machining (ECM)_ Process, Working & Diagram*, The Engineer's Post, India, 2023, [Online]. Available: https://www.theengineerspost.com/electrochemical-machining/.

44. Zhang, H., Liu, S., Yue, W., Xiao, H., Zhang, P., Experimental study of surface characteristic in electrochemical machining of 35CrMo steel. *Metals (Basel).*, 8, 7, 509, 2018, doi: 10.3390/ met8070509.

45. Gupta, K., Jain, N.K., Laubscher, R.F., Electrochemical hybrid machining processes. *Springer Briefs Appl. Sci. Technol.*, 9783319259208, 9–32, 2016, doi: 10.1007/978-3-319-25922-2_2.

46. Dhar, N.R., Development of an Electrochemical Grinding (Ecg) Machine. *Proceedings of the 2nd International Conference and 7th Annual Paper Meet*, At: Bangladesh, July, 2016.

47. College, K., *Electro-chemical Grinding - Advantages And Disadvantages - Mechanical Education*, 2022, KCG College of Technology, India, [Online]. Available: https://kcgcollege.ac.in/pdf/mech/studymaterials/UNIT4ECG-min.pdf.

48. Han, W. and Kunieda, M., Wire electrochemical grinding of tungsten micro-rods using neutral electrolyte. *Precis. Eng.*, 52, November 2017, 458–468, 2018, doi: 10.1016/j.precisioneng.2018.02.006.

49. Li, H., Fu, S., Zhang, Q., Niu, S., Qu, N., Simulation and experimental investigation of inner-jet electrochemical grinding of GH4169 alloy. *Chin. J. Aeronaut.*, 31, 3, 608–616, 2018, doi: 10.1016/j.cja.2017.08.014.

50. Wang, F., He, Y., Wu, X., Kang, M., Flow field characteristics and experimental research on inner jet electrochemical face grinding of SUS420J2 stainless steel. *Sci. Rep.*, 12, 1, 11789, 2022, doi: 10.1038/s41598-022-16099-1.

51. Kong, H., Liu, Y., Zhu, X., Peng, T., *Study on Ultrasonic Assisted Electrochemical Drill-Grinding of Superalloy*, 2020.

52. Zhu, X., Liu, Y., Zhang, J., Wang, K., Kong, H., Ultrasonic-assisted electrochemical drill-grinding of small holes with. *J. Adv. Res.*, 23, 151–161, 2020, doi: 10.1016/j.jare.2020.02.010.

53. Kirk, G.A., *Pulsed Electrochemical Machining_Achieved Through Chemistry_Orthopedic Design Technology*, Orthopedic Design & Technology Magazine, New Jersey, 2022, [Online]. Available: https://www.odtmag.com/issues/2022-02-01/view_features/pulsed-electrochemical-machining-achieved-through-chemistry/.

54. Niu, S., Qu, N., Li, H., *Investigation of electrochemical mill-grinding using abrasive tools with bottom insulation*, The International Journal of Advanced Manufacturing Technology. vol. 97, pp. 1371–1382, 2018.

55. N., Q.U. *et al.*, Macro electrochemical milling and its hybrid variants. *Chin. J. Aeronaut.*, December, 2023, doi: 10.1016/j.cja.2023.12.015.

56. Hu, Z., Jiao, F., Niu, Y., Ma, X., Li, C., Jie, Y., Heliyon Study on the surface quality of bearing raceway in plunge electrolytic internal grinding. *Heliyon*, 9, 3, e14273, 2023, doi: 10.1016/j. heliyon.2023.e14273.

57. Narayan, S.B.K.A., Experimental setup development and parametric study of electrochemical face grinding process using Ni-based superalloy Shyam Bihari Kaushal * and Audhesh Narayan. *Int. J. Abras. Technol.*, 10, 1, 1–15, 2020.

58. Wang, F., Zhao, J., Kang, M., *Investigation of inner-jet electrochemical face grinding of thin-walled rotational parts. Int. J. Adv. Manuf. Tech.,* 115, 9, 3269–3287, 2021.

59. Zhong, J., Han, S., Lu, H., Kan, X., Effect of tip geometry and tip clearance on aerodynamic performance of a linear compressor cascade. *Chin. J. Aeronaut.*, 26, 3, 583–593, 2013, doi: 10.1016/j.cja.2013.04.020.

60. Liu, J., Hui, L., Jia, D., Liu, Y., Zhu, D., An electrochemical machining method for aero-engine blades based on four-directional synchronous feeding of cathode tools. *Chin. J. Aeronaut.*, 36, 9, 380–391, 2023, doi: 10.1016/j.cja.2022.10.003.

61. Pradhan, S., Singh, S., Prakash, C., Królczyk, G., Pramanik, A., Pruncu, C., II, Investigation of machining characteristics of hard-to-machine Ti-6Al-4V-ELI alloy for biomedical applications. *J. Mater. Res. Technol.*, 8, 5, 4849–4862, 2019, doi: 10.1016/j.jmrt.2019.08.033.

62. Utriainen, M., Application, F., Data, P., Oy, E., (12) Patent Application Publication (10) Pub. No.: US 2009 / 0312954 A1 (D Patent Application Publication. 1, 19, 1–6, 2009.

63. Kuster, F. and Dalaee, M., CIRP Encyclopedia of Production Engineering. *CIRP Encycl. Prod. Eng.*, 1–5, Springer, 2014, 2016, doi: 10.1007/978-3-642-35950-7.

64. Chen, Z., Zhan, S., Zhao, Y., Electrochemical jet-assisted precision grinding of single-crystal SiC using soft abrasive wheel. *Int. J. Mech. Sci.*, 195, December 2020, 106239, 2021, doi: 10.1016/j.ijmecsci.2020.106239.

65. Chmir, M.Y., Timofeev, Y.S., Poluyanov, V.S., Diamond ECM grinding of ceramic-metal tungsten. *Procedia - Soc. Behav. Sci.*, 6, 408–410, 2013, doi: 10.1016/j.procir.2013.03.104.

66. Krzysztof, P., Electrochemical ECG grinding of ceramic and tungsten sinter. 01001, 1–5, 2019.

67. Hua, J.Z,., Jiaoa, F,., Niua, Y,., Maa, X,., Lia, C,., Y., *S*tudy on surface quality of bearing raceway in plunge electrolytic internal grinding, *Heliyon,* 2021.

68. Bosem, G.K., Analysis of Electrochemical Grinding Process While Machining Alumina-Aluminium Interpenetrating Phase-composites Using Grey Taguchi Method. *J. Eng. Appl. Sci.*, *5*, 5, 354–360, 2010.

69. Ullas Bhalani, P.A.H.J. and Shah, V., *Electrochemical grinding _ PPT*, Slideshare, California, 2017.

70. *Electrochemical Grinding Services Explained_ Advantages and Applications - HyTech Spring and Machine Corp*, VAAGDEVI COLLEGE, India, 2021, [Online]. Available: https://www.mechanicaleducation.com/electro-chemical-grinding-advantages-and-disadvantages/.

Note

*Corresponding author: chikau@uj.ac.za

14
Photochemical Machining

Sandip Kunar[1]*, Jagadeesha T.[2], Gurudas Mandal[3], Norfazillah Talib[4], Akhilesh Kumar Singh[5] and Itha Veeranjaneyulu[1]

[1]Department of Mechanical Engineering, Aditya University, Surampalem, India

[2]Department of Mechanical Engineering, National Institute of Technology, Calicut, India

[3]Department of Metallurgical Engineering, Kazi Nazrul University, Asansol, India

[4]Department of Manufacturing Engineering, Universiti Tun Hussein Onn Malaysia, Johor, Malaysia

[5]Department of Mechanical Engineering, Aditya College of Engineering & Technology, Surampalem, India

Abstract

One of the key elements in the production of microcomponents is surface topography. The most often helpful technique for low-cost micromanufacturing is photochemical machining (PCM). The history and evolution of PCM are discussed in this chapter. The PCM process, mechanism of etching, and steps for experimental design are explored in this chapter. The pertinent research on PCM and the parametric impact are also covered. Additionally, a scientific explanation for the impact is provided along with a comprehensive parametric effect on the response measurements. The gaps and scope of the work are then stated.

***Keywords*:** Photochemical machining, Inconel 718, brass, surface topography

14.1 Introduction

The traditional machining methods are unable to meet the exacting dimensional requirements, high surface polish, and complicated forms. Additionally, the hard materials limit the use of traditional machining techniques. Additionally, for some applications, the increase in temperature and residual stresses that typical machining procedures create in the work piece might not be acceptable. Consequently, non-traditional machining techniques are now widely employed in the production of a large range of products. Abrasive jet machining, photochemical machining (PCM), and other non-conventional machining techniques are among them. Photochemical etching is the relatively little researched non-conventional machining method [1]. The combination of chemical etching and photoresist imaging forms the basis of the PCM process [2]. A regulated chemical reaction is used in the PCM method to precisely shape any particular form without the need for physical force. The process of microscopic electrochemical cell action, which is also responsible for metal corrosion and chemical dissolution, etching of material.

In addition to other benefits, PCM produces challenging light metal components that are free from stress, burr, and inexpensive, and requires shorter supply time. Since this method controls the machining's complexity, it can produce metal components with complex designs more quickly, efficiently, and affordably than any other traditional metal forming method. The method also has the advantage of being able to etch a wide variety of materials, including metals and alloys. On the other hand, PCM makes it simple to etch metals and alloys such as aluminum, steel, nickel, Monel, and Kovar. Owing to the variety of materials that may be utilized in the PCM method, this method is

becoming a major player in the production of précised parts for a variety of industries, including jewelry, electronics, optical, and medicine. Production of gaskets for mobile phones, watch part ornamentation, suspension head assemblies, and jewelry are examples of typical uses [3]. Various multiple criteria decision making (MCDM) approaches are utilized in this study to optimize performance measures such as etch factor, undercut, and surface roughness for the PCM process [4]. A range of control constraints are investigated when PCM is used for stainless steel. While surface roughness and depth of engraving are performance measures, time and temperature are control limitations. This study compares the surface roughness and engraving depth of two different etchants, ferric and cupric chloride on stainless steel under various control constraints [5]. The primary emphasis of the research for PCM is on geometric topographies on Monel 400 with two etchants, *i.e.*, $FeCl_3$ and $CuCl_2$ at various temperatures and etchant concentrations. Responses including undercut, surface roughness (R_a), depth of etch, and geometric characteristics such aspect ratio and etch factor are compared. The impacts of geometry type and perimeter on PCM process behavior are also implicated in this study [6].

The parametric effect problems of the less studied PCM technique are presented in this chapter. This section is followed by a discussion of the contextual, which focuses on the brief history and the selected literature study. Additionally, the details of the PCM process and the experimental settings are provided in the section that follows. Next, it is detailed how the process parameters affect the PCM's performance metrics. The surface characteristics of the machined specimens are discussed to disclose the influence of process parameters. After the

chapter summary, the opportunity of future work for PCM is briefly discussed.

14.2 Contextual

The understanding of how acid attacks metals, which leads to the development of the PCM technique. As far back as 2500 BC, there are records of this technology in the ancient histories of the Greeks and Egyptians. An etchant consisting of charcoal, ordinary salt, and vinegar operating through a hand-engraved mask of linseed oil paint is used to the PCM technique. Using scribed wax as a resist, the appealing designs were also etched onto the blades. Although the first mention of photoetching dates back to 1826, William Fox Talbot was granted the first patent in 1852 for a method using ferric chloride to etch copper using photoetching. However, experts have not done much research on this mechanism recently. Different types of study on PCM are explored as follows:

Few researchers have reported on their simulation work linked to etching. The 2D simulation model has been created for etching and conducted an experimental examination of the process parameters on micro geometry [7]. Additionally, using a computer model, a single crystal silicon has been evaluated for 3D anisotropic wet etching. The 3D simulation model for the anisotropic wet etching of single-crystal silicon is created and stated that it holds potential for a detailed examination of complex 3D micro electro mechanical systems (MEMS) [8]. A parametric analysis is conducted and used PCM to manufacture the microstructures on carbon steel surfaces [9]. The PCM is used to create the surface textures on Monel 400 sheets and investigate the effects of temperature and etching time on the etched pattern as well as the impact of spinning speed on the photoresist layer [10].

Using two distinct etchants, ferric chloride and cupric chloride, the chemical machining is conducted on copper and reported that the ferric chloride etchant produced a higher etching rate, while the cupric chloride etchant produced a better surface quality [11]. In addition, the investigation of the chemical machining is conducted on aluminum to examine the impact of etching temperature and duration on etching rate and surface finish [12]. The cupric chloride regeneration mechanism is explored [13]. The PCM of Inconel 600 is performed using ferric chloride etchant and discussed the parametric influences on the performance measures [14]. The effect of sodium hydroxide concentration at constant temperature has been studied on the shape of alumina nanowires and nanotubes [15]. The PCM is accomplished on OFHC copper using ferric chloride etchant to measure the parametric effect on surface roughness, etch factor, and undercut. Gray rational analysis was then used for optimization [16]. Grey analysis method and artificial neural networks were used to optimize the process parameters for undercut and etch rate [17, 18]. The 3D photochemical process is used for stent production and the impact of magnetic field on the SS316L etch rate [19]. The rolling operation is affected on the PCM of Monel 400 [20, 21]. The PCM investigation for the Inconel 718 alloy is carried out and reported how a surface topography analysis revealed the impact of grain size and other selected factors on the surface roughness [22]. Using the response surface approach and grey analysis method, the process parameter optimization for PCM of German silver, brass, and SS316L steel has been completed for the prediction of surface roughness, undercut, and etch rate. Three factors have been identified as control parameters: temperature, time, and concentration [23–25]. This method is used as a texturing technique to create channels [26]. Moreover, PCM is used to create the microchannels [27].

It is evident from the literature mentioned above that several researchers have reported on their findings from PCM studies for various materials. The mechanism of etching and the parametric impact have been studied. A brief overview of PCM and the process parameters are covered in this chapter. The causes of the surface roughness, etch rate are revealed by a thorough parametric effect and a systematic justification for the same of two different materials, such as brass and Inconel 718. The surface topography analysis for brass and Inconel 718 provides validity to the findings.

14.3 PCM Process

One type of chemical machining that combines chemical etching and photography is called photochemical machining (PCM). It is a chemical etching technique using a photoresist stencil to remove material from the specimen in the designated places. The steps of PCM are displayed in Figure 14.1. The technique is relatively new, having been identified as a manufacturing method some years ago. The steps of process are outlined below:

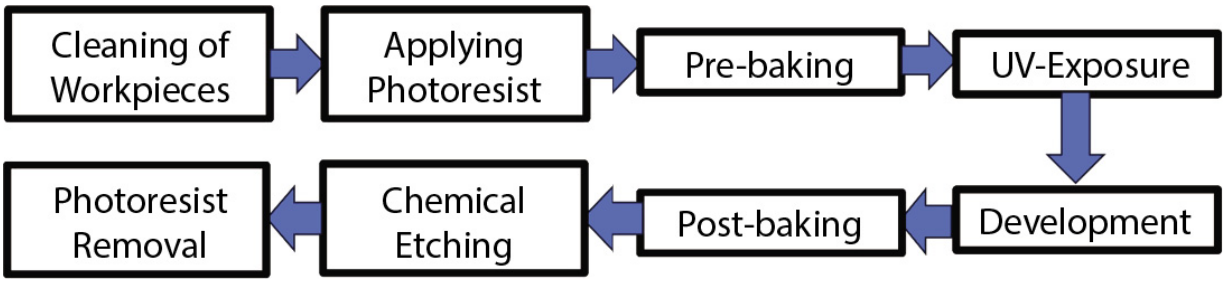


Figure 14.1 Various steps in PCM process.

i. **Fabrication of Photo Tool**

It functions as a PCM tool. The creation of oversized artwork or paper is the first step. To reduce dimensional inaccuracy, artwork is typically made at a

certain magnification factor. Art can be created by computer-aided drafting, precise coordination graph plotting, or manual drafting. The artwork is captured on camera using a precise reduction tool. Several image masters are utilized in large volume production to expose, develop, and etch multiple parts. The product is master film with the engraved pattern on it. Film sets are designed to allow for simultaneous exposure from both perspectives. Provisions for portion reclamation following etching are included in the master's preparation.

ii. **Selection of Metal**

The goal with metals is to have the smallest possible grain size because larger grains result in less smooth edges. It is best to select a metal that dissolves in etchant. A material needs to have a consistent thickness and be flat. There should be no inclusions, embedded particles, or scratches on the surface, and the finish should be consistent.

iii. **Preparation of Work Piece**

The metal surface needs to be clean for the photoresist to adhere well to the metal. The best way to remove the work piece is to spray water on the metal surface and see if each droplet spreads out to create a thin layer of water. A film's formation suggests sufficient cleaning. After that, the work item is dried and rinsed.

iv. **Masking with Photoresists**

A photosensitive surface that thwarts the etchant action is provided by photoresists. Positive or negative masking can be used for the photoresist. Areas of the positive acting system that are exposed to light fade away as they mature. Exposure zones in a negative system become insoluble in the developing solutions.

Applying photoresists can be done by spraying, whirling coating, or dipping. After allowing the resists to air dry, they are baked at a maximum temperature of 120°C for 15 min. Photoresists are exposed to ultraviolet (UV) light, which polymerizes the exposed portions of light-sensitive resin and increases their resistance to developer chemicals.

v. **Etching**

Etching involves exposing the produced and post-baked metal panel to hot acid. When exposed metal encounters acid, it oxidizes and forms a soluble reaction product. Etching can be carried out by either spraying heated acid or submerging in an agitated chemical bath. The breakthrough happens when the etching has advanced to a point when penetration from each surface has penetrated halfway through the sheet. Etching machines are designed to resist etchant-induced corrosion. The etchant is in a section near the base of machines. The etchant temperature is kept consistent with the use of a heating element and cooling coil. Processing can go on continuously with an etcher that has a conveyor system. One sheet is processed at a time with batch type machines.

vi. **Stripping and Inspection**

Panels that have had their photoresist coating removed (stripped) are still coated after etching. The photoresist needs to be eliminated without leaving any stains on the metal. When pieces are still attached to the metal sheet, handling them during stripping is made easier. The positioning of connecting tabs ensures that they do not impede the part’s functionality. Examined is the etched work piece’s thickness. Plug gauges and a horizontal optical comparator are the ideal tools for inspection.

14.4 Mechanism of Etching

The three primary steps of chemical etching process, which removes material, are as follows:

1. Diffuse ions from an etchant solution moved through the boundary layer toward the exposed region on the workpiece.
2. Gaseous and soluble byproducts produced when the exposed specimen surface reacts chemically with the etchant.
3. A surface by-product of the work piece diffuses into the etchant solution through the boundary layer.

14.5 Steps for Experimental Designing

i. **Recognition and Statement of the Problem**

While this may seem like an obvious concept, it is frequently difficult to identify problems that call for testing and to formulate a concise, widely recognized description of them. It is essential to develop every concept regarding the experiment's goals.

ii. **Choice of Factors, Levels, and Range**

Upon examining the variables that could impact a process or system's performance, the investigation typically finds that these variables fall into one of two categories, *i.e.*, prospective design variables or nuisance factors. The variables that the researcher may want to change for the experiment are known as potential design elements. Held-constant, allowed-to-vary, and design factors are a few helpful classifications. Often, noise factors are divided into

three categories: controllable, uncontrollable, and noise factors. One whose levels the researcher can regulate is a controlled nuisance factor.

iii. **Selection of the Response Variable**

The researcher should make sure that the response variables are high for the investigation. The response variable is typically the measured characteristic's average, standard deviation, or both. It is not rare to receive multiple responses.

iv. **Choice of Experimental Design**

This stage is rather simple if the pre-experimental planning tasks are carried out correctly. The selection of an appropriate run order for the experimental trials, the calculation of sample size (number of repetitions), and the decision about the involvement of blocking or other randomization constraints are all factors in the choice of design.

v. **Performing the Experiment**

It is crucial to closely monitor the experiment's operation to make sure everything is going as planned. At this point, technique errors in the experiment will typically eliminate the validity of the results. Effective planning is essential to success. The logistics and planning complexities of conducting a planned experiment in a sophisticated manufacturing or research and development setting are often underestimated.

vi. **Statistical Analysis of the Data**

The data should be analyzed using statistical techniques to ensure that the conclusions and outcomes are factual rather than subjective. The statistical techniques needed are simple if the

experiment has been well planned and carried out in accordance with the plan.

vii. **Conclusions and Recommendations**

After the data has been analyzed, the experiments need to suggest a course of action and make useful judgments regarding the findings. At this point, the graphical techniques are frequently helpful, especially when presenting the findings to others. Confirmation testing and repeat runs ought to be carried out to verify the experiment's outcomes.

14.6 Process Parameters

The output parameters and control parameters that affect the process are included in the process parameters. Fixed parameters are those that are maintained at a fixed value during an experiment.

i. **Control Parameters:** several parameters affect PCM performance, and how these parameters depends on the operator's background and the parameters. Selecting the input parameters is therefore the main duty. The selection of input parameters is typically based on a survey of the literature, the experience of the operator, and some pilot trials. Another name for these input parameters is control parameters. The input parameters are adjusted across a range during experiments to examine their impact on the output characteristics. The input parameters are etchant temperature, etchant concentration and time for etching. The UV light intensity, photo tool properties, photoresist thickness, etc., also have an impact on PCM operation in addition to these primary input parameters. Additionally, various etchants and addition

of acids to the etchant affect PCM performance metrics.

ii. **Response parameters:** the experiment's output parameters are those that have an impact on the chosen control parameters. The selection of response parameters shall be based on their respective relevance to the work or application. The following variables determine how well any PCM technique performs:

    i. **Material removal rate (etch rate):** the homogeneity of the solution temperature, the specimen's chemical and metallurgical uniformity determine the etching rate, also known as the rate of material removal. The biggest grain sizes in castings typically result in the roughest surface together with the lower machining rate. Rolled metal sheets often provide the best surface quality together with the highest rate of machining rate. Hard metals have lower etching rates, whereas softer metals have higher etching rates.

    ii. **Surface finish:** the machining is seen at the borders between the grains as well as on each individual grain's surface. Therefore, for a good surface quality and homogeneous appearance, a homogenous metallurgical structure and tiny grain size are required. The surfaces that were photochemically machined lack a consistent lay pattern. Photochemical machining for a specific amount of time results in a fundamental surface finish for each material based on the heat treatment, grain size and orientation. Any previous surface flaws, such as waviness, scratches, and dents will be partially adjusted and replicated in the machined surface, even though PCM cannot remove them.

iii. **Undercut:** during the machining process, material is removed both inwardly and depth-wise beneath the photoresist in the unexposed region. The distance etched in the exposed area is referred to as the undercut, and the distance etched beneath the photoresist as cut's depth. Because of the undercut, a larger slot than needed is created after etching. To obtain precise dimensions, the undercut must be considered prior to etching.

iv. **Etch factor:** this refers to the undercut to etch depth ratio. When scribing the mask using templates for chemical etching, this ratio needs to be considered.

v. **Edge deviation:** edge deviation (ED) is the variance of the machined component's edge. It speaks of the edge's straightness that is created during milling. When fabricating microcomponents, such as heat sinks and microchannels, where the accuracy of the produced geometry greatly affects the part's or device's performance, edge deviation is essential.

vi. **Etchants:** in PCM, several etchants are utilized for various materials. These etchants include sodium hydroxide, cupric chloride, and the addition of acids such as hydrofluoric acid and nitric acid for improved performance. A common etching material for materials such as steel, aluminum and its alloys, copper and its alloys, and nickel is ferric chloride ($FeCl_3$). It is dependable, affordable, and has a high etch rate.

14.7 Parametric Effect

The effectiveness of PCM is affected by several control parameters. The previous section covered the various PCM response parameters. However, surface roughness and material removal rate (MRR) are the two main factors that control PCM performance. Numerous researches have also reported on these two parameters.

i. **Workpiece Substance**

The material of the workpiece could be made of glass, ceramics, metal, or an alloy. The etch rate and surface roughness are significantly influenced by the components' makeup and type (crystalline or amorphous). Another crucial factor to consider is the shape of the component that needs to be made. The specimen's thickness and shape also have an impact.

ii. **Photoresist Masking**

Photoresists come in four different varieties: positive, negative, wet, and dry. There are two options for applying the wet photoresist: dipping and spin coating. The photoresist application technique determines the homogeneity and resist thickness in microns on the specimen. In this instance, the workpiece's geometry to be machined, thickness, and shape all affect how well it performs. There are various kinds of photoresists with varying adhesion strengths available. As a result, photoresist application essentially controls PCM performance.

iii. **Machine for Etching**

The etching process can be done in a beaker or an etching machine, depending on how many specimens need to be produced. The etching machine provides

spray etching, which improves PCM process performance. Etching time, nozzle packing density, spray jet pressure, nozzle type, spray jet angle, drop velocity, drop size, etchant quantity, nozzle oscillation, and workpiece oscillation are some of the critical characteristics of an etching machine.

iv. **Etchant**

The solution known as the etchant is where the substance dissolves. Different materials can be etched using different etchants. Consequently, choosing the right etchant is crucial for improving etching rate. The PCM process is heavily dependent on the etchant concentration, temperature, and etching duration, which also significantly affect the rate of material removal and surface roughness. Furthermore, the surface tension, viscosity, redox potential, and pH index are useful factors for etchants.

v. **Effect of Concentration**

One of the key factors influencing the PCM's performance is the etching concentration. The concentration of the solution determines how many molecules are in the etchant solution. When molecules collide on the specimen's surface, a chemical reaction takes place. Less etching and better surface quality since fewer molecules will clash on the specimen's surface at lower etch concentrations. This reduces surface diffusion. The molecules in the etchant will increase as the concentration rises. Reactive collisions are therefore more likely to happen when there are more reactant molecules present per unit volume in the etchant. More molecules will cause more reactive collisions to happen at the surface of the specimen. Better etching and increased diffusion as a result will lead to a higher rate of material removal, but the

uneven surface will result in a lower surface finish. The etch rate and surface roughness are significantly impacted by concentration increases up to a certain point. As concentration increases, the etch rate and surface roughness will both decrease. The viscosity effect is the primary cause of this. The viscosity of the etchant solution increases, hindering the flow of the produced product and further degrading the fresh etchant.

vi. **Effect of Temperature**

When molecules contact with one another energetically, chemical reactions take place. Temperature controls molecular motion because it is a measure of the kinetic energy of molecules. Only when the molecules have enough energy to undergo a reaction will they do so. As the etchant's temperature rises, the molecular energy intensity will also rise, resulting in more particle collisions and a faster reaction rate. Etching rate often increases as temperature rises. An increase in temperature causes the molecular energy level to rise, which causes reactive molecular collisions on the specimen surface and improves diffusion. A rougher surface will result from removing a larger amount of material from the surface. Better MRR and greater surface roughness follow because of this when temperature rises.

vii. **Effect of Etching Time**

If the molecules collide on the specimen surface for a shorter amount of time, diffusion will be diminished. Due to decreased material dissolution in the etchant solution, there is a decrease in MRR but an improvement in surface polish. Diffusion and MRR will be enhanced by longer-term molecular collisions on the specimen's surface. However, a longer interval

between collisions results in a greater R_a, which could contribute to an uneven surface. As a result, the surface roughness and rate of material removal increase continuously over time.

14.8 Analysis of Machined Surfaces

i. **Photochemical Machining of Brass**

A study describes the PCM of brass. The impact of process parameters on the rate of material removal and surface roughness are examined. Lower MRR with a better surface roughness has been found at lower concentrations because there are fewer molecules attacking the specimen's surface. Intragranular corrosion, which is the first stage of diffusion, occurs at grain borders, while trans-granular corrosion is the next stage of diffusion that occurs within the grain. For brass, the dendritic structure has been documented. For an etchant with a higher concentration, a rougher surface and more molecules attacking it will lead to an increased MRR. It is reported that void formation results from higher concentrations of combined intergranular and trans granular corrosion. It has also been acknowledged that increasing the temperature and etching duration increases the rate of material removal and the roughness of the surface [24].

ii. **Photochemical Machining of Inconel 718**

The PCM investigation is carried out on Inconel 718. It has been documented how the grain size and process parameters affect the rate of material removal and surface roughness. According to research on the impact of grain sizes at various temperatures, smaller grain sizes cause higher material rates and surface roughness than bigger grain sizes. The etching rate

increases because of an improved reaction rate at temperatures up to 65°C. This is because there is more kinetic energy and better collisions at the grain boundaries, which leads to more corrosion there. Therefore, it has been noted that as temperature rises, surface roughness, and MRR also increase [22].

14.9 Conclusion

The least studied unconventional machining method, PCM, is covered in detail, along with several associated features. The first section of the chapter introduces the PCM process and its steps. The basis of the PCM process, the history of PCM, and current PCM trends are discussed. The etch rate and surface roughness are highlighted as the two most important performance characteristics after a discussion of the many control and performance parameters. A summary of the several elements influencing surface roughness and material clearance rate is provided. The mechanism is explained in depth along with the impact of the three most crucial parameters, which are temperature, etching duration, and etchant concentration, on the etch rate and surface roughness. The recommendations for additional PCM work are provided, with an emphasis on the challenging parts of the field.

14.10 Scope for Future Work

One of the least studied unconventional machining techniques is PCM, which can create parts with intricate shapes and geometries and is useful in a variety of contexts. In this context, the future study on the following areas of PCM may be viable given on various aspects of PCM.

- Comparative PCM analysis of various alloys (such as copper and aluminum alloys), as well as parametric optimization for PCM of various materials and estimation of the ideal ranges of process parameters,
- UV exposure’s impact on PCM properties,
- Photoresist thickness’s effect on PCM performance,
- Etchant regeneration,
- Nanoparticle production and characterization from the dissolved metal in etchant.

References

1. Gamage, J.R. and DeSilva, A.K.M., Assessment of research needs for sustainability of unconventional machining processes. *Procedia CIRP*, 26, 385–390, 2015.
2. Allen, D.M., Photochemical machining: From ‘manufacturing’s best kept secret’ to a $6 billion per annum, rapid manufacturing process. *CIRP Annals-Manufacturing Technol.*, 53, 2, 559– 572, 2004.
3. Yadav, R.P. and Teli, S.N., A Review of issues in photochemical machining. *Int. J. Mod. Eng. Res.*, 4, 7, 49–53, 2014.
4. Sapkota, G., Ghadai, R.K., Cep, R., Shanmugasundar, G., Kalita, K., Enhancing Efficiency in Photo Chemical Machining: A Multivariate Decision-Making Approach. *Front. Mech. Eng.*, 10, 2024, doi: 10.3389/fmech.2024.1325018.
5. Vikash Ruhela, R., Imran Ansari, M., Jadhav, P.V. *et al.*, An experimental investigation of photo chemical machining process for stainless-steel material by using

different etchants. *Mater. Today: Proc.*, 2023, https://doi.org/10.1016/j.matpr.2023.03.324.

6. Patil, D.K., Thorat, S., Sadaiah, M., Study of the effect of PCM process parameters on geometry type, Ra, depth of etch, undercut comparing FeCl3 and CuCl2 etchants on Monel 400. *Adv. Mater. Process. Technol.*, 10, 3, 1956–1976, 2024, https://doi.org/10.1080/2374068X.2023.2205668.

7. Bruzzone, A.A.G. and Reverberi, A.P., An experimental evaluation of an etching simulation model for photochemical machining. *CIRP Ann.*, 59, 1, 255–258, 2010, doi: 10.1016/j.cirp. 2010.03.070.

8. Lee, J.G. and Won, T., Three-dimensional numerical simulation for anisotropic wet chemical etching process. *Mol. Simul.*, 33, 7, 593–597, 2007, doi: 10.1080/08927020601067508.

9. Zhang, J. and Meng, Y., A study of surface texturing of carbon steel by photochemical machining. *J. Mater. Process. Technol.*, 212, 10, 2133–2140, 2012, doi: 10.1016/j.jmatprotec.2012.05.018.

10. Mudigonda, S. and Patil, D.H., Some investigations on surface texturing on monel 400 using photochemical machining, in: *ASME 2015 International Manufacturing Science and Engineering Conference*, pp. V001T02A045-V001T02A045, American Society of Mechanical Engineers, 2015, 10.1115/MSEC2015-9294.

11. Çakır, O., Temel, H., Kiyak, M., Chemical etching of Cu-ETP copper. *J. Mater. Process. Technol.*, 162, 275–279, 2005, doi: 10.1016/j.jmatprotec.2005.02.035.

12. Çakır, O., Chemical etching of aluminium. *J. Mater. Process. Technol.*, 199, 1-3, 337–340, 2008, doi:

10.1016/j.jmatprotec.2007.08.012.

13. Cakir, O., Copper etching with cupric chloride and regeneration of waste etchant. *J. Mater. Process. Technol.*, 175, 1-3, 63–68, 2006.

14. Wagh, D.V., Dolas, D.R., Dhagate, M.D., Experimental investigation of photochemical machining on Inconel 600 using ferric chloride. *Int. J. Eng. Res. Technol.*, 4, 2, 289–293, 2014.

15. Sadeghpour-Motlagh, M., Mokhtari-Zonouzi, K., Aghajani, H., Kakroudi, M.G., Effects of etching time and NaOH concentration on the production of alumina nanowires using porous anodic alumina template. *J. Mater. Eng. Perform.*, 23, 6, 2007–2014, 2014, doi: 10.100711665-014-1011-y.

16. Chaudhari, K., Patil, A., Kolekar, M., Patil, A., Photochemical machining. *Int. J. Recent Innovation Trends Comput. Commun.*, 4, 4, 132–136, 2016.

17. Saraf, A.R. and Sadaiah, M., Application of artificial intelligence for the prediction of undercut in photochemical machining. *Int. J. Mechatron. Manuf. Syst.*, 6, 2, 183–194, 2013, doi: 10.1504/IJMMS.2013.053829.

18. Misal, N.D. and Sadaiah, M., Comparison of Design of Experiments and Gray Rational Analysis of Photochemical Machining. *Int. J. Innovations Eng. Technol.*, 3, 121–126, 2013.

19. Saraf, A.R. and Sadaiah, M., Magnetic field-assisted photochemical machining (MFAPCM) of SS316L. *Mater. Manuf. Processes*, 32, 3, 327–332, 2017, doi: 10.1080/10426914.2016.1198014.

20. Patil, D.H. and Mudigonda, S., The effect of the rolling direction, temperature, and etching time on the photochemical machining of Monel 400 microchannels. *Adv. Mater. Sci. Eng.*, 6751305, 2016, https://doi.org/10.1155/2016/6751305.

21. Patil, D.H. and Mudigonda, S., Investigation on effect of grain orientation in photochemical machining of Monel 400. *Mater. Manuf. Processes*, 32, 16, 1831–1837, 2017, doi: 10.1080/10426914.2017.1291953.

22. Misal, N.D., Saraf, A.R., Sadaiah, M., Experimental investigation of surface topography in photochemical machining of Inconel 718. *Mater. Manuf. Processes*, 32, 15, 1756–1763, 2017, doi: 10.1080/10426914.2017.1317786.

23. Wagh, D.V. and Dolas, D.R., Multi Response Optimization of Process Parameters in PCM of Inconel 600 Using Desirability Function Approach of RSM. *Int. J. Engine Res.*, 5, 2, 127–130, 2016.

24. Wangikar, S.S., Patowari, P.K., Misra, R.D., Effect of process parameters and optimization for photochemical machining of brass and German silver. *Mater. Manuf. Processes*, 32, 15, 1747– 1755, 2017, doi: 10.1080/10426914.2016.1244848.

25. Wangikar, S.S., Patowari, P.K., Misra, R.D., Parametric Optimization for Photochemical Machining of Copper using Overall Evaluation Criteria. *Mater. Today Proc.*, 5, 2, 4736–4742, 2018, doi: 10.1016/j.matpr.2017.12.046.

26. Gao, Q., Lizarazo-Adarme, J., Paul, B.K., Haapala, K.R., An economic and environmental assessment model for microchannel device manufacturing: Part 2–Application.

J. Cleaner Prod., 120, 146–156, 2016, doi: 10.1016/j.jclepro.2015.04.141.

27. Das, S.S., Tilekar, S.D., Wangikar, S.S., Patowari, P.K., Numerical and experimental study of passive fluids mixing in micro-channels of different configurations. *Microsyst. Technol.*, 23, 12, 5977–5988, 2017, doi: 10.100700542-017-3482-x.

Note

*Corresponding author: sandip.sandip.kunar@gmail.com

15
Abrasive-Assisted Micromachining

Rayappa Shrinivas Mahale[1]*, Krishnamurthy Goggi[2], Vaibhav Raibole[2], K.B. Jagadeeshgouda[2] and Prashant Kakkamari[3]

[1]Department of Automation and Robotics, JSPMs Rajarshi Shahu College of Engineering, Pune, Maharashtra, India

[2]Department of Mechanical Engineering, Jain College of Engineering and Research, Udyambag, Belagavi, Karnataka, India

[3]Department of Mechanical Engineering, KLS Gogte Institute of Technology, Belagavi, Karnataka, India

Abstract

Abrasive-assisted machining (AAM) stands as a paramount domain within advanced manufacturing, wielding a transformative influence on precision machining processes. This paper systematically explores the fundamentals, techniques, and advancements in AAM, addressing its industrial relevance and nuanced applications. The discourse begins by elucidating the foundational principles of abrasive machining, delving into abrasive types, characteristics, and material removal mechanisms. Subsequently, an in-depth analysis of prominent techniques, including abrasive-assisted micromachining (AAMM), abrasive jet machining (AJM), and abrasive flow machining (AFM), is presented, encompassing operational intricacies, applications, and comparative evaluations. Materials compatibility and the expansive application landscape of AAM are scrutinized, with a focus on real-world case studies and successful implementations across

diverse industries. Technological advancements are explored, highlighting recent innovations in abrasive materials, process integration, and their collective impact on machining precision. The optimization paradigm is investigated through a meticulous examination of key machining parameters, performance-influencing factors, and strategies for enhancing operational efficiency. Moreover, challenges inherent in AAM are identified, and analytical frameworks for their mitigation are proposed, providing valuable insights into future trends and research directions. A comparative analysis with conventional machining techniques offers a nuanced perspective on the efficiency and limitations of AAM. The discussion extends to encompass safety protocols and environmental considerations, underlining the importance of occupational health measures and sustainable machining practices. This study synthesizes comprehensive insights into the evolving landscape of AAM, encapsulating conclusive findings and their implications for future research and technological development. The presented work contributes a holistic understanding of AAM's technical intricacies, positioning it as a key player in advancing precision manufacturing methodologies.

***Keywords*:** Abrasive-assisted machining, precision machining, technological advancements, optimization strategies, industrial applications, comparative analysis, occupational safety, environmental sustainability

15.1 Introduction

Evolution of micromachining and the rise of abrasive-assisted micromachining (AAMM). For centuries, artisans and engineers have sought methods to craft increasingly intricate and precise structures. Traditional machining techniques, however, struggled to achieve the

miniaturization required for the burgeoning field of microfluidics and MEMS (microelectromechanical systems). Enter micromachining, a collection of techniques capable of creating features on the micrometer scale. Initially, methods like photolithography and wet chemical etching dominated, offering high resolution but often limited to specific materials or geometries. Abrasive-assisted micromachining (AAMM) emerged as a versatile alternative, able to tackle challenging materials and achieve complex 3D structures. This paragraph could delve into the historical context of micromachining, the limitations of earlier techniques, and the key advantages that propelled AAM to prominence.

Unveiling the mechanism: how AAM works its magic. At its core, AAM harnesses the erosive power of abrasive particles. These tiny warriors, ranging from sand to diamond grit, are propelled towards the target material, chipping away at its surface. But unlike traditional sandblasting, AAM employs additional techniques for precise control. This paragraph could explore the different methods used in AAM, such as fluid jets, ultrasonics, electrochemical processes, and magnetic fields. You could explain how each method imparts unique properties to the abrasive particles, influencing their impact, penetration depth, and directionality. A symphony of parameters: optimizing the AAM process. Just like any fine-tuned instrument, the success of AAM hinges on the careful orchestration of various parameters. This paragraph could delve into the critical factors that influence the AAM process, such as: abrasive particle selection: material, size, shape, and concentration all play a role in the material removal rate and surface finish. Carrier medium: gas jets, water jets, and even slurries can be used, each offering different advantages in terms of control, precision, and cleaning efficiency. Process parameters: flow rate,

pressure, standoff distance, and scanning strategy all impact the final feature shape and accuracy. By understanding the interplay of these parameters, researchers and engineers can tailor the AAM process for specific materials and desired microfeatures.

Pushing the boundaries: advanced applications of AAM. The versatility of AAM has led to its adoption in diverse fields. This paragraph could showcase some cutting-edge applications, such as: microfluidics: fabricating intricate microchannels for lab-on-a-chip devices, enabling rapid diagnostics and drug testing. MEMS: creating high-precision sensors and actuators, crucial for miniaturized medical devices and microrobots. Micro-optics: shaping lenses, filters, and waveguides for advanced optical systems used in communication and biomedical imaging. Microneedles: fabricating painless microneedles for minimally invasive drug delivery and blood glucose monitoring. Each application highlights a unique aspect of AAM's capabilities, demonstrating its potential to revolutionize various industries. Looking ahead: the future of AAM. While AAM has made significant strides, further advancements are on the horizon. This paragraph could discuss potential areas of development, such as: hybrid approaches: combining AAM with other micromachining techniques for even greater flexibility and control. *In-situ* monitoring: real-time monitoring of the AAM process for improved accuracy and defect detection. Nanoparticle abrasives: utilizing nanoparticles for even higher resolution and intricate feature creation. By addressing these challenges and exploring new avenues, AAM promises to remain a vital tool for pushing the boundaries of miniaturization and enabling groundbreaking innovations in various fields. In the intricate world of microfabrication, where precision and miniaturization reign supreme, the quest for versatile and efficient techniques continues.

Abrasive-assisted micromachining (AAM) emerges as a frontrunner, offering a unique blend of flexibility, affordability, and effectiveness, making it a valuable asset for established and emerging industries alike. This comprehensive exploration delves into the core principles, applications, and potential of AAM, equipping you with the knowledge to harness its capabilities for your microfabrication needs.

Unveiling the core: delving into the fundamentals of AAM. At its heart, AAM relies on a focused jet, carrying a cocktail of abrasive particles and a carrier fluid, to meticulously sculpt microfeatures on a surface. This seemingly simple principle unlocks a world of possibilities, as the choice of abrasive material, carrier fluid, jet parameters, and mask design all contribute to shaping the desired microstructures.

Two primary variations of AAM dominate the microfabrication landscape: abrasive jet machining (AJM): compressed air or nitrogen propels the abrasive particles in this technique, generating a high-velocity jet that erodes the target material. The abrasive particles, ranging from aluminum oxide and silicon carbide to diamond, provide the cutting edge, while the gas jet serves as the delivery vehicle. Abrasive water jet machining (AWJM): here, water takes center stage as the carrier fluid, offering several advantages. Its incompressibility ensures consistent jet characteristics, while its cooling properties minimize thermal damage. Additionally, water's versatility allows for the incorporation of various additives, further tailoring the machining process [1–5].

Beyond the basics: exploring the diverse applications of AAM. The true value of AAM lies in its adaptability across various industries and applications. Its ability to handle diverse materials, including brittle ceramics, hard metals,

and even delicate polymers, makes it a universal player in the microfabrication arena. Let us explore some key domains where AAM shines:

Microfluidics: from microchannels for drug delivery to intricate lab-on-a-chip devices, AAM's ability to create precise fluidic pathways with high aspect ratios makes it a preferred choice for microfluidic device fabrication. Microelectromechanical systems (MEMS): the intricate structures and delicate features of MEMS devices often require precise and versatile machining techniques. Abrasive-assisted micromachining (AAM) excels in creating microgears, nozzles, and other crucial components with high accuracy and minimal damage. Optics: from diffractive lenses to micromirrors, the ability to create complex micro-optical structures with smooth surface finishes is crucial. Abrasive-assisted micromachining (AAM), with its precise control and diverse abrasive options, effectively addresses this need. Medical devices: the medical field benefits significantly from AAM's ability to micromachine biocompatible materials like polymers and ceramics. This opens doors for creating microneedles, microsurgical tools, and even microfluidic implants with exceptional precision and biocompatibility.

Unveiling the advantages: why choose AAM for your microfabrication needs? Versatility: AAM's ability to handle a wide range of materials and create diverse features makes it a versatile tool for various applications. Cost-effectiveness: compared to other microfabrication techniques, AAM offers a relatively lower setup and operational cost, making it an attractive option for both large-scale and small-scale projects. Simplicity: the basic principles of AAM are relatively straightforward, making it easier to learn and implement compared to complex lithography or laser-based techniques. Accuracy and Precision: With proper control over jet parameters and

mask design, AAM can achieve high accuracy and precision in feature creation, crucial for demanding applications. Good surface finish: depending on the chosen abrasives and process parameters, AAM can achieve smooth surface finishes, reducing the need for further polishing steps [6–10].

15.1.1 Literature Survey

Title	Authors	Year	Focus
Abrasive Assisted Micro Electric Discharge Machining on ‘Inconel 718’: An Experimental Exploration	Sivaprakasam, P., & Hariharan, P.	2023	Combining abrasive assistance with micro-EDM for improved material removal rate in Inconel 718.
Cryogenically assisted abrasive jet micromachining of polymers	Dahotre, N. B., & Datta, S.	2022	Utilizing cryogenic cooling to enhance micromachining of polymers like PDMS, ABS, and PTFE.
Investigation on surface integrity and microchannel fabrication of soda-lime glass using abrasive water jet micromachining	Zhang, Y., *et al*.	2023	Studying the impact of abrasive water jet micromachining on surface quality and microchannel formation in soda-lime glass.
Research on micro-abrasive jet micromachining for fabrication of microfluidic chips	Liang, Y., *et al*.	2022	Exploring the use of micro-abrasive jet micromachining for creating microfluidic chips.
Experimental investigation of microchannel fabrication in borosilicate glass	Kumar, V., *et al*.	2022	Analyzing the process parameters for fabricating microchannels in borosilicate glass

Title	Authors	Year	Focus
using abrasive jet micromachining			using abrasive jet micromachining.
Abrasive jet micromachining of silicon carbide for microfluidic applications	Patil, V. B., *et al*.	2023	Evaluating the feasibility of abrasive jet micromachining for creating microfluidic features in silicon carbide.
A review of micro-abrasive jet micromachining technology and its applications	Zhang, Y., *et al*.	2022	Comprehensive review of micro-abrasive jet micromachining technology and its diverse applications.
Experimental and numerical investigation of surface integrity in micro-abrasive jet micromachining	Li, C., *et al*.	2023	Combining experimental and numerical analysis to understand the impact of micro-abrasive jet micromachining on surface integrity.
Development of micro-abrasive jet micromachining system for high-precision and high-efficiency	Sun, Y., *et al*.	2022	Proposing a novel micro-abrasive jet micromachining system for efficient and precise

Title	Authors	Year	Focus
microfluidic chip fabrication			microfluidic chip fabrication.
A study on the machinability of silicon nitride using abrasive jet micromachining	Liang, Y., *et al*.	2023	Investigating the machinability of silicon nitride using abrasive jet micromachining techniques.

15.2 Erosion Mechanism

15.2.1 Abrasive Particle Characteristics

Particle Size and Shape

The size and shape of abrasive particles are fundamental factors affecting erosion. Smaller particles generally result in higher erosion rates due to their ability to penetrate material surfaces more effectively. Larger particles, on the other hand, tend to cause more surface abrasion and less penetration. Moreover, the shape of abrasive particles, whether angular or rounded, can influence their cutting and erosion capabilities. Angular particles may have a greater impact on material removal, while rounded particles can lead to smoother surface finishes [11, 12].

Particle Hardness

Abrasive particle hardness is another critical attribute. Harder particles are more effective at removing material but can also lead to more significant wear on the nozzle and other components of the AAM system. The choice of abrasive material with the appropriate hardness is vital to strike a balance between efficient material removal and preserving equipment.

Particle Velocity and Concentration

The velocity of abrasive particles in the water jet stream and their concentration in the abrasive mixture are vital parameters. Higher particle velocity can increase erosion rates while adjusting particle concentration can be used to control the rate of material removal. These parameters are often fine-tuned to achieve the desired cutting or profiling results while managing erosion effectively.

Material Composition

The composition of abrasive particles, whether they are composed of garnet, aluminum oxide, or other materials, can significantly impact erosion. Different abrasive materials have distinct cutting characteristics and wear rates. Understanding how the material composition influences the erosion process is critical for optimizing AAM for specific applications [13–16].

Particle Velocity Distribution

In addition to the average particle velocity, the distribution of particle velocities within the jet can have a notable impact on erosion. Variations in particle velocity can result in uneven erosion patterns on the workpiece, affecting the overall quality of the cut. Analyzing the particle velocity distribution is important for achieving consistent results.

Understanding these abrasive particle characteristics is integral to developing erosion prediction models that can accurately depict the erosion process in AAM. Moreover, this knowledge aids in the selection of optimal abrasive materials and the fine-tuning of process parameters to achieve the desired machining outcomes while minimizing the adverse effects of erosion. In the subsequent sections, we will further explore the factors that influence erosion in

AAM, enabling a more comprehensive understanding of this complex phenomenon [17–20].

15.2.2 Material Properties

The properties of the workpiece material being machined in abrasive-assisted micromachining (AAM) are integral to understanding and predicting erosion in the process. Different materials exhibit varying responses to the high-velocity abrasive jet, and their specific properties can significantly influence erosion rates, patterns, and the overall efficiency of the machining operation. In this section, we explore the key material properties that play a central role in the erosion process within AAM.

Material Hardness

The hardness of the workpiece material is a critical factor that affects erosion. Softer materials are generally more susceptible to erosion due to their lower resistance to abrasive particle impact. Harder materials, in contrast, tend to withstand erosion better. The relative hardness of the workpiece compared to the abrasive particles can determine the extent of material removal and surface damage.

Material Toughness

Material toughness is another essential property to consider. Tougher materials can absorb and dissipate energy more effectively, which can mitigate the extent of erosion. In contrast, brittle materials are more prone to cracking and chipping when subjected to high-velocity abrasive particles, leading to increased erosion rates.

Porosity and Microstructure

The porosity and microstructure of the workpiece material can significantly impact erosion. Highly porous materials may experience greater erosion as abrasive particles can penetrate the material more deeply. Additionally, the microstructure, such as grain size and distribution, can affect the erosion behavior, with finer-grained materials generally being more erosion-resistant.

Material Density and Thermal Conductivity

Material density and thermal conductivity also play a role in erosion. Materials with higher densities and better thermal conductivity can dissipate the heat generated during the erosion process more efficiently, reducing the risk of thermal damage to the workpiece.

Material Composition and Phase Changes

The composition of the workpiece material, including its chemical constituents and impurities, can influence erosion rates and patterns. Some materials may undergo phase changes, such as melting or recrystallization, when exposed to the high-velocity abrasive jet, impacting erosion behavior.

Surface Roughness

The initial surface roughness of the workpiece can affect erosion. A rough surface may provide more areas for abrasive particles to impact, potentially increasing erosion rates. Conversely, a smoother surface may reduce erosion due to the reduced surface area available for abrasive interaction.

Understanding these material properties is crucial for optimizing the AAM process and managing erosion effectively. The selection of the right material for a specific

application, as well as the adjustment of process parameters based on material properties, can significantly impact erosion rates and the overall quality of the machining operation. In the subsequent sections, we will further explore additional factors that influence erosion in AAM, contributing to a comprehensive understanding of this complex phenomenon [21–25].

15.2.3 Micromachining Parameters

The parameters of the water jet, such as pressure, velocity, and nozzle design, are critical elements that influence erosion in abrasive-assisted micromachining (AAM). These parameters control the characteristics of the abrasive jet and, consequently, impact the rate and pattern of erosion on the workpiece. Understanding how these water jet parameters influence the erosion process is essential for optimizing the AAM operation and achieving the desired machining results. In this section, we delve into the key water jet parameters and their effects on erosion in AAM. Water pressure: water pressure is a fundamental parameter in AAM, and it plays a significant role in erosion. Higher water pressure results in a more powerful jet, increasing the velocity and kinetic energy of the abrasive particles. This can lead to higher erosion rates, but it must be carefully controlled to avoid excessive tool wear and reduce operational costs. Water velocity: the velocity of the water jet determines the speed at which the abrasive particles impact the workpiece. Higher water velocities can lead to increased erosion rates. However, the relationship between velocity and erosion is not always linear, and achieving a balance between material removal and preserving equipment is crucial. Nozzle design and geometry: the design and geometry of the nozzle through which the abrasive jet is expelled can significantly impact erosion. Nozzle geometry affects the focusing and

dispersion of the abrasive particles. The shape and size of the nozzle orifice can influence the distribution of particle impacts on the workpiece, which in turn affects erosion patterns. Abrasive particle concentration: the concentration of abrasive particles in the water jet is a key parameter. Higher concentrations of abrasive particles result in increased erosion, as more abrasive particles are impacting the workpiece. Adjusting particle concentration can be used to control material removal rates and achieve desired machining outcomes.

Jet stability and consistency: the stability and consistency of the water jet are essential to achieving predictable erosion patterns. Variations in jet stability can lead to uneven erosion on the workpiece, affecting cut quality. Maintaining a stable and consistent jet is vital in achieving precise and repeatable results. Jet standoff distance: the distance between the nozzle and the workpiece, known as the jet standoff distance, influences erosion. Varying the standoff distance can change the impact angle of abrasive particles, affecting the extent and pattern of erosion on the workpiece.

Mixing tube design: the design of the mixing tube, where the abrasive particles are introduced into the water jet, can influence erosion. The design of this component can impact the distribution and concentration of abrasive particles in the jet. Understanding and controlling these water jet parameters is essential for optimizing AAM processes. It allows for the fine-tuning of machining parameters to achieve the desired material removal rates, cut quality, and tool wear while managing erosion effectively. In the subsequent sections, we will further explore the development of erosion prediction models and the assessment of practical implications, providing a comprehensive understanding of erosion in AAM [26–30].

15.2.4 Interaction Between Abrasive Particles and Workpiece

The interaction between abrasive particles and the workpiece is at the heart of the erosion process in abrasive-assisted micromachining (AAM). This intricate interaction dictates the rate and pattern of material removal, which, in turn, impacts the efficiency and precision of the machining operation. Understanding the dynamics of this interaction is crucial for predicting erosion behavior and optimizing the AAM process. In this section, we delve into the complexities of the interaction between abrasive particles and the workpiece.

Impact Mechanism

The abrasive particles entrained in the water jet impact the workpiece surface with considerable kinetic energy. Understanding the impact mechanism, including the angle, velocity, and force of impact, is essential for comprehending how erosion occurs. The kinetic energy transfer from the particles to the workpiece material is what ultimately leads to material removal and erosion.

Material Removal Mechanisms

Several material removal mechanisms come into play during the interaction. These mechanisms can include abrasion, cutting, and fracture. Abrasion involves the removal of material through repeated particle impacts, cutting involves the formation of a channel by the abrasive jet, and fracture can occur in brittle materials when the stress exceeds the material’s strength, leading to material chipping or cracking.

Erosion Patterns

The interaction between abrasive particles and the workpiece gives rise to erosion patterns. These patterns can vary based on the material properties, particle characteristics, and process parameters. Understanding how these variables influence erosion patterns is critical for achieving the desired surface finish and cut quality.

Surface Temperature Effects

The interaction between abrasive particles and the workpiece generates heat due to friction and impact. This temperature rise can affect material properties and lead to thermal damage. Understanding the thermal effects of the interaction is important for managing erosion and minimizing unwanted alterations in the workpiece material.

Material Specificity

Different workpiece materials respond uniquely to abrasive particle impact. Understanding how specific materials react to erosion is essential for selecting the most suitable material for a given application and optimizing the AAM process accordingly.

Wear and Tool Life

The interaction between abrasive particles and the workpiece also has implications for tool wear and the service life of nozzles and other system components. Monitoring wear and understanding its mechanisms is crucial for maintaining equipment and controlling operational costs.

Comprehending the complex interplay between abrasive particles and the workpiece is instrumental in developing accurate erosion prediction models and optimizing the AAM process for specific applications. By considering the

impact mechanism, material removal mechanisms, erosion patterns, surface temperature effects, material specificity, and wear, engineers and operators can fine-tune parameters to achieve precise, efficient, and cost-effective AAM. This understanding is a fundamental component in managing and mitigating erosion in AAM effectively [31–35].

15.3 Erosion Mechanisms in AAM Explanation

In this chapter, we dive deep into the intricate world of erosion mechanisms within the context of abrasive-assisted micromachining (AAM). The goal is to unravel the multifaceted ways in which abrasive particles interact with materials, leading to erosion and material removal.

15.3.1 Particle Impact and Cutting Mechanisms

In this section, we delve into two fundamental mechanisms of erosion within abrasive-assisted machining (AAM): particle impact and cutting. These mechanisms describe how abrasive particles interact with the material surface, resulting in material removal.

Particle impact mechanism: we explain that particle impact occurs when high-velocity abrasive particles strike the material's surface. The kinetic energy of these particles upon impact dislodges material particles from the surface, leading to erosion. The force generated by the impact depends on the particle's velocity, size, and hardness. This mechanism is particularly relevant when the abrasive particles strike the surface at angles or velocities that do not lead to cutting.

Cutting mechanism: we introduce the concept of cutting, which is driven by the penetration of abrasive particles into

the material. When the particles penetrate the surface, they physically separate material particles from the bulk. The depth of penetration is influenced by the particle's kinetic energy, angle of impact, and material properties. This mechanism is especially prominent when abrasive particles impact the surface at angles that facilitate material penetration.

Combined action of impact and cutting: readers learn that in real-world scenarios, both particle impact and cutting mechanisms often coexist. The combined action of these mechanisms depends on factors like particle velocity, angle of impact, material hardness, and process parameters. This interplay contributes to the complexity of the overall erosion process.

Effect on material removal rate: we emphasize that the material removal rate due to particle impact and cutting mechanisms depends on the abrasive particle's velocity, hardness, and angle of impact. Higher velocities and harder particles generally result in more efficient material removal. Understanding these mechanisms is essential for predicting the rate and nature of material removal during AAM.

By the end of this section, readers will have a clear understanding of how particle impact and cutting mechanisms contribute to material erosion in the AAM process. These mechanisms form the basis for the subsequent exploration of erosion rates, material responses, and the development of specialized erosion models in later sections of the chapter [36–40].

15.3.2 Fatigue Damage from Repetitive Impacts

In this section, we delve into the concept of fatigue damage that arises as a result of repetitive impacts from abrasive particles during abrasive-assisted micromachining (AAM).

This phenomenon highlights the cumulative effect of erosive interactions on the material's surface.

Understanding fatigue damage: we begin by explaining that repetitive impacts of abrasive particles on the material surface can lead to fatigue damage. Just as repeated bending of material can lead to cracks over time, the cyclic impacts of abrasive particles can result in microcracks, surface degradation, and even changes in material properties.

Microcracking and surface degradation: readers learn that the repetitive impacts create stress cycles within the material. Over time, these cycles lead to the initiation and propagation of microcracks in the material. These microcracks can significantly impact the structural integrity of the material, reducing its strength and potentially leading to failure.

Effect on material properties: we highlight that fatigue damage does not just affect the material's surface. It can extend deeper into the material, leading to changes in properties such as hardness, toughness, and resilience. These changes can influence how the material responds to subsequent impacts and stresses.

Role in erosion mechanisms: this section emphasizes that fatigue damage contributes to the overall erosion process. The presence of microcracks and degraded surfaces can accelerate erosion rates, making the material more susceptible to material removal through particle impact and cutting.

Mitigation strategies: we briefly touch upon strategies to mitigate fatigue damage, such as controlling process parameters to reduce impact intensity, using protective coatings, and employing post-machining treatments to restore material integrity.

By the end of this section, readers will have gained insight into the long-term effects of repetitive impacts on material surfaces in AAM. Understanding the concept of fatigue damage adds another layer of complexity to the erosion mechanisms, highlighting the need for accurate erosion models and strategies to manage material degradation. This knowledge serves as a foundation for understanding how these mechanisms are incorporated into erosion models and their practical implications in the subsequent sections of the chapter [41–45].

15.3.3 Factors Influencing Erosion Rate

In this section, we explore the various factors that significantly influence the rate of erosion within the context of abrasive-assisted machining (AAM). These factors play a pivotal role in determining the intensity and extent of material removal during the machining process.

Abrasive particle attributes: we explain that the attributes of the abrasive particles, such as their size, shape, and hardness, directly impact erosion rates. Larger and harder particles tend to induce higher erosion rates due to their increased impact force and penetration capability.

Particle velocity: readers learn that the velocity at which abrasive particles are propelled onto the material surface has a direct influence on the rate of erosion. Higher particle velocities result in greater kinetic energy upon impact, leading to more efficient material removal. Material properties: we emphasize that the inherent properties of the material being machined are crucial. Harder materials may exhibit lower erosion rates due to their resistance to abrasive impacts. Material characteristics like hardness, density, and toughness influence how the material responds to erosive forces.

Process parameters: this section covers the significance of process parameters, including pressure, standoff distance, and abrasive flow rate. Manipulating these parameters directly affects the intensity of the erosive jet and the resulting material removal rates.

Nozzle geometry: readers discover that the design and geometry of the nozzle play a role in shaping the erosive jet's behavior. Nozzle attributes like shape, diameter, and angle impact the focusing and dispersion of the abrasive particles, affecting erosion rates.

The interplay of factors: we emphasize that erosion rates are not determined by a single factor but by the interplay of all these factors. Their combined influence leads to intricate erosion dynamics that require careful consideration and accurate modeling.

By the end of this section, readers will have gained a comprehensive understanding of the multiple factors that contribute to erosion rates within AAM. This knowledge equips readers with insights into the complexity of the erosion process and prepares them to appreciate the significance of erosion modeling in predicting and optimizing material removal in the subsequent sections of the chapter [46–50].

15.3.4 Variability of Erosion Across Materials

In this section, we explore how different materials respond to erosive forces within the context of abrasive-assisted machining (AAM). The variability in material properties leads to varying levels of susceptibility to erosion, impacting the efficiency and outcomes of the machining process (Figure 15.1).

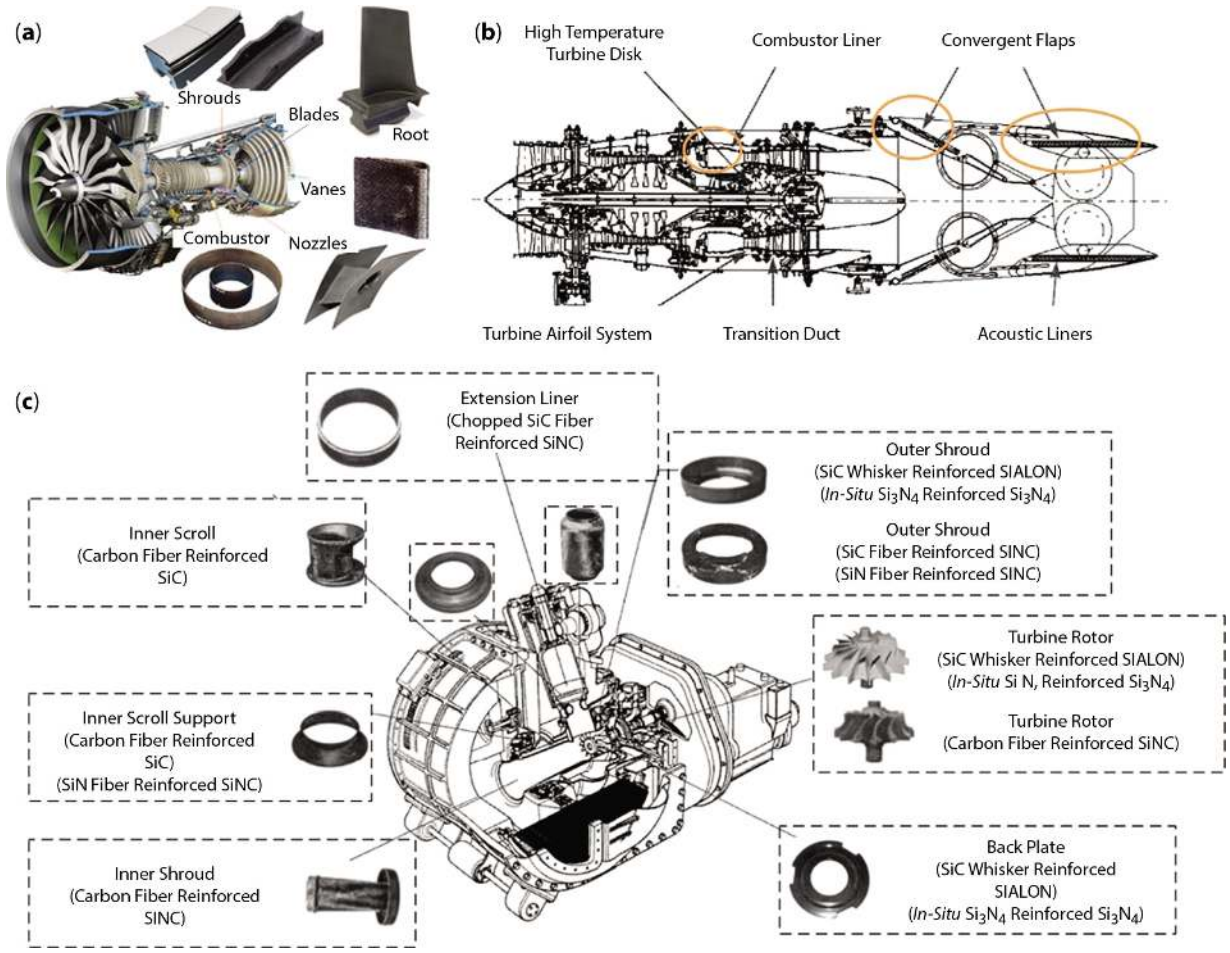


Figure 15.1 The application of CMCs: (a) high-temperature parts of aero-engines; (b) hot zone of the jet engine; (c) main CMCs components of CGT [50].

Material response to erosive forces: we begin by explaining that different materials exhibit varying responses to erosive forces due to their unique properties. Some materials may resist erosion more effectively, while others may be more prone to material removal.

Material hardness: readers learn that material hardness is a significant factor in determining erosion resistance. Harder materials are generally more resilient to abrasive impacts and cutting, leading to lower erosion rates compared to softer materials.

Material toughness: we discuss how material toughness, which relates to a material's ability to absorb energy before fracturing, can influence erosion susceptibility. Tougher materials can withstand the impact of abrasive particles better, reducing erosion rates.

Material microstructure: this section touches on how the microstructure of a material can impact its erosion behavior. Materials with fine-grained microstructures may exhibit enhanced erosion resistance due to improved particle deflection and energy absorption.

Material composition: we explain that the composition of a material, including the presence of alloys or composite reinforcements, can significantly influence erosion rates. Certain compositions may lead to enhanced erosion resistance, making them suitable for specific machining applications.

Practical implications: readers gain insight into the practical implications of material variability in AAM. Manufacturers must carefully consider material properties and tailor machining parameters to achieve optimal results and minimize excessive material removal.

By the end of this section, readers will have a comprehensive understanding of how different materials respond to erosive forces within AAM. This understanding highlights the importance of material selection, process parameter adjustment, and the development of accurate erosion models to predict and optimize material removal rates for specific materials. This knowledge sets the stage for exploring erosion modeling techniques and applications in subsequent sections of the chapter [51–55].

15.4 Existing Erosion Models

In this chapter, we delve into the landscape of erosion modeling, exploring the existing models used in various industries and discussing their relevance to the context of abrasive-assisted machining (AAM). The goal is to provide readers with an overview of the broader erosion modeling field before delving into AAM-specific models in later sections.

Introduction to erosion models: we begin by introducing the concept of erosion models. These are mathematical representations that aim to predict and quantify the material removal and erosion processes caused by various forces, including abrasive impacts and cutting.

Overview of existing models: we discuss a range of erosion models that have been developed for various applications, such as soil erosion, riverbed erosion, and erosion in industrial processes. These models serve as a foundation for understanding how different industries have approached erosion prediction.

Relevance to AAM: we highlight that while existing erosion models have been successful in their respective domains, applying them directly to AAM may be challenging due to the unique characteristics of the process. AAM involves specific erosive forces, particle interactions, and material responses that demand tailored models.

Limitations and gaps: this section explores the limitations of applying existing erosion models to AAM. We address challenges related to particle velocities, impacts, material interactions, and the need for accuracy in high-precision machining.

Importance of specialized models: readers gain an understanding of the need for specialized erosion models

for AAM. Tailoring models to the process's intricacies will lead to more accurate predictions and improved optimization strategies.

By the end of this chapter, readers will have gained insight into the broader landscape of erosion modeling and its relevance to AAM. This knowledge prepares them to delve into the subsequent sections, where the development and validation of customized erosion models specifically designed for AAM will be discussed in detail [56–60].

15.4.1 Introduction to Erosion Models

In this section, we provide readers with an introduction to the concept of erosion models, which are fundamental to understanding how material removal occurs due to abrasive forces within the context of abrasive-assisted machining (AAM).

Defining erosion models: we start by explaining that erosion models are mathematical representations that attempt to predict and quantify the erosion process. These models are used to understand how materials are removed from surfaces due to external forces, such as abrasive particle impacts, cutting, and wear.

Physical processes in erosion: readers learn that erosion models are developed based on a solid understanding of the underlying physical processes involved in the erosion phenomenon. These models aim to capture the interplay of variables that influence material removal, such as particle velocity, impact angle, material properties, and process parameters.

Prediction and optimization: the section highlights that erosion models have practical applications in predicting erosion rates, optimizing process parameters, and understanding the effects of material responses to erosive

forces. These models enable manufacturers to make informed decisions for efficient and effective machining.

Types of erosion models: we mention that there are various types of erosion models, including empirical models based on experimental data, mechanistic models that incorporate fundamental physics, and numerical simulations that use computational techniques to simulate erosive interactions.

Challenges in modeling: this section briefly touches upon the challenges of developing accurate erosion models, including the complexity of interactions between particles and surfaces, the influence of multiple variables, and the need for validation against real-world data.

By the end of this section, readers will have a clear understanding of what erosion models are and their significance in predicting material removal in the AAM process. This understanding serves as a foundation for exploring the development of specialized erosion models tailored to the complexities of AAM in later sections of the chapter [61].

15.4.2 Overview of Existing Erosion Models

In this section, we provide readers with an overview of the existing erosion models that have been developed for various industries and applications. This exploration sets the stage for understanding the broader landscape of erosion modeling before focusing on models relevant to abrasive-assisted machining (AAM).

Types of industries: we begin by introducing readers to the diverse range of industries that have utilized erosion models. These include fields like geology, hydrology, and industrial processes. Each industry has developed models to understand erosion phenomena specific to their domain.

Soil erosion models: we delve into soil erosion models used in agriculture and land management. These models predict the movement of soil particles due to factors like water flow and wind, providing insights into soil conservation and erosion control.

Riverbed erosion models: this section briefly explains riverbed erosion models, which are relevant in predicting how water currents and sediment transport lead to changes in riverbed morphology and channel erosion.

Industrial erosion models: readers learn about models used in industrial processes, where the erosion of machinery and equipment due to abrasive wear is a concern. These models aid in optimizing equipment design and maintenance strategies.

Applicability to AAM: we highlight that while these models have been successful in their respective fields, direct application to AAM may be limited due to the unique conditions and factors involved in the process.

Importance of tailored models: the section emphasizes that developing tailored erosion models for AAM is essential to account for the specific particle interactions, material responses, and process parameters unique to the machining process.

By the end of this section, readers will have gained insight into the diversity of existing erosion models and their applications across various industries. This knowledge prepares them to appreciate the challenges and nuances of developing AAM-specific erosion models, which will be discussed in detail in the subsequent sections of the chapter [62].

15.4.3 Relevance of Existing Erosion Models to AAM

In this section, we explore the relevance of the existing erosion models from various industries to the context of abrasive-assisted micromachining (AAM). We discuss the challenges and limitations of applying these models to AAM due to the unique characteristics of the machining process.

Challenges of direct application: we start by acknowledging that while existing erosion models have been successful in their respective industries, directly applying them to AAM can be challenging. Abrasive-assisted micromachining involves specific erosive forces, particle interactions, and material responses that differ from those in other applications.

Particle velocities and impacts: we discuss how the high velocities of abrasive particles in AAM can result in different erosive effects compared to other industries (Figure 15.2). The impacts of these particles on the material surface need to be understood in the context of AAM’s unique parameters.

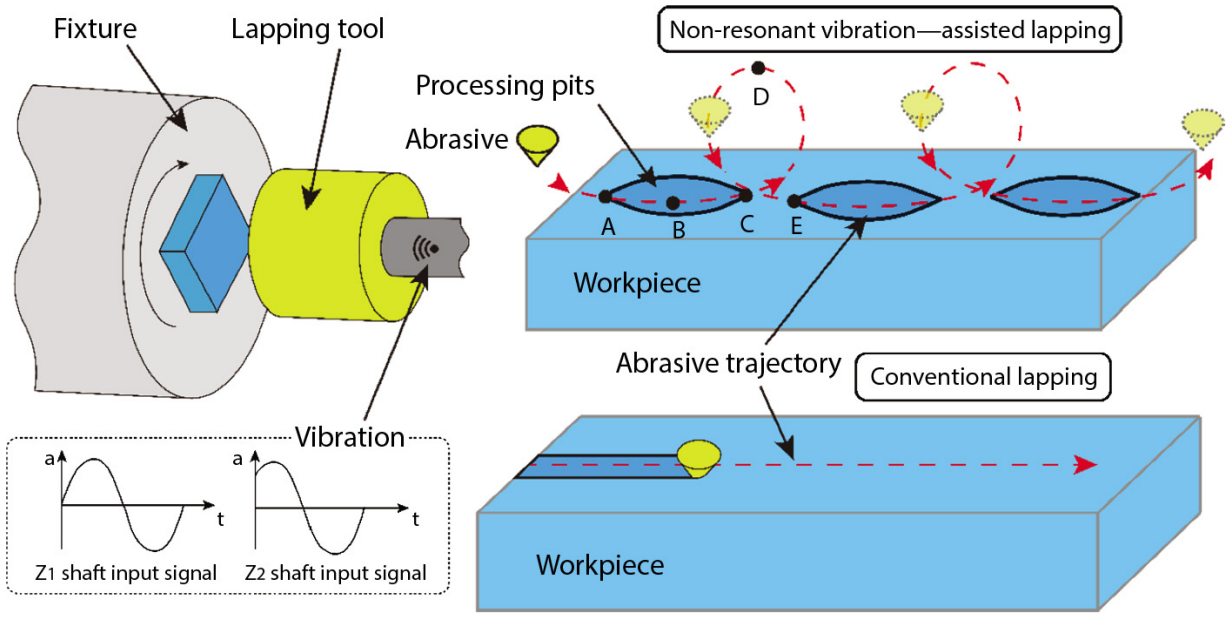


Figure 15.2 Schematic diagram represents ultrasonic lapping device [62].

Material responses: the section highlights that AAM materials may have different responses to erosive forces compared to materials in other applications. The material's hardness, toughness, and microstructure can influence the erosion process in distinct ways.

Process parameters: we mention that the process parameters in AAM, such as pressure, standoff distance, and abrasive flow rate, have a direct impact on erosive forces. These parameters need to be accounted for when adapting existing models or developing new ones.

Need for tailored models: we emphasize that the intricacies of AAM demand the development of specialized erosion models that consider the unique characteristics of the process. These models need to capture the interplay of factors specific to AAM for accurate predictions.

Model validation: the section touches on the importance of validating adapted or customized models for AAM through

experimental data and measurement techniques specific to the process.

By the end of this section, readers will have a clear understanding of the challenges and limitations of directly applying existing erosion models to AAM. This knowledge prepares them to appreciate the significance of developing tailored erosion models that accurately account for the intricacies of the AAM process, which will be discussed in detail in the subsequent sections of the chapter [63].

15.4.4 Importance of Specialized Erosion Models for AAM

In this section, we explore the importance of developing specialized erosion models that are specifically tailored to the unique characteristics of abrasive-assisted micromachining (AAM). These customized models are crucial for accurately predicting material removal and optimizing the machining process (Figure 15.3).

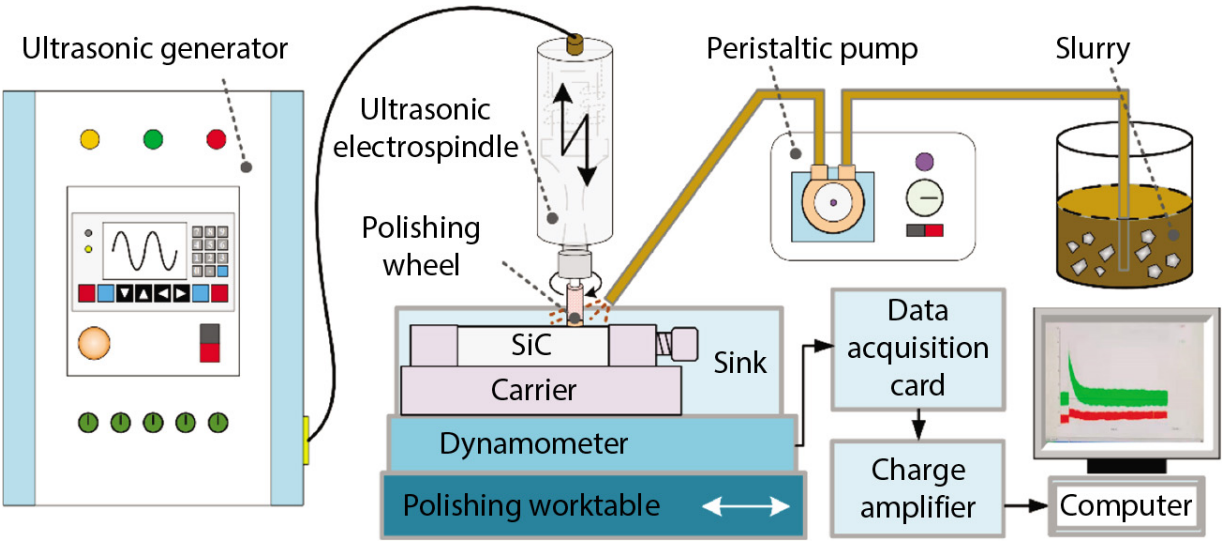


Figure 15.3 Basic tool path in the X-Y plane for cylindrical holes. The “forward” direction is shown [63].

Precision in prediction: we emphasize that AAM involves precise material removal for intricate shapes and high-

quality finishes. Generic erosion models may not capture the intricacies of AAM’s erosive forces and material responses accurately.

Process complexity: the section highlights that AAM encompasses multiple parameters, such as particle velocity, pressure, standoff distance, and material properties, which interact in complex ways. Specialized models can capture these interactions effectively.

Material variability: we discuss how different materials used in AAM may have varying responses to erosive forces due to differences in hardness, toughness, and microstructure. Specialized models can account for this variability.

Optimization strategies: readers learn that accurate erosion models are essential for optimizing process parameters and predicting material removal rates. These models aid manufacturers in achieving desired machining outcomes efficiently.

Process control: the section mentions that specialized models can contribute to better process control by providing insights into how different parameters influence material removal. This helps in achieving consistent and repeatable results.

Future advancements: we briefly touch upon the potential for advancements in erosion modeling techniques, such as combining experimental data with computational simulations for more accurate predictions.

By the end of this section, readers will understand the critical need for developing specialized erosion models for AAM. These models are integral to achieving precise material removal, optimizing process parameters, and ensuring the quality and efficiency of the machining process. This understanding paves the way for the

exploration of AAM-specific erosion modeling techniques in the subsequent sections of the chapter [64].

15.5 Development of AAM Erosion Models

In this chapter, we delve into the process of developing erosion models tailored specifically to the context of abrasive-assisted micromachining (AAM). The focus is on creating models that accurately capture the unique erosive forces, particle interactions, and material responses inherent to the AAM process.

Introduction to model development: we begin by introducing the concept of developing erosion models specifically for AAM. This involves creating mathematical representations that simulate how abrasive particles interact with the material surface and lead to material removal.

Incorporating process parameters: readers learn that the development of AAM erosion models requires the incorporation of process parameters such as pressure, standoff distance, and abrasive flow rate. These parameters significantly influence the behavior of erosive forces.

Material response consideration: the section highlights that AAM erosion models must take into account how different materials respond to erosive impacts due to variations in hardness, toughness, and other material properties.

Data collection and analysis: we touch upon the importance of collecting experimental data from actual AAM processes and analyzing them to calibrate and validate the developed models.

Modeling techniques: readers gain insight into the various modeling techniques that can be employed, including

empirical models based on experimental data, mechanistic models that involve fundamental physics principles, and numerical simulations that use computational methods to simulate particle interactions.

Iterative process: this section explains that model development is often an iterative process involving refining and adjusting the model based on experimental results until it accurately predicts material removal in AAM.

By the end of this chapter, readers will have a clear understanding of the process involved in developing erosion models specifically tailored to the AAM process. This knowledge prepares them to appreciate the intricacies of modeling erosion in AAM and sets the stage for understanding how these models are validated, verified, and applied in subsequent sections of the chapter [65].

15.5.1 Introduction to Model Development

In this section, we provide readers with an introduction to the concept of developing erosion models specifically for abrasive-assisted micromachining (AAM). The focus is on creating mathematical representations that simulate how erosive forces interact with the material surface, leading to material removal.

Purpose of model development: we begin by explaining that the primary purpose of developing AAM erosion models is to gain insights into how abrasive particles interact with materials during the machining process. These models help predict material removal rates, optimize process parameters, and enhance machining precision.

Capturing complex interactions: readers learn that erosion models aim to capture the complex interactions between abrasive particles, material surfaces, and process parameters. By representing these interactions

mathematically, models can provide valuable predictions and insights.

Importance of realism: the section highlights the importance of realism in model development. The more accurately the model represents the real-world behavior of erosive forces, the more reliable its predictions will be for AAM applications.

Balancing complexity and simplicity: we mention that while models need to be detailed enough to capture the relevant physics and parameters, they also need to be practical and efficient for computational simulations and predictions.

Iterative nature of model development: readers gain insight into the iterative nature of model development. As experimental data is collected and compared with model predictions, adjustments, and refinements are made to improve the accuracy of the model over time.

By the end of this section, readers will have a clear understanding of the purpose and principles behind the development of AAM erosion models. This understanding serves as a foundation for exploring the specific steps, considerations, and challenges involved in developing accurate and effective erosion models for AAM in the subsequent sections of the chapter [66].

15.5.2 Incorporating Process Parameters Into Models

In this section, we delve into the process of incorporating process parameters into erosion models developed specifically for abrasive-assisted micromachining (AAM). These parameters play a crucial role in shaping the behavior of erosive forces and material removal during the machining process.

Significance of process parameters: we begin by emphasizing that process parameters, such as pressure, standoff distance, and abrasive flow rate, directly influence the intensity of erosive forces and the resulting material removal rates in AAM.

Pressure and erosion: readers learn how pressure affects the velocity of abrasive particles and the overall kinetic energy of the erosive jet. Higher pressure leads to increased impact force, influencing both particle impact and cutting mechanisms.

Standoff distance impact: this section explains how the standoff distance, which is the space between the nozzle and the material surface, affects the focusing and dispersion of the erosive jet. Different standoff distances result in varying material removal depths and precision. Abrasive flow rate influence: the section covers how the abrasive flow rate determines the concentration of abrasive particles in the erosive jet. Higher flow rates lead to more abrasive particles, affecting the density of impact and cutting forces on the material surface.

Complex interactions: we discuss the complex interactions between these process parameters and how they affect each other. For instance, increasing pressure might require adjustments to standoff distance to maintain optimal material removal rates.

Modeling challenge: this section also highlights the modeling challenge of accurately representing these parameter interactions in the erosion model. The model must account for how changes in one parameter influence the behavior of other parameters and overall erosion dynamics.

By the end of this section, readers will have gained an understanding of how crucial process parameters are in the

development of accurate erosion models for AAM. These parameters dictate the intensity of erosive forces and material removal rates, making their incorporation into models essential for predicting and optimizing the machining process. This knowledge prepares readers to appreciate the complexities of modeling parameter interactions in subsequent sections of the chapter [67].

15.5.3 Considering Material Responses in Models

In this section, we explore the importance of considering how different materials respond to erosive forces and how these responses influence the development of erosion models tailored for abrasive-assisted micromachining (AAM).

Material variability: we begin by emphasizing that AAM often involves machining different materials, each with its unique properties. Some materials might be harder, more brittle, or tougher than others, leading to varying responses to erosive impacts.

Impact on erosion rate: readers learn that material responses significantly impact erosion rates. Harder materials may resist erosive forces better, leading to lower removal rates, while softer materials may experience faster material removal.

Material hardness and erosion: this section explains how material hardness, which indicates a material’s resistance to deformation, plays a role in determining erosion susceptibility. Harder materials tend to withstand erosive impacts more effectively.

Material toughness and erosion: we discuss how material toughness, which measures a material’s ability to absorb

energy without fracturing, influences the ability of a material to withstand impacts and resist erosion.

Microstructure and composition: the section touches on the importance of considering material microstructure and composition. Fine-grained microstructures or certain alloy compositions can impact how materials respond to erosive forces.

Model customization: we highlight that erosion models for AAM need to account for these material variations by incorporating relevant material properties and responses. Models must adapt to the specific material being machined to provide accurate predictions.

By the end of this section, readers will have gained insight into the role of material responses in the development of tailored erosion models for AAM. Understanding how different materials interact with erosive forces prepares readers to appreciate the complexity of modeling these interactions accurately and effectively in the subsequent sections of the chapter [68].

15.5.4 Data Collection and Analysis for Model Development

In this section, we delve into the crucial process of data collection and analysis for the development of erosion models tailored to abrasive-assisted micromachining (AAM). Accurate and reliable data serve as the foundation for creating models that can predict material removal rates and optimize the machining process.

Data collection importance: we start by highlighting the significance of collecting realworld experimental data from actual AAM processes. These data provide insights into how abrasive particles interact with materials and enable the calibration and validation of erosion models.

Experimental setup: readers learn that data collection involves setting up controlled experiments that replicate AAM conditions. This includes varying process parameters, material types, and other factors to capture a wide range of scenarios.

Data points and variability: this section emphasizes that collecting a sufficient number of data points is essential to ensure the accuracy and reliability of the model. Variability in data helps account for the complexity and uncertainties of the machining process.

Data analysis techniques: we discuss various techniques for analyzing collected data, such as statistical analysis, regression analysis, and curve fitting. These techniques help identify trends, correlations, and patterns that inform model development.

Calibrating and validating models: the section mentions that the collected data are used to calibrate and validate the developed erosion models. Calibration ensures that the model's parameters match real-world behavior, while validation tests the model's accuracy against new data.

Data-model interaction: readers gain insight into the iterative nature of data collection, model development, and validation. Adjustments to the model are made based on how well it aligns with experimental data.

By the end of this section, readers will understand the pivotal role of data collection and analysis in the development of erosion models tailored to AAM. This knowledge prepares them to appreciate the meticulous process of aligning model predictions with real-world observations, ensuring the model's accuracy and reliability in predicting material removal rates and optimizing the machining process [69].

15.6 Verification and Validation of AAM Erosion Models

In this chapter, we dive into the essential steps of verifying and validating the erosion models that have been developed specifically for abrasive-assisted micromachining (AAM). These steps are crucial to ensuring that the models accurately predict material removal rates and provide reliable insights for process optimization.

Introduction to verification and validation: we begin by explaining the importance of these two distinct processes. Verification involves checking whether the developed model is correctly implemented and matches the mathematical representation. Validation, on the other hand, assesses how well the model’s predictions align with real-world experimental data.

Verification process: readers learn that verification focuses on internal consistency. It ensures that the equations, calculations, and code of the model are accurate and errorfree. This process confirms that the model behaves as intended and has been implemented correctly.

Validation process: this section emphasizes that validation involves comparing the model’s predictions with experimental data collected from actual AAM processes. The goal is to assess the model’s accuracy and reliability in predicting material removal rates and erosion behavior.

Challenges in validation: the section touches on challenges in validation, such as the need for sufficient and diverse experimental data, dealing with uncertainties in the machining process, and addressing the complexity of erosive interactions.

Model adjustments: readers gain insight into the iterative nature of model development, verification, and validation.

Adjustments to the model are made based on how well it aligns with experimental data, leading to an improved model over time.

Importance for process optimization: we discuss how accurate and validated erosion models are instrumental in process optimization. They provide manufacturers with insights into parameter adjustments, material selection, and quality control for achieving desired machining outcomes.

By the end of this chapter, readers will have a clear understanding of the critical steps involved in verifying and validating AAM erosion models. These steps ensure that the models accurately represent the AAM process and provide reliable predictions for material removal rates and process optimization. This knowledge prepares readers to appreciate the rigor required to develop erosion models that can be effectively applied in real-world AAM scenarios [70].

15.6.1 Introduction to Verification and Validation

In this section, we introduce the concepts of verification and validation within the context of abrasive-assisted micromachining (AAM) erosion models. These two distinct processes are crucial in ensuring the accuracy, reliability, and effectiveness of the developed models.

Purpose of verification: we start by explaining that verification is the process of confirming that the developed erosion model has been correctly implemented. It involves checking whether the mathematical equations, algorithms, and code of the model have been accurately translated into the computational framework.

Internal consistency: readers learn that verification focuses on internal consistency. It ensures that the model's calculations, logic, and numerical methods are error-free and behave as intended. The goal is to confirm that the model behaves according to its design specifications.

Purpose of validation: the section then introduces validation, which is the process of assessing how well the developed model's predictions align with real-world experimental data. Validation involves comparing the model's outputs to actual observations from AAM processes to evaluate its accuracy and reliability.

Real-world accuracy: we emphasize that the ultimate goal of validation is to determine whether the model accurately predicts material removal rates, erosion behavior, and other relevant outcomes that occur in the actual machining process.

Iterative nature: the section touches on the iterative nature of verification and validation. As models are developed and refined, they undergo multiple rounds of verification to ensure correct implementation and validation to ensure accurate predictions.

Importance of both processes: this section concludes by highlighting the importance of both verification and validation in building effective AAM erosion models. Verification ensures the model's internal consistency, while validation ensures its external accuracy and relevance to real-world scenarios.

By the end of this section, readers will have gained an understanding of the fundamental concepts of verification and validation in the context of AAM erosion models. This knowledge sets the stage for exploring the specific steps and challenges involved in each of these processes in subsequent sections of the chapter [71].

15.6.2 Verification Process for AAM Erosion Models

In this section, we delve into the verification process for the erosion models developed specifically for abrasive-assisted micromachining (AAM). Verification is crucial to ensuring that the models have been correctly implemented and behave according to their intended design.

Internal consistency: we begin by reiterating that verification focuses on internal consistency. It involves checking the model's equations, calculations, algorithms, and code to ensure that they have been accurately translated into the computational framework.

Code review and testing: readers learn that verification often involves a thorough review of the model's code to identify errors, discrepancies, or unintended behaviors. Rigorous testing is performed to ensure that the calculations and logic produce the expected results.

Mathematical rigor: this section highlights the importance of ensuring that the mathematical equations and methods used in the model are accurate and well-founded. Any errors in the mathematical representation can lead to incorrect predictions.

Benchmarking: the section touches on the practice of benchmarking, where the model's outputs are compared against known analytical solutions or reference data to confirm its accuracy under specific conditions.

Model limitations: we discuss how identifying the limitations of the model is an important aspect of verification. Models are simplifications of real-world phenomena, and acknowledging their limitations is essential for understanding the scope of their applicability.

Iterative process: readers gain insight into the iterative nature of verification. As errors or inconsistencies are identified and corrected, the model undergoes multiple rounds of testing and validation to ensure its accuracy.

By the end of this section, readers will have a clear understanding of the verification process for AAM erosion models. This process ensures that the models are internally consistent, accurate in their calculations, and reliable in predicting material removal rates. This knowledge prepares readers to appreciate the significance of internal validation and sets the stage for understanding the external validation process in subsequent sections of the chapter [72].

15.6.3 Experimental Techniques for Measuring Erosion

Experimental techniques play a crucial role in measuring erosion and validating erosion models within the context of abrasive-assisted micromachining (AAM). These techniques provide real-world data that help researchers and engineers understand erosive interactions and validate the accuracy of their models.

Erosion measurement importance: we start by highlighting the significance of accurately measuring erosion. Experimental data provide insights into material removal rates, surface wear, and the effects of erosive forces, which are essential for calibrating and validating erosion models.

Direct observations: one common approach involves direct observations of the material surface before and after AAM. Techniques such as optical microscopy, scanning electron microscopy (SEM), and 3D surface profilometry are used to measure erosion pits, material removal, and surface damage.

Surface profilometry: readers learn that surface profilometry provides quantitative measurements of surface roughness, depth, and features, offering insights into the extent of material removal and wear.

Weight loss measurements: this section explains weight loss measurements, where the change in mass of a sample before and after machining is used to calculate material removal rates. This technique is suitable for understanding material loss due to erosive forces.

Particle velocity and impact measurements: we touch upon techniques that involve measuring particle velocity and impact angles during AAM processes. High-speed cameras and specialized sensors help capture particle behavior, aiding in model validation.

Microhardness testing: the section highlights microhardness testing, which assesses the hardness of a material before and after machining. Changes in hardness provide information about material alterations due to erosive impacts.

Comparison with model predictions: readers gain insight into how the collected experimental data are compared with the predictions of erosion models. This comparison helps researchers validate the models' accuracy and reliability.

By the end of this explanation, readers will understand the various experimental techniques used to measure erosion and validate erosion models in the context of AAM. These techniques provide valuable data that enhance our understanding of the erosion process and contribute to the development of accurate and effective erosion models for optimizing the machining process [73].

15.6.4 Comparison of Model Predictions with Experimental Data

Comparing model predictions with experimental data is a crucial step in validating the accuracy and reliability of erosion models within the context of abrasive-assisted micromachining (AAM). This comparison provides insights into the model's performance and helps assess its ability to predict real-world material removal rates and erosion behavior.

Validation process: we start by emphasizing that comparing model predictions with experimental data is a fundamental aspect of the validation process. The collected experimental data serve as a benchmark against which the model's predictions are evaluated.

Quantitative metrics: readers learn that quantitative metrics are often used to quantitatively assess the similarity between model predictions and experimental data. Metrics such as mean absolute error, root mean square error, and correlation coefficients provide objective measures of how well the model performs.

Accuracy assessment: this section explains that comparing model predictions with experimental data allows researchers and engineers to assess the model's accuracy across a range of scenarios and parameter combinations. It helps identify areas where the model performs well and areas where adjustments might be needed.

Visual comparison: we touch upon the importance of visual comparison, where graphs, plots, and charts are used to overlay the model predictions and experimental data. Visual representation helps researchers identify trends, deviations, and patterns.

Identifying discrepancies: the section discusses how discrepancies between model predictions and experimental

data provide valuable insights. These discrepancies might indicate areas where the model’s assumptions, parameters, or equations need refinement.

Model improvement: readers gain insight into how the comparison process guides the iterative improvement of the model. Adjustments and refinements are made to enhance the model’s accuracy based on how well it aligns with experimental observations.

By the end of this explanation, readers will understand the importance of comparing model predictions with experimental data for validating erosion models in the context of AAM. This comparison process ensures that the models accurately replicate real-world material removal rates and erosion behavior, providing researchers and engineers with confidence in the reliability of their models for optimizing the machining process [74].

15.7 Applications of Erosion Models

Erosion models developed within the context of abrasive-assisted micromachining (AAM) have a wide range of practical applications that contribute to process optimization, material selection, and quality control. These models provide valuable insights into erosive forces, material removal rates, and machining outcomes.

Optimizing process parameters: we start by highlighting how erosion models are used to optimize process parameters such as pressure, standoff distance, and abrasive flow rate. By simulating different parameter combinations, manufacturers can identify optimal settings for achieving desired material removal rates and machining precision.

Predicting material removal rates: readers learn that erosion models help predict material removal rates for

different materials under varying conditions. This information guides manufacturers in estimating machining times, planning production schedules, and optimizing resource utilization.

Selecting materials: this section explains how erosion models aid in material selection by assessing how different materials respond to erosive forces. Manufacturers can choose materials that withstand abrasion and erosion for longer tool lifespans and improved machining quality.

Quality control and inspection: the section touches on how erosion models contribute to quality control by predicting the surface finish, wear, and damage that results from the machining process. This information helps ensure consistent product quality.

Design optimization: we discuss how erosion models influence the design of intricate parts and components. By predicting how erosive forces will interact with specific designs, manufacturers can create parts that maintain structural integrity and desired surface finishes.

Process improvement: readers gain insight into how erosion models contribute to continuous process improvement. Analyzing model predictions and comparing them with realworld outcomes helps identify areas for process enhancement.

Research and development: the section highlights how erosion models aid in research and development efforts. They help researchers explore new materials, refine machining techniques, and understand the complex interactions between erosive forces and materials.

By the end of this explanation, readers will understand the diverse applications of erosion models in the context of AAM. These models serve as powerful tools for optimizing

processes, selecting materials, ensuring quality, and driving innovation in the field of AAM [75].

15.7.1 Role of Erosion Models in Process Optimization

Erosion models play a pivotal role in the process optimization of abrasive-assisted micromachining (AAM), providing valuable insights into the intricate dynamics of the machining process. These models assist in achieving efficient material removal, precise machining, and improved overall performance.

Parameter exploration: we start by highlighting that erosion models allow manufacturers to explore a wide range of process parameters, such as pressure, standoff distance, and abrasive flow rate. By simulating different parameter combinations, manufacturers can identify the optimal settings for achieving desired material removal rates and machining quality.

Optimal material removal rates: readers learn that erosion models predict material removal rates for various materials and process conditions. Manufacturers can use these predictions to determine the most efficient machining strategies, reducing unnecessary material wastage and maximizing productivity.

Reducing tool wear: this section explains how erosion models can assist in reducing tool wear. By predicting the effects of erosive forces on tool surfaces, manufacturers can make informed decisions about tool material selection and machining parameters to extend tool lifespans.

Surface finish prediction: the section discusses how erosion models provide insights into the resulting surface finish after machining. Manufacturers can adjust parameters to

achieve desired surface qualities, reducing the need for post-processing and improving overall part quality.

Minimizing energy consumption: we touch upon how erosion models contribute to energy-efficient machining. By identifying parameter settings that result in optimal material removal rates while minimizing energy consumption, manufacturers can achieve sustainable machining processes.

Quick iterative testing: readers gain insight into how erosion models enable manufacturers to quickly test different scenarios without the need for extensive experimental trials. This accelerates the process optimization cycle and reduces costs.

Scenario testing: the section highlights how erosion models allow manufacturers to test hypothetical scenarios and evaluate their feasibility. This helps in decision-making and strategic planning for complex machining projects.

By the end of this explanation, readers will understand how erosion models serve as indispensable tools in the process optimization of AAM. These models provide the ability to explore various machining parameters, predict outcomes, and make informed decisions to achieve efficient material removal, improved surface finishes, and overall enhanced performance of the machining process [76].

15.7.2 Tool Wear Prediction and Management

Tool wear prediction and management are crucial aspects within the context of abrasive-assisted micromachining (AAM) to ensure efficient and effective machining processes. Predicting tool wear and implementing strategies to manage it are essential for maintaining machining accuracy, quality, and cost-effectiveness.

Significance of tool wear: we start by highlighting that tool wear directly impacts machining outcomes. As tools degrade, they can lead to reduced precision, increased material removal rates, and poor surface finishes. Managing tool wear is essential for maintaining consistent quality.

Predictive modeling: readers learn that erosion models play a significant role in predicting tool wear. These models simulate the interactions between abrasive particles and tool surfaces, providing insights into how wear accumulates over time.

Material removal rate: this section explains that tool wear is closely related to the material removal rate. As tool wear increases, material removal rates can change, affecting both machining efficiency and the lifespan of the tool.

Tool material selection: the section discusses how erosion models can aid in tool material selection. By simulating different tool materials and their responses to erosive forces, manufacturers can choose materials that offer optimal wear resistance.

Parameter optimization: we touch upon how erosion models help optimize machining parameters to reduce tool wear. Adjusting parameters such as pressure, standoff distance, and abrasive flow rate can minimize wear while maintaining desired material removal rates.

Monitoring and maintenance: readers gain insight into how tool wear prediction guides monitoring and maintenance schedules. Predictive models help manufacturers plan timely tool replacements, minimizing downtime and avoiding unexpected tool failures.

Cost savings: the section highlights that effective tool wear management leads to cost savings. Reduced tool

replacement frequency, improved quality, and minimized material wastage contribute to overall process efficiency.

By the end of this explanation, readers will understand the importance of tool wear prediction and management in AAM. Erosion models serve as valuable tools for predicting wear, optimizing machining parameters, and making informed decisions to extend tool lifespans, maintain machining accuracy, and achieve cost-effective and high-quality machining outcomes [77].

15.7.3 Quality Improvement Through Erosion Modeling

Erosion modeling plays a significant role in improving the quality of products and components within the context of abrasive-assisted micromachining (AAM). By accurately predicting material removal rates, surface finishes, and erosion behavior, these models contribute to enhancing the overall quality of machined parts (Figure 15.4).

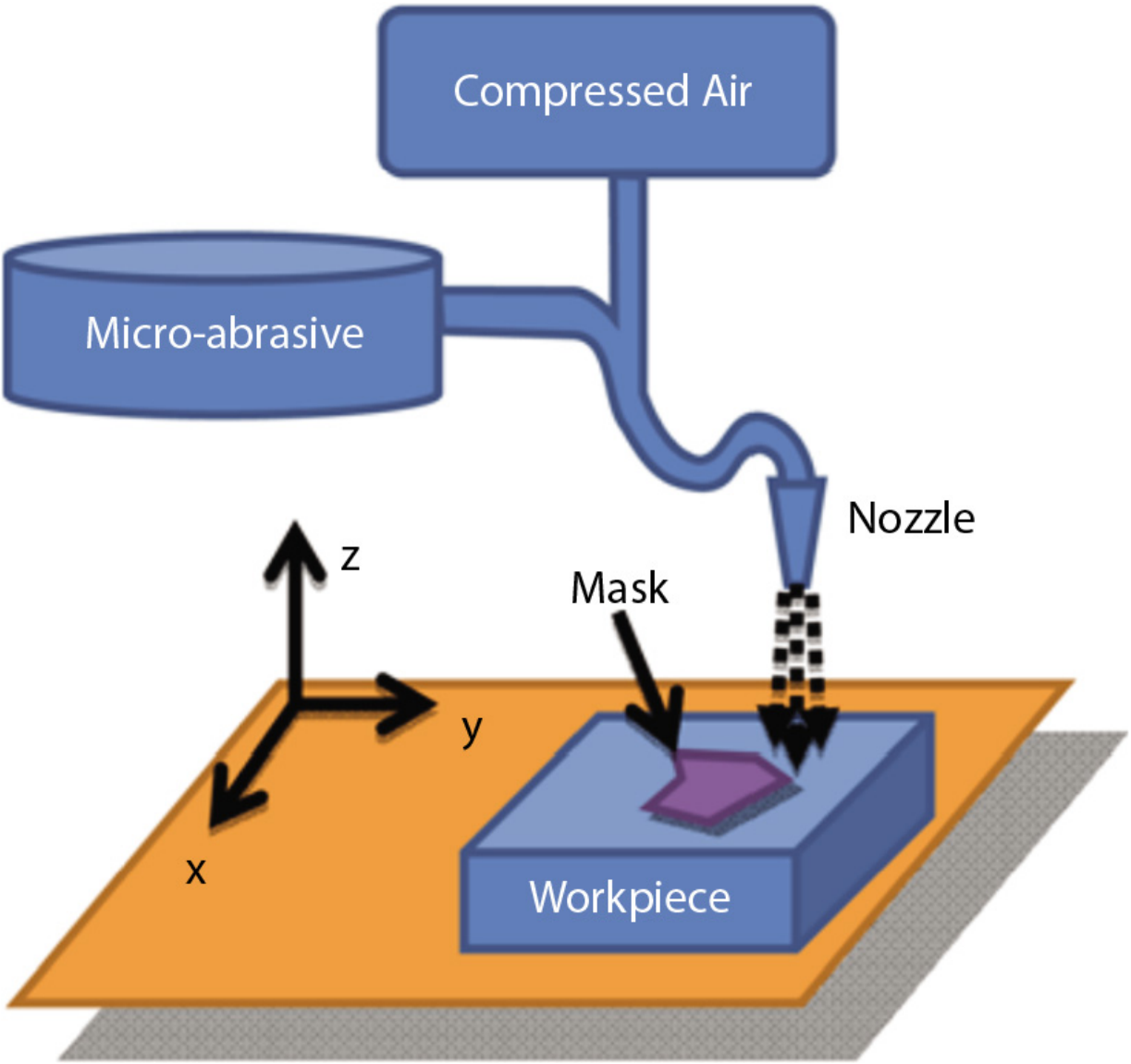


Figure 15.4 Schematic of the LN_2 pressurizing and dispensing equipment [77].

Surface finish enhancement: we start by emphasizing that erosion models provide insights into the resulting surface finish after machining. Manufacturers can adjust process parameters to achieve desired surface qualities, reducing the need for post-processing and enhancing part aesthetics.

Consistent material removal: readers learn that erosion models predict material removal rates accurately, helping manufacturers achieve consistent material removal across

different machining operations. This consistency contributes to uniform part dimensions and enhanced quality.

Minimized defects: this section explains that accurate erosion modeling helps minimize defects caused by uneven material removal or excessive erosion. Manufacturers can identify optimal parameter settings that reduce the likelihood of defects and improve overall part integrity.

Improved dimensional accuracy: the section discusses how erosion models contribute to improved dimensional accuracy. By predicting material removal rates and accounting for erosion behavior, manufacturers can fine-tune parameters to achieve precise part dimensions.

Reduced rework and scrap: we touch upon how erosion models assist in reducing rework and scrap. Predictive models help manufacturers identify parameters that yield the desired quality on the first attempt, minimizing the need for corrective actions and reducing waste.

Enhanced process control: readers gain insight into how erosion models enable enhanced process control. Manufacturers can adjust parameters based on model predictions to ensure that machining outcomes consistently meet quality standards.

Optimal parameter selection: the section highlights how erosion models guide optimal parameter selection for specific machining tasks. Manufacturers can select parameters that achieve the desired quality while minimizing wear, energy consumption, and material wastage.

By the end of this explanation, readers will understand how erosion modeling contributes to quality improvement in AAM. These models provide manufacturers with insights into surface finishes, material removal rates, and erosion

behavior, enabling them to optimize parameters, enhance consistency, and deliver high-quality machined components [78].

15.8 Advancements in Erosion Modeling Techniques

Advancements in erosion modeling techniques have significantly enhanced our ability to accurately simulate and predict erosive interactions within the context of abrasive-assisted micromachining (AAM). These techniques leverage computational power, data-driven approaches, and an improved understanding of erosive mechanisms to provide more accurate and reliable predictions.

Introduction to advancements: we start by highlighting the importance of continuous advancements in erosion modeling techniques. These advancements enable researchers and engineers to tackle complex erosive interactions and improve the accuracy of model predictions.

Computational fluid dynamics (CFD): readers learn about the integration of computational fluid dynamics in erosion modeling. Computational fluid dynamics techniques simulate fluid flow and particle interactions, allowing for a detailed representation of the erosive jet and its impact on the material surface.

Finite element analysis (FEA): this section discusses how finite element analysis can be coupled with erosion models to account for material deformation and stress distribution during the machining process. This integrated approach provides a more comprehensive understanding of erosive mechanisms.

Machine learning and data-driven approaches: the section emphasizes the role of machine learning in erosion modeling. Machine learning algorithms can learn from large datasets of real-world observations to predict erosion behavior and material removal rates accurately.

Multiscale modeling: we touch upon multiscale modeling, where different lengths and time scales are considered in the model. This approach captures the complexity of erosive interactions occurring at various levels and provides more accurate predictions.

Physics-informed models: this section highlights the development of physics-informed models that combine physical principles with computational techniques. These models enhance the accuracy of predictions by incorporating a fundamental understanding of erosive mechanisms.

Material response models: readers gain insight into the integration of material response models into erosion simulations. These models consider how different materials respond to erosive forces, improving the accuracy of material removal rate predictions.

Validation and data quality: the section discusses how advancements in erosion modeling techniques also require high-quality experimental data for validation. Accurate validation data contribute to refining and improving the models.

By the end of this explanation, readers will understand the significance of advancements in erosion modeling techniques for AAM. These techniques leverage computational tools, data-driven approaches, and an improved understanding of erosive mechanisms to provide more accurate, reliable, and comprehensive predictions. These advancements contribute to enhancing the accuracy

of material removal rate predictions, optimizing machining processes, and guiding effective decision-making in AAM [79].

15.8.1 Future Directions in Erosion Modeling for AAM

This section explores the potential future directions and trends that are likely to shape the field of erosion modeling for abrasive-assisted micromachining (AAM). As technology and research continue to evolve, these directions offer opportunities to enhance the accuracy, applicability, and effectiveness of erosion models.

Advancements in computational techniques: we start by discussing how computational techniques, such as finite element analysis, computational fluid dynamics, and multiscale modeling, are likely to see continued advancements. These techniques enable more detailed and comprehensive simulations of erosive interactions.

Integration of machine learning: readers learn about the increasing role of machine learning in erosion modeling. Machine learning algorithms can harness large datasets to enhance predictions, leading to more accurate material removal rate estimates and erosion behavior simulations.

Real-time predictive models: this section emphasizes the potential for developing real-time predictive models for AAM. These models could provide immediate insights into material removal rates and erosion behavior during ongoing machining processes, facilitating dynamic process adjustments.

Material-process interaction models: the section discusses the potential for models that incorporate the interactions between materials and the AAM process. This would lead to

a more accurate representation of material responses, enhancing overall modeling accuracy.

Virtual prototyping and optimization: we touch upon how erosion models could be used for virtual prototyping and optimization of machining processes. Manufacturers can simulate different designs and parameters to identify optimal setups before physical machining even begins.

Environmental impact assessment: the section explores the possibility of using erosion models to assess the environmental impact of AAM processes. This includes predicting the generation of waste materials, energy consumption, and other factors.

Industry 4.0 integration: readers gain insight into how erosion models could be integrated into Industry 4.0 initiatives, contributing to the development of smart manufacturing processes that optimize machining based on real-time data and predictions.

By the end of this section, readers will have gained an understanding of the potential future directions in the field of erosion modeling for AAM. These directions highlight the ongoing evolution of computational techniques, the increasing role of machine learning, and the potential for real-time predictions and dynamic process adjustments. These trends offer exciting opportunities to enhance the accuracy, efficiency, and sustainability of AAM processes in the years to come [80].

15.9 Concluding Remarks and Implications for AAM Erosion Modeling

This concluding section summarizes the key insights and implications discussed throughout the chapter on erosion

modeling for abrasive-assisted micromachining (AAM). It reflects the significance of erosion modeling, its challenges, and the potential impact on the field of machining.

Summary of key points: we start by summarizing the key points and takeaways from the previous sections, emphasizing the importance of erosion models in predicting material removal rates, optimizing parameters, and enhancing machining quality.

Challenges and opportunities: the section acknowledges the challenges faced in accurately modeling erosive interactions. It highlights the opportunities for advancement through computational techniques, data-driven approaches, and an improved understanding of erosive mechanisms.

Interdisciplinary collaboration: this section discusses the interdisciplinary nature of erosion modeling. Engineers, physicists, material scientists, and computational experts collaborate to develop comprehensive models that bridge theoretical understanding and real-world observations.

Impact on AAM field: readers gain insight into the broader implications of erosion modeling on the AAM field. Accurate models have the potential to revolutionize machining processes, reduce material wastage, enhance part quality, and improve overall operational efficiency.

Driving innovation: the section explores how erosion modeling drives innovation by enabling virtual prototyping, dynamic parameter adjustments, and the exploration of new machining techniques. This innovation contributes to the continuous advancement of the machining industry.

Ongoing research: we touch upon the need for ongoing research to address challenges, refine models, and explore new avenues for improvement. Research efforts will

continue to shape the accuracy and applicability of erosion modeling in the future.

Collaboration and knowledge sharing: readers learn that collaboration and knowledge sharing within the AAM community are essential for the progress of erosion modeling. Researchers and practitioners can collectively contribute to refining models and pushing the boundaries of the field.

By the end of this section, readers will have gained a comprehensive understanding of the implications and significance of erosion modeling in the context of AAM. This chapter concludes by highlighting the potential of erosion models to transform machining processes, drive innovation, and contribute to the ongoing advancement of the machining industry.

References

1. Madić, M. and Radovanović, M., Mathematical modeling and analysis of AWJ cutting of carbon steel S275JR using ANN. *Acad. J. Manuf. Eng.*, 9, 49–54, 2011.

2. Caydaş, U. and Hasçalik, A., A study on surface roughness in abrasive waterjet machining process using artificial neural networks and regression analysis method. *J. Mater. Proces. Technol.*, 202, 574–582, 2008.

3. Srinivasu, D.S. and Ramesh Babu, N., A neuro-genetic approach for selection of process parameters in abrasive waterjet cutting considering variation in diameter of focusing nozzle. *Appl. Soft Comp.*, 8, 809–819, 2008.

4. Jegaraj, J.J.R. and Ramesh Babu, N., A soft computing approach for controlling the quality of cut with abrasive waterjet cutting system experiencing orifice and focusing

tube wear. *J. Mater. Proces. Technol.*, 185, 217–227, 2007.

5. Lu, Y., Li, X., Jiao, B., Liao, Y., *Application of artificial neural networks in abrasive waterjet cutting process*. *International Symposium on Neural Networks*, Chongqing, China, pp. 877–882, 2005.

6. Ciupan, C., Ciupa, E., Ferenţ-Pipaş, S., Neural model for abrasive water jet cutting machine. *Nonconv. Technol. Rev.*, 17, 25–29, 2013.

7. Feng, C.X., Yu, Z.G., Kusiak, A., Selection and validation of predictive regression and neural network models based on designed experiments. *IIE Trans.*, 38, 13–23, 2006.

8. Zain, A.M., Haron, H., Sharif, S., Review of ANN technique for modeling surface roughness performance measure in the machining process, in: *Proceedings- 2009 3rd Asia Intl. Conf. on Modelling and Simulation*, vol. 5071954, pp. 35–39, AMS 2009.

9. Chinu, K., Sanjay, K.C., A review on magnetically assisted abrasive finishing and their critical process parameters. *Manuf. Rev.* 5, 13, 2018, https://doi.org/10.1051/mfreview/2018010.

10. Lei, Y.Y., Jia, Q., Yang, G.L., Qiu, G., Ma, C., Song, Q.J., Abrasive water jet precise machining based on ANN. *J. Sichuan Univ. Eng., (Eng. Sci. Ed.)*, 37, 6, 155–159, 2005.

11. Parikh, P.J. and Lam, S.S., Parameter estimation for Abrasive Assisted Micromachining process using neural networks. *Int. J. Adv. Manuf. Technol.*, 40, 5–6, 497–502, 2009.

12. Yang, L., Peng, Z., Tang, C., Zhang, F., Numerical model of abrasive water jet cutting speed based on ANN. *Trans. Chin. Soc. Agric. Mach.,* 36, 5, 117–120, 2005.

13. Levenberg, K., A Method for the Solution of Certain Non-Linear Problems in Least Squares. *Q. Appl. Math.*, 2, 164–168, 1944.

14. Chakravarthy, P.S. and Ramesh Babu, N., A semi-empirical model for cutting granite with abrasive waterjets, in: *Proc. of 17th AIMTDR*, pp. 259–262, 1997.

15. Chakravarthy, P.S. and Ramesh Babu, N., A hybrid approach for selection of optimal process parameters in abrasive water jet cutting. *I. Mech. E, J. Eng. Manufact., Part B*, 214, 781–791, 2000.

16. Zain, A.M., Haron, H., Sharif, S., Estimation of the minimum machining performance in the AAM using integrated ANN-SA. *Int. J. Expert Syst. Appl.,* 38, 8316–8326, 2011.

17. Cornel, C., Emilia, C., Siliva, F.P., Neural model for abrasive water jet cutting machine, Nonconventional Technologies Review, in: *Romanian Association of Nonconventional Technologies*, 2013.

18. Ficko, M., Begic-Hajdarevic, D., Cohodar Husic, M., Berus, L., Cekic, A., Klancnik, S., Prediction of Surface Roughness of an Abrasive Water Jet Cut Using an Artificial Neural Network. *Materials*, 14, 3108, 2021.

19. Bławucki, S., Zaleski, K., Leleń, M., Analysis of capabilities of cutting thin-walled structures of EN AW-2024 T351 alloy using an abrasive water-jet. *Mechanik*, 8, 1078–1079, 2016.

20. Copertaro, E., Assessment of Resistive Strain Gauges Measurement Performances in Experimental Modal Analysis and Their Application to the Diagnostics of Abrasive Waterjet Cutting Machinery. *Measurement*, 188, 110626, 2022.

21. Ochal, P., Kuczmaszewski, J., Kłonica, M., Assessment of surface finish quality of metal/ composite compound structures as cut by abrasive water-jet. *Mechanik*, 90, 436–438, 2017.

22. Moldovan, M., Boșca, A., Roman, C., Prejmerean, C., Prodan, D., Bere, P., Cosma, C., Rotaru, H., Bone Reaction to a Newly Developed Fiber-Reinforced Composite Material for Craniofacial Implants. *Mater. Plast.*, 57, 131–139, 2020.

23. Bere, P., Dudescu, M., Neamțu, C., Cocian, C., Design, Manufacturing and Test of CFRP Front Hood Concepts for a Light-Weight Vehicle. *Polymers*, 13, 1374, 2021.

24. Ganovska, B., Molitoris, M., Hosovsky, A., Pitel, J., Krolczyk, J.B., Ruggierio, A., Krolczyk, G.M., Hloch, S., Design of the Model for the On-Line Control of the AWJ Technology Based on Neural Networks. *Indian J. Eng. Mater. Sci.*, 23, 279–287, 2016.

25. Duspara, M. and Starčević, V., Samardžić, I. Analysis of Zones Created with Waterjet Cutting of AISI 316 L Corrosion Resistant Steel. *Teh. Vjesn.—Tech. Gaz.*, 25, 199165, 2018.

26. Duspara, M. and Palatinuš, T., Samardžić, I.; Marić, D.; Starčević, V.; Stoić, A. Influence of Abrasive Feeding and Cutting Direction on the Surface Roughness. *Procedia Eng.*, 149, 48–55, 2016.

27. Bere, P. and Krolczyk, J.B., Determination of Mechanical Properties of Carbon/Epoxy Plates by Tensile Stress Test. *E3S Web Conf.*, 19, 03018, 2017.

28. Deaconescu, A. and Deaconescu, T., Response Surface Methods Used for Optimization of Abrasive Waterjet Machining of the Stainless Steel X2 CrNiMo 17-12-2. *Materials*, 14, 2475, 2021.

29. Müller, M., Kolář, V., Šulc, J., Mishra, R.K., Hromasová, M., Behera, B.K., Effect of Waterjet Machining Parameters on the Cut Quality of PP and PVC-U Materials Coated with Polyurethane and Acrylate Coatings. *Materials*, 14, 7542, 2021.

30. Löschner, P., Jarosz, K., Niesłony, P., Investigation of the Effect of Cutting Speed on Surface Quality in Abrasive Water Jet Cutting of 316L Stainless Steel. *Procedia Eng.*, 149, 276–282, 2016.

31. Pytka, J., Budzyński, P., Józwik, J., Michałowska, J., Tofil, A., Łyszczyk, T., Błażejczak, D., Application of GNSS/INS and an Optical Sensor for Determining Airplane Takeoff and Landing Performance on a Grassy Airfield. *Sensors*, 19, 5492, 2019.

32. Biruk-Urban, K., Zagórski, I., Kulisz, M., Leleń, M., Analysis of Vibration, Deflection Angle and Surface Roughness in Water-Jet Cutting of AZ91D Magnesium Alloy and Simulation of Selected Surface Roughness Parameters Using ANN. *Materials*, 16, 3384, 2023.

33. Maneiah, D., Shunmugasundaram, M., Raji Reddy, A., Zareena Begum Optimization of Machining Parameters for Surface Roughness during Abrasive Assisted Micromachining of Aluminium/Magnesium Hybrid Metal

Matrix Composites. *Mater. Today Proc.*, 27, 1293–1298, 2020.

34. Copertaro, E., Perotti, F., Castellini, P., Chiariotti, P., Martarelli, M., Annoni, M., Focusing Tube Operational Vibration as a Means for Monitoring the Abrasive Waterjet Cutting Capability. *J. Manuf. Process.*, 59, 1–10, 2020.

35. Oleksik, M., Dobrotă, D., Tomescu, M., Petrescu, V., Improving the Performance of Steel Machining Processes through Cutting by Vibration Control. *Materials*, 14, 5712, 2021.

35. Peko, I., Marić, D., Nedić, B., Samardžić, I. Modeling and Optimization of Cut Quality Responses in Plasma Jet Cutting of Aluminium Alloy EN AW-5083. *Materials*, 14, 5559, 2021.

36. Leleń, M., Ruggiero, A., Józwik, J., Geometric Features of a Multilayer Surface After Water Jet Cutting in Variable Cutting Conditions. *Manuf. Technol.*, 22, 713–723, 2023.

37. Tyč, M., Hlaváčová, I.M., Barták, P., Analyses of Vibration Signals Generated in W. Nr. 1.0038 Steel during Abrasive Water Jet Cutting Aimed to Process Control. *Materials*, 15, 345, 2022.

38. Wala, T. and Lis, K., Influence of Selected Diagnostic Parameters on the Quality of AWJ Cutting Surface. *Adv. Sci. Technol. Res. J.*, 16, 129–140, 2022.

39. Selvam, R., Karunamoorthy, L., Arunkumar, N., Investigation on Performance of Abrasive Water Jet in Machining Hybrid Composites. *Mater. Manuf. Process.*, 32, 700–706, 2017.

40. Adam Khan, M. and Gupta, K., Machinability Studies on Abrasive Assisted Micromachining of Low Alloy Steel for Different Thickness. *IOP Conf. Ser. Mater. Sci. Eng.*, 709, 044099, 2020.

41. Józwik, J., Ruggiero, A., Leleń, M., Microscopic Analysis of the Surface Morphology of Multilayer Structures of the AluminumAlloy—Silicon Type after Water Jet Cutting. *Manuf. Technol.*, 22, 693–702, 2023.

42. Monno, M. and Ravasio, C., The Effect of Cutting Head Vibrations on the Surfaces Generated by Waterjet Cutting. *Int. J. Mach. Tools Manuf.*, 45, 355–363, 2005.

43. Xiu, C., Weng, Y., Shi, W., Vision, and Vibration Data Fusion-Based Structural Dynamic Displacement Measurement with Test Validation. *Sensors*, 23, 4547, 2023.

44. Hreha, P., Radvanská, A., Hloch, S., Peržel, V., Królczyk, G., Monková, K., Determination of Vibration Frequency Depending on Abrasive Mass Flow Rate during Abrasive Water Jet Cutting. *Int. J. Adv. Manuf. Technol.*, 77, 763–774, 2015.

45. Peržel, V., Hreha, P., Hloch, S., Tozan, H., Valíček, J., Vibration Emission as a Potential Source of Information for Abrasive Waterjet Quality Process Control. *Int. J. Adv. Manuf. Technol.*, 61, 285–294, 2012.

46. Krenický, T. and Rimár, M., Monitoring of Vibrations in the Technology of AWJ. *Key Eng. Mater.*, 496, 229–234, 2011.

47. Karmiris-Obratański, P., Karkalos, N.E., Kudelski, R., Papazoglou, E.L., Markopoulos, A.P., Experimental Study on the Correlation of Cutting Head Vibrations and Kerf

Characteristics during Abrasive Waterjet Cutting of Titanium Alloy. *Procedia CIRP*, 101, 226–229, 2021.

48. Michałowska, J., Tofil, A., Józwik, J., Pytka, J., Legutko, S., Siemiątkowski, Z., Łukaszewicz, A., Monitoring the Risk of the Electric Component Imposed on a Pilot During Light Aircraft Operations in a High-Frequency Electromagnetic Field. *Sensors*, 19, 5537, 2019.

49. Dziedzic, K., Pashechko, M., Barszcz, M., Józwik, J., Structure and Construction Assessment of the Surface Layer of Hardfaced Coating after Friction. *Adv. Sci. Technol. Res. J.*, 11, 253–260, 2017.

50. Zhang, H., Zhao, Z., Li, J., Ye, L., Liu, Y., Review on Abrasive Machining Technology of SiC Ceramic Composites. *Micromachines*, 15, 1, 106, 2024, https://doi.org/10.3390/mi15010106.

51. Opěla, P., Schindler, I., Kawulok, P., Kawulok, R., Rusz, S., Sauer, M., Shallow and Deep Learning of an Artificial Neural Network Model Describing a Hot Flow Stress Evolution: A Comparative Study. *Mater. Des.*, 220, 110880, 2022.

52. Churyumov, A., Kazakova, A., Churyumova, T., Modelling of the Steel High-Temperature Deformation Behaviour Using Artificial Neural Network. *Metals*, 12, 447, 2022.

53. Honysz, R., Modeling the Chemical Composition of Ferritic Stainless Steels with the Use of Artificial Neural Networks. *Metals*, 11, 724, 2021.

54. Rymarczyk, T., Kozłowski, E., Kłosowski, G., Electrical Impedance Tomography in 3D Flood Embankments Testing—Elastic Net Approach. *Trans. Inst. Meas. Control*, 42, 680–690, 2020.

55. Duspara, M., Starčević, V., Samardžić, I., Horvat, M., Optimization of Abrasive Waterjet Machining Process Parameters. *Teh. Glas.*, 11, 4, 143–149, 2017.

56. Stoić, A., Duspara, M., Kosec, B., Stoić, M., Samardžić, I., The Influence of Mixing Water and Abrasives on the Quality of Machined Surface. *Metal.-Sisak Then Zagreb.*, 53, 239–242, 2014.

57. Ke, G., Meng, Q., Finley, T., Wang, T., Chen, W., Ma, W., Ye, Q., Liu, T.-Y., LightGBM: A Highly Efficient Gradient Boosting Decision Tree, in: *Proceedings of the 31st Conference on Neural Information Processing Systems (NIPS 2017)*, Long Beach, CA, USA, 4–9 December, 2017.

58. Storn, R. and Price, K., Differential Evolution—A Simple and Efficient Heuristic for Global Optimization over Continuous Spaces. *J. Glob. Optim.*, 11, 341–359, 1997.

59. Madić, M., Janković, P., Slătineanu, L., Radovanović, M., Artificial Intelligence Model for the Prediction of Cut Quality in Abrasive Water Jet Cutting. *Applied Mechanics Materials*, 657, 206–210, 2014, https://doi.org/10.4028/www.scientific.net/amm.657.206Gupta.

60. T., Ramkumar, J., Tandon, P., Vyas, N., Application of Artificial Neural Networks in Abrasive Water Jet Milling. *Procedia CIRP*, 37, 225–229, 2015, https://doi.org/10.1016/j.procir.2015.08.076.

61. Natarajan, Y., Murugesan, P.K., Mohan, M., Liyakath Ali Khan, S.A., Abrasive Assisted Micromachining process: A state of the art of the review. *J. Manuf. Processes*, 49, 271–322, 2020, https://doi.org/10.1016/j.jmapro.2019.11.030.

62. Zhao, H., Gu, Y., Xi, Y., Fu, X., Gao, Y., Wang, J., Xie, L., Liang, G., Simulation and Experimental Study of Non-Resonant Vibration-Assisted Lapping of SiCp/Al. *Micromachines*, *15*, 113, 2024, https://doi.org/10.3390/mi15010113.

63. Chen, X., Xu, S., Meng, F., Yu, T., Zhao, J., Multi-Objective Optimization in Ultrasonic Polishing of Silicon Carbide via Taguchi Method and Grey Relational Analysis. *Materials*, *16*, 5673, 2023, https://doi.org/10.3390/ma16165673.

64. Arola, D. and Ramulu, M., Material removal in abrasive waterjet machining of metals Surface integrity and texture. *Wear*, 210, 1–2, 50–58, 1997, https://doi.org/10.1016/s0043-1648(97)00087-2.

65. Meng, H. and Ludema, K., Wear models and predictive equations: their form and content. *Wear*, 181–183, 443–457, 1995. https://doi.org/10.1016/0043-1648(95)90158-2.

66. Kulekci, M.K., Processes and apparatus developments in industrial waterjet applications. *Int. J. Mach. Tools Manuf.*, 42, 12, 1297–1306, 2002, https://doi.org/10.1016/s0890-6955(02)00069-x.

67. Akkurt, A., Kulekci, M.K., Seker, U., Ercan, F., Effect of feed rate on surface roughness in abrasive waterjet cutting applications. *J. Mater. Process. Technol.*, 147, 3, 389–396, 2004, https://doi.org/10.1016/j.jmatprotec.2004.01.013.

68. Arola, D., McCain, M., Kunaporn, S., Ramulu, M., Waterjet and abrasive waterjet surface treatment of titanium: a comparison of surface texture and residual

stress. *Wear*, 249, 10–11, 943– 950, 2001, https://doi.org/10.1016/s0043-1648(01)00826-2.

69. Chen, F., Siores, E., Patel, K., Momber, A., Minimizing particle contamination at abrasive waterjet machined surfaces by a nozzle oscillation technique. *Int. J. Mach. Tools Manuf.*, 42, 13, 1385–1390, 2002, https://doi.org/10.1016/s0890-6955(02)00081-0.

70. Leleń, M., Biruk-Urban, K., Józwik, J., Tomiło, P., Modeling and Machine Learning of Vibration Amplitude and Surface Roughness after Waterjet Cutting. *Materials*, 16, 19, 6474, 2023, https://doi.org/10.3390/ma16196474.

71. Hashish, M. and Zalzala, A.M.S., A study of abrasive-waterjet machining. *Int. J. Mach. Tool Des. Res.*, 23, 3, 187–197, 1983.

72. Pandalai, K.A. and Pashby, I.R., A study of surface finish and accuracy in Abrasive Assisted Micromachining. *J. Mater. Process. Technol.*, 37, 3, 381–390, 1993.

73. Hashish, M. and Mohamed, S., II, Development of an expert system for abrasive waterjet machining. *Int. J. Mach. Tools Manuf.*, 37, 2, 205–218, 1997.

74. Hashish, M., Surface integrity of materials machined by abrasive waterjet. *Int. J. Mach. Tools Manuf.*, 40, 12, 1703–1714, 2000.

75. Hashish, M. and Fawzy, M., Process capabilities of abrasive waterjet machining. *J. Mater. Process. Technol.*, 153, 1000–1007, 2004.

76. Hashish, M., Recent developments in abrasive waterjet technology. *Int. J. Mach. Tools Manuf.*, 47, 13, 1867–1873, 2007.

77. Kim, H., Lee, I., Ko, T.J., 3D tool path generation for micro-abrasive jet machining on 3D curved surface. *Int. J. Precis. Eng. Manuf.*, 14, 1519–1525, 2013, https://doi.org/10.1007/s12541-013-0205-9.

78. Heaney, D.F. and Hashish, M., Effects of abrasive waterjet cutting on the fatigue life of aerospace materials. *Int. J. Mach. Tools Manuf.*, 66, 1-4, 121–132, 2013.

79. Hashish, M. and El-Sayed, M., A review of abrasive water jet cutting. *Int. J. Adv. Manuf. Technol.*, 80, 1-4, 545–550, 2015.

80. Liu, H. and Chen, Y., Experimental study on surface quality and precision of Abrasive Assisted Micromachining. *Procedia CIRP*, 62, 493–498, 2017.

Note

**Corresponding author*: rayappamahale@gmail.com

16
Abrasive Water Jet Micromachining: Pushing the Micro-Frontier Further—A Glimpse at Recent Advancements

M. Abdur Rahman[1]*, Mohamed Bak Kamaludeen[1], T. R. Tamilarasan[2], N. Rajmohan[2] and S. Loganathan[1]

[1]Department of Mechanical Engineering, B.S. Abdur Rahman Crescent Institute of Science & Technology, Chennai, India

[2]Department of Automobile Engineering, B.S. Abdur Rahman Crescent Institute of Science & Technology, Chennai, India

Abstract

This chapter presents an in-depth examination of abrasive water jet micromachining (AWJMM), an advanced material removal process that synergizes the erosive force of high-velocity water with the abrasive action of particulate matter to achieve precise material cutting with minimal thermal deformation. Central to AWJMM is its capability to efficaciously section a diverse array of materials, ranging from metals to composite structures, by propelling water at supersonic speeds while integrating abrasive granules, such as garnet, into the jet stream. This amalgamation not only ensures elevated cutting efficacy but also promotes the reduction of material wastage and environmental detriment, positioning it as a superior alternative to conventional machining paradigms. The merits of AWJMM are multifaceted, encompassing its non-thermal nature, eco-friendliness, capability to execute intricate cuts with reduced material loss, and its adaptability across a multitude of industrial sectors. Subsequently, the discourse extends to the examination of the applications of AWJMM within various domains such as aerospace, automotive, and electronics, where the prerequisites of precision and material integrity are paramount. The attribute of AWJMM to function devoid of inducing thermal damage or mechanical stresses unveils novel pathways for fabricating complex components with heightened precision and minimal necessity for post-processing interventions. This section delves into key research within the AWJMM field, summarizing technological progress and insights from scholarly articles. It highlights advancements in abrasive materials, jet propulsion, and optimization techniques, aiming to enhance AWJMM's efficiency, precision, and environmental sustainability. These developments are pushing the boundaries of AWJMM's applications and economic viability. Looking ahead, the text forecasts significant innovations in automation, material science, and computational fluid dynamics, expected to improve AWJMM's precision, efficiency, and adaptability across industries. This forward-looking perspective underscores AWJMM's potential to revolutionize precision engineering and sustainable manufacturing, marking its critical contribution to the evolution of modern manufacturing.

***Keywords*:** Abrasive water jet micromachining (AWJMM), precision engineering, sustainability, technological innovations

16.1 Introduction

Abrasive water jet micromachining (AWJMM) represents a cutting-edge technology in the realm of microscale machining, offering precision and versatility in the fabrication of intricate components with unparalleled intricacy and accuracy. This cutting-edge method utilizes the force of high-pressure water streams combined with abrasive particles to accurately eliminate material from objects, facilitating the creation of microstructures and features with remarkable precision and quality. Abrasive water jet micromachining

(AWJMM) has emerged as a cornerstone technique in various industries, including aerospace, automotive, electronics, and biomedical engineering, where intricate microscale components are indispensable [1].

At its core, AWJMM operates on the principle of combining a high-pressure water jet with abrasive particles, typically garnet or aluminum oxide, to create a highly potent cutting tool. When abrasive particles are integrated into the water flow, they enhance the cutting capability of the jet, allowing it to effectively erode a wide variety of materials, including composites, ceramics, metals, and polymers. This process is particularly well-suited for machining materials that are difficult to cut using conventional methods due to their hardness, brittleness, or thermal sensitivity [2].

Essential elements of an AWJMM system comprise a high-pressure pump, a system for delivering abrasives, a mixing chamber, a focusing nozzle, and a CNC (computer numerical control) controller. The high-pressure pump generates the requisite pressure, typically ranging from 30,000 to 90,000 pounds per square inch (psi), to propel the water through the system. The system responsible for delivering abrasives feeds the abrasive particles into the water flow, where they are captured and propelled toward the workpiece. The mixing chamber guarantees an even spread of abrasive particles throughout the water flow, enhancing the precision and effectiveness of the cutting process [3].

A crucial element within the AWJMM system, the focusing nozzle plays a key role in concentrating the high-pressure water jet and abrasive particles into a tightly controlled beam. This feature enables the accurate elimination of materials and supports complex machining processes. The nozzle design, including its geometry and aperture size, significantly influences the cutting performance and quality of the machined features. Additionally, the CNC controller orchestrates the movement of the nozzle relative to the workpiece, facilitating complex machining operations with exceptional precision and repeatability [3].

One of the distinct advantages of AWJMM is its ability to achieve microscale machining with unparalleled precision and accuracy. The fine abrasive particles, typically in the range of 10–50 µm in diameter, enable the fabrication of microstructures and features with dimensions as small as a few micrometers. This level of precision is critical for applications requiring high-resolution components, such as microelectromechanical systems (MEMS), microfluidic devices, and medical implants [4].

Furthermore, AWJMM offers several inherent benefits over traditional machining methods. Unlike conventional machining processes that generate heat-affected zones, mechanical stresses, and burrs, AWJMM is a cold-cutting technique that minimizes thermal distortion and mechanical damage to the workpiece. This is particularly advantageous when machining heat-sensitive materials or delicate components that require precise dimensional tolerances and surface finishes [5]. Moreover, AWJMM is a versatile and cost-effective machining solution capable of processing a wide range of materials with varying hardness and complexity. From soft polymers and elastomers to hard metals and ceramics, AWJMM can effectively machine virtually any material with exceptional precision and surface quality. This versatility makes AWJMM a preferred choice for prototyping, rapid manufacturing, and production of custom-designed components across diverse industries.

Thus, AWJMM represents a transformative technology in the field of microscale machining, offering unmatched precision, versatility, and efficiency in the fabrication of intricate components and microstructures. Its ability to achieve high-resolution machining with minimal thermal and mechanical effects makes it an indispensable tool in modern manufacturing and engineering applications. As advancements in technology continue to drive innovation in microscale fabrication, AWJMM is poised to play a pivotal role in

shaping the future of precision manufacturing across a myriad of industries [6]. In addition to providing a comprehensive overview of AWJMM as a pivotal technology in precision engineering, this chapter delves into the multifaceted benefits, diverse applications, and the cutting-edge research that continue to propel this field forward. Through an exploration of its operational principles, advantages, and the nuanced control of its machining parameters, we gain insights into why AWJMM stands as a critical tool in the micromanufacturing landscape. The chapter highlights several key benefits that make AWJMM a preferred choice for a wide array of machining tasks. These benefits include its non-thermal cutting process, which eliminates heat-affected zones, thus preserving the integrity of the workpiece material. This aspect is particularly beneficial for materials that are susceptible to thermal distortion. Moreover, the minimal mechanical stress imparted on the workpiece ensures the preservation of material properties post-machining, an essential factor for high-precision components. Another significant advantage discussed is the versatility of AWJMM. Capable of machining a broad spectrum of materials with high precision, from soft polymers to hard ceramics and metals, AWJMM enables manufacturers to tackle a diverse range of projects with a single machining tool. The process's ability to produce complex microscale features with high aspect ratios and smooth surface finishes is also underscored, illustrating its superiority over traditional machining methods [7].

The applications of AWJMM are vast and varied, reflecting its adaptability to different industry needs. This chapter provides a detailed examination of its applications in fields such as aerospace, automotive, electronics, and biomedical engineering. In the aerospace and automotive industries, AWJMM is utilized for producing lightweight structural components with complex geometries, contributing to fuel efficiency and performance enhancements. In the electronics sector, it facilitates the miniaturization of components, while in biomedical engineering, AWJMM is instrumental in creating intricate features on implants and medical devices, which are critical for patient-specific treatments [5].

A pivotal section of this chapter is dedicated to discussing recent research developments in AWJMM. Innovations in process optimization, nozzle design, and abrasive materials are at the forefront of enhancing AWJMM's capabilities. Studies focusing on the environmental impact of AWJMM, aiming to reduce waste and improve recycling of used abrasive materials, reflect the growing emphasis on sustainability within the field. Additionally, research into hybrid machining processes, which combine AWJMM with other machining techniques, reveals efforts to push the boundaries of what can be achieved in terms of precision, efficiency, and material properties [8].

Emerging technologies such as machine learning and artificial intelligence are also being integrated into AWJMM systems to improve process control, predictability, and automation. These advancements not only enhance the efficiency and accuracy of the machining process but also open new avenues for custom and on-demand manufacturing of microscale components. In conclusion, this chapter not only serves as an introduction to the principles and operation of AWJMM but also showcases its significant benefits, wide-ranging applications, and the dynamic research landscape that continues to evolve and expand its capabilities. Through ongoing innovation and exploration, AWJMM is set to remain at the forefront of micromanufacturing technology, offering solutions to some of the most challenging and intricate machining needs across various industries.

16.2 The Essence of AWJMM: A Powerful Blend of Water and Grit

At its core, AWJMM harnesses the combined power of a high-pressure water jet and a stream of fine abrasive particles. Imagine a focused beam of water, pressurized to tens of thousands of times the atmospheric pressure, laden with microscopic garnet, aluminum

oxide, or other abrasive materials. This potent mixture, propelled through a precisely controlled nozzle, becomes a formidable sculpting tool, capable of etching delicate features on a variety of materials, from brittle silicon to tough ceramics.

16.2.1 Abrasive Water Jet Micromachining Setup

The high-velocity water jet acts as the carrier, propelling the abrasive particles towards the workpiece. Upon impact, the abrasive grains erode the material through a combination of scratching, gouging, and microfracturing. By meticulously managing elements like nozzle geometry, size, flow rate, abrasive type, and water pressure, targeted material removal is achieved. This precision allows for the creation of detailed microchannels, microfluidic devices, and other miniaturized components with outstanding accuracy and surface finish [9].

16.2.2 Advantages of AWJMM

Compared to traditional micromachining methods like laser ablation or microelectrical discharge machining (EDM), AWJMM boasts several unique advantages [10]:

- Versatility: a truly universal tool, AWJMM can handle a diverse range of materials, including ceramics, polymers, metals, and even composites.
- Precision and control: the narrow jet stream and precise control over process parameters enable the creation of features with exceptional accuracy and surface finish, often on the order of micrometers.
- No thermal influence: unlike laser or EDM, AWJMM is a cold machining process, generating minimal heat. This eliminates thermal deformations and preserves the material’s properties, making it ideal for heat-sensitive materials.
- Contactless process: the non-contact nature of AWJMM minimizes tool wear and tear, leading to lower maintenance costs and increased productivity.
- Environmentally friendly: AWJMM utilizes water as the primary medium, making it a clean and sustainable alternative to processes that generate hazardous waste.

The following Table 16.1 summarizes the applications of AWJMM in various industries. This table provides a concise overview of how AWJMM is applied across different industries, showcasing its adaptability and versatility in addressing various manufacturing needs [11].

16.2.3 Unveiling the Applications of AWJMM

The applications of AWJMM extend across various industries, each benefitting from its unique capabilities [5, 12–14]:

- Electronics: AWJMM fabricates intricate microcircuits, MEMS devices, and other miniaturized electronic components with high precision and minimal heat impact.

Table 16.1 Uses of abrasive water jet micromachining (AWJMM) across different industries.

Industry	Applications
Aerospace	– Production of lightweight structural components
	– Creation of complex geometries
	– Contribution to fuel efficiency and performance
Automotive	– Manufacturing lightweight structural components
	– Creating complex geometries
	– Enhancing fuel efficiency and overall performance
Electronics	– Facilitating miniaturization of components
	– Precision machining of electronic parts
	– Producing intricate features on microelectronic devices
Biomedical engineering	– Creating intricate features on implants
	– Precision machining of medical devices
	– Contributing to patient-specific treatments

- Medical: AWJMM creates microfluidic devices for medical diagnostics, surgical stents, and other delicate medical implants with exceptional surface finish and biocompatibility.
- Aerospace: AWJMM manufactures lightweight and high-strength aerospace components with complex geometries, contributing to fuel efficiency and performance.
- Automotive: AWJMM enables the production of precise fuel injector nozzles, intricate cooling channels, and other critical automotive components.
- Microplastics research: AWJMM can be used to precisely cut and analyze microplastics, aiding in environmental research and pollution control.

The following Table 16.2 provides a concise overview of how AWJMM is applied in various industries, showcasing its adaptability and contribution to diverse manufacturing needs.

These are just a glimpse of the diverse applications where AWJMM finds its mark. As research and development progress, the potential of AWJMM continues to expand, pushing the boundaries of miniaturization and paving the way for innovative products and technologies across various fields.

Table 16.2 Overview of how AWJMM is applied in various industries.

Industry	Applications
Electronics	– Fabrication of intricate microcircuits
	– Manufacturing MEMS devices
	– Production of miniaturized electronic components
	– High precision with minimal heat impact
Medical	– Creation of microfluidic devices
	– Fabrication of surgical stents
	– Production of delicate medical implants
	– Exceptional surface finish and biocompatibility
Aerospace	– Manufacturing lightweight and high-strength components
	– Production of parts with complex geometries
	– Contribution to fuel efficiency and overall performance
Automotive	– Production of precise fuel injector nozzles
	– Creation of intricate cooling channels
	– Manufacturing other critical automotive components
Microplastics research	– Precise cutting and analysis of microplastics
	– Contribution to environmental research and pollution control

16.3 Some Prominent Research Works on Abrasive Water Jet Micromachining

16.3.1 The Intricacies of Submerged and Dry Abrasive Water Jet (AWJ) Micromilling

Haghbin *et al.* [15] investigated both submerged and dry conditions in micromilling with abrasive water jet (AWJ), specifically for creating microchannels in metals. The study centered on 316L stainless steel and 6061-T6 aluminum. The exploration delved into the impact of nozzle angles and standoff distances on erosion rates and the shapes of the channels. Results showed deeper channels reduce centerline erosion due to jet spread and stagnation, a trend unaffected by submergence. Submerged operations yielded narrower channels, as water confines the jet's spread, unlike in air where wider channels form. This study highlights that submerged AWJ micromilling produces more precise features without compromising erosion rate, offering advantages for precise microfabrication tasks.

16.3.2 Predicting Microfeature Profiles in ASJM of Borosilicate Glass

Nouraei and collaborators [16] verified the precision of a surface evolution model in the context of abrasive slurry jet micromachining (ASJM) on borosilicate glass, yielding microchannels with variations in depth and width of under 3%. The ASJM system showcased remarkable accuracy, achieving an inter-channel repeatability of within 5%. The study enhanced an existing model for abrasive air jet micromachining by incorporating measured erosion rates of borosilicate glass. Remarkably, this model accurately predicted the profiles of microchannels, with a maximum deviation of 7% even for aspect ratios as high as 5. This research contributes to leveraging surface evolution models for ASJM, offering potential enhancements in microfeature design and fabrication on borosilicate glass.

G. Hailu [17] research introduces cryogenically assisted abrasive jet micromachining (CAJM), enhancing the machining of elastomers like PDMS for micro-devices in microfluidics and MEMS. This innovative approach improves erosion rates and reduces particle embedment compared to traditional abrasive jet micromachining (AJM). Through finite element analysis, Hailu investigates the effects of erosion, cooling, and thermal distortion on machining accuracy. The study also addresses particle embedment, proposing effective cleaning methods like glass bead blasting combined with freezing, achieving up to 100% particle removal. This work significantly advances AJM's application in fabricating polymer and elastomer-based microdevices.

16.3.3 Micromilling Metals with Water: Submerged or Not?

This investigation delves into the intricacies of abrasive water jet (AWJ) micromilling, drawing comparisons between submerged and "dry" conditions applied to 316L stainless steel and 6061-T6 aluminum. Varying nozzle angles and standoff distances reveal deeper channels with reduced centerline erosion, irrespective of submergence. Water shapes the jet's impact, yielding narrower features when submerged, yet influences erosion rates to decrease with channel depth. The study unveils nuanced differences, highlighting submerged AWJ's advantage of achieving narrower features without compromising the centerline etch rate. This insight has implications for optimizing AWJ micromachining in applications requiring precise material removal at the microscopic level [15].

16.3.4 High-Aspect-Ratio Fins via Abrasive Water Jet Micromachining

This research investigates the application of abrasive water jet micromachining (AWJMM) in producing high-aspect-ratio fins from Al6061-T6 aluminum, with the goal of improving

heat sink efficiency through increased fin density. Utilizing micro-nozzles to carve straight channels, the process leaves behind slender, free-standing fins. The study examined how various machining parameters, such as abrasive flow rate, channel offset, water jet pressure, number of passes, and nozzle speed, affected the quality of the produced fins. A notable challenge encountered was the “leveling” effect, where the tops of fins were eroded by stray abrasive particles and secondary channel flows. Optimal conditions that fostered deeper channel cuts—high water pressure, slow nozzle speed, and increased abrasive flow—were found to mitigate this issue by maintaining a minimum offset distance. Unexpectedly, the research demonstrated that the jet could maintain its erosive power over larger effective standoff distances than previously thought, provided that the abrasive particles were of sufficient size. The findings enabled the successful fabrication of high-quality, high-aspectratio fins, with ratios surpassing 40, heralding advancements in heat sink design through improved thermal management capabilities [18].

16.3.5 Narrowing Down AWJ Micromachining with Metal Masks

Naser Haghbin *et al.* [19] explored using metal masks to reduce the minimum feature width in AWJ micromachining, traditionally limited to 600 µm, on aluminum and borosilicate glass. Their approach yielded features two to three times narrower than unmasked methods, with 11% smoother and 44% less wavy surfaces. Adjusting mask thickness allowed for control over channel depth and width, enhancing surface quality. The technique demonstrated a unique reduction in centerline erosion rate with depth for masked channels, attributed to changes in abrasive flow and stagnation zones. This innovation enables creating features as narrow as 150 µm, expanding AWJ’s applicability in micro fabrication.

16.3.6 Predicting Microchannel Profiles in ASJM of Ductile Materials

H. Nouraei *et al.* [20] introduced a novel numerical-empirical model aimed at predicting microchannel profiles in ductile materials through the use of ASJM. Addressing limitations in existing models, this approach considers material-specific erosion rates, incorporates computational fluid dynamics (CFD) corrections for particle impact variations, and employs 3D CFD models for erosion prediction in deeper profiles. Experimental validation confirms the accurate prediction of channel widening and cross-sections, particularly in materials like polymethyl methacrylate (PMMA). The model provides valuable insights for optimizing design and process control in ASJM of ductile materials, enhancing microchannel fabrication precision [20].

16.3.7 Predicting Microchannel Machining with Abrasive Water Jets: A New Model Emerges

L. Kong *et al.* [3] introduce a pioneering “integral modeling process” for predicting microchannel profiles in AWJMM, addressing previous model limitations. Key features include fluid dynamics integration and enhanced accuracy through consideration of factors like particle divergence angles and material-specific insights for stainless steel and aluminum. With an average prediction error of only 4.5% in channel width, the model represents a significant advancement in AWJMM understanding, promising optimized machinability and precise microchannel fabrication across different materials.

16.3.8 Air’s Influence on Abrasive Micromachining: Less Waviness, Narrower Channels

Naser Haghbin and colleagues [21] performed a comparative study AJWMM and high-pressure slurry jet micromachining, focusing on the effects of air entrapment. Despite identical particle velocities, HASJM produced microchannels with 3.4 times less centerline waviness and 26% narrower profiles than AWJMM, attributed to the absence of air-

induced abrasive flow rate variations. Roughness was similar under certain conditions. However, HASJM's erosion rate was 27% lower, due to its narrower channels. This research highlights entrained air's significant influence on microchannel profiles, with high pressure abrasive slurry jet micro-machining (HASJM) offering advantages in reducing waviness and achieving narrower features.

Ehsan Azarsa and colleagues [18] investigated the application of AWJMM for fabricating high aspect ratio free-standing structures, specifically heat sink fins from Al6061-T6. The process involved using a micro-nozzle to machine adjacent channels, examining the effects of different parameters. The study noted that increasing erosion rates by raising water jet pressures, reducing traverse speeds, and augmenting abrasive mass flow rates effectively countered the adverse 'leveling' phenomenon. Interestingly, in contrast to previous studies, the jet maintained its energy even at stand-off distances greater than 10 mm. The study effectively showcased the capacity to produce well-crafted, self-supporting structures with aspect ratios surpassing 40.

Abrasive water jet systems designed for micromachining, featuring jet diameters spanning 30 to 70 µm, exhibit versatility in slotting, cutting, profiling, drilling, and milling a wide array of materials. Trials with 40-µm jets and nanometer-sized aluminum oxide particles suggest the feasibility of cutting with diameters less than 10 µm. The need for rapid stopping and starting of cutting jets becomes crucial, especially during hole drilling. Diamond seated valves are discussed as a potential solution, capable of executing tens of jet on/off cycles per second [22].

R. Jafar and colleagues [23] studied the effects of kinetic energy from alumina particles and the angle of jet impact on channel roughness and erosion rates in borosilicate glass using ASJM. Through computational fluid dynamics, they determined that slurry jets with higher particle energies generate more extensive lateral cracks, resulting in increased channel roughness and higher erosion rates. The research found that material removal predominantly occurred through brittle erosion, with the roughness and erosion rate at perpendicular angles dependent solely on particle kinetic energy. Research findings on abrasive water jet micromachining from selected research papers are summarized in Table 16.3.

Table 16.3 Research findings on abrasive water jet micromachining from selected research papers.

Composition	Tests performed	Research findings	Reference
316L stainless steel, 6061-T6 aluminum	Submerged and dry AWJ micromilling with various nozzle angles and standoff distances	Erosion lessens as channel depth increases, unaffected by submergence; water narrows jet footprint, enabling finer channels without losing etch efficiency.	A. Naser Haghbin, J. Kenneth Spelt, and M. “Abrasive waterjet micromachining of chann metals: Comparison between machining in a submerged in water,” International Journal Tools and Manufacture, vol. 88, pp. 108-117 https://doi.org/10.1016/J.IJMACHTOOLS.20 https://doi.org/10.1016/J.IJMACHTOOLS.20 [15]
Borosilicate glass	ASJM with water slurry and aluminum oxide particles	The model for surface evolution accurately predicts the contours of microchannels and holes, with a variation of up to 7% for aspect ratios reaching 5.	H. Nouraei, K. Kowsari, J. K. Spelt, and M. P “Surface evolution models for abrasive slurr micromachining of channels and holes in gla vol. 309, pp. 65-73, 2014: https://doi.org/10.1016/J.WEAR.2013.11.00 https://doi.org/10.1016/J.WEAR.2013.11.00
Polymeric materials, elastomers	AJM with various parameters	Cryogenic AJM allows precise elastomer machining, using FE analysis for erosion, heat, and distortion studies, with SEM tracking particle embedding.	G. Hailu. “Abrasive Jet Micro-Machining Of Materials.” (2012): https://doi.org/10.32920/ryerson.14660466 https://doi.org/10.32920/ryerson.14660466
Al6061-T6	AWJ micromachining of free-standing structures	Minimizing leveling requires higher jet pressures, slower speeds, and more abrasives.	Ehsan Azarsa, L. Cinco and M. Papini. “Fabr high aspect ratio free-standing structures us abrasive water jet micro-machining.” Journa Materials Processing Technology, 275 (2020 https://doi.org/10.1016/J.JMATPROTEC.201 https://doi.org/10.1016/J.JMATPROTEC.201 [18]

Composition	Tests performed	Research findings	Reference
		Proper offset avoids leveling, allowing highquality, highaspect structures from distances over 10mm.	
Al6061-T6, borosilicate glass	Masked AWJ micromachining	Channels created using masks were 2-3 times narrower and exhibited lower roughness and waviness compared to those that were unmasked.	Ally, S., J. K. Spelt, and M. Papini. “Predictio machined surface evolution in the abrasive j micromachining of metals.” *wear* 292 (2012) [25]

Adapted for ASJM with minor adjustments, two analytical models originally formulated for air-driven abrasive jet micromachining demonstrated their predictive capabilities, yielding average errors of 12% for erosion rates and 17% for roughness. Furthermore, a numerical simulation initially designed for air-driven jets found successful application in ASJM, providing accurate forecasts of channel roughness, shape, and depth across various conditions.

Kowsari, K *et al*. [24] investigated how a low-concentration, high-molecular-weight polymer solution influences the features of micro-holes in materials like borosilicate glass, 6061-T6 aluminum alloy, 110 copper, and 316 stainless steel using low-pressure ASJM. Utilizing aqueous jets that contained 1 wt% of 10-µm Al_2O_3 particles, it was found that incorporating 50 wppm of polyethylene oxide (PEO) resulted in the creation of blind holes in glass that exhibited approximately 20% reduced width and 30% shallower depth compared to those formed without PEO. The introduction of PEO and the resultant normal stresses were observed to produce more defined and V-shaped cross-sectional profiles in the holes. Symmetric through-holes were produced in 3-mm-thick borosilicate glass using ASJM, achieving chipping-free symmetry at depths ranging from 80–900 µm. Lateral oscillations of jets with dissolved PEO were observed, reaching amplitude of 20 µm. In the case of metals, the depths of symmetric blind holes were confined to approximately 150 µm; at depths beyond this, the holes transformed into highly asymmetric forms, creating subsurface slots. The study found that ductile materials were particularly susceptible to the alignment of the jet, with the addition of PEO causing the formation of less circular holes due to the polymer-induced random jet oscillations. The hole depths exhibited a sequence across materials as follows: borosilicate glass, 6061-T6 aluminum, 110 copper, and 316 stainless steel. Additionally, when machining through a sacrificial layer of glass or epoxy, the borosilicate glass holes displayed sharper edges.

Surface evolution models, conventionally utilized to predict microchannel profiles in AJM on glass and polymeric substrates, have been newly adapted for the AJM process on metallic substrates in a study conducted by Ally, S. *et al*. [25]. Investigating the dependence of erosion rates on abrasive jet inclination angles for aluminum 6061-T6, Ti–6Al–4V alloy, and 316L stainless steel, the study employed 50-µm Al_2O_3 abrasive powder with an average velocity of 106 m/s. Maximum erosion rates occurred when the jet angle was set between 20° and 35° to the surface in all examined systems.

Metallic materials exhibited a considerably lower AJM etch rate compared to glass and polymers, with noticeable particle embedding observed in 316L stainless steel. Utilizing erosion data in an AJM surface evolution model, the predicted cross-sectional profiles of both unmasked and masked channels closely aligned with the measured profiles up to an aspect ratio of 1.25. This underscores the feasibility of predicting surface evolution in AJM of metals using models initially formulated for glass and polymers.

In their research, Hou *et al*. [26] integrated ultrasonic vibration to improve the abrasive water micromachining of glass by activating it directly at the nozzle of the abrasive water jet. This introduction of ultrasonic energy enhances flow quality, elevates abrasive velocity, and notably enhances the depth of erosion and the removal of material in glass. Experimental findings underscore the impact of parameters such as vibration amplitude, system pressure, standoff distance, and abrasive size on glass material removal. Both system pressure and vibration amplitude prove significant, contributing to heightened erosion depth and increased material removal. The presence of uplifts at the edge of the erosion pit suggests the importance of the plastic method in the abrasive water jet machining process aided by ultrasonic vibration.

Smart materials, known for their ability to self-repair in response to environmental changes, find diverse applications in industries such as biomedical, aerospace, defense, and energy. These materials, characterized by high hardness, strength, melting point, and low creep behavior, present challenges in micron-scale manufacturing. While AWJMM is a non-traditional method capable of machining hard and brittle materials like ceramics and glasses, machining in the air can compromise quality. In their work, James *et al*. [27] investigate the application of submerged abrasive water jet machining (SAWJMM) for the micromachining of intelligent ceramic materials. The objective is to improve machining quality by eliminating water jet spreading, thereby reducing noise and minimizing debris. Experimental studies with a custom-built SAWJMM setup show that SAWJMM effectively machines smart materials, including shape memory alloys and piezoelectric materials, at the micron scale. The process produces surfaces free of thermal stresses and edge cracking. Key factors like stand-off distance and abrasive grit size have a major impact on machining results, altering cavity dimensions, kerf angle, and the rate of material removal.

Table 16.4 Research findings on abrasive water jet micromachining from selected research papers.

Composition	Tests performed	Research findings	Reference
Various materials (metals, glass, ceramics, polymers, composites)	Micromachining with abrasive water jets using 30–70-µm jet diameters	Cutting with jet diameters less than 10 µm should be possible using nanometer sized particles. Diamond seated valves can significantly improve the control over the jet for precise operations like drilling.	Miller, D. S., "Micromachining with abrasive waterjets," Journal of Materials Processing Technology, 149(1-3), (2004): 37-42. [22]
Borosilicate glass	Abrasive slurry jet micromachining (ASJM) focusing on the kinetic energy of alumina particles and the impact angle of the jet.	The texture and wear rate of channels are influenced by the impacting particles' kinetic energy. Greater energy results in more uneven channels and increased wear rates, stemming from more extensive lateral fractures.	R. Jafar, H. Nouraei, M. Emamifar, M. Papini, J. K. Spelt, "Erosion modeling in abrasive slurry jet micromachining of brittle materials," Journal of Manufacturing Processes, 17 (2015): 127-140. [23]
Borosilicate glass, 6061-T6 aluminum alloy, 110 copper, 316 stainless steel	Low-pressure abrasive slurry jet micromachining (ASJM) with and without highmolecular-weight polymer (PEO)	Incorporating PEO into the abrasive slurry jet modifies the micro-holes' dimensions, resulting in shallower and more narrow formations. This inclusion enhances symmetry in glass drilling and alters the erosion dynamics in metallic materials.	Kowsari, K., H. Nouraei, D. F. James, J. K. Spelt, M. Papini, "Abrasive slurry jet micro-machining of holes in brittle and ductile materials," Journal of Materials Processing Technology 214, no. 9 (2014): 1909-1920. [24]
Aluminum 6061-T6, Ti–6Al–4V alloy, 316L stainless steel	Abrasive jet micromachining (AJM) with a focus on the inclination angle of the abrasive jet	The maximum erosion rate occurs at jet angles ranging from 20° to 35° relative to the surface. Metals show a slower etching rate compared to glass and polymers, with significant particle embedding observed in 316L stainless steel.	Ally, S., J. K. Spelt, M. Papini, "Prediction of machined surface evolution in the abrasive jet micro-machining of metals," wear 292 (2012): 89-99. [25]

Ghobeity *et al*. [28] conducted a comprehensive comparison between microfluidic chips produced through AJM and wet etching. Their study explores the characteristics of these chips, emphasizing efficiency, precision, and surface quality. Abrasive jet micromachining demonstrates versatility and precise control over chip geometry, while wet etching excels

in creating smooth surfaces. The research aims to guide the selection of fabrication methods based on specific application requirements. By evaluating the pros and cons of each technique, the study provides valuable insights for optimizing the manufacturing process of microfluidic chips to meet diverse needs in fields such as lab-on-a-chip technology and microfluidic-based devices.

Lari *et al.* [29] research introduces a rotating mask apparatus (RMA) for AJM, enhancing microfabrication flexibility. This innovative approach allows precise control over the size and shape of the erosive footprint, enabling the creation of complex 3D microchannel geometries crucial for microfluidics. The RMA not only offers the ability to produce diverse and intricate shapes but also increases mask durability and supports precise straight-line etching. Experimental results confirm the RMA's capability to achieve both asymmetric and symmetric designs with high precision, marking a significant advancement in microscale manufacturing technologies.

Table 16.5 Research findings on abrasive water jet micromachining from selected research papers.

Composition	Tests performed	Research findings	References
High aspect ratio free-standing structures	Studied effect of process parameters on quality	At higher erosion rates, leveling minimizes, requiring minimum offset to prevent it. Jets, energized by higher pressure and larger particles, erode effectively even at great distances, enabling structures with aspect ratios above 40.	Ehsan Azarsa, L. Cinco and M. Papini. "Fabrication of high aspect ratio freestanding structures using abrasive water jet micro-machining." Journal of Materials Processing Technology, 275 (2020): 116318. [18]
Micromachining abrasive water jet systems	-	Micromachining abrasive water jet systems can cut with jet diameters as small as 10 µm. Diamond seated valves can potentially be used for frequent jet on/off cycles.	Miller, D. S. (2004). Micromachining with abrasive waterjets. Journal of Materials Processing Technology, 149(1-3), 37-42. [22]
Abrasive slurry jet micromachining (ASJM)	Investigated the influence of particle energy and angle on channel roughness and erosion rate.	Above the cracking threshold, particle kinetic energy dictates roughness and erosion rate; higher energy increases both. Brittle erosion predominates, with models accurately predicting outcomes.	R. Jafar, H. Nouraei, M. Emamifar, M. Papini and J. K. Spelt. "Erosion modeling in abrasive slurry jet micromachining of brittle materials." Journal of Manufacturing Processes, 17 (2015): 127-140. [23]
A dilute high-molecular-weight polymer solution	Examined the impacts of elasticity and viscosity on the shape, depth, and diameter of holes.	Polymer solution sharpens and symmetrizes glass holes, but metals show less circularity and more asymmetry; depth varies by material.	Kowsari, K., H. Nouraei, D. F. James, J. K. Spelt, and M. Papini. "Abrasive slurry jet micromachining of holes in brittle and ductile materials." Journal of Materials Processing Technology 214, no. 9 (2014): 1909-1920. [24]

Abhishek, Kumar *et al*. [30] devised an innovative approach for crafting precise cylindrical micro-holes in brittle materials using micro-abrasive jet machining (µ-AJM), with the aim of refining microfluidic devices such as lab-on-chip systems. Typically, µ-AJM leads to conical holes with tapered sidewalls. However, by maintaining a constant nozzle stand-off distance (NSD) throughout the machining process, they achieved a noteworthy reduction in taper angle and an enhancement in hole cylindricity. Evaluations using a coordinate measuring machine (CMM) confirmed a 56% decrease in taper angle and a 57% increase in cylindricity, showcasing the method's potential to elevate micromanufacturing precision. Abrasive jet micromachining contributes to precise processing of brittle materials like SiO_2 glass and Si_3N_4. Polishing with a micro slurry jet notably improves material surface, resulting in reduced roughness. Silicate glass Ra decreases from 2.32 µm to 0.35 µm, while Si_3N_4 Ra decreases from 2.63 µm to 0.34 µm. The investigation

explores the processes of material elimination and surface generation mechanisms, exploring factors that influence surface morphology, quality, and roughness to enhance overall quality and diminish roughness [31].

Table 16.6 Research findings on abrasive water jet micromachining from selected research papers.

Composition	**Tests performed**	**Research findings**	**References**
Channels with non-conventional shaped cross sections	N/A	AJM with a novel rotating mask creates diverse 3D microfluidic channels, improving shape control, mask life, and straight traverses.	Lari, MR Sookhak, A. Ghazavi, and M. Papini. "A rotating mask system for sculpting of three-dimensional features using abrasive jet micro-machining." Journal of Materials Processing Technology 243 (2017): 62-74. [29]
Brittle materials	Studied effect of constant nozzle stand-off distance on hole cylindricity	Maintaining consistent nozzle stand-off in µ-AJM decreased taper angle by 56%, enhancing cylindricity by 57% in microfluidic applications with cylindrical micro holes.	Abhishek, Kumar, Somashekhar S. Hiremath, and S. Karunanidhi. "A novel approach to produce holes with high degree of cylindricity through Micro-Abrasive Jet Machining (µ-AJM)." CIRP Journal of Manufacturing Science and Technology 21 (2018): 110-119. [30]
Hard-brittle materials (silicate glass, silicon nitride)	Polishing experiments using micro slurry jet	Micro slurry jet polishing notably enhanced surface evenness, reducing the roughness of silicate glass from 2.32 µm to 0.35 µm and that of Si_3N_4 from 2.63 µm to 0.34 µm. Studies on material removal and the formation of the surface were undertaken.	Liu, Zeng Wen, and R. Y. Liu. "Study on polishing technology for hard-brittle materials by a micro abrasive water jet." Advanced Materials Research 1027 (2014): 52-57. [31]
Glass	Investigated effect of polymer concentration and nozzle design on jet stability	Abrasive slurry micromachining: Higher polymer concentration shrinks, but destabilizes footprint. Tapered nozzle design cuts oscillation, yielding 11% narrower channels.	Van Wijk, E., D. F. James, M. Papini, and J. K. Spelt. "Micro-machining with abrasive slurry-jets: effects of dissolved polymer concentration and nozzle design." The International Journal of Advanced Manufacturing Technology 102 (2019): 317-331. [32]

The resolution in ASJM depends on erosion footprint diameter and jet stability. Increased polymer concentration reduces footprint size but raises jet oscillation. Nozzle design impact on jet stability was explored using various acrylic nozzles with a 180-µm sapphire orifice. Fluorescent streak photography revealed unstable vortices, contributing to oscillation. Jet oscillation, measured photographically, nonlinearly increased with polymer concentration for all nozzles.

The implementation of a novel steel nozzle featuring a 30° tapered entrance successfully mitigated oscillations. Using polymer slurries, microchannels were created on glass plates, yielding channels that were 11% more narrow compared to standard reference channels. This optimization of footprint size while minimizing oscillation was reported in the study [32].

16.4 Conclusion

In conclusion, this chapter has thoroughly explored the intricacies and advancements of AWJMM, highlighting its role as a cutting-edge material removal technique that harmonizes the kinetic energy of high-velocity water with the abrasive potential of particulate matter for precise and thermally undistorted material cutting. Central to AWJMM's appeal is its unparalleled versatility in processing a wide spectrum of materials, from metals to composites, with remarkable efficiency and minimal environmental impact. This method stands out for its non-thermal cutting process, eco-friendly approach, ability to perform complex cuts with minimal material wastage, and its broad applicability across various industrial sectors. The exploration of AWJMM's applications in fields that demand high precision and material integrity, such as aerospace, automotive, and electronics, underscores its capacity to produce complex components without thermal or mechanical compromises, thereby reducing the need for additional processing.

The chapter has also presented a synthesis of current research and developments within the AWJMM domain, pointing to enhancements in abrasive materials, jet technology, and process optimization that collectively aim to elevate the method's cutting performance and environmental sustainability. These advancements are not only extending the practical applications of AWJMM but are also improving its economic feasibility.

Looking forward, the anticipation of breakthroughs in automation, material science, and computational techniques holds promise for further elevating the precision, efficiency, and versatility of AWJMM. Such advancements are poised to redefine the paradigms of precision engineering and sustainable manufacturing, affirming AWJMM's pivotal role in the ongoing evolution of modern manufacturing technologies. The ongoing journey of AWJMM from a novel machining process to a cornerstone of sustainable and precision manufacturing exemplifies its potential to meet the emerging challenges and requirements of future manufacturing landscapes.

16.5 A Glimpse Into the Future: What Lies Ahead for AWJMM?

The horizon for AWJMM is vast and full of potential, poised for groundbreaking advancements that promise to redefine the realms of precision, efficiency, and application diversity. Key areas of development like innovative nozzle technology, advanced abrasive materials, and refined process control mechanisms are set to push the boundaries of what is achievable in terms of cutting speed, accuracy, and surface integrity. The integration of sophisticated robotics and automation systems is expected to unlock new dimensions in micromachining capabilities, facilitating the production of more complex and detailed microstructures than ever before. Further exploration into novel abrasive substances and the development of hybrid machining processes, which amalgamate AWJMM with other

fabrication techniques, are anticipated to broaden the spectrum of materials that can be effectively machined. This evolution could open doors to new industries and applications, ranging from bespoke microelectronics to customized biomedical devices, offering unprecedented opportunities for innovation.

Abrasive water jet micromachining stands out not only for its operational excellence but also for its contribution to sustainable manufacturing practices. Its ability to cut through materials without generating heat or toxic byproducts exemplifies the kind of environmentally friendly technology that modern industries seek to adopt, marrying efficiency with ecological responsibility. Looking ahead, the synergy between AWJMM technology and emerging fields such as nanotechnology, smart materials, and green manufacturing is set to catalyze a new era of microfabrication. This fusion promises to yield not just incremental improvements but potentially transformative breakthroughs, offering smarter, more sustainable, and highly customized solutions across a spectrum of applications. In essence, AWJMM represents a beacon of innovation in the micromachining landscape, promising a future where the limitations of today become the conquered challenges of tomorrow. As we stand on the cusp of these advancements, the journey of AWJMM is indeed an unfolding saga, one that promises to captivate and inspire as it progresses, shaping the microscopic contours of our future world.

References

1. El-Shorbagy, R.M., El-Baradie, Z.M., Abdel-Aziz, A.I., Microstructure and Mechanical Properties of 2024 Aluminum Alloy with and Without Rare-Earth and Thermomechanical Treatment after Multi-pass Stir Friction Processing. *Int. J. Metalcast.*, 18, 1–17, 2023, https://doi.org/10.1007/s40962-023-01191-7.

2. Wang, H., Yuan, R., Zhang, X., Zai, P., Deng, J., Research Progress in Abrasive Water Jet Processing Technology. *Micromachines*, 14, 8, 1526, 2023, https://doi.org/10.3390/mi14081526.

3. Kong, L., Wang, Y., Lei, X., Feng, C., Wang, Z., Integral modeling of abrasive waterjet micromachining process. *Wear*, 482, 203987, 2021, https://doi.org/10.1016/j.wear.2021.203987.

4. Azarsa, E., Ibrahim, A., Papini, M., Abrasive water and slurry jet micro-machining techniques for fabrication of molds containing raised free-standing micro-features. *Precis. Eng.*, 65, 197– 215, 2020, https://doi.org/10.1016/j.precisioneng.2020.05.009.

5. Anu Kuttan, A., Rajesh, R., Dev Anand, M., Abrasive water jet machining techniques and parameters: a state of the art, open issue challenges and research directions. *J. Braz. Soc. Mech. Sci. Eng.*, 43, 1–145, 2021, 10.1007/s40430-021-02898-6.

6. Natarajan, Y., Murugesan, P.K., Mohan, M., Ali Khan, S.A.L., Abrasive Water Jet Machining process: A state of art of review. *J. Manuf. Processes*, 49, 271–322, 2020, DOI:10.1016/j. jmapro.2019.11.030.

7. Sharma, R., Maurya, S., Saini, R., A Review Paper on Current Research and Development in Abrasive Waterjet Machining. *Math. Stat. Eng. Appl.*, 71, 4, 4160–4169, 2022, https://doi.org/10.17762/msea.v71i4.991.

8. Gembalová, L., Hlaváč, L.M., Spadło, S., Geryk, V., Oros, L., Notes on the Abrasive Water Jet (AWJ) Machining. *Materials*, 14, 22, 7032, 2021, https://doi.org/10.3390/ma14227032.

9. Nouraei, H., Wodoslawsky, A., Papini, M., Spelt, J.K., Characteristics of abrasive slurry jet micro-machining: a comparison with abrasive air jet micro-machining. *J. Mater. Process. Technol.*, 213, 10, 1711–1724, 2013, DOI:10.1016/J.JMATPROTEC.2013.03.024.

10. Jagadish, and Gupta, K., *Abrasive Water Jet Machining of Engineering Materials*, Springer Nature, Switzerland AG, 2020, Abrasive Water Jet Machining of Engineering Materials | SpringerLink.

11. Khan, M.A., Soni, H., Mashinini, P.M., Uthayakumar, M., Abrasive water jet cutting process form machining metals and composites for engineering applications: A review. *Eng. Res. Express*, 3, 2, 022004, 2021, 10.1088/2631-8695/abfe98.

12. Llanto, J.M., Tolouei-Rad, M., Vafadar, A., Aamir, M., Recent progress trend on abrasive waterjet cutting of metallic materials: a review. *Appl. Sci.*, 11, 8, 3344, 2021, DOI:10.3390/APP11083344.

13. Kale, A., Singh, S.K., Sateesh, N., Subbiah, R., A review on abrasive water jet machining process and its process parameters. *Mater. Today: Proc.*, 26, 1032–1036, 2020, DOI:10.1016/j. matpr.2020.01.309.

14. Dehghanghadikolaei, A., Mohammadian, B., Namdari, N., Fotovvati, B., Abrasive machining techniques for biomedical device applications. *J. Mater. Sci.*, 5, 1–11, 2018, DOI:10.19080/ JOJMS.2018.04.555654.

15. Haghbin, N., Spelt, J.K., Papini, M., Abrasive waterjet micro-machining of channels in metals: Comparison between machining in air and submerged in water, *Int. J. Mach. Tools Manuf.*, 88, 108–117, 2015, https://doi.org/10.1016/J.IJMACHTOOLS.2014.09.012.

16. Nouraei, H., Kowsari, K., Spelt, J.K., Papini, M., Surface evolution models for abrasive slurry jet micro-machining of channels and holes in glass. *Wear*, 309, 65–73, 2014, https://doi.org/10.1016/J.WEAR.2013.11.003.

17. Hailu, G., *Abrasive Jet Micro-Machining Of Polymeric Materials*, Ottawa: Library and Archives Canada = Bibliothèque et Archives Canada, 2013, 2012, https://doi.org/10.32920/ryerson.14660466.v1.

18. Azarsa, E., Cinco, L., Papini, M., Fabrication of high aspect ratio free-standing structures using abrasive water jet micro-machining. *J. Mater. Process. Technol.*, 275, 116318, 2020, https://doi.org/10.1016/J.JMATPROTEC.2019.116318.

19. Haghbin, N., Ahmadzadeh, F., Papini, M., Masked micro-channel machining in aluminum alloy and borosilicate glass using abrasive water jet micro-machining. *J. Manuf. Processes*, 35, 307–316, October 2018, https://doi.org/10.1016/J.JMAPRO.2018.08.017.

20. Nouraei, H., Kowsari, K., Samareh, B., Spelt, J.K., Papini, M., Calibrated CFD erosion modeling of abrasive slurry jet micro-machining of channels in ductile materials. *J. Manuf. Processes*, 23, 90–101, 2016, https://doi.org/10.1016/J.JMAPRO.2016.06.007.

21. Haghbin, N., Ahmadzadeh, F., Spelt, J.K., Papini, M., Effect of entrained air in abrasive water jet micro-machining: Reduction of channel width and waviness using slurry entrainment. *Wear*, 344–345, 99–109, 2015, https://doi.org/10.1016/J.WEAR.2015.10.008.

22. Miller, D.S., Micromachining with abrasive waterjets. *J. Mater. Process. Technol.*, *149*, 1-3, 37–42, 2004, https://doi.org/10.1016/j.jmatprotec.2004.02.041.

23. Jafar, R., Nouraei, H., Emamifar, M., Papini, M., Spelt, J.K., Erosion modeling in abrasive slurry jet micro-machining of brittle materials. *J. Manuf. Processes*, 17, 127–140, 2015, https://doi.org/10.1016/J.JMAPRO.2014.08.006.

24. Kowsari, K., Nouraei, H., James, D.F., Spelt, J.K., Papini, M., Abrasive slurry jet micromachining of holes in brittle and ductile materials. *J. Mater. Process. Technol.*, 214, 9, 1909– 1920, 2014, https://doi.org/10.1016/J.JMATPROTEC.2014.04.008.

25. Ally, S., Spelt, J.K., Papini, M., Prediction of machined surface evolution in the abrasive jet micro-machining of metals. *Wear*, 292, 89–99, 2012, https://doi.org/10.1016/j.wear.2012.05.029.

26. Hou, R., Wang, T., Lv, Z., Liu, Y., Experimental study of the ultrasonic vibration-assisted abrasive waterjet micromachining the quartz glass. *Adv. Mater. Sci. Eng.*, 2018, 1–9, 2018, http://dx.doi.org/10.1155/2018/8904234.

27. James, S. and Mahajan, A., Experimental study of machining of smart materials using submerged abrasive waterjet micromachining process, in: *International Manufacturing Science and Engineering Conference*, vol. 51388, American Society of Mechanical Engineers, p. V004T03A012, 2018, http://dx.doi.org/10.1155/2018/8904234.

28. Ghobeity, A., John Crabtree, H., Papini, M., Spelt, J.K., Characterisation and comparison of microfluidic chips formed using abrasive jet micromachining and wet etching. *J. Micromech. Microeng.*, 22, 2, 025014, 2012, https://doi.org/10.1088/0960-1317%2F22%2F2%2F025014.

29. Sookhak Lari, M.R., Ghazavi, A., Papini, M., A rotating mask system for sculpting of three-dimensional features using abrasive jet micro-machining. *J. Mater. Process. Technol.*, 243, 62–74, 2017, https://doi.org/10.1016/J.JMATPROTEC.2016.12.006.

30. Abhishek, K., Hiremath, S.S., Karunanidhi, S., A novel approach to produce holes with high degree of cylindricity through Micro-Abrasive Jet Machining (μ-AJM). *CIRP J. Manuf. Sci. Technol.*, 21, 110–119, 2018, https://doi.org/10.1016/j.cirpj.2018.02.002.

31. Liu, Z.W. and Liu, R.Y., Study on polishing technology for hard-brittle materials by a micro abrasive water jet. *Adv. Mater. Res.*, 1027, 52–57, 2014, DOI:10.4028/www.scientific.net/AMR.1027.52.

32. Van Wijk, E., James, D.F., Spelt, J.K., Micro-machining with abrasive slurry-jets: effects of dissolved polymer concentration and nozzle design. *Int. J. Adv. Manuf. Technol.*, 102, 317–331, 2019, https://doi.org/10.1007/s00170-018-3173-5.

Note

*Corresponding author: abdurrahman@crescent.education

17
Micro-Electrical Discharge Machining: State of Art

M. Sivakumar[1]*, C. T. Justus Panicker[1], R. Karthikeyan[1] and G. Suresh[2]

[1]Department of Production Engineering, National Institute of Technology Tiruchirappalli, Tiruchirappalli, India

[2]Department of Mechanical Engineering, Mount Zion College of Engineering and Technology, Pudukkottai, Tiruchirappalli, India

Abstract

This chapter delves into the evolution, principles, and advancements in micro-electrical discharge machining (micro-EDM) process which is a non-traditional precision-based machining technique which is critical for microscale manufacturing. Originating from conventional EDM processes, micro-EDM stands out for its capability to fabricate intricate geometries and superior surface qualities in hard-to-machine materials. This chapter outlines the fundamental working principle of micro-EDM, emphasizing the role of electrical discharges in material removal and the critical aspects of process parameters that influence machining efficiency. It explores the differentiation between macro-EDM and micro-EDM, detailing the specific requirements for achieving high precision and accuracy in micro-machining. The text further examines the major components and process parameters of micro-EDM, including discharge energy, peak current, gap and discharge voltage, pulse duration, and non-electrical factors like workpiece materials and

dielectric fluids. Additionally, the chapter highlights the significance of machining characteristics such as electrode wear ratio (EWR), surface roughness, and material removal rate (MRR) in evaluating micro-EDM performance. Various micro-EDM variants and hybrid approaches, including simultaneous micro-EDM and micro-ECM (SEDCM) and ultrasonic cavitation-assisted micro-EDM, are presented, showcasing the technology's adaptability and potential for innovation in precision manufacturing.

***Keywords*:** Micro-electrical discharge machining (micro-EDM), process parameters, hybrid micromachining, material removal rate (MRR)

17.1 Introduction

Micromachining encompasses a variety of techniques, each with its own set of advantages and limitations. Traditional machine tools are used for well-known operations *viz.*, grinding, milling, turning, and drilling; effective for larger-scale manufacturing, often fall short when precision at the microscale is required [1, 2]. Similarly, energy-beam machining methods, including electron, laser, and focused ion beam techniques, while offering non-contact advantages, struggle with issues related to 3D structure control, material removal rates, and achieving high aspect ratios [3]. The search for solutions to these challenges has propelled the development and application of chemical and electrophysical processes, notably electrochemical machining (ECM) and electric discharge machining (EDM). Nowadays, micromachining is important for improving microfeatures in additive manufacturing components. Additive manufacturing is a modern technology that creates components layer by layer for various applications [4, 5], enhancing the integration of micromachining techniques to refine and add detailed features to these

components, thereby expanding the possibilities and applications of additive manufacturing in modern industries.

Electric discharge machining stands out as a cornerstone non-traditional manufacturing process, having been refined and evolved over more than six decades from its initial application in simple die-sinking operations. Its journey from an obscure, inefficient process to a sophisticated, precision-driven machining technique mirrors the broader evolution of manufacturing technologies. Initially conceptualized for removing broken tools from workpieces, EDM's scope has expanded dramatically, driven by innovations in control systems, power supply technologies, and machining strategies. Today, EDM is not only capable of shaping complex geometries in hard-to-machine materials but also plays a crucial role in microscale manufacturing [6].

Micro-EDM represents a significant advancement, offering the capability to produce microscale features with high precision. This process variation is a testament to the ongoing refinement of EDM technologies, catering to the demands for miniaturization while overcoming the limitations of traditional machining methods [7]. The development and application of micro-EDM have been bolstered by research and industrial practices aimed at optimizing process parameters, enhancing machining efficiency, and expanding the range of applications. The combination of hybrid micromachining approaches, which integrate micro-EDM with additional techniques like laser machining or micro-milling, further highlights its significance [2]. This hybrid approach leverages the strengths of each technique, enabling the production of complex geometries and superior surface qualities, while also reducing processing times and improving material properties at the microscale.

This book chapter provides an in-depth exploration of micro-EDM, shedding light on its fundamental principles and the forefront of advancements in process parameters, machining strategies, and its applications. It delves into the core of micro-EDM, elucidating the process parameters essential for its operation, the machining parameters crucial for enhancing performance, and the spectrum of emerging micro-EDM techniques. Moreover, the chapter underscores the applications of micro-EDM across various industries, spotlighting its significance in precision manufacturing. It also examines the burgeoning potential of hybrid micro-EDM technologies in pushing the frontiers of precision, thereby addressing the demands of modern manufacturing and facilitating the ongoing trend toward product miniaturization.

17.2 Principles of Micro-EDM

17.2.1 Working Principle

The process of micro-EDM is used for shaping electrically conductive materials through a controlled process of electric sparks. This method operates under the fundamental principle of material erosion induced by repeated electrical discharges, as shown in Figure 17.1. These discharges occur in a meticulously controlled environment between an electrode and the material being machined, submerged within the dielectric fluid that is specific to the micro-EDM process. The working principle of micro-EDM is given below:

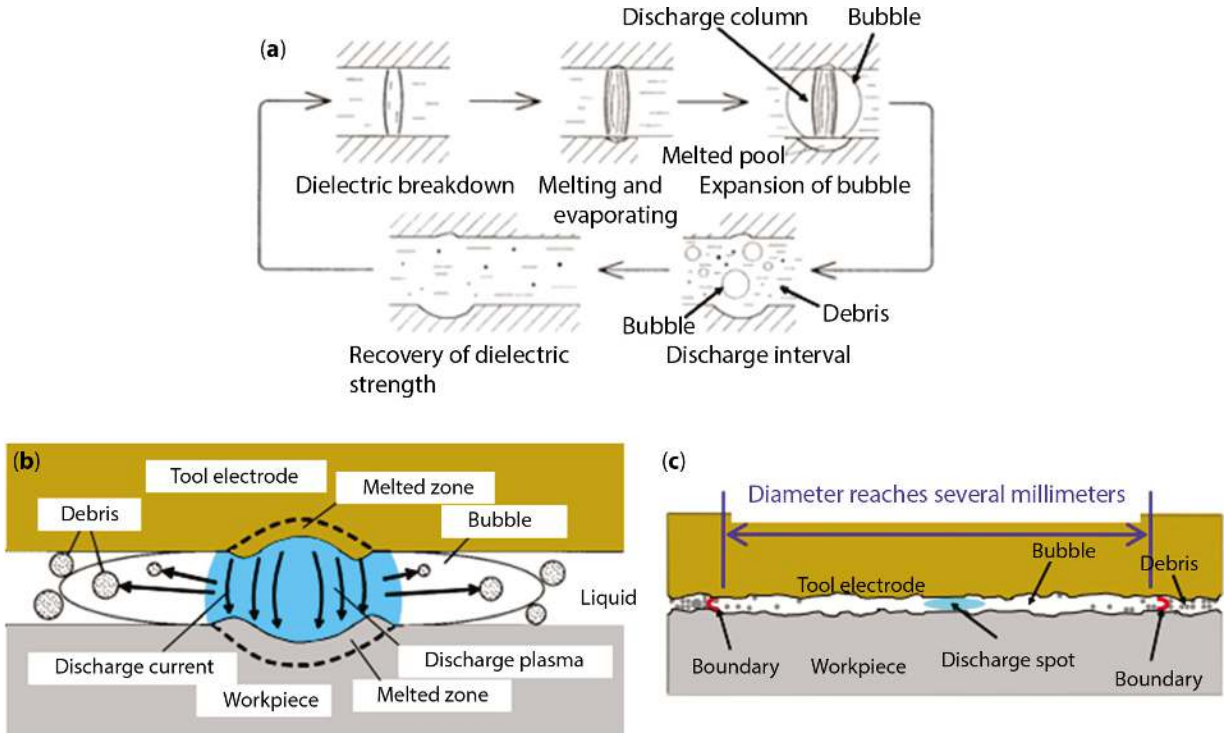


Figure 17.1 Working principle of micro-EDM. (a) EDM gap dynamics, (b) EDM discharge gap schematic with tool electrode and debris, and (c) post-discharge bubble and debris interaction in EDM [8].

i. Initial Setup

The process begins with the positioning of a specially designed electrode near the workpiece. Both the workpiece and electrode are electrically conductive, and the entire setup is immersed in a dielectric fluid. This fluid acts as an insulator until a specific voltage is exceeded, facilitating spark generation.

ii. Generation of Electrical Sparks

When the voltage applied exceeds the dielectric capacity of the fluid in between, a regulated spark leaps over the shortest path from the electrode to the workpiece. This spark, which is precisely concentrated, takes place where the gap between the two is smallest.

iii. Material Erosion and Removal

The extreme temperature produced by every spark causes a tiny quantity of substance to melt and evaporate from both the electrode and the workpiece. Finally, upon solidification electrode and workpiece surface are slightly pitted due to dielectric fluids ejection of liquefied material.

iv. Progression of Machining

At the point of discharge, the gap between electrode and workpiece increases during material removal. This dynamic variation in separation distance results in automatic movement to the nearest point of closeness, enabling the step-by-step, accurate, and regulated removal of material.

v. Thermal Nature of Material Removal

Micro-EDM operates primarily through a thermal process. The primary mechanism for removing material hinges on the thermal energy discharged in the sparks, which cause the material to melt and vaporize. This characteristic highlights the emphasis on thermal dynamics over mechanical forces in micro-EDM, setting it apart from conventional machining techniques.

17.2.2 Gap Phenomena of Micro-EDM

The phenomena associated with sparking and the gap in micro-EDM are crucial for understanding the intricacies of this precision machining process, as shown in Figures 17.1(b&c). These phenomena involve complex interactions within the machining gap between the electrode, workpiece, debris particles, and dielectric fluid [8]. Below, we explore these interactions and their implications for the micro-EDM process, ensuring clarity and originality while preserving the technical terminology.

i. Initial misconceptions and clarifications: traditional depictions suggest that the sparking gap is filled primarily with fine debris and minute bubbles, with the arc column diameter being smaller than the gap width. However, this representation does not fully capture the reality. In contrast, gas occupying the gap, and the fragment particles removed is comparable to the separation distance and the electrode surface roughness. This discrepancy highlights the need for a nuanced understanding of gap dynamics.

ii. Mechanisms of dielectric breakdown: dielectric breakdown during consecutive pulse discharges typically starts at locations where debris accumulates or is inside the bubbles. As the discharge continues, the diameter of the arc column widens, aligning with the dimensions of the resulting discharge crater. Such expansion highlights the evolving aspect of the sparking mechanism.

iii. Bubble dynamics and material removal: the rapid vaporization of electrode materials and dielectric fluid leads to bubble creation and its eventual expansion within the gap. The bubble’s growth is limited by the dielectric fluid’s inertia and viscosity, causing the internal pressure to soar. The interaction between the expanding bubble and the dielectric fluid generates a high-pressure and high-velocity field, crucial for material removal. The dielectric fluid, therefore, plays a dual role in facilitating material removal and in the subsequent cooling and stabilization of the machining process.

iv. Post-discharge recovery and debris formation: following the discharge, electron and ions recombine, restoring the dielectric strength. Evaporated substances solidify or condense, forming debris

particles. Notably, gases produced during the discharge (*e.g.*, hydrogen and methane) contribute to bubble formation. Debris particles, encapsulated by these bubbles, are eventually flushed from the gap by the dielectric fluid, preventing their reattachment to the electrode surfaces.

v. Cooling and machining stability: the dielectric fluid also serves to cool the electrodes through heat convection at the boundary layers. This cooling effect, alongside the flushing of debris, is instrumental in maintaining the stability of the micro-EDM process.

The spark glinting phenomena based on gap in micro-EDM involve a dynamic interplay resulting in debris due to the workpiece and electrode immersed in the dielectric fluid, characterized by a series of interactions. These interactions are pivotal in shaping the material removal mechanisms, influencing the machining process's efficiency and precision. By understanding these complex phenomena, advancements in micro-EDM technology can continue to evolve, pushing the boundaries of precision machining.

Table 17.1 Differentiate between macro-EDM and micro-EDM [9, 10].

Feature	Macro-EDM	Micro-EDM
Plasma channel radius	Larger electrode size, resulting in a smaller relative plasma channel radius.	Comparable size of electrode and plasma channel radius, indicating a nuanced control at the micro level.
Electrode size and heat dissipation	Larger electrodes, facilitating better heat dissipation.	Uses smaller electrodes (*e.g.*, Ø5 mm for micro-WEDG and <Ø20 mm for BEDG), reducing heat transfer and raising the chance of damage from sparks.
Flushing pressure and debris removal	Larger gap and electrode size simplify debris removal and reduce the sensitivity to flushing pressure variations.	Smaller gaps and electrode sizes complicate debris removal due to higher dielectric viscosity and pressure drop in microvolumes, coupled with increased risk of electrode breakage.
Precision and accuracy	Achieved through controlled electrode vibrations and wear.	Naturally higher due to finer control over machining parameters, leading to superior final product quality.
Electrode wear	Lower proportional wear per discharge, with electrode	Higher wear per discharge necessitates careful management of spark energy to prevent

Feature	Macro-EDM	Micro-EDM
	durability being more manageable.	excessive wear and damage.
Energy control and crater size	Higher peak energy is permissible, creating larger craters.	To manage the rate of unit removal per spark and facilitate the use of smaller electrodes, it is necessary to cap the peak energy, which leads to the creation of smaller crater sizes.

17.2.3 Contrasting Macro-EDM from Micro-EDM

Macro-EDM and micro-EDM work alike in principle, considering spark erosion, yet they diverge significantly in application specifics. Micro-EDM distinguishes itself by necessitating higher precision in control over discharge energy, gap, voltage, and frequency to achieve its characteristic fine machining quality, as shown in Table 17.1. Unlike macro-EDM, micro-EDM requires adjustments in tool size, tool fabrication techniques, power supply, machine tool movement resolution, and flushing methods to cater to the unique demands of micro-level machining. Techniques such as wire electrical discharge grinding (WEDG), micro-EDM milling, and pattern transfer that repeats are explicitly tailored for micro-EDM, highlighting their specialized nature.

17.3 Major Components of Micro-Electrical Discharge Machining

Several pivotal components synergize into a micro-EDM system that works in harmony to perform precision machining tasks [11]. The core component of these systems

is the central control unit (CCU). This unit in the system ensures the communication between the operator and the machinery, as well as coordinating the activities of the different subsystems. This unit is crucial for managing operations, encompassing the storage of program instructions in memory units, and overseeing the electrical discharges through the electrical unit supplying power.

The closed-loop servo plays a critical role in precisely managing the electrode's approach toward the workpiece, ensuring optimal machining conditions and accuracy. It employs feedback mechanisms to adjust the electrode's position dynamically, maintaining the desired gap for effective material removal. Within the work tank, the workpiece is securely fastened and submerged in a dielectric fluid that mitigates fire risks by cooling and flushing away disintegrated materials. This setup is essential for the safety and efficiency of the machining process.

The position control system, equipped with high-precision servo motors, dictates the tool electrode's movement along the X, Y, Z, and rotational axes. This subsystem is fundamental for achieving the intricate geometries typical of micro-EDM applications, enabling the controlled descent of the electrode based on servo parameters.

The dielectric tank serves as a reservoir for the dielectric fluid, equipped with electro-valves and pumps to regulate the fluid's flow into the work tank, thus ensuring a consistent machining environment. An innovative addition to some micro-EDM systems is the rotating unit, which facilitates the electrode's rotation, enhancing machining efficiency and surface finish.

Figure 17.2 shows the schematic overview of these foundational units, illustrating their interconnections and functionality within both EDM and micro-EDM systems.

This section will delve into the intricacies of three major components, further elucidating their significance in the micro-EDM system.

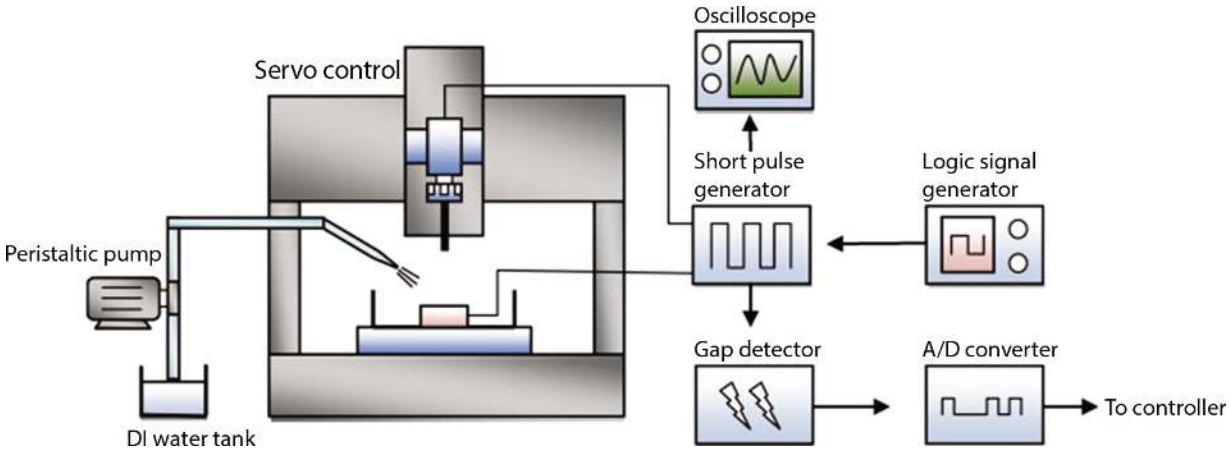


Figure 17.2 Basic components of electrical discharge micromachining [11].

17.3.1 Resistor-Capacitor (RC) Pulse Generators

The operational principle is similar to common oscillator circuit, influenced fundamentally by two main components [8]: the wire inductance and charge retention of capacitance that connects the capacitor both to the tool and the workpiece. These elements primarily govern the duration of the discharge pulse within this circuit. Additionally, discharges over specific time, or the rate at which the dissipation occurs, depends on the duration needed for the capacitor to recharge. The circuit has resistance (R) that controls recharging duration. Maintaining the resistance at a level that is neither too low to prevent the undesirable transition from sparking to arcing is crucial, thereby identifying an optimal resistance level that effectively mitigates the risk of arcing.

The resistor-capacitor (RC) circuit releases energy during discharge which is not just influenced by the selected

capacitance but also by the residual capacitance that prevails among electrical feeders, the worktable, electrode holder and among and tool electrode. This stray capacitance establishes the lowest limit for the energy discharged per pulse. In situations where it is critical to minimize discharge energy, such as in final finishing operations, the machining process can be carried out using only the stray capacitance, eliminating the need for an externally connected capacitor.

This type of pulse generator is adept at generating pulses characterized by high peak current values and brief durations. Such capabilities are instrumental in facilitating precise material removal, thereby achieving the desired surface quality. Optimal surface finish is attributed to pulse conditions with higher peak currents and shorter discharge durations, resulting in smaller discharge craters.

This pulse generator (Figure 17.3), despite these advantages, is often critiqued for its relatively low machining, attributed to the low frequency of discharge stemming from the requisite capacitor charging time. This limitation is evident from uneven surface finishes, since energy discharged varies based on the capacitor’s charge stored prior to dielectric breakdown. The design of the RC pulse generator lacks the capability to regulate the pulse duration, posing a risk of thermal harm to the workpiece should the dielectric strength fail to recover prior to the next discharge. This could result in a continuous flow of current through the identical plasma channel without the capacitor being recharged.

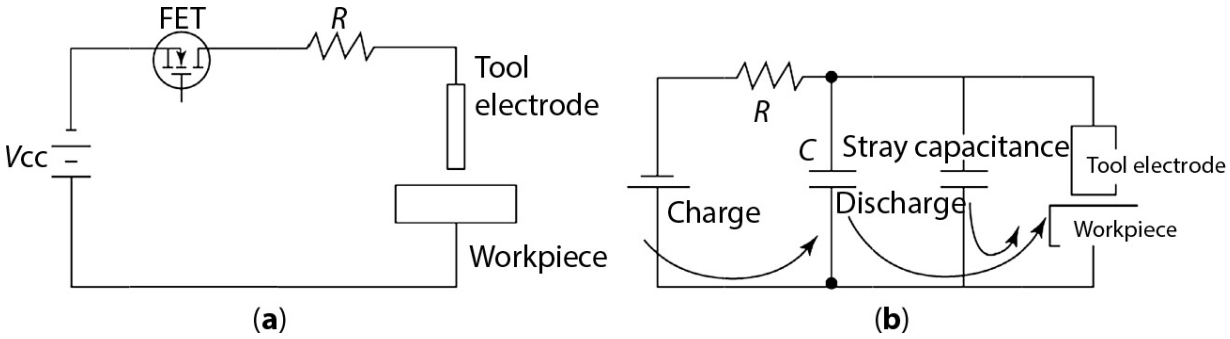


Figure 17.3 Fundamental circuit configurations for (a) transistor type and (b) resistor-capacitor pulse generators [8].

17.3.2 Servo Control System

Figure 17.4 provides a detailed schematic overview of a control system specifically engineered for high precision micro- and nano-EDM enabled by servos [12]. This system incorporates a tri-modal approach to servo control to optimize the EDM process's precision and efficiency. The synergy of both z-axis controls and the piezo table is achieved by the respective servo feed control of the machine tools in the z-axis and that of the piezo table, additionally with the integrated cooperative control.

The methodology critically compares the mean operational gap voltage and a set reference servo voltage for the piezo table servo feed control. The discrepancy between these values is subsequently amplified and fed into the piezo drive as an input signal. This action causes a proportional adjustment of the piezo table according to the voltage input, thus enabling meticulous control over the machining gap width.

In the z-axis servo feed control scenario, a similar comparative analysis is conducted between the mean operational voltage and the reference servo voltage. The resultant differential is then used to modulate the control drive of the z-axis, facilitating precise gap adjustments.

The hybrid or cooperative control strategy augments the capability of z-axis control and piezo table. Although the piezo table offers a rapid response capability, its movement range is limited to about 18 mm. The integration of both control mechanisms under the cooperative strategy ensures a swift response capability over a broader movement range, significantly enhancing the micro-EDM process's efficiency and precision. This comprehensive control system exemplifies the cutting-edge advancements in EDM technology, aiming for optimal accuracy and operational efficiency.

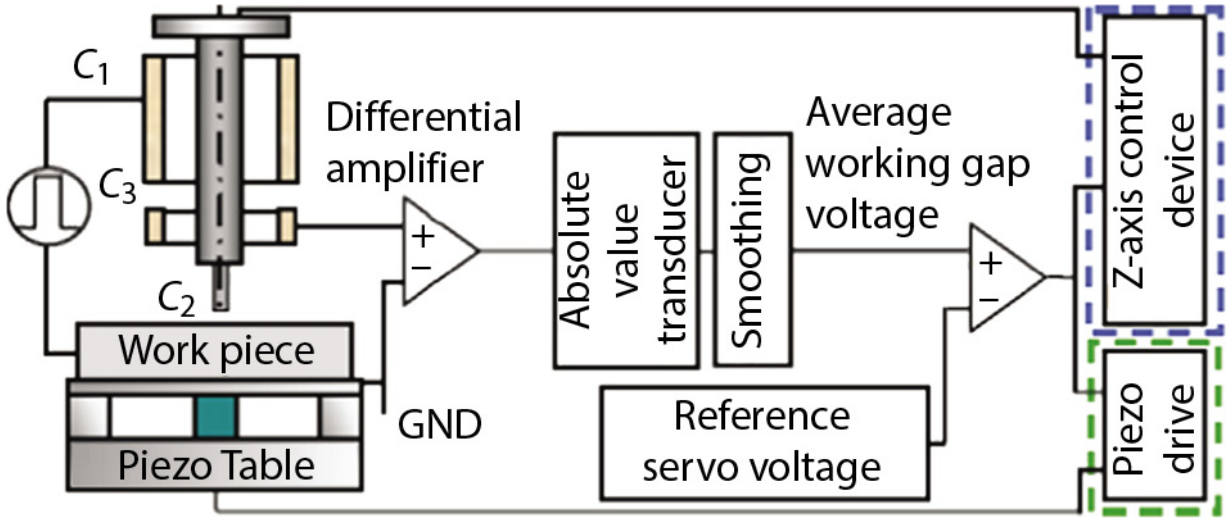


Figure 17.4 Servo feed control system overview [12].

17.3.3 Dielectric Circulation System

Micro-electrical discharge machining stands out for its exceptional ability to machine complex features on hard materials, largely due to its advanced dielectric circulation system. This system, a cornerstone of micro-EDM, consists of an intricately designed assembly. The system includes a dielectric fluid, a reservoir for storage, a pump designed to inject the fluid into the machining area, and an advanced filtration system for removing debris. This ensures a favorable machining zone by steadily flowing filtered

dielectric fluid. Required flushing pressure with valves and proper orientation of dielectric fluid between the electrode and workpiece is possible by nozzles and conduits. The major component of the machinery are conduits and nozzles, which are designed to accurately direct the dielectric fluid into the space between the workpiece and the electrode, along with a valve that allows for the adjustment of the flushing pressure. The dielectric fluid, the system's linchpin, serves as an electrical insulator to prevent direct contact between the workpiece and the tool, while also expediting the removal of eroded particles from the spark gap.

This dielectric circulation system fulfils critical roles to enhance the micro-EDM process's efficiency [8]. Its primary function is to evacuate gaseous and solid debris produced during machining, achieved by maintaining a consistent dielectric flow through the spark gap. This not only purifies the machining environment but also ensures the introduction of fresh, clean dielectric fluid, facilitating optimal discharge conditions. Furthermore, the system adeptly removes metal particles from the spark gap, thereby preserving the machining process's integrity.

Additionally, the dielectric circulation system is instrumental in thermal management within the micro-EDM framework. It keeps the dielectric fluid's temperature significantly below its flash point, thereby averting potential thermal risks. This cooling capacity extends to both the electrode and the workpiece, thus maintaining their structural integrity and prolonging their operational lifespan. Through these functions, the dielectric circulation system ensures precision of micro-EDM process, its safety, and overall efficiency, highlighting its indispensable role in the dominion of advanced manufacturing.

17.4 Process and Machining Parameters of Micro-Electrical Discharge Machining

Micro-electrical discharge machining (micro-EDM) is a highly precise method of material removal, governed by key parameters that significantly impact its performance, precision, and surface finish quality. This process mainly involves the discharge of energy, which is influenced by elements such as pulse generators. These elements play a crucial role in determining the material removal rate (MRR) and tool wear rate (TWR), both of which are essential for attaining high precision in microfeatures and achieving an optimal surface finish [8, 13]. Peak current, pivotal for energy per discharge, influences MRR and surface quality, where higher currents increase MRR at the expense of surface finish and TWR. Gap voltage and discharge voltage play essential roles in spark energy and inter-electrode gap (IEG) control, impacting debris removal and discharge stability. Pulse duration and frequency directly affect material removal and surface quality, with longer durations and higher frequencies potentially enhancing MRR but affecting surface smoothness and thermal damage.

17.4.1 Process Parameters of Micro-EDM

i. Discharge Energy

In micro-EDM, discharge energy stands out as a pivotal parameter, encapsulating various operational factors that contribute to the energy discharged between electrodes across the IEG. Different pulse generators alter the computation of this energy, which in turn influences the MRR and the TWR, affecting the microfeature precision and surface finish.

ii. Peak Current

The ampere flowing per unit time per discharge pulse, is a crucial factor in determining the energy or power used during each discharge. A higher peak current lead to a greater MRR, but this benefit is offset by a decrease in surface quality and an increase in the TWR.

iii. Gap and Discharge Voltage

The voltage across the electrodes, or gap voltage, is instrumental in defining the spark's total energy. Through servo control adjustments, this voltage establishes the IEG, affecting debris flushing and subsequent discharge stability. A higher IEG can enhance MRR but may compromise surface quality due to enlarged crater sizes.

iv. Pulse Duration

The duration of the pulse-on time, which permits current to pass through the IEG, is pivotal in the process of material degradation and removal. An increase in pulse durations is directly associated with an enhanced MRR; however, it leads to a coarser surface texture owing to the formation of broader and greater craters.

v. Pulse Frequency

The frequency of pulses, which denotes the count of cycles in a second, affects the quality of the surface finish. Settings with higher frequencies result in briefer pulse durations, which produce smaller craters and reduce thermal damage.

vi. Duty Factor

The duty factor, defined as the percentage ratio of pulse duration to the total cycle time, influences machining conditions significantly. A higher duty factor

reduces flushing times, potentially causing short circuits, whereas a lower duty factor suggests more off time and reduced machining rates.

17.4.2 Non-Electrical Process Parameters of Micro-Electrical Discharge Machining

Non-electrical parameters, such as workpiece material properties, tool electrode characteristics, vibration techniques, dielectric fluids, flushing methods, and flushing pressure, also significantly impact machining performance [8, 13]. These factors influence the efficiency of debris removal, cooling, and electrical discharge stability, thereby affecting MRR, surface finish, and the creation of high-aspect-ratio microfeatures.

i. Workpiece Materials

The conductivity of the material to be machined influences the EDM process. Other critical properties include thermal conductivity, specific heat, and melting or vaporization points, which collectively influence the machining efficiency.

ii. Tool Electrodes

The effectiveness of EDM largely depends on the tool electrode used. The material's thermal properties are vital, given the process's reliance on thermal energy. High melting points, thermal conductivity, and specific material characteristics such as erosion resistance, machining ease, cost, availability, electrical conductivity, thermal diffusivity, and mechanical properties dictate the suitability of materials like copper, brass, tungsten, and alloys for tool fabrication.

iii. Workpiece and Tool Vibration

Vibration techniques, applied to either the tool or workpiece, enhance EDM performance by improving debris removal and flushing efficiency through constant changes in the discharge gap and dielectric fluid pressure.

iv. Dielectric Fluids

Dielectric fluids play a multifaceted role in EDM, affecting everything from cooling to the stability of electrical discharges. The choice of fluid is influenced by its viscosity, dielectric strength, cooling capabilities, and chemical composition, which are essential for a stable machining process and optimal MRR.

v. Types of Dielectric Flushing

Flushing methods, including pressure and suction flushing, are vital for debris removal and maintaining stable discharge conditions. Techniques vary based on the machining operation, with jet and side flushing being common approaches.

vi. Flushing Pressure

Adequate flushing pressure is essential for removing eroded particles and cooling the machining zone, contributing to stable machining conditions and the generation of high-aspect-ratio microfeatures, although high pressures must be managed to avoid tool deflection.

17.4.3 Machining Characteristics of Micro-Electrical Discharge Machining

Machining characteristics like MRR, EWR, overcut, surface roughness, diametral variance at entry and exit holes, circularity, and machining time are critical for assessing micro-EDM performance [8, 13]. These characteristics are influenced by a complex interplay of electrical and non-

electrical process parameters, highlighting the importance of optimizing these parameters to achieve desired outcomes in terms of productivity, accuracy, and surface integrity in micro-EDM processes.

i. Material Removal Rate (MRR)

   Material removal rate (MRR) quantifies the volume of material eroded from the workpiece per unit time, serving as a measure of the machining speed. This rate is crucial for gauging productivity, balancing the need for quick machining against maintaining dimensional accuracy and surface integrity. The MRR is influenced by several process parameters including discharge voltage, peak current, pulse duration, and duty cycle, and it is calculated by measuring the weight difference of the workpiece before and after machining over the machining time. Optimizing these parameters can enhance MRR while considering other essential machining outcomes like surface finish, tool wear, and accuracy.

ii. Electrode Wear Ratio (EWR)

   The EWR or TWR compares the volume of material worn away from the electrode to that removed from the workpiece. High TWR can detract from the machined features' precision and surface quality. Tool wear, especially in micro-EDM drilling, affects tool length and, consequently, machining accuracy. This ratio is significantly influenced by the electrical and thermal properties of the tool material, as well as the machining parameters. Minimizing TWR is essential for maintaining the geometrical accuracy and integrity of machined features.

iii. Surface Roughness

Surface roughness in micro-EDM is primarily determined by the size of craters formed by each discharge. Efficient dielectric flushing in the discharge gap minimizes the resolidification of molten material on the machined surface, improving the surface finish. The surface roughness is also dependent on the pulse energy and various machining parameters, with effective flushing techniques playing a critical role in achieving a smoother surface.

iv. Overcut (OC)

Overcut represents the dimensional discrepancy beyond the intended geometry of the machined feature, particularly notable in micro-hole drilling. This difference is affected by the machining settings and how effectively debris is cleared from the machining area. Reducing overcut is crucial to attaining the required geometric accuracy in micro-EDM operations.

v. Diametral Variance at Entry and Exit Holes

This criterion measures the difference in diameter between the entry and exit points of drilled micro-holes, with significant variance indicating potential inaccuracies in the drilling process. Factors such as pulse duration, peak current, and flushing pressure can affect this variance, impacting the uniformity and accuracy of the drilled holes.

vi. Circularity

Circularity assesses the roundness of drilled micro-holes, with deviations from perfect circularity indicating potential issues in the drilling process. This performance metric is crucial for evaluating the geometric precision of micro-holes, with factors such as flushing pressure and tool vibration affecting the outcome.

vii. Machining Time

Machining time refers to the entire time needed to create a particular microfeature on the workpiece. It has a strong connection to the MRR, with different process parameters playing a significant role in the operation’s efficiency. Cutting down on machining time without compromising quality is essential for boosting productivity in micro-EDM processes.

17.5 Major Varieties of Electrical Discharge Micromachining

Table 17.2 summarizes the variants of micro-EDM, highlighting their operational mechanisms and the significance of each in micro-manufacturing processes. These variants extend the capabilities of traditional EDM to the micro-scale, offering precision and flexibility for producing micro-sized features and parts across various industries.

17.5.1 Micro-Wire Electro-Discharge Machining (µ-WEDM)

Jarin *et al.* [18] conducted a detailed experimental study to examine the impact of nanopowder on the micro-wire electro-discharge machining (µ-WEDM) process, specifically when machining gold-coated silicon. The µ-WEDM is a precision machining process used to produce complex structures in various industrial applications. The study focuses on the use of gold as a temporary coating on silicon to enhance electrical conductivity and enable µ-WEDM. Nanopowder mixed dielectric medium is introduced to improve machining accuracy and stability. The research found that adjusting nanopowder concentrations in the dielectric medium could significantly

improve the MRR and spark gap (SG), demonstrating the potential for enhanced µ-WEDM performance.

Figure 17.5 shows the experimental setup for µ-WEDM with a circulation process designed to prevent nanopowder sedimentation. A submersible pump circulates nanopowder mixed dielectric oil in the EDM tank, ensuring consistent machining conditions. This setup is pivotal for the research as it maintains the stability and quality of the machining process by evenly distributing the nanopowder throughout the dielectric medium, thus facilitating the study of its effects on µ-WEDM performance.

Table 17.2 Variant types of electrical discharge micromachining.

Type of variant	Working	Significance
Die-sinking micro-EDM [14]	Uses an electrode to produce mirror images on the workpiece by sinking into it.	Earliest and most common type, suitable for intricate shapes and microfeatures.
Micro-wire electro-discharge machining [13]	Employs a moving microwire as the electrode to cut through the material precisely.	Allows for precise cutting of complex shapes with high precision.
Dry and near-dry micro-EDMs [13]	Employs gas or air as the dielectric medium instead of liquid or uses a mixture of liquid and gas.	Reduces pollution and waste management costs, suitable for green manufacturing.
Micro-EDM drilling [15]	Employs micro-electrodes for the purpose of creating micro-holes within the workpiece.	It solves the difficulty of clamping long electrodes, which is ideal for creating micro-holes with high aspect ratios.
Micro-electro-discharge	Involves the erosion of material from the workpiece to	Used to fabricate microelectrodes with high aspect ratios, essential for

Type of variant	Working	Significance
grinding [16]	produce micro-shafts or features.	creating precise microtools and features.
Planetary or orbital micro-EDM [13]	Integrates orbital motion into the electrode mechanism to enhance flushing capabilities and improve the removal of debris.	Improves the precision of machining operations, increases the rate at which material is removed, and minimizes wear on the electrode. This is particularly advantageous for the creation of blind micro-holes.
Reverse micro-EDM [17]	Reverses the polarity to erode material from a larger diameter rod, creating micro-electrodes.	Enables the fabrication of complex electrode shapes and multiple electrodes simultaneously.

The study by Yukui Wang *et al.* [19] investigates a processing defect in micro gears produced by μ-WEDM, characterized by non-intact tooth profiles as shown in Figure 17.6. Through real-time CCD camera observation, they identified the defect's main cause as the gravity affecting the micro gear, leading to differential stresses on an ultrathin cantilever beam formed during machining. Despite modifying the liquid flushing strategy, the defect persisted, primarily due to the material's lower tensile strength (X153CrMoV12), which fractures under stress before the completion of machining, highlighting the challenge in micro-gear fabrication.

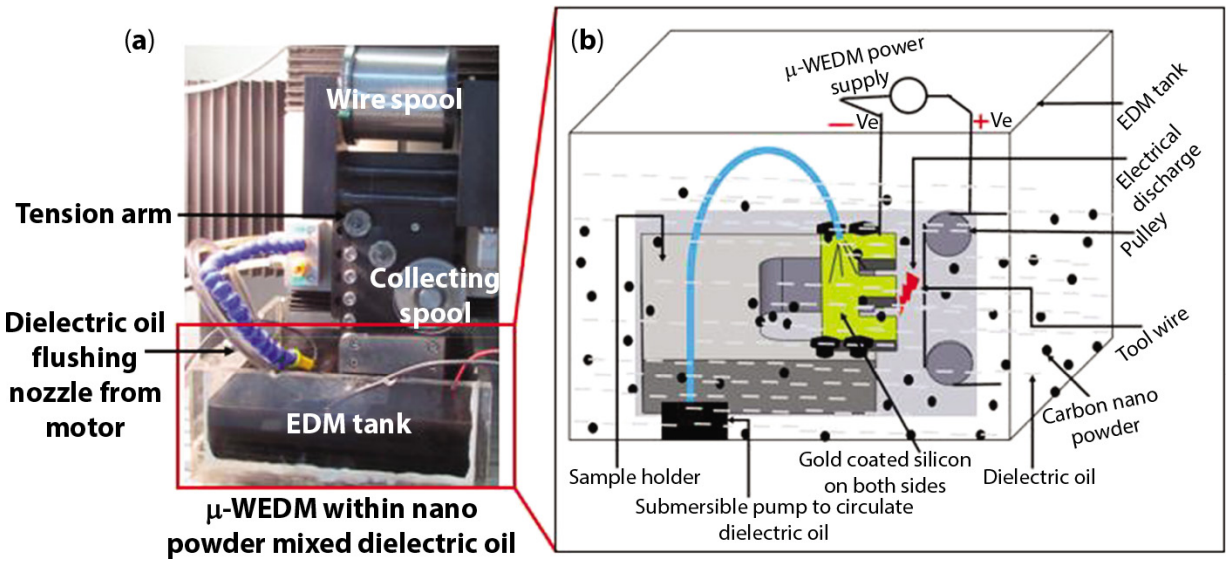


Figure 17.5 μ-WEDM setup and experimental methodology [18].

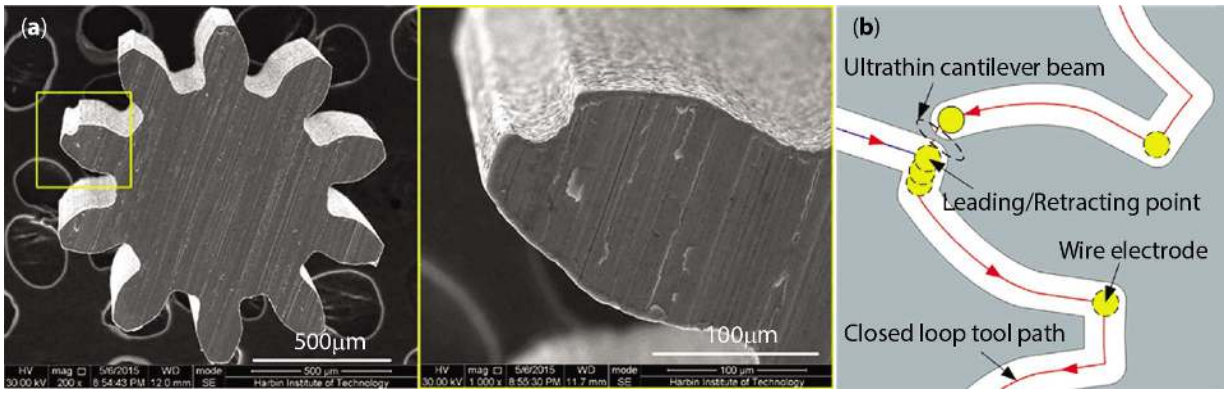


Figure 17.6 Microscale gear fabricated using micro-EDM: (a) displays SEM images, (b) illustrates the schematic representation of the machining defect [19].

17.5.2 Micro-Electrical Discharge Grinding (Micro-EDG)

Micro-EDG is a specialized form of EDG tailored for micro-machining, utilizing electrical discharges to erode material from the workpiece. Figure 17.7 illustrates three distinct types of micro-EDG processes:

i. Wire electrical discharge grinding (WEDG): this method employs a continuously fed wire as the electrode to erode the material, facilitating the production of microrod electrodes with high precision. The continuous feeding compensates for electrode wear, maintaining machining accuracy.

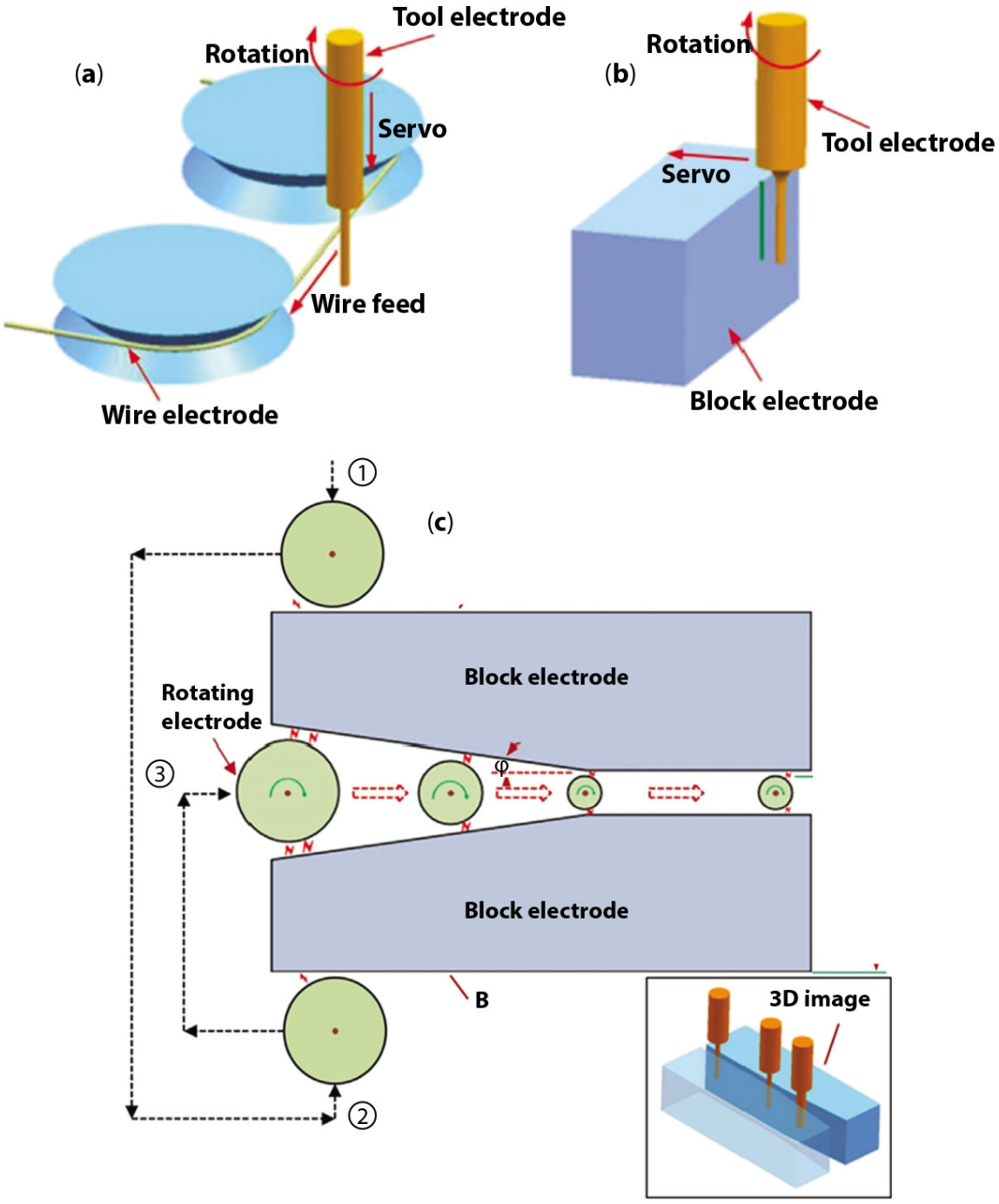


Figure 17.7 Various micro-EDM machining approaches: (a) wire electrical discharge grinding (WEDG), (b) block electrical discharge grinding (BEDG), and (c) electrical discharge grinding using two block electrodes (EDG-TBE) [16].

ii. Block electrode discharge grinding (BEDG): here, a

block electrode is used to grind the microrod electrode. While BEDG offers higher machining efficiency due to the larger electrode contact area, it suffers from accuracy issues due to the wear of the block electrode, affecting dimensional consistency.

iii. Electrical discharge grinding using two block electrodes (EDG-TBE): this novel approach involves feeding a rod electrode through a narrow gap between two block electrodes. The width of the gap and the discharge parameters control the final diameter of the rod, eliminating the need for in-process measurement and thereby simplifying the equipment. EDG-TBE has been shown to offer higher machining efficiency and accuracy compared to BEDG, with reduced equipment complexity.

These techniques signify progress in the field of micro-machining, facilitating the accurate creation of micro rod electrodes (Figure 17.7), which are crucial for use in microelectromechanical systems (MEMS) and various other areas that demand small-scale, high-accuracy parts.

17.6 Hybrid Type of Electrical Discharge Micromachining

17.6.1 Simultaneous Micro-EDM and Micro-ECM (SEDCM)

Simultaneous micro-EDM and micro-ECM (SEDCM) is a hybrid machining process that combines the material removal mechanisms of both EDM and ECM [11]. It is designed to utilize the precise material removal and complex shape capabilities of micro-EDM with the smooth surface finishes and no-tool-wear advantages of micro-ECM. This procedure is conducted within a distinct setting,

employing deionized water with low resistivity. This water serves a dual purpose: it functions as a dielectric medium for EDM and as a conductive electrolyte for ECM.

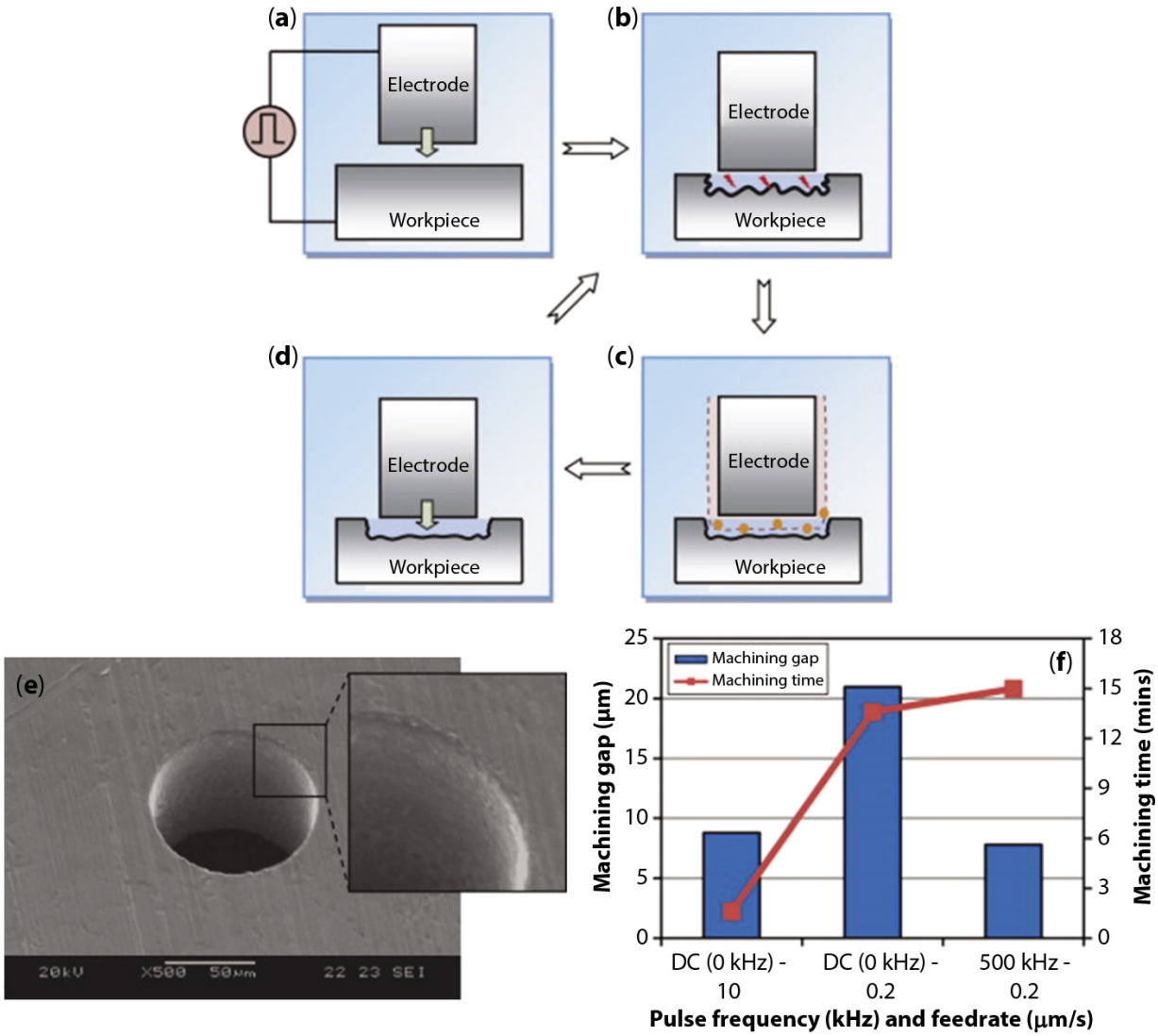


Figure 17.8 Illustration of the simultaneous micro-EDM and micro-ECM (SEDCM) process: (a) initiation of the SEDCM process, (b) discharge phase, (c) dissolution phase, (d) electrode feeding stage, (e) microscopic view of a micro-hole created using SEDCM with 500 kHz pulses, 30% duty cycle, and a feed rate of 0.2 mm/s, (f) comparison of machining gap and time across various SEDCM conditions [11].

When the electrode is gradually moved closer to the workpiece, thereby reducing the space between them as illustrated in Figure 17.8(a), there comes a point where this distance becomes minimal enough to disrupt the

stability of the deionized water, triggering spark formation as shown in Figure 17.8(b). This process involves removing material from the workpiece by melting and vaporizing it, leading to a surface marked by overlapping pits. As the gap subsequently increases, the discharge process halts, allowing the mild conductivity of the deionized water to facilitate electrochemical processes, as demonstrated in Figure 17.8(c). These processes lead to the anodic dissolution on the surface of the workpiece, enhancing the surface quality by removing imperfections. The utilization of brief voltage pulses focuses on this dissolution activity, promoting accurate machining as represented by the dashed line in Figure 17.8(c). The procedure is repetitive, with the electrode moving forward in small steps to start a new spark, as illustrated in Figure 17.8(d). This necessitates a regulated feed rate to allow sufficient time for the electrochemical reactions to enhance the surface finish efficiently.

The micro-hole shown in Figure 17.8(e), created with pulses of 500-kHz frequency and a 0.2-mm/s feed rate, demonstrates the SEDCM process's capability to produce a smooth surface free of craters and without unwanted diameter expansion or micro-pits near the rim. Figure 17.8(f) compares different machining conditions, highlighting how the use of short voltage pulses, low feed rate, and low-resistivity deionized water are integral to the process, achieving a delicate balance between the machining gap and time for an optimized outcome.

The significance of this study is in the development of SEDCM as a novel process that combines the material removal mechanisms of micro-ECM and micro-EDM. Particularly, it is effective when a low feed rate is applied, leading to the transformation from pure micro-EDM to a hybrid process. The three critical factors for successful SEDCM implementation are identified as the use of low-

resistivity deionized water, short voltage pulses, and low feed rate, which together enable the delivery of high-precision machining with excellent surface finishes, desirable for micro- and nanofabrication.

17.6.2 Ultrasonic Cavitation-Assisted Micro-EDM

In the progress of precision manufacturing methods, the introduction of a hybrid micro-EDM approach offers considerable promise for improving the creation of high aspect ratio micro-holes in extremely hard materials such as reaction-bonded silicon carbide (RB-SiC). This innovative method is centered around combining ultrasonic cavitation and incorporating carbon nanofibers into the dielectric fluid, as illustrated in Figure 17.9(a).

A probe-type oscillator horn then introduces ultrasonic vibrations above the workpiece, instigating cavitation—a process involving the formation and implosive collapse of microbubbles in the fluid [20]. This cavitation effect supersedes the traditional bubble escape mechanism [21] by efficiently removing the debris created during the discharge process. The focused ultrasonic energy from the oscillator horn ensures that only the region of interest experiences intense cavitation, minimizing energy dispersion and promoting an efficient debris removal process at lower energy levels.

Furthermore, carbon nanofibers are identified as a critical component in machining low-conductivity materials like RB-SiC [22]. Their enhanced electrical conductivity reduces the fluid’s dielectric strength and increases the spark gap, which facilitates a greater MRR and enhances the surface finish quality. The ultrasonic vibration ensures the carbon nanofibers remain evenly distributed, preventing

aggregation and enhancing the frequency of electrical discharges during the process.

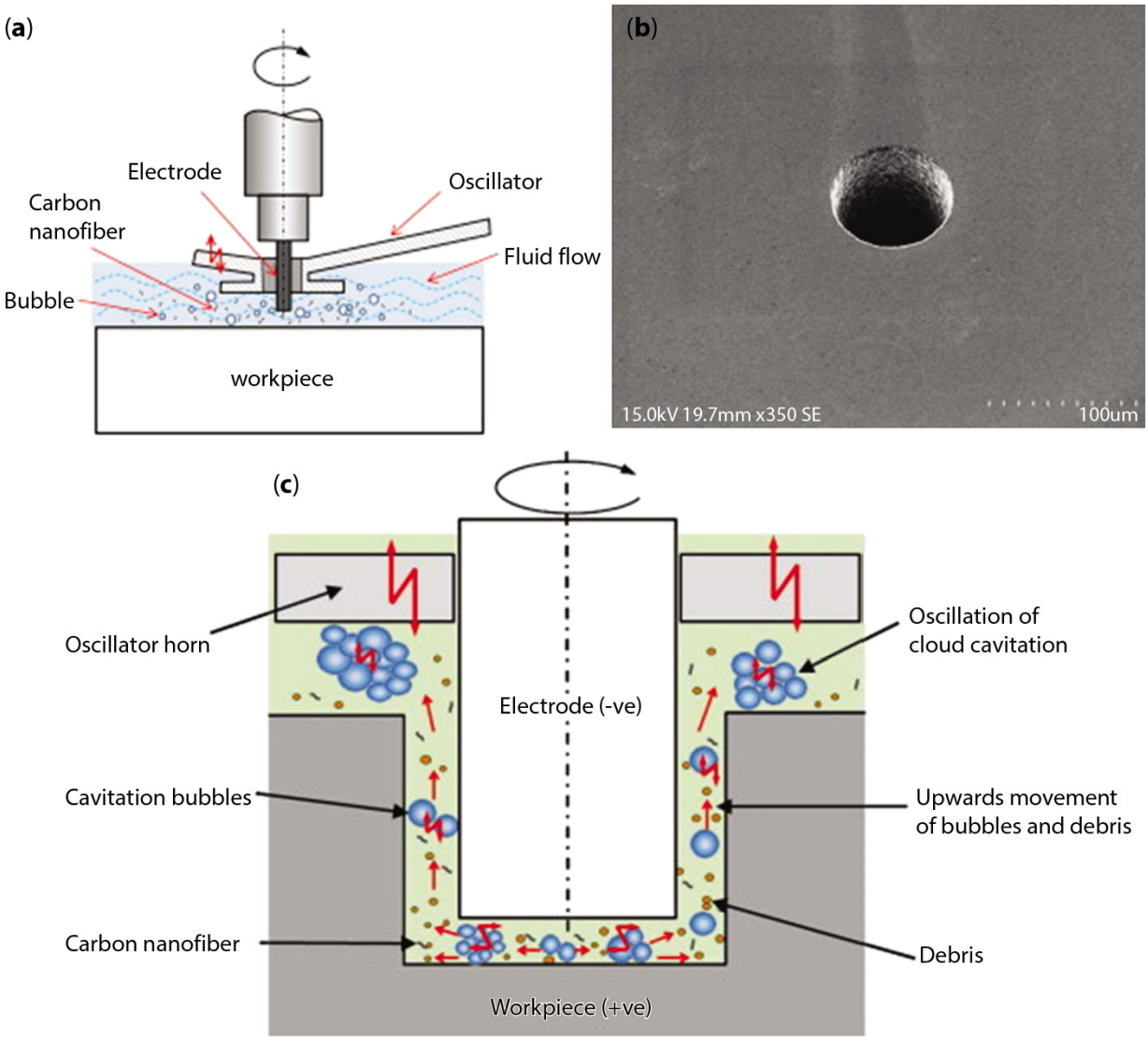


Figure 17.9 (a) Diagram of the hybrid micro-EDM setup with carbon nanofibers and electrode. (b) Microhole made with a 50-μm tool electrode. (c) Model of debris removal by cavitation [20].

To evaluate the quality of the inner surfaces of the micro-holes, as observed in Figure 17.9(b), scanning electron microscopy (SEM) was used. The conceptual model for debris ejection via cavitation-assisted micro-EDM is seen in Figure 17.9(c). The application of ultrasonic vibrations is

anticipated to produce two primary benefits: the stirring action for the homogenous distribution of carbon nanofibers and the generation of cavitation bubbles to facilitate debris clearance. These combined effects are designed to decrease the chance of short circuits and improve the stability of the machining process, possibly resulting in significant enhancements in EDM efficiency.

17.7 Summary

The book chapter “Electrical Discharge Micromachining: State of Art” provides an in-depth analysis of micro-EDM, a precision machining process that utilizes electrical discharges to fabricate microscale features in electrically conductive materials. It covers the evolution of EDM from traditional machining to its crucial role in micro-manufacturing, detailing the working principles, process parameters, and the differentiation between micro-EDM and macro-EDM. The chapter emphasizes the importance of various components and parameters that influence machining efficiency, accuracy, and surface quality. It also explores several micro-EDM variants and hybrid approaches, highlighting the technique’s adaptability and potential for innovation. Through discussions on machining characteristics such as material removal rate, electrode wear ratio, and surface roughness, the text underscores micro-EDM’s significance in meeting the demands for miniaturization and precision in modern industries.

References

1. Balaji, N.S., Velmurugan, C., Kumar, M.S., Sivakumar, M., Asokan, P., Experimental investigation on mechanical properties of FDM-based nylon carbon parts using ANN approach. *Surf. Let.*, *30*, 2350028, 2023.

2. Hyacinth Suganthi, X., Natarajan, U., Ramasubbu, N., A review of accuracy enhancement in micro-drilling operations. *Int. J. Adv. Manuf. Tech.*, 81, 199, 2015.

3. Jahan, M.P., Micro-electrical discharge machining, in: *Nontraditional Machining Processes: Research Adva*, vol. 111, 2013.

4. Jahan, M.P. and Wong, Y.S., A study on the fine-finish die-sinking micro-EDM of tungsten carbide using different electrode materials. *J. Mater. Process. Tech., 209*, 3956, 2009.

5. Jarin, S., Saleh, T., Rana, M., Muthalif, A.G.A., Ali, M.Y., An Experimental Investigation on the Effect of Nanopowder for Micro-Wire Electro Discharge Machining of Gold Coated Silicon. *Procedia Eng., 184*, 171, 2017.

6. Katz, Z. and Tibbles, C.J., Analysis of micro-scale EDM process. *Int. J. Adv. Manuf. Tech., 25*, 923, 2005.

7. Kim, B.H., Park, B.J., Chu, C.N., Fabrication of multiple electrodes by reverse EDM and their application in micro-ECM. *J. Micromech. Microeng., 16*, 843, 2016.

8. Kumar, D., Singh, N.K., Bajpai, V., Recent trends, opportunities and other aspects of micro-EDM for advanced manufacturing: a comprehensive review. *J. Braz. Soc. Mech. Sci. Eng., 42*, 1, 2020.

9. Kunieda, M., Hayasaka, A., Yang, X.D., Sano, S., Araie, I., Study on Nano EDM Using Capacity Coupled Pulse Generator. *CIRP Ann., 56*, 213, 2007.

10. Sivakumar, M., Jerald, J., Balaji, N.S., Rajesh Kannan, G., Prediction of Mechanical Properties on Wire Arc Additive Manufacturing 316l Stainless Steel Using Fuzzy

Logic, in: *Optimization of Advanced Manufacturing Processes*, S. Kunar (Ed.), Apple Academic Press, Florida, 2024.

11. Liew, P.J., Yan, J., Kuriyagawa, T., Experimental investigation on material migration phenomena in micro-EDM of reaction-bonded silicon carbide. *App. Surf. Sci., 276*, 731, 2013.

12. Liew, P.J., Yan, J., Kuriyagawa, T., Fabrication of deep micro-holes in reaction-bonded SiC by ultrasonic cavitation assisted micro-EDM. *Inter. J. Mach. Tools Mfg., 76*, 13, 2014.

13. Munusamy, S. and Jerald, J., Effect of *in-situ* Intrinsic Heat Treatment in Metal Additive Manufacturing: A Comprehensive Review. *Met. Mater. Internat.*, 29, 3423, 2021.

14. Nguyen, M.D., Rahman, M., Wong, Y.S., Simultaneous micro-EDM and micro-ECM in low-resistivity deionized water. *Int. J. Mach. Tools Manuf.*, 54, 55, 2012.

15. Qingfeng, Y., Xingqiao, W., Ping, W., Zhiqiang, Q., Lin, Z., Yongbin, Z., Fabrication of micro rod electrode by electrical discharge grinding using two block electrodes. *J. Mater. Process. Tech., 234*, 143, 2016.

16. Rahman, M., Asad, A.B.M.A., Masaki, T., Wong, Y.S., Lim, H.S., Integrated Hybrid Micro/ Nano-Machining, in: *Prcd. of the ASME International Manufacturing Science and Engineering Conf*, vol. 2007, p. 197, 2009.

17. Saleh, T. and Bahar, R., Near Net Shape Machining by Micro-EDM and Micro-WEDM, in: *Micro-electrical Discharge Machining Processes*, G. Kibria (Ed.), pp. 231–264, Springer, Germany, 2019.

18. Sivakumar, M., Jerald, J., Shriram, S., Jayanth, S., Balaji, N.S., Hybrid Laser-Assisted Jet Electrochemical Micromachining Process, in: *Hybrid Micromachining and Microfabrication Technologies: Principles, Varieties and Applications*, S. Kunar (Ed.), pp. 179–203, John Wiley & Sons, Hoboken, 2023.

19. Song, K.Y., Chung, D.K., Park, M.S., Chu, C.N., Micro electrical discharge drilling of tungsten carbide using deionized water. *J. Micromech. Microengg., 19*, 045006, 2009.

20. Uhlmann, E., Mullany, B., Biermann, D., Rajurkar, K.P., Hausotte, T., Brinksmeier, E., Process chains for high-precision components with micro-scale features. *CIRP Ann., 65*, 549, 2016.

21. Wang, J., Han, F., Cheng, G., Zhao, F., Debris and bubble movements during electrical discharge machining. *Intl. J. Mach. Tools Manuf., 58*, 11, 2012.

22. Wang, Y., Chen, X., Wang, Z., Dong, S., Fabrication of micro gear with intact tooth profile by micro wire electrical discharge machining. *J. Mater. Process. Tech., 252*, 137, 2018.

Note

**Corresponding author*: siva.sky06@gmail.com

18
Electrochemical Micromachining

Bikash Ghoshal* and Daya Shankar Diwakar
Department of Mechanical Engineering, Guru Gobind Singh Educational Society's Technical Campus, Bokaro, Jharkhand, India

Abstract

In this chapter, several important aspects of the latest developments in electrochemical micromachining are highlighted. Mass removal rate (MRR) in electrochemical micromachining (EMM) is described in detail for a selection of proper microtool feed rate and to determine machining time for a microfeature. Prediction of shape evolution in EMM is a challenging task which mainly depends on tool shape and current density distribution. It requires solution of Laplace's equation, $\nabla^2 V = 0$. Simulation procedures are discussed for shape prediction. Shaping in EMM through mask and effects of end shapes of microtool like conical, reverse conical and cylindrical on shape evolution are highlighted. Selection of electrolyte is a major area particularly for successful EMM of superalloy. Electrolyte has severe influence on the metal/alloy to be machined by EMM. Electrical double layer, electrolyte resistance, MRR, sludge formation, accuracy of machining are directly influenced by electrolyte. Fabrication and use of cylindrical, conical, reverse conical and disk shaped microtools are discussed for enhancement of EMM. Finally, advanced measurement techniques utilizing scanning electron microscope (SEM), non-contact 3D surface profiler, atomic force microscope (AFM), scanning and

transmission electron microscope (STM), and micro coordinate measuring machine (CMM) are described.

***Keywords*:** Micromachining, microtool, shape evolution

18.1 Introduction

18.1.1 Electrochemical Machining Process Overview

Electrochemical machining (ECM) is a non-contact type of machining based on Michael Faraday's laws of electrolysis. Anodic workpiece and cathode tool are separated by electrolytic gap of 100 to 600 μm. Electrolyte may be neutral salt solution or mild acidic solution or mixture of both. The electrolyte is pumped at high pressure approximately 1.4 MPa to 2.4 MPa with high velocities between the anodic workpiece and cathode electrode. It plays a critical task of allowing electric current flow between anode and cathode. It also removes the reaction products, hydrogen bubble and dissipates heat generated.

The tool of ECM is made of high electrical and thermal conductive material with high corrosive resistance. General purpose tool materials are copper, aluminum, brass, bronze, titanium, stainless steel, cupronickel, etc. The size of tool is slightly smaller than the size of cavity because in the time of machining overcut occurs on workpiece.

The supply power in ECM is the function of direct or pulse current, relatively low voltage ranging from 10 to 30 V to reduce the arcing problem between the gaps. Current densities up to 1.5–8.0 A/mm^2 is applied to achieve better surface finish. When voltage is applied, reactions take place at the anodic workpiece, cathode tool, and within the electrolyte. Material dissolution occurs at the anodic workpiece near the tool and generated shape on the

workpiece is the replica of the cathode tool. Electrochemical machining creates multifaceted shapes and closed tolerances that would be very complicated or likely impossible to accomplish with conventional machining processes. Figure 18.1 shows a workpiece (*e.g.*, iron) and a round shaped tool having central hole for flow of electrolyte (*e.g.*, aqueous solution of NaCl). Ionization of iron, water, and sodium chloride occur with the application of potential difference as shown below:

$$Fe \rightarrow Fe^{++} + 2e^{-} \quad (18.1)$$

$$H_2O \leftrightarrow H^{+} + OH^{-} \quad (18.2)$$

$$NaCl \leftrightarrow Na^{+} + Cl^{-} \quad (18.3)$$

Electrons released by anodic iron go through external circuit to the cathode to be accepted by hydrogen ions (H^+) to produce hydrogen gas at cathode. Iron ions reacts with Cl^- and $(OH)^-$ to form $FeCl_2$ and $Fe(OH)_2$, respectively, and finally, these are converted to sludge. The flowing electrolyte between workpiece and tool carries away the sludge. The current flows through the electrolytic gap/inter-electrode gap and regional dissolution of anodic metal (Fe) occurs. Tool is given steady downward feed depending on dissolution rate maintaining equilibrium inter-electrode gap. Thus, a blind hole is machined.

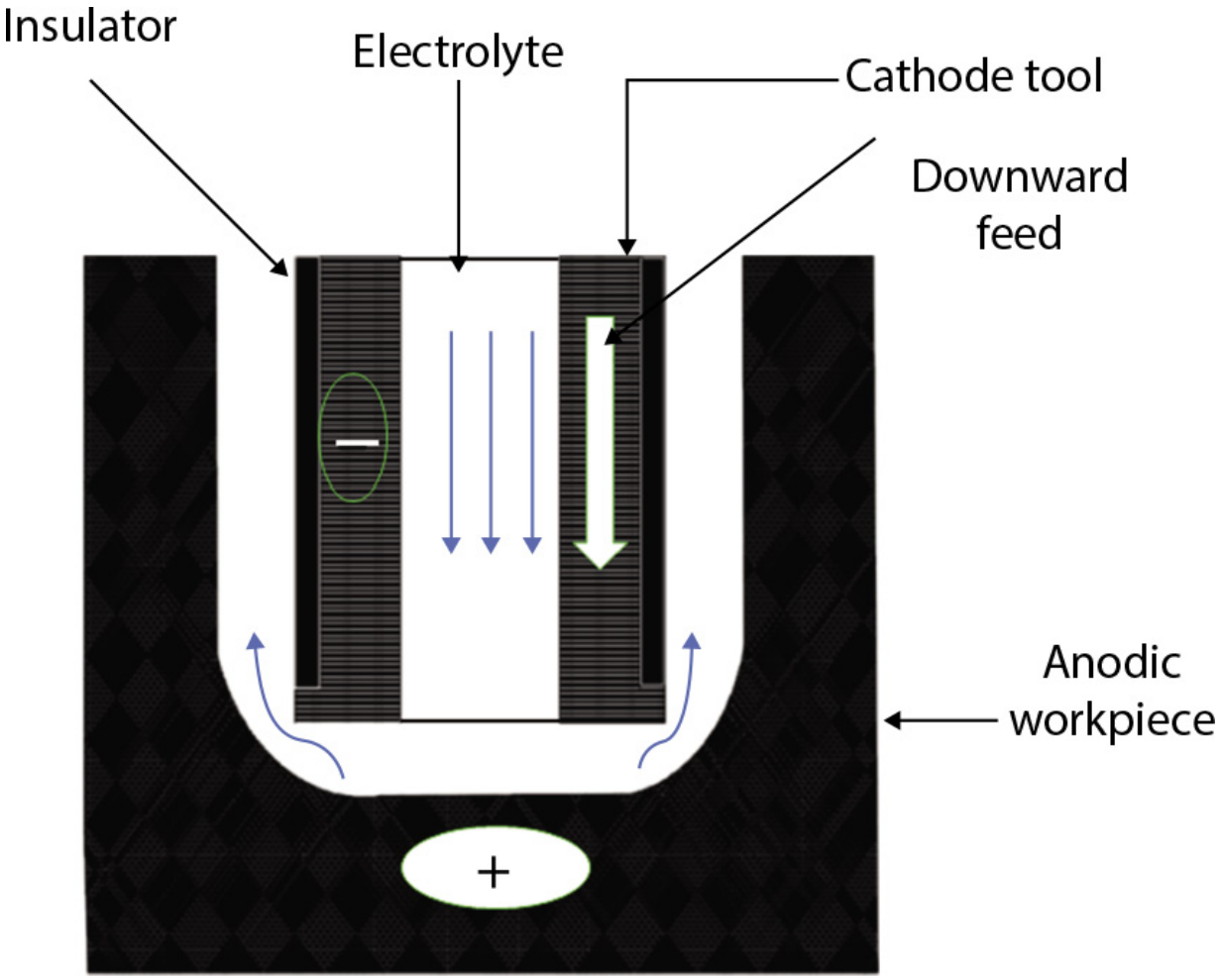


Figure 18.1 Schematic diagram of electrochemical machining.

If an intricate shape is to be machined on the workpiece, the designed tool with matching shape is moved in vertical axis with appropriate feed during ECM until proper depth of machining is realized. Figure 18.2 shows the initial position of the workpiece and tool in ECM. The final shape of the workpiece evolved in ECM is shown in Figure 18.3. It is worth mentioning that all the sharp corners on the workpiece are rounded due to higher current density. Rate of dissolution of metal is higher at the region of higher current density. At the initial position of ECM, region 'A' and region 'B' marked on the tool (protruded portions) will be very close to the workpiece. Current density at these

two zones of workpiece will be much higher due to lowest inter-electrode gap (IEG). Ohmic resistance to current flow will be lowest at these regions and as a result, metal will be dissolved at these two regions only. At the final position of ECM, steady gap (equilibrium gap) will be maintained throughout the whole region of machining, as shown in Figure 18.3.

W. Gusseff first patented controlled ECM process in 1929. Later on, it was established as a viable and commercially suitable machining process in aircraft industries for deburring and smooth finishing operations in 1940. Gradually, it gained popularity as a machining process due to no tool wear, high quality surface finish, stress-free machined surface, and capability to machine hard material. Metal removal rate (MRR) depends on voltage, type, concentration and flow rate of electrolyte, atomic weight of the workpiece, and IEG. Voltage and electrolyte highly influence surface finish.

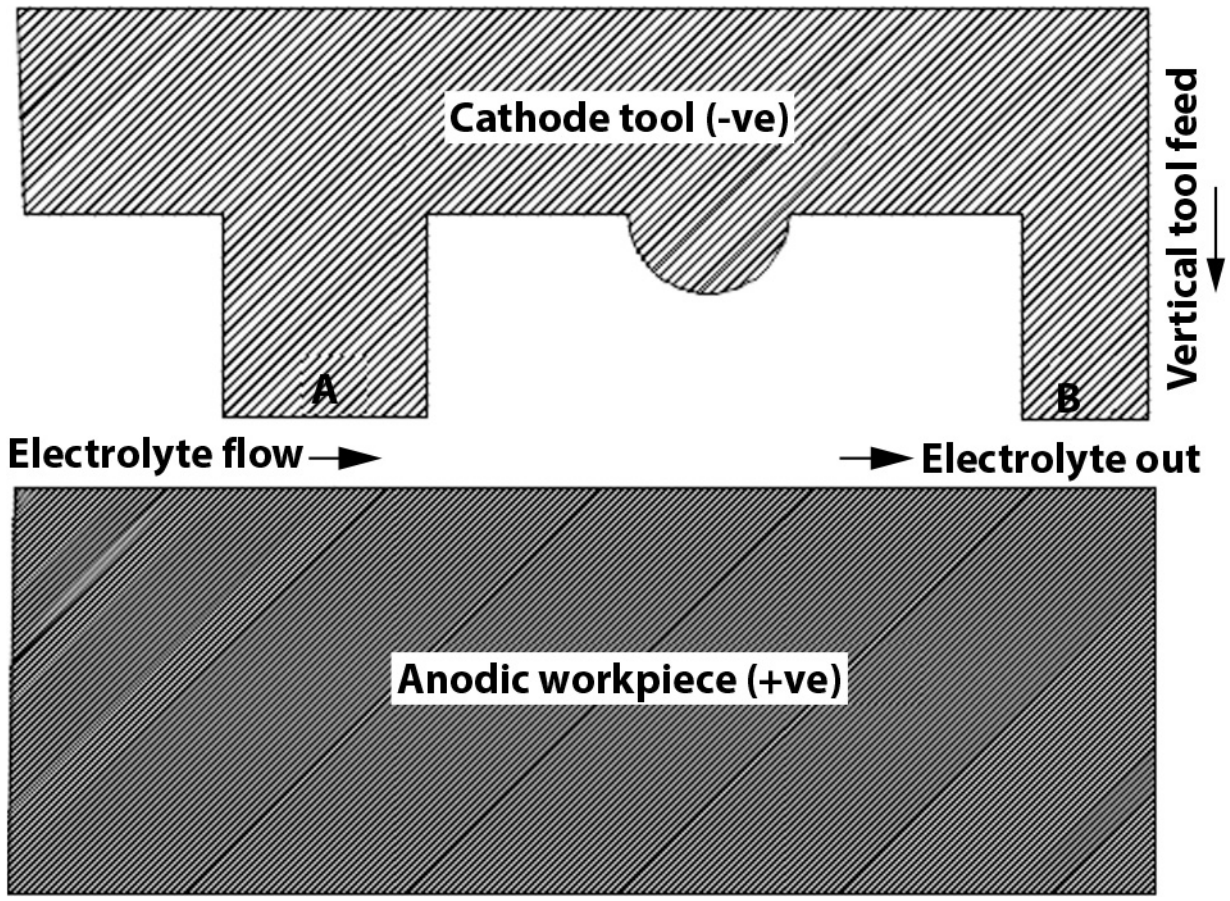


Figure 18.2 Initial positions of tool and workpiece in ECM.

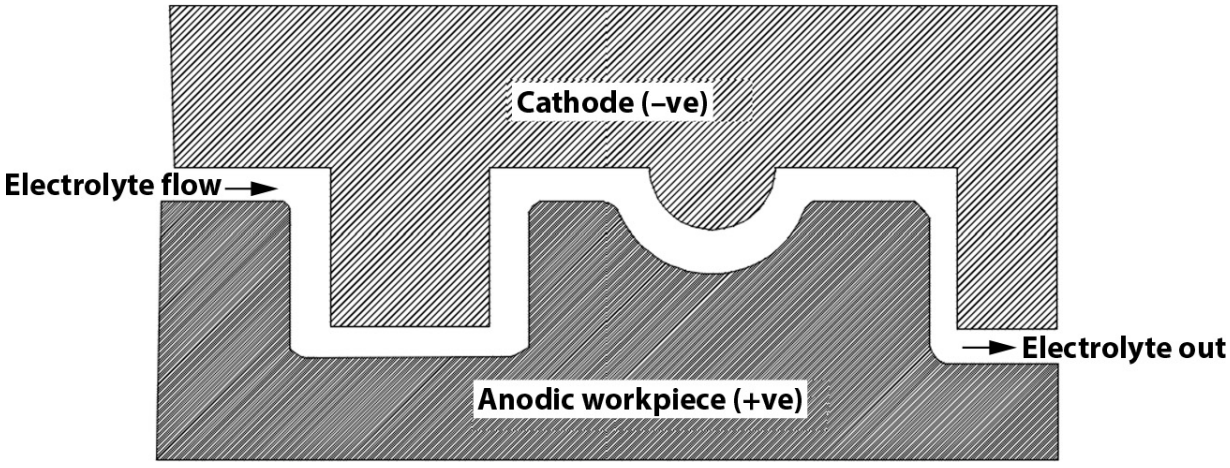


Figure 18.3 Final shape evolution in ECM of workpiece.

18.2 Overview of Electrochemical Micromachining

Ultra-precision devices are extensively used in industries in synchronization with the development of innovative micromachining activities like machining of micro-holes, microprofiles, free form surfaces, etc. Miniaturization of constituents in microelectromechanical systems (MEMS), electronics, sensors, mobile, and the computer industry is the need of the hour to accommodate microproducts in limited space. This is essential to serve the huge populations within limited resources. Micromachining technologies help in saving material and energy in addition to enhancing functionalities of microproducts. There is huge demand for microproducts made of titanium, nickel and cobalt based superalloys in electronics, communication industry and aerospace industry due to their high hardness. In traditional machining, drilling of circular or non-circular micro-hole in superalloys is very difficult [1]. Tool materials coming in contact with superalloy develop very high temperature and strong bonding leading to welding and failure of cutting tool edge. In recent years, electrochemical micromachining (EMM) has been used to solve existing difficulties for the fabrication and production of microparts. The term micromachining means material removal in the range of 1 to 999 μm [2–4]. Generally, it means material removal in the range of micron or submicron. In this process, anodic workpiece and cathode microtool separated by very narrow gap of 5–15 μm are immersed in electrolyte for passing of current. Dissolution of anodic metal takes place atom by atom. Electrochemical micromachining is in the limelight as it has many advantages compared to other non-conventional micromachining technologies. The same microtool can be repeatedly used without wear as it is noncontact machining. As material dissolution occurs atom by atom, no stress is developed during machining and hence, most suitable for micromachining hard materials like superalloys. Pulse power is used in EMM for better

accuracy of machining. Applied voltage, pulse frequency, pulse width along with Ohmic resistance of electrolyte mainly controls MRR.

18.3 Electrochemistry of Electrochemical Micromachining

When the applied voltage is greater than overpotentials involved in EMM, electrochemical reactions take place at the anode, cathode, and electrolyte. The type of anodic metal and nature of electrolyte determine the reactions at cathode and anode described below:

a. Cathode reactions

Hydrogen gas evolves at the cathode by the following reactions:

$$\text{Acidic electrolyte produces hydrogen gas by } 2H^+ + 2e^- \rightarrow H_2\uparrow \tag{18.4}$$

$$\text{Alkaline/neutral electrolyte produces hydrogen gas by } 2H_2O + 2e^- \rightarrow H_2\uparrow + 2(OH)^- \tag{18.5}$$

b. Anode reactions

Two possible reactions may occur at the anodic workpiece:

i. Dissolution of metal ions

ii. Evolution of oxygen

Dissolution of metal occurs by the following reaction:

$$M \rightarrow M^{n+} + ne^- \tag{18.6}$$

Once metal ions get sufficient energy from applied voltage, they cross the double layer barrier to the bulk electrolyte

and react with hydroxide ions as given below (Jain (2002)) [5].

$$M^{n+} n\,(OH)^- \rightarrow M\,(OH)_n \tag{18.7}$$

Evolution of oxygen may occur due to the following reactions.

$$2H_2O \rightarrow O_2\uparrow + 4H^+ + 4e^- \text{(When acidic electrolyte is used)} \tag{18.8}$$

$$4(OH)^- \rightarrow 2H_2O + O_2\uparrow + 4e^- \text{ (When alkaline electrolyte is used)} \tag{18.9}$$

To understand the type of reactions in acidic electrolyte, let us consider EMM of stainless steel work piece (SS-304) with H_2SO_4 as electrolyte. When appropriate voltage is applied, the following reactions will take place:

$$\text{Anode: } Fe \rightarrow Fe^{3+} + 3e^- \tag{18.10}$$

$$Cr \rightarrow Cr^{3+} + 3e^- \tag{18.11}$$

$$\text{Cathode: } 2H_2O + 2e^- \rightarrow 2(OH)^- + H_2\uparrow \tag{18.12}$$

$$\text{Electrolyte: } H_2SO_4 \rightarrow 2H^+ + (SO_4)^{2-} \tag{18.13}$$

$$2Fe^{3+} + 3(SO_4)^{2-} = Fe_2(SO_4)_3 \tag{18.14}$$
$$2Cr^{3+} + 3(SO_4)^{2-} = Cr_2(SO_4)_3$$

To understand the type of reactions in neutral electrolyte, let us consider EMM of iron work piece in aqueous $NaNO_3$ electrolyte. When appropriate voltage is applied, the following reactions will take place:

$$\text{Anode:} \quad Fe \rightarrow Fe^{++} + 2e^{-} \tag{18.15}$$

$$\text{Cathode:} \quad 2H_2O + 2e^{-} \rightarrow H_2\uparrow + 2(OH)^{-} \tag{18.16}$$

$$\text{Electrolyte:} \quad NaNO_3 \rightarrow Na^{+} + (NO_3)^{-} \tag{18.17}$$

$$Fe^{++} + 2(OH)^{-} \rightarrow Fe(OH)_2 \tag{18.18}$$

$$Fe^{++} + 2(NO_3)^{-} \rightarrow Fe(NO_3)_2 \tag{18.19}$$

$$4\,Fe(OH)_2 + 2H_2O + O_2 \rightarrow 4\,Fe(OH)_3\downarrow \text{ (Sludge)} \tag{18.20}$$

Only anodic metal is dissolved at the cost of electrical energy. Current flows through the movement of free electrons in metal while electrolyte performs the carrier of ions between work piece and tool. Shape of cathode tool remains same.

18.3.1 Metal Removal Mechanism in Electrochemical Micromachining

Faraday's laws of electrolysis are well known and given as below:

i. The quantity of any substance dissolved is proportional to the quantity of current passed through the electrolyte.

ii. The amount of different substances dissolved by the same amount of electric energy are proportional to their chemical equivalent weights.

Quantitatively mass dissolved or deposited is

$$m = \frac{MIt}{Fz} \tag{18.21}$$

Where m is the mass (in grams) dissolved, I is the current (in amperes) passed for the time t (second), M is the atomic weight (in grams), F is Faraday's constant, and z is the valency of cation.

Mathematical modeling for predicting MRR is so helpful that corrective approach can be initiated before actual micromachining/experimentation. Planning for variation of the parameters involved in the modeling can also be done beforehand and subsequently modified to achieve the desired results.

18.3.1.1 Metal Removal Rate Based on the Double Layer Model

The MRR in ECM is governed by Faraday's laws of electrolysis. But in the case of EMM, IEG is kept very small (5–15 µm) for better accuracy. Hence, several additional factors are to be considered while governing MRR equation is developed. As soon as a metal is immersed in electrolyte, ionization starts. The metal molecules go to the electrolyte as metal ions and electrons are left in the metal. Again, metal ions are discharged to metal in backward reaction maintaining an equilibrium condition. A voltage is to be applied for anodic dissolution of metal so that the reactions are in forward direction only. The associated resistance overcome in irreversible charge transfer is called charge transfer resistance. The double layer capacitance is defined as two parallel layers of charges aligned adjacent to the metal immersed in electrolyte, as shown in Figure 18.4. The first layer consists of generally negative ions adsorbed into the metal and the second layer consists of generally positive ions attracted to the surface. At the bulk electrolyte away from the metal, free ions of both positive and negative are available during machining. The flow

velocity of electrolyte is negligible in the case of EMM. Therefore, adequate transfer of mass will not occur from one electrode to the other electrode. This impedes current flow through the electrolyte due to diffusion layer formation and this component is called Warburg impedance. While developing MRR equation for EMM, the following factors are taken into consideration: (a) charge transfer resistance, (b) double layer capacitance, (c) Warburg impedance, and (d) Ohmic resistance of electrolyte.

Let us consider an electrical circuit model of EMM cell based on Randles circuit (Bard and Faulkner, 2001) [6], as shown in Figure 18.5. Warburg resistance, R_W, and charge transfer resistance, R_{ct}, are in series and in parallel arrangement with double-layer capacitance, C_{dl}. Electrolyte resistance, R_e, is in series with combined resistances at both ends of anode and cathode.

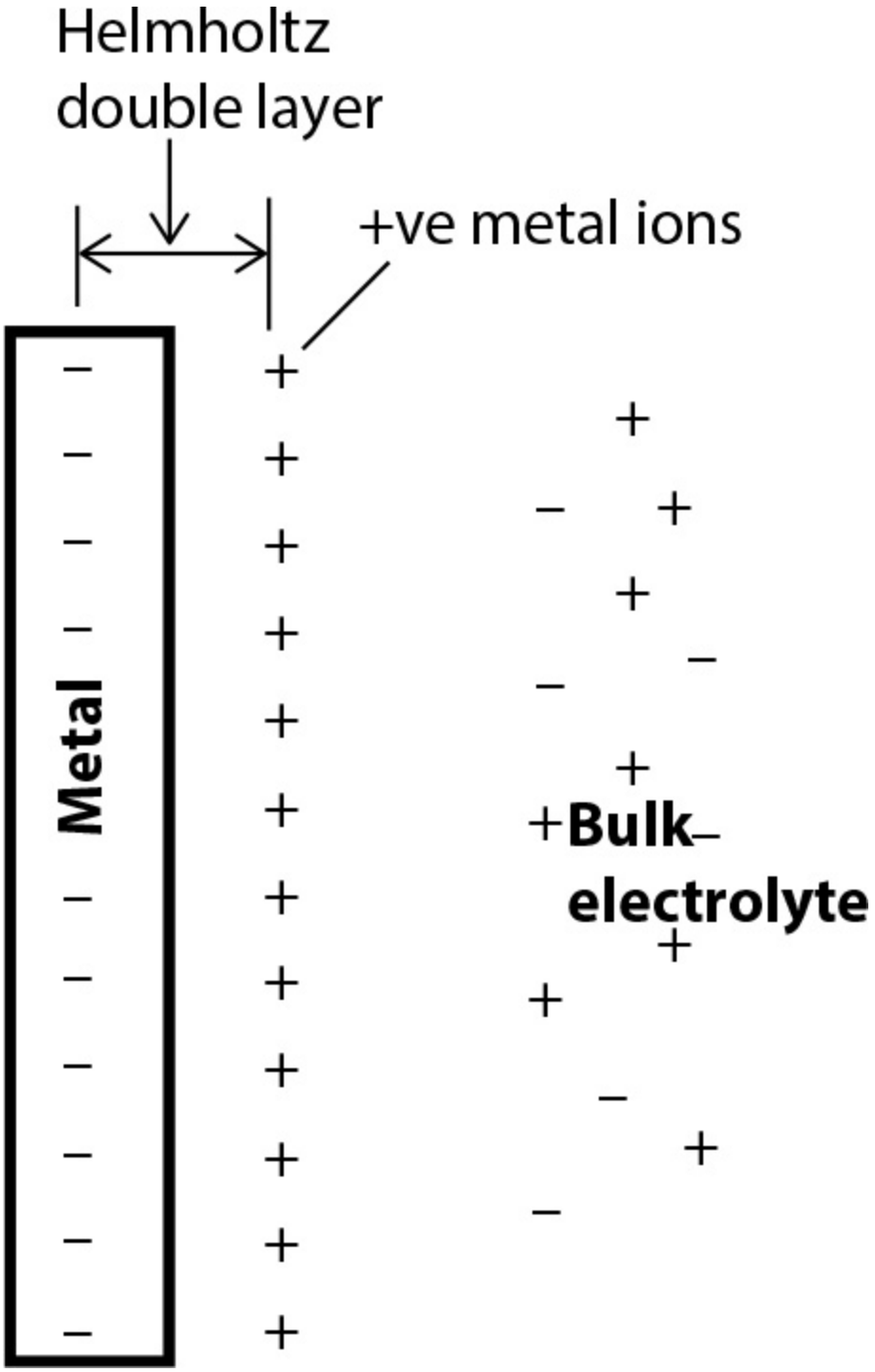


Figure 18.4 Electrical double layer.

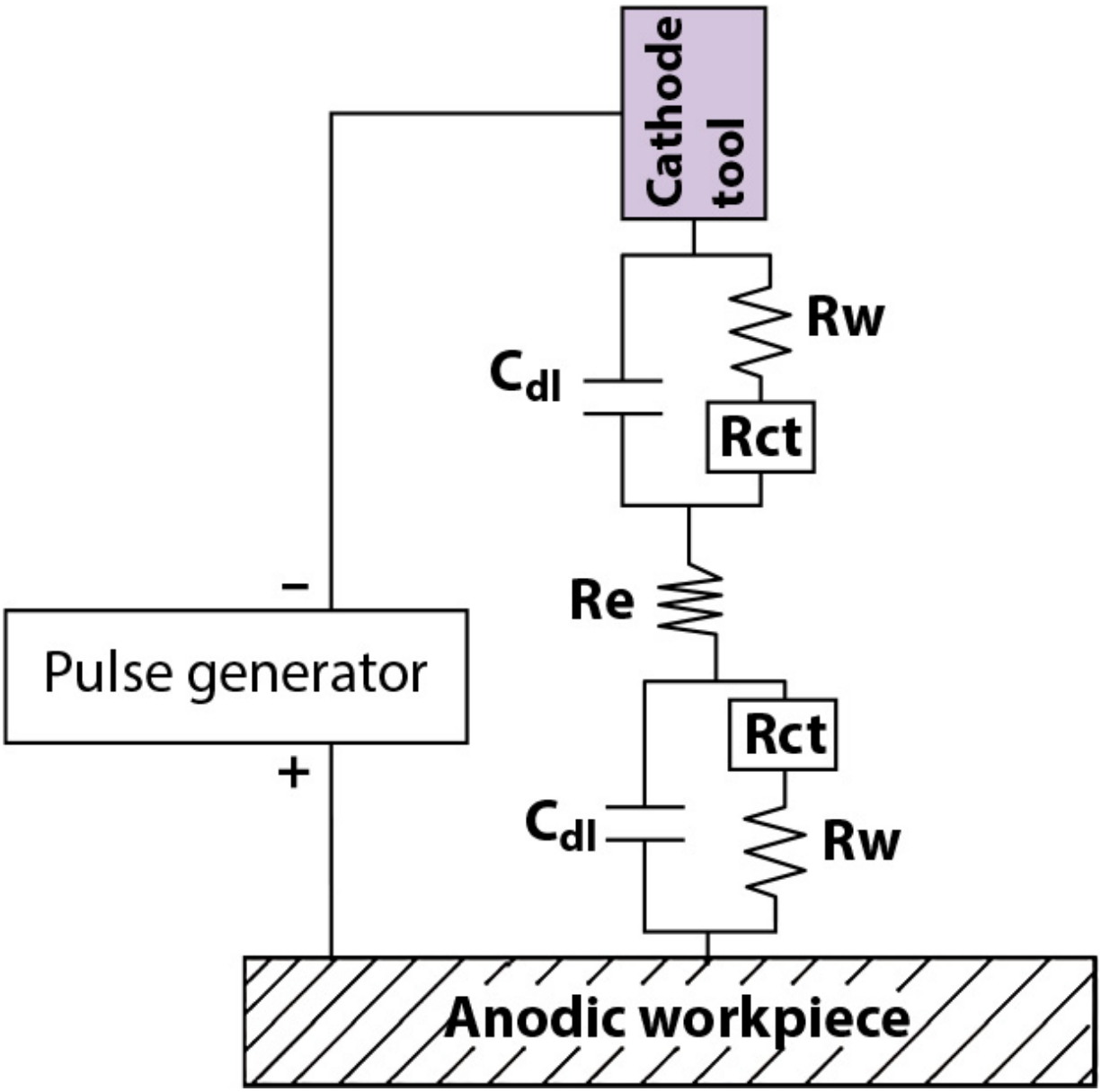


Figure 18.5 Electrical circuit model of EMM cell.

Gouy-Chapman-Stern model (Mc Geough, 1974) [7] and (K.B. Oldham, 2008) [8] defines specific double layer capacitance, C_{sp} as follows:

$$C_{sp} = \frac{\varepsilon_s \varepsilon_0}{\delta} \tag{18.22}$$

Where δ is Stern layer thickness in meter, ε_0 is permittivity of vacuum in farad/meter, and ε_s is relative permittivity of

the electrolytic solution.

$$C_{dl} = A \times C_{sp} \tag{18.23}$$

Where C_{dl} is double layer capacitance, A is active tool surface area in m^2.

$$R_{C_{dl}} = \frac{1}{\omega C_{dl}} \tag{18.24}$$

Where $R_{C_{dl}}$ is resistance of double layer and ω is radial frequency.

Warburg impedance is very small at high frequencies, as there is no scope for diffusing reactants to move too far. It increases at low frequencies, as the reactants need to diffuse further than previous one.

$$\text{Warburg Impedance}, R_W = \frac{\sqrt{2}}{\sqrt{\omega}}\alpha \tag{18.25}$$

Where α is Warburg coefficient defined as expressed below:

$$\alpha = \frac{RT}{n^2F^2A\sqrt{2}}\left(\frac{1}{C^*\sqrt{D_O}} + \frac{1}{C^*\sqrt{D_R}}\right) \tag{18.26}$$

Where R is universal gas constant (8.314 J/K mole), C* is bulk concentration of the diffusing species (moles/cm^3), n is number of electrons transferred, D_R is diffusion coefficient of the reductant, D_O is diffusion coefficient of the oxidant, and T is temperature in K.

Charge transfer resistance, R_{ct} is calculated based on Butler-Volmer equation as given below:

$$R_{ct} = \frac{RT}{nFi_0} \tag{18.27}$$

Where i_0 is the exchange current density.

So, equivalent resistance of $R_{C_{dl}}$, R_{ct}, and R_W is as follows:

$$R_{eq} = R_{C_{dl}} \times \frac{(R_W + R_{ct})}{(R_{C_{dl}} + R_W + R_{ct})} \tag{18.28}$$

The total equivalent circuit resistance is given by,

$$R_{teq} = R_e + 2R_{eq} \tag{18.29}$$

$$\text{From Equation 18.21 MRR, } \frac{dm}{dt} = \frac{VM}{R_{teq}\, z\, F} \tag{18.30}$$

Where V is applied voltage.

Charging time constant of the double layer,

$$\tau = \rho_S\, C_{dl}\, h \text{ (Schuster } \textit{et al.}\text{) [9]}$$

Where ρ_S is specific resistance of electrolyte, h is length of IEG and C_{dl} is double layer capacitance. Pulsed power is supplied in EMM for better accuracy in micromachining. Current flows through electrolyte only after appropriate charging of double layer. The definite timing of starting of the current flow is unpredictable. Assuming non-faradaic/ non-dissolution time as $\tau/3$, a theoretical graph is fitted with experimental graph, as shown in Figure 18.6 (Ghoshal *et al*, 2014) [10].

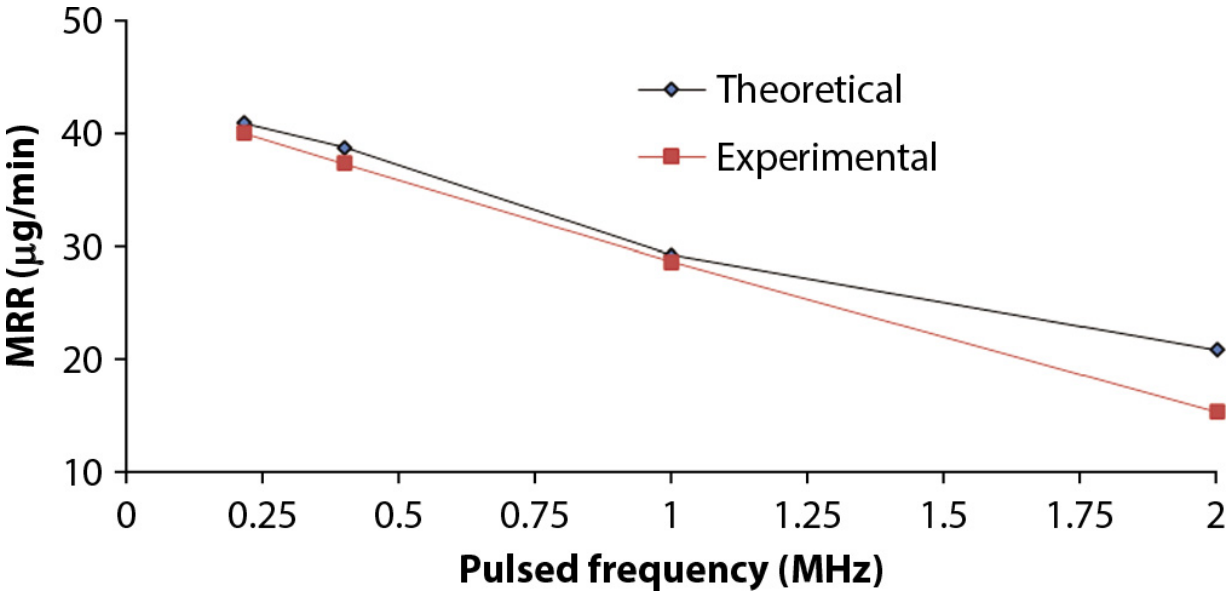


Figure 18.6 Comparison of theoretical and experimental MRR.

$$\text{MRR} = \text{Pulse frequency (Hz)} \times \text{Faradaic time} \times \frac{dm}{dt} \qquad (18.31)$$

18.3.1.2 MRR Equation for EMM Based on Pulsed Wave Form

The total current passed during a pulse on time is the sum of faradaic current and nonfaradaic current (Mithu *et al*, 2011) [11]. Figure 18.7 explains pulse on time, T_{on} and pulse off time, T_{off} during each cycle of pulsed power. At the starting of the pulse, maximum voltage, V_{max} charges the double layer capacitance without dissolution of metal from the anodic workpiece for the time t* and corresponding current is called non-faradaic current. After the suitable charging of double layer, voltage becomes flat and it is called faradaic voltage, $V_{faradaic}$. Faradaic current flows during rest of the pulse on time for dissolution of anodic metal. Since the material removal occurs for the faradaic currents only during each cycle, the MRR per cycle can be calculated as follows:

$$MRR_{cycle} = \int_{t^*}^{T_{on}} \frac{IM}{z\,F} dt \tag{18.32}$$

$$\text{Ohm's law states that } V = IR \tag{18.33}$$

Where R is resistance in the IEG and calculated by

$$R = \frac{h\rho_s}{A} \tag{18.34}$$

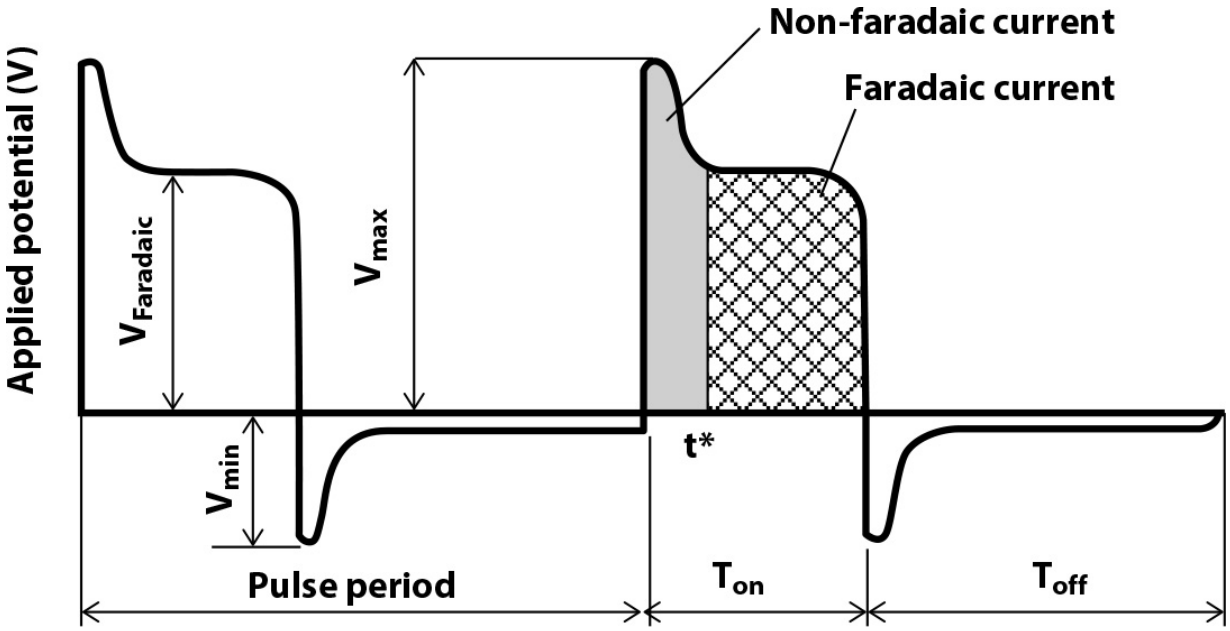


Figure 18.7 Pulse wave form during EMM.

Therefore,

$$MRR_{cycle} = \int_{t^*}^{T_{on}} \frac{V_{faradaic} A M}{\rho_s h z F} dt \quad (18.35)$$

$$\text{or, } MRR_{cycle} = \frac{V_{faradaic} A M}{\rho_s h z F}(T_{on} - t^*)$$

$$MRR = \frac{V_{faradaic} A M}{\rho_s h z F}(T_{on} - t^*)f$$

Where, f is pulse frequency in Hertz. $V_{faradaic}$, t*, and T_{on} are acquired from oscilloscope as displayed during EMM operation.

18.3.2 Evolution of Shape in Electrochemical Micromachining

$$\text{Equation 18.21 can be expressed as volume removal, } Q = \frac{MIt}{F\rho z} \quad (18.36)$$

Where ρ is density of the metal.

$$\text{Or} \frac{dA\, dy}{dt} = \frac{MI}{F\rho z}$$

Where dA is the elemental area on the machining zone of anode and dy is elemental dissolution of metal normal to dA.

$$\text{Hence, rate of recession,} \frac{dy}{dt} = \frac{JM}{F\rho z} \quad (18.37)$$

Where, J is net current density arising out of diffusion, migration, and convection of ions. Equation 18.37 clearly explains that generation of shape in EMM is highly influenced by current density, J.

$$J = J_{mt} + J_{et} \quad (18.38)$$ [10]

Butler-Volmer equation gives J_{et}, current density due to electron transfer, and current density due to mass transfer is given by

$$J_{mt} = z^2 dc\left(\frac{F^2}{RT}\right) \times \frac{\partial V}{\partial y} + Fzd \times \frac{\partial c}{\partial y} \quad (18.39)$$ Bard and Faulkner (2001) [6]

Where d denotes diffusivity, c denotes concentration of anodic ions, $\frac{\partial V}{\partial y}$ is potential gradient in the direction of recession of metal, and $\frac{\partial c}{\partial y}$ is concentration gradient of ions in the direction of recession of metal. The concentration of metal ions increases during the pulse on time and reduces during pulse off time. But due to high pulse frequency (MHz), chances of built up of concentration gradient is not there and hence,

$$J_{mt} = z^2 dc\left(\frac{F^2}{RT}\right) \times \frac{\partial V}{\partial y} \quad (18.40)$$

Movement of ions or migration is controlled by rate of change of voltage (dV/dy) along the direction of dissolution of metal. It is also known that potential, V in the IEG controls electric field distribution satisfying Laplace's equation as follows.

$$\nabla^2 V = 0 \quad (18.41)$$

Solution of Laplace's equation is needed for getting the value of dV/dy and thus calculating current density utilizing Equation 18.40. Once current density distribution at the machining zone is known, shape can be predicted utilizing Equation 18.37. Many authors have taken different

approaches for the prediction of shape during EMM. Moving boundary algorithm is applied after solving the current density distribution at the anodes. Only boundary faces were discretized and then, automatic refinement of the mesh took place based on current density distribution as the workpiece was progressively machined. Analysis was done in discrete time steps (Δt, y). Each node was moved by distance Δd, the recession alongside the flux line and thereby workpiece shape was determined after each time step, Δt. Boundary element method was applied by Pattavanitch *et al.* [12] to model the evolution of shape in EMM. Figure 18.8 explains the shape evolution in three-time steps (three passes). At the discrete points of 1, 2, 3, 4, 5 of first pass, current density is calculated and points are moved to corresponding points at second pass based on amount of recession along the flux line utilizing Equation 18.37. Similarly, after time step Δt, the points 1, 2, 3, 4, 5 are moved to corresponding points at third pass. Thus, final shape of the profile is generated. Purcar *et al.* [13] solved the potential model numerically and applied boundary element method to simulate model of three-dimensional (3D) anodic shape change during electrochemical machining. All the above simulation results agreed with the experimental results of anodic shape change. Shape can also be predicted through finite element simulation and corroborated by the experimental observations. General steps involved in programming of shape evolution are shown in Figure 18.9.

The shape can be produced by three techniques. Designed tool already shown in Figure 18.3 is fit for reasonably larger shapes so that it is easy to fabricate the tool. The designed tool is moved in vertical axis till proper depth of machining is realized during machining. Shape can be produced by sinking and milling method in the second case where a microtool of simple shape (*e.g.*, round shape) is

drilled to the required depth of workpiece and followed by milling along the designed path to produce the same shape as produced by the designed tool. This process is suitable for generation of shapes where no of products is small as extra cost is involved in design and fabrication of the tool. Desired shape can also be generated by a third technique through mask EMM. For fabrication of microstructures like micro-hole array/micro-dimple array on a single piece of metal, photoresist patterning is done on the anodic workpiece. Metal is removed at the exposed surface only and thereby pattern is transferred to the anodic surface. For mass production, an inert patterned metal mask (*e.g.*,, platinum plate) is generally attached to the anodic workpiece but not bonded, as shown in Figure 18.10. Electrolyte flows through the IEG. While voltage is applied between anodic metal and cathode, dissolution of metal occurs only from the exposed anodic metal surface. Mask contains array of uncovered hole of diameter B and after machining B′ represents entry diameter. Then, undercut is defined as B′–B. The machining zone can be simulated as stated earlier and shape of profile of array of micro-holes can be predicted. The rate of dissolution of metal is higher at the mask edge as current density is higher at the mask edge (Li *et al* (2010)) [14]. Evolution of profile shape is influenced by spacing to opening ratio and mask aspect ratio. Mask aspect ratio is defined as the d/B, *i.e.*, ratio of depth to hole diameter. Where d is the thickness of mask. Undercut is more when aspect ratio is small. Removal of reaction products becomes difficult when aspect ratio is high. Generally, aspect ratio is kept greater than 1 to keep undercut within limit.

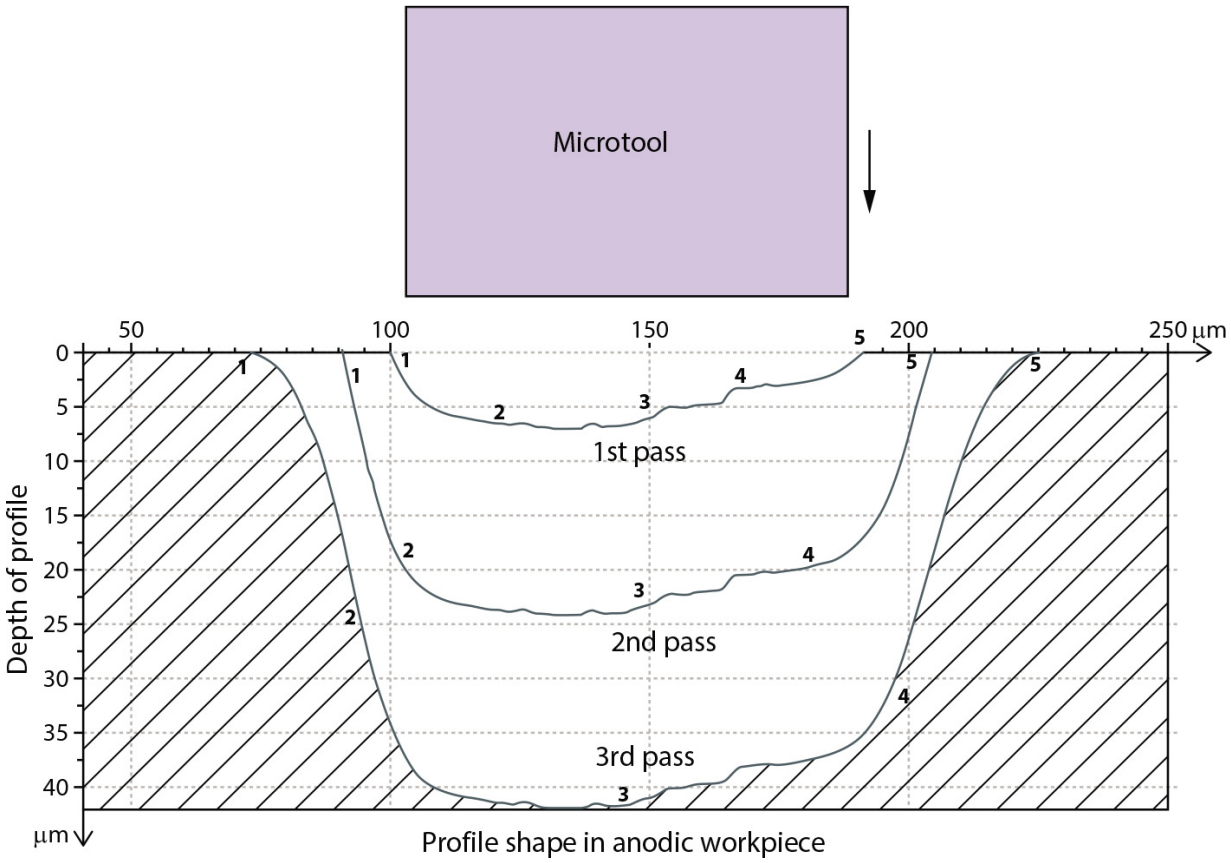


Figure 18.8 Generation of profile shape.

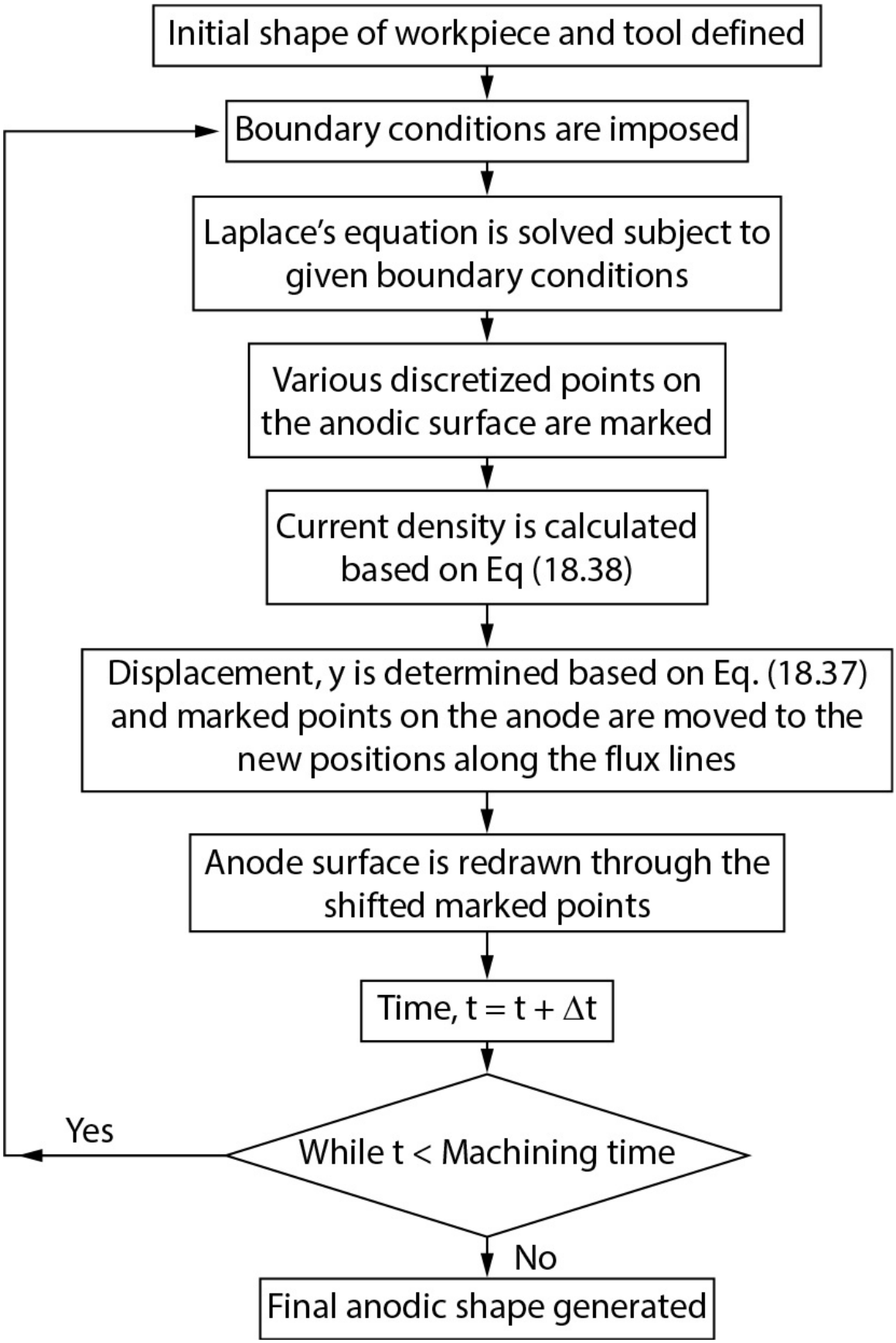

Initial shape of workpiece and tool defined
Boundary conditions are imposed
Laplace's equation is solved subject to given boundary conditions
Various discretized points on the anodic surface are marked
Current density is calculated based on Eq (18.38)
Displacement, y is determined based on Eq. (18.37) and marked points on the anode are moved to the new positions along the flux lines
Anode surface is redrawn through the shifted marked points
Time, t = t + Δt
While t < Machining time
Yes
No
Final anodic shape generated

Figure 18.9 Shape evolution flow chart.

Sometimes, patterned insulation mask plate is attached to cathode, but not bonded. Anodic metal surface is fully exposed as substrate, as shown in Figure 18.11. This technique can be used repetitively for mass production (I. Schonenberger and S. Roy (2005)) [15].

Shape of cross section of blind microprofiles generated in EMM using straight, conical, and reversed taper microtool were explored (Ghoshal and Bhattacharyya (2015)) [16]. Initially, shapes were simulated and predicted. Later, it was verified by experiments that cross sectional profile generated by reversed taper microtool were either taperless or least tapered subject to reversed taper angle of the microtool. Conical microtool produces a cross sectional profile of microchannel of lesser taper angle than that generated by cylindrical microtool. It is worth mentioning that the sinking and milling method of microchannel generation produces lesser taper angle of profile than that of microchannel produced by the scanning machining layer by layer method (Ghoshal and Bhattacharyya (2013)) [17]. Figure 18.12 explains both the approaches of microchannel generation. The microtool continues back and forth motion while machining goes on in the scanning machining layer by layer method. Before each scan, a small vertical feed of microtool is given at both ends. Thus, layer-by-layer metal removal occurs. In sinking and milling method, sinking at the initial point is done to a considerable depth or final depth and subsequently, milling is continued along the designed path. The front lateral face of the microtool actively participates in micromachining. The microtool proceeds very slowly over the path of micro profile generation. This method is suitable in terms of lower machining time, smaller overcut, and lesser taper angle of the micro profile.

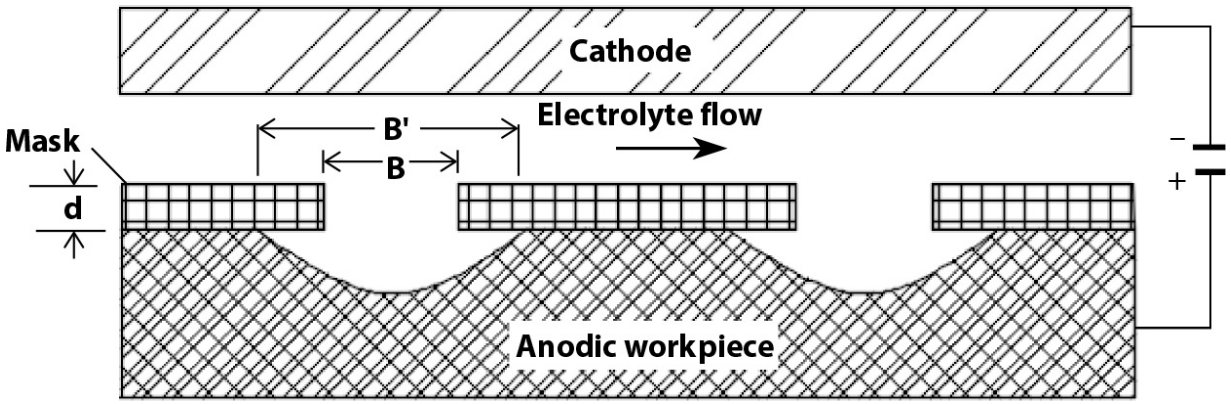


Figure 18.10 Shaping in EMM through mask attached to anode.

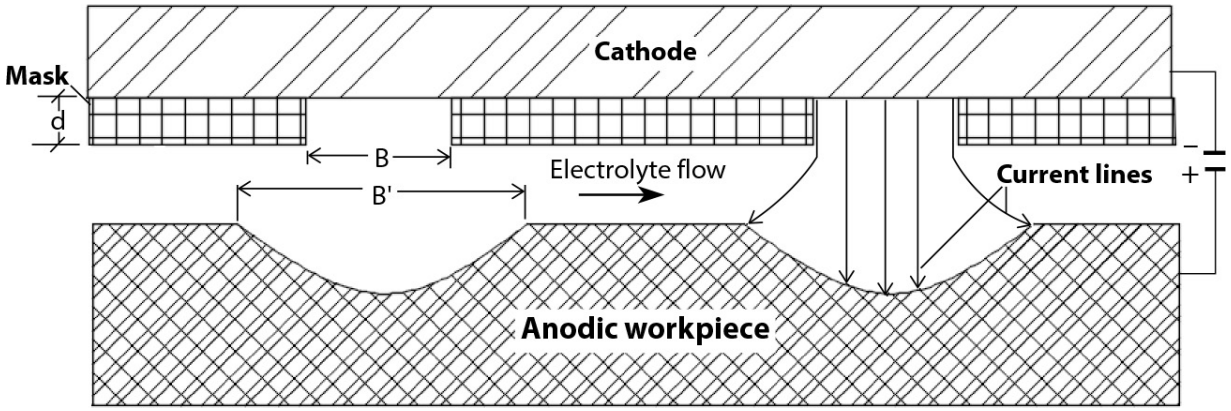


Figure 18.11 Shaping in EMM through mask attached to cathode.

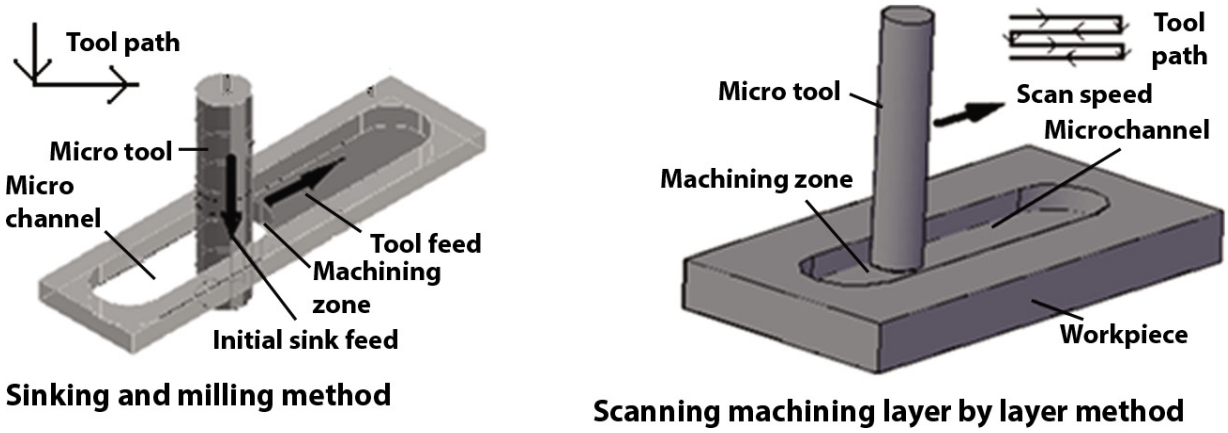


Figure 18.12 Methods of microchannel generation.

For the shaping through micro-hole, *i.e.*, taper less, the IEG of 10 µm is simulated with conical microtool. The following

are the assumptions:

i. The conductivity of the electrolyte remains constant.

ii. The electric parameters are stable.

iii. The concentration gradient in the bulk electrolyte is negligible.

Boundary conditions are as follows:

$$V|\,\Gamma_{3*4*5*6} = 3\ \text{V (at the anodic surface)} \tag{18.42}$$

$$V|\,\Gamma_{1*2} = 0\ \text{V (at the cathodic tool)} \tag{18.43}$$

$$\frac{\partial V}{\partial N}|\,\Gamma_{7*8*9*10} = 0\ \text{(the boundary conditions)} \tag{18.44}$$

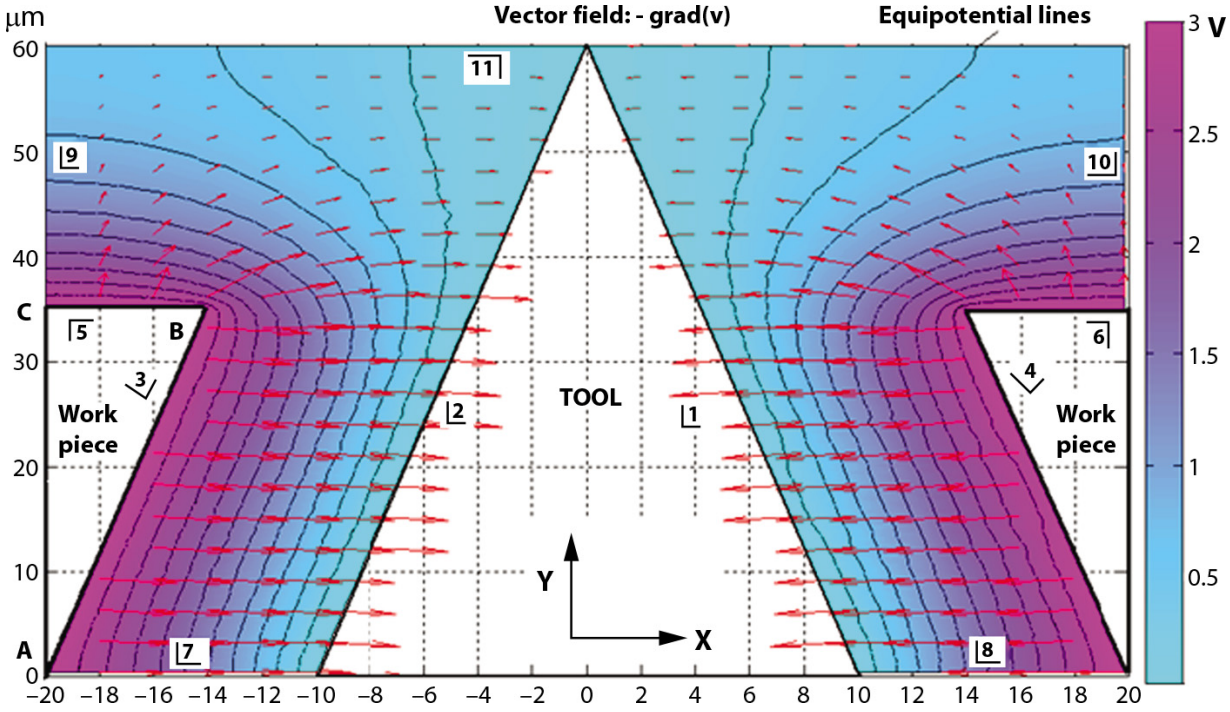


Figure 18.13 Distribution of equipotential lines for conical microtool.

Where 3 V is applied between anodic workpiece and cathode microtool, N is the surface normal. Thickness of

workpiece is 35 µm and IEG is 10 µm. The Laplace's equation, *i.e.*, Equation (18.41) is solved subject to the stated boundary conditions in MATLAB. Figure 18.13 exhibits equipotential lines distribution in the IEG when the tip of conical microtool is 25 µm below the bottom surface of the work piece. The diameter of the micro-hole at the entry side is 40 µm and initially, tapered after perforation is complete. It is clear from the distribution of equipotential lines that on the bottom surface of workpiece and at the bottom edge marked 'B,' gap (y) between lines is small, *i.e.*, dV/dy is more. Hence, current density will be high at these zones, as explained by Equation 18.40. Therefore, the microhole will be taperless if machining is continued for a few minutes at this position after perforation is complete. This has been corroborated by experimentation [10].

18.4 Machining Conditions in Electrochemical Micromachining

A precise EMM in the range of micron can be carried out using the optimal parametric combinations, controlled pulsed power supply and using electrolyte of less corrosive. The goal of higher machining rate of the anode can also be was achieved [10].

18.4.1 Power Supply in Electrochemical Micromachining

In EMM, pulsed power is applied to increase resolution and accuracy of machining. Electrochemical micromachining is carried out at a very low voltage ranging from 3 V to 10 V. Very small IEG is maintained (5–15 µm). Each cycle of pulsed power consists of pulse on time and pulse off time. Short pulse on time increases the precision and accuracy [9, 18]. Resolution of machining is decided by the charging

time of double layer, $\tau = \rho_s C_{dl} h$. Where ρ_s is specific resistivity, C_{dl} is double-layer capacitance, and h is IEG. Charging time constant, τ for regions of higher IEG is greater. In case it is greater than pulse on time, there will be no dissolution and thus restricting the metal dissolution within very close region of microtool. Setting of pulse off time is very important during machining for clearance of machining debris from machining zone. A too short pulse on time decreases MRR and hence, balance is required between on and off time. A pulse generator or function generator is required to produce pulses of various shapes like rectangular voltage wave form (RVW), triangular voltage waveform (TVW), and sinusoidal voltage waveform (SVW). The RVW has been used by maximum researchers. It has been reported that TVW followed by SVW has better accuracy than RVW in terms of kerf width (overcut) while wire EMM was done on stainless steel 304 of thickness 100 μm with tungsten wire of ϕ 30 μm. The reason behind is input energy of triangular and sinusoidal pulses are lesser than that of a rectangular pulse for the same peak voltage, frequency, and duty ratio (Sharma *et al.* (2021)) [19].

18.4.2 Electrolytes in Electrochemical Micromachining

Electrolyte plays the role of medium for carrying current between workpiece and microtool in ECM or EMM. Removal of heat and sludge from the machining zone is also performed by electrolyte. Selection of electrolyte is mainly guided by priority of machining outputs like MRR, accuracy and surface finish. Electrolytes should have the following properties:

a. It must be chemically active for better MRR. Degree of dissociation of ions is high in strong electrolyte. Only dissociated ions can carry current in an electrolyte.

Sometimes, positive and negative ions make ions pairs due to electrostatic attraction. These pairs are unable to carry current in weak electrolytes like organic acids. That is why organic acids are not used in ECM/EMM.

b. Electrolyte must be chemically stable.

c. It should be non-corrosive and non-toxic.

d. It should be cheap and easily available in the market.

Electrolytes used in EMM may be passivating or non-passivating. Anodic metal reacts with oxygen or hydrogen during EMM and thereby passive film of oxides and hydroxide of metal is created on the workpiece (J. W. Schultze, M. M. Lohrengel (2000)) [20]. A passive layer reduces MRR and needs higher potential for breaking the layer to continue machining.

Electrolytes may be classified to (i) neutral aqueous salt, (ii) aqueous acid, and (iii) aqueous alkalis.

i. Neutral aqueous salt: these are of very low cost and environment friendly and hence, the first choice of researchers as electrolyte in ECM/EMM. The aqueous solution of NaCl disrupts the growth of passive layer resulting in higher MRR and bright surface on stainless steel [21, 22]. Sodium bromide (NaBr) as an electrolyte has been effectively used for machining of titanium with the application of higher voltage to break passive film produced in case of simple chloride and nitrate electrolyte [23]. One disadvantage of using aqueous salt is the formation of sludge in the IEG which sometimes creates short-circuit during machining.

ii. Aqueous acid: acidic electrolyte of low concentration is chosen for EMM so that the least damage is done to the environment. Moreover, reaction products remain dissolved and hence, very small IEG can be maintained

for better accuracy of machining. Low concentration of H_2SO_4 is suitable for EMM of nickel and stainless steel.

iii. Aqueous alkalis are rarely used for electrochemical micromachining due to formation of passive layer on workpieces and metal hydroxides causing congestion in the IEG [9]. NaOH or KOH are used for machining tungsten or tungsten carbide.

Concentration of electrolyte highly influences MRR and surface finish. More ions are present within the working solution of higher concentration for carrying higher current and as a result, higher MRR occurs [24]. Concentration of electrolyte is generally expressed as gram moles per liter of solution. Thus, 1M aqueous solution of H_2SO_4 has 98 grams of H_2SO_4 per liter of solution since the molecular weight of H_2SO_4 is 98, *i.e.*, 98 = 2x1+32+4x16. Ghoshal *et al.* has shown that with increase in concentration, overcut of microchannel on stainless steel increases. At the same time surface roughness improves which is evident from decrease in R_a value from 0.103 µm at 0.1M H_2SO_4 to 0.048 µm at 0.3M H_2SO_4. The authors describe that 0.2M electrolyte is appropriate for micromachining of stainless steel considering lesser overcut, lesser machining time and improved surface quality (Ghoshal & Bhattacharyya (2015)) [25].

Generally, mixed electrolyte is suitable for machining of alloy. Sulfuric acid mixed with nitric acid was used as electrolyte for generating microstructures with better surface finish and sharp edges on WC–Co alloy (Choi *et al.*) [26]. Aqueous NaCl mixed with potassium dichromate ($K_2Cr_2O_7$) was used for investigating the machining output of alloy steel $20MnCr_5$ [27]. The aqueous solution of NaCl and HCl was used as electrolyte for drilling of deep hole in

nickel based superalloy [28]. Electrochemical micromachining of titanium alloy with electrolytes of three different blends of sodium chloride are reported. Sodium chloride and glycerol electrolyte produced optimal overcut while best circularity was obtained from the mixture of sodium chloride and citric acid and maximum MRR was obtained from sodium chloride and sodium nitrate combination of electrolyte (Thangamani *et al.*) [29]. Metal removal rate of stainless steel is higher when acid is added to sodium nitrate electrolyte than the normal sodium nitrate electrolyte. Authors also point out that lesser overcut is generated in acidified sodium nitrate electrolyte in comparison to only sodium nitrate electrolyte (R. Thanigaivelan *et al.*) [30].

18.4.3 Role of Inter-Electrode Gap in Machining Accuracy

The IEG has a major role to play in EMM for stable material removal, accuracy and precision. To maintain high accuracy and good surface finish, IEG is maintained below 15–20 μm. When IEG is reduced, localization of resolution also increases [31]. Machining accuracy is inversely proportional to the IEG size. Direct measurement of IEG in EMM is still a challenge as the gap is extremely small. In EMM, the complex and short-lived process occurs within the small gap of electrodes. A linear relationship between the deviation of pulse signal and gap size is maintained for online monitoring. In EMM, electrical conduction method is suitable for measurement of gap between the electrodes. Charging of double layer followed by discharging is necessary for the built up of circuit during EMM and overpotentials at anode and cathode are involved at each cycle. Faradaic current or dissolution current shown in Figure 18.7 is stable current and this current can be utilized for the measurement of IEG. Programming can be

done with boundary conditions as limit of gap so that stable machining occurs. In EMM, tool feed rate in vertical and horizontal direction must be judiciously decided based on volume removal rate and accordingly put at computerized numerical control (CNC) programming which controls machining. When the tool feed rate and the machining rate match, an equilibrium gap is maintained and stable machining continues. When tool feed rate is more compared to the dissolution rate, the gap reduces and current increases. If the feed is not stopped, the tool and the workpiece get damaged. To avoid this situation, a control mechanism can be devised which monitors the circuit current. Once maximum current limit is reached, the tool is retreated for the adjustment of IEG. Again, when lower limit of current value is reached due to increased IEG, the tool feed is provided for machining to continue. This close loop control system will be ideal for EMM cell.

18.5 Electrochemical Micromachining Set Up

A schematic model of an EMM system is shown in Figure 18.14.

18.5.1 Machining Unit

Microtool movement in the range of micron/submicron is necessary for EMM. XYZ movement stage supports the machining chamber containing holding devices for workpiece and electrolyte. X and Y movements of the stage is necessary for locating the workpiece under the microtool at preferred position and also for feed movement. Microtool is mounted on the Z-axis slide for vertical feed. The stepper motors actuate the movement of the three axes which are controlled by programming software. Therefore, appropriate programs are to be developed for machining of

microchannels, micro-holes and free-form surfaces. The machining chamber is fabricated from non-conductive and non-corrosive perspex sheet.

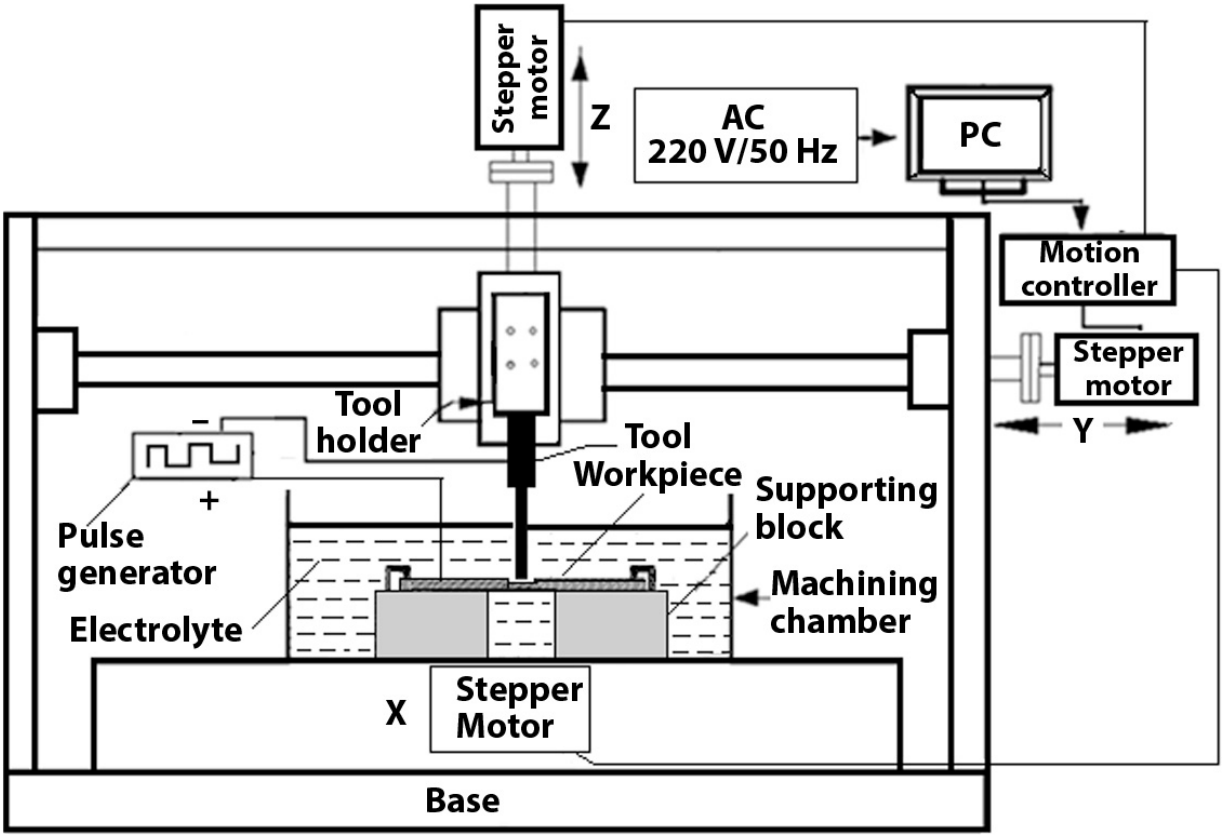


Figure 18.14 Schematic electrochemical micromachining set up.

18.5.2 Power Supply Unit

The main supply of 230V/50 Hz single phase is connected to pulse generator/function generator for generating pulses at definite frequency. Then, positive terminal is supplied to anodic workpiece and negative terminal to cathode tool. Sometimes, a vibratory unit of piezo-actuator is also connected to 230-V main power supply. An amplifier module in the range –20 V to 130 V is used for creating longitudinal vibration of microtool. Feed control in the nanometer range in Z direction is also possible. Another function generator is to be connected to 230-V main power

supply for getting modulated output voltage at a particular frequency for controlling frequency and amplitude of vibration of microtool. A multimeter is used to measure the modulated voltage, frequency and also for measuring current at the machining zone.

18.5.3 Data Collection System

A digital storage oscilloscope continuously monitors the EMM processes. Pulse shape indicates machining conditions like normal machining, short circuit or micro sparking. After setting of initial gap of <10 µm between microtool and workpiece, electrolyte is supplied to appropriate level and automatic feed system is followed through running programs. During micromachining operation, various data such as peak to peak voltage, faradaic voltage, mean voltage, pulse width, and duty ratio are observed. Voltage drop is too much during microsparking and the nature of pulse shape during short circuit is detected, as shown in Figure 18.15.

18.6 Fabrication of Different Microtools in Electrochemical Micromachining

Microtool is crucial for conducting micromachining activities. At the initial state of development of micromachining technology, electro discharge machining (EDM) and sometimes wire electro discharge grinding (EDG) methods were applied for fabrication of microtool above the diameter of 100 µm. Micro cracks on surface and residual stress caused by thermal effects are common drawbacks of these methods. Nowadays, microtool of below 10-µm diameter is also being used. Currently, there is significant development in fabrication of microtool by ECM

at low cost. Microtool can be fabricated with the application of direct current (DC) and pulsed power both. Direct current can be applied between an anodic rod (*e.g.*,, tungsten rod) and a cathodic rod (*e.g.*, platinum) kept side-by-side maintaining a suitable IEG. The anodic rod is to be rotated for uniform reduction in diameter and for the reduction of diffusion layer thickness during the fabrication of microtool (Fan *et al.* (2010)) [32]. In case of pulsed power, the shape of microtool depends on two important parameters of duty ratio (on time/cycle time) and voltage. Excess voltage forms a thick diffusion layer around the anodic tool and thereby creates barrier to current flow at the location of thick diffusion layer. Suitable 'off time' during each pulse will be helpful for removing sludge away from the machining zone reducing thickness of diffusion layer (Fan *et al.* (2009)) [33]. For fabrication of tungsten microtool, strong NaOH/KOH solution (2M to 5M) is generally used.

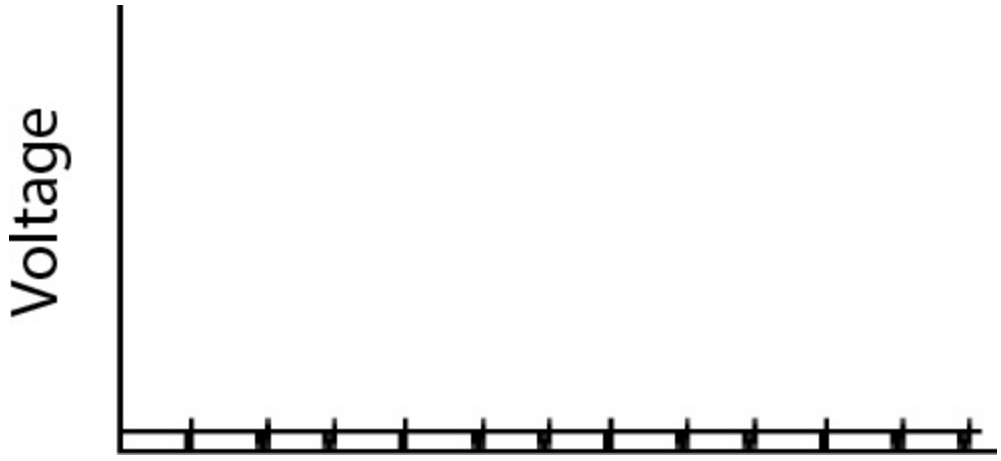


Figure 18.15 Pulse shape during short circuit.

To avoid rotation of tool, a rod to be etched is centered over the inner hole of cathode ring and etched with the application of DC voltage. Cylindrical microtool can be fabricated typically around 5-V applied voltage. Conical shape is generated when less than 5 V is applied while

reverse conical shape tool is formed in the range of more than 5 V. This typical voltage varies depending on diameter of inner hole of cathode and concentration of electrolyte. Machining time may be 20 min for producing small diameter microtool from ϕ 300 µm tungsten rod (Wang *et al.* (2008)) [34].

To reduce machining time, vibration is applied and fabrication can be achieved within 1–2 min (Ghoshal B. *et al.* (2013)) [35]. Authors used a centrally located straight anodic tungsten rod of ϕ 300 µm within cathode stainless steel ring of diameter 1600 µm. Oscillatory vibration was applied to the anodic tungsten rod with the help of piezoelectric transducer and 2M NaOH electrolyte was used, as shown in Figure 18.16. Vibration plays vital role for improved convection and diffusion of ions due to bubble collapse during the fabrication of microtool. The tool is vibrated longitudinally with definite amplitude of vibration below 230Hz frequency of vibration. The micro jets generated from bubble collapse interrupt the diffusion layer and increase the convective mass transport. Diffusion layer thickness increases with increase in applied voltage. Hence, greater amplitude of vibration is required for the increased applied voltage to remove the diffusion layer. Uniform diameter of microtool and conical microtools can be fabricated by applying appropriate amplitude of vibration corresponding to each voltage starting from 3 V to 9 V, as shown in Figure 18.17. Combinations of voltage and amplitude of vibrations for the generation of conical microtool of 4°, 10°, and 16° taper angle are also presented in the figure. For a particular voltage, higher amplitude of vibration is required to fabricate microtool of higher taper angle. Fabrication time highly reduces with increased voltage and amplitude of vibration. Figure 18.18 (a) exhibits a 6.5° conical microtool and Figure 18.18 (b) exhibits reversed taper microtool fabricated by the authors.

Conical microtool is stronger than reversed taper microtool in terms of rigidity. Conical tools are more effective and accurate for taperless through and blind microchannel generation during EMM (Ghoshal B. *et al.* (2015)) [36].

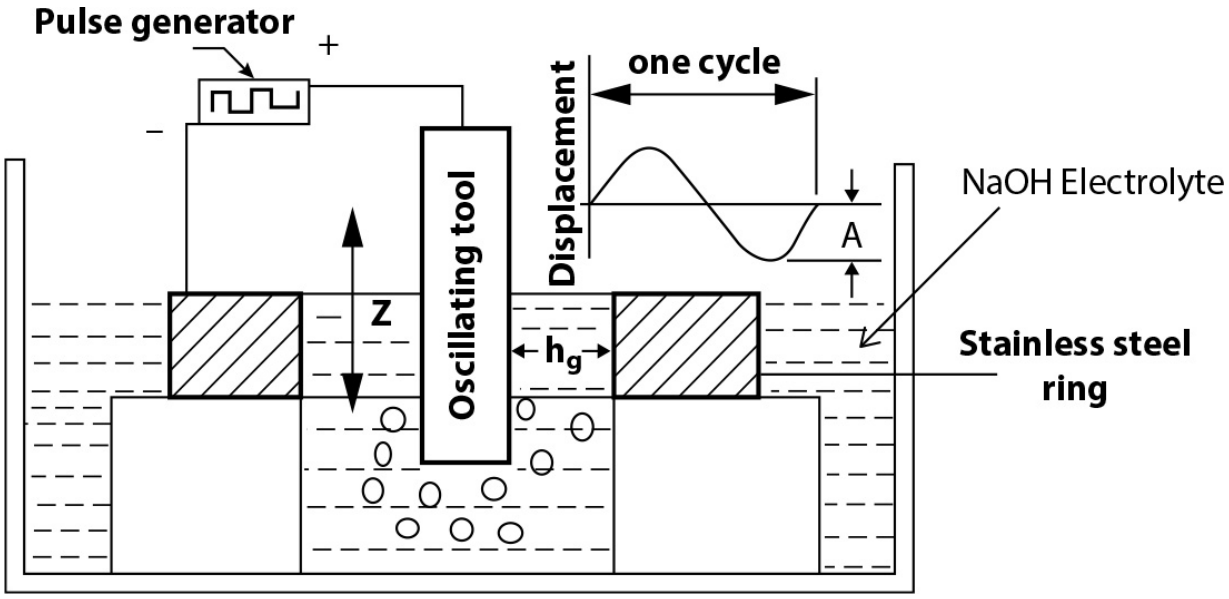


Figure 18.16 Schematic diagram for fabricating microtool.

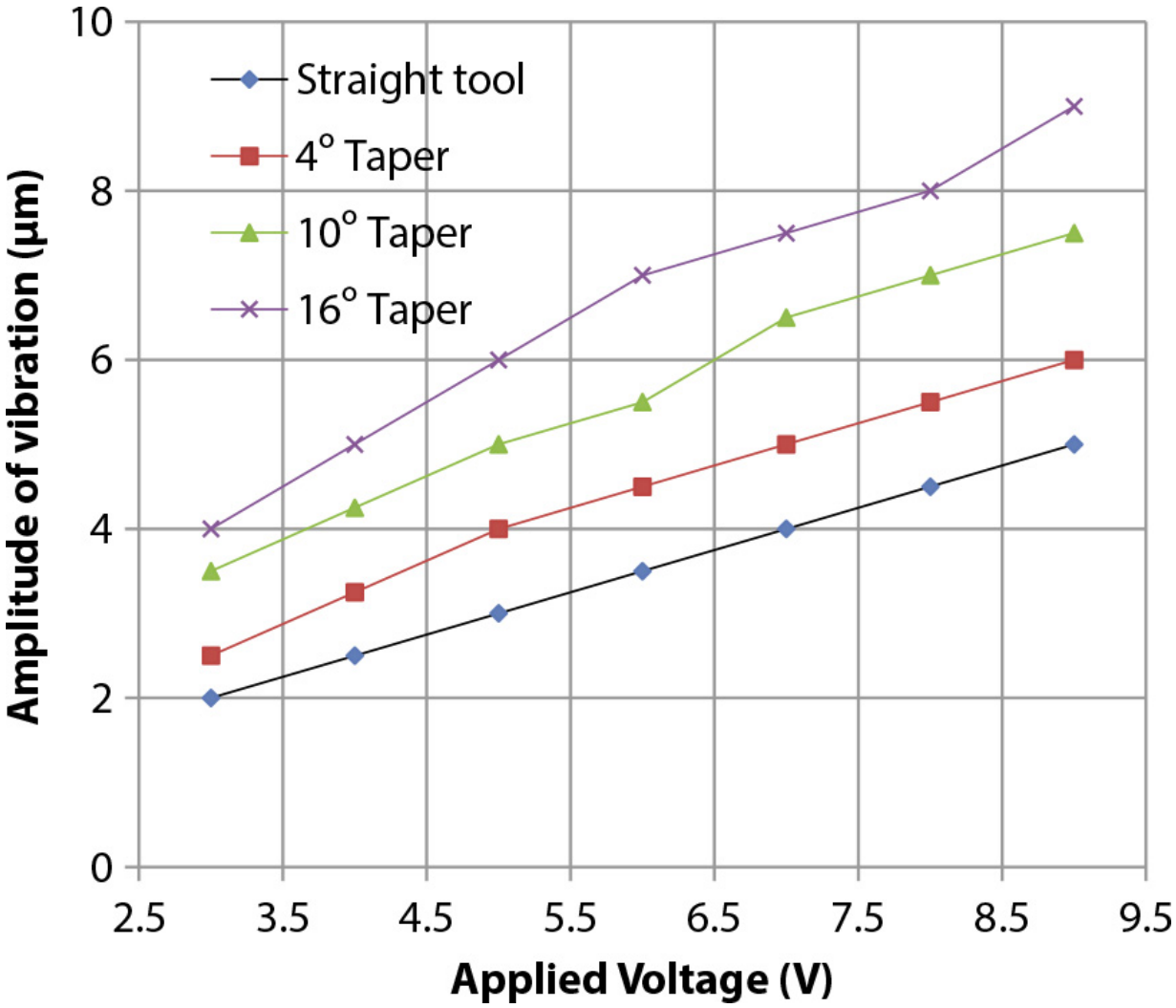
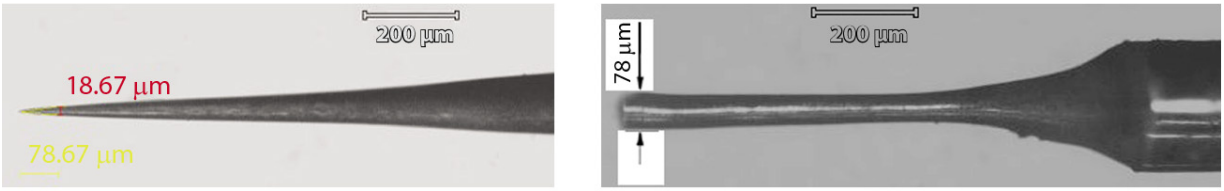


Figure 18.17 Voltage and amplitude combinations for tool fabrication.



(a) (b)

Figure 18.18 (a) 6.5° conical microtool. (b) Slightly reversed taper 78 µm at tip.

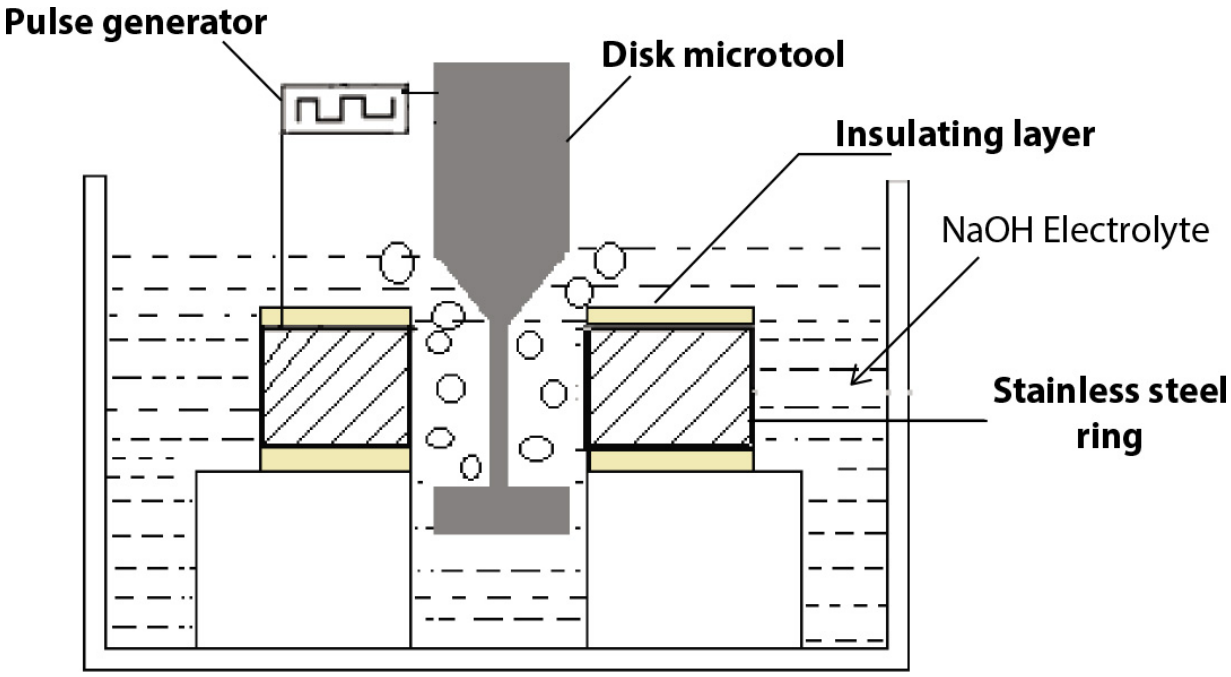


Figure 18.19 Fabrication of disk microtool.

Disk-shaped microtool can also be fabricated by EMM, as shown in Figure 18.19. Top and bottom surfaces of the stainless steel ring are insulated and thus, current passes through the side wall of the hole dissolving tungsten rod at specific location. Disk-shaped microtool is used for 3D micromachining with sharp vertical wall.

18.7 Process of Measurement of Microfeatures

Development in micro-measurement technology is indispensable for the development of micromachining technologies. Aerospace, auto, and electronic industries are reducing sizes day by day keeping in mind the reduction of weight. Measuring microparts or microfeatures which are invisible has its own challenges. Optics play a major role in micrometrology. Optical methods of imaging by means of camera and thereafter using image analysis software is one of the predominant methods of dimensional measurement.

Advanced measurement techniques include effective use of scanning and transmission electron microscope (STM), scanning electron microscope (SEM), atomic force microscope (AFM), non-contact 3D surface profiler working on the principle of coherent correlation interferometry (*e.g.*, Taylor Hobson Talysurf CCI sunstar), and micro coordinate measuring machine (CMM). Scanning electron microscope is very popular among researchers in this field as high resolution 3D images produced by it provide topographical, textural, and compositional information. Figure 18.20 exhibits magnified SEM micrograph of a micro nozzle generated on stainless steel sheet (SS-304) with the microtool of taper angle 5.71°. Machining conditions are tool feed rate 2.66 μm/min, duty ratio 30%, electrolyte 0.05 M/L H_2SO_4, pulse frequency 10 MHz, and average voltage 3 V. Micro nozzle is 10.3° tapered. Entry and exit diameter of the micro nozzle is 160 μm and 40 μm, respectively.

Scanning and transmission electron microscope produces high resolution image at the atomic level by scanning a sharp metallic wire tip over a surface while a voltage is applied to the tip. Atomic force microscope works on the principle of scanning probe microscopy and is used to measure below nm range.

Figure 18.21 shows the application of Taylor Hobson Talysurf CCI sunstar. Figure 18.21 (a) exhibits 3D surface of blind microchannel generated on SS-304 by sinking and milling method with the help of conical microtool of taper angle 9.54°. Machining conditions are duty ratio 30%, pulse frequency 5 MHz, electrolyte 0.2 M/L H_2SO_4, vertical feed rate 0.211 μm/s during sinking up to a depth of 232 μm, and horizontal feed rate 0.104 μm/s. Total machining time for the microchannel of 500-μm length is 1 h 46 min. Figure 18.21 (b) shows the cross-sectional profile of the

above-mentioned blind microchannel. Entry width is 142 µm with entry overcut 29 µm. *i.e.,* (142–84)/2. Diameter of conical microtool at 232 µm from the tip is 84 µm. Width of microchannel at bottom of cross-sectional profile is 70 µm. Figure 18.21 (c) exhibits the roughness profile at the bottom surface with Ra 0.17 µm and Rz 1.28 µm. Micro coordinate measuring machine is used to measure 3D microfeatures. Online microscope and digital storage oscilloscope may be used for continuous monitoring of EMM processes.

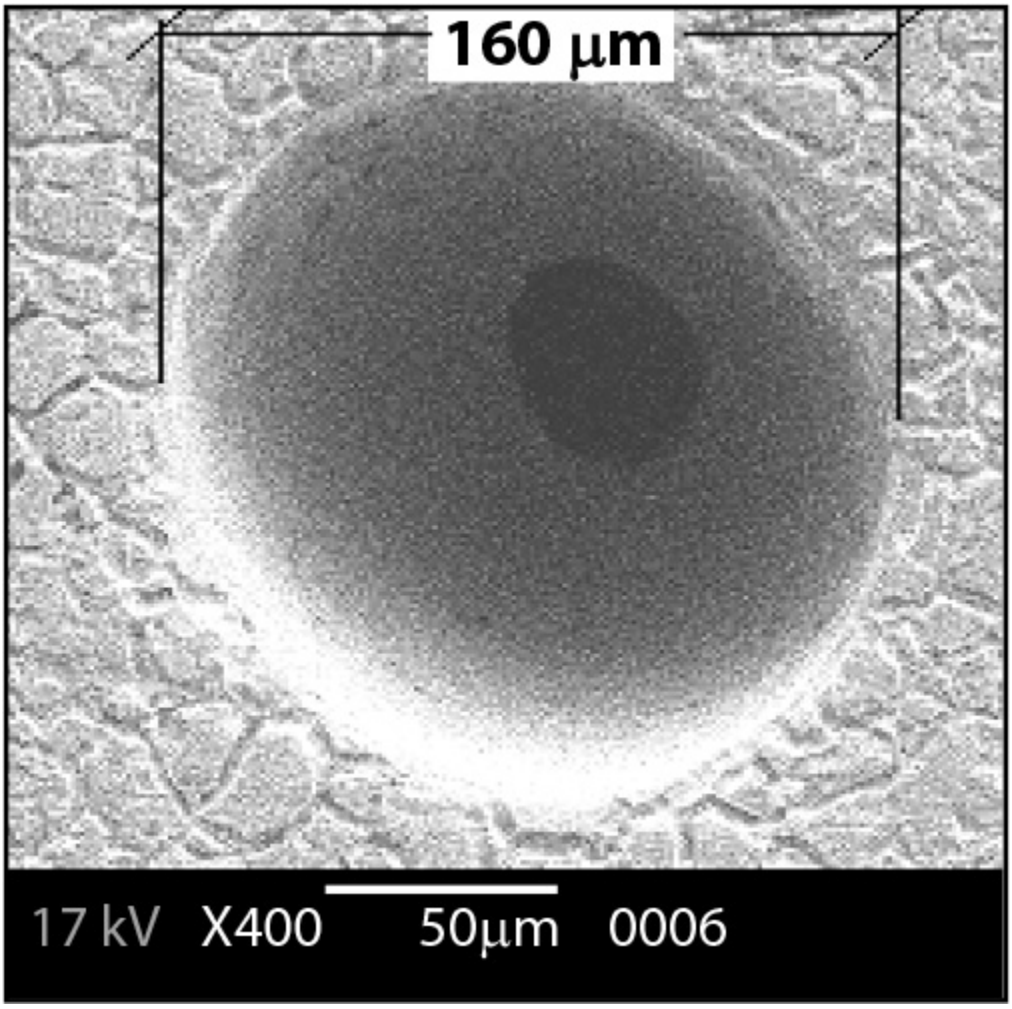


Figure 18.20 SEM micrograph of micro nozzle.

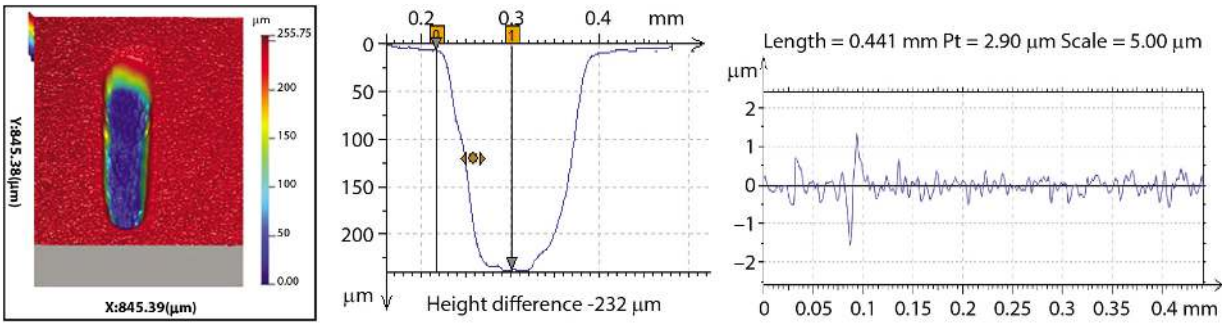


Figure 18.21 (a) 3D surface of channel. (b) Cross-sectional profile. (c) Roughness profile at bottom surface.

18.8 Application of Electrochemical

Micromachining

Microfeatures produced by EMM have wide applications in MEMS, printed circuit board microfluidic systems, etc. Some of the typical applications of EMM are described here. Microfuel injection nozzles are used for atomization of liquid fuels so that oxygen of air quickly comes in contact with fuel atom and thereby ensure quick and complete burning. Stress-free micro-holes are drilled on turbine blades by EMM for cooling purpose. Microprofiles and microchannels are widely used in fuel cell technology, aerodynamics, and biomedical sectors. Array of micro-holes in artificial body parts made of titanium helps in quick assimilation with bone of human body. Through-mask EMM has been done for fabrication of an array of precision micro nozzles in thin stainless-steel sheet and copper sheet for application in inkjet printer heads. Electrochemical micromachining finds wide application in metamaterials where restructuring of surface with precise geometrical shape and orientation is done such that surface achieves smart properties capable of manipulating electromagnetic waves by absorbing, blocking, and bending waves. Thereby, aircraft or missiles evades radar system as receiver antenna of radar fails to receive the reflected wave from them supposed to be detected by it.

18.9 Conclusions

In this chapter, starting from basic ECM process to important aspects of latest developments in EMM is discussed. Mass removal rate in EMM is described in detail for the selection of proper microtool feed rate and to determine machining time for a microfeature. Prediction of shape evolution in EMM is a challenging task which mainly depends on tool shape and current density distribution. It

requires solution of Laplace's equation, $\nabla^2 V = 0$. Application of finite element method (FEM), MATLAB simulations are discussed for shape prediction. Shaping in EMM through mask is also described. Effects of end shapes of microtool like conical, reverse conical, and cylindrical on shape evolution are highlighted. Selection of electrolyte is a major area particularly for successful EMM of superalloy. Electrolyte has severe influence on the metal/alloy to be machined by EMM. Electrical double layer, electrolyte resistance, MRR, sludge formation, and accuracy of machining are directly influenced by electrolyte. Fabrication of cylindrical, conical, reversed conical, and disk-shaped microtools by ECM are discussed elaborately. Uses of different shaped microtools are also discussed for enhancement of EMM. Accurate measurement of microparts or microfeatures is a challenging task. Advanced measurement techniques utilizing SEM, non-contact 3D surface profiler, AFM, STM, and CMM are described.

18.10 Future Research Opportunities

Some of the authors reported ultrasonic method of measurement of IEG and some reported measurement of IEG by measuring current between electrodes. Highly reliable methods of controlling IEG are still missing. Monitoring and control of IEG still needs further research as low IEG is preferred for better accuracy in 3D EMM and accurate IEG control is necessary for smooth continuation of EMM along with preservation of quality of machined features. Scientific selection of electrolyte for a particular metal is still a major area of research. For EMM of superalloys, mixed electrolytes may be more fruitful for smooth machining and an important area for further research. Further research in micro fabrication of

superalloys will open up many challenging possibilities. Electrochemical micromachining of superalloys will be more popular considering their wide use in aircraft engine parts, automobile, and medical fields due to high strength, corrosion resistance, and good mechanical properties.

References

1. Mishra, P.K., *Nonconventional Machining*, Narosa Publishing House, New Delhi, India, 2010.
2. Bhattacharyya, B., Munda, J., Malapati, M., Advancement in electrochemical micromachining. *Int. J. Mach. Tools Manuf.*, 44, 15, 1577–1589, 2004.
3. Corbett, J., McKeown, R.A., Peggs, G.N., Whatmore, R., Nanotechnology: International developments and emerging products. *CIRP Ann. - Manuf. Technol.*, 49, 2, 523–545, 2000.
4. Taniguchi, N., Current Status in, and Future Trends of, Ultraprecision Machining and Ultrafine Materials Processing. *CIRP Ann. - Manuf. Technol.*, 32, 2, 573–582, 1983.
5. Jain, V.K., *Advanced Machining Process*, Allied Publishers Pvt Ltd, New Delh, 2002.
6. Bard, A.J. and Faulkner, L.R., *Electrochemical methods: fundamentals and applications*, 2nd, John Wiley & Sons, New York, 2001.
7. McGeough, J.A., *Principles of Electrochemical Machining*, Chapman and Hall, London, 1974.
8. Oldham, K.B., A Gouy-Chapman-Stern model of the double layer at a metal ionic liquid interface. *J.*

Electroanal. Chem., 613, 131–138, 2008.

9. Schuster, R., Kirchner, V., Allongue, P., Ertl, G., Electrochemical micromachining. *Science*, 289, 5476, 98–101, 2000.

10. Ghoshal, B. and Bhattacharyya, B., Shape control in micro borehole generation by EMM with the assistance of vibration of tool. *Precis. Eng.*, 38, 127–137, 2014.

11. Mithu, M.A.H., Fantoni, G., Ciampi, J., Santochi, M., On how tool geometry, applied frequency and machining parameters influence electrochemical microdrilling. *CIRP J. Manuf. Sci. Technol.*, 5, 202–213, 2012.

12. Pattavanitch, J., Hinduja, S., Atkinson, J., Modeling of the Electrochemical Machining Process by the Boundary Element Method. *CIRP Ann.–Manuf. Technol.*, 59, 243–246, 2010.

13. Purcar, M., Bortels, L., Bossche, B.V., Deconinck, J., 3 D Electrochemical Machining Computer Simulations. *J. Mater. Process. Technol.*, 149, 472– 478, 2004.

14. Wang, L., Wang, Q., Hao, X., Ding, Y., Lu, B., Finite Element Simulation and Experimental Study on the Through-mask Electrochemical Micromachining (EMM) Process. *Int. J. Adv. Manuf. Technol.*, 51, 155–162, 2010.

15. Schonenberger, I. and Roy, S., Microscale pattern transfer without photolithography of substrates. *Electrochim. Acta*, 51, 809–819, 2005.

16. Ghoshal, B. and Bhattacharyya, B., Investigation on Profile of Microchannel generated by Electrochemical Micromachining. *J. Mater. Process. Technol.*, 222, 410–42, 2015.

17. Ghoshal, B. and Bhattacharyya, B., Micro electrochemical sinking and milling method for generation of micro features. *Proc. Inst. Mech. Eng., Part B : J. Eng. Manuf.*, 227, 11, 1651–1663, 2013.

18. Ahn, S.H., Ryu, S.H., Choi, D.K., Chu, C.N., Electro-chemical micro drilling using ultra short pulses. *Precis. Eng.*, 28, 2, 129–134, 2004.

19. Sharma, V., Patel, D., Agrawal, V., Jain, V.K., Ramkumar, J., Investigations into machining accuracy and quality in wire electrochemical micromachining under sinusoidal and triangular voltage pulse condition. *J. Manuf. Processes*, 62, 348–367, 2021.

20. Schultze, J.W. and Lohrengel, M.M., Stability, reactivity and breakdown of passive films: Problems of recent and future research. *Electrochem. Acta*, 45, 2499–2513, 2000.

21. Macdonald, D.D., Passivity- The key to our metals-based civilization. *Pure Appl. Chem.*, 71, 6, 951–978, 1999.

22. Datta, M., Anodic dissolution of metals at high rates. *IBM J. Res. Dev.*, 37, 2, 207–226, 1993.

23. Dhobe, S.D., Doloi, B., Bhattacharyya, B., Surface characteristics of ECMed titanium work samples for biomedical applications. *Int. J. Adv. Manuf. Technol.*, 55, 1-4, 177–188, 2011.

24. Kozak, J., Rajurkar, K.P., Makkar, Y., Study of Pulse Electrochemical Micromachining. *J. Manuf. Processes*, 2001, 7–14, 2004.

25. Ghoshal, B. and Bhattacharyya, B., Generation of Microfeatures on Stainless Steel by Electrochemical

Micromachining. *Int. J. Adv. Manuf. Technol.*, 76, 39–50, 2015.

26. Choi, S.H., Kim, B.H., Shin, H.S., Chang, D.K., Chu, C.N., Analysis of the electrochemical behaviors of WC – Co alloy for micro ECM. *J. Mater. Process. Tech.*, 213, 4, 621–630, 2013.

27. Ayyappan, S.K. and Sivakumar, K., Investigation of electrochemical machining characteristics of 20MnCr5 alloy steel using potassium dichromate mixed aqueous NaCl electrolyte and optimization of process parameters. *Proc. Inst. Mech. Eng., Part B : J. Eng. Manuf.*, 229, 11, 2014.

28. Bilgi, D.S., Jain, V.K., Shekhar, R., Mehrotra, S., Electrochemical deep hole drilling in super alloy for turbine application. *J. Mater. Process. Tech.*, 149, 1, 445–452, 2004.

29. Thangamani, G., Thangaraj, M., Moiduddin, K., Mian, S.H., Alkhalefah, H., Umer, U., Performance Analysis of Electrochemical Micro Machining of Titanium (Ti-6Al-4V) Alloy under Different Electrolytes Concentrations. *Metals*, 11, 247, 2021.

30. Thanigaivelan, R., Arunachalam, R.M., Karthikeyan, B., Loganathan, P., Electrochemical micromachining of stainless steel with acidified sodium nitrate electrolyte. *Procedia - Soc. Behav. Sci.*, 6, 351–355, 2013.

31. Xu, Z., Chen, X., Zhou, Z., Qin, P., Zhu, D., Electrochemical machining of high-temperature titanium alloy Ti60. *Procedia CIRP*, 42, 125–130, 2016.

32. Fan, Z.W. and Hourng, L.W., Wang, C.Y., Fabrication of Tungsten Micro-electrodes Using Pulsed Electrochemical Machining. *Precis. Eng.*, 34, 489–496, 2010.

33. Fan, Z.W. and Hourng, L.W., The analysis and investigation on the microelectrode fabrication by electrochemical machining. *Int. J. Mach. Tools Manuf.*, 49, 659–666, 2009.

34. Wang, M.H., Zhu, D., Peng, W., Experimental Research on Electrochemical Micromachining. *Adv. Des. Manufacture to Gain Competitive Edge*, 6, 775–783, 2008.

35. Ghoshal, B. and Bhattacharyya, B., Influence of vibration on micro-tool fabrication by electrochemical machining. *Int. J. Mach. Tools Manuf.*, 64, 49–59, 2013.

36. Ghoshal, B. and Bhattacharyya, B., Vibration Assisted Electrochemical Micromachining of High Aspect Ratio Micro features. *Precis. Eng.*, 42, 231–24, 2015.

Note

**Corresponding author*: ghoshal_bikash@rediffmail.com

19
Ultrasonic Micromachining

Pradeepkumar Krishnan
Mechanical and Industrial Engineering Department, National University of Science and Technology, Muscat, Sultanate of Oman

Abstract

Ultrasonic micromachining (USM) is a non-traditional machining process utilized extensively in microfabrication and microengineering applications. This chapter provides a comprehensive overview of USM, covering its principles, equipment, process parameters, applications, advantages, and limitations. The discussion also includes recent advancements and emerging trends in the field of USM. By understanding the intricacies of USM, researchers and practitioners can harness its potential for precise and efficient microscale material removal.

***Keywords*:** Ultrasonic micromachining, microfabrication, microengineering, non-traditional machining, microscale material removal

19.1 Introduction

Ultrasonic micromachining (USM) stands at the forefront of non-traditional machining processes, playing a pivotal role in the realm of microfabrication and microengineering applications. This chapter serves as a comprehensive guide to USM, offering an in-depth exploration of its fundamental principles, essential equipment components, critical process parameters, diverse applications, notable advantages, and inherent limitations [1]. Moreover, the

discourse extends to encompass recent advancements and emerging trends within the field of USM.

Ultrasonic micromachining operates on the principle of utilizing ultrasonic vibrations to achieve precise and efficient material removal at the microscale, making it a preferred choice for fabricating intricate microcomponents and structures with exceptional accuracy [2]. By delving into the intricacies of USM, researchers and practitioners can unlock its full potential and leverage its capabilities for achieving high precision in microscale material removal tasks.

Throughout this chapter, we will navigate through the core aspects of USM, shedding light on its underlying principles, the significance of equipment configuration, the critical influence of process parameters on machining outcomes, the diverse array of applications where USM excels, the advantages it offers in terms of precision and material compatibility, as well as the limitations that necessitate careful consideration and optimization [3].

Furthermore, the chapter will delve into the realm of recent advancements in USM, highlighting the development of cutting-edge tool materials, innovative slurry formulations, enhanced process monitoring techniques, and the integration of USM with additive manufacturing technologies [4]. Emerging trends in the field will also be explored, focusing on enhancing process efficiency, sustainability, and scalability through novel configurations, automation, and digitalization.

By embarking on this exploration of USM, readers will gain a profound understanding of this transformative machining process, paving the way for harnessing its capabilities to achieve precise and efficient material removal at the microscale. The insights provided in this chapter aim to equip researchers and practitioners with the knowledge

and tools necessary to leverage USM effectively in their microfabrication and microengineering endeavors, driving innovation and advancement in the field.

19.2 Principles of Ultrasonic Micromachining

Ultrasonic micromachining involves a meticulous process of generating microfeatures, starting from the fabrication of microtools. In the realm of micro-ultrasonic micromachining (micro-USM), the process differs from conventional USM in terms of tool size and attachment to the horn or tool holder, emphasizing the creation of precise and intricate microfeatures [4]. Unlike regular USM processes where tools are prepared separately and then attached to the horn, micro-USM necessitates the production of microtools directly on the setup using techniques like wire electrode discharge machining (WEDM) or wire electrode discharge grinding (WEDG) to ensure stability and accuracy during machining [5]. In micro-USM, a low-frequency signal is converted into high-frequency vibrations through magnetostrictive or piezoelectric transducers, transmitting ultrasonic vibrations (typically in the range of 30–50 kHz) to the tool holder and subsequently to the tool or sonotrode [6]. The tool in micro-USM is meticulously designed to mirror the shape of the desired end product, ensuring optimal machining efficiency and consistent resonance with high amplitude. Prior to machining, a narrow gap is maintained between the tool and the workpiece, which is then flooded with an abrasive slurry comprising various abrasives suspended in a liquid medium [6].

During each vibrating cycle, the abrasive particles in the slurry are driven towards the work surface by the downward stroke of the sonotrode, leading to material

removal through mechanisms such as microchipping, mechanical abrasion, cavitation erosion, and chemical action [7]. These mechanisms work synergistically to remove material by impact, abrasion, cavitation, and chemical reactions, with cavitation erosion being more pronounced in machining porous materials like graphite compared to harder materials such as ceramics or hardened steels.

19.3 Equipment for Ultrasonic Micromachining

The schematic diagram of micro-USM system shown in Figure 19.1 typically includes the following components:

1. Microtool rotating mechanism with spindle: consists of a motor, mandrel, and bearings to provide the required rotations per minute for the microtool.
2. Ultrasonic frequency generator: involves a resonance circuit that converts low-frequency electrical power to high-frequency electrical power, which is then transmitted to the transducer for conversion into mechanical motion.
3. Acoustic head: comprising the transducer and horn, responsible for transmitting high-frequency vibrations to the tool for material removal.
4. Computer numerical control (CNC) axis: provides controlled movement in multiple axes for precise machining operations.
5. Slurry circulation unit: ensures the continuous flow and distribution of abrasive slurry during the machining process.

6. Machining chamber: holds the workpiece and the slurry, providing a controlled environment for the machining operation.

The micro-USM setup integrates these components to enable the precise and efficient machining of microfeatures using ultrasonic vibrations and abrasive action. The system is designed to achieve high accuracy, intricate geometries, and controlled material removal at the microscale.

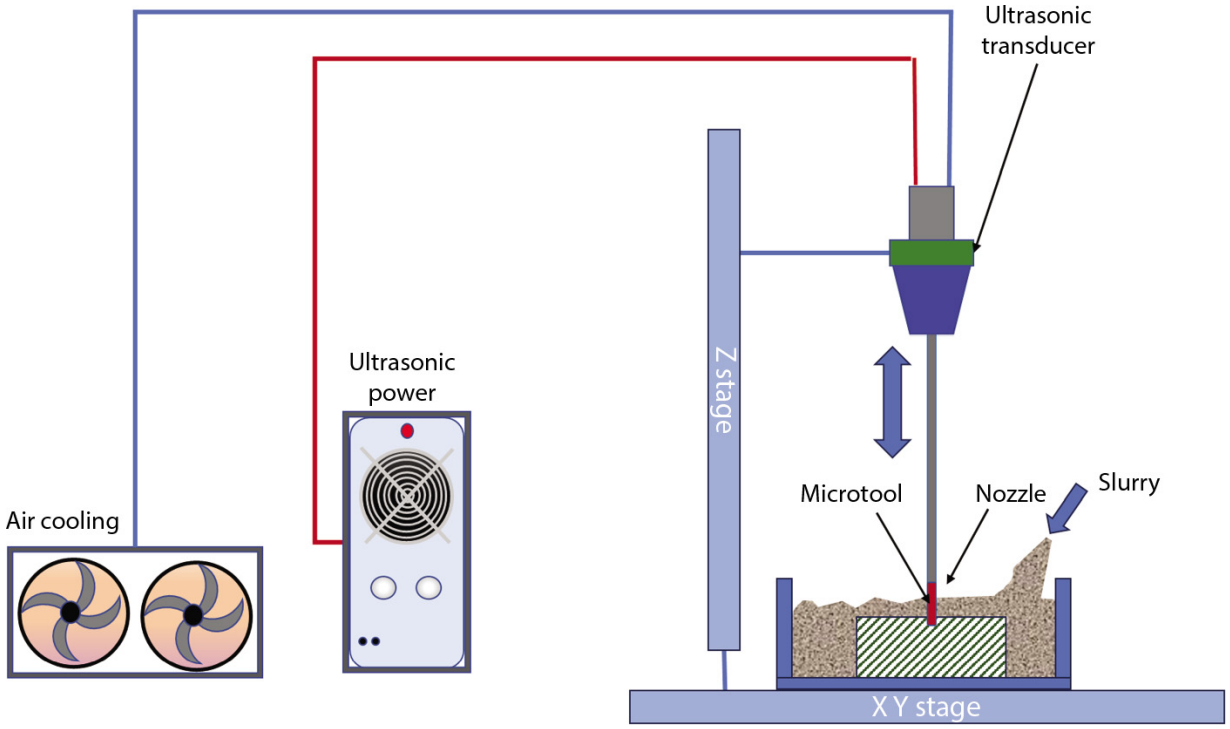


Figure 19.1 Schematic diagram of micro-USM setup.

19.4 Process Parameters in Ultrasonic Micromachining

In micro-USM, the process parameters play a crucial role in determining the machining efficiency and quality of the final product. The complexity of the parametric relationship in micro-USM arises from the interplay of various factors and related parameters that influence the process outputs.

Various operating parameters, machining conditions and their influence can be represented through a diagram, as shown in Figure 19.2. These influencing parameters can be categorized into four main groups: acoustic system, abrasive and slurry, microtool, and workpiece characteristics [8].

1. **Abrasive particle type and size:** the type and size of abrasive particles significantly impact the machining rate in micro-USM. The machining rate tends to increase with larger abrasive particles, as they facilitate faster material removal. Additionally, the machining speed can be enhanced by increasing the average static load and utilizing tool rotation. Tool rotation aids in the swift removal of debris, thereby boosting machining speed [8].
2. **Tool wear:** tool wear is influenced by the hardness and coarseness of the abrasive particles. Harder and coarser abrasives lead to increased tool wear. In micro-USM, tool wear escalates notably with a decrease in tool diameter. Consequently, materials like stainless steel and thoriated tungsten, commonly used in conventional USM, may not be suitable for micro-USM applications [9].
3. **Oscillation amplitude and machining load:** machining speed and tool wear are affected by the oscillation amplitude and machining load. An increase in these parameters can lead to higher machining speeds but may also result in increased tool wear [9].
4. **Surface finish:** the type and size of abrasive particles also influence the surface finish in micro-USM. Generally, surface finish improves with larger abrasive particles. Tungsten carbide has been reported to produce a rougher surface compared to titanium

carbide and boron carbide. Smaller abrasive particles are typically used in micro-USM, but improper distribution of these particles in the gap can lead to increased surface roughness [9].

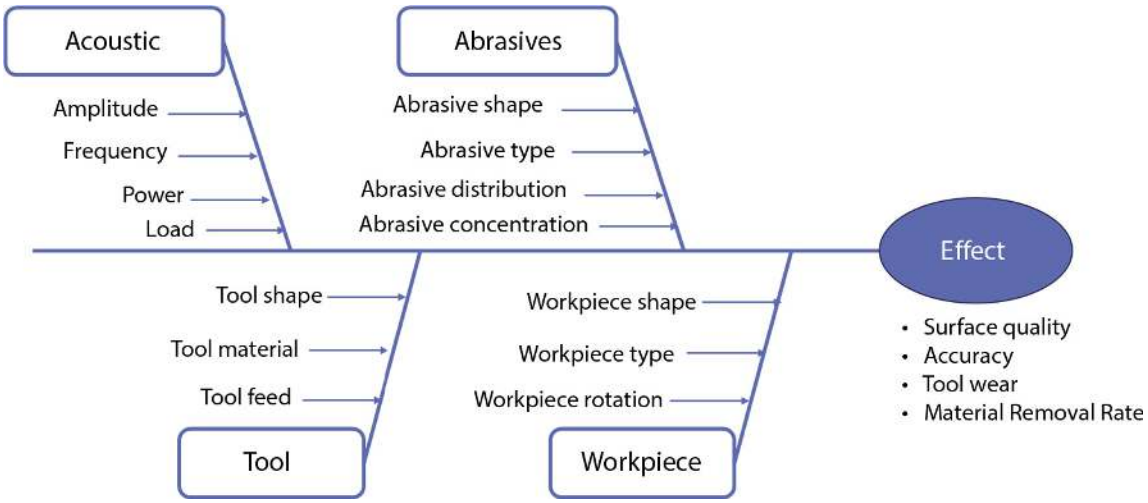


Figure 19.2 Process parameters in micro-USM.

5. **Material removal mechanisms:** the material removal mechanisms in micro-USM, including microchipping, abrasion, cavitation, and chemical reactions, are intricate and not fully understood. Further research is needed to elucidate these mechanisms and enhance the understanding of material removal in micro-USM processes.

Understanding and optimizing these process parameters are essential for achieving desired machining outcomes, such as surface finish, dimensional accuracy, material removal rate, and tool longevity in micro-ultrasonic machining applications.

19.5 Applications of Ultrasonic Micromachining

Ultrasonic micromachining (USM) has a wide range of applications across various industries due to its ability to fabricate intricate microcomponents and structures with high precision and accuracy. Some of the common applications of USM include micro-milling, micro-drilling, micro-turning, micro-grinding, micro-abrasive jet machining, micro-laser machining, and micro-electro discharge machining [10].

One of the latest applications of micro-machining by USM involves the fabrication of microchannels required in bio-MEMS (microelectromechanical systems). Bio-MEMS are devices that integrate biological components with microelectronics and are used in various biomedical applications such as drug delivery systems, lab-on-a-chip devices, and biosensors. The precise machining of microchannels in bio-MEMS using USM enables the creation of intricate fluidic pathways essential for the functioning of these devices [11].

This application highlights the versatility of USM in addressing the growing demand for miniaturized and complex components in the field of biomedical engineering and microfluidics. By leveraging the capabilities of USM, researchers and practitioners can continue to explore new avenues for enhancing bio-MEMS devices and advancing biomedical technologies.

19.6 Advantages and Limitations of Ultrasonic Micromachining

Ultrasonic micromachining (USM) offers several advantages that make it a preferred choice for fabricating

microcomponents and structures with high precision and accuracy. However, like any machining process, USM also has its limitations that need to be considered for optimal performance.

19.6.1 Advantages

1. **High precision:** USM enables the machining of intricate geometries and small features at the microscale with exceptional precision, allowing for the production of complex microcomponents with tight tolerances.
2. **Intricate feature generation:** the process of USM allows for the generation of intricate features and patterns on various materials, making it suitable for applications that require detailed and precise machining.
3. **Minimal heat-affected zone:** USM is a non-thermal machining process, which means that it generates minimal heat during material removal. This characteristic helps in preventing thermal damage to the workpiece and maintaining material properties.
4. **Compatibility with various materials:** USM is compatible with a wide range of materials, including brittle and hard-to-machine materials such as ceramics, glass, and advanced composites. This versatility makes it suitable for diverse machining applications.

19.6.2 Limitations

1. **Limited material removal rates:** one of the limitations of USM is its relatively low material removal rate compared to some traditional machining processes. This can impact productivity, especially when machining larger volumes of material.

2. **Tool wear:** USM is susceptible to tool wear, particularly when machining hard materials or using abrasive slurry. Tool wear can affect machining accuracy and surface finish, necessitating frequent tool maintenance or replacement.
3. **Challenges in controlling surface roughness:** achieving desired surface roughness can be challenging in USM, especially when dealing with complex geometries or varying material properties. Controlling surface finish requires careful optimization of process parameters.
4. **Edge quality control:** maintaining consistent edge quality in USM can be difficult, especially in applications where sharp edges or precise edge profiles are critical. Variations in tool wear or process conditions can affect edge integrity.

By understanding the advantages and limitations of USM, manufacturers and researchers can effectively leverage this technology for specific applications while addressing its inherent challenges to optimize machining outcomes.

19.7 Recent Advancements and Emerging Trends

Micro-ultrasonic micromachining (micro-USM) has witnessed significant advancements and is at the forefront of emerging trends in the field of microfabrication and microengineering. These developments have expanded the applications and capabilities of micro-USM, paving the way for innovative solutions in various industries such as electronics, medical, aerospace, and more [8].

19.7.1 Latest Advancements

1. **Fabrication of microtools:** the ability to fabricate microtools within the same setup as micro-USM has enhanced the applicability of the process. This advancement enables the creation of micro holes, 3D micro cavities, and micro slots with precise geometries, contributing to the production of intricate microcomponents [12].
2. **Rotary tool integration:** incorporating rotary tools in micro-USM has introduced a material removal mechanism that combines diamond grinding and USM. This hybrid approach enhances the impact, indentation, and rate of material removal, leading to improved machining accuracy, tool life, and efficiency [13].
3. **Integration with turning:** combining micro-USM with turning processes has shown benefits such as strain hardening, removal of residual stress, reduction of machining time, enhancement of surface quality, and extended tool life. This integration has opened up new possibilities for achieving complex machining tasks with improved outcomes [13].
4. **Microfluidics applications:** micro-USM is increasingly being utilized in the field of microfluidics for developing microchannels, micro cavities, and other structures on both conductive and non-conductive materials. These microfluidic components are essential for applications in microsensors, microheat exchangers, and MEMS [14].

19.7.2 Emerging Trends

1. **Innovative microfeature fabrication:** the trend towards fabricating intricate 3D microfeatures and

channels on advanced materials like polymers and ceramics for MEMS applications is gaining momentum. Micro-USM's ability to work on a wide range of materials makes it a promising technology for creating complex microstructures [15].

2. **Enhanced tool control and stability:** addressing challenges related to microtool handling, fixing, and wear is a key trend in micro-USM. Innovations in tool fabrication, fixing techniques, and tool wear monitoring are essential for maintaining process stability, accuracy, and overall machining efficiency.
3. **Implementation of piezo vibration:** the recent introduction of piezo vibration in the workpiece has shown promise in improving the flushing condition of the slurry and enhancing stirring during micro-USM. This innovation contributes to better machining efficiency and process control, highlighting the importance of integrating new technologies for optimization [16].
4. **Focus on process monitoring and control:** emphasizing the accuracy of measurement, quality of surface finish, and implementation of online monitoring and control systems are critical trends in micro-USM. Real-time monitoring and control mechanisms are essential for ensuring consistent machining outcomes and enhancing the overall performance of the process.

By staying abreast of these latest advancements and emerging trends in micro-USM, researchers and practitioners can harness the full potential of this technology for pushing the boundaries of microscale material removal and fabrication.

19.8 Conclusions

The field of micro-USM is witnessing rapid advancements and embracing emerging trends that are reshaping the landscape of microfabrication and microengineering. The latest developments in micro-USM, such as the fabrication of microtools, integration with rotary tools and turning processes, and its applications in microfluidics, are expanding the horizons of precision machining at the microscale. These advancements are enabling the production of intricate microcomponents and structures with enhanced accuracy and efficiency.

Moreover, the emerging trends in micro-USM, including innovative microfeature fabrication, enhanced tool control and stability, implementation of piezo vibration, and a focus on process monitoring and control, underscore the continuous evolution and optimization of micro-USM processes. By embracing these trends, researchers and practitioners can unlock the full potential of micro-USM for diverse applications in industries such as electronics, medical devices, aerospace, and beyond.

As micro-USM continues to evolve, it is essential for stakeholders to collaborate, innovate, and invest in research and development efforts to further enhance the capabilities and scalability of this technology. By leveraging the latest advancements and staying attuned to emerging trends, the potential of micro-USM in achieving precise and efficient microscale material removal and fabrication can be fully realized, paving the way for groundbreaking innovations in microengineering and beyond.

Acknowledgment

The authors thank the management of the National University of Science and Technology (NUST) for the

support and encouragement.

References

1. Banu, A., Ali, M.Y., Rahman, M.A., Konneh, M., Investigation of process parameters for stable micro dry wire electrical discharge machining. *Int. J. Adv. Manuf. Technol.*, 103, 1, 723–741, 2019. https://doi.org/10.1007/s00170-019-03603-7

2. Khuri-Yakub, B.T., Ergun, A.S., Oralkan, O., Yaralioglu, G.G., Ultrasonic Transduction. *Compr. Microsys.*, 2, 517–539, 2007, doi: 10.1016/B978-044452190-3.00046-X.

3. Masuzawa, T., State of the art of micromachining. *CIRP Ann. - Manuf. Technol.*, 49, 2, 473–488, 2000, doi: 10.1016/S0007-8506(07)63451-9.

4. Guldiken, R. and Onen, O.m. 5 - MEMS ultrasonic transducers for biomedical applications, in: *Woodhead Publishing Series in Biomaterials*. S. Bhansali and A. B. T.-M. for B. A. Vasudev (Eds.), pp. 120–149, Woodhead Publishing, 2012. https://doi.org/https://doi.org/10.1533/9780857096272.2.120

5. Zarepour, H., Yeo, S.H., Tan, P.C., Aligiri, E., A new approach for force measurement and workpiece clamping in micro-ultrasonic machining. *Int. J. Adv. Manuf. Technol.*, 53, 5–8, 517–522, 2011, doi: 10.1007/s00170-010-2845-6.

6. Nad, M., Ultrasonic horn design for ultrasonic machining technologies. *Appl. Comput. Mech.*, 4, 1, 79–88, 2010.

7. Debnath, S., Kunar, S., Anasane, S.S., Bhattacharyya, B., Non-traditional micromachining processes: opportunities

and challenges. *Non-traditional Micromachining Processes: Fundamentals and Applications*, 1–59, 2017.

8. Jain, V., Sharma, A.K., Kumar, P., Recent Developments and Research Issues in Microultrasonic Machining. *ISRN Mech. Eng.*, 2011, 1–15, 2011. doi: 10.5402/2011/413231.

9. Wang, J., Shimada, K., Mizutani, M., Kuriyagawa, T., Tool wear mechanism and its relation to material removal in ultrasonic machining. *Wear*, 394–395, 96–108, 2018, doi: 10.1016/j. wear.2017.10.010.

10. Nithin, H.R. and Kiran, N., Parameter Affecting Ultrasonic Machining. *International Journal of Engineering Research & Technology (IJERT)*, 8, 11, 353–367, 2019. https://www.ijert.org

11. Chircov, C. and Grumezescu, A.M., *Microelectromech. Syst. (MEMS) Biomed. Appl.*, 13, 2, 2022, https://doi.org/10.3390/mi13020164.

12. Yu, Z.Y., Rajurkar, K.P., Tandon, A., Study of 3D micro-ultrasonic machining. *J. Manuf. Sci. Eng.*, 126, 4, 727–732, 2004, doi: 10.1115/1.1813482.

13. Singh, R.P. and Singhal, S., Rotary Ultrasonic Machining: A Review. *Mater. Manuf. Process.*, 31, 14, 1795–1824, 2016, doi: 10.1080/10426914.2016.1140188.

14. Scott, S.M. and Ali, Z., Fabrication methods for microfluidic devices: An overview. *Micromachines*, 12, 3, 319, 2021, https://doi.org/10.3390/mi12030319.

15. Qin, Y. *et al.*, Micro-manufacturing: Research, technology outcomes and development issues. *Int. J. Adv. Manuf. Technol.*, 47, 9–12821–837, 2010, doi: 10.1007/s00170-009-2411-2.

16. Haiqal, U., Khaidir, U., Mohid, Z., A Review on Chip Formation Characteristics Under Dry and Flood Cutting. *Research Progress in Mechanical and Manufacturing Engineering*, 2, 2, 611–618, 2021. http://publisher.uthm.edu.my/periodicals/index.php/rpmme

Note

Email: pradeepkrishnan@nu.edu.om

20
Laser Surface Modification of Implant Materials: An Insight

V. K. Bupesh Raja[1]*, Sathish Kannan[2], Jayaprakash Jeyaraju[3], V. Selvarani[4], Abel J. Francis[5] and A. Jayaganthan[1]

[1]School of Mechanical Engineering, Sathyabama Institute of Science and Technology, Chennai, India

[2]Engineering, Architecture and Interior Design, Amity University, Dubai, UAE

[3]Department of Mechanical Engineering, Advanced Research Institution (ARI), Dr. M. G. R. Educational and Research Institute, Chennai, Tamil Nadu, India

[4]Department of Chemistry, St. Joseph's Institute of Technology, Chennai, India

[5]Department of Surface Treatment, Eltechnologies, Chennai, India

Abstract

Laser surface modification techniques have emerged as powerful tools for enhancing the performance of implant materials in medical applications. This book chapter provides a comprehensive overview of laser-based surface modification methods, including laser ablation, surface melting, alloying, cladding, and patterning. The chapter discusses the principles, methodologies, and applications of these techniques, emphasizing their role in improving the biocompatibility, bioactivity, and antimicrobial properties of implant surfaces. Key factors influencing the efficacy of laser surface modification, such as laser parameters and material properties, are examined, and case studies from

orthopedic, dental, and cardiovascular implants are presented to illustrate their clinical relevance. Furthermore, the chapter discusses future trends and prospects in the field, including advancements in laser technology and integration with additive manufacturing processes. Overall, this book chapter serves as a valuable resource for researchers, clinicians, and industry professionals interested in optimizing implant therapies through laser surface modification.

***Keywords*:** Implant materials, laser surface modification, biocompatibility, osseointegration

20.1 Introduction

Implant materials have revolutionized modern medicine by offering effective solutions to a wide range of medical conditions, including bone fractures, joint replacements, dental restorations, and cardiovascular interventions [1–3]. These materials serve as vital components in prosthetic devices, providing structural support, facilitating tissue integration, and restoring function to impaired or diseased areas of the body [4]. The success of implant therapies depends significantly on the biocompatibility, mechanical properties, and surface characteristics of the materials used, which profoundly influence their performance and longevity *in vivo* [5–8].

Surface modification techniques play a crucial role in enhancing the performance of implant materials by improving their biocompatibility, osseointegration, and long-term functionality [9, 10]. By altering the surface properties, these techniques aim to optimize the interaction between the implant and the surrounding biological environment, thereby improving clinical outcomes. Laser surface modification techniques offer unique advantages in

this regard, allowing precise control over surface morphology, chemistry, and topography [11]. These techniques utilize high-energy laser beams to induce structural and chemical changes on the surface of implant materials, enhancing their biocompatibility, corrosion resistance, and mechanical properties [12, 13].

In this chapter, we provide an overview of implant materials and their significance in medical applications. We discuss the importance of surface modification techniques in enhancing implant performance and briefly introduce laser surface modification techniques and their advantages. The objective of this chapter is to explore the principles, methods, and applications of laser surface modification in the context of implant materials, highlighting their potential to improve the clinical efficacy and longevity of implant therapies.

20.2 Fundamentals of Laser Surface Modification

Laser surface modification techniques have garnered significant attention for their ability to enhance the properties of implant materials, thereby improving their performance in medical applications. In this section, we delve into the fundamental principles underlying laser-material interaction, including the processes of laser ablation, melting, and solidification. Additionally, we discuss the various factors influencing laser-material interaction and provide an overview of different types of lasers commonly used for surface modification.

Laser-material interaction involves the absorption of laser energy by the material’s surface, leading to physical and chemical changes. The interaction primarily depends on the wavelength, intensity, and duration of the laser pulse.

When the laser beam strikes the material's surface, it can be reflected, transmitted, absorbed, or scattered [14]. Absorption of laser energy results in heating of the material, leading to various thermal and chemical effects [15, 16].

Laser ablation is a process wherein high-intensity laser pulses are used to remove material from the surface through vaporization or expulsion [17, 18]. This process is highly dependent on the laser fluence and material properties [19]. Laser melting occurs when the absorbed laser energy surpasses the material's melting threshold, causing localized melting and subsequent solidification upon cooling. Laser solidification involves the rapid cooling of melted material, leading to the formation of a modified surface layer with altered microstructure and properties [20, 21].

Several factors influence laser-material interaction, including laser parameters such as wavelength, pulse duration, fluence, and repetition rate [22, 23]. Material properties such as absorption coefficient, thermal conductivity, and melting point also play a crucial role in determining the outcome of laser surface modification processes [24, 25]. Additionally, environmental factors such as ambient temperature and pressure can influence interaction dynamics.

A variety of lasers are employed for surface modification of implant materials, each offering unique capabilities and advantages. Commonly used lasers include Nd:YAG (neodymium-doped yttrium aluminum garnet), CO_2 (carbon dioxide), and excimer lasers. Nd:YAG lasers are widely used for their versatility, high power output, and precise control over parameters [6, 26, 27]. CO_2 lasers are preferred for their ability to efficiently vaporize organic materials and polymers. Excimer lasers, on the other hand,

are well-suited for precision micromachining and surface patterning due to their short wavelength and high pulse energy [28].

20.3 Laser Surface Modification Techniques

Laser technology has revolutionized the field of surface modification of implant materials, offering precise control over surface properties to enhance biocompatibility, wear resistance, and mechanical strength. In this chapter, we explore various laser surface modification techniques, including laser surface melting and re-solidification, laser ablation, laser cladding and alloying, laser surface texturing, laser-induced surface patterning, and laser surface alloying and nitriding. We also provide a comparative analysis of these techniques, highlighting their advantages, limitations, and applications in the field of implant materials.

20.3.1 Laser Surface Melting and Re-Solidification

Laser surface melting involves the localized heating of the material's surface above its melting temperature, followed by rapid cooling and solidification. This process leads to the formation of a refined microstructure with improved mechanical properties and surface finish [29–32]. Laser surface melting is particularly effective for enhancing the wear resistance and corrosion resistance of implant materials, such as titanium alloys, magnesium alloys/ composites and stainless steel [33].

20.3.2 Laser Ablation

Laser ablation is a non-contact, material removal process wherein high-energy laser pulses are used to vaporize or remove material from the surface. This technique is employed to create precise surface features, such as microchannels or roughened textures, for improving osseointegration and tissue adhesion [34]. Laser ablation is commonly used in dental implantology and orthopedic applications to promote faster bone healing and implant stability [35].

20.3.3 Laser Cladding and Alloying

Laser cladding and alloying involve the deposition of a thin layer of material onto the substrate surface to improve its properties. In laser cladding, a powdered or wire feedstock material is melted and fused onto the substrate surface, forming a metallurgically bonded layer. Laser alloying, on the other hand, involves the introduction of alloying elements into the substrate surface through laser-induced melting and mixing [36]. These techniques are utilized to enhance the surface hardness, wear resistance, and corrosion resistance of implant materials [37, 38].

20.3.4 Laser Surface Texturing

Laser surface texturing involves the precise ablation of material from the surface to create micro- or nanoscale patterns or features [39]. These textured surfaces can improve tribological properties, reduce friction, and promote cell adhesion for enhanced osseointegration [5, 40]. Laser surface texturing is employed in dental implants, orthopedic implants, and cardiovascular stents to optimize tissue integration and implant stability [2, 41, 42].

20.3.5 Laser-Induced Surface Patterning

Laser-induced surface patterning encompasses a range of techniques for creating periodic or non-periodic surface patterns using laser irradiation. These patterns can be tailored to control surface wettability, adhesion, and biological response [43–45]. Laser-induced surface patterning is utilized in dental implants, orthopedic implants, and biomedical devices to modulate cell behavior and tissue regeneration [46–48].

20.3.6 Laser Surface Alloying and Nitriding

Laser surface alloying involves the introduction of alloying elements into the surface layer to improve its mechanical and chemical properties. Similarly, laser surface nitriding involves the diffusion of nitrogen into the surface to form hard nitride layers with enhanced wear and corrosion resistance [13]. These techniques are employed to enhance the surface properties of implant materials, such as titanium and stainless steel, for orthopedic and dental applications [49].

20.3.7 Comparison of Different Laser Surface Modification Techniques

Each laser surface modification technique offers unique advantages and limitations, making them suitable for specific applications [33, 50–52]. Laser surface melting and resolidification, laser cladding, and alloying are effective for enhancing surface hardness and wear resistance, while laser ablation and texturing are valuable for creating tailored surface topographies to improve tissue integration [53]. Laser-induced surface patterning and alloying offer precise control over surface chemistry and morphology, enabling advanced customization of implant surfaces for specific clinical requirements [54–56, 58].

20.4 Applications of Laser Surface Modification in Implant Materials

Laser surface modification techniques offer versatile solutions for enhancing the performance of implant materials in various medical applications. In this chapter, we explore the applications of laser surface modification in metallic and polymer-based implants, focusing on the enhancement of biocompatibility, osteointegration, and controlled drug delivery. Additionally, we present case studies and examples highlighting the successful implementation of laser techniques in implant materials.

20.4.1 Surface Modification of Metallic Implants Using Laser Techniques

Metallic implants, such as titanium and stainless steel, are widely used in orthopedic and dental applications due to their excellent mechanical properties and biocompatibility. Laser surface modification techniques, including laser surface melting, ablation, and alloying, are employed to enhance the surface characteristics of metallic implants [57–60]. These techniques improve surface roughness, wettability, and bioactivity, promoting faster osseointegration and long-term implant stability [23, 61]. For example, laser surface texturing of titanium implants has been shown to enhance osteoblast adhesion and proliferation, leading to improved bone formation and implant integration [62, 63].

20.4.2 Enhancement of Biocompatibility and Osteointegration Through Laser Surface Modification

Biocompatibility and osteointegration are critical factors determining the success of implant therapies. Laser surface

modification techniques offer precise control over surface properties, allowing for the creation of implant surfaces tailored to promote cell adhesion, proliferation, and differentiation [64]. By modulating surface chemistry and topography, laser-treated implants exhibit improved interactions with surrounding tissues, resulting in enhanced biocompatibility and osteointegration [65]. For instance, laser-induced surface patterning of titanium implants has been shown to promote the formation of a stable oxide layer, facilitating protein adsorption and cell attachment for improved osseointegration [66, 67].

20.4.3 Surface Modification of Polymer-Based Implants Using Laser Techniques

Polymer-based implants, such as polyethylene and polyetheretherketone (PEEK), offer advantages such as flexibility, biocompatibility, and low density. Laser surface modification techniques, including laser ablation and surface patterning, are utilized to improve the surface properties of polymer implants [68–70]. These techniques enhance surface roughness, porosity, and bioactivity, enabling better cell adhesion and tissue integration [11, 71]. Lasertreated polymer implants have shown promise in orthopedic and soft tissue applications, where improved bio-integration and mechanical stability are crucial for long-term success [72].

20.4.4 Laser Surface Modification for Controlled Drug Delivery from Implant Surfaces

Laser surface modification techniques can be employed to create drug-releasing implant surfaces for localized and sustained drug delivery. By incorporating drug-loaded coatings or microstructures onto implant surfaces, laser-treated implants enable controlled release of therapeutic agents directly at the implant site [20, 30, 73]. This

approach has significant potential in orthopedic and dental implants, where localized drug delivery can mitigate inflammation, infection, and implant-related complications [74, 75]. For example, laser-induced surface patterning of drug-eluting coatings on titanium implants has been demonstrated to enhance antibacterial efficacy and promote tissue regeneration [64, 76].

Several case studies and examples demonstrate the successful implementation of laser surface modification techniques in implant materials. The osseointegration and biomechanical stability of laser-treated titanium implants has been proved in rabbit model [77]. Laser clad titanium implants exhibit promising results in simulated physiological environments [38].

20.5 Characterization of Laser-Modified Surfaces

Laser surface modification techniques impart specific changes to the surface properties of implant materials, thereby necessitating thorough characterization to understand and optimize their performance. In this chapter, we explore various techniques for characterizing laser-modified surfaces, including scanning electron microscopy (SEM), atomic force microscopy (AFM), X-ray photoelectron spectroscopy (XPS), and X-ray diffraction (XRD) [11, 78, 79]. We discuss the analysis of surface morphology, roughness, and composition, as well as the evaluation of mechanical properties and surface wettability. Furthermore, we emphasize the importance of surface characterization in assessing the effectiveness of laser surface modification techniques.

20.5.1 Techniques for Characterizing Laser-Modified Surfaces

20.5.1.1 Scanning Electron Microscopy (SEM)

Scanning electron microscopy (SEM) is a powerful tool for visualizing surface morphology and topography at high magnifications and resolutions. It provides detailed information about surface features, such as microstructures, cracks, and pores, enabling qualitative and quantitative analysis of laser-modified surfaces [62].

20.5.1.2 Atomic Force Microscopy (AFM)

Atomic force microscopy (AFM) offers high-resolution imaging of surface topography and roughness at the nanoscale level. It utilizes a sharp probe to scan the surface and measure surface features, including height variations and surface roughness parameters [51, 80]. Atomic force microscopy is particularly useful for characterizing laser-induced surface textures and patterns.

20.5.1.3 X-Ray Photoelectron Spectroscopy (XPS)

X-ray photoelectron spectroscopy (XPS) is a surface-sensitive technique used to analyze the elemental composition and chemical state of the surface. It provides information about the chemical composition, bonding configurations, and surface contaminants present on laser-modified surfaces [6, 41].

20.5.1.4 X-Ray Diffraction (XRD)

X-ray diffraction (XRD) is employed to analyze the crystalline structure and phase composition of laser-modified surfaces. It can identify crystallographic phases, grain sizes, and residual stresses induced by laser

processing, offering insights into the microstructural changes occurring in the material [41, 81].

20.5.2 Analysis of Surface Morphology, Roughness, and Composition

Surface morphology and roughness play crucial roles in determining the functional properties of laser-modified surfaces, such as adhesion, wear resistance, and bioactivity. Scanning electron microscopy and AFM are commonly used to characterize surface morphology and roughness parameters, including average roughness (Ra), root mean square roughness (Rq), and surface skewness (Rsk) [27, 80, 82–84]. X-ray photoelectron spectroscopy provides information about the elemental composition and chemical states present on the surface, aiding in the understanding of surface chemistry and modifications induced by laser processing.

20.5.3 Evaluation of Mechanical Properties and Surface Wettability

The mechanical properties and surface wettability of laser-modified surfaces are important factors influencing their performance in implant applications. Techniques such as nanoindentation and microhardness testing are utilized to evaluate mechanical properties, including hardness, elastic modulus, and indentation resistance [66]. Contact angle measurements are employed to assess surface wettability and surface energy, which affect the interactions between the implant surface and biological fluids or tissues [27, 41, 66, 85, 86].

Surface characterization plays a pivotal role in assessing the effectiveness of laser surface modification techniques and optimizing process parameters to achieve desired surface properties. By comprehensively analyzing surface

morphology, roughness, composition, mechanical properties, and wettability, researchers can gain valuable insights into the structure-property relationships of laser-modified surfaces [23, 87]. This knowledge facilitates the design and development of tailored implant surfaces with enhanced biocompatibility, osteointegration, and long-term performance.

20.6 Challenges and Future Perspectives

Laser surface modification techniques have demonstrated significant potential for enhancing the properties of implant materials, yet they are not without challenges and limitations. In this chapter, we discuss the current challenges associated with laser surface modification techniques, strategies for overcoming these challenges, and future perspectives in the field. We explore emerging trends, potential advancements, and innovations that may shape the future of laser surface modification of implant materials.

20.6.1 Challenges and Limitations Associated with Laser Surface Modification Techniques

i. **Precision and Control**

   Achieving precise control over laser parameters and ensuring uniformity in surface modification remain challenges. Variations in laser beam intensity, scanning speed, and spot size can lead to non-uniform surface modifications and inconsistent results [88].

ii. **Heat-Affected Zone (HAZ)**

   Laser processing generates heat, which can result in the formation of a heat-affected zone (HAZ) around the

treated area. Excessive heat can induce undesirable changes in material properties, such as phase transformations, residual stresses, and microstructural alterations [89].

iii. **Material Compatibility**

Not all implant materials are suitable for laser surface modification. Some materials may exhibit poor laser absorption or thermal conductivity, limiting the effectiveness of laser processing. Additionally, certain materials may be prone to degradation or chemical reactions under laser irradiation.

iv. **Surface Contamination**

Laser surface modification processes may introduce surface contaminants or induce chemical reactions with surrounding gases, leading to surface contamination or undesirable chemical modifications. Contaminants can adversely affect surface properties and compromise the biocompatibility of implant materials.

20.6.2 Strategies for Overcoming Challenges and Optimizing Laser Surface Modification Processes

20.6.2.1 Process Optimization

Optimization of laser parameters, such as laser fluence, pulse duration, and repetition rate, is crucial for achieving desired surface modifications while minimizing undesirable effects. Advanced control systems and real-time monitoring techniques can enhance process stability and repeatability [90].

20.6.2.2 Multi-Step Processing

Implementing multi-step processing strategies, such as sequential laser treatments or combined laser techniques (*e.g.*, laser ablation followed by laser surface alloying), can overcome limitations associated with individual laser processes and enable the tailored modification of implant surfaces [75, 91, 92].

20.6.2.3 Material Selection and Design

Choosing implant materials with favorable properties for laser processing and surface modification is essential. Material composition, microstructure, and thermal properties should be carefully considered to ensure compatibility with laser processing techniques.

20.6.2.4 Surface Pre-Treatment

Pre-treating implant surfaces through methods such as cleaning, polishing, or surface activation can improve laser absorption, enhance surface cleanliness, and mitigate the effects of surface contamination during laser processing [93].

20.6.3 Emerging Trends and Future Directions in Laser Surface Modification of Implant Materials

20.6.3.1 Advanced Laser Technologies

Advancements in laser technologies, including ultrafast lasers, picosecond lasers, and femtosecond lasers, offer opportunities for precise and efficient surface modification with minimal heat-affected zones and improved control over surface features.

20.6.3.2 Functional Surface Designs

Future research may focus on developing functional surface designs with tailored properties for specific biomedical applications. Functionalized surfaces with controlled topographies, chemistries, and release profiles can promote enhanced tissue integration, antibacterial activity, and therapeutic efficacy [85, 94].

20.6.3.3 Innovative Materials and Composites

Exploration of novel materials and composites with superior properties for laser surface modification is anticipated. Bio-inspired materials, smart polymers, and bioactive ceramics may offer unique advantages for implant applications, enabling the development of next-generation implant materials with enhanced performance and functionality [38, 95–97].

20.7 Conclusion

In this chapter, we delved into the realm of laser surface modification of implant materials, exploring its potential to enhance the performance and functionality of biomedical implants. As we conclude, let us recapitulate the key points discussed and reflect on the significance of laser surface modification in the field of implantology.

Throughout this chapter, we examined various aspects of laser surface modification techniques, including their principles, applications, challenges, and future perspectives. We discussed the fundamentals of laser-material interaction, different types of laser surface modification techniques, and their applications in modifying metallic and polymer-based implant materials. Furthermore, we explored techniques for characterizing laser-modified surfaces and highlighted the importance of

surface characterization in assessing the effectiveness of laser processing.

Laser surface modification holds immense significance in improving the performance of implant materials across a wide range of biomedical applications. By precisely altering surface characteristics such as morphology, roughness, chemistry, and wettability, laser techniques can enhance the biocompatibility, osteointegration, and long-term stability of implants. Laser-treated surfaces exhibit tailored properties that promote favorable interactions with biological tissues, thereby reducing implant failure rates and improving patient outcomes.

As we look to the future, it is evident that laser surface modification will continue to play a pivotal role in advancing the field of implantology. Emerging trends such as advanced laser technologies, functional surface designs, and innovative materials hold promise for further enhancing the performance and functionality of implant materials. Future research efforts should focus on addressing the challenges associated with laser processing, optimizing process parameters, and translating laboratory findings into clinical practice.

In conclusion, laser surface modification represents a powerful tool for tailoring the properties of implant materials to meet the evolving needs of modern healthcare. By harnessing the capabilities of laser technology, researchers and clinicians can pave the way for the development of next-generation implants with improved biocompatibility, functionality, and longevity, ultimately transforming the landscape of implantology and benefiting patients worldwide.

References

1. Luke Yeo, I.S., Dental Implants: Enhancing Biological Response Through Surface Modifications. *Dent. Clin. North Am.*, 66, 4, 627–642, 2022, doi: 10.1016/j.cden.2022.05.009.

2. Saran, R., Ginjupalli, K., George, S.D., Chidangil, S., V K, U., LASER as a tool for surface modification of dental biomaterials: A review. *Heliyon*, 9, 6, e17457, 2023, doi: 10.1016/j.heliyon.2023. e17457.

3. Madeira, S., Buciumeanu, M., Nobre, D., Carvalho, O., Silva, F.S., Development of a novel hybrid Ti6Al4V–ZrO2 surface with high wear resistance by laser and hot pressing techniques for dental implants. *J. Mech. Behav. Biomed. Mater.*, 136, September, 105508, 2022, doi: 10.1016/j. jmbbm.2022.105508.

4. Pothala, S. and Jagannadha Raju, M., Recent advances of metallic bio-materials in additive manufacturing in biomedical implants–A review. *Mater. Today Proc.*, xxxx, 2023, ISSN 2214-7853, doi: 10.1016/j.matpr.2023.07.109.

5. Costa, M.M. *et al.*, NiTi laser textured implants with improved *in vivo* osseointegration: An experimental study in rats. *J. Mater. Sci. Technol.*, 114, 120–130, 2022, doi: 10.1016/j. jmst.2021.11.014.

6. Gnilitskyi, I. *et al.*, Cell and tissue response to nanotextured Ti6Al4V and Zr implants using high-speed femtosecond laser-induced periodic surface structures. *Nanomed. Nanotechnol., Biol. Med.*, 21, 102036, 2019, doi: 10.1016/j.nano.2019.102036.

7. Singh, V., Katyal, P., Kumar, K., Kumar, R., Surface Integrity and Biological Response of Ti-Alloy Implants after Surface Modification. *Mater. Today Proc.*, 56, 2451–2468, 2022, doi: 10.1016/j. matpr.2021.08.235.

8. Basova, T.V., Vikulova, E.S., Dorovskikh, S., II, Hassan, A., Morozova, N.B., The use of noble metal coatings and nanoparticles for the modification of medical implant materials. *Mater. Des.*, 204, 109672, 2021, doi: 10.1016/j.matdes.2021.109672.

9. Chowdhury, S. and Arunachalam, N., Surface functionalization of additively manufactured titanium alloy for orthopaedic implant applications. *J. Manuf. Process.*, 102, July, 387–405, 2023, doi: 10.1016/j.jmapro.2023.07.015.

10. Emmelmann, C., Scheinemann, P., Munsch, M., Seyda, V., Laser additive manufacturing of modified implant surfaces with osseointegrative characteristics. *Phys. Procedia*, 12, PART 1, 375–384, 2011, doi: 10.1016/j.phpro.2011.03.048.

11. Venkatesan, K. *et al.*, Development of bioactive and antimicrobial nano-topography over selective laser melted Ti6Al4V implant and its *in-vitro* corrosion behavior. *J. Mech. Behav. Biomed. Mater.*, 149, October 2023, 106210, 2024, doi: 10.1016/j.jmbbm.2023.106210.

12. Jambhulkar, N., Jaju, S., Raut, A., Surface modification techniques for different materials used in dental implants review. *Mater. Today Proc.*, 60, 2266–2269, 2022, doi: 10.1016/j. matpr.2022.04.683.

13. Travessa, D.N., Guedes, G.V.B., de Oliveira, A.C., da Silva Sobrinho, A.S., Roche, V., Jorge, A.M., Corrosion performance of the biocompatible β-Ti12Mo6Zr2Fe alloy

submitted to laser and plasma-nitriding surface modifications. *Corros. Sci.*, 209, article id. 110740, March, 2022, 10.1016/j.corsci.2022.110740.

14. Trtica, M., Stasic, J., Batani, D., Benocci, R., Narayanan, V., Ciganovic, J., Laser-assisted surface modification of Ti-implant in air and water environment. *Appl. Surf. Sci.*, 428, 669–675, 2018, doi: 10.1016/j.apsusc.2017.09.185.

15. Al Harbi, N., Benyounis, K.Y., Looney, L., Stokes, J., Laser Surface Modification of Ceramic Coating Materials. *Encycl. Smart Mater.*, 1, 445–461, 2021, doi: 10.1016/B978-0-12-803581-8.11386-4.

16. Villapún, V.M., Man, K., Carter, L., Penchev, P., Dimov, S., Cox, S., Laser texturing of additively manufactured implants: A tool to programme biological response. *Biomater. Adv.*, 153, January, 213574, 2023, doi: 10.1016/j.bioadv.2023.213574.

17. Bereznai, M. *et al.*, Surface modifications induced by ns and sub-ps excimer laser pulses on titanium implant material. *Biomaterials*, 24, 23, 4197–4203, 2003, doi: 10.1016/ S0142-9612(03)00318-1.

18. Jones, S.E., Nichols, L., Elder, S.H., Priddy, L.B., Laser microgrooving and resorbable blast texturing for enhanced surface function of titanium alloy for dental implant applications. *Biomed. Eng. Adv.*, 5, January, 100090, 2023, doi: 10.1016/j.bea.2023.100090.

19. Frerichs, H., Stricker, J., Wesner, D.A., Kreutz, E.W., Laser-induced surface modification and metallization of polymers. *Appl. Surf. Sci.*, 86, 1–4, 405–410, 1995, doi: 10.1016/0169-4332(94)00431-5.

20. Bandyopadhyay, A., Balla, V.K., Roy, M., Bose, S., Laser surface modification of metallic biomaterials. *Jom*, 63, 6,

94–99, 2011, doi: 10.1007/s11837-011-0099-x.

21. Farber, E., Nazarov, D., Mitrofanov, I., Sufiiarov, V., Popovich, A., Maximov, M., Development of the titanium meshes by selective laser melting and chemical etching for using as medical implants. *Mater. Today Proc.*, 30, 746–751, 2019, doi: 10.1016/j.matpr.2020.01.558.

22. Boyd, J.D., Stromberg, A.J., Miller, C.S., Grady, M.E., Biofilm and cell adhesion strength on dental implant surfaces via the laser spallation technique. *Dent. Mater.*, 37, 1, 48–59, 2021, doi: 10.1016/j.dental.2020.10.013.

23. Eghbali, N., Naffakh-Moosavy, H., Sadeghi Mohammadi, S., Naderi-Manesh, H., The influence of laser frequency and groove distance on cell adhesion, cell viability, and antibacterial characteristics of Ti-6Al-4V dental implants treated by modern fiber engraving laser. *Dent. Mater.*, 37, 3, 547–558, 2021, doi: 10.1016/j.dental.2020.12.007.

24. Tunakova, V., Hrubosova, Z., Tunak, M., Kasparova, M., Mullerova, J., Laser surface modification of electrically conductive fabrics: Material performance improvement and design effects. *Opt. Laser Technol.*, 98, 178–189, 2018, doi: 10.1016/j.optlastec.2017.07.017.

25. Hu, Y. *et al.*, *In situ* preparation of nano cone-like structures of rutile titanium oxides on titanium implants by one-step femtosecond laser irradiation for enhanced mechanical properties and biocompatibility. *J. Mater. Res. Technol.*, 27, 2684–2694, 2023, doi: 10.1016/j.jmrt.2023.09.316.

26. Ciganovic, J. *et al.*, Surface modification of the titanium implant using TEA CO2 laser pulses in controllable gas

atmospheres - Comparative study. *Appl. Surf. Sci.*, 258, 7, 2741–2748, 2012, doi: 10.1016/j.apsusc.2011.10.125.

27. jun Wang, J., Zhang, M., jie Wang, Y., ni Jia, L., jun Yang, J., Zhang, Q., The effects of using Nd:YAG laser on the surface modification and cell adhesion/spreading on zirconia discs: An *in vitro* study. *Mater. Lett.*, 324, June, 132602, 2022, doi: 10.1016/j.matlet.2022.132602.

28. García-de-Albeniz, N., Jiménez-Piqué, E., Roa, J.J., Mas-Moruno, C., A review of surface topographical modification strategies of 3Y-TZP: Effect in the physicochemical properties, microstructure, mechanical reliability, and biological response. *J. Eur. Ceram. Soc.*, 43, 8, 2977–3004, 2023, doi: 10.1016/j.jeurceramsoc.2023.02.043.

29. Furlan, V., Demir, A.G., Previtali, B., Micro and sub-micron surface structuring of AZ31 by laser re-melting and dimpling. *Opt. Laser Technol.*, 75, 164–172, 2015, doi: 10.1016/j. optlastec.2015.06.030.

30. Bupesh Raja, V.K. *et al.*, Influence of Laser Treatment Medium on the Surface Topography Characteristics of Laser Surface-Modified Resorbable Mg3Zn Alloy and Mg3Zn1HA Nanocomposite. *Met. (Basel).*, 13, 5, 850, 2023, doi: 10.3390/met13050850.

31. Comita, P.B., Surface modification with lasers. *Adv. Mater.*, 2, 2, 82–90, 1990, doi: 10.1002/ adma.19900020204.

32. Sypniewska, J., Szkodo, M., Majkowska-Marzec, B., Mielewczyk – Gryń, A., Effect of hybrid modification by ceramic layer formation in MAO process and laser remelting on the structure of titanium bio-alloy

Ti13Nb13Zr. *Ceram. Int.*, 49, 11, 16603–16614, 2023, doi: 10.1016/j. ceramint.2023.02.018.

33. Pulido-González, N., Torres, B., Zheludkevich, M.L., Rams, J., High Power Diode Laser (HPDL) surface treatments to improve the mechanical properties and the corrosion behaviour of Mg-Zn-Ca alloys for biodegradable implants. *Surf. Coat. Technol.*, 402, June, 126314, 2020, doi: 10.1016/j.surfcoat.2020.126314.

34. Vidyasagar, K.E.C., Aggarwal, V., Sinha, S.S., Saha, S.K., Kalyanasundaram, D., Laser based micro texturing of freeform surfaces of implants using a Stewart platform. *Precis. Eng.*, 72, April, 294–303, 2021, doi: 10.1016/j.precisioneng.2021.05.004.

35. Jambhulkar, N., Jaju, S., Raut, A., Bhoneja, B., A review on surface modification of dental implants among various implant materials. *Mater. Today Proc.*, 72, 3209–3215, 2023, doi: 10.1016/j.matpr.2022.12.022.

36. Kostrubiec, F., Pawlak, R., Walczak, M., Division, M.S., Laser modification of properties of materials and elements for electronics of conducting materials. *Proceedings of SPIE - The International Society for Optical Engineering*, 5229, 197–205, 2003.

37. Unune, D.R., Brown, G.R., Reilly, G.C., Thermal based surface modification techniques for enhancing the corrosion and wear resistance of metallic implants: A review. *Vacuum*, 203, June, 111298, 2022, doi: 10.1016/j.vacuum.2022.111298.

38. Deng, Z. *et al.*, Laser cladding preparation of HA-Ag gradient bioactive ceramic coating: A feasibility study. *Surf. Coat. Technol.*, 427, September, 127848, 2021, 10.1016/j.surfcoat.2021.127848.

39. Li, W. *et al.*, A novel method to fabricate micro-nano hierarchical topographies on zirconia dental implant using femtosecond laser. *Mater. Lett.*, 345, 22, 134454, 2023, doi: 10.1016/j. matlet.2023.134454.

40. Hajam, M., II and Khan, M.M., Effect of laser surface texturing on the corrosion behaviour and biocompatibility of zinc hydroxyapatite implant material. *Mater. Today Commun.*, 38, January, 108110, 2024, doi: 10.1016/j.mtcomm.2024.108110.

41. Priyanka, C.P., Keerthi Krishnan, K., Sudeep, U., Ramachandran, K.K., Osteogenic and antibacterial properties of TiN-Ag coated Ti-6Al-4V bioimplants with polished and laser textured surface topography. *Surf. Coat. Technol.*, 474, July, 130058, 2023, doi: 10.1016/j. surfcoat.2023.130058.

42. Menci, G., Demir, A.G., Waugh, D.G., Previtali, B., Laser surface texturing of β-Ti alloy for orthopaedics: Effect of different wavelengths and pulse durations. *Appl. Surf. Sci.*, 489, February, 175-186, 2019, doi: 10.1016/j.apsusc.2019.05.111.

43. Picraux, S.T., Pope, L.E., Tailored surface modification by ion implantation and laser treatment. *Science*, 9, 226, 4675, 615–22, 1984 Nov, doi: 10.1126/science.226.4675.615.

44. Garcia-de-Albeniz, N., Ginebra, M.P., Jimenez-Piqué, E., Influence of nanosecond laser surface patterning on dental 3Y-TZP: Effects on the topography, hydrothermal degradation and cell response. *Dent. Mater.*, 40, January 2023, 139–150, 2023, doi: 10.1016/j.dental.2023.10.026.

45. Huraib, W.M. *et al.*, Influence of rough micro-threaded and laser micro-textured implant-neck on peri-implant

tissues: A systematic review. *Saudi Dent. J.*, 35, 6, 602–613, 2023, doi: 10.1016/j. sdentj.2023.05.025.

46. Trtica, M., Gakovic, B., Batani, D., Desai, T., Panjan, P., Radak, B., Surface modifications of a titanium implant by a picosecond Nd:YAG laser operating at 1064 and 532 nm. *Appl. Surf. Sci.*, 253, 5, 2551–2556, 2006, doi: 10.1016/j.apsusc.2006.05.024.

47. Kalakuntla, N. *et al.*, Laser patterned hydroxyapatite surfaces on AZ31B magnesium alloy for consumable implant applications. *Materialia*, 11, 100693, May, 2020, doi: 10.1016/j. mtla.2020.100693.

48. Ho, Y.H., Vora, H.D., Dahotre, N.B., Laser surface modification of AZ31B-Mg alloy for bio-wettability. *J. Biomater. Appl.*, 29, 7, 915–928, 2015, doi: 10.1177/08853282145511 56.

49. Shirazi, H.A., Chan, C.W., Lee, S., Elastic-plastic properties of titanium and its alloys modified by fibre laser surface nitriding for orthopaedic implant applications. *J. Mech. Behav. Biomed. Mater.*, 124, May, 104802, 2021, doi: 10.1016/j.jmbbm.2021.104802.

50. Wei, X. *et al.*, Surface modification of Co-Cr-Mo implant alloy by laser interference lithography. *Tribol. Int.*, 97, 212–217, 2016, doi: 10.1016/j.triboint.2016.01.039.

51. Yao, H. *et al.*, Femtosecond laser-induced nanoporous layer for enhanced osteogenesis of titanium implants. *Mater. Sci. Eng., C*, 127, June, 112247, 2021, doi: 10.1016/j.msec.2021.112247.

52. C.-H.Y. and Natarajan Jeyaprakash, D.R.K., We are IntechOpen, the world’s leading publisher of Open Access books Built by scientists, for scientists TOP 1 %. *Intech*, 11, tourism, 13, 2016, [Online]. Available:

https://www.intechopen.com/books/advanced-biometric-technologies/liveness-detection-in-biometrics.

53. Wang, Y. *et al.*, Influence of femtosecond laser pulse sequence on the morphology and roughness of titanium surface micro-patterns. *J. Manuf. Process.*, 97, January, 248–259, 2023, doi: 10.1016/j.jmapro.2023.05.003.

54. Tan, C.Y., Wen, C., Ang, H.Q., Influence of laser parameters on the microstructures and surface properties in laser surface modification of biomedical magnesium alloys. *J. Magnes. Alloy.*, 12, 1, 1–26, 2024, doi: 10.1016/j.jma.2023.12.008.

55. Wang, M., Yang, Z., Yang, C., Zhang, D., Tian, Y., Liu, X., The investigation of mechanical and thermal properties of super-hydrophobic nitinol surfaces fabricated by hybrid methods of laser irradiation and carbon ion implantation. *Appl. Surf. Sci.*, 527, June, 146889, 2020, doi: 10.1016/j.apsusc.2020.146889.

56. Mukherjee, S., Optimization of Slurry and Process Parameter on, in: *1st Int. Electron. Conf. Mater*, pp. 0–3, [Online]. Available: http://sciforum.net/conference/ecm-1%0AReview.

57. Chen, Z.C., Chang, T.L., Wu, Q.X., Liu, C.C., Chen, H.C., Huang, C.H., Surface modification of bio-orderly CrTiN thin films with periodic corrugated nanopod structures by picosecond laser ablation. *J. Alloys Compd.*, 938, 168193, 2023, doi: 10.1016/j.jallcom.2022.168193.

58. Slađana, L., Rakin, M., Čairović, A., Maksimović, V., *Slađana Laketić 2019*, Srpski arhiv za celokupno lekarstvo, 147, 7–8, 497–501, 2019, https://doi.org/10.2298/SARH181126054L I. C.-

A[Online]. Available: doi: https://doi.org/10.2298/SARH181126054L.

59. Khoo, L.K. *et al.*, Titanium fixture implants treated by laser in dentistry: Review article. *J. Oral Maxillofac. Surgery, Med. Pathol.*, 31, 6, 381–385, 2019, doi: 10.1016/j.ajoms.2019.08.001.

60. Gupta, R., Naveena A, H., Vadali, M., Bhatia, D., Enhancement of cell attachment on Ti6Al4V via surface modifications using pulsed laser surface melting. *Surf. Coat. Technol.*, 474, October, 130080, 2023, doi: 10.1016/j.surfcoat.2023.130080.

61. Ackerl, N., Bork, A.H., Hauert, R., Müller, E., Rottmar, M., Rationally designed ultra-short pulsed laser patterning of zirconia-based ceramics tailored for the bone-implant interface. *Appl. Surf. Sci.*, 545, January, 149020, 2021, doi: 10.1016/j.apsusc.2021.149020.

62. Shah, F.A., Grandfield, K., Palmquist, A., *Laser surface modification and the tissue-implant interface*, Elsevier Ltd, 2016, doi: 10.1016/B978-0-08-100883-6.00009-5.

63. Liu, Q. *et al.*, Response of MG63 Osteoblast Cells to Surface Modification of Ti-6Al-4V Implant Alloy by Laser Interference Lithography. *J. Bionic Eng.*, 14, 3, 448–458, 2017, doi: 10.1016/ S1672-6529(16)60410-9.

64. Zhang, F. *et al.*, Surface modification of titanium implants by pH-Responsive coating designed for Self-Adaptive antibacterial and promoted osseointegration. *Chem. Eng. J.*, 435, P2, 134802, 2022, doi: 10.1016/j.cej.2022.134802.

65. Harawaza, K., Cousins, B., Roach, P., Fernandez, A., Modification of the surface nanotopography of implant devices: A translational perspective. *Mater. Today Bio*,

12, October, 100152, 2021, doi: 10.1016/j.mtbio.2021.100152.

66. Simões, I.G., dos Reis, A.C., da Costa Valente, M.L., Analysis of the influence of surface treatment by high-power laser irradiation on the surface properties of titanium dental implants: A systematic review. *J. Prosthet. Dent.*, 129, 6, 863–870, 2023, doi: 10.1016/j.prosdent.2021.07.026.

67. Nisar, S.S., Arun, S., Choe, H.C., Plasma electrolytic oxidation coatings on femtosecond lasertreated Ti-6Al-4V alloy for bio-implant use. *Surf. Coat. Technol.*, 464, February, 129553, 2023,, doi: 10.1016/j.surfcoat.2023.129553.

68. Ghosh, S., Abanteriba, S., Wong, S., Houshyar, S., Selective laser melted titanium alloys for hip implant applications: Surface modification with new method of polymer grafting. *J. Mech. Behav. Biomed. Mater.*, 87, July, 312–324, 2018, doi: 10.1016/j.jmbbm.2018.07.031.

69. Zheng, W. *et al.*, Multifunctional modifications of polyetheretherketone implants for bone repair: A comprehensive review. *Biomater. Adv.*, 154, July, 213607, 2023, doi: 10.1016/j. bioadv.2023.213607.

70. Chayanun, S., Chanamuangkon, T., Boonsuth, B., Boccaccini, A.R., Lohwongwatana, B., Enhancing PEEK surface bioactivity: Investigating the effects of combining sulfonation with sub-millimeter laser machining. *Mater. Today Bio*, 22, July, 100754, 2023, doi: 10.1016/j. mtbio.2023.100754.

71. Abdal-hay, A. *et al.*, Fabrication of micropores on titanium implants using femtosecond laser technology: Perpendicular attachment of connective tissues as a pilot

study. *Opt. Laser Technol.*, 148, April 2021, 107624, 2022, doi: 10.1016/j.optlastec.2021.107624.

72. Obilor, A., Sainsbury, W., Pacella, M., Wilson, A., Silberschmidt, V.V., Laser Processing of Polymers for Surface Energy Control of Biomedical Implants. *Procedia CIRP*, 113, March, 558– 563, 2022, doi: 10.1016/j.procir.2022.09.174.

73. Park, J. *et al.*, Improving hydroxyapatite coating ability on biodegradable metal through laser-induced hydrothermal coating in liquid precursor: Application in orthopedic implants. *Bioact. Mater.*, 25, June 2022, 796–806, 2023, doi: 10.1016/j.bioactmat.2022.06.020.

74. Biçer, F. and Toker, S.M., Effects of surface micro-deformation on the cellular response to metallic implant materials. *Mater. Today Commun.*, 37, October, 107273, 2023, doi: 10.1016/j. mtcomm.2023.107273.

75. Wan, Y. *et al.*, Osteogenic and antibacterial ability of micro-nano structures coated with ZnO on Ti-6Al-4V implant fabricated by two-step laser processing. *J. Mater. Sci. Technol.*, 131, 240– 252, 2022, doi: 10.1016/j.jmst.2022.04.046.

76. Xiong, J., Zhang, L., Yu, L., Dai, J., Lv, Q., Using laser etched-array periodic structure surface to construct silver loaded titanium implants with combined efficient antibacterial and osteogenic properties. *Appl. Surf. Sci.*, 641, July, 158533, 2023, doi: 10.1016/j.apsusc.2023.158533.

77. Faeda, R.S., Tavares, H.S., Sartori, R., Guastaldi, A.C., Marcantonio, E., Biological Performance of Chemical Hydroxyapatite Coating Associated With Implant Surface Modification by Laser Beam: Biomechanical Study in

Rabbit Tibias. *J. Oral Maxillofac. Surg.*, 67, 8, 1706–1715, 2009, doi: 10.1016/j.joms.2009.03.046.

78. Vishnu, J. *et al.*, Insights into the surface and biocompatibility aspects of laser shock peened Ti-22Nb alloy for orthopedic implant applications. *Appl. Surf. Sci.*, 586, February, 152816, 2022, doi: 10.1016/j.apsusc.2022.152816.

79. A, R., Das, M., Balla, V.K., Sen, D.D.D., Manivasagam, G., Surface engineering of LENS-Ti-6Al-4V to obtain nano- and micro-surface topography for orthopedic application. *Nanomed. Nanotechnology, Biol. Med.*, 18, 157–168, 2019, doi: 10.1016/j.nano.2019.02.010.

80. Ozturk, A., Anıl€Ozt€urk 2024.pdf, *J. Stomatol. Oral Maxillofac. Surg.*, 2024.

81. Braga, F.J.C., Marques, R.F.C., Filho, E.A., Guastaldi, A.C., Surface modification of Ti dental implants by Nd:YVO 4 laser irradiation. *Appl. Surf. Sci.*, 253, 23, 9203–9208, 2007, doi: 10.1016/j.apsusc.2007.05.048.

82. Kang, S.H., Bengtson, B.P., Heo, C.Y., Various Properties of Silicone Breast Implant Surfaces and Multimodal Techniques for the Functional Surface Modification. *Clin. Plast. Surg.*, 48, 1, 87–99, 2021, doi: 10.1016/j.cps.2020.08.003.

83. Choudhury, D. *et al.*, The impact of surface and geometry on coefficient of friction of artificial hip joints. *J. Mech. Behav. Biomed. Mater.*, 72, May, 192–199, 2017, doi: 10.1016/j. jmbbm.2017.05.011.

84. Milovanović, D.S., Radak, B.B., Gaković, B.M., Batani, D., Momčilović, M.D., Trtica, M.S., Surface morphology modifications of titanium based implant induced by 40

picosecond laser pulses at 266 nm. *J. Alloys Compd.*, 501, 1, 89–92, 2010, doi: 10.1016/j.jallcom.2010.04.047.

85. Carvalho, A. *et al.*, Femtosecond laser microstructuring of alumina toughened zirconia for surface functionalization of dental implants. *Ceram. Int.*, 46, 2, 1383–1389, 2020, doi: 10.1016/j. ceramint.2019.09.101.

86. Tardelli, J.D.C., Loyolla, C.D., Ferreira, I., Kreve, S., dos Reis, A.C., Influence of surface modifications on the fracture resistance of aged zirconia implants: A systematic review of *in vitro* experimental studies. *J. Oral Maxillofac. Surgery, Med. Pathol.*, 36, 1, 1–10, 2024, doi: 10.1016/j. ajoms.2023.06.001.

87. Lei, P. *et al.*, Research status of laser surface texturing on tribological and wetting properties of materials: A review. *Opt. (Stuttg).*, 298, December 2023, 171581, 2024, doi: 10.1016/j. ijleo.2023.171581.

88. Atieh, M.A., Fadhul, I., Shah, M., Hannawi, H., Alsabeeha, N.H.M., Diode Laser as an Adjunctive Treatment for Peri-implant Mucositis: A Systematic Review and Meta-analysis. *Int. Dent. J.*, 72, 6, 735–745, 2022, doi: 10.1016/j.identj.2022.06.026.

89. Hashmi, A.W. *et al.*, A comprehensive review on surface post-treatments for freeform surfaces of bio-implants. *J. Mater. Res. Technol.*, 23, 4866–4908, 2023, doi: 10.1016/j.jmrt.2023.02.007.

90. Amuda, M.O.H. and Akinlabi, E.T., *Trend and Development in Laser Surface Modification for Enhanced Materials Properties*, pp. 92–120, IGI Global, 2016, doi: 10.4018/978-1-5225-0329-3. ch005.

91. De Damborenea, J., Surface modification of metals by high power lasers. *Surf. Coat. Technol.*, 100–101, 1–3,

377–382, 1998, doi: 10.1016/S0257-8972(97)00652-X.

92. Das, K., Balla, V.K., Bandyopadhyay, A., Bose, S., Surface modification of laser-processed porous titanium for load-bearing implants. *Scr. Mater.*, 59, 8, 822–825, 2008, doi: 10.1016/j. scriptamat.2008.06.018.

93. Guan, K., Zhou, Y., Yu, J., Guan, Y., Dosimetry verification of *in vitro* radiotherapy dose via laser polishing of 3D-printed metallic implant surface. *Opt. Lasers Eng.*, 170, 107788, July 2023, doi: 10.1016/j.optlaseng.2023.107788.

94. Sahm, B.D., da Costa Valente, M.L., dos Reis, A.C., Use of surface nanotechnology in 3D implants for antimicrobial action: A systematic review. *J. Oral Maxillofac. Surgery, Med. Pathol.*, 3, 273–277, July, 2023, doi: 10.1016/j.ajoms.2023.08.016.

95. Obayi, C.S. and Nnamchi, P.S., *Surface modification and functionalization of ceramic composites for bone implantation*, Elsevier Ltd, 2023, doi: 10.1016/B978-0-323-85883-0.00020-X.

96. Kr, D., Haldar, N., Kumar, C., Technology, N., *Synthesis and fabrication of magnesium based biomedical implant*, 2nd, Elsevier Ltd, 2024, doi: 10.1016/B978-0-323-96020-5.00269-7.

97. Peng, B., Xu, H., Song, F., Wen, P., Tian, Y., Zheng, Y., Additive manufacturing of porous magnesium alloys for biodegradable orthopedic implants: Process, design, and modification. *J. Mater. Sci. Technol.*, 182, 79–110, 2024, doi: 10.1016/j.jmst.2023.08.072.

Note

*Corresponding author: bupesh.v.k@gmail.com

21
Ion Beam Processing: A Brief Review

Pravin Pawar[1]*, Amaresh Kumar[2] and Raj Ballav[2]

[1]Department of Mechanical Engineering, National Institute of Technology Goa, Cuncolim, Goa, India

[2]Department of Production & Industrial Engineering, National Institute of Technology Jamshedpur, Jharkhand, India

Abstract

Ion beam processing is one of the powerful processes to fabricate nanoscale structures on a variety of materials, specifically, hard and brittle materials. This process can be utilized for various fields like communication, electronics, automobile, and medicine. This technology is used to manufacture micromachining of tools, surgical instruments, probes and different micro/nanosized components. The various ion beam processes such as milling, etching, implantation, and depositions are used to manufacture micro- and nanostructures. In this chapter, a literature review based on focused ion beam process, ion beam process, developed ion beam process, and combined ion beam process are explained briefly.

***Keywords*:** Focused ion beam (FIB), ion beam machining (IBM), ion beam etching, combined ion beam process, ion beam figuring

21.1 Introduction

The ion beam techniques are used for manufacturing special surfaces and coatings. It has a wide range of applications like the manufacturing of medical implants,

screws, catheters, sensors, the creation of nanostructures, surface modification, and micromachining of micromechanical devices [1]. Ion beam machining (IBM) and focused ion beam machining (FIBM) are methods that use ion impact to eliminate surface atoms of material, although they can also involve chemical reactions to create volatile products. These procedures take place in a low-pressure environment to raise the mean free path of the ions between collisions [2]. In ion beam processing, there are several processes like reactive ion etching, plasma etching, reactive ion beam machining, IBM, FIBM, and ion beam-assisted etching that are used for ultrafine machining [3]. In ion beam processing, there are methods like reactive ion beam-assisted chemical etching, Ar ion beam etching, and oxygen reactive ion beam etching [4]. The most widely used ion species for microfabrication are Ga, Si, As, and Be [5]. In this chapter, a brief review of past-to-present research work carried out on various ion beam processing is studied.

21.2 Focused Ion Beam Process

In this section, various types of focused ion beam processes are explained. The focused ion beam process (FIB) is reviewed in terms of focused ion beam (FIB) milling, FIB machining, FIB fabrication, FIB etching, FIB sputtering, FIB deposition, and FIB irradiation.

21.2.1 Introduction of Focused Ion Beam

In the semiconductor industry, the FIB process is a valuable process for photomask repair, integrated circuits, surface probing of substrate materials, semiconductor doping, and lithography. This process used to analyze the microstructure, which are made from methods such as three-dimensional (3D) tomographic imaging, transmission

electron microscopy, 3D electron channeling contrast imaging, 3D electron backscatter diffraction, micromechanical testing techniques, and probe tomography [6, 7]. Focused ion beam systems are a very effective process for precision micromachining in various applications. This type of machining process involves ion beam-induced surface chemistry for deposition and etching, micro- and nanomachining through physical sputtering, and scanning ion microscopy. Focused ion beam microfabrication methods, including ion beam-induced deposition and physical sputtering, provide a highly flexible and accurate method for fabricating micron and submicron-scale structures. The FIB sputter-etching is an efficient process for repairing prototypes and restructuring prototypes of developed devices, as well as for preparing samples for imaging or analyzing specific regions. This process can be applied in microelectronics, biosciences, and micromechanics [8]. Focused ion beam processes have been extensively utilized in failure analysis, micro- and nanofabrication, and prototyping for research. The components of an FIB system are an ion optical system for concentrating a spot down to a few nanometers, a source that emits ions from a very small location, and a scanning device for precise positioning of the focused beam in lateral directions. The ion beam interaction with the workpiece material changes its surface properties and surface structure by using different methods like ion beam-induced etching, ion milling, deposition, and ion implantation. This technology offers the ability to create nanoscale structures with high precision without a mask or direct focused beam writing [9, 10]. Focused ion and electron beams are employed to selectively deposit conducting or insulating films in specific locations. The primary uses of this process include designing integrated circuits, making modifications to prototypes, repairing masks, and machining microsystems. The effectiveness of this technology has

been proven in various applications, including mask repair, maskless lithography, modification of integrated circuits (IC's), tip of tool modification, micromechanical applications, micromachining, creation of 3D structures, and production of microelectromechanical system (MEMS) sensors, transmission electron microscopy (TEM) samples that retain most of the microstructural details of stress corrosion cracks in austenitic alloys [8, 11–13].

Focused ion beam technology is set to have a significant effect on nanofabrication due to its exceptional advantages in terms of precision, resolution, flexibility, and cost. Moreover, it possesses the unique capability to both add materials through implantation and deposition, as well as remove materials through milling and etching. Focused ion beam-based nanofabrication includes four major methods, such as implantation, milling, ion assisted etching, and ion-induced deposition of material [14]. The commercially available ion sources utilized in FIB are classified into three types: gas field ion sources, plasma ion sources, and liquid metal ion sources [15]. The FIB technology was utilized to fabricate samples at the micro/nanoscale by deposition and milling processes. The various input parameters in this process are: ion dose, precursor gas, ion energy, dwell time, current density, incidence angle, overlapping, refresh time, spot size, ion current, and ion species. The FIB-CVD technology was used to manufacture complex 3D micro- and nanoscale structures [16]. In microfabrication, it offers benefits compared to current photolithography and other micromachining methods. These benefits include improved resolution with minimal lateral scattering, the ability to work without masks, better resolution of small features, and flexibility with different materials and shapes [5]. Focused ion beam milling is known to be a highly accurate and flexible technique for creating prototypes or custom structures. This technology provides a precise and flexible

means of producing small structures at micron and sub-micron scales [17].

21.2.2 Focused Ion Beam Milling

Dai *et al.* [18] fabricated two-dimensional (2D) metal ferroelectric metal nanocapacitor arrays through FIB milling with serial and synchronal modes. They observed that more uniform arrays were obtained in the synchronal mode compared to the serial mode; however, the surface of the arrays was significantly damaged. In Dorronsoro *et al.* [19], a novel method was created to measure residual stress on the surface of difficult-to-cut parts with greater precision compared to traditional X-ray diffraction methods. This method involves measuring surface displacements that occur after stresses are moderately relieved through machining a thin slit perpendicular to the surface. The displacements around the slit were then measured by a new digital image correlation algorithm that utilizes Fourier analysis. Inkson *et al.* [20] examined the changes in stress levels in alumina samples with concentrated residual stresses near nano-indents and scratches. It was discovered that the number of cracks near the nano-indentation sites in alumina material. Martynowycz *et al.* [21] created lamellae of macromolecular protein crystals, which is an effective method for continuous rotation microcrystal electron diffraction. They obtained ideal thickness and were not severely affected by this process. The obtained structure size was between 100 and 300 nm. Martynowycz *et al.* [22] developed a protocol used for FIB milling in the creation of crystalline lamellae microcrystal electron diffraction. Polovinkin *et al.* [23] found that using FIB milling at cryogenic temperatures can effectively eliminate excess host lipidic mesophase matrix. They observed that

cryogenic FIB milling can generate excellent lamellae from crystals grown in lipidic mesophases.

Drobne *et al.* [24] utilized FIB/scanning electron microscope (SEM) to mill and capture images of digestive gland cells. The purpose of the research was to record how FIB interacted with the surface of the biological specimen during analysis. In Pekin *et al.* [25], there were sections discussing electron transparent Al and Si alloys using both Ne and Ga ion beams for a direct comparison. The use of Ne FIB milling does not greatly decrease the undesirable effects caused by the FIB. Though, the Ne ion beam allows for more accurate milling. Presser *et al.* [26] found that FIB milling has proven effective in preparing metallurgical samples and various multilayer thin films for electron microscopy. Although the semiconductor industry frequently utilizes FIB processes, Also, it is used for selectively preparing small features for SEM and potentially TEM analysis. In Lehrer *et al.* [27], the technique presented for fabricating metal coated atomic force microscopy probes using FIB milling allows for quick and consistent production of superior-quality aperture probes. The smallest aperture size achieved was 50 nm. Savenko *et al.* [28] created customizable and exchangeable tips for atomic force microscopy with extremely high aspect ratios using lateral FIB milling. The aspect ratios reached were as high as 45 and the tip diameters were as small as 9 nm through a deformation-suppressing writing strategy. Liao *et al.* [29] used a reliable technique to produce nanometer notches on 3Y-TZP, ensuring uniformity across the specimen’s width. The nanometer-wide notch tip was lower than the grain size of 3Y-TZP. Tanaka *et al.* [13] created a micromanufacturing technique that has exceptional micro-assembly ability through the use of FIB milling. In Wilhelmi *et al.* [30], the intricate and large nanopatterns can be created using FIBs, allowing for

precise control over the depth, width, height, and placement of patterns across multiple writing areas. In Han *et al.* [31], a mathematical FIB milling model was used to predict the height of nanopatterns on a silicon surface by varying the overlap. The simulation results showed that the developed model was more accurate in predicting the height. Goswami *et al.* [32] found that optimal parameters for single crystal silicon material were a current of dwell time of 1.15 µs, 30.15 pA, and an overlap of 73.81% during the FIB milling process. The resulting optimized output results were a surface roughness of 1.90 nm and a material removal rate of 7.414×10^{-3} $\mu m^3/s$. Chen *et al.* [33] examined the effect of He-FIB line scanning on the silicon substrate. They observed that helium bubbles initially appear in the lower portion of the amorphous area. As the dose increases with a constant beam energy and the helium bubbles had a greater. Ridder *et al.* [34] found that selecting an appropriate ion beam scanning method can greatly enhance the quality of circular holes created in a silicon substrate through FIB milling as compared to linear raster scan. In Vermeij *et al.* [35], an innovative method of masking has been implemented to prevent damage caused by FIB. The superiority of the topmost surface of multiple micro pillars was monitored using high angular resolution 3D electron backscatter diffraction. The high angular resolution 3D electron backscatter diffraction offers a precise assessment of the level of FIB damage on the surface. The clear diffraction patterns were achieved near the hole by using the umbrella method. Therefore, the umbrella approach proves to be an effective and adaptable tool to assist various FIB techniques. Li *et al.* [36] investigated a new technique, *i.e.*, the moire technique, that was suggested and shown to be effective in determining the strain in MEMS structures. This method involves creating nano grating lines with a 140-nm spacing

and 70-nm width on the MEMS structures using ion milling. This FIB moire approach has various possible uses in the mechanical measurement of MEMS devices. In Li *et al.* [37], a new method for measuring residual strain in microstructures using the FIB moire technique was developed and demonstrated. This method involves directly writing a nanograting on the microstructures using ion milling. The FIB moire pattern was created through the interference of raster scan lines and specimen grating. The FIB moire technique shows potential for various mechanical metrology applications in MEMS. In Chen *et al.* [38], a process known as “sketch and peel” was proposed and demonstrated to facilitate FIB milling for the direct and quick production of plasmonic nanoparticles and structure. The reliability of this method was maintained by the creation of a sidewall coating through ion milling induced redeposition. In comparison to electron-beam lithography, this FIB-based approach offers additional functionality for the fabrication of plasmonic materials. Li *et al.* [39] suggested an approach for determining the FIB processing microstructure contour under specific process and device conditions, using minimal experimental data. They investigated how redeposition and sputtering affect profile formation during focused ion beam scanning, describing the distribution of these effects at each pixel with Gaussian equations (single-Gaussian and double-Gaussian models). Stoyanov *et al.* [40] developed a framework for modeling that combines computational models to simulate FIB milling of specific shapes, assess process capability, conduct risk analysis, and optimize the process. Yoon *et al.* [41] examined the effect of new path generation algorithms on FIB milling. These algorithms, based on traditional machining techniques used to determine the FIB scanning paths. It was found that the scanning path played a crucial role in the quality of the end

product without significant time loss. The balanced raster and backstitch raster patterns were identified as producing the highest quality results in terms of squareness and smoothness of the pocket. The appropriate scanning path can be chosen based on the desired squareness, surface roughness, or efficiency. Buchnev *et al.* [42] demonstrated that utilizing prior manufacturing experience in deep learning can accurately forecast the final appearance of structures created through FIB milling with over 96% accuracy. The predictions are generated quickly, in just a few milliseconds, allowing for real-time deployment of the methodology to speed up optimization and enhance the reproducibility of FIB processing. A neural network has the ability to predict with precision the appearance of samples in scanning electron microscope images. Kim *et al.* [43] presented the code AMADEUS 3D, a program that can recreate surface topography in three-dimensional space while considering redeposition and sputtering. The program accurately predicts the maximum depth and overall shape of structures. Hofmann [44] investigated defects and the residual lattice strains generated by glancing-incidence FIB machining. The findings revealed that using 30 keV glancing incidence FIB milling resulted in lesser significant defects. Korsunsky *et al.* [45] created ring-shaped trenches on samples with residual stress, leading to controlled strain relief at the surface by FIB milling. The digital image FE modeling confirms that strain changes on the surface match experimental results as the depth of ring drilling increases. This new technique offers a significant advancement in accurately evaluating residual stress at the submicron level. Dovidenko *et al.* [46] modified surfaces on a millimeter scale with nanopatterns as small as 30 nm. The precision of FIB nanoscale patterning was demonstrated in millimeter-scale regions, *i.e.*, Au films were sputtered on quartz substrates, showing

surface modification. This method can be used on both bulk materials and ultrathin films. It was noted that the modified surface was clean of contaminants, except for those inside the individual wells. Charandabi *et al.* [47] studied the major factors influencing the parameters for the sputter yield of a nanoporous material. They found that porosity and roughness were the most dominant factors in the sputter yield. The nanoporous structure was a more significant factor in the characterization of the sputter yield of materials than the porosity itself. Luo *et al.* [48] examined the effect of atom redeposition in focused ion beam manufacturing of nanodots using a theoretical simulation that utilizes the 3D surface structure model and experimental research. The results indicate that over one-third of the milling depth is decreased as a result of the redeposition consequence during the focused ion beam nanofabrication procedure. The atom's redeposition plays a crucial role in surface creation during nanoscale fabrication. Dhamodaran *et al.* [49] explored how different factors influence the creation of nanodots during the processing GaAs without as well as with XeF_2 gas flow. The use of a reactive gas such as XeF_2 can regulate the formation of nanodots on the GaAs surface during FIB processing. Bhavsar *et al.* [50] analyzed the machinability of high-speed steel by FIB milling. They found that the most influencing factors for maximum material removal were a high beam current, high angle of incidence, a maximum extraction voltage, minimal overlap between beam diameters, and dwell time has a lesser impact on material removal rate (MRR). The lowest achievable surface roughness was below 12.3 nm, and the higher material removal rate was 0.3984 m^3/s. The beam current was identified as the most influential factor in determining both surface roughness and MRR. As discussed in Bhavsar *et al.* [51], FIB milling is a manufacturing process on a micro-

and nanoscale that is used to fabricate components with high resolution. This process is commonly used to create microsurgical instruments, micromachining tools, scanning probe microscopy probes. They investigated the results of the deposition effect of high speed steel (HSS) work material during FIB milling. It was discovered that redeposition had a significant effect on HSS material during FIB milling of square trenches. The modified mathematical model provides more accurate simulated results for sputtering depth. Li *et al.* [52] found that when the ion beam fluence increased, the sputtering rate reduced in a non-linear manner. They observed that the sputtering rate improved as the beam current increased. They successfully created nano-grooves with an aspect ratio greater than 3. Sabouri *et al.* [53] investigated the influence of varying the pixel dwell time during Ga-focused ion beam milling on a crystalline Si surface. It was noted that longer dwell times resulted in reduced damage and a higher sputter yield. Lebedev *et al.* [54] developed the method for manufacturing arrays of nano-channels in silicon glass chips with the help of FIB milling. They found etching time was the most influencing factor on the width and depth of the produced nano-channels also the effective diameter of the nano-channels was 1.5 mC/m^2 and 20 nm, respectively. Borgardt *et al.* [55] observed that the focused ion milling rate intended for the redeposited workpiece material was 1.3 times more in comparison to crystalline silicon material. Tseng *et al.* [6] found that the FIB milling was effectively processed on a two-layer substrate. The material used in this research was a two-layer substrate with a 60-nm thick gold layer on a silicon wafer. It was found that the depth of the channel increased as the dwell time raised. Salvati *et al.* [56] developed innovative technique to analyze the amorphous layer formed in a silicon material when exposed to a Ga-ion beam. The

findings suggest that the development of eigenstrain in the amorphous layer is not primarily due to the transformation of volume that takes place in the amorphous layer. In Bhavsar *et al.* [57]: FIB milling is a fast and precise method used for micro- and nanofabrication of devices. They studied how cemented carbide can be machined using FIB milling. They observed that the most influencing factors are high beam current, minimal overlap, increased angle of incidence, and high extraction voltage for a higher MRR. Conversely, a larger angle of incidence and lower beam current resulted in smoother surfaces. The surface roughness obtained a minimum of 5.6 nm, while the maximum material removal rate was measured at 0.4836 mm^3/s. The dwell time was found to have a lesser effect on surface roughness and material removal rate. Bhavsar *et al.* [58] determined that the MRR and surface roughness during FIB micromilling of cemented carbide. It was found that the beam current was the most important factor in this process. They achieved a surface roughness of 5.6 nm and a material removal rate of 0.4836 $\mu m^3/s$. Martin *et al.* [59] machined single crystal diamond without a mask by using a focused oxygen ion beam. The resulting damage layer from the oxygen ions can be eliminated using non-invasive postprocessing techniques like localized electron beam induced chemical etching. The damaged layer can also be removed through carbon etching induced by an electron beam with the assistance of H_20. In Wu *et al.* [60], a cost-effective technique was created to produce surfaces that are highly hydrophobic and anisotropic. This technique involves computerized numerical control (CNC) machining with diamond tools that have been microstructured by an FIB process. This allows for parallelization and results in a machining speed that is at least four times faster than alternative methods. Ono *et al.* [61] explained a technique for sharpening the edge of a single crystal diamond cutting

tool. The method not only sharpens the edge but also creates a flat surface known as the “new rake face” by adjusting the beam angle. This newly created surface can act as the “effective rake face” during precision cutting. The results of machining were influenced by factors like beam current and voltage, which influence the beam intensity and therefore the etching rate changes. Yan *et al.* [62] examined how different FIB processing parameters impact the tip morphology of the multi-tip diamond tool. A higher beam current and acceleration voltage significantly enhance processing efficiency. Nevertheless, it becomes challenging to maintain machining accuracy with a high beam current. Conversely, precision was better achieved with a relatively low beam current. The dwell time does result in material redeposition but does not influence processing efficiency. Burns *et al.* [63] considered the FIB microscope to be beneficial when used for machining and patterning ferroelectric materials. Wicki *et al.* [64] manufactured lenses by FIB milling to mill all apertures, ensuring precise alignment within a tolerance of around 300 nm. Chen *et al.* [65] investigated how the profile error was formed and how it can be compensated for in focused ion beam bitmap milling of 3D optical microstructure. They observed that increasing the beam current can make FIB milling more efficient, but it can decrease processing accuracy. The process of having a higher beam overlap ratio can lead to a smoother surface. Fu *et al.* [66] describe the development, fabrication, and evaluation of diffractive optical elements (DOEs) with smooth surfaces for fiber coupling. They successfully created minimum diameter of 65 µm through FIB process. The experimental study revealed a coupling efficiency of 75%, demonstrating the effectiveness of the DOEs in meeting application specifications and being produced with FIB. In Huson *et al.* [67], an ion beam with a specific focus has been utilized to

cut individual carbon fibers and fibers within an epoxy composite in order to create flat surfaces for nano-indentation. The process of FIB milling causes surface damage to the carbon fibers and spreads disordered carbon debris to the surrounding areas. This debris has been found up to 100 mm away from the milling location. In Li *et al.* [68], a method for micromachining photonic bandgap fiber (PBGF) by FIB milling process was investigated. The PBGF gas cell was used to measure the absorption of C_2H_2 and CH_4 gases. The longer PBGF resulted in higher sensitivity and improved signal quality for weak absorption lines. Hu *et al.* [69] investigated particles generated through FIB milling on glassy carbon material. It was observed that nanosized particles were frequently present on the surface-machined patterns. The fast-repetitive scan mode was preferable because it produced fewer particles. Youn *et al.* [70]: in an experimental study, repetitive pass milling was employed with FIB to create glassy carbon (GC) molds without the need for masks or resist. These GC molds were then used to imprint glass for the production of microfluidic components and it was observed that there were dimensional discrepancies among the glass and the GC mold materials. Youn *et al.* [71] utilized a focused ion beam to create micro-molds made of glassy carbon (GC). They observed that by employing a repetitive pass technique during FIB milling, nano- and microstructures were achieved with flat channel bottoms and almost perpendicular sidewalls. It was observed that utilized FIB milling was the slowest process, but it resulted in the highest machined surface quality, with a surface roughness value ranging from 4 to 30 nm depending on the depth of milling. When femtosecond lasers were used in conjunction with FIB milling, it allowed for the fast production of superior quality microstructures over a large region. Taniguchi *et al.* [72] successfully machined a lens with a

depth of 203 nm and a diameter of 2.93 µm on a GC material using FIB with dwell time changing. Sarkar *et al.* [73] discovered ultrafine grains in the subsurface of a focused ion beam machined tantalum surface. The findings indicate that FIB imaging methods can effectively detect ultrafine grains at a nano scale level. Xiao *et al.* [74] fabricated ultrafine-grained aluminum and single-crystalline aluminum by using xenon and/or gallium ions in FIB milling. The yield strength of the material remains unaffected by the different ions. In contrast, the strength of ultrafine-grained aluminum decreases as the Ga dose increases, leading to noticeable variations in the resulting microstructures and deformation patterns. Jamaludin *et al.* [75] observed that the aspect ratio of microholes was dissimilar for various materials like zinc, copper, silicon, and aluminum. The sputter yield of materials plays a major role in the depth of the FIB milling. The long dwell time, low beam current, and acceleration voltage parameters provide a high aspect ratio of a microhole. In Ay *et al.* [76] a method was developed to mill deep grating structures in KGLW:Yb^{3+} using FIB. They observed that redeposition effects were minimized by varying pixel resolution distribution and dwell time for the same dose per area. Hambe *et al.* [77] developed a unique approach to producing ferroelectric nanostructures without any damage by using an FIB process. In this approach, by applying a conventional e-beam photoresist and then treating it with a dilute acid solution, nanostructures of varying sizes between 1 µm and 250 nm were formed in a lead zirconate titanate material. Kim *et al.* [78] studied the ion beam sputtering system to reduce the surface roughness of the backlight unit die and mold material. The mold material and surface roughness of die was found to decrease from around 900 nm to 500 nm through the application of a uniform Ar ion beam sputtering process. Hung *et al.* [79]

examined the micromachinability of silicon using FIB sputtering at a normal incident angle. They observed that increasing the dwell time, pixel spacing, ion dose, and accelerating voltage resulted in greater sputtering depth, and they achieved a surface roughness of 2–5 nm. In Ali *et al.* [80], a micromilling tool created by using FIB sputtering was utilized for machining microchannels. The microstructures were able to achieve the greatest aspect ratio of 13:1. The FIB sputtering manufacturing processes were used for micromilling of tools, nanopillars, sharp AFM tips, and nanopores for applications in micro-opto-electromechanical systems (MOEMS), MEMS, Bio-MEMS, and more. In Picard *et al.* [81], tools were produced using high speed steel material, tungsten carbide material, and single crystal diamond with various face designs like triangular, rectangular, and complex shapes. The focused ion beam tools were used in ultra-precision microgrooving experiments, and they found that the machined groove closely replicates the face of the microtool. The cutting of microgrooves on polymer rods having a pitch of 40–150 µm and diameter of 3 mm results in groove arc lengths exceeding 12 cm and groove roughness usually below 0.2µm. Choi *et al.* [82] examined FIB milling diamond cutting tool edge sharpness. The platinum coating layer on diamond tool protected as well as reduce damage during FIB milling process. In Lee *et al.* [83], a novel approach was presented to minimize the geometric error in FIBM. They suggested in this study involved using a process control strategy. An algorithm was developed to measure the amount of redeposition after to each production cycle then adjust the subsequent process plan accordingly. This algorithm could generate an accurate computer-aided design file to be used in the machining process. The experiments showed a significant enhancement in micro-sized pocket machining.

21.2.3 Focused Ion Beam Machining

In Prewett *et al.* [84], focused ion beams are utilized to remove undesired material from IC circuits and masks through micromachining. A study conducted experimentally identifies various challenges primarily linked to the elevated energies of beams needed for precise micromachining. In Sun *et al.* [85], a prototype fiber side optical sensor created effectively by using FIB machining. The sensor includes an extremely precise reflective mirror measuring 10 µm x 10 µm having a surface roughness of 10 nm. In Chkhalo *et al.* [86], a high-performance facility was discussed. This facility allows for the production of optical surfaces in various shapes, such as complex concave or convex shapes. The precision of the effective roughness and surface shape achieved through this facility was at a sub nanometer level. In Han *et al.* [87], an optical fiber tip was engraved with a phase hologram using an FIB system, resulting in the emergence of a ring-shaped beam from the tip of the fiber. The process of FIB machining was carried out for about 45 min at 30 kV and 200 pA. Madison *et al.* [88] applied a layer of chromia, Cr_2O_3, onto silica substrates, SiO^2, which was found to dissipate charge when exposed to an electron beam. The chromia film was observed to be mostly amorphous with nanometer-level roughness. These findings indicate that using sacrificial masking could facilitate the rapid prototyping of intricate devices. Hosokawa *et al.* [89] created a micro-die with a very smooth surface at the nanometer level for Co-less polycrystalline tungsten carbide. The Vickers hardness of Co-less tungsten carbide was significantly greater than that of tungsten carbide with 10 wt% Co. This means that the Co-less tungsten carbide micro-die made with FIB machining was well-suited for use as a die in micro-forging. Joe *et al.* [90] suggested the detection of material

interfaces through monitoring of secondary electron images obtained during the FIB process. To determine endpoints for the FIB processes, the mean and skewness of the gray-level histograms of the secondary electron images were assessed. Miyamoto *et al.* [91] investigated the process of creating micro-mechanical components using Ga^+ and Au^+-focused ion beams at 30 keV. It also looked into the properties of polycrystalline silicon and developed a computer simulation method to predict changes in patterns etched into a polycrystalline silicon wafer. The sample treated with Au^+ ions at ion incidence angles ranging from 0° to 70° exhibited a smooth surface. Hung *et al.* [92] observed that the process factors of gallium FIB machining were optimized to improve micromachining of single-crystal silicon. When increasing the ion dose, accelerating voltage, extending dwell time, and shortening pixel spacing, it led to increased sputtering depth. The same factors also influenced MRR. They achieved surface roughness between 2–5 nm. Motz *et al.*, [93] formed micro-sized bending copper beams ranging in thickness from 7.5 to 1.0 um by using FIB process. In Hosokawa *et al.* [94], the nanocrystalline and sub-microcrystalline nickel samples were processed using a focused Ga^+ ion beam at various doses. The roughness of the surface increased as the ion dose increased. The nanocrystalline nickel surfaces were found to be smoother compared to the sub-microcrystalline nickel surfaces. In Davies *et al.* [95] the focused ion beam deposition (FIBD) and focused ion beam micromachining (FIBM) methods were utilized to modify various materials at the nanoscale. The resolution in the direction of the beam was influenced by the scan input parameters used for beam deflection. They achieved a control resolution of 10 nm during machining and deposition rates around 0.1 nm/s. Yang *et al.* [96] investigated the method for controlling micro/nano components at the micro/nanoscale,

which involves utilizing a combined FIB system consisting of a micro manipulator, gas injection system and scanning electron microscope. This integrated FIB approach effectively created micro gears, significantly enhancing precision by over thirty times when compared to conventional gear production methods. This micromanufacturing process serves as a valuable tool for constructing and integrating micromachines. Madison *et al.* [97] studied the fundamental trade space of throughput and resolution. The process involves creating and analyzing intricate test structures using chromia and silica to observe how the bilayer responds to a focused beam of gallium cations. In Lalev *et al.* [98], a new and effective method for preparing data was suggested for layer-based FIB processing of intricate three-dimensional (3D) micro/nanostructures using 3D CAD data directly. The technique allows for the easy design of complex surfaces in any 3D CAD software and after that transforming them into GDSll streams for FIBD or sputtering. The experiments demonstrated that there was minimal deviation from the lateral dimensions. Sun *et al.* [99] utilized a predictive divergence compensation technique that can assist in achieving precise 3D structures with FIB bitmap milling, and selecting the appropriate pixel spacing can minimize the overlap effect. This method significantly enhances the accuracy of the machined surface. In experiments with FIB milling, various microstructures like parabolic, sinusoidal, hemispherical, and nano-hemispherical structures have been successfully produced using traditional bitmap milling and proposed divergence compensation methods. In Felicis *et al.* [100], a novel method was created for generating intricate patterns on a micro- and nanoscale with great precision. A distinct sampling strategy was employed to enhance the transformation process from a e3D-meshed CAD model to the FIB digital to analog converter. A

pyramid and a hemisphere were machined and distinguished from shapes produced by traditional methods. They observed that the approach was highly efficient in creating intricate shapes. The results demonstrate that a spatial resolution of less than 100 nm can be achieved by using this methodology. In Sun *et al.* [101], a new innovative approach was successfully developed for micro- and nanofabrication, focusing on process planning, haptic design, and manufacturing. This method offers a real-time 30 solution for efficient production of micro- and nano-gratings using FIBM. They observed that by integrating virtual haptics simulation into FIBM, users can effectively optimize and plan fabrication process factors for the cost-effective and precise manufacture of micro- and nano-gratings. Wollschläger *et al.* [102] investigated how the depth of the damaged layer in a thin-film piezoelectric lead zirconate titanate was influenced by FIB machining parameters. The findings demonstrate that the depth of the Ga^{+}-implanted layer decreases as the inclination angle decreases, while the Ga concentration in the implanted layers can be linked to ion energy and ion dose. In Lehrer *et al.* [103], FIB processing can lead to the creation of defects, which can vary from amorphization to gallium precipitation. The study explored gallium contamination and implantation, along with defect formation during FIB processing. The formation of defects was examined using TEM. In Chao *et al.* [104], zinc oxide nanowire ultraviolet sensors were created through the process of machining and the thermal oxidation of metallic zinc structures. In Jud *et al.* [105], FIB technology is a useful process for examining specific properties of materials at the micro/nanometer scale through processes such as cross sectioning, marking, and structuring.

21.2.4 Focused Ion Beam Fabrication

In Orbons *et al.* [106], using the macro-channeling technique, Rutherford backscattering spectrometry was used to analyze high aspect ratio sub-micrometer periodic structures created through FIB lithography. Bass *et al.* [107] created a new method to accurately define and insulate Nb/Al-AlOx/Nb superconducting insulating-superconducting (SIS) tunnel junctions as small as 0.2 μm^2. This innovative technique enables the production of sub- and half-micron SIS junctions using FIB technology. Kim *et al.* [108] explored a promising method for creating 3D micro- and nanostructures using 3D FIB fabrication. This method allows for precise control through the scanning and etching of ion beams. The three-dimensional focused ion beam etching process demonstrated in the study shows potential for producing complex 3D devices. The results suggested that this newly developed FIB etching system could be valuable for manufacturing nanoscale 3D structures. In Kitamura *et al.* [109], a 3D characteristic was created in an optical microlens by FIB process. The shape of the lens was achieved by controlling the dwell time and beam positions during the sputter machining process. The lens, which has a slightly curved surface having a radius of 1.88 mm was produced through FIB machining. In Nesprías *et al.* [110], the 3D micromachining was conducted on x-cut lithium niobate crystals by a high-energy, heavy-ion beam. The structures created exhibited precise outlines, nearly vertical edges, and smooth surfaces. Wang *et al.* [111] made a nanoscale dual-step by FIB process. Modrzynski *et al.* [112] created new samples using various materials and methods to enhance efficiency. They experimented with a novel approach using FIB patterning for quickly prototyping PhC patterns on scintillators. In Guenol *et al.* [113], molecular dynamics (MD) simulations were done to

study the effects of Ga^+ irradiation on silicon using two different geometries. In unstrained silicon, the amorphized areas have a lower density compared to amorphous silicon created through the standard melt-quench process. Kim *et al.* [114] studied the charging effect on a ZrO_2 sintered body caused by Ga ion beam irradiation by closely examining SIM images and changes in Ga ion intensity. As the intensity of Ga ions increased, the charging effect on the ZrO_2 sintered body improved.

21.2.5 Focused Ion Beam Etching

Focused Ion Beam etching in Salut *et al.* [115]: FIB techniques have been effectively used to create high frequency surface acoustic wave (SAW) devices. There is potential for further advancing the technology to produce SAW devices with a 500-nm wavelength. In Hansel *et al.* [116], ion beam etching technology for surface finishing is highly reliable and predictable. The efficiency of the machine and quality of results confirm that ion beam etching is an excellent and effective tool for precision surface processing in current and upcoming technology. In Kuball *et al.* [117], FIB etching was utilized in the creation of nanoscale GaN structures. It required gallium ion beam currents ranging from 1 to 4 pA to manufacture such small GaN structures. The fabrication process involved creating GaN structures as 20–30 nm in diameter through the use of FIB etching.

21.2.6 Focused Ion Beam Deposition

Lipp *et al.* [118] focused ion and electron beams were utilized to deposit conducting or insulating films in specific areas. They are commonly used in designing integrated circuits, modifying prototypes, fixing masks, and fabricating microsystems. The material deposition

efficiency in electron beam induced deposition is influenced by beam energy in a similar manner as the secondary electron yield induced by the electron beam. Fu *et al.* [119] microfabricated a lens on the emitting surface of the laser diode with a wavelength of 635 nm using FIB deposition. This technique involves depositing SiO_2 directly on the emitting surface of the laser diode using FIB. The direct deposition of SiO_2 in one step allows for the incorporation of specific micro optical elements at precise locations on micro-devices like micro-opto-electro-mechanical systems (MOEMS), making it suitable for post-processing surface-relief microstructures.

21.3 Ion Beam Process

The ion beam process includes several techniques such as machining, etching, deposition, figuring processes which are explained in this section.

21.3.1 Ion Beam Machining

Arimatsu *et al.* [120] developed an ion beam milling machine intended for precise, very fine and high-speed machining. This machine was tested on aluminum and copper materials. The high level of precision and exceptional throughput can be achieved by keeping machining deviations at +3% or below. In Davies *et al.* [121], the developed ion beam (IB) milling apparatus, which was a Kaufman type source and was used to give argon ions with energy of 1.5 kV also current densities up to 25 mA/cm^2. They developed algorithms for computer control to control the rotation, position, and orientation of the workpiece. They successfully made surface texture, polishing, holes, grooves, and slots on refractory metals. They controlled process parameters like point of incidence

on the workpiece, angle of incidence, dwell time, current density, and ion energy. In Miyamoto *et al.* [122], a technique was developed for the IB fabrication using masks created through wet etching and lift-off approaches in order to create intricate patterns in a die. They successfully fabricated dies with a surface roughness of 0.1 µm and a flatness of under 0.5 µm. Miyamoto *et al.* [123] developed a new simulation technique for forecasting the changes in profiles and angles of facets on hemispherical objects when they were rotated at a consistent tilt angle during IB machining. Bauer *et al.* [124] created dot and nanoscopic ripple patterns on titanium materials through exposing them to 1.5 keV argon ions at a perpendicular angle. Miyamoto *et al.* [125] fabricated opto-mechanical and opto-electrical devices by IB fabrication process. They machine-cement carbide chips, which had a grain size of 0.5 µm and a 1.0-keV argon ion, and gave a fine surface finish. In Liang *et al.* [126] the rate at which amorphous SiO_2 (fused silica) was removed by Ar^+ ions with 600 to 1200 volts rises as the dwell time and ion energy increase to varying degrees, but reduces exponentially as the work distance increases. The high-precision mirror figure shape, after machining, has a surface roughness ranging from 0.43–0.44-nm root mean square. In Besserer *et al.* [127], a technique for preparing samples using ion beam-slope cutting was employed. The method enables the successful preparation of voids as small as 10 nm for examination by SEM. They observed improved detection of voids smaller than 0.04 mm^2. In Tsuchiya *et al.* [128], ion beam machining was carried out on gauge block alloy steel using oxygen and argon ions to study how the residual oxidized layer impacts surface roughness enhancement. The research revealed that utilizing oxygen-ion beam machining is successful in enhancing surface roughness. In Shima *et al.* [129], ion-beam machining was utilized to analyze how it affects the surface roughness of

ally steel. The depth of machining increases in a linear fashion as time progresses. However, during the initial stages of machining (until a depth of approximately 30 nm), the surface roughness was unchanged. As the process continues, the surface roughness starts to increase over time. It was observed that lower ion current density and ion energy result in decreased surface roughness. The optimal beam angle for maximum machining depth was found to be around 50°, whereas the minimum surface roughness was achieved at angles exceeding 70°. In Levinson *et al.* [130], ion beams and thermal processes are now considered important in the field of lithography. One example of their importance is using an ion beam to reduce line edge roughness (LER) in photoresists. He *et al.* [131] investigated ion beam lithography as a potential method for micro/nano and nanomachining polymeric materials. The findings indicated that utilizing masked ion beam lithography has the capability to change both the hydrophobic properties and surface topography. In Carter *et al.* [132], the principles of wavefront propagation were used to explain how surface structure changes through ion bombardment induced sputtering erosion of solids. This method was also applied to IB polishing of rough surfaces and shaping desired contours on both large and small area systems. In Akel *et al.* [133], the results indicate that the mean energy of the beam ions was influenced due to the type of gas, and it rises as the mass of the gas ions increases. Miyamoto [134] formed or sharpened diamond tools by using ion beam machining. They observed that combining mechanical pre-finishing and IB machining can be beneficial for the sharpening or formation of diamond tools. Reference [3] implemented a novel method for enhancing the sharpness of diamond knives through the use of different type of beam sputtering. They observed that the material removal time with the O^+/O_2^+ beam was

better than the Ar^+ beam. In Miyamoto *et al.* [135], the process involves sharpening diamond tools that were pre-finished using mechanical lapping process and creating small negative lands on the cutting edges of these tools through the IBM process. This process also improved the straightness of the cutting edge. In Drummond *et al.* [136], the beam diameter can be decreased to less than 0.5 µm, enabling even more precise machining. It is important to consider that when using fine beams for deep cuts, the redeposition of sputtered material on the edges of the hole or groove can impact the sputtering rate. In Dong *et al.* [137], surface modification using ion beams has been demonstrated. This process has significant potential for enhancing the tribological characteristics and mechanical properties of polymeric materials. In Bayly *et al.* [138], ion beam sputtering can efficiently utilize existing masking methods to precisely define surface characteristics within the limits of the masks. Ion beam machining plays a key role in creating optical devices, and this method is expected to see more widespread use in the future. Factors that affect the sputtering rate include the sample's temperature, surface impurities, the presence of impurities, the angle at which the ion beam hits the surface, stresses from polishing during sample preparation, and surface cracks. Hashimoto *et al.* [139] created an IB sputtering machine with a better deposition rate and solved the low deposition rate issue seen in traditional machines. They achieved a deposition rate of 340 nm/min, which were significantly higher than those of conventional ion beam sputtering machines. In Davies *et al.* [140], ion beam sputter machining allows for precise control over material removal in the production of micromechanical structures, surface profiling, and the finishing of surfaces. The profiles observed in the cam-shaped case during the experiment closely match the computer predictions made using a

simple model of stock removal. Remnev *et al*. [141] described a technique for finishing medical needles using large-area ion beam sputtering. They observed that by using a mixture of Ar and dry air (37/6), there has been a noticeable enhancement in the surface morphology related to using pure Ar sputtering. The puncture force of the needle after grinding was decreased by approximately 50%, and a significant improvement in needle sharpness was achieved through this method. Liu *et al.* [142] explored the effect of simultaneous Al co-deposition on the surface roughness of SiO_2. The root mean square (RMS) roughness was observed to increase as the Al content increased, when transitioning from normal to oblique incident angles. In Castellano *et al.* [143] the research has proven that RIBM is an effective method for creating detailed patterns with multiple levels of resistance. The use of reactive ion beam milling (RIBM) with an oxygen beam can produce resist profiles that are highly anisotropic at fast etch rates of up to 100 nm/min. This process results in edge profiles that are highly anisotropic, with no undercutting and no leftover materials deposited. In Xiao *et al*. [144], MD simulations were utilized to analyze the behavior of material removal and surface development on a nanoscale level when polishing silicon with ion beams. An increased ion dose resulted in improved surface quality but also led to a thicker amorphous layer being formed. The surface roughness, material removal rate, and formation of amorphous structures were all found to be closely linked to energy of the Ar ions. In Wang *et al.* [145], a new approach that combines mechanical lapping with ion beam polishing has been suggested to produce a sharp nt-cBN cutting edge. This method was ideal for creating cutting tools having uncomplicated shapes and extremely sharp cutting edges. In Xu *et al.* [146], ion beam irradiation was utilized to treat the surface of the micropunch made through

precision machining. The process involved using Ar plasma for ion irradiation. This method can enhance the quality reduce surface roughness of the micropunch's surface.

21.3.2 Ion Beam Etching

In Li *et al*. [147], ion beam processing technology is a new form of high-energy beam technology, along with photon beam processing and electron beam processing. It is commonly utilized in various fields, like ion beam injection, ion beam etching (IBE), ion beam deposition, and ion beam exposure. The ion beam etching technology is particularly prevalent in physical experiments, microelectronics, MEMS, and optical manufacturing. Ion beam processing utilizes the principle of ion sputtering to remove surface material at the atomic level through high-energy ion beam bombardment. In IBE technology, ion beam generation can be categorized into reaction ion etching, ion sputter etching, and plasma etching based on the action mechanism. Ion sputter etching involves using the sputter effect to dislodge surface atoms when ions with energy strike the workpiece surface. To prevent chemical reactions, inert gases such as krypton, argon, and xenon are utilized as the ion medium. In Scherer *et al.* [148], ion beam etching was utilized to create exceptionally even vertical sidewalls in III-V semiconductors, resulting in significant anisotropy. The purpose of this is to manufacture mirrors and redirect light within lnGaAs and GaAs waveguide configurations. Brun *et al*. [149] investigated the process of etching polytetrafluoroethylene (PTFE) with an oxygen ion beam irradiation in the MeV energy series. They created micro-patterns on PTFE by using masks with two different ion fluences and successfully obtained a better aspect ratio and excellent verticality and edge quality. In Taniguchi *et al*. [4], the researchers analyzed different attributes of ion beam

etching on diamond. They successfully created conical diamond field electron emitter arrays with height of 5.86 mm, a curvature radius of 30 nm, and a base radius of 2.58 mm. In Tagg *et al.* [150], a theory was developed to simulate the growth of surfaces in both 2D and 3D while considering changes in the orientation of the surface-beam. This theory demonstrates how surface gradient discontinuities can occur when inert gas ions bombard static samples. The erosion of surfaces during ion bombardment has also been investigated theoretically, particularly in cases where the sample is tilted or rotated. It was found that rocking and rotating the sample can allow for more flexibility in determining the final surface profile. Li *et al.* **[**151] noticed that the surface roughness of diamond-turned NiP could be greatly diminished by using a combination of ion beam etching and resist coating. The surface roughness decreased from 30% to 40% of the original diamond-turned surface. Hence, the IBP process could serve as the final step in the process to decrease the surface roughness of diamond faces. Bauer *et al.* [152] investigated a surface figuring technique using reactive ion beam etching (RIBE) with oxygen gas instead of standard argon ion beam figuring (IBF) processing. The surface topography was preserved very well with this method. The quality of the surface after ion beam processing was mostly dependent on the initial topography. The RIBE machining was reliable and did not produce any harmful by-products, making it appropriate for various usage.

21.3.3 Ion Beam Deposition

In Lee *et al.* [153], thin films of calcium phosphate were created on titanium using the ion beam assisted deposition technique. The ratio of calcium to phosphorus in the film, which can be adjusted by the type of evaporants or ion beam current, greatly influenced both the rate of

dissolution in a saline solution and the crystal structure under physiological conditions. Linß *et al.* [154] created Si samples using Ar ion beam erosion with low ion energy. In this work, they used co-deposition materials such as Mo, Cu, Al, steel, Ni, Cr, Ta, Ti, Si, and Zn. The Si samples and co-deposition materials were irradiated simultaneously using a broad beam ion source. The study revealed that the formation of structures on the substrate was influenced by the metals that form silicides, leading to increased surface roughness. In contrast, metals that do not form silicides do not exhibit patterning, resulting in lower surface roughness. In Horino *et al.* [155], a novel low energy ion beam deposition machine has been created to produce films with extremely high purity. Using this new concept, carbon nitride (CN) films were deposited onto silicon wafers. The CN films exhibited no peaks that were observed that may have originated from crystalline material. Yatsui *et al.* [156] crystallized B_4C thin films were effectively produced on glass at room temperature using ion beam evaporation without the need for substrate heating or post-annealing. The films exhibited a Vickers hardness of 2,300.

21.3.4 Ion Beam Figuring

In Zeuner *et al.* [157], IBF is becoming more popular for accurately shaping and polishing optical components, including spheres, aspheres, and free-form surfaces on lenses and mirrors. This technology can also be used to shape the molds for producing optical lenses. In Kurashima *et al.* [158], the roughness of the ultra-low expansion glass substrate surface was measured after being treated with an Ar^+ ion beam with energies ranging from 3 to 10 keV. The surface roughness of a machined surface to a depth of 50 nm remained similar to that of an untreated surface. The roughness of the machined surface tended to rise with

higher Ar^+ ion beam energies. In Arnold *et al.* [159], a novel approach and design for a multiaxis IB figuring machine specifically used for the precise correction of silicon spheres were introduced. This technique involves transforming dwell time information into machining instructions, with the sphere being shaped with a continuous spiral route instead of a sequential raster path.

21.4 Developed Ion Beam Process

Nabhiraj *et al.* [160] developed a micromachining system using an inductively coupled plasma ion source. The process parameters, particularly the ion energy spread, brightness, and size of the source, were optimized to improve efficiency. The potential for microfabrication on copper and silicon targets was investigated. The different patterns, like gratings with a 20-μm period and spirals, had been successfully produced on silicon wafers. The current setup has achieved milling rates of around 5 μm^3/sec. Zhou *et al.* [161] proposed a new process called low energy pulsed ion beam (LPIB) which allows for better material removal by adjusting the pulse frequency and duty cycle. When applied to monocrystalline silicon, the duty cycle and pulse frequency are set at 1% and 100 Hz, respectively. In comparison to IBF, which has a removal resolution of approximately 0.01 nm, LPIB technology offers a more precise and consistent removal tool for material surface treatment across different scales. It has the potential for various applications, including ultra-precision manufacturing, special surface processing, ion beam sputtering deposition, and adjustment of inertial device quality. Toyoda *et al.* [162] examined the efficiency of a gas cluster ion beam (GCIB) process in creating a small mold made of tungsten carbide that cannot be machined. In this process they utilized collimated GCIB with controlled

target positions and ion dosage, small free-surface molds can be produced. The surface of the irradiated GCIB displays a smooth texture devoid of any scratches. Ando *et al.* [163] produced patterns by using multiple ion beam machines. They found that focus voltage and demagnification ratio were theoretically important process parameters. The creation of multiple ion beams was achieved through a screen lens. In Wang *et al.* [164], a method for creating nanostructured speckle patterns on polymers through broad-ion beam milling has been developed. This technique was cost-effective. Using an argon ion beam, random patterns were effectively generated on the surfaces of four different types of polymers, such as polyester, carbon fiber reinforced plastic epoxy matrix, polyimide, and polyvinyl formal-acetal. The resulting speckle patterns exhibit excellent time stability.

21.5 Combined Ion Beam Process

In Kawasegi *et al.* [165], the process used for creating a textured diamond cutting tool involved a combination of heat treatment and FIB process. This resulted in the successful creation of a texture on the rake face of the tool. This approach was found to be more efficient compared to using femtosecond laser method for diamond cutting tools. The cutting performance of the tool improved and providing the quality of the machined surface. Barienti *et al.* [166] discovered that the interface zone of metallic composites could be made ready for a specific analytical task by using a combination of ion beam processing and metallographic methods. The ion beam processing can significantly enhance the quality of sample preparation. Eichhorn *et al.* [167] introduced a novel technology using a focused ion beam for modifying carbon nanotubes (CNTs) in terms of their orientation, length, and diameter. These

CNTs are placed on an atomic force microscope probe by way of a pick-and-place method using a nanorobotic microgripper. In Milani *et al.* [168], the combination of the simultaneous scanning electron microscopy and focused ion beam methods was utilized to manipulate and image unprepared (fresh) cells at a submicron level. This was done to showcase the capabilities of the combined SEM/FIB process for ultramicroscopic studies and they successfully achieved sectioning at the nanoscale level. In Miller *et al*. [169], a thin film strain-sensor with a 20 mm x 100 mm active sensing area was created using both pulsed laser deposition and FIBM to achieve the desired shape. The indium-tin-oxide thin films, ranging from 100 to 246 nm in thickness, were used to make the sensors. The active strain-sensors had gage factors between –0.3 and –8.7 and exhibited a linear response at room temperature with very little hysteresis. In Kaur *et al.* [170], zinc oxide (ZnO) donor films with a thickness of 1 m were initially created using the FIB method to a depth of 0.8 µm. From these prepared donors, debris-free micropellets of ZnO with very even edges and surface consistency were then produced using laser-induced forward transfer. Rajput *et al.* [171] examined the influence of various beam process factors, including mode of deposition, beam dwell time, deposition of nanopillars, and pattern size, using an FIB process. During the fabrication of nanopillars using circular and serpentine deposition modes, long tails of deposited material were detected. The quantity of material deposited in these tails was determined to be influenced by both the beam dwell time and the diameter of the pillar. The presence of the tail was no longer evident at increased beam dwell time and pillar diameter. In Inkson *et al.* [172], Ti and Pt nanowires were created using a combination of ultra-high vacuum molecular beam epitaxy deposition for Ti thin films and FIB deposition for Pt thin films. A cross-

sectional FIB sputtering process was then used to create electron-transparent nanowires. The microstructure of Ti nanowires on Al_20_3 substrates remains stable at temperatures ranging from 550°C to 600°C. Similarly, the amorphous platinum wires deposited using FIB exhibit stability up to temperatures between 580°C and 650°C. Lee *et al.* [173] suggested a new technique for rapidly and cost-effectively producing large-diameter micropillars using a hybrid approach. To determine the effectiveness of this technique, a total of 76 coarse single crystal copper micropillars were created through micro-electrical discharge machining with WC-Co microtools. The hybrid method involved combining micro-electrical discharge machining with annular milling. In Fujiwara *et al.* [174], the Zerodur substrate had a thin carbon layer applied using the ion beam sputtering deposition method. The surface roughness of the carbon layer was dependent on ion energy and machined depth. Specifically, with a 1.0-keV Ar+ ion beam and a machined depth between 10 nm and 50 nm, the surface roughness of the carbon layer decreased significantly up to 10 nm. Assayag *et al.* [175] designed a coupled SEM/FIB system that was utilized to create precise mirror facets in various laser structures. The enhanced machining technique was effectively utilized to create a double heterostructure laser butt-coupled device connected to its optical waveguide. Frey *et al.* [176] explored how the interaction among the ion beam and solid material affects the creation of small structures through techniques such as chemically assisted material deposition, ion-beam sputtering, and etching. It examines how focused ion beams can be used to process structures smaller than 100 µm. The process of material removal influences when change in swelling and composition, reflected ions, and an angle-dependent sputter rate. In Adams *et al.* [177], the use of combined ultra-precision machining and FIB

sputtering processes was employed for the manufacture of polymers and metal alloys. Ga-ion beam sputtering was used to create micro-end mills with a cylindrical tool shank. These microtools were capable of fabricating fine channels that are 26–28 microns wide in materials such as brass, 6061 aluminum, and polymethyl methacrylate. The tools produced through FIB sputtering were able to successfully machine a variety of materials.

21.6 Conclusion

The focused ion beam has become a popular technology to fabricate nanoscale structures. The nanofabrication based on this technology involves four major approaches such as milling, implantation, ion-induced deposition, and ion assisted etching of materials. The FIB processing is used to remove specific site of materials. It includes a number of processes such as milling, machining, fabrication, etching, deposition, sputtering and irradiation. From this, milling is most effective method in the semiconductor industry because it is simple and the low-cost process also provides results with minimum requirements. The ion beam process is mostly applied in electronics fields. This process has a high level of accuracy, high speed, high deposition rate, and provide fine surface finish to the material. For this process mostly, applied ion is argon ion. A potential method named ion beam lithography is used for micro/nano- and nanomachining polymeric materials. This process has ability to modify the surface topography and hydrophobic properties. Some researchers tried to upgrade this FIB processing through which they achieved high-resolution material removal by adjusting different input parameters. The developed FIB is cost-effective technique and provides a more precise and consistent removal tool for material surface treatment across different scales. This process is

mostly applied in ultra-precision manufacturing and special surface processing.

References

1. Wolf, G.K. and Ensinger, W., Ion Beam Techniques, in: *Ullmann's Encyclopedia of Industrial Chemistry*, 6th electronic ed, Wiley-VCH, Weinheim Germany, 2003.

2. Allen, D.M., Shore, P., Evans, R.W., Fanara, C., O'Brien, W., Marson, S., O'Neill, W., Ion beam, focused ion beam, and plasma discharge machining. *CIRP Ann. Manuf. Technol.*, 58, 647, 2009.

3. Fukuyama, R. and Taniguchi, J., Ion beam sharpening of a single-crystal diamond knife without facet and ripple formations by swinging motion of knife. *Microelectron. Eng.*, 141, 245, 2015.

4. Taniguchi, J., Ohno, H., Kawabata, Y., Miyamoto, I., Ion-beam processing of single crystal diamond using SOG mask. *Vacuum*, 80, 793, 2006.

5. Tseng, A.A., Recent developments in micromilling using focused ion beam technology. *J. Micromech. Microeng.*, 14, R15–R34, 2004.

6. Tseng, A.A., Insua, I.A., Park, J.S., Chen, C.D., Milling yield estimation in focused ion beam milling of two-layer substrates. *J. Micromech. Microeng.*, 15, 20, 2005.

7. Huang, J., Alqahtani, A., Viegas, J., Dahlem, M.S., Fabrication of optical fiber gratings through focused ion beam techniques for sensing applications, in: *2012 Photonics Global Conference (PGC), Singapore*, pp. 1–4, IEEE, 2012.

8. Driesel, Y.W., Micromachining Using Focused Ion Beams phys. *Stat. sol. (a)*, 146, 523, 1994.

9. Machalett, F. and Seidel, P., Focused Ion Beams and Some Selected Applications, in: *In digital Encyclopedia of Applied Physics*, KGaA (Ed.), vol. 1, Wiley-VCH Verlag GmbH & Co, Weinheim, Germany, 2024.

10. Atiqah, N., Jaafar, I.H., Ali, M.Y., Asfana, B., Application of focused ion beam micromachining: A review. *Adv. Mat. Res.*, 576, 507, 2012.

11. Science, B., Huang, Y.Z., Lozano-perez, S., Langford, R.M., Titchmarsh, J.M., Jenkins, M.L., Preparation of transmission electron microscopy cross-section specimens of crack tips using focused ion beam milling. *J. Microsc.*, 207, 129, 2002.

12. Narayan, K. and Subramaniam, S., Focused ion beams in biology, in: *Nat. Methods*, vol. 12, p. 1021, Nature Publishing Group, United Kingdom, 2015.

13. Tanaka, T., Irisawa, T., Fujiwara, M., Gennai, N., Micrometer-scale fabrication and assembly using focused ion beam. *Thin Solid Films*, 509, 113, 2006.

14. Tseng, A.A., Recent developments in nanofabrication using focused ion beams. *Small*, 1, 924, 2005.

15. Kong, C., Cheong, S., Tilley, R.D., Recent development in focused ion beam nanofabrication, in: *Comprehensive nanoscience and nanotechnology*, 2nd, D. Andrews, T. Nann, R.H. Lipson (Eds.), pp. 327–356, Elsevier Science & Technology, San Diego, 2019.

16. Kim, C.S., Ahn, S.H., Jang, D.Y., Review: Developments in micro/nanoscale fabrication by focused ion beams. *Vacuum*, 86, 1014, 2012.

17. Young, R.J., Micro-machining using a focused ion beam. *Vacuum*, 44, 353, 1993.

18. Dai, Y., Yang, L., Wang, L., Tian, B., Zou, L., Cheng, H., Huang, D., Addressable metal-ferroelectric-metal nanocapacitor arrays fabricated by focused ion beam milling. *Integr. Ferroelectr.*, 132, 99, 2012.

19. Dorronsoro, A., Navarrete, J., Pan, A., Castaño, E., Sánchez, J.M., Alkorta, J., Digital image correlation after focused ion beam micro-slit drilling: A new technique for measuring residual stresses in hardmetal components at local scale. *Int. J. Refract. Hard Mater.*, 112, 106155, 2023.

20. Inkson, B.J., Leclere, D., Elfallagh, F., Derby, B., The effect of focused ion beam machining on residual stress and crack morphologies in alumina, in: *J. Phys. Conf. Ser*, vol. 26, p. 219, Institute of Physics Publishing, University of Leeds, UK, 2006.

21. Martynowycz, M.W., Zhao, W., Hattne, J., Jensen, G.J., Gonen, T., Collection of Continuous Rotation MicroED Data from Ion Beam-Milled Crystals of Any Size. *Structure*, 27, 545, 2019.

22. Martynowycz, M.W. and Gonen, T., Protocol for the use of focused ion-beam milling to prepare crystalline lamellae for microcrystal electron diffraction (MicroED). *STAR Protoc.*, 2, 100686, 2021.

23. Polovinkin, V., Khakurel, K., Babiak, M., Angelov, B., Schneider, B., Dohnalek, J., Andreasson, J., Hajdu, J., Demonstration of electron diffraction from membrane protein crystals grown in a lipidic mesophase after lamella preparation by focused ion beam milling at

cryogenic temperatures Polovinkin Vitaly. *J. Appl. Crystallogr.*, 53, 1416, 2020.

24. Drobne, D., Milani, M., Lešer, V., Tatti, F., Surface damage induced by FIB milling and imaging of biological samples is controllable. *Microsc. Res. Tech.*, 70, 895, 2007.

25. Pekin, T.C., Allen, F.I., Minor, A.M., Evaluation of neon focused ion beam milling for TEM sample preparation. *J. Microsc.*, 264, 59, 2016.

26. Presser, N. and Hilton, M.R., Applications of focused ion beam machining to the characterization of carbide, nitride and oxide films. *Thin Solid Films*, 308–309, 369, 1997.

27. Lehrer, C., Frey, L., Petersen, S., Sulzbach, T., Ohlsson, O., Dziomba, T., Danzebrink, H.U., Ryssel, H., Fabrication of silicon aperture probes for scanning near-field optical microscopy by focused ion beam nano machining. *Microelectron. Eng.*, 57–58, 721, 2001.

28. Savenko, A., Yildiz, I., Petersen, D.H., Bøggild, P., Bartenwerfer, M., Krohs, F., Oliva, M., Harzendorf, T., Ultra-high aspect ratio replaceable AFM tips using deformation-suppressed focused ion beam milling. *Nanotechnology*, 24, 465701, 2013.

29. Liao, Y., Gruber, M., Lukic, H., Chen, S., Megremis, S., Fracture toughness of zirconia with a nanometer size notch fabricated using focused ion beam milling. *J. Biomed. Mater. Res. B Appl. Biomater.*, 108, 3323, 2020.

30. Wilhelmi, O., Roussel, L., Faber, P., Reyntjens, S., Daniel, G., Focussed ion beam fabrication of large and complex nanopatterns. *J. Exp. Nanosci.*, 5, 244, 2010.

31. Han, J., Lee, H., Min, B.K., Lee, S.J., Prediction of nanopattern topography using two-dimensional focused ion beam milling with beam irradiation intervals. *Microelectron. Eng.*, 87, 1, 2010.

32. Goswami, A., Singh, K., Aravindan, S., Rao, P.V., Optimizing FIB milling process parameters for silicon and its use in nanoreplication. *Mater. Manuf. Process.*, 32, 1052, 2017.

33. Chen, Q., Shao, T., Xing, Y., Zhou, Z., Machine Learning-Based Damage Predicion Method for the Micro/Nano Structures Fabricated by Helium Focused Ion Beam, in: *2021 21st International Conference on Solid-State Sensors, Actuators and Microsystems (Transducers)*, Orlando, FL, USA, pp. 1052–1055, IEEE, 2021.

34. De Ridder, R.M., Hopman, W.C.L., Ay, F., Focused-Ion-Beam Processing for Photonics, in: *2007 9th International Conference on Transparent Optical Networks*, Rome, Italy, pp. 212–215, IEEE, 2007.

35. Vermeij, T., Plancher, E., Tasan, C.C., Preventing damage and redeposition during focused ion beam milling: The “umbrella” method. *Ultramicroscopy*, 186, 35, 2018.

36. Li, B., Xie, H., Zhang, X., Focused Ion Beam Nano-Machined Structures For Strain Analysis By A Moiré Technique. *MRS Online Proc. Lib.*, 761, 5484, 2002.

37. Biao, L., Tan, X., Xiel, H., Zhang, X., Focused ion beam (FIB) nano-machining and FIB Moire technique for strain analysis in MEMS/NEMS structures and devices, in: *The Sixteenth Annual International Conference on Micro*

Electro Mechanical Systems, 2003. MEMS-03 Kyoto. IEEE, Kyoto, Japan, pp. 674–677, 2003.

38. Chen, Y., Bi, K., Wang, Q., Zheng, M., Liu, Q., Han, Y., Yang, J., Chang, S., Zhang, G., Duan, H., Rapid Focused Ion Beam Milling Based Fabrication of Plasmonic Nanoparticles and Assemblies via “sketch and Peel” Strategy. *ACS Nano*, 10, 11228, 2016.

39. Li, Y., Xing, Y., Fang, C., Chen, Q., Qiu, X., An experiment-based method for focused ion beam milling profile calculation and process design. *Sens. Actuators A Phys.*, 286, 78, 2019.

40. Stoyanov, S., Tang, Y.K., Bailey, C., Evans, R., Marson, S., Allen, D., Modelling and Process Capability Analysis of Focused Ion Beam, in: *2009 32nd International Spring Seminar on Electronics Technology*, Brno, Czech Republic, pp. 1–6, IEEE, 2009.

41. Yoon, H.S., Kim, C.S., Lee, H.T., Ahn, S.H., Advanced scanning paths for focused ion beam milling. *Vacuum*, 143, 40, 2017.

42. Buchnev, O., Grant-Jacob, J.A., Eason, R.W., Zheludev, N.I., Mills, B., Macdonald, K.F., Deep-Learning-Assisted Focused Ion Beam Nanofabrication. *Nano Lett.*, 22, 2734, 2022.

43. Kim, H.B., Hobler, G., Steiger, A., Lugstein, A., Bertagnolli, E., Full three-dimensional simulation of focused ion beam micro/nanofabrication. *Nanotechnology*, 18, 245303, 2007.

44. Hofmann, F., Harder, R.J., Liu, W., Liu, Y., Robinson, I.K., Zayachuk, Y., Glancing-incidence focussed ion beam milling: A coherent X-ray diffraction study of 3D nano-

scale lattice strains and crystal defects. *Acta Mater.*, 154, 113, 2018.

45. Korsunsky, A.M., Sebastiani, M., Bemporad, E., Focused ion beam ring drilling for residual stress evaluation. *Mater. Lett.*, 63, 1961, 2009.

46. Dovidenko, K., Potyrailo, R.A., Tarte, L.L., Millimeter-scale surface nano-structuring using focused ion beam milling. *MRS Online Proc. Lib.*, 901, 516, 2005.

47. Charandabi, S.C., Sabouri, A., Ostadi, H., Anthony, C.J., Prewett, P.D., Characterisation of nanoporous materials using Focused Ion Beam milling method, in: *2012 12th IEEE International Conference on Nanotechnology (IEEE-NANO)*, pp. 1–4, IEEE, Birmingham, UK, 2012.

48. Sun, J., Luo, X., Ritchie, J.M., Chang, W., Wang, W., An investigation of redeposition effect for deterministic fabrication of nanodots by focused ion beam. *Precis. Eng.*, 36, 31, 2012.

49. Dhamodaran, S. and Ramkumar, J., Controlling the nanodot formation on GaAs surface during focused ion beam processing. *Radiat. Eff. Defects Solids*, 165, 889, 2010.

50. Bhavsar, S.N., Aravindan, S., Rao, P.V., Machinability study of high speed steel for focused ion beam (FIB) milling process - An experimental investigation at micron/nano scale. *Precis. Eng.*, 38, 168, 2014.

51. Bhavsar, S.N., Aravindan, S., Rao, P.V., Experimental investigation of redeposition during focused ion beam milling of high speed steel. *Precis. Eng.*, 36, 408, 2012.

52. Li, W., Lalev, G., Dimov, S., Zhao, H., Pham, D.T., A study of fused silica micro/nano patterning by focused-

ion-beam. *Appl. Surf. Sci.*, 253, 3608, 2007.

53. Sabouri, A., Anthony, C.J., Bowen, J., Vishnyakov, V., Prewett, P.D., The effects of dwell time on focused ion beam machining of silicon. *Microelectron. Eng.*, 121, 24, 2014.

54. Lebedev, D., Malyshev, G., Ryzhkov, I., Mozharov, A., Shugurov, K., Sharov, V., Panov, M., Tumkin, I., Afonicheva, P., Evstrapov, A., Bukatin, A., Mukhin, I., Focused ion beam milling based formation of nanochannels in silicon-glass microfluidic chips for the study of ion transport. *Microfluid. Nanofluid.*, 25, 51, 2021.

55. Borgardt, N.I., Rumyantsev, A.V., Volkov, R.L., Chaplygin, Y.A., Sputtering of redeposited material in focused ion beam silicon processing. *Mater. Res. Express*, 5, 025905, 2018.

56. Salvati, E., Brandt, L.R., Papadaki, C., Zhang, H., Mousavi, S.M., Wermeille, D., Korsunsky, A.M., Nanoscale structural damage due to focused ion beam milling of silicon with Ga ions. *Mater. Lett.*, 213346, 2018, 2018.

57. Bhavsar, S.N., Aravindan, S., Rao, P.V., Machinability study of cemented carbide using Focused Ion Beam (FIB) milling. *Mater. Manuf. Process.*, 27, 1029, 2012.

58. Bhavsar, S.N., Aravindan, S., Rao, P.V., Investigating material removal rate and surface roughness using multi-objective optimization for focused ion beam (FIB) micro-milling of cemented carbide. *Precis. Eng.*, 40, 131, 2015.

59. Martin, A.A., Randolph, S., Botman, A., Toth, M., Aharonovich, I., Maskless milling of diamond by a focused oxygen ion beam. *Sci. Rep.*, 5, 8958, 2015.

60. Wu, R., Tauhiduzzaman, M., Ravi Selvaganapathy, P., Anisotropic wetting surfaces machined by diamond tool with tips microstructured by focused ion beam. *Mater. Des.*, 210, 110014, 2021.

61. Ono, T., Sharpening of the diamond tool edge by the Ar ion beam machine tool. *Procedia Manuf.*, 53, 246, 2021.

62. Yan, Y., Wang, Y., Wu, W., Lou, Z., Geng, Y., Fabrication of sinusoidal-shaped multi-tip diamond tools by a focused ion beam machining process. *Proc. Inst. Mech. Eng. B J. Eng. Manuf.*, 237, 1115–1121, 2023.

63. Burns, S.R., Gregg, J.M., Nagarajan, V., Nanostructuring Ferroelectrics via Focused Ion Beam Methodologies. *Adv. Funct. Mater.*, 26, 8367, 2016.

64. Wicki, F., Longchamp, J.N., Escher, C., Fink, H.W., Design and implementation of a micron-sized electron column fabricated by focused ion beam milling. *Ultramicroscopy*, 160, 74, 2016.

65. Chen, X., Ren, Z., Zhu, Y., Wang, Y., Zhang, J., Wang, X., Xu, J., Formation mechanism and compensation methods of profile error in focused ion beam milling of three-dimensional optical microstructures. *SN Appl. Sci.*, 2, 758, 2020.

66. Fu, Y., Kok, N., Bryan, A., Investigation of single mode fiber coupling using diffractive optical element with continuous relief fabricated by focused ion beam technology, in: *OFC 2001. Optical Fiber Communication Conference and Exhibit. Technical Digest Postconference Edition (IEEE Cat. 01CH37171)*, Anaheim, CA, USA, pp. ThC3–1-ThC3-3, 2001.

67. Huson, M.G., Church, J.S., Hillbrick, L.K., Woodhead, A.L., Sridhar, M., Van De Meene, A.M.L., Focused ion

beam milling of carbon fibres. *Mater. Chem. Phys.*, 168, 193, 2015.

68. Li, X., Liang, J., Ueda, T., Applied technique of focused ion beam milling based on microstructure of photonic bandgap fiber. *Int. J. Adv. Manuf. Technol.*, 68, 465, 2013.

69. Hu, Q. and O'Neill, W., Occurrence of particle debris field during focused Ga ion beam milling of glassy carbon. *Appl. Surf. Sci.*, 256, 5952, 2010.

70. Youn, S.W., Takahashi, M., Goto, H., Maeda, R., A study on focused ion beam milling of glassy carbon molds for the thermal imprinting of quartz and borosilicate glasses. *J. Micromech. Microeng.*, 16, 2576, 2006.

71. Youn, S.W., Takahashi, M., Goto, H., Maeda, R., Microstructuring of glassy carbon mold for glass embossing - Comparison of focused ion beam, nano/femtosecond-pulsed laser and mechanical machining. *Microelectron. Eng.*, 83, 2482, 2006.

72. Taniguchi, J., Satake, S., II, Oosumi, T., Fukushige, A., Kogo, Y., Dwell time adjustment for focused ion beam machining. *Nucl. Instrum. Methods Phys. Res. B*, 307, 248, 2013.

73. Sarkar, J. and Gilman, P.S., Imaging ultrafine grains in machined tantalum subsurface using a focused ion beam. *Scr. Mater.*, 59, 301, 2008.

74. Xiao, Y., Wehrs, J., Ma, H., Al-Samman, T., Korte-Kerzel, S., Göken, M., Michler, J., Spolenak, R., Wheeler, J.M., Investigation of the deformation behavior of aluminum micropillars produced by focused ion beam machining using Ga and Xe ions. *Scr. Mater.*, 127, 191, 2017.

75. Jamaludin, F.S., Mohd Sabri, M.F., Said, S.M., Controlling parameters of focused ion beam (FIB) on high aspect ratio micro holes milling. *Microsyst. Technol.*, 19, 1873, 2013.

76. Ay, F., Iñurrategui, I., Geskus, D., Aravazhi, S., Pollnau, M., Integrated lasers in crystalline double tungstates with focused-ion-beam nanostructured photonic cavities. *Laser Phys. Lett.*, 8, 423, 2011.

77. Hambe, M., Wicks, S., Gregg, J.M., Nagarajan, V., Creation of damage-free ferroelectric nanostructures via focused ion beam milling. *Nanotechnology*, 19, 175302, 2008.

78. Kim, B.Y., Lee, J.S., Lee, J.H., A Study on Improving the Surface Roughness by Ion Beam Sputtering, in: *Proceedings of the Korean Nuclear Society Conference, Korean Nuclear Society*, vol. 1104-1105, 2005.

79. Hung, N.P., Ali, M.Y., Fu, Y.Q., Ong, N.S., Tay, M.L., Surface integrity and removal rate of silicon sputtered with focused ion beam. *Mach. Sci. Technol.*, 5, 239, 2001.

80. Ali, M.Y., Hung, W., Yongqi, F., A review of focused ion beam sputtering. *Int. J. Precis. Eng. Manuf.*, 11, 157, 2010.

81. Picard, Y.N., Adams, D.P., Vasile, M.J., Ritchey, M.B., Focused ion beam-shaped microtools for ultra-precision machining of cylindrical components. *Precis. Eng.*, 27, 59, 2003.

82. Choi, W.K. and Baek, S.Y., Study on platinum coating depth in focused ion beam diamond cutting tool milling and methods for removing platinum layer. *Materials*, 82015, 6498, 2015.

83. Lee, H., Han, J., Min, B.K., Lee, S.J., Geometric compensation of focused ion beam machining using image processing. *Appl. Phys. Express*, 1, 127002, 2008.

84. Prewett, P.D., Marriott, P., Bishop, H.E., Microcircuit machining using focused ion beams—a note on the role of SIMS for end point detection. *Microelectron. Eng.*, 10, 1, 1989.

85. Sun, J., Li, J., Maier, R.R.J., Hand, D.P., Macpherson, W.N., Miller, M.K., Ritchie, J.M., Luo, X., Fabrication of a side aligned optical fibre interferometer by focused ion beam machining. *J. Micromech. Microeng.*, 23, 105005, 2013.

86. Chkhalo, N.I., Kaskov, I.A., Malyshev, I.V., Mikhaylenko, M.S., Pestov, A.E., Polkovnikov, V.N., Salashchenko, N.N., Toropov, M.N., Zabrodin, I.G., High-performance facility and techniques for high-precision machining of optical components by ion beams. *Precis. Eng.*, 48, 338, 2017.

87. Han, J., Sparkes, M., O'Neill, W., Controlling the optical fiber output beam profile by focused ion beam machining of a phase hologram on fiber tip. *Appl. Opt.*, 54, 890, 2015.

88. Madison, A.C., Villarrubia, J.S., Liao, K.-T., Schumacher, J., Siebein, K., Ilic, B.R., Liddle, J.A., Stavis, S.M., An Unconventional Tradespace of Focused-Ion-Beam Machining, in: *The 2022 International Conference on Frontiers of Characterization and Metrology for Nanoelectronics*, Monterey, CA, US, 2022.

89. Hosokawa, H., Shimojima, K., Mabuchi, M., Surface roughness of a Co-less WC micro-die fabricated by

focused-ion-beam machining. *Philos. Mag. Lett.*, 84, 149, 2004.

90. Joe, H.E., Lee, W.S., Jun, M.B.G., Park, N.C., Min, B.K., Material interface detection based on secondary electron images for focused ion beam machining. *Ultramicroscopy*, 184, 37, 2018.

91. Miyamoto, I. and Taniguchi, N., Focused Ion Beam Fabrication of Micro-Mechanical Parts — Machining Characteristics of Polycrystalline Silicon and Computer Simulation of Profile Changes of Patterns. *CIRP Ann.*, 39, 205, 1990.

92. Hung, N.P., Fu, Y.Q., Ali, M.Y., Focused ion beam machining of silicon. *J. Mater. Process. Technol.*, 127, 256, 2002.

93. Motz, C., Schöberl, T., Pippan, R., Mechanical properties of micro-sized copper bending beams machined by the focused ion beam technique. *Acta Mater.*, 53, 4269, 2005.

94. Hosokawa, H., Shimojima, K., Iwasaki, H., Mabuchi, M., Nanomachining of nanocrystalline nickel by focused ion beam. *Philos. Mag. Lett.*, 84, 713, 2004.

95. Davies, S.T. and Khamsehpour, B., Focused ion beam machining and deposition for nanofabrication. *Vacuum*, 47, 455, 1996.

96. Yang, H. and Rachev, S., Focused Ion Beam Micro Machining and Micro Assembly, in: *Precision Assembly Technologies and Systems*, vol. 315, S. Ratchev, (Ed.), p. 81, IFIP Advances in Information and Communication Technology, Springer, Berlin, Heidelberg, 2010, IPAS 2010.

97. Madison, A.C., Villarrubia, J.S., Liao, K.T., Copeland, C.R., Schumacher, J., Siebein, K., Ilic, B.R., Liddle, J.A., Stavis, S.M., Unmasking the Resolution–Throughput Tradespace of Focused-Ion-Beam Machining. *Adv. Funct. Mater.*, 32, 2111840, 2022.

98. Lalev, G., Dimov, S., Kettle, J., Van Delft, F., Minev, R., Data preparation for focused ion beam machining of complex three-dimensional structures. *Proc. Inst. Mech. Eng. B J. Eng. Manuf.*, 222, 67, 2008.

99. Sun, J., Luo, X., Ritchie, J., Hrncir, T., A predictive divergence compensation approach for the fabrication of three-dimensional microstructures using focused ion beam machining. *Proc. Inst. Mech. Eng. B J. Eng. Manuf.*, 226, 229, 2012.

100. De Felicis, D., Mughal, M.Z., Bemporad, E., A method to improve the quality of 2.5 dimensional micro-and nano-structures produced by focused ion beam machining. *Micron*, 101, 8, 2017.

101. Sun, J., Liu, Y., Ritchie, J.M., Luo, X., A haptic digital tool to assist the design, planning and manufacture of micro- and nanostructures. *Proc. Inst. Mech. Eng. E: J. Process Mech. Eng.*, 229, 290, 2015.

102. Wollschläger, N., Österle, W., Häusler, I., Stewart, M., Ga+ implantation in a PZT film during focused ion beam micro-machining. *Phys. Status Solidi C*, 12, 314–317, 2015.

103. Lehrer, C., Frey, L., Petersen, S., Mizutani, M., Takai, M., Ryssel, H., Defects and Gallium-Contamination During Focused Ion Beam Micro Machining, in: *2000 International Conference on Ion Implantation Technology*

Proceedings. Ion Implantation Technology - 2000 (Cat. No.00EX432), Alpbach, Austria, pp. 695–698, 2000.

104. Chao, L.C., Ye, C.C., Chen, Y.P., Yu, H.Z., Facile fabrication of ZnO nanowire-based UV sensors by focused ion beam micromachining and thermal oxidation. *Appl. Surf. Sci.*, 282, 384, 2013.

105. Jud, P.P., Nellen, P.M., Sennhauser, U., Micromachining by Focused Ion Beam (FIB) for materials characterization. *Adv. Eng. Mater.*, 7, 384, 2005.

106. Orbons, S.M., van Dijk, L., Bozkurt, M., Johnston, P.N., Reichart, P., Jamieson, D.N., Focused ion beam machined nanostructures depth profiled by macrochannelling ion beam analysis. *Nucl. Instrum. Methods Phys. Res. B*, 249, 747, 2006.

107. Bass, R.B., Zhang, J.Z., Lichtenberger, A.W., Machine-Aligned Fabrication of Submicron SIS Tunnel Junctions Using a Focused Ion Beam. *IEEE Trans. Appl. Supercond.*, 9, 3240, 1999.

108. Kim, S.J. and Iwasaki, K., Development of focused ion beam machining systems for fabricating three-dimensional structures. *Jpn. J. Appl. Phys.*, 47, 5120, 2008.

109. Kitamura, M., Koike, E., Takasu, N., Nishimura, T., Focused ion beam machining for optical microlens fabrication. *Jpn. J. Appl. Phys.*, 41, 4019–4021, 2002.

110. Nesprías, F., Venturino, M., Debray, M.E., Davidson, J., Davidson, M., Kreiner, A.J., Minsky, D., Fischer, M., Lamagna, A., Heavy ion beam micromachining on $LiNbO_3$. *Nucl. Instrum. Methods Phys. Res. B*, 267, 69, 2009.

111. Wang, C.Y., Yang, S.M., Jing, W.X., Lin, Q.J., Han, F., Structure analysis of nano-scale dual-step fabricated by Focused Ion Beam, in: *2013 13th IEEE International Conference on Nanotechnology (IEEE-NANO 2013)*, pp. 829–832, IEEE, Beijing, China, 2013 August.

112. Modrzynski, P., Gotszalk, T., Knapitsch, A., Kunicki, P., Lecoq, P., Moczala, M., Papakonstantinou, I., Auffray, E., Light Extraction from Scintillating Crystals Enhanced by Photonic Crystal Structures Patterned by Focused Ion Beam. *IEEE Trans. Nucl. Sci.*, 63, 644, 2016.

113. Guénolé, J., Prakash, A., Bitzek, E., Atomistic simulations of focused ion beam machining of strained silicon. *Appl. Surf. Sci.*, 416, 86, 2017.

114. Kim, K.H., Kim, J.J., Suzuki, T., Shindo, D., Characterization of the charging effect in a ZrO2 sintered body by Ga ion beam irradiation. *J. Electron Microsc.*, 57, 53, 2008.

115. Salut, R., Majjad, H., Daniau, W., Ballandras, S., P3N-1 Direct Writing Of High Frequency Surface Acoustic Waves Using Focus Ion Beam Etching, in: *2006 IEEE Ultrasonics Symposium*, pp. 2285–2288, IEEE, Vancouver, BC, Canada, 2006.

116. Hänsel, T., Frost, F., Nickel, A., Schindler, T., Ultra-precision Surface Finishing by Ion Beam Techniques. *Vak. Forsch. Prax.*, *19*, 24, 2007.

117. Kuball, M., Morrissey, F.H., Benyoucef, M., Harrison, I., Korakakis, D., Foxon, C.T., Nano-Fabrication of GaN Pillars Using Focused Ion Beam Etching. *Phys. Stat. Sol. (a).*, 176, 355, 1999.

118. Lipp, S., Frey, L., Lehrer, C., Demm, E., Pauthner, S., Ryssel, H.A., Comparison of Focused Ion Beam and

Electron Beam Induced Deposition Processes. *Microelectron. Reliab.*, 36, 1779, 1996.

119. Fu, Y. and Bryan, N.K.A., A Novel One Step Integration of Edge-Emitting Laser Diode With Micro-Elliptical Lens Using Focused Ion Beam Direct Deposition. *IEEE Trans. Semicond. Manuf.*, 15, 2, 2002.

120. Arimatsu, K., Hashimoto, I., Ooishi, S., Tanaka, S., Sato, T., Gejyo, T., Development of large scale ion beam milling machines. *Nucl. Instrum. Methods Phys. Res. B: Beam Interact. Mater. At.*, *37*, 833, 1989.

121. Davies, S.T. and Bowen, D.K., An apparatus for batch fabrication of micromechanical elements by ion beam machining. *J. Vac. Sci. Technol., B*, 5, 337, 1987.

122. Miyamoto, I., Shuhara, A., Taniguchi, N., Ion-Beam Machining of Tungsten Carbide Chips — Fabrication of Fine Patterns. *CIRP Ann.*, 40, 187, 1991.

123. Miyamoto, I., Davies, S.T., Whitehouse, D.J., Computer Simulation of Profile Changes of Hemi-Spherical Diamond Styli During Ion Beam Machining. *CIRP Ann.*, *37*, 171, 1988.

124. Bauer, J. and Frost, F., Orientation-dependent nanostructuring of titanium surfaces by low-energy ion beam erosion. *Surf. Interface Anal.*, 52, 1071, 2020.

125. Miyamoto, I. and Taniguchi, N., Ion beam fabrication of ultrafine patterns on cemented carbide chips with ultrafine grains. *CIRP Ann.*, *42*, 239, 1993.

126. Liang, X., Gu, Y., Wang, X., Ma, Z., Sui, Y., Zheng, J., Study on mechanism and process of ion beam machining on high-precision large optical surfaces, in: *Proc. SPIE 9281, 7th International Symposium on Advanced Optical*

Manufacturing and Testing Technologies: Advanced Optical Manufacturing Technologies, (AOMATT 2014), Harbin, China, 2014, SPIE, 9281, 92810V.

127. Besserer, H.B., Gerstein, G., Maier, H.J., Nürnberger, F., Specimen preparation by ion beam slope cutting for characterization of ductile damage by scanning electron microscopy. *Microsc. Res. Tech.*, 79, 321, 2016.

128. Tsuchiya, K., Shima, T., Horisawa, H., Yasunaga, N., Improvement of surface roughness by oxygen ion beam machining. *Nanotechnology*, 6, 158, 1995.

129. Shima, T. and Inoue, N., A study on surface roughness in ion-beam machining. *Precis. Eng.*, 12, 157, 1990.

130. Levinson, H.J. and Brunner, T.A., Ion Beams, Thermal Processes and Lithographic Challenges, in: *2014 20th International Conference on Ion Implantation Technology (IIT)*, Portland, OR, USA, pp. 1–4, 2014.

131. He, W., Poker, D.B., Gonsalves, K.E., Batina, N., Micro/nano machining of polymeric substrates by ion beam techniques. *Microelectron. Eng.*, 65, 153, 2003.

132. Carter, G., Nobes, M.J., Katardjiev, I.V., The theory of ion beam polishing and machining. *Vacuum*, 44, 303, 1993.

133. Akel, M., Salo, S.A., Saw, S.H., Lee, S., Ion beam features produced by two plasma focus machines operated with different gases. *IEEE Trans. Plasma Sci.*, 42, 2202, 2014.

134. Miyamoto, I., Ultra fine finishing of diamond tools by ion beams. *Precis. Eng.*, 9, 71, 1987.

135. Miyamoto, I., Ezawa, T., Nishimura, K., Ion beam machining of single-point diamond tools for nano-precision turning. *Nanotechnology*, *1*, 44, 1990.

136. Drummond, I.W. and Long, J.V.P., Scanning ion microscopy and ion beam micro-machining. *Nature*, *215*, 950, 1967.

137. Dong, H. and Bell, T., State-of-the-art overview: ion beam surface modification of polymers towards improving tribological properties. *Surf. Coat. Technol.*, 111, 29, 1999.

138. Bayly, A.R. and Townsend, P.D., Optical applications of ion beam machining. *Opt. Laser Technol.*, 5, 205, 1973.

139. Hashimoto, I., Arimatsu, K., Ishikawa, Y., Tanaka, S., Gejyo, T., Development of a high deposition rate machine by ion beam sputtering. *Nucl. Instrum. Methods Phys. Res. B: Beam Interact. Mater. At.*, *37-38*, 838, 1989.

140. Davies, S.T. and Bowen, D.K., Ion Beam Machining of Micromechanical Structures. *MRS Online Proc. Lib.*, 76, 135, 1986.

141. Remnev, A.G., Nagato, K., Uemura, K., Effect of working gas composition in medical needle sharpening by ion beam sputtering. *Biomed. Phys. Eng. Express*, 4, 025033, 2018.

142. Liu, Y., Hirsch, D., Fechner, R., Hong, Y., Fu, S., Frost, F., Rauschenbach, B., Nanostructures on fused silica surfaces produced by ion beam sputtering with Al co-deposition. *Appl. Phys. A Mater. Sci. Process.*, 124, 73, 2018.

143. Castellano, R.N., A comparison of reactive ion beam milling and reactive ion etching for multilevel resist

patterning. *J. Electrochem. Soc.*, *131*, 2340, 1984.

144. Xiao, H., Dai, Y., Duan, J., Tian, Y., Li, J., Material removal and surface evolution of single crystal silicon during ion beam polishing. *Appl. Surf. Sci.*, 544, 148954, 2021.

145. Wang, J., Chen, J., Jin, T., Guo, B., Yuan, J., Zhao, Q., Preparation of nanotwinned cBN cutting edge by combining mechanical lapping and ion beam polishing. *Diam. Relat. Mater.*, 105, 107801, 2020.

146. Xu, J., Wang, C.J., Guo, B., Shan, D.B., Sugiyama, Y., Ono, S., Surface finish of micro punch with ion beam irradiation. *Trans. Nonferrous Met. Soc. China*, 19, s526, 2009.

147. Li, S. and Dai, Y., Ion Beam Figuring Technology, in: *Large and Middle-Scale Aperture Aspheric Surfaces*, John Wiley & Sons Singapore Pte. Ltd, 2016.

148. Scherer, A., Soole, J., Beebe, E., Orenstein, M., Bhat, R., Ion Beam Machining of Optoelectronic Components, in: *LEOS 1991 Summer Topical Meetings on Epitaxial Materials and In-Situ Processing for Optoelectronic Devices. Photonics and Optoelectronics*, pp. 8–9, IEEE, Newport Beach, CA, USA, 1991.

149. Brun, S., Guibert, G., Meunier, C., Guibert, E., Keppner, H., Mikhailov, S., Rapid and direct micro-machining/patterning of polymer materials by oxygen MeV ion beam irradiation through masks. *Nucl. Instrum. Methods Phys. Res. B.*, 269, 2422, 2011.

150. Tagg, M.A., Smith, R., Walls, J.M., Sample rocking and rotation in ion beam etching. *J. Mater. Sci.*, 21, 123, 1986.

151. Li, Y., Takino, H., Frost, F., Characteristics of diamond turned NiP smoothed with ion beam planarization technique. *J. Eur. Opt. Soc.-Rapid Publ.*, 13, 27, 2017.

152. Bauer, J., Frost, F., Arnold, T., Reactive ion beam figuring of optical aluminium surfaces. *J. Phys. D: Appl. Phys.*, 50, 085101, 2017.

153. Lee, I.S., Zhao, B., Lee, G.H., Choi, S.H., Chung, S.M., Industrial application of ion beam assisted deposition on medical implants. *Surf. Coat. Technol.*, 201, 5132, 2007.

154. Linß, F., Bundesmann, C., Frost, F., Low-energy ion beam erosion of Si with simultaneous co-deposition of metallic surfactants: Experimental and simulated data. *Appl. Surf. Sci.*, 646, 158923, 2024.

155. Horino, Y., Tsubouchi, N., Enders, B., Heck, C., Chayahara, A., Kinomura, A., Fujii, K., Development of a New Ion-Beam Deposition Technology for Ultra-High-Purity Film Fabrication. *Phys. Stat. Sol. (a)*, 160, 583, 1997.

156. Yatsui, K., Jiang, W., Suematsu, H., Suzuki, T., Kinemuchi, Y., Yang, S.C., Quick preparation of thin films and nanosize powders by high-density ablation plasma produced by intense pulsed ion beam, in: *IEEE Conference Record - Abstracts. PPPS-2001 Pulsed Power Plasma Science 2001. 28th IEEE International Conference on Plasma Science and 13th IEEE International Pulsed Power Conference (Cat. No.01CH37)*, p. 476, IEEE, Las Vegas, NV, USA, 2001.

157. Zeuner, M. and Kiontke, S., Ion Beam Figuring Technology in Optics Manufacturing. *Opt. Photonik*, 7, 56, 2012.

158. Kurashima, Y., Miyachi, S., Miyamoto, I., Ando, M., Numata, A., Evaluation of surface roughness of ULE® substrates machined by Ar+ ion beam. *Microelectron. Eng.*, *85*, 1193, 2008.

159. Arnold, T. and Pietag, F., Ion beam figuring machine for ultra-precision silicon spheres correction. *Precis. Eng.*, 41, 119, 2015.

160. Nabhiraj, P.Y., Menon, R., Rao, G.M., Mohan, S., Bhandari, R.K., Micro fabrication by low energy ion beam from plasma based ion sources, in: *2011 IEEE International Vacuum Electronics Conference (IVEC)*, pp. 395–396, IEEE, Bangalore, India, 2011.

161. Zhou, G., Tian, Y., Shi, F., Song, C., Tie, G., Zhou, G., Xie, L., Shao, J., Wu, Z., Low-energy pulsed ion beam technology with ultra-high material removal resolution and widely adjustable removal efficiency. *Micromachines*, 12, 1370, 2021.

162. Toyoda, N., Houzumi, S., Mashita, T., Mitamura, T., Mochiji, K., Yamada, I., Novel precision machining using gas cluster ion beams. *Surf. Coat. Technol.*, 201, 8624, 2007.

163. Ando, M., Matsuzaka, M., Saita, M., Experimental study of multiple ion beam machine. *Microelectron. Eng.*, 11, 431, 1990.

164. Wang, Q., Kishimoto, S., Tanaka, Y., Naito, K., Fabrication of nanoscale speckle using broad ion beam milling on polymers for deformation analysis. *Theor. Appl. Mech. Lett.*, 6, 157, 2016.

165. Kawasegi, N., Ozaki, K., Morita, N., Nishimura, K., Yamaguchi, M., Development and machining performance of a textured diamond cutting tool

fabricated with a focused ion beam and heat treatment. *Precis. Eng.*, 47, 311, 2017.

166. Barienti, K., Kahra, C., Herbst, S., Nürnberger, F., Maier, H.J., Ion Beam Processing for Sample Preparation of Hybrid Materials with Strongly Differing Mechanical Properties. *Metallogr. Microstruct. Anal.*, 9, 54, 2020.

167. Eichhorn, V., Bartenwerfer, M., Fatikow, S., Nanorobotic assembly and focused ion beam processing of nanotube-enhanced AFM probes. *IEEE Trans. Autom. Sci. Eng.*, 9, 679, 2012.

168. Milani, M. and Drobne, D., Focused ion beam manipulation and ultramicroscopy of unprepared cells. *Scanning*, 28, 148, 2006.

169. Miller, T.M., Fang, H., Magruder, R.H., Weller, R.A., Fabrication of a micro-scale, indium-tin-oxide thin film strain-sensor by pulsed laser deposition and focused ion beam machining. *Sens. Actuators A Phys.*, 104, 162, 2003.

170. Kaur, K.S., Feinaeugle, M., Banks, D.P., Ou, J.Y., Di Pietrantonio, F., Verona, E., Sones, C.L., Eason, R.W., Laser-induced forward transfer of focussed ion beam pre-machined donors. *Appl. Surf. Sci.*, 257, 6650, 2011.

171. Rajput, N.S., Singh, A.K., Verma, H.C., Beam scanning effect on focused-ion-beam-induced processing. *Radiat. Eff. Defects Solids*, 168, 472, 2013.

172. Inkson, B.J., Dehm, G., Wagner, T., Thermal stability of Ti and Pt nanowires manufactured by Ga + focused ion beam. *J. Microsc.*, 214, 252, 2004.

173. Lee, U.S., Kim, B.H., Kim, S.M., Oh, C.S., Rapid manufacturing of large diameter Cu micropillars by

micro-electrical discharge machining and focused ion beam. *Int. J. Adv. Manuf. Technol.*, 113, 1153, 2021.

174. Fujiwara, K., Pahlovy, S.A., Miyamoto, I., Ar+ ion beam machining of the carbon thin layer deposited on the Zerodur® substrate for EUVL projection optics. In. *Microelectron. Eng.*, 88, 2527, 2011.

175. Assayag, G.B., Sudraud, P., Gierak, J., Remiens, D., Menigaux, L., Dugrand, L., Focused ion beam machining of mirror facets of a monolithically integrated GaAs/GaAlAs double heterojunction (DH) laser and its optical waveguide. *Microelectron. Eng.*, 11, 413, 1990.

176. Frey, L., Lehrer, C., Ryssel, H., Nanoscale effects in focused ion beam processing. *Appl. Phys. A Mater. Sci. Process.*, 6, 1017, 2003, (2003, May).

177. Adams, D.P., Benavides, G.L., Vasile, M.J., Micrometer-scale machining of metals and polymers enabled by focused ion beam sputtering. *MRS Online Proc. Lib.*, 546, 201, 1998.

Note

*Corresponding author: pravinpawar@nitgoa.ac.in; pravin.1900@gmail.com

22
Parametric Optimization in Electrochemical Discharge Machining of Microchannel on Glass Using Multiple Tool Passes

Rithwik Shankar Raj[1], Neeraj Bagi[2], Jinka Ranganayakulu[1]*, A. Bharatish[1] and K. Venkata Rao[3]

[1]Dept. of Mechanical Engineering, RV College of Engineering, Bengaluru, Karnataka, India

[2]MeuKron Technologies, Belagavi, Karnataka, India

[3]Vignan's Foundation for Science, Technology & Research (Deemed to be University), Guntur, Andhra Pradesh, India

Abstract

The demand for glass-based devices such as microreactors, microelectromechanical systems and especially in the production of microfluidic devices is increasing. It is mainly due to properties of glass such as chemical resistance, minimal thermal expansion, high toughness, and optical transference. Also, glass can be bonded anodically to silicon wafer to form closed microfluidic channels for biomedical applications. But glass machining poses significant challenges due to its brittleness and susceptibility to cracks and fractures. Electrochemical discharge machining is a promising technique for precise and efficient glass machining. In this chapter, micromachining of channels on glass workpiece was carried out using mixed electrolyte of NaOH and KOH. In addition, a three-pass tool feed was implemented to avoid tool bending issues, and the process

parameters were optimized Taguchibased grey relational analysis.

***Keywords*:** Mixed electrolyte, multi-tool pass, grey relational analysis, microchannel

22.1 Introduction

Glass has extensive uses in the micromanufacturing industry, especially in the production of microfluidic devices, microreactors, microelectromechanical systems (MEMS), and bio-medical devices, due to favorable properties such as its capacity to anodically bond with silicon wafers, chemical inertness, minimal thermal expansion, high toughness, and optical transference. Glass machining poses significant challenges due to its brittleness and susceptibility to cracks and fractures. Electrochemical discharge machining (ECDM) emerges as a promising technique to ensure precise and efficient glass machining. Electrochemical discharge machining is a machining technique introduced in 1968 by Kurafuji *et al*. [1] as a hybrid process. The process has several terms in literature, including ‘electrochemical arc machining’ [2], ‘electrochemical spark machining’ [3], and ‘spark-assisted chemical engraving (SACE)’ [4]. The choice of glass material depends on the desired quality. Borosilicate glass is commonly preferred for its capacity to anode bond to silicon [5] and its excellent biocompatibility, which is essential for bio-MEMS devices [6]. The advent of lab-on-chip devices and applications demands high pressures and temperatures coupled with the use of volatile fluids, which necessitates the use of glass [7]. Other methods used for the micromachining of glass include plasma etching and laser ablation methods [8–10]. These methods generally require more elaborate infrastructure in case of laser ablation and masking layers in plasma etching, representing current constraints. Therefore, simpler and cost-effective methods are required for etching glass-based microdevices [11].

Electrochemical discharge machining is a suitable alternative method as it is capable of machining micro-holes on non-conductive materials irrespective of their strength and hardness [12, 13]. Higher speed machining is observed when using ECDM compared to dry and wet etching and ultrasonic drilling processes [10]. Several machining parameters can increase the performance and efficiency of the ECDM machining process. The ECDM process is a hybrid method that combines electrochemical machining (ECM) and electric discharge machining (EDM) [11] and has been used for the machining of nonconducting materials, including polymer matrix composites, SiC, quartz, alumina, and zirconia [11, 12, 14, 15].

This chapter focuses on the study of microchannels machined with multi (three) tool passes using mixed electrolytes of NaOH and KOH. The detailed literature review is presented on applications of glass-based microfluidic devices, mechanics of material removal, electrolyte types, and their influence and optimization of process parameters.

22.1.1 Applications of Glass-Based Microfluidic Devices

Lab-on-a-chip devices require machining microchannels with dimensions within the range of 10–100µm [16]. Glass substrates preferred generally in microfluidic devices include borosilicate, soda lime, fused quartz and Pyrex glass, a type of borosilicate glass, comprises 80% silicon dioxide (SiO_2), 12% boron trioxide (B_2O_3), 3% aluminum oxide (Al_2O_3), and 4% sodium oxide (Na_2O) by weight. Notably, Pyrex glass exhibits a low coefficient of thermal expansion of 3.3×10^{-6} K^{-1} until 400°C, and it offers transparency across a range of wavelengths, including those visible to the human eye, near-ultraviolet (UV), and near-infrared (IR), rendering it suitable for optical analysis or fluorescent radiation testing

[16]. Quartz only contains silicon oxide (SiO_2) and is well-suited for insulating microfluidic devices integrated with electronic circuits or electrodes due to its high electrical resistivity [17].

Microfluidic devices based on glass can be used to capture important cells for visualization from a variety of orientations, with the capacity to regulate the single-cell angle visibility to a minimum of 0.72°. Microchips based on silicon-Pyrex facilitate experimental trials at elevated pressures (up to 300 bar) and high temperatures (up to 400°C) [18]. These experimental conditions enable rapid attainment of phase equilibrium in fluid mixtures within microfluidic devices, facilitating the exploration of phase transport phenomena in microchannels [19]. Glass microfluidic devices find application in monitoring chemical reactions [20], analyzing bio-samples [21], and visualizing complex flow dynamics. They are particularly useful for studying multiphase flow [22], interactions among oil, water, and solid phases [23], gas dynamics [24], and porous networks [25–27]. They are also used for microreactor applications such as monodisperse gold nanoparticles [28] and small sample volume synthesis of proteins [29]. Glass-based devices are preferred for manufacturing opto-fluidic detection devices, micro-mixers, micro-valves, micro-pumps, micro-sensors, cell culturing applications, and particle filters [30].

22.1.2 Material Removal in ECDM

Numerous investigations have explored the material removal mechanism in ECDM. Ghosh and Basak [31] formulated a theoretical model to predict the material removal rate (MRR), which was subsequently validated through experimental data. Unlike discharge occurring due to the breakdown of a thin gas film, it was studied as a switching process. Studies indicated an augmentation in the MRR with

higher electrolyte concentration and inductance. Material erosion in glass is attributed not only to thermal effects from spark generation but also to chemical erosion resulting from the interaction of the alkali solution with glass [32]. Further analysis of the chemical aspect of material removal suggested a high-temperature etching process [33]. The electrochemical discharge phenomenon mirrors what is seen in arc discharge valves. Spark energy and the approximate size of hydrogen gas bubbles are inferred from the proposed model. Jain *et al*. [12] determined the MRR by treating the process as a 3D unsteady-state heat conduction problem. The ECDM mechanism model has been refined through experimental observation of the circuit's time-varying current [34], where the interplay between thermal energy from the spark and chemical etching by the electrolyte jointly governs MRR in ECDM.

22.1.3 Electrolyte Type and Influence of Electrolytes

The choice and concentration of the electrolyte are crucial factors in the machining of glass by ECDM. Numerous studies have analyzed the impact of electrolyte parameters on the machining process. NaOH and KOH electrolytes are mainly focused on research due to their significant influence on MRR, surface roughness, discharge stability, and machining depth. The study by Yang *et al*. [33] reports a higher MRR when alkaline electrolytes have a higher pH value. Machining slits in glass using wire electrochemical discharge machining (WECDM) revealed that slit expansion was less pronounced when employing KOH electrolyte compared to NaOH. This discrepancy is attributed to denser bubble formation with KOH electrolyte, leading to a more stable discharge [35]. Furthermore, using NaCl as an electrolyte for machining soda lime glass rods demonstrated that the applied voltage significantly affects the width and depth of machined grooves and the machined area's surface

roughness [36]. Glass microstructuring using KOH and NaOH electrolytes revealed that holes machined in KOH solutions exhibited smaller diameters compared to those in NaOH solutions of the same concentration. This disparity is attributed to the higher hydrogen bubble density in KOH solutions, stemming from their superior conductivity, which also contributes to a more stable isolation layer [37]. Additionally, higher concentrations of NaOH electrolyte result in increased viscosity and yield smoother channels on the glass workpiece [38]. A comparative study between KOH and NaCl electrolytes for glass machining revealed a higher MRR with KOH due to its greater reactivity with glass [39]. Experimental findings suggested that NaOH was more effective than $NaNO_3$ for machining soda lime glass, with MRR showing an increasing trend with applied voltage. However, NaOH electrolytes may produce harmful fumes if ventilation is inadequate, unlike $NaNO_3$, which does not generate such fumes [40]. Moreover, higher concentrations of NaOH electrolyte result in more frequent vaporization of borosilicate glass surface material by high-energy sparks, whereas lower concentrations lead to smaller hole sizes with surface wrinkling due to chemical etching predominance [41]. Commonly used electrolytes in ECDM processes are KOH, NaOH, NaCl, and KCl, among which KCl and NaCl often form precipitates of heavy salt, necessitating frequent electrolyte solution replacement. Therefore, KOH and NaOH are preferred electrolytes for the ECDM process [42]. Furthermore, $NaNO_3$ exhibits a significantly higher critical voltage than NaOH and KOH alkaline electrolytes [43].

22.1.4 ECDM Process Parameters and Statistical Analysis

Recent studies have focused more on research efforts to investigate the quality aspects of the ECDM process. The MRR during ECDM of soda lime glass was found to be

directly influenced by electrolyte concentration, higher duty factor, and energy partition [44]. Kim *et al.* [45] and Rajurkar *et al.* [46] observed that achieving excellent surface quality is possible without the need for surface treatments. Kirchner [47] demonstrated the potential for creating microstructures on hard metals by avoiding tool wear using ECM with extremely small pulses. Additionally, Ghosh *et al.* [47] proposed utilizing the electrochemical discharge phenomenon for the micro-welding of workpieces. However, it becomes essential to identify the ideal combination of process parameters. Statistical tools and methods prove to be essential tools for this purpose. Taguchi's methodology [49–51] effectively determines the optimal settings for process parameters pertaining to drilling to enhance output response. The signal-to-noise ratios (S/N ratios) are generally considered to optimize the responses with respect to the input parameters. However, this method fails to consider the concurrent effects of multiple parameters for optimization. Grey relational analysis (GRA) was introduced for ECDM first by Deng [52], which is meant to tackle the limitations. Moreover, GRA can be utilized for multi-response optimization of the ECDM process [53–59].

The literature shows that most of the parametric study was done with a single tool pass and a single type of electrolyte. Hence, the present work focuses on the optimization process parameters to machine the microchannels with multi-tool passes (three) with mixed electrolytes of NaOH and KOH considering the responses like the MRR, heat affected zone (HAZ), and overcut, using an in-house prototype machining setup. The process parameters were optimized using Taguchi-based GRA.

22.2 Methodology Adopted to Machine Microchannel

The overview of the methodology adopted to machine microchannel and optimization of process parameters is presented in Figure 22.1.

22.3 Experimentation

In the present work, three factors were taken as input parameters, namely, electrolyte concentration, voltage, and duty factor each at three levels. The responses taken were MRR, HAZ and overcut. Experiments were conducted according to design of experiments. Degree of freedom is calculated for the factors. As each factor has three levels, the degree of freedom is 7. Therefore, at three factors and three levels and with degree of freedom of 7, L_9 orthogonal array was selected for conducting experiments. An in-house developed experimental set-up as shown in Figure 22.2 was used to conduct the experiments. The electrolyte cell with close-up view with anode and spark generation is presented in Figure 22.3. A mixed electrolyte of NaOH and KOH helps to machine deeper channels [43]. Also, it increases electrical conductivity of the electrolyte due to higher ionic mobility of K+ ions [59]. In addition, a pulsed direct current (DC) was implemented with T_{on} and T_{off} of 2 ms and 1 ms, respectively, with pulse frequency of 333 Hz to allow the fresh electrolyte to reach the machining zone and as well as to cool the tool [5]. The properties of the borosilicate glass workpiece along with its values are shown in Table 22.1. A stainless-steel tool of 0.3 mm was used separately for each experiment. A graphite plate of size 40 mm x 40 mm x 5 mm was used as an auxiliary electrode (anode).

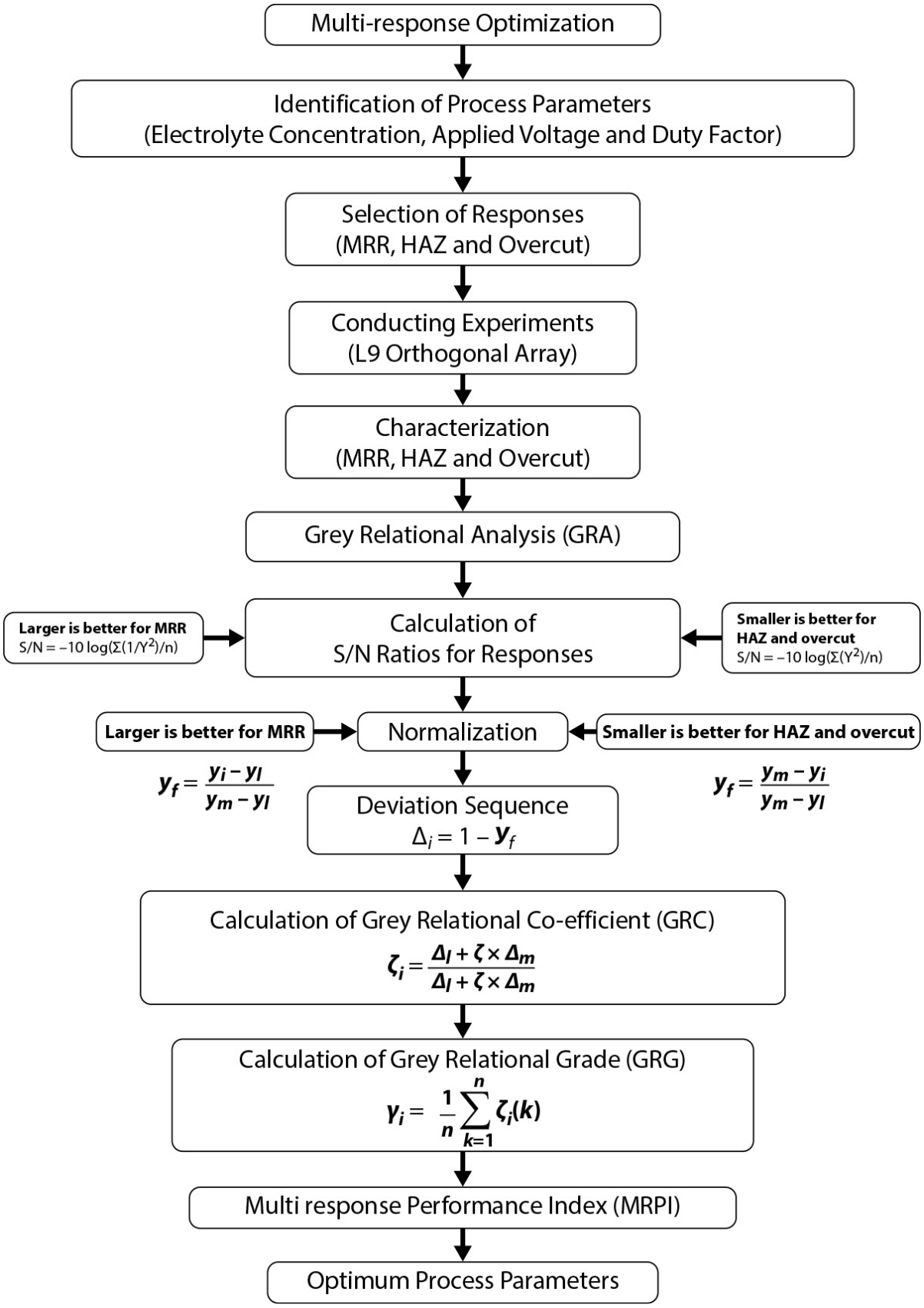

Multi-response Optimization
Identification of Process Parameters
(Electrolyte Concentration, Applied Voltage and Duty Factor)
Selection of Responses
(MRR, HAZ and Overcut)
Conducting Experiments
(L9 Orthogonal Array)
Characterization
(MRR, HAZ and Overcut)
Grey Relational Analysis (GRA)
Larger is better for MRR
S/N = −10 log(Σ(1/Y2)/n)
Calculation of
S/N Ratios for Responses
Smaller is better for
HAZ and overcut
S/N = −10 log(Σ(Y2)/n)
Larger is better for MRR
Normalization
Smaller is better for HAZ and overcut
$y_f = \frac{y_i - y_I}{y_m - y_I}$
$y_f = \frac{y_m - y_i}{y_m - y_I}$
Deviation Sequence
$\Delta_i = 1 - y_f$
Calculation of Grey Relational Co-efficient (GRC)
$\zeta_i = \frac{\Delta_I + \zeta \times \Delta_m}{\Delta_I + \zeta \times \Delta_m}$
Calculation of Grey Relational Grade (GRG)
$\gamma_i = \frac{1}{n}\sum_{k=1}^{n} \zeta_i(k)$
Multi response Performance Index (MRPI)
Optimum Process Parameters

Figure 22.1 Overview of the methodology adopted to optimize process parameters.

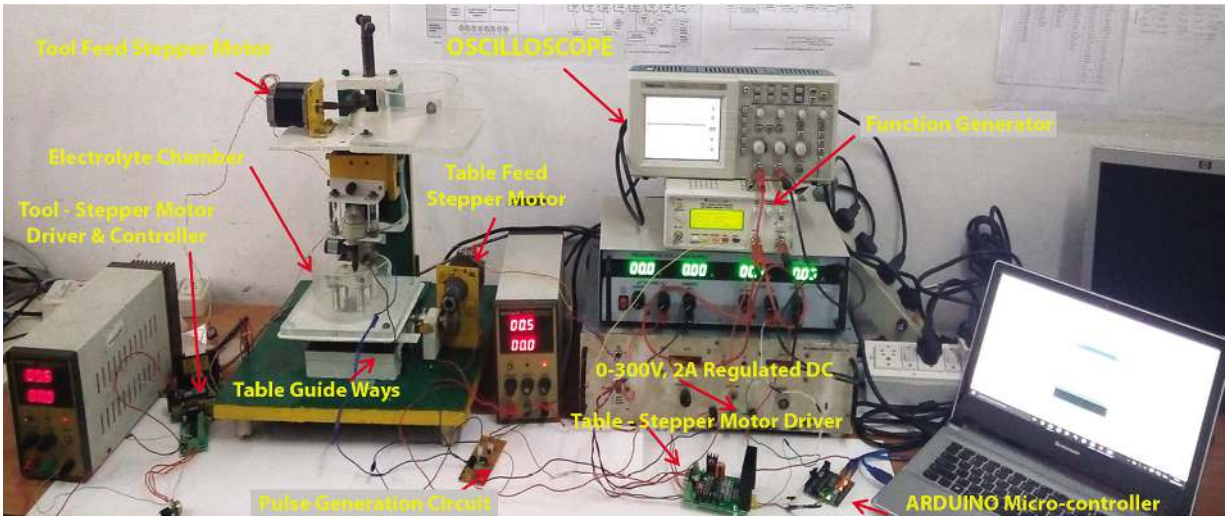


Figure 22.2 In-house ECDM experimental set-up.

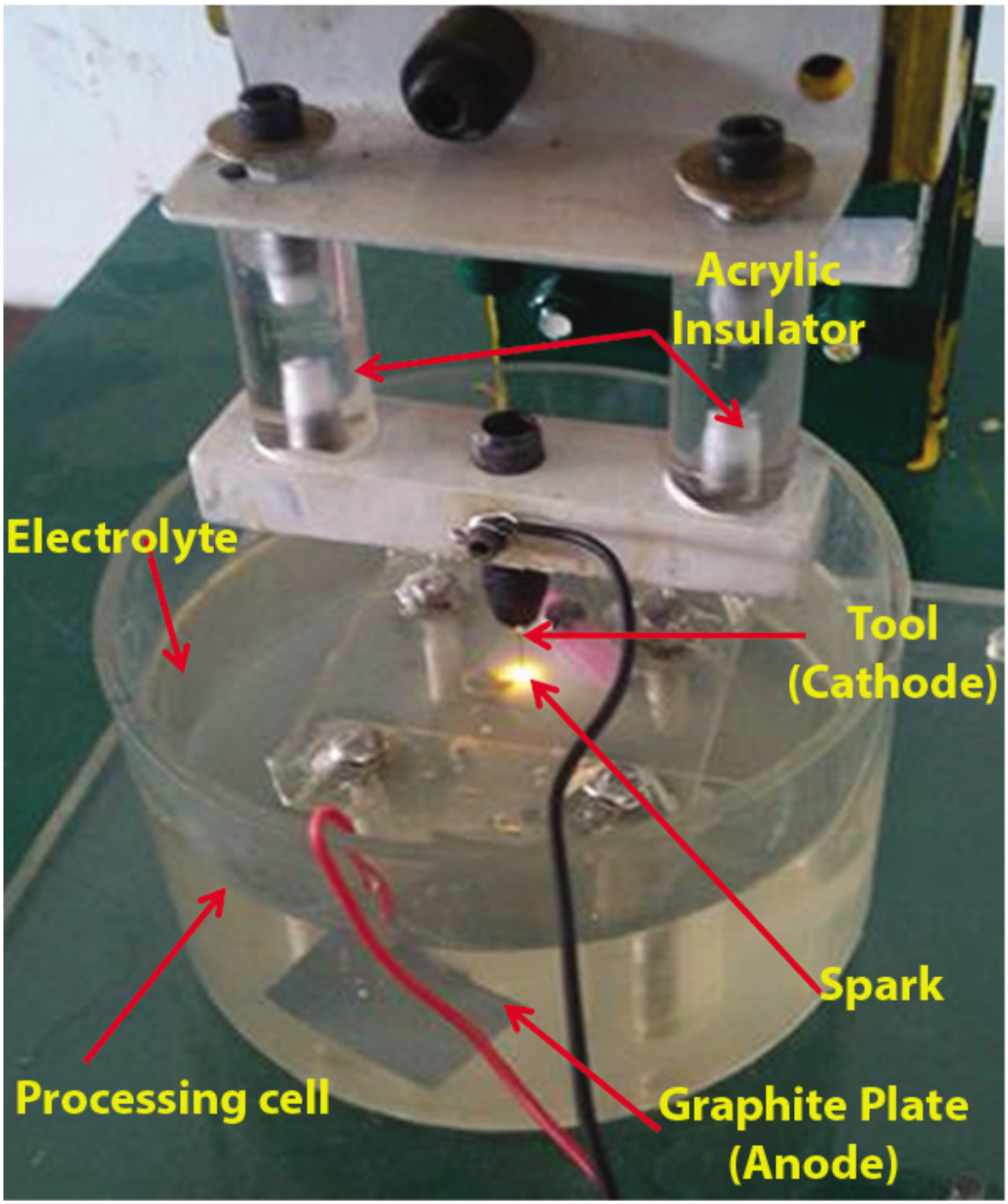


Figure 22.3 Electrolyte (processing) cell arrangement.

Table 22.1 Properties of borosilicate glass.

Property	**Values**
Density at 25 °C	2.23 g/cm^3

Property	Values
Young's modulus E	63 x 10^3 N/mm^2
Thermal conductivity, λ, at 90°C	1.2 $W.m^{-1}.K^{-1}$
Poisson's ratio, μ	0.2
Transformation temperature, T	525°C
Softening point	820°C

When the voltage is increased across the anode and cathode, the electrolysis of water takes place and forms H_2 gas bubbles at cathode (tool) and O_2 bubbles at anode as shown in Equations 22.1 and 22.2, respectively [60].

Cathodic reactions (at tool):

$$2H_2O + 2e^- \rightarrow 2OH^- + H_2\uparrow \quad (22.1)$$

Anodic reactions (at auxiliary electrode, graphite):

$$4OH^- \rightarrow 2H_2O + O_2\uparrow + 4e^- \quad (22.2)$$

With increase in voltage the H_2 bubble density increases at cathode and finally forms gas blanket between tool and electrolyte. At critical voltage the breakdown of voltage takes place across the gas blanket and the intensity of the spark melts and vaporizes the work material.

The chemical reactions of the electrolytes follow Equations 22.3 and 22.4, respectively [33]. The chemicals attack the glass and weakens silicon bonding and starts chemical etching.

$$SiO_2 + 2KOH + H_2O \rightarrow Si(OH)_4 + K_2O \quad (22.3)$$

$$SiO_2 + 2NaOH + H_2O \rightarrow Si(OH)_4 + Na_2O \quad (22.4)$$

The three process parameters at three levels as shown in Table 22.2 were used for the experimentation. The

experimental plan based on L_9 orthogonal array as shown in Table 22.3 was used to conduct the experiments. Once the experiments were done, the characterization was done to calculate the MRR, overcut and HAZ. Finally, the responses were optimized using Taguchi-based experimental plan and S/N ratios with GRA method and using multi-response performance index (MRPI), the optimal process parameters were identified.

Table 22.2 Process parameters at three levels.

Factor	Level 1	Level 2	Level 3
Electrolyte concentration (EC) (wt.%) (NaOH + KOH)	(12+3) 15	(17+3) 20	(22+3) 25
Voltage, (V)	40	45	50
DF (%)	65	70	75

Table 22.3 Experimental plan.

Trial no.	EC (wt. by %)	V	DF (%)
1	15	40	65
2	15	45	70
3	15	50	75
4	20	40	70
5	20	45	75
6	20	50	65
7	25	40	75
8	25	45	65
9	25	50	70

22.3.1 Step-by-Step Procedure for Conducting the Experiments

The procedure for conducting experiments is described as follows,

1. All the workpieces to be machined were cleaned and dried. Weight of workpieces were measured before machining.
2. Electrolyte was prepared based on weight by percentage by mixing different combinations of NaOH and KOH with distilled water.
3. Workpiece was clamped and electrolyte was poured in the chamber. Tool was immersed in the electrolyte to 2-mm depth and an initial clearance of 25 µm was set between tool tip and the surface of workpiece.
4. Electrodes (anode and cathode) were separated at 35 mm during experiments.
5. Constant table feed rate of 0.49 mm/min was maintained using stepper motor and the tool was made to move in downward direction to a depth of 0.04 mm for each pass. The channel machining length was fixed at 8 mm.
6. When all the three passes were done, workpiece was removed and cleaned well. The weight of workpiece was measured after machining.
7. Characterization of microchannels made on workpiece was done using scanning electron microscope.

22.3.2 Experimental Results

Experiments were done based on design of experiments and L_9 orthogonal array. The results for MRR, HAZ, and overcut obtained using Equations 22.5–22.7, respectively, as shown in Table 22.4. The measurements of channel width and HAZ are shown in Figure 22.4.

Table 22.4 Experimental results.

Trial no.	MRR (mg/min)	HAZ (mm)	Overcut (mm)
1	0.0409	0.0958	0.0583
2	0.2090	0.2100	0.0866
3	0.2586	0.2573	0.0966
4	0.1520	0.1065	0.1101
5	0.2459	0.2355	0.1298
6	0.1844	0.1985	0.1919
7	0.1455	0.2069	0.1339
8	0.1680	0.2769	0.1815
9	0.2377	0.2933	0.2033

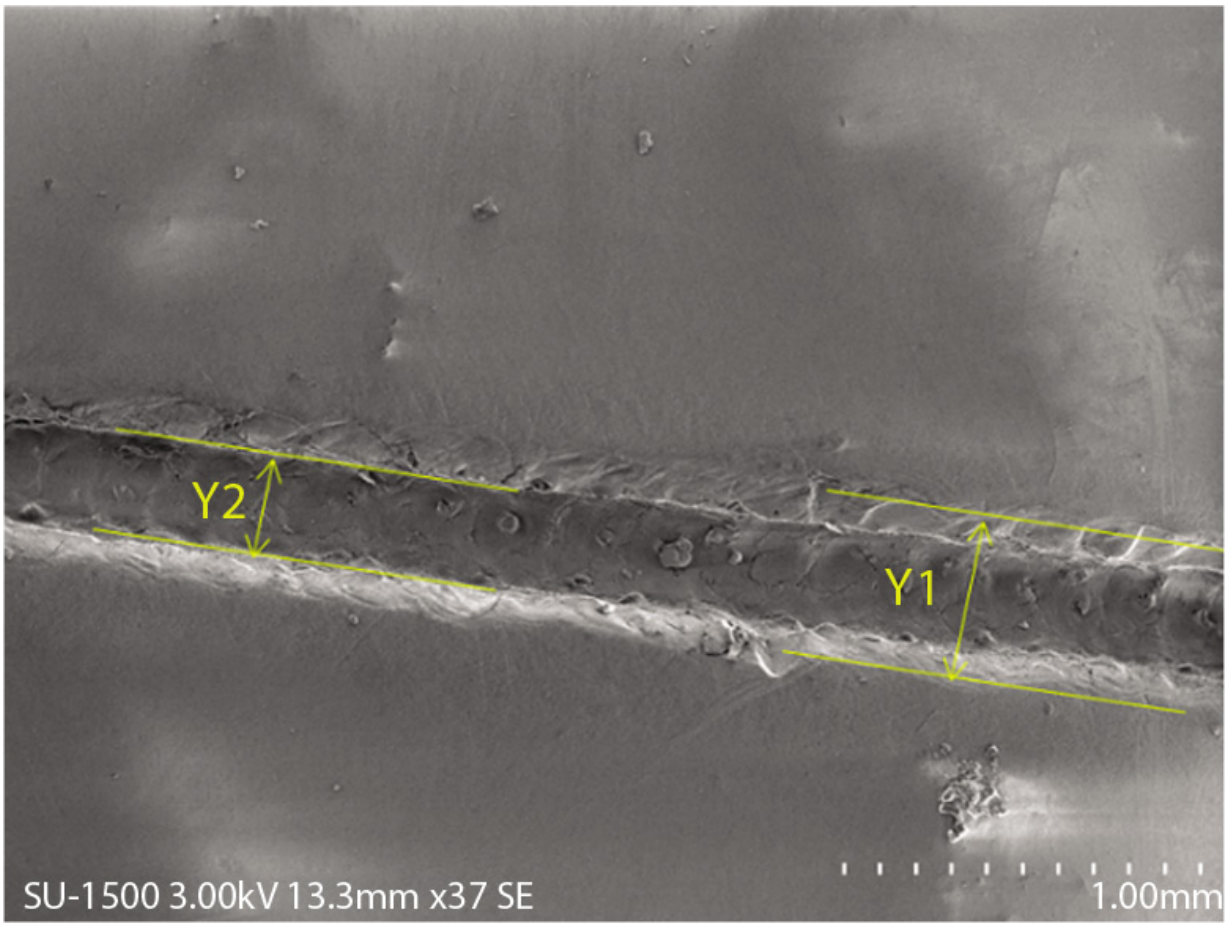


Figure 22.4 SEM image of microchannel.

22.3.2.1 Characterization of Microchannels

- **Material Removal Rate**

  MRR was calculated using Equation 22.5

$$MRR = (W_1 - W_2) / T \quad (22.5)$$

  Where W_1 and W_2 are the weight of the workpieces before and after machining, and T = time in minutes.

- **Heat Affected Zone**

  HAZ was calculated using Equation 22.6

$$HAZ = (Y_1 - Y_2)/2 \quad (22.6)$$

Where Y_1 = width of HAZ, Y_2 = width of machined microchannel.

- **Overcut**

  Overcut was calculated using Equation 22.7.

$$Overcut = (Y_2 - Z_2)/2 \quad (22.7)$$

Where Y_2= width of machined microchannel and Z_2 = tool diameter.

22.3.3 Grey Relational Analysis

In this method, all responses are combined into a single grey relational grade, and a ranking is assigned. The grey relational grade with the highest rank provides the optimal process parameters. During data normalization, Equation 22.8, higher is better, and is used for MRR, and lower is better for HAZ and overcut, as shown in Equation 22.9.

Step 1: before GRA is performed, the data is normalized and the original sequence is converted to values between 0 and 1.

Higher is better, the normalization of data can be performed for MRR.

$$y_f = \frac{y_i - y_l}{y_m - y_l} \quad (22.8)$$

Lower is better, the normalization of data can be performed for HAZ and overcut.

$$y_f = \frac{y_m - y_i}{y_m - y_l} \quad (22.9)$$

where, y_f = normalized value, y_i = original value, y_m = highest value in the original sequence and, y_l = lowest value

in the original sequence.

Step 2: after performing normalization, the highest value 1 is taken as the reference value and the difference between the normalized values in the sequence and the reference values are found.

$$\Delta_i = 1 - y_f \tag{22.10}$$

Step 3: calculation of the grey relational coefficient (GRC)

$$\zeta_i = \frac{\Delta_l + \zeta \times \Delta_m}{\Delta_i + \zeta \times \Delta_m} \tag{22.11}$$

where, ζ_i = grey relational coefficient, ζ = distinguishing or identification coefficient = 0.5, Δ_l = lowest difference = 0 and Δ_m = highest difference = 1

Step 4: calculation of the grey relational grade (GRG) is done by taking the average of the GRC of the responses.

$$\gamma_i = \frac{1}{n} \Sigma_{k=1}^{n} \zeta_i(k) \tag{22.12}$$

22.4 Multi-Response Optimization

The Taguchi method mainly deals with single-response optimization problems where only one response is considered. To overcome this, multi-responses were combined into a single response to obtain optimal levels. In the present work, GRA is used on the S/N ratios to solve multi-response problem and is solved as follows:

22.4.1 Calculation of S/N Ratio for the Responses

The S/N ratio for responses were calculated using larger is better for MRR and smaller is better for HAZ and over cut

using Equations 22.13 and 22.14, respectively, as indicated in Table 22.5.

Table 22.5 S/N ratio for the responses.

Trial no.	S/N ratios		
	MRR	**HAZ**	**Overcut**
1	–27.7655	20.3700	24.6822
2	–13.5971	13.555	21.2496
3	–11.7474	11.7905	20.3005
4	–16.3631	19.4530	19.1643
5	–12.1848	12.5569	17.7292
6	–14.6848	14.0435	14.3344
7	–16.7427	13.6848	17.4644
8	–15.4938	11.1535	14.8225
9	–12.4794	10.6532	13.8373

Larger is better for MRR:

$$S/N = -10 \log(\Sigma(1/Y^2)/n) \quad (22.13)$$

Smaller is better for HAZ and overcut:

$$S/N = -10 \log(\Sigma(Y^2)/n) \quad (22.14)$$

where Y = responses and n = number of responses for the given factor level combination.

22.4.2 Normalization of S/N Ratio Values

The obtained S/N ratios are normalized using Equation 22.13 for MRR and Equation 22.14 for HAZ and overcut, respectively, as shown in Table 22.6.

22.4.3 Calculation of GRC and GRG

Finally, normalized values of S/N ratios were used to calculate deviation sequence, GRC, and GRG using Equations 22.10–22.12, respectively, as shown in Table 22.7.

22.4.4 Calculation of Optimal Levels for Process Parameters Using Multi-Response Performance Index (MRPI)

Figure 22.5 shows the main effects plot for means on GRG. The MRPI were calculated using GRG values for calculating optimal process parameters, as shown in Table 22.8.

Table 22.6 Normalized values of S/N ratios.

Trial no.	Normalized values of S/N ratios		
	MRR	**HAZ**	**Overcut**
1	1	0	0
2	0.11547	0.70130	0.31651
3	0	0.88295	0.40403
4	0.28815	0.09437	0.50880
5	0.02730	0.80408	0.644113
6	0.18338	0.65108	0.95416
7	0.31185	0.68800	0.66554
8	0.23388	0.94851	0.90915
9	0.04569	1	1

Table 22.7 Deviation sequence, GRC, and GRG.

Exp. no.	Deviation sequence			GRC			GRG
	MRR	HAZ	Overcut	MRR	HAZ	Overcut	
1	0	1	1	1	0.3333	0.3333	0.5555
2	0.8845	0.2987	0.6834	0.3611	0.6260	0.4224	0.4698
3	1	0.1170	0.5959	0.3333	0.8103	0.4562	0.5332
4	0.7118	0.9056	0.4912	0.4125	0.3557	0.5044	0.4242
5	0.9727	0.1959	0.3558	0.3395	0.7185	0.5842	0.5473
6	0.8166	0.3489	0.0458	0.3797	0.5889	0.9160	0.6282
7	0.6881	0.3120	0.3344	0.4208	0.6158	0.5992	0.5452
8	0.7661	0.0051	0.0091	0.3949	0.9898	0.8462	0.7436
9	0.9543	0	0	0.3438	1	1	0.7813

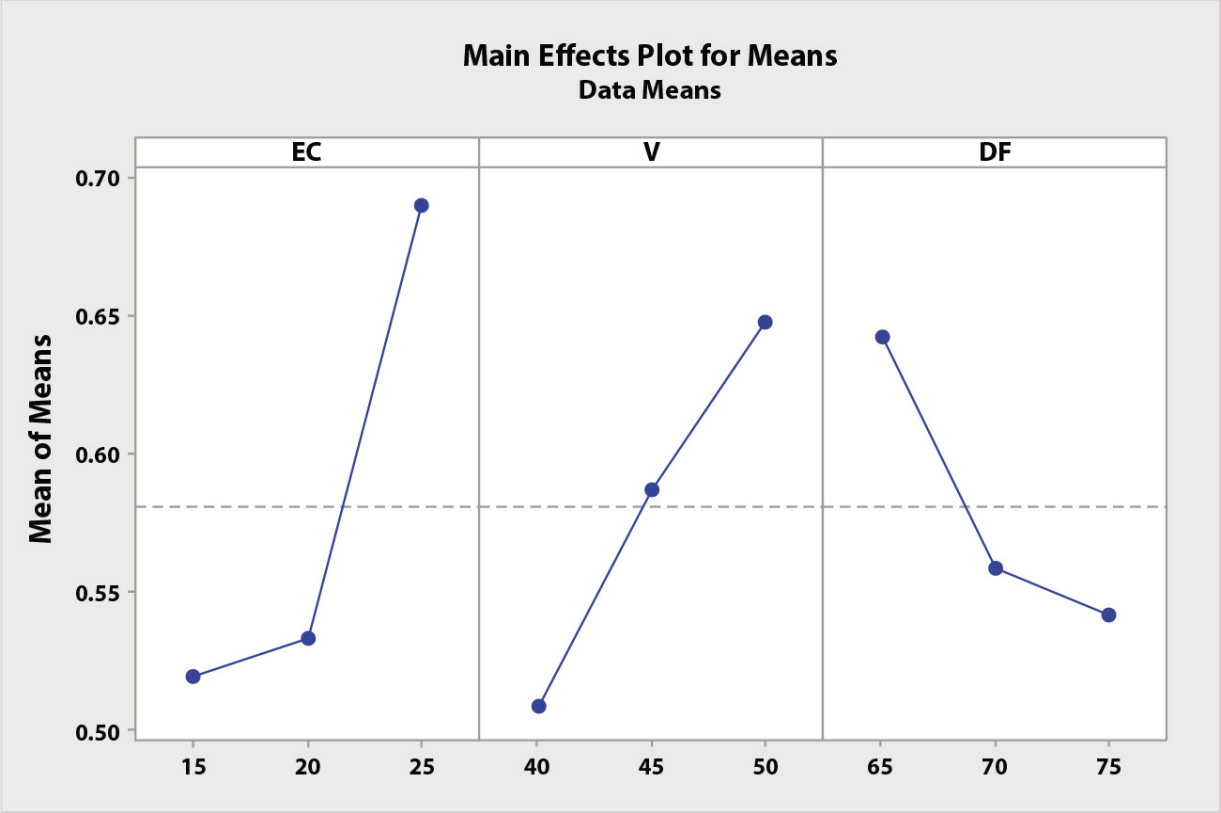


Figure 22.5 Main effects plot for means on GRA.

From Table 22.8, it was found that optimal levels for achieving maximum MRR, minimum HAZ, and overcut were EC at 25% wt., voltage at 50V, DF at 65%, respectively. A well-defined microchannel is achieved at optimal process parameters, as shown in Figure 22.4.

Table 22.8 MRPI on GRG values.

Factors	**Levels**		
	1	**2**	**3**
Electrolyte concentration (EC) (wt.%) (NaOH + KOH)	0.51956	0.53329	0.69005
Voltage, (V)	0.50834	0.58696	0.64756
DF (%)	0.64248	0.55845	0.54197

22.5 Conclusions

- In this chapter, microchannels were machined using three tool passes to avoid tool bending and damages to the workpiece.
- Mixed electrolyte of NaOH was implemented to increase the electrical conductivity of the electrolyte.
- Pulsed DC was implemented to stabilize the spark and to cool the workpiece and tool.
- A Taguchi-based GRA was implemented to optimize the process parameters.
- From the GRA, it was found that optimal levels for achieving maximum MRR, minimum HAZ, and minimum overcut were electrolyte concentration at 25% wt., voltage at 50V, and duty factor at 65%, respectively. Experiments based on optimal values of the process parameters have resulted to a well-defined microchannel.

References

1. Kurafuji, H., Electrical discharge drilling of glass. *Ann. CIRP*, 16, 415–419, 1968.
2. Kubota, M., Japan Society of Precision Engineering, *Proc. Int. Conf. Production Engineering Tokyo*, p. 51, Tokyo, 1974.
3. Tandon, S., Jain, V.K., Kumar, P., Rajurkar, K.P., Investigations into machining of composites. *Precis. Eng.*, 12, 227–238, 1990.
4. Langen, H., Fascio, V., Wüthrich, R., Viquerat, D., Three-dimensional structuring of pyrex glass devices—trajectory control *Int. in Conf. European Society for Precision*

Engineering and Nanotechnology (EUSPEN)(Eindhoven), vol. 2, pp. 435–8, 2002.

5. Wüthrich, R. and Fascio, V., Machining of non-conducting materials using electrochemical discharge phenomenon—an overview. *Int. J. Mach. Tools Manuf.*, 45, 9, 1095–1108, 2005.

6. Iliescu, C., Tay, F.E.H., Miao, J., Strategies in deep wet etching of Pyrex glass. *Sens. Actuators A Phys.*, 133, 395–400, 2007.

7. Sinton, D., Energy: The microfluidic frontier. *Lab Chip*, 14, 3127–3134, 2014.

8. Brusberg, L., Queisser, M., Gentsch, C., Schroder, H., Lang, K.D., Advances in CO2-laser drilling of glass substrates. *Physics Procedia*, 39, 548–555, 2012, doi: 10.1016/j.phpro.2012.10.072.

9. Lin, L., Zhang, M., Qiu, D., Jing, X., Jiang, F., Yu, D., Dry etching of fused silica glass in C4F8/ Ar inductively coupled plasmas for through glass via (TGV) applications, in: *2014 15th International Conference on Electronic Packaging Technology*, Chengdu, China, pp. 334–339, 2014, doi: 10.1109/ICEPT.2014.6922667.

10. Hof, L.A. and Ziki, J.A., Micro-hole drilling on glass substrates-a review. *Micromachines*, 8, 2, 53, 2017, doi: 10.3390/mi80200.

11. Singh, T. and Dvivedi, A., Developments in electrochemical discharge machining: A review on electrochemical discharge machining, process variants and their hybrid methods. *Int. J. Mach. Tools Manuf.*, 105, 1–13, 2016, doi: 10.1016/j.ijmachtools.2016.03.004.

12. Jain, V.K., Dixit, P.M., Pandey, P.M., On the analysis of the electrochemical spark machining process. *Int. J. Mach.*

Tools Manuf., 39, 1, 165–186, 1999, doi: 10.1016/S0890-6955(98)00010-8.

13. Wuthrich, R. and Fascio, V., Machining of non-conducting materials using electrochemical discharge phenomenon - An overview. *Int. J. Mach. Tools Manuf.*, 45, 9, 1095–1108, 2005, doi: 10.1016/j.ijmachtools.2004.11.011.

14. Singh, Y.P., Jain, V.K., Kumar, P., Agrawal, D.C., Machining piezoelectric (PZT) ceramics using an electrochemical spark machining (ECSM) process. *J. Mater. Process. Technol.*, 58, 1, 24–31, 1996, doi: 10.1016/0924-0136(95)02102-7.

15. Wang, J., Guo, Y.B., Fu, C., Jia, Z., Surface integrity of alumina machined by electrochemical discharge assisted diamond wire sawing. *J. Manuf. Processes*, 31, 96–102, 2018, doi: 10.1016/j. jmapro.2017.11.008.

16. Hwang, J., Cho, Y.H., Park, M.S. *et al.*, Microchannel Fabrication on Glass Materials for Microfluidic Devices. *Int. J. Precis. Eng. Manuf.*, 20, 479–495, 2019, https://doi.org/10.1007/s12541-019-00103-2.

17. Iliescu, C., Taylor, H., Avram, M., Miao, J., Franssila, S., A practical guide for the fabrication of microfluidic devices using glass and silicon. *Biomicrofluidics*, 6, 16505, 2012.

18. Marre, S., Adamo, A., Basak, S., Aymonier, C., Jensen, K.F., Design and packaging of microreactors for high pressure and high temperature applications. *Ind. Eng. Chem. Res.*, 49, 11310– 11320, 2010, https://doi.org/10.1021/ie101346u.

19. Basha, S., Keane, D., Morrissey, A., Nolan, K., Oelgemoller, M., Tobin, J., Studies on the adsorption and kinetics of photodegradation of pharmaceutical

compound, indomethacin using novel photocatalytic adsorbents (IPCAs). *Ind. Eng. Chem. Res.*, 49, 11302–11309, 2010, https://doi.org/10.1021/ie101304a.

20. Sarrazin, F., Salmon, J.B., Talaga, D., Servant, L., Chemical reaction imaging within microfluidic devices using confocal raman spectroscopy: the case of water and deuterium oxide as a model system. *Anal. Chem.*, 80, 1689–1695, 2008, https://doi.org/10.1021/ac7020147.

21. Ota, N., Yalikun, Y., Tanaka, N., Shen, Y., Aishan, Y., Nagahama, Y., Oikawa, M., Tanaka, Y., Simple isolation of single cell: thin glass microfluidic device for observation of isolated single Euglena gracilis cells. *Anal. Sci.*, 35, 577–583, 2019, https://doi.org/10.2116/analsci.18p568.

22. Yalikun, Y., Aishan, Y., Mosha, A., Sumiyama, K., Tanaka, Y., Oocyte all-surfaces' imaging method using micro-scale rotational flow. *Micro Nano Lett.*, 13, 306–311, 2018, https://doi.org/10.1049/mnl.2017.0731.

23. Aishan, Y., Yalikun, Y., Funano, S., Shen, Y., Tanaka, Y., Accurate rotation of ultrathin glass chamber for single-cell multidirectional observation. *Appl. Phys. Express*, 13, 026502, 2020, https://doi.org/10.7567/1882-0786/ab626d, 026502.

24. Xu, K., Liang, T., Zhu, P., Qi, P., Lu, J., Huh, C., Balhoff, M., A 2.5-D glass micromodel for investigation of multi-phase flow in porous media. *Lab Chip*, 17, 640–646, 2017, https://doi.org/10.1039/c6lc01476c.

25. Tangirala, S. and Sheng, J.J., Investigation of oil production and flowback in hydraulically fractured water-wet formations using the Lab-on-a-Chip method. *Fuel*, 254, 115543, 2019, https://doi.org/10.1016/j.fuel.2019.05.126.

26. Grate, J.W., Kelly, R.T., Suter, J., Anheier, N.C., Silicon-on-glass pore network micromodels with oxygen-sensing fluorophore films for chemical imaging and defined spatial structure. *Lab Chip*, 12, 4796–4801, 2012, doi: https://doi.org/10.1039/c2lc40776k.

27. Anbari, A., Chien, H.T., Datta, S.S., Deng, W., Weitz, D.A., Fan, J., Microfluidic model porous media: fabrication and applications. *Small*, 14, 1–15, 2018, doi: https://doi.org/10.1002/smll.201703575.

28. Yagyu, H., Tanabe, Y., Takano, S., Hamamoto, M., Continuous flow synthesis of monodisperse gold nanoparticles by liquid-phase reduction method on glass microfluidic device. *Micro Nano Lett.*, 12, 536–539, 2017, https://doi.org/10.1049/mnl.2017.0126.

29. Tanaka, Y. and Shimizu, Y., Integration of a reconstituted cell-free protein-synthesis system on a glass microchip. *Anal. Sci.*, 31, 67–71, 2015, https://doi.org/10.2116/analsci.31.67.

30. Tang, T., Yuan, Y., Yalikun, Y., Hosokawa, Y., Li, M., Tanaka, Y., Glass based micro total analysis systems: Materials, fabrication methods, and applications. *Sens. Actuators B Chem.*, 339, 129859, 2021. ISSN 0925-4005, https://doi.org/10.1016/j.snb.2021.129859.

31. Basak, I. and Ghosh, A., Mechanism of material removal in electrochemical discharge machining: a theoretical model and experimental verification. *J. Mater. Process. Technol.*, 71, 350–359, 1997, https://doi.org/10.1016/S0924-0136(97)00097-6.

32. Fascio, V., Wuthrich, R., Viquerat, D., Langen, H., 3D microstructuring of glass using electrochemical discharge machining (ECDM). MHS’99, in: *Proceedings of 1999 International Symposium on Micromechatronics and*

Human Science (Cat. No.99TH8478), pp. 179–183, 1999, doi: 10.1109/MHS.1999.820003.

33. Yang, C., Ho, S.-S., Yan, B., Micro Hole Machining of Borosilicate Glass through Electrochemical Discharge Machining (ECDM), *Key Eng. Mater.*, 196, 149–166, 2001, Doi:10.4028/www.scientific.net/KEM.196.149..

34. Kulkarni, A., Sharan, R., Lal, G.K., An experimental study of discharge mechanism in electrochemical discharge machining. *Int. J. Mach. Tools Manuf.*, 42, 1121–1127, 2002.

35. Yang, C.T., Song, S.L., Yan, B.H., Huang, F.Y., Improving machining performance of wire electrochemical discharge machining by adding SiC abrasive to electrolyte. *Int. J. Mach. Tools Manuf.*, 46, 15, 2044–2050, 2006. ISSN 0890-6955, https://doi.org/10.1016/j.ijmachtools.2006.01.006.

36. Furutani, K. and Maeda, H., Machining Glass Rod with Lathe Type Electro-Chemical Discharge Machine. *J. Micromech. Microeng.*, 18, 065006, 2008, doi: 10.1088/0960-1317/18/6/065006.

37. Cao, X., Kim, B.H., Chu, C., Micro-structuring of glass with features less than 100µm by electrochemical discharge machining. *Precis. Eng.*, 33, 459–465, 2009, doi: 10.1016/j.precisioneng. 2009.01.001.

38. Jana, D., Ziki, A., Didar, T.F., Wüthrich, R., Micro-texturing channel surfaces on glass with spark assisted chemical engraving. *Int. J. Mach. Tools Manuf.*, 57, 66–72, 2012. ISSN 0890-6955, https://doi.org/10.1016/j.ijmachtools.2012.01.012.

39. Jawalkar, C., Kumar, P.,, Sharma, A., Investigations on performance of ECDM process using NaOH and NaNO3 electrolytes while micro machining soda lime glass. *Int. J.*

Manuf. Technol. Manage., 28, 80–93, 2014, https://doi.org/10.1504/IJMTM.2014.064623.

40. Kolhekar, K.R. and Sundaram, M., A Study on the Effect of Electrolyte Concentration on Surface Integrity in Micro Electrochemical Discharge Machining. *Procedia CIRP*, 45, 355–358, 2016. ISSN 2212-8271, https://doi.org/10.1016/j.procir.2016.02.146.

41. Saranya, S., Nair, A., Ravi Sankar, A., Experimental investigations on the electrical and 2D-machining characteristics of an electrochemical discharge machining (ECDM) process. *Microsyst. Technol.*, 23, 1453–1461, 2017, https://doi.org/10.1007/s00542-016-3027-8.

42. Zhang, Z., Huang, L., Jiang, Y. *et al.*, A study to explore the properties of electrochemical discharge effect based on pulse power supply. *Int. J. Adv. Manuf. Technol.*, 85, 2107–2114, 2016, https://doi.org/10.1007/s00170-015-8302-9.

43. Sabahi, N. and Razfar, M.R., Investigating the effect of mixed alkaline electrolyte (NaOH + KOH) on the improvement of machining efficiency in 2D electrochemical discharge machining (ECDM). *Int. J. Adv. Manuf. Technol.*, 95, 643–657, 2018, https://doi.org/10.1007/s00170-017-1210-4.

44. Bhondwe, K.L., Yadava, V., Katherisan, G., Finite element prediction of material removal rate due to electrochemical spark machining. *Int. J. Mach. Tools Manuf.*, 46, 1699–1706, 2006.

45. Rajurkar, K.P., Zhu, D., McGeough, J., Kozak, J., De Silva, A., New developments in electro-chemical machining. *Ann. CIRP*, 48, 567–579, 1999.

46. Kim, B.H., Ryu, S.H., Choi, D.K., Chu, C.N., Micro electrochemical milling. *J. Micromech. Microeng.*, 15, 124–129, 2005.

47. Kirchner, V., *Electrochemical micro structuring with ultrashort voltage pulses*, Free University of Berlin, Berlin, Germany, 2001.

48. Ghosh, A., Muju, M.K., Parija, S., Allesu, Micro welding using electrochemical discharge. *Int. J. Mech. Tools Manuf.*, 37, 1303–1311, 1997.

49. Singh, S., Singh, A., Singh, I., Dvivedi, A., Optimization of the Process Parameters for Drilling of Metal Matrix Composites (MMC) Using Taguchi Analysis. *Adv. Mater. Res.*, 410, 249–252, 2012.

50. Muthuramalingam, T., Vasanth, S., Vinothkumar, P., Geethapriyan, T., Rabik, M.M., Multi criteria decision making of abrasive flow oriented process parameters in abrasive water jet machining using Taguchi–DEAR methodology. *Silicon*, 10, 5, 2015–2021, 2019, https://doi.org/10.1007/s12633-017-9715-x.

51. Antil, P., Singh, S., Singh, P., Taguchi's methodology based parametric analysis of material removal rate during ECDM of PMCs. *Procedia Manuf.*, 26, 469–473, 2018.

52. Julong, D., Introduction to Grey system theory. *J. Grey Syst.*, 1, 1–24, 1989.

53. Antil, P., Singh, S., Manna, A., Electrochemical discharge drilling of SiC reinforced polymer matrix composite using taguchi's grey relational analysis. *Arabian J. Sci. Eng.*, 43, 1257–1266, 2017, doi: 10.1007/s13369-017-2822-6.

54. Goud, M.M. and Sharma, A.K., On performance studies during micromachining of quartz glass using electrochemical discharge machining. *J. Mech. Sci.*

Technol., 31, 1365–1372, 2017, doi: https://doi.org/10.1007/s12206-017-0236.

55. Antil, P., Modelling and multi-objective optimization during ECDM of silicon carbide reinforced epoxy composites. *Silicon*, 12, 275–288, 2019, doi: https://doi.org/10.1007/s12633-019-00122-8.

56. Kumar, J.S. and Kalaichevlan, K., Taguchi-Grey multi-response optimization on structural parameters of honeycomb Core Sandwich structure for low velocity impact test. *Silicon*, 10, 3, 879–889, 2018.

57. Kumar, P.N., Rajadurai, A., Muthuramalingam, T., Multiresponse optimization on mechanical properties of silica Fly ash filled polyester composites using Taguchi-Grey relational analysis. *Silicon*, 10, 4, 1723–1729, 2018.

58. Rajput, V., Pundir, S.S., Goud, M. *et al.*, Multi-Response Optimization of ECDM Parameters for Silica (Quartz) Using Grey Relational Analysis. *Silicon*, 13, 1619–1640, 2021, https://doi.org/10.1007/s12633-020-00538-7.

59. Ranganayakulu, J. and Srihari, P.V., Multi-objective Optimization Using Taguchi's Loss Function-Based Principal Component Analysis in Electrochemical Discharge Machining of Micro-channels on Borosilicate Glass with Direct and Hybrid Electrolytes. *Adv. Manuf. Processes*, Volume/edition 1, pages 349-360, 2019, https://doi.org/10.1007/978-981-13-1724-8_34.

60. Bhattacharyya, B., Doloi, B.N., Sorkhel, S.K., Experimental investigations into electrochemical discharge machining (ECDM) of non-conductive ceramic materials [J]. *J. Mater. Process. Technol.*, 95, 1–3, 145–154, 1999.

Note

*Corresponding author: jinka.ranganayakulu@gmail.com

23
Abrasive Water Jet Machining

Ashok K.G.[1]*, Ajith D.[2], Raju M.[1] and Thiagarajan S.[1]

[1]Department of Mechanical Engineering, Easwari Engineering College, Chennai, India

[2]Department of Mechanical Engineering, Saveetha School of Engineering, Saveetha Institute of Medical and Technical Sciences, Chennai, India

Abstract

Abrasive water jet machining (AWJM) is a non-traditional machining process that utilizes a high-velocity stream of water mixed with abrasive particles to cut and shape a variety of materials. This book chapter provides a comprehensive overview of the principles, applications, and recent advances in the field of AWJM. The chapter begins with the fundamental principles underlying AWJM, including the generation of high-pressure water jets, the introduction of abrasives, and their combined effect on material removal. Through a detailed exploration of the process parameters, such as pressure, abrasive flow rate, and traverse speed, the chapter outlines the key factors influencing the machining efficiency and quality.

The subsequent sections explore into the diverse applications of AWJM across different industries. From the precision cutting of metals and composites to the intricate profiling of brittle materials like ceramics, the versatility of AWJM is highlighted. Furthermore, the environmental advantages, such as reduced heat-affected zones and minimal material wastage, are discussed, emphasizing the sustainable aspects of this machining technique. In addition

to its current applications, the chapter explores the latest advancements and innovations in AWJM technology. This includes developments in nozzle design, control systems, and automation, which enhance precision, speed, and overall process efficiency. Furthermore, the integration of artificial intelligence and machine learning algorithms for process optimization and predictive maintenance is explored, showcasing the cutting-edge research in this field.

To conclude, the book chapter provides readers with a holistic understanding of AWJM, from its foundational principles to its contemporary applications and emerging trends. Researchers, engineers, and practitioners in the field of manufacturing and materials processing will find this comprehensive overview invaluable for both academic study and practical implementation.

***Keywords*:** Abrasive particles, stand of distance, mechanical erosion, nozzle

23.1 Introduction

In the realm of modern manufacturing processes, precision cutting plays a pivotal role in shaping materials with unparalleled accuracy and efficiency. Abrasive water jet machining (AWJM) stands out as a revolutionary technology that combines the force of high-pressure water jets with abrasive particles, offering a versatile and precise method for cutting a wide array of materials [1]. The origins of water jet cutting can be traced back to the mid-20th century when high-pressure water jets were first employed for industrial cutting purposes. Over time, this technology has evolved into the sophisticated process recognized as AWJM [2]. The integration of abrasive particles into the high-speed water stream enhances the

cutting capabilities, allowing for the precise shaping of materials that range from soft polymers to robust metals [3]. Abrasive water jet machining (AWJM) harnesses the kinetic energy of a high-velocity water jet to propel abrasive particles towards a workpiece, eroding the material and creating intricate cuts. The precision of the cutting process is facilitated by computer-controlled systems that govern the movement of the water jet and regulate the abrasive flow [4]. Understanding the underlying principles of this process is crucial for optimizing cutting parameters and achieving the desired quality in the final product.

The versatility of AWJM is reflected in its diverse range of applications across industries. From aerospace and automotive manufacturing to the intricacies of medical device production, AWJM proves its efficacy in cutting materials of varying thicknesses and complexities [5]. Its non-thermal nature eliminates the risk of heat-induced deformities, making it ideal for materials that are sensitive to temperature changes. The absence of mechanical stress and the ability to cut without creating a heat affected zone (HAZ) are some of the key advantages that set AWJM apart from traditional cutting methods. The evolution of AWJM has been marked by advancements in pump technology, abrasive delivery systems, and control mechanisms, making it a dynamic field with broad applications.

As technology progresses, the landscape of AWJM continues to evolve. Innovations in nozzle design, abrasive mixing, and control systems contribute to enhanced precision, speed, and cost-effectiveness. Additionally, sustainability considerations and environmental impact are driving research into eco-friendly abrasives and water recycling methods, positioning AWJM as a green alternative in the manufacturing field.

This chapter explores the intricate world of AWJM, its principles, applications, advantages, and the evolving landscape of this cutting-edge technology. The evolution of AWJM has been marked by advancements in pump technology, abrasive delivery systems, and control mechanisms, making it a dynamic field with broad applications. As manufacturing demands become more stringent, the precision and flexibility offered by AWJM make it a compelling choice in the quest for efficient and sustainable cutting solutions.

23.2 Elements of Abrasive Water Jet Machining

Abrasive water jet machining (AWJM) is a non-traditional machining method that utilizes a high-velocity stream of liquid containing abrasive particles to cut, shape, and machine several materials. The key elements of AWJM are:

23.2.1 High-Pressure Hydro Jet Production

In AWJM, high-pressure hydro jet production is a method that uses a pressurized water jet combined with abrasive particles to machine, shape, or cut a variety of materials [6]. This technology is widely used in industries such as manufacturing, aerospace, automotive, and more, due to its versatility in cutting a wide range of materials.

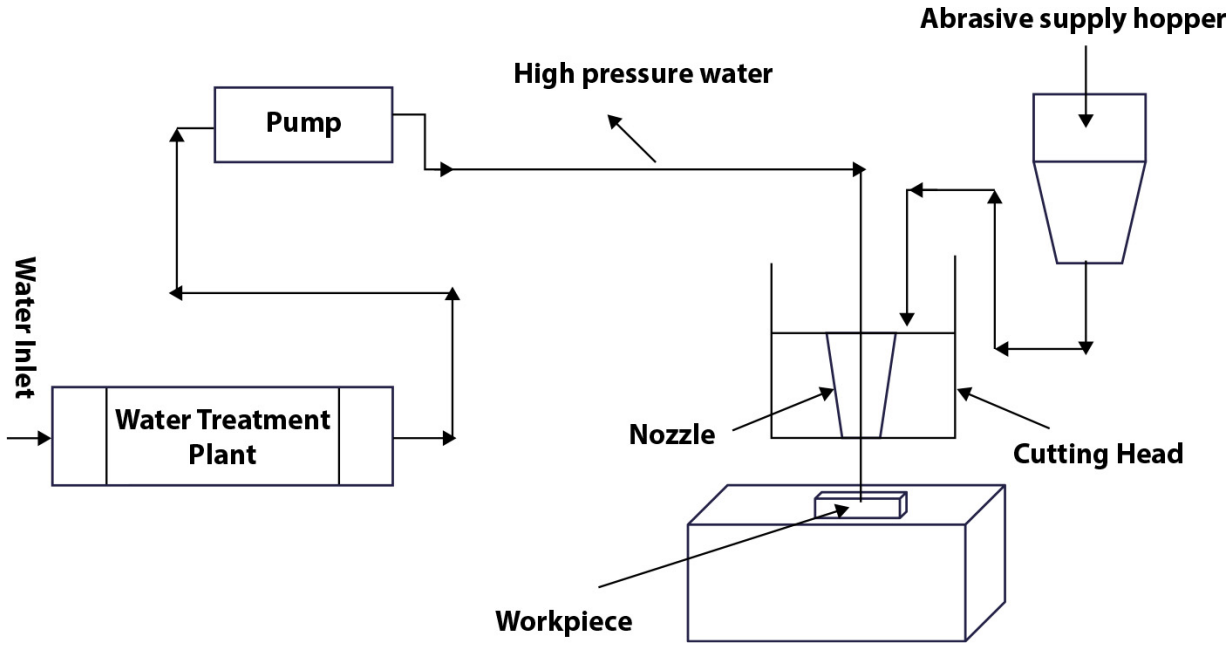


Figure 23.1 Elements of abrasive water jet machining.

The process begins with a high-pressure water pump that generates pressures typically extending from 30,000 to 90,000 pounds per square inch (psi). The water pump pressurizes water to a very high level, creating a powerful stream [4]. Abrasive particles, usually garnet, are mixed with the high-pressure water stream in a mixing chamber. Garnet is a common choice for its hardness and ability to maintain its sharp edges during the cutting process [7]. The mixture of water and abrasive is then directed through a specialized nozzle assembly. The nozzle design is crucial as it regulates the velocity and focus of the abrasive water jet. The material to be machined or cut is subjected to the high-velocity abrasive water jet. The abrasive particles in the jet help to erode and cut through the material by removing small particles at a high speed. In many applications, the cutting process is controlled by computer numerical control (CNC) systems. Computer numerical control systems precisely control the movement of the abrasive water jet, allowing for intricate and accurate cuts. High-pressure hydro jet production in AWJM provides an

efficient and precise method for cutting a variety of materials, making it a valuable tool in modern manufacturing processes. The elements of AWJM are depicted in Figure 23.1.

23.2.2 Hydro Pump Systems

In AWJM, the hydro pump system plays a crucial role in generating and delivering high-pressure liquid mixed with abrasive particles to machine materials. The hydro pump system is responsible for pressurizing water to the required levels and supplying it to the cutting nozzle [8]. There are two main types of hydro pump systems used in AWJM: intensifier pumps and direct drive pumps. Intensifier pumps operate on the principle of hydraulic intensification. They use a hydraulic cylinder to amplify the pressure of a smaller volume of oil or water to generate the high-pressure water needed for cutting. The process involves two cylinders, a large low-pressure cylinder, and a small high-pressure cylinder connected by a plunger or piston. The main components of an intensifier pump include a hydraulic intensifier, a hydraulic accumulator, a high-pressure cylinder, and a low-pressure cylinder.

Direct drive pumps use a high-speed motor to directly drive a plunger or piston, pressurizing the water to the required level. These pumps are more compact and simpler in design compared to intensifier pumps. The key components of a direct drive pump include a motor, a plunger or piston, and a check valve system to control the flow of water. The hydro pump system is responsible for mixing abrasive particles with water to create a slurry. This abrasive slurry is then directed through the cutting nozzle to enhance the cutting capabilities of the water jet.

23.2.3 Pressure Amplifiers

Pressure amplifiers play a crucial role in AWJM by boosting the pressure of the water before it mixes with abrasives. In AWJM, a high-pressure water jet is used to propel abrasive particles at a workpiece to cut or erode the material. Pressure amplifiers are employed to increase the pressure of the water, which enhances the cutting efficiency and speed of the process. The pressure intensifier is a key component that further boosts the pressure of the water. It typically consists of a hydraulic system and a reciprocating pump. The hydraulic system is used to drive the reciprocating pump, which in turn increases the pressure of the water. The intensified water is then directed to the cutting head, where it passes through a small orifice. The high-pressure water stream is now ready for the addition of abrasives. Higher pressure results in a more powerful and efficient cutting action. This allows for faster material removal and the ability to cut through thicker or harder materials. The increased pressure helps in achieving finer and more precise cuts, enhancing the overall quality of the machined parts.

23.2.4 Abrasive Particles

The abrasive particles play a crucial role in enhancing the cutting ability of the water jet. Various types of abrasive particles can be used in AWJM, depending on the application requirements. Some common types of abrasive particles include:

- **Garnet:** garnet is one of the most widely used abrasives. It is a natural mineral with high hardness and sharp edges, making it effective for cutting a variety of materials, including metals, ceramics, and composites [7].

- **Aluminum oxide:** aluminum oxide is another commonly used abrasive material in AWJM. It is a synthetic abrasive with high hardness and is suitable for cutting materials like metals and ceramics. Aluminum oxide abrasives are known for their durability [2].
- **Silicon carbide:** silicon carbide is a hard and brittle abrasive material that is suitable for cutting hard and brittle materials. It is often used for applications involving ceramics, glass, and certain composites [9].
- **Crushed glass:** crushed glass abrasive particles are environmentally friendly and can be used for cutting applications where minimizing environmental impact is a concern. It is a recycled abrasive material with moderate hardness [10].
- **Olivine:** olivine is a natural mineral that is used as an abrasive in AWJM. It is relatively soft compared to some other abrasives but is suitable for cutting applications where a softer abrasive is preferred.
- **Diamond:** in some specialized applications, synthetic diamond particles can be used as abrasives. Diamond is extremely hard and is suitable for cutting hard and abrasive materials such as ceramics and certain metals.

Abrasive selection is influenced by various factors, including the material to be cut, the desired surface finish, cutting speed, and environmental factors. The grain size, or size of the abrasive particles, is a major factor in the AWJM. Fine grain is usually for smoothing and finishing operations, while coarse grain is generally used for cutting. Abrasives with a lower mesh number also typically have fewer particles per unit weight and a larger average particle size [8, 11]. For the purpose of cutting the workpiece in AWJM, the abrasive’s flow is dependent on

water pressure. Because of their higher kinetic energy, abrasive particles have a greater capacity to remove material and reduce surface roughness, which also tends to shorten process times. Particle speed and disintegration within the abrasive nozzle are therefore enhanced by higher water pressure, which also enhances surface quality. On the other hand, excessive water pressure could have a detrimental effect on the material. When abrasive particles are too broken up by extreme water pressure, they lose their cutting power. The rate at which material is removed is accelerated by extremely high-water pressure. Each type of abrasive has its own set of characteristics, making it suitable for specific applications. The micrograph images of abrasive particles are shown in Figure 23.2.

The standoff distance is another important parameter in the machining process. The space between the work surface and the nozzle tip is known as the standoff distance. The jet can expand before it hits the work surface if the standoff distance is greater. Because of the increased standoff distance, the cutting process causes the jet diameter to increase. This leads to ineffective cutting and inferior part quality by lowering the jet's kinetic energy at impingement. Wear zone distortion during material removal is impacted by reductions in standoff distance and cut depth [12]. In the end, the cutting process is more efficient because it produces a smoother surface because of its higher kinetic energy.

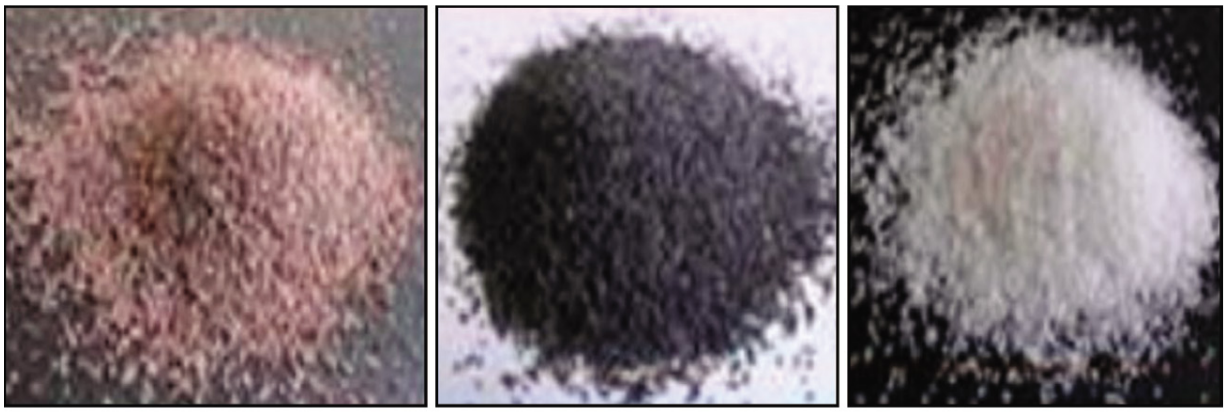


Figure 23.2 Abrasive particles (a) garnet [6], (b) silicon carbide [6], and (c) aluminum oxide [6].

23.2.5 Nozzle Geometry

In AWJM, the nozzle geometry plays a crucial role in determining the performance and efficiency of the cutting process. The nozzle is a critical component that directs the high-pressure water and abrasive mixture towards the workpiece. Here are some key aspects of nozzle geometry in AWJM:

- **Orifice shape:** the opening that allows the abrasive water jet to leave the nozzle is known as the orifice. Common orifice shapes include round, elliptical, and rectangular. Round orifices are widely used and offer good performance for general cutting applications. Elliptical orifices may be employed for specific applications where a more focused or widened jet stream is required. Rectangular orifices can provide a rectangular-shaped cutting pattern, suitable for specific cutting needs.
- **Orifice size:** the size of the orifice significantly affects the cutting capability. Smaller orifices generally produce finer and more precise cuts, while larger orifices are suitable for faster material removal. The

material being cut, the intended cutting speed, and the needs of the application all influence the orifice size selection.

- **Orifice material:** nozzle orifices are commonly made of materials like sapphire, tungsten carbide, or diamond. Sapphire orifices are known for their wear resistance and are suitable for cutting softer materials. Tungsten carbide orifices are more durable and are often used for cutting harder materials.
- **Nozzle angle:** the angle at which the abrasive water jet exits the nozzle is known as the nozzle angle. Common angles are 90° and 45°. The nozzle angle affects the shape and penetration of the cutting stream. Lower angles may provide better precision, while higher angles can be used for faster material removal.

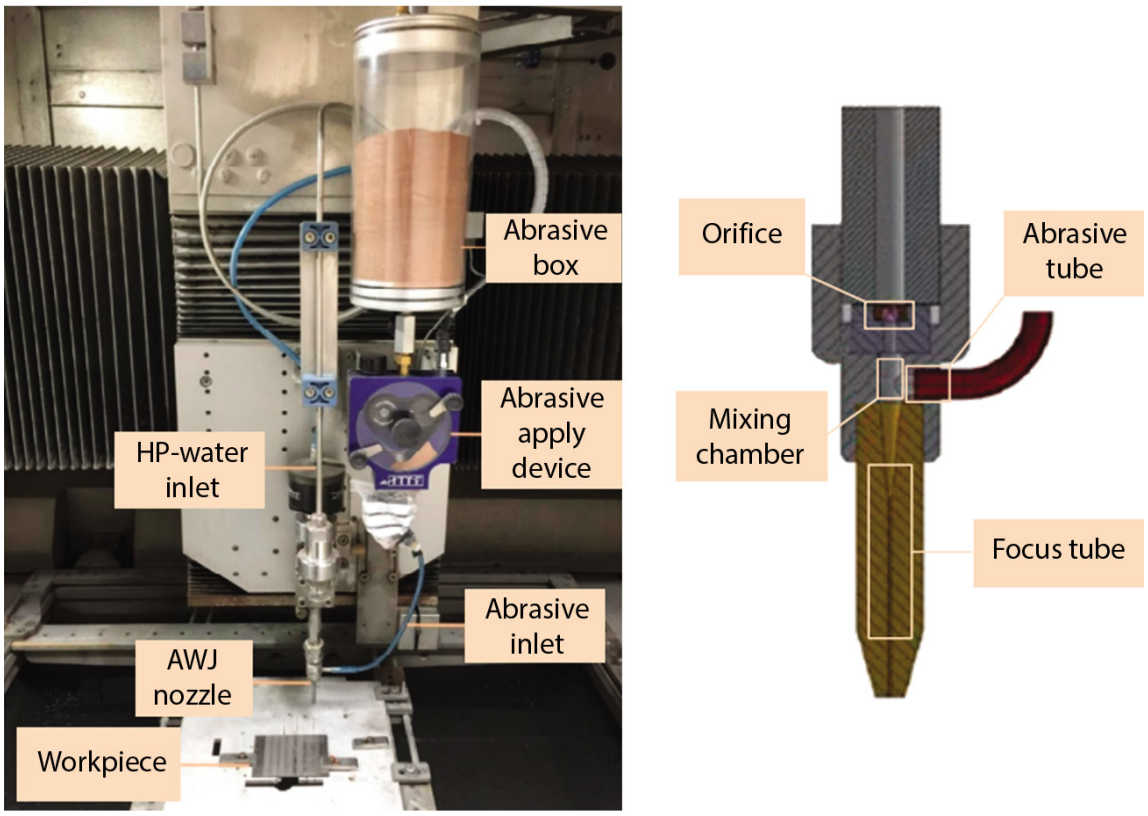


Figure 23.3 The abrasive focusing tube and its parts [13].

- **Abrasive focusing tube:** abrasive granules in the water stream can be concentrated with the aid of an abrasive focusing tube, which increases cutting efficiency in certain nozzles. The design and length of the focusing tube can influence the abrasive water jet's cutting performance. The abrasive focusing tube is shown in Figure 23.3.

23.2.6 Abrasive Blending and Distribution

An abrasive hopper, a metering valve, and a delivery hose comprise the abrasive feed system. The abrasive particles are transported to the abrasive inlet on the nozzle system by a delivery hose that is connected to the metering valve. By regulating the abrasive mass flow rate, the metering valve acts as an ON/OFF switch. The hopper is regarded as

a storage container for abrasives. The nozzle assembly and abrasive hopper must be as close to one another as possible in order to maximize cutting efficiency. The experimental setup of AWJM is shown in Figure 23.4.

The cutting head also called the nozzle assembly, is made up of the orifice, the fluid jet nozzle, and the mixing container. The nozzle assembly, also called the cutting head, is made up of an abrasive water jet nozzle, an orifice, and a mixing chamber. The high-pressure water jet is provided and controlled by the cutting head [14]. The orifice, which has diameters that normally range from 1 to 5 mm, is in charge of transferring high-pressure water into a high-velocity water jet. Among the materials most frequently used for orifices are sapphire and diamond. The working life of a sapphire orifice is limited to 200 h, whereas a diamond orifice can last up to 2000 h. The mixing chamber is positioned between the orifice and the nozzle, creating a space where water and abrasive particles are combined and drawn in by vacuum suction [15]. The combination of the water jet inside the mixing container accelerates abrasive particles through the nozzle. The main material used in the nozzle is tungsten carbide. Optimal cutting performance can be attained by rigidly setting the nozzle’s length and diameter.

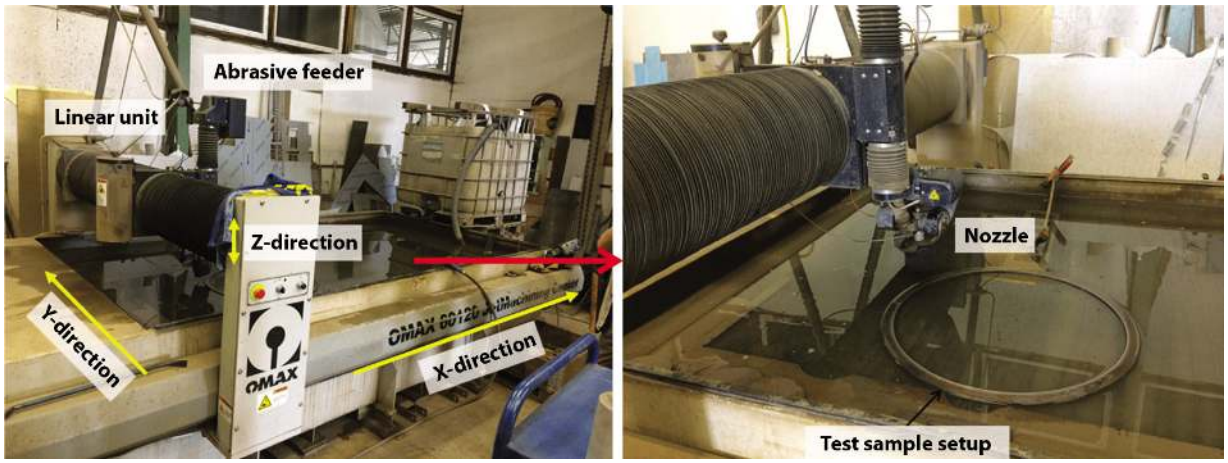


Figure 23.4 Experimental set up of AWJM [16].

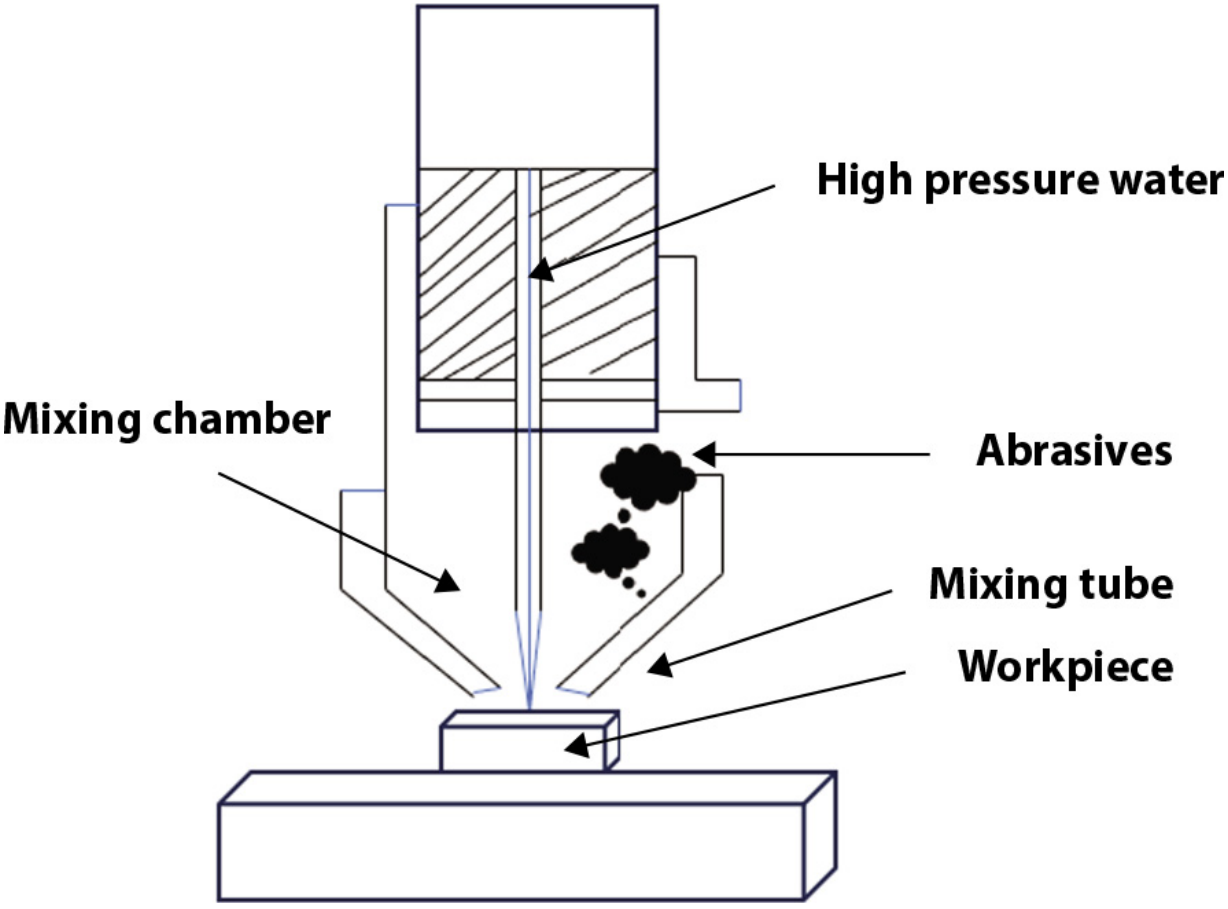


Figure 23.5 Abrasive blending and distribution system.

The technique of removing or cutting material from a workpiece through AWJM is based on mechanical attrition. Using a high-velocity water jet stream and abrasive

particles, this technique targets a particular specimen. The specimen will be subjected to high stress due to the kinetic energy converting into pressure energy when the induced stress reaches its peak and particles from the target material are removed. The abrasive blending and distribution systems are illustrated in Figure 23.5.

23.3 Process Variables and Operating Factors in AWJM

Abrasive water jet machining (AWJM) is a non-traditional machining technique that shapes, cuts, and machines a variety of materials using a high-velocity stream of water infused with abrasive particles. The effectiveness and results of AWJM are influenced by a number of process variables and operational factors. The process variables of AWJM are depicted in Figure 23.6.

23.3.1 Water Flow Rate and Pressure

The pressure of the water jet is a critical factor in AWJM. Higher pressures generally result in increased cutting speeds and the ability to cut through harder materials. Typical pressure ranges for AWJM are between 60,000 psi (415 MPa) to 90,000 psi (620 MPa) [18]. Water flow rate in machining processes refers to the volume of water that passes through the nozzle aperture per unit of time. The flow rate affects the cutting performance, including cutting depth, kerf width, surface roughness, energy carrying capacity of the jet, influencing the material removal rate and the cooling of the process zone. Optimal flow rates are based on the material to be machined and the intended cutting properties [19]. The cutting depth improves as the abrasive flow rate increases, with a significant increase observed when the flow rate is raised from 70 to 130 g/min. This indicates that the dissimilarity in abrasive flow

rate has a substantial effect on the cutting performance. Additionally, the changes in abrasive flow rate influence the energy distribution and the cutting ability of the AWJM process. Furthermore, the effect of abrasive flow rate on the kerf width and the surface roughness of the cut. It states that the top kerf width is insensitive to abrasive flow rate, while the kerf width ratio is sensitive to changes in flow rate. The surface roughness on the kerf walls is also observed to decrease with an increase in flow rate [20].

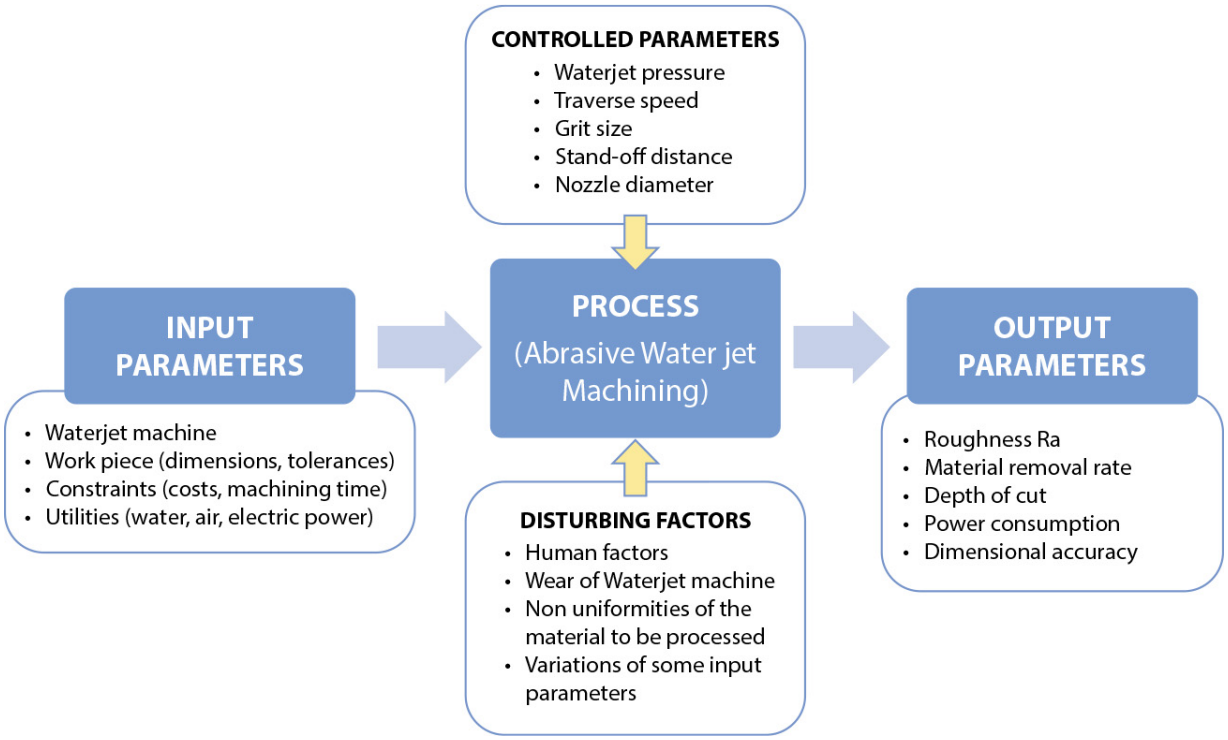


Figure 23.6 Process variables and operating factors in abrasive water jet machining [17].

The pressure of the water jet is another critical parameter in unconventional machining processes. The relationship between water pressure and performance has been widely investigated. Higher pressures result in increased cutting force, allowing for more efficient material removal. However, excessive pressure can cause damage to the workpiece or lead to excessive erosion of the nozzle [21]. Higher water pressure in AWJM generally leads to

increased cutting speeds. There is a direct relationship between the water pressure and the energy imparted to the workpiece material and abrasive particles. Consequently, faster material removal rates and higher cutting speeds are a result of higher water pressure. Higher water pressures enable the abrasive waterjet to effectively cut through thicker and harder materials, expanding the range of materials that can be machined using this technology. Controlling the water pressure is crucial for achieving precise and accurate cuts. Higher water pressure can lead to better control over the cutting stream and improve the overall accuracy of the machining process. The water pressure influences the quality of the cut surface. Optimal water pressure parameters can result in smoother cut surfaces with reduced roughness and minimal taper, contributing to the overall quality of the machined parts. The water pressure also affects the operational efficiency of the AWJM process. Understanding the optimal water pressure parameters can contribute to maximizing the efficiency of material removal, minimizing abrasive consumption, and reducing cutting times [7].

23.3.2 Abrasive Particle Size and Velocity

The choice of abrasive material and its particle size influence the cutting characteristics. Common abrasives include garnet, aluminum oxide, and silicon carbide. Finer abrasives may produce smoother finishes, while coarser abrasives are more effective for rapid material removal. The size of abrasive particles plays a critical role in the quality of the machined surface. Particle size is selected based on the requirements for surface finish and cutting effectiveness. The velocity at which abrasive particles travel affects their kinetic energy and subsequent material removal rate [22]. Abrasive velocity is a variable that operators control to optimize performance, with the

influence of particle velocity on cutting processes. The velocity of abrasive particles directly affects cutting efficiency and the ability to penetrate different materials [23].

23.3.3 Standoff Length

Standoff length (SOL) is the distance between the nozzle tip and the workpiece surface. Standoff length is crucial as it affects the jet spread and, consequently, the cutting kerf and precision. For instance, the standoff distance affects factors such as kerf width and cutting depth. When adjusting the standoff distance, it can impact the energy dissipation and penetration process, ultimately influencing the cutting performance [24]. Moreover, the standoff distance, in combination with other variables like pump pressure and abrasive flow rate, plays a vital role in determining the kerf width ratio. Additionally, the relationships between abrasive properties such as hardness, roundness, and cutting ability are also influenced by the SOL. For instance, as the abrasive hardness rises from a certain level, a drop in cutting ability occurs, likely due to abrasive fracture and its negative effects on flow stability. In summary, the SOL is intricately linked with various aspects of AWJM and plays a crucial role in overall cutting performance and quality. The process variable of AWJM is shown in Figure 23.7.

23.3.4 Traverse Velocity

The amount of heat produced during the machining process is determined by the rate at which the water jet nozzle passes over the surface of the workpiece. It also affects the quality of the cut and the efficiency of material removal. The transverse speed of the workpiece can significantly affect the material removal rate in abrasive jet machining (AJM) [25]. Faster transverse speeds typically lead to

higher material removal rates, as the abrasive jet has more time to remove material from the workpiece. However, slower transverse speeds can result in lower material removal rates, as the abrasive jet may not have enough time to remove material completely. The transverse speed of the workpiece can also impact the flow of the abrasive material used in AJM [10]. Faster transverse speeds can create turbulent flow conditions, which can improve abrasive flow and material removal. Slower transverse speeds, on the other hand, can result in less turbulent flow conditions, which can lead to poorer abrasive flow and material removal. The transverse speed of the workpiece can affect the cutting pressure in AJM. Increasing the transverse speed can increase the cutting pressure, leading to deeper cuts and improved material removal. However, if the transverse speed is too high, it can result in excessive cutting pressure, which can negatively impact the quality of the machined surface. The transverse speed of the workpiece can also impact the jet standoff distance in AJM [6]. Faster transverse speeds can result in a shorter jet standoff distance, which can improve material removal and surface finish. Slower transverse speeds, on the other hand, can result in a longer jet standoff distance, which can lead to poorer material removal and surface finish. Faster transverse speeds can lead to higher vibration levels, which can negatively impact the machining process's outcome. Slower transverse speeds, on the other hand, can result in lower vibration levels, which can improve the quality of the machined surface [3]. By understanding the factors that affect material removal rate, abrasive flow, cutting pressure, jet standoff distance, and workpiece vibration, machinists can optimally select the appropriate transverse speed for their specific AJM application to achieve the desired quality and efficiency. The process parameters are listed in Table 23.1.

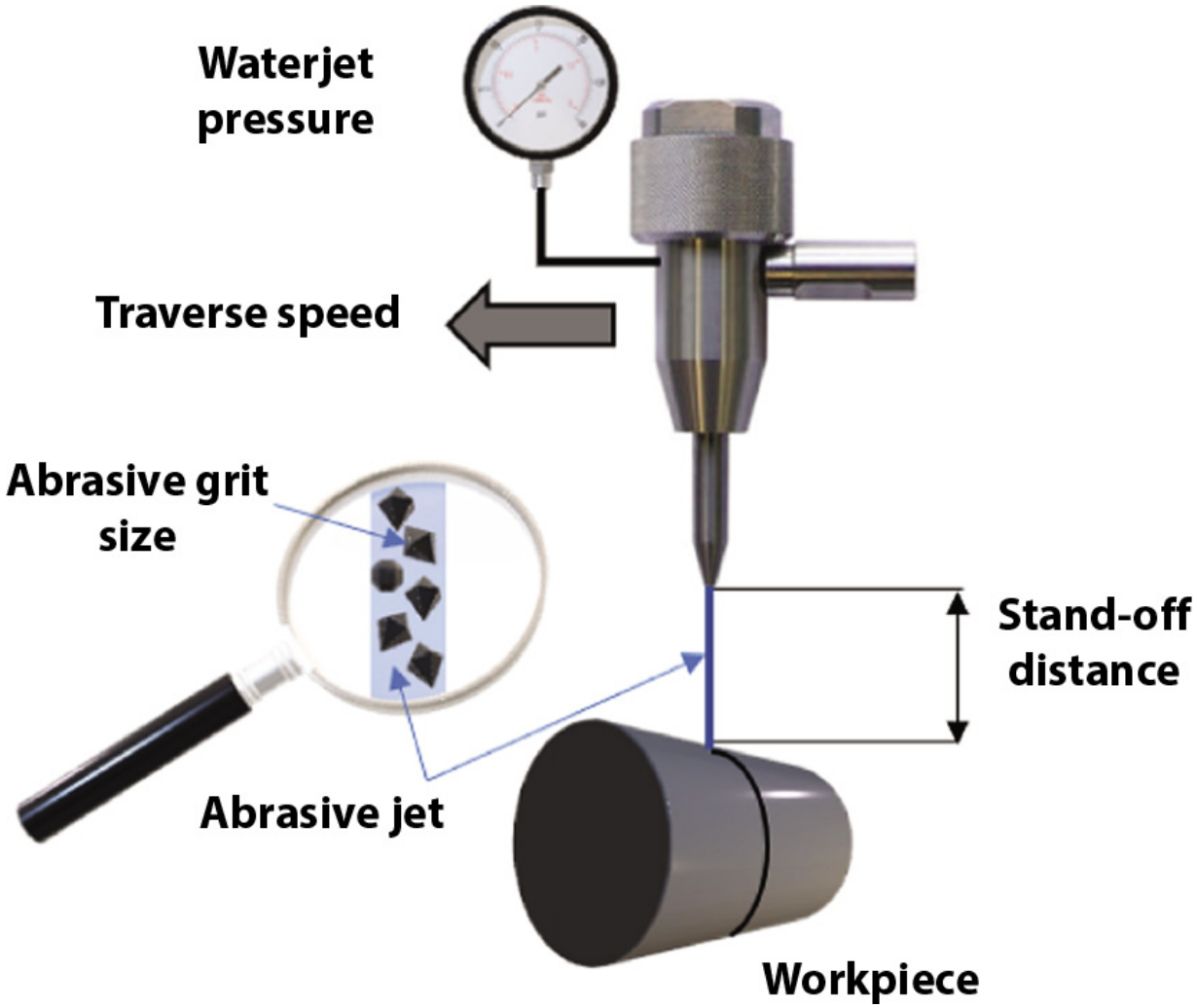


Figure 23.7 The process variable of AWJM [17].

Table 23.1 The process parameters of AWJM process [17].

S. no.	Traverse speed (mm/min)	Pressure (MPa)	Stand-off distance (mm)	Grit size
1	40	250	1	80
2	50	300	1.5	100
3	60	350	2	120

23.4 Abrasive Water Jet Machining Applications

Due to its adaptability, precision, environmental friendliness, and ability to cater to a wide range of materials and applications, AWJ has become increasingly popular in many machining operations. Among these, the following are the broad ranges: automotive, aerospace, construction, microelectronics, marine, and medical [2, 4]. The applications of AWJM process are listed in Table 23.2.

23.4.1 Automotive Industry

Abrasive water jet machining (AWJM) is used for cutting various automotive components such as sheet metal, composite materials, glass, and ceramics. It can cut intricate shapes with high precision without causing heat-affected zones or material deformation, making it suitable for producing car body panels, interior components, and structural parts. Abrasive water jet machining (AWJM) is employed for trimming excess material and deburring sharp edges from automotive parts. It ensures smooth and precise edges, improving the quality and appearance of components like door panels, dashboard trim, and engine parts. With the increasing use of composite materials in automotive manufacturing for their lightweight and strength properties, AWJM is utilized for machining these materials. It enables precise shaping and drilling of composite parts used in body panels, chassis components, and interior trim. Prototype parts for engines and engine components, such as flanges, sensor housings, and manifolds. Other components include hinges, latches, tabs, and brackets for doors and entry points; spacers, washers, rims, brakes, and wheel assemblies. Furthermore, gears, linkages, and bearings for drive trains, transmissions, and power train assemblies. Gaskets and seals are cut out of

many different types of materials for all kinds of sealing applications.

Table 23.2 Applications of AWJM [6].

Materials		**Industrial application**
Type	**Work piece**	
Natural	Concrete, cement, ceramics, graphite, stone or rock.	Mining, manufacturing, and processing of ceramics and graphite, building, construction, housing, and tile industry.
Metals	Titanium, aluminum, stainless steel, and alloys.	Automotive, marine, aerospace, architecture, civil, medical, and electronics industries.
Composites	Wire glass, laminated glass, optic glass, composites, and magnetic materials.	Aerospace, automotive, electronics industry, glass, decorations, optical fiber, and medical industry.

23.4.2 Aerospace Industry

Abrasive water jet machining (AWJM) is a flexible manufacturing process that finds several applications in the aerospace industry due to its ability to precisely cut various materials while maintaining high tolerances. Composite materials, such as carbon fiber-reinforced polymers (CFRP) and fiberglass, are widely used in aerospace due to their lightweight and high strength properties. Abrasive water jet machining (AWJM) is effective in cutting and shaping these materials without causing delamination or other damage, making it suitable for manufacturing components like aircraft fuselages, wings, and interior panels. Abrasive

water jet machining (AWJM) can efficiently cut aluminum and titanium alloys used in aerospace manufacturing. It is often used to produce parts like brackets, fittings, and structural components due to its ability to cut complex shapes accurately without inducing heat-affected zones or metallurgical changes. Abrasive water jet machining (AWJM) can be used to precisely machine critical components of aircraft engines, such as turbine blades, compressor blades, and fuel nozzles. The process allows for intricate designs and tight tolerances, contributing to the efficiency and performance of aircraft engines. Abrasive water jet machining (AWJM) is employed in aerospace for repair and maintenance tasks, such as removing damaged sections of aircraft components or repairing worn parts. It can be used to remove coatings, corrosion, and other surface imperfections without causing additional damage to the underlying material. Abrasive water jet machining (AWJM) is utilized in the production of various aerostructures, including aircraft skins, stringers, ribs, and bulkheads. Its ability to cut thick materials accurately makes it suitable for fabricating these structural components with minimal material waste.

23.4.3 Profiling and Metal Cutting

Abrasive water jet machining (AWJM) is a versatile and precise manufacturing process used in various industries for profiling and cutting a wide range of materials, including metals. Abrasive water jet machining (AWJM) can create intricate and precise profiles on metal surfaces, allowing for the production of complex shapes with tight tolerances. The abrasive water jet can be directed to create beveled or chamfered edges on metal parts, facilitating assembly and improving aesthetics. It is used to contour metal surfaces, particularly useful in industries such as aerospace and automotive for shaping components with

aerodynamic or ergonomic profiles. Abrasive water jet machining (AWJM) is valuable in rapid prototyping processes, allowing designers to quickly iterate and refine metal parts before final production. It can cut through a wide range of metal thicknesses, from thin sheets to thick plates, with minimal heat-affected zones and no risk of thermal distortion, can effectively cut hardened metals such as stainless steel, tool steel, and titanium without compromising material properties. It is particularly advantageous for cutting non-conductive metals like aluminum, copper, and brass, where traditional methods like laser or plasma cutting may encounter difficulties.

23.4.4 Machining of Composite Materials

Abrasive water jet machining (AWJM) is a versatile and effective method for machining fiber composite materials. Fiber composites, such as CFRP or glass fiber-reinforced polymers (GFRP), are commonly used in aerospace, automotive, marine, and other industries due to their lightweight and high strength properties. However, machining these materials can be challenging due to their anisotropic and heterogeneous nature. Fiber composite materials are susceptible to delamination, fiber pullout, and other forms of damage during conventional machining processes like milling or drilling. Abrasive water jet machining (AWJM), however, is a non-contact process, which reduces the risk of such damage. However, there might be some limitations while machining composite materials with AWJM. The limitations such as rough edge finish, delamination, and high-pressure causing separation of fiber and matrix, resulting in weaker parts. Proper control of process parameters, such as nozzle angle and standoff distance, is crucial to minimize delamination in fiber composite materials. The photograph images of

machined fiber composite materials are illustrated in Figure 23.8.



Figure 23.8 Machining of composite materials [21].

23.4.5 Glass Machining

Abrasive water jet machining (AWJM) can precisely cut-glass sheets into desired shapes with high accuracy and minimal material wastage. This is particularly useful in industries such as automotive, electronics, and construction where glass components need to be cut with intricate designs. Abrasive water jet machining (AWJM) can be used for etching or engraving designs, patterns, or texts onto glass surfaces. This is commonly seen in decorative glass products, signage, and architectural glass applications. Abrasive water jet machining (AWJM) can efficiently drill precise holes in glass materials without causing cracks or chipping. This is valuable in industries like electronics for making holes in glass substrates for electrical components. In the automotive and architectural industries, laminated glass is commonly used for safety and security purposes. Abrasive water jet machining (AWJM) can trim laminated glass layers to precise dimensions without damaging the integrity of the laminate. Artists and sculptors utilize AWJM for creating intricate glass

sculptures and artworks due to its ability to precisely shape and sculpt glass materials.

23.5 Advantages of Abrasive Water Jet Machining

- AWJM can cut through a wide range of materials, including metals, composites, ceramics, glass, stone, and even some plastics. This versatility makes it suitable for diverse applications across industries.
- Unlike traditional machining methods such as laser cutting or plasma cutting, the AWJM method uses cold cutting. As a result of its lack of thermal generation during cutting, there is less chance of the workpiece suffering thermal damage like warping, melting, or changes in material properties.
- The precise cutting technique known as AWJM results in reduced kerf widths. Because there is less material wasted, this is an economical choice— especially when using expensive components.
- AWJM relieves the workpiece of mechanical stresses and distortions during the cutting process because it is a non-contact cutting method. When working with thin or delicate materials, this is especially beneficial.
- AWJM can cut intricate shapes and contours with high precision, allowing for the production of complex parts and components without the need for secondary finishing operations.
- AWJM is considered an environmentally friendly machining method compared to some other cutting processes. It does not produce hazardous fumes, gases, or by-products, and the abrasive material used in the process is typically recyclable.

- Unlike traditional cutting methods that involve the use of cutting tools subject to wear and tear, AWJM does not use cutting tools. This eliminates the need for tool changes and reduces maintenance costs associated with tool wear.
- AWJM is particularly well-suited for cutting thin and brittle materials that may be difficult to machine using conventional methods. It can cut such materials without causing cracks, chips, or other forms of damage.
- AWJM can achieve high levels of precision and accuracy, with tolerances typically in the range of ±0.1 mm or better, depending on the specific application and machine setup.
- Setting up an AWJM system for a new job is relatively quick and straightforward compared to some traditional machining methods. This helps reduce downtime and increase overall productivity.

23.6 Challenges and Limitations

23.6.1 Challenges

- The abrasive particles used in AWJM are consumed during the cutting process, leading to the need for frequent replenishment. This can increase operating costs and downtime for refilling abrasive supplies.
- The disposal of abrasive slurry generated during the machining process can pose environmental challenges. Proper handling and disposal methods are necessary to mitigate any environmental impact.
- AWJM systems require regular maintenance to ensure optimal performance. Components such as nozzles,

pumps, and filters may wear out over time and need to be replaced or refurbished.

- It can be difficult to achieve high-quality edges, particularly when working with thicker materials or intricate geometries. Abrasive water jet machining may leave behind a slightly rough edge or a taper angle, which may require additional finishing operations.

23.6.2 Limitations

- Compared to other cutting techniques like plasma or flame cutting, AWJM can create surfaces that are reasonably smooth; however, extra post-processing procedures like grinding or polishing may be necessary to achieve a mirror-like finish.
- Achieving high levels of accuracy and precision can be challenging with AWJM, especially for intricate or fine features. Factors such as jet divergence, abrasive wear, and material properties can affect dimensional accuracy.
- AWJM is capable of cutting through thick materials, there are practical limitations to the thickness that can be effectively machined. Beyond a certain thickness, the cutting speed may decrease significantly, or the quality of the cut may diminish.

23.7 Recent Trends and Developments in AWJM

- Abrasive water jet machining has been continuously evolving with advancements aimed at improving efficiency, precision, and versatility. Some recent trends and developments in the field of AWJM are listed.

- Recent developments in AWJM focus on improving the precision of the machining process. This includes advancements in nozzle design, control systems, and abrasive delivery mechanisms to achieve finer cuts and intricate patterns. High-precision AWJM systems are increasingly being used in industries such as aerospace, automotive, and medical device manufacturing.
- The growing trend towards multi-axis AWJM systems that enable cutting complex 3D shapes with greater accuracy. These systems incorporate advanced software algorithms and robotic arms to manipulate the cutting head along multiple axes, allowing for more intricate geometries and improved part quality. The photographic image of multi axis machining is shown in Figure 23.9.

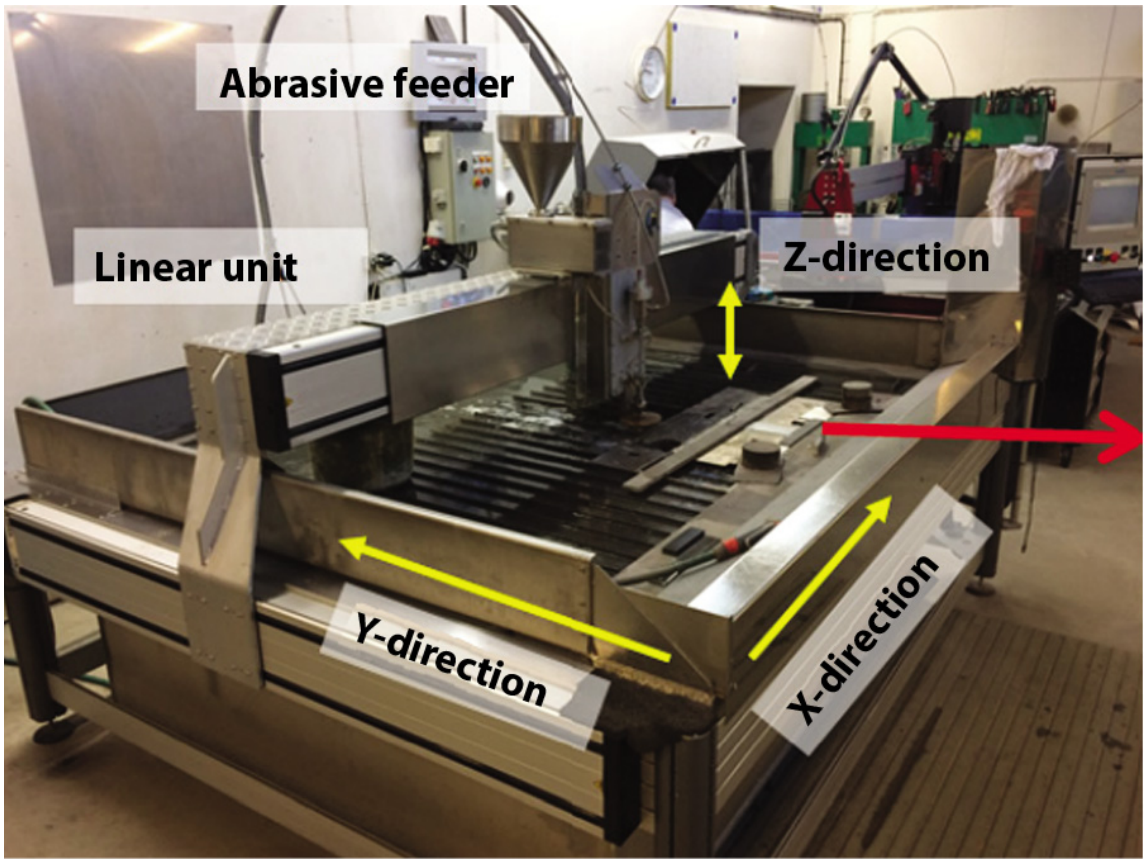


Figure 23.9 Multi-axis AWJM process [16].

- Automation is playing a significant role in the evolution of AWJM, with increased integration of robotics and computer numerical control systems. Automated loading and unloading of workpieces, tool changing, and realtime monitoring enhance productivity and reduce downtime, making AWJM more competitive in high-volume manufacturing environments.
- The use of new types of abrasives and abrasive recycling techniques were employed to improve efficiency and sustainability in AWJM. Innovations in abrasive materials, such as nano-sized particles and composite abrasives, offer the potential for higher cutting speeds and improved surface finish. Additionally, efforts to recycle and reuse abrasives are

gaining traction to minimize waste and reduce operating costs.

- There is a growing interest in integrating AWJM with additive manufacturing processes, such as 3D printing. Combining these technologies allows for the fabrication of complex hybrid structures with high accuracy and minimal post-processing. Abrasive water jet machining (AWJM) can be used for precision finishing, surface texturing, and support structure removal in additive manufacturing applications.
- As sustainability is important in manufacturing, there is a focus on reducing the environmental impact of AWJM. Efforts are underway to optimize process parameters, minimize water and abrasive consumption, and develop eco-friendly abrasive materials. Additionally, the use of closed-loop water recycling systems and filtration technologies helps mitigate the environmental footprint of AWJM operations.
- Advances in sensor technology and data analytics enable real-time monitoring and control of AWJM processes. By collecting and analyzing data on cutting parameters, material properties, and machine performance, manufacturers can optimize process efficiency, detect defects, and prevent unplanned downtime. Intelligent control systems adjust cutting parameters dynamically to maintain consistent quality and maximize throughput.

23.8 Conclusion

Abrasive water jet machining is a flexible and efficient manufacturing technique that is used in many different industries to drill, shape, and cut a broad variety of

materials. Here are some key conclusions drawn from the application and study of AWJM:

Abrasive water jet machining (AWJM) can achieve high precision cuts with minimal material wastage. This makes it suitable for applications where intricate shapes or tight tolerances are required. One of the significant advantages of AWJM is its ability to cut a wide range of materials, including metals, ceramics, composites, glass, and even some heat-sensitive materials like plastics and foams. This versatility makes it a preferred choice in industries where multiple materials need to be processed. Unlike some traditional machining methods like laser cutting or plasma cutting, AWJM is a non-thermal process. This means it does not induce heat-affected zones or thermal stress in the material being cut, preserving its structural integrity. Abrasive water jet machining (AWJM) is considered an environmentally friendly machining process as it does not involve the use of hazardous chemicals or generate harmful fumes. Additionally, it produces minimal dust or waste, making it a cleaner option compared to some other machining techniques. Abrasive water jet machining (AWJM) enables the cutting of complex shapes and contours with ease. This capability is particularly beneficial in industries such as aerospace, automotive, and medical devices, where intricate designs are common. Since AWJM does not involve direct contact between the cutting tool and the workpiece, tool wear is minimal compared to conventional machining processes. This results in longer tool life and reduced maintenance costs. Continuous research and development efforts are focused on optimizing AWJM parameters such as pressure, abrasive flow rate, nozzle design, and standoff distance to improve cutting efficiency, surface finish, and minimize operating costs.

References

1. Kale, A., Singh, S.K., Sateesh, N., Subbiah, R., A review on abrasive water jet machining process and its process parameters. *Mater. Today Proc.*, 26, 1032–1036, 2019, https://doi.org/10.1016/j.matpr.2020.01.309.

2. Wang, H., Yuan, R., Zhang, X., Zai, P., Deng, J., Research Progress in Abrasive Water Jet Processing Technology. *Micromachines*, 14, 1526–1559, 2023, https://doi.org/10.3390/mi14081526.

3. Chenrayan, V., Manivannan, C., Shahapurkar, K., Zewdu, G.A., Maniselvam, N., Alarifi, I.M., Alblalaihid, K., Tirth, V., Algahtani, A., An experimental and empirical assessment of machining damage of hybrid glass-carbon FRP composite during abrasive water jet machining. *J. Mater. Res. Technol.*, 19, 1148–1161, 2022, https://doi.org/10.1016/j.jmrt.2022.05.042.

4. Natarajan, Y., Murugesan, P.K., Mohan, M., Liyakath Ali Khan, S.A., Abrasive Water Jet Machining process: A state of art of review. *J. Manuf. Process.*, 49, 271–322, 2020, https://doi.org/10.1016/j.jmapro.2019.11.030.

5. Bañon, F., Sambruno, A., González-Rovira, L., Vazquez-Martinez, J.M., Salguero, J., A review on the abrasive water-jet machining of metal–carbon fiber hybrid materials. *Met. (Basel)*, 11, 1–29, 2021, https://doi.org/10.3390/met11010164.

6. Llanto, J.M., Tolouei-Rad, M., Vafadar, A., Aamir, M., Recent progress trend on abrasive waterjet cutting of metallic materials: A review. *Appl. Sci.*, 11, 3344–3368, 2021, https://doi.org/10.3390/app11083344.

7. Thakur, R.K. and Singh, K.K., Abrasive waterjet machining of fiber-reinforced composites: a state-of-the-art review. *J. Braz. Soc. Mech. Sci. Eng.*, 42, 381–406, 2020, https://doi.org/10.1007/s40430-020-02463-7.

8. Saravanan, S., Vijayan, V., Jaya Suthahar, S.T., Balan, A.V., Sankar, S., Ravichandran, M., A review on recent progresses in machining methods based on abrasive water jet machining, Mater. *Today Proc.*, 212020, 116–122, 2020, https://doi.org/10.1016/j.matpr.2019.05.373.

9. Li, H. and Wang, J., An experimental study of abrasive waterjet machining of Ti-6Al-4V. *Int. J. Adv. Manuf. Technol.*, 81, 361–369, 2015, https://doi.org/10.1007/s00170-015-7245-5.

10. Arunkumar, P., Muthukumaran, N., Muthu Samy, M., Prabhu, L., Rajeshwari, R., Investigation on effect of process parameters in abrasive Jet Machining process using full factorial design. *Mater. Today Proc.*, 47, 5395–5400, 2021, https://doi.org/10.1016/j.matpr.2021.06.169.

11. Vigneshwaran, S., Uthayakumar, M., Arumugaprabu, V., Abrasive water jet machining of fiber-reinforced composite materials. *J. Reinf. Plast. Compos.*, 37, 230–237, 2018, https://doi.org/10.1177/0731684417740771.

12. Melentiev, R. and Fang, F., Recent advances and challenges of abrasive jet machining. *CIRP J. Manuf. Sci. Technol.*, 22, 1–20, 2018, https://doi.org/10.1016/j.cirpj.2018.06.001.

13. Zou, X., Fu, L., Wu, L., Zuo, W., Research on Multiphase Flow and Nozzle Wear in a High-Pressure Abrasive Water Jet Cutting Head. *Machines*, 11, 614–633, 2023, https://doi.org/10.3390/machines11060614.

14. Khan, M.A., Soni, H., Mashinini, P.M., Uthayakumar, M., Abrasive water jet cutting process form machining metals and composites for engineering applications: A review. *Eng. Res. Express*, 3, 1–24, 2021, https://doi.org/10.1088/2631-8695/abfe98.

15. Jagadish, K.G., *Abrasive Water Jet Machining of Ceramic Composites*, 51–71, SpringerBriefs in Applied Sciences and Technology, 2020, https://doi.org/10.1007/978-3-030-36001-6_4.

16. Holmberg, J., Wretland, A., Berglund, J., Abrasive Water Jet Milling as An Efficient Manufacturing Method for Superalloy Gas Turbine Components. *J. Manuf. Mater. Process.*, 6, 124–146, 2022, https://doi.org/10.3390/jmmp6050124.

17. Deaconescu, A. and Deaconescu, T., Response surface methods used for optimization of abrasive waterjet machining of the stainless steel x2 crnimo 17-12-2. *Mater. (Basel).*, 14, 2475–2491, 2021, https://doi.org/10.3390/ma14102475.

18. Chen, M., Zhang, S., Zeng, J., Chen, B., Correcting shape error located in cut-in/cut-out region in abrasive water jet cutting process. *Int. J. Adv. Manuf. Technol.*, 102, 1165–1178, 2019, https://doi.org/10.1007/s00170-018-3123-2.

19. Hlavacek, P., Hloch, S., Nag, A., Petru, J., Muller, M., Hromasová, M., Srníček, P., Effect of rotation direction, traverse speed, and abrasive type during the hydroabrasive disintegration of a rotating Ti6Al4V workpiece. *Proc. Inst. Mech. Eng. Part B J. Eng. Manuf.*, 235, 1848–1860, 2021, https://doi.org/10.1177/0954405420971226.

20. Sasikumar, K.S.K., Arulshri, K.P., Ponappa, K., Uthayakumar, M., A study on kerf characteristics of hybrid aluminium 7075 metal matrix composites machined using abrasive water jet machining technology. *Proc. Inst. Mech. Eng. Part B J. Eng. Manuf.*, 232, 690–704, 2018, https://doi.org/10.1177/0954405416654085.

21. Murthy, B.R.N., Makki, E., Potti, S.R., Hiremath, A., Bolar, G., Giri, J., Sathish, T., Optimization of Process Parameters to Minimize the Surface Roughness of Abrasive Water Jet Machined Jute/ Epoxy Composites for Different Fiber Inclinations. *J. Compos. Sci.*, 7, 498–516, 2023, https://doi.org/10.3390/jcs7120498.

22. Perec, A., Research into the disintegration of abrasive materials in the abrasive water jet machining process. *Mater. (Basel)*, 14, 3940–3954, 2021, https://doi.org/10.3390/ma14143940.

23. Pahuja, R., Ramulu, M., Hashish, M., Surface quality and kerf width prediction in abrasive water jet machining of metal-composite stacks. *Compos. Part B Eng.*, 175, 107134, 2019. https://doi.org/10.1016/j.compositesb.2019.107134.

24. Dhanawade, A., Kumar, P., Kumar, S., Experimental study on abrasive water jet machining of carbon epoxy composite. *Adv. Mater. Process. Technol.*, 6, 40–53, 2020, https://doi.org/10.1080/2374068X.2019.1703338.

25. Srinivasu, D.S., Axinte, D.A., Shipway, P.H., Folkes, J., Influence of kinematic operating parameters on kerf geometry in abrasive waterjet machining of silicon carbide ceramics. *Int. J. Mach. Tools Manuf.*, 49, 1077–1088, 2009, https://doi.org/10.1016/j.ijmachtools.2009.07.007.

Note

*Corresponding author: ashok6733@gmail.com

24
Effect of Ultrasonic Vibration-Assisted Micromachining on the Surface Properties of Difficult-to-Machine Materials

P. Jeyapandiarajan, Joel J., S. Arulvel, E. Venkatesaperumal, D. Vignesh and Sreethul Das*
School of Mechanical Engineering, Vellore Institute of Technology, Vellore, Tamil Nadu, India

Abstract

Miniaturization of components in the modern manufacturing scenario necessitates machining of complex features on advanced materials. Machining hard materials with conventional methods like turning, milling, and grinding can be challenging due to high cutting forces, temperatures, tool wear, and poor surface quality. In order to address these challenges, a frequency vibration is introduced in the machining process to improve the surface properties of the material. Ultrasonic vibration-assisted micromachining (UVAMM) is a technique that involves transmitting of high frequency vibration to the cutting tool or workpiece to enhance the machining performance. The tool-workpiece contact become a fluctuating process that allows chip separation and minimize cutting force, while machining difficult-to-cut materials such as titanium, nickel alloys, ceramics, and composites. This chapter discusses UVAMM technology and highlights the applications, capabilities, and limitations of UVAMM on difficult to cut materials.

***Keywords*:** Ultrasonic vibration, cutting force, surface roughness, micromachining

Nomenclature

VAM	Vibration-assisted machining
UVAMM	Ultrasonic vibration-assisted micromachining
MMC	Metal matrix composites
CFRP	Carbon fiber reinforcement composites
RUM	Rotary ultrasonic machining
EVC	Elliptical vibration-assisted cutting
CNC	Computer numerical control
DTM	Difficult-to-Machine
TMM	Traditional micro-milling
UVAI	Ultrasonic vibration-assisted Hertzian indentation

24.1 Introduction

Recent advancement in manufacturing techniques and material science discipline are extensively utilized in modern materials, characterized by high hardness, wear, and temperature resistance. As technology moves towards developing new materials such as high strength superalloys, metal matrix composites (MMC), and carbon fiber reinforcement composites (CFRP), it imposes limitations with respect to the tools and machining processes currently available for material processing [1]. Even with the advent of technologies like additive manufacturing, machining remains an unavoidable means for shaping materials to the final functional requirements. Traditional machining processes encounter several challenges while processing advanced materials such as generation of excessive cutting force and temperatures, leading to excessive tool wear and reduced surface integrity that adversely affects the productivity and quality requirements of the machined surface. Miniaturization in various scientific and technological domains has led to the emergence of micromachining for the precise and reliable creation of precision components with intricate features. Micromachining involves a plethora of techniques for fabricating ultra-precision geometrical features with dimensions in the micrometer range. Conventional methods like micromilling, microturning, and microgrinding have

established themselves as reliable processing methods for diverse applications. Micromachining on specific features has routed its application through aerospace, optics, medical devices, automotive and electronic industries [2]. Even with all the technological advancements, micromachining faces difficulties while machining difficult-to-cut materials.

For the advanced materials, there is a need for adapting the process of machining beyond the traditional means to achieve better performance. In the recent years, researchers are highly interested in enhancing the machinability of difficult-to-cut materials by developing and experimenting on hybrid mode machining. Hybrid machining involves application of external energy sources such as thermal, vibrational, magnetic, pulsed, abrasive particle, high pressure air/water jet and coolant to assist conventional machining processes. Each form of energy has some special advantages over the other [3] and vibrational energy has been extensively used to assist the micromachining processes. As research and development push the boundaries of miniaturization, demand for superior accuracy and development of novel materials intensifies and novel micromachining approaches like ultrasonic vibration-assisted micromachining (UVAMM) draws attention. Ultrasonic vibration-assisted micromachining (UVAMM) has shown to outperform the conventional micromachining process with improved tool life, surface integrity, reduction of micro-cracks and lower residual stress. Ultrasonic vibration-assisted micromachining (UVAMM) enactment depends on optimizing parameters as frequency and amplitude, this requirement varies based on the work-material added to this machining process variables such as cutting speed, feed rate and depth of cut [4]. This chapter deals with the UVAMM performance and the factors that helps in enlightening the surface quality and tool life.

24.2 The Technique of UVAMM

Ultrasonic vibration-assisted micromachining (UVAMM) can be considered to be evolved from the technology of vibration-assisted machining (VAM). The concept of VAM was first established in the early 1950s, and it has been implemented into different machining methods, both conventional and non-conventional. In the late

1990s, micromachining techniques were developed to produce small parts with a high degree of precision. Since then, the two-dimensional (2D) elliptical vibration [5] and three-dimensional (3D) VAM processes have evolved, and the UVAMM process has been widely adopted across various industries. By integrating VAM with additive manufacturing, it is possible to attain faster, efficient, and accurate manufacturing processes [6]. A roadmap showing the evolution of VAM technologies is shown in Figure 24.1.

Vibration-assisted machining (VAM) entails integrating external energy into the traditional machining technique to produce high frequency with low amplitude vibrations into the workpiece or tool, allowing for periodic separation across a workpiece and the tool. This can result in reduced cutting force and the production of thinner chips, leading to increased processing performance, extended tool life span, improved surface finish, and minimized burr formation [7]. It can be classified into two categories: one based on vibration direction (1D, 2D, and 3D), and the other based on frequency range (ultrasonic VAM and non-ultrasonic VAM). Ultrasonic VAM operates at a high frequency of vibration, typically more than 20 kHz, and employs a resonant vibration mechanism to maintain an appropriate vibration amplitude. The cutting efficiency of difficult-to-machine materials is significantly enhanced by high vibration frequency [8]. In a non-ultrasonic VAM, vibration frequencies obtained are typically less than 10 kHz by using a mechanical linkage that transfers power, causing the device to expand and contract [9].

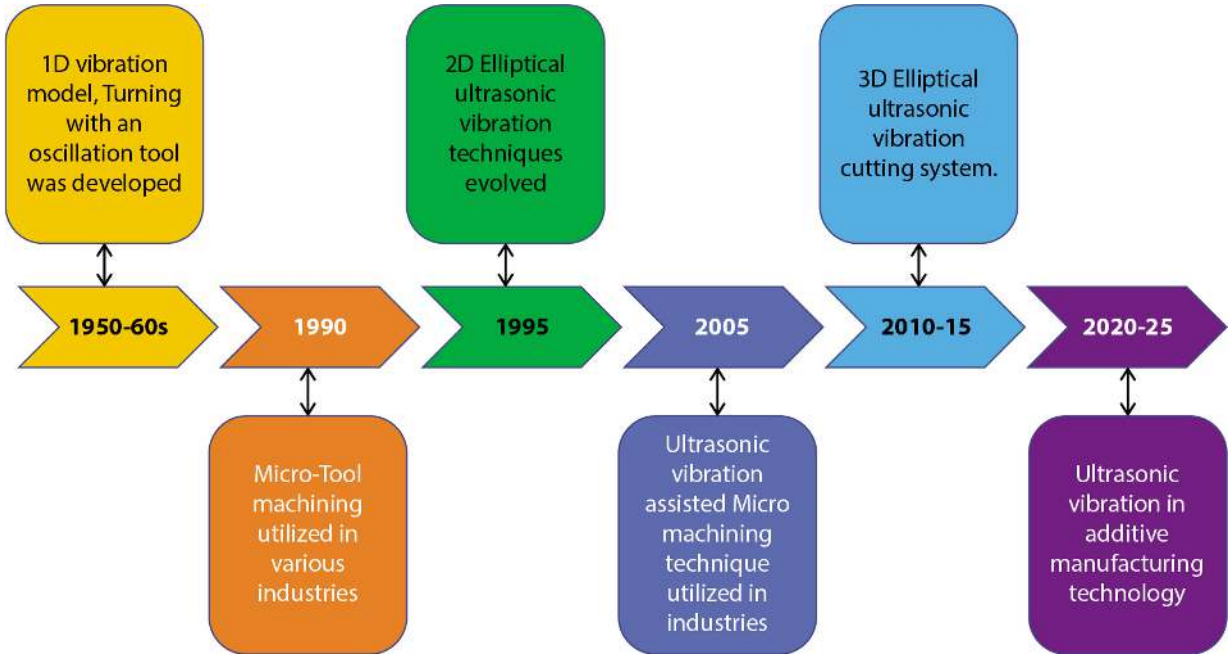


Figure 24.1 Evolution of UVAMM.

The vibration devices are broadly classified into two groups based on the operating frequencies of the system: the resonant mode and the non-resonant mode. In a non-resonant vibration system, the vibration actuators normally vibrate below its natural frequency. In order to increase stability and decrease dynamic error in the vibration platform, adjustable hinge structures are often adopted for greater dynamic responsiveness with reduced friction. In a resonant system, a sonotrode (stated as a horn or concentrator) transfers and amplifies a specific vibration from a vibration source by vibrating at its natural frequency. This system can obtain a greater operating frequency with improved energy consumption than a non-resonant system [10]. Figure 24.2 shows the classification of VAM systems. Table 24.1 lists the characteristic features and complexity of parts for different VAM systems. In a VAM system, an ultrasonic generator transforms electrical energy into a high-frequency signal, which is then transferred to a transducer to turn the frequency signal into mechanical vibration. The sonotrode/concentrator amplifies mechanical vibration, which is then transferred to the tool holder containing the cutting tool [11]. The process of UVAMM (refer to Figure 24.3) involves configuring the vibration parameters such as frequency, amplitude, and vibration direction, along with machine parameters such as spindle rotation, feed rate, and depth of cut. Once the

parameters are set, the workpiece is fixed in place, and the ultrasonic vibration is activated along with the computer numerical control (CNC) program to process the material.

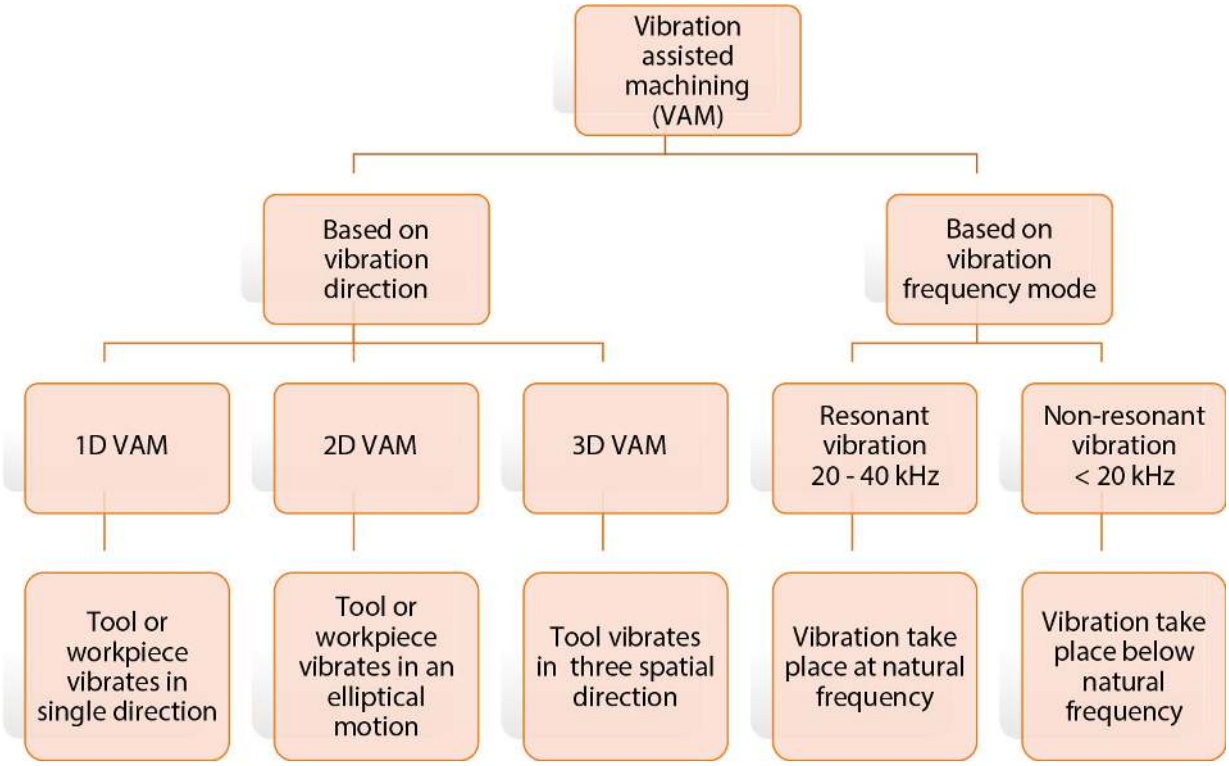


Figure 24.2 Classification VAM.

Table 24.1 Characteristics of vibration-assisted micromachining.

Features	**1D UAM**	**2D UAM**	**3D UAM**	**RUM (rotary ultrasonic machining)**
Frequency	Reciprocating motion of tool in ultrasonic range	Elliptical tool trajectory using simultaneous ultrasonic vibration in two directions	Three different modes of ultrasonic frequencies	Rotary motion + vibration of tool
Feature complexity	Flat and cylindrical surfaces	Grooves, slots, pattern/texture development	Complex shapes, optical freeform surfaces	Complex shapes, free-form surfaces

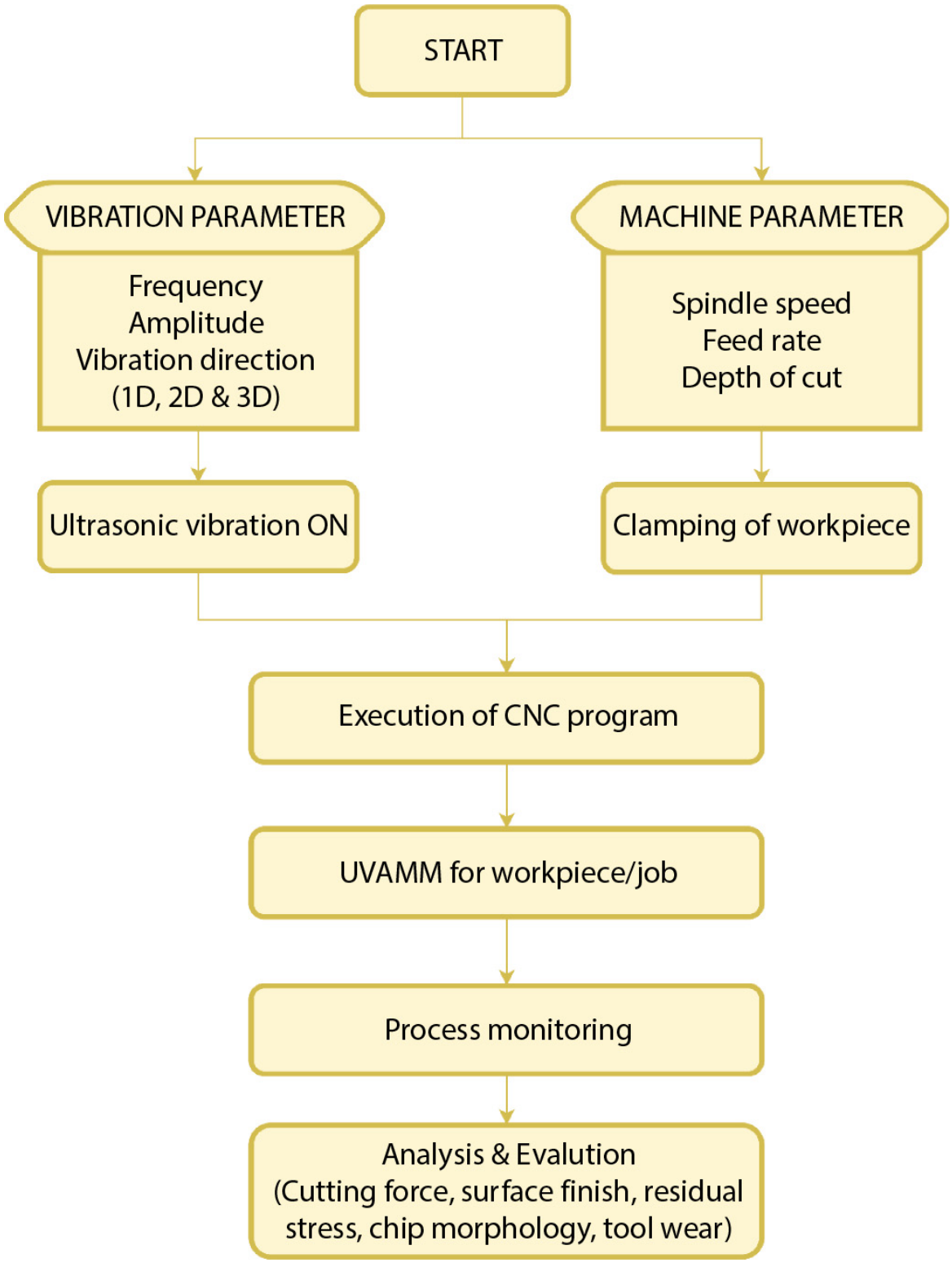


Figure 24.3 Methodology of UVAMM.

24.3 UVAMM of Difficult-To-Machine

Materials

Research on ultrasonic vibration-assisted machining (UVAM or UAM) has attracted enormous attention due to its capability to enhance the machining quality of difficult-tomachine (DTM) materials [12, 13]. The periodic separation among the tool rake face and workpiece as the unique characteristic feature of UVAM which leads to the reduction of cutting force, enhancing the machinability and improving the surface quality when compared with conventional machining processes. Several researchers have obtained significant reduction of the machining force and extended tool life, while employing UVAM [14, 15].

Figure 24.4 compares surface roughness between different hard-to-cut materials. During the micromilling operation of Ti6Al4V and Inconel 718 [16], the surface roughness obtained is 0.1 µm and 0.14 µm, respectively. However, with the aid of ultrasonic vibration, the surface irregularity is significantly reduced by 0.071 µm for titanium and 0.09 µm for Inconel. Surface roughness values for borosilicate glass (BK7) using micromilling and rotary ultrasonic vibration milling were reported as 0.23 µm and 0.11 µm, respectively [17].

The state of the art on UVAMM and its application to advanced materials is discussed in the subsequent sections.

24.3.1 UVAMM of Traditional Metallic Alloys

Aluminum alloys are commonly used in military, aerospace, and automotive equipment, but UVAMM is becoming increasingly important owing to its better accuracy and efficiency in micromanufacturing [18]. UVAMM technique was investigated for aluminum 6061 T6. The method employs longitudinal vibration of the workpiece by adjusting the amplitude and feed rate during the milling process. Compared to regular milling, the UVAMM process reduced the cutting force by 12% and resulted with better surface finish [19]. During machining operations, burr development is a frequently occurring phenomenon. The application of abrasive UVAMM of Al6061 material has reduced surface irregularity from 8.97 to 6.63 nm and improved surface smoothness by 26% [20].

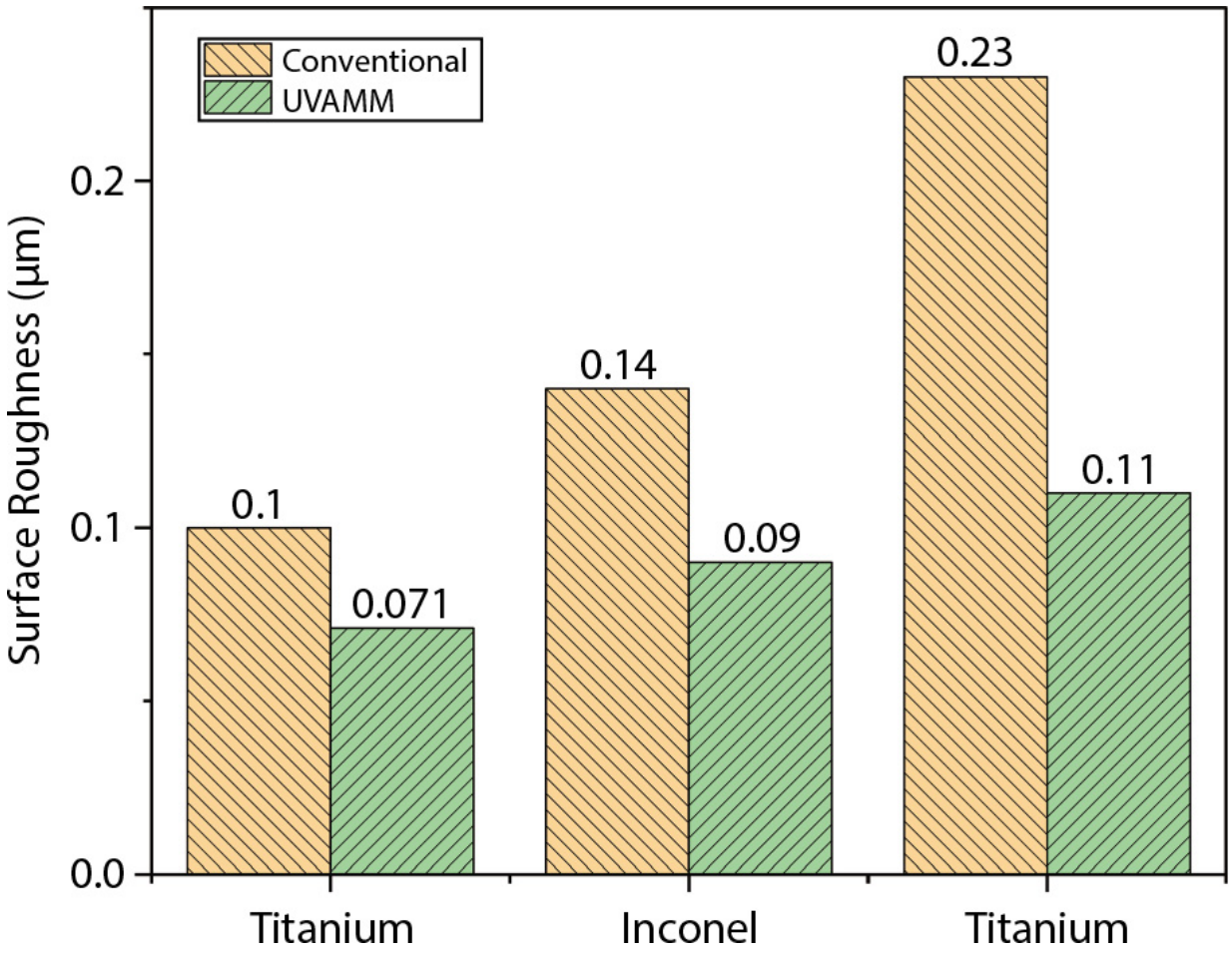


Figure 24.4 Comparison of surface roughness of conventional vs UVAMM [16, 17].

Chern *et al.* [21] proposed the strategy of vibrating the work holder during microdrilling operation. For this purpose, a worktable capable of providing vibrations of frequency ranging from 1 to 10 kHz has been configured. Drilling experiments have been carried out on Al 6061-T6 and SS41 using a 0.5-mm diameter twist drill in lubricated conditions. Parameters like roundness, machining force, and wall profile of the drilled hole have been found to improve when drilling is carried out at higher values of vibration frequency and amplitude. Due to the presence of high frequency vibration, the tool has been found to align properly while contacting the workpiece, which improves the accuracy of the drilled hole. The vibrations increased the cutting velocity and enabled separation of drill-workpiece contact, which allowed the lubricant to reach the cutting zone. This has reduced the cutting force and temperature during the drilling process. This ensures

that the drill maintains its hardness and sharpness, making it stable and uniform with each revolution. As a result, the variation of radial force is minimized, and the roundness is improved. The versatility of two vibration schemes for UVAMM, namely, linear and elliptical, were compared by Zhang *et al.* [22]. The experiments were conducted on 0Cr18Ni9 stainless steel using carbide inserts. The machining schemes have been found to be effective for turning microgrooves on cylindrical workpieces, thereby confirming the capability of ultrasonic vibration cutting to generate intricate microscale features.

24.3.2 UVAMM of Superalloys

In VAM, the effects of vibration parameters on Ti6Al4V were investigated with the objective of producing burrs. Slot milling experiments are carried out with 1 mm diameter uncoated carbide end mills on Ti-6Al-4V. Traditional micromilling produces burr heights of about 36 µm for down milling and 28 µm for up milling. However, when vibration is incorporated into the process, the burr height on the up-milling side is reduced by 58% and on the down milling side by about 50%. The experimental results reveal that vibration-assistance minimizes burr production and enhances machining precision [23]. A unique 2D ultrasonic transducer design was developed for high-frequency VAM. The resonance frequency of the intended 2D ultrasonic transducer was determined through analytical, numerical, and experimental methods, resulting in values of 27,770 Hz, 28,460 Hz, and 27,900 Hz, respectively. The machining trials were conducted for titanium alloy in two directions: feed-axial (XZ) and feed-cross feed (XY). In the XZ direction, an improved surface smoothness (Ra) value of 0.02 µm was achieved at a low vibration amplitude of 2 µm, high spindle revolution of 30000 rpm, and low feed rate of 5mm/min [24].

The research investigates the use of UVAMM with a maximum amplitude of 15 µm for horizontal vibration of workpieces of aluminum alloy 6061T6 and titanium alloy TC4. The experiment results indicate that ultrasonic vibrations efficiently reduces the milling force by 12% and 17% compared to traditional milling, therefore resulting in better machining performance and prolonged tool life [25]. Longitudinal torsional ultrasonic vibration

microhole drilling (LTUAD) experiment was conducted for chip geometry, thrust force, and top burr size, and data reveals that the average thrust force in LTUAD reduced from 1.98% to 24.9%. The exit burr height was spread equally with little extension in LTUAD than the traditional drilling, which diminished from 17.2% to 44.9% [26]. This study explores the process of dual-direction VAM on Ti6Al4V and its effect on tool life extension, back chipping, and chip formation. It focuses on the significance of vibration assistance in enhancing surface integrity and reducing tool runout frequency. The study exposes that, vibration assistance improves the surface profile, resulting in a lower surface roughness value of Ra 25 nm. The frequency and amplitude of vibration prove to have a substantial impact on surface quality and shape accuracy. Higher vibration frequencies and amplitudes lead to improved surface roughness and shape accuracy. However, excessively high vibration frequencies could damage the primary shaft and accelerate surface roughness [27]. Rotary ultrasonic elliptical end milling (RUEEM) is a machining technique used for high-performance side milling of Ti6Al4V alloy. The experiment aimed to analyze the surface integrity of titanium in the RUEEM under varying vibration amplitudes and cutting velocities. The vibration amplitude and cutting speed increases lead to an increase in surface roughness values, which went from Ra 0.160 mm to Ra 0.758 mm. At low cutting speeds, the surface compressive residual stress decreased with vibration amplitudes, while at high cutting speeds, it exhibited an opposite tendency [28].

High temperature applications, such as those in the chemical energy, turbine engine, and aerospace industries, are the main uses for alloys based on nickel. Strong creep resistance, improved corrosion resistance, and increased fatigue strength are among the excellent mechanical qualities of alloys based on nickel. Even still, greater cutting force is required throughout the machining process and the good qualities indicate significant tool damage [29]. For producing very accurate micro parts, micromachining is favored. That being said, the material’s surface quality is impacted by the Inconel alloy’s greater fluidity when subjected to micromachining. The utilization of ultrasonic-assisted micromachining presents a viable solution in lowering tool wear and nickel alloy cutting pressure. One useful technology for lowering tool wear and nickel

alloy cutting pressure is ultrasonic assisted micromachining [30]. Because of their limited thermal conductivity and tendency to work harden, Inconel alloys, which are renowned for their strength and heat resistance present difficulties for traditional micromachining. One approach that shows promise is ultrasonic-aided micromachining (UAMM), which has benefits in terms of residual stress and surface roughness [31]. Surface defects reduce dramatically if the feed rate (Fz) increases. When the frequency is above 4 Hz, the impact of ultrasonic vibration on the surface integrity becomes smaller. The minimum burr size on the down milling side is 50.23 µm, while on the up-milling side is 36.57 µm. The use of UVAMM efficiently prevents the built-up edge formation and improves the micromilling process. Compared to traditional micro-milling (TMM), thrust force (Fx), radial stress (Fy), and axial stress (Fz) of UVAMM were reduced by 7.6%, 11.5% & 1.3%, respectively [32].

24.3.3 UVAMM of Brittle Materials

A 2D vibration powered by piezoelectricity, to provide vibration to the workpiece during the micromilling of optical glass. The directions, amplitudes, and frequencies of vibrations are investigated in relation to their impacts on surface finish and profile form. The surface quality is improved by increasing the vibration amplitude from 2 µm to 4 µm. When vibration assistance is given in the normal direction, the Ra value reduced by 45%, whereas surface finish does not change notably in the feed direction [33]. An experimental study was conducted on the effect of ultrasonic vibration and tool inclination on microgrinding of glassy carbon. The combined use of ultrasonic vibration and tool inclination enhance the surface quality, resulting in a surface finish of 200-nm Ra [34].

Microchannels in zirconium oxide and rotary ultrasonic machining (RUM) improve surface quality, prevent edge chipping, and enhance dimensional accuracy during machining. The input parameters used were cutting speed set at 3000 rpm, feed rate at 0.5mm/ min, depth of cut at 0.0125mm, frequency at 26 KHz, and amplitude at 35µm, achieving surface roughness of 0.26 µm. The experimental results indicate that high dimensional precision and surface roughness is linearly proportional to the cutting depth and

feed rate and opposite to cutting speed, frequency, and amplitude [35]. A study was conducted to investigate the material removal mechanism of micro-cylindrical SiC surfaces using ultrasonic vibration-assisted polishing (UVAP). The correlation between ultrasonic vibration, friction force, and the quality of micro-cylindrical surfaces affected by the parameters of polishing, including the polishing force, the speed of polishing, and the parameters of ultrasonic vibration. The grinding process resulted in a surface irregularity of 109.2 nm (Ra) and 1.3978 µm (Rt) for the workpiece by applying ultrasonic vibration, the Ra and Rt values can be reduced to 4.3 nm and 25.4 nm, respectively. The results indicate that the implementation of ultrasonic vibration can effectively reduce the friction force during the polishing process of the SiC micro-cylindrical surface, leading to an enhancement in surface finish [36]. The research presents a layered elliptical vibration-assisted cutting (LEVC) approach for creating deep microgrooves with various forms. The LEVC technique produces less residual stress than the layered conventional cutting (LCC) process when the machining stress is compared using finite element analysis. Machining experiments results reveal that the LEVC approach is effective in creating micro grooves with adjustable shape and depth [37].

Processing bio-ceramics becomes challenging due to their inherent brittleness and hardness. Diamond grinding, a form of abrasive machining, is extensively employed for bio-ceramic materials. During regular grinding, the resulting edge chips are larger, rougher, and longer, with an average size of about 0.64–0.68 mm. However, in UVAG (ultrasonic-assisted grinding), the chips are thinner, smoother, and shorter, with an average size of 0.05–0.07 mm. The ultrasonic vibration-assisted Hertzian indentation (UVAI) approach results in a substantial reduction of around 50% in the edge chipping size [38]. An ultrasonic vibration-assisted microgrinding process was developed to prevent crack damage in biological bones during grinding. A spherical grinding head was used to achieve this by examining the morphology and height measurements of abrasive particles produced by the grinding head. The researchers created a microgrinding force prediction model by examining the relationship between cutting depth and grinding force. The theoretical model agreed well with

experimental observations, with average variances of 10.37% on the x-axis, 6.85% on the y-axis, and 7.81% on the z-axis. The findings indicated that the application of ultrasonic vibration reduced the maximum thickness of chips that remained undeformed, increased the elimination of bone meal and ductile materials, and reduced the amount of grinding force [39].

24.3.4 UVAMM for Generation of Textured Surfaces

Ultrasonic vibrations may be utilized to form sophisticated micro-nano structured surfaces possessing specialized functional features. Textured surfaces are used in a variety of engineering applications to provide functional properties to surfaces. Vibration-assisted micromachining is considered to be one of the most suitable options for generating textured surfaces. In VAM, ultrasonic vibration can be modulated to generate different surface textures. The scheme can be used in grinding, turning, or milling to obtain various micro/nano textures by selecting a suitable combination of vibration modes, machining parameters and tool geometry [40]. Using a 3D resonant vibration-assisted machining system, Ali *et al.* [41] successfully generated micro-dimples on a cylindrical surface. Functionally, these micro-dimples have improved the ani-icing property of the cylindrical surface. In another work [42], the same system was used to generate wavy patterns, which improved the wettability property of the surface. Hence, by suitable selection of process parameters, UVAMM system may be utilized to obtain surface properties for different applications. The suitability of ultrasonic vibration-assisted diamond turning to create free-form surfaces has been successfully demonstrated by Xing *et al*. [43] by machining a bidirectional sinusoidal wave grid surface with high precision on a die steel mold meant for mass production of optical systems. Micromilling has been utilized to obtain various patterns in a controlled manner on copper surfaces [44]. This is accomplished using a 2D VAMM system by modulating the vibration frequency and feed per tooth during the milling process. However, the vibration stage designed for the experiment utilized frequencies in the order of 2000 Hz. Altering the optical properties of structural surfaces by controlling the reflectivity using micro/nano features for providing apparent colors has widespread applications. Elliptical vibration texturing in

which vibrations are superimposed with the cutting velocity can create overlapping patterns which can induce optical interference property to the surface leading to surface coloring. This principle has been used to create 2D nano-pyramid features on aluminum surface by using a nano indentation process by controlling the machining parameters in the presence of vibration [45]. The researchers were able to replicate images which exhibited two different colors when viewed from orthogonal directions. Elliptical vibration texturing also has the capability to process brittle materials such as ceramics, glass etc. due to the intermittent cutting nature. This method provides an alternative to laser-based techniques for surface patterning and is proposed to produce better iridescent effects and can generate complex patterns with higher efficiency [46]. Mechanical processing through vibration texturing also eliminates the need for sample pre-machining and post-processing associated with laser texturing.

24.4 Conclusion

Machining of hard materials becomes less difficult through the assistance of vibration to the conventional micromachining process, which improves surface properties of the materials. Ultrasonic vibration-assisted micromachining (UVAMM) decreases cutting forces, enhances surface smoothness by reducing chip adhesion and facilitates smoother chip formation. Its performance depends on optimizing machine and vibration parameters such as depth of cut, feed rate, frequency and amplitude results through minimum heat generation, reduced burr formation and improved surface integrity.

24.4.1 Salient Points

- 1D and 2D UVAMM mechanisms differs by varying the chip geometry and produce shorter and thinner chips, which lowers cutting force and reduces the stress, causing better lubrication.
- Periodic fluctuation between the tool and workpiece allows to dissipate heat faster, which lowers the temperature and enhances the lubrication than conventional machining.

- In UVAMM, the tool and work material have intermittent contact, which reduces cutting force, tool wear, and extends the lifespan of the tool.
- Uniform alternate cycles between tool and workpiece facilitates to provide smaller subsurface crack and also irregular chips minimizes surface irregularity.
- Burr formation occurs during machining and can cause edge deformation. This can be significantly reduced with the use of UVAMM.

24.4.2 Challenges and Future Scope

- The large-scale application of UVAMM is limited by the unavailability of efficient vibration systems that can generate a wide range of amplitudes and vibration modes. The theoretical research in this field as well as the development of hardware still needs to go a long way to overcome the limitations in this field [19]. Synchronization between the vibration system and machine tool, and the selection of actuators suitable for micromachining are still challenging aspects of UVAMM.
- Sustainability issues are a significant aspect of present-day manufacturing operations. One of the areas under investigation of the UVAMM process to fabricate components for microfluidic applications. The manufacture of microchannels on ceramics, glass and silicon for micro-heat exchanger and sensor applications using the UVAMM technique is an area of interest for researchers.
- The development of versatile UVAMM systems to machine free-form surfaces remains a scarcely explored area. Modification of surface to impart functional properties to the surface can be explored further considering the wide variety of applications in that area.

References

1. Gavalda Diaz, O., Garcia Luna, G., Liao, Z., Axinte, D., The new challenges of machining ceramic matrix composites (CMCs):

Review of surface integrity. *Int. J. Mach. Tools Manuf.*, 139, 24–36, 2019.

2. Debnath, S., Kunar, S., Anasane, S.S., Bhattacharyya, B., *Non-traditional Micromachining Processes: Opportunities and Challenges*, Springer, Cham, pp. 1–59, 2017.
3. Unune, D.R. and Mali, H.S., Current status and applications of hybrid micro-machining processes: A review. *Proc. Inst. Mech. Eng. Part B J. Eng. Manuf.*, 229, 10, 1681–1693, 2015.
4. Das, S., Doloi, B., Bhattacharyya, B., *Recent Advancement on Ultrasonic Micro Machining (USMM) Process*, Springer, Cham, pp. 61–91, 2017.
5. Moriwaki, T. and Shamoto, E., Ultrasonic Elliptical Vibration Cutting. *CIRP Ann. - Manuf. Technol.*, 44, 1, 31–34, 1995.
6. Hehr, A. and Dapino, M.J., Dynamics of ultrasonic additive manufacturing. *Ultrasonics*, 73, 49–66, 2017.
7. Brehl, D.E. and Dow, T.A., Review of vibration-assisted machining. *Precis. Eng.*, 32, 3, 153–172, 2008.
8. Xu, W.X. and Zhang, L.C., Ultrasonic vibration-assisted machining: principle, design and application. *Adv. Manuf.*, 3, 3, 173–192, 2015.
9. Chen, W., Huo, D., Shi, Y., Hale, J.M., State-of-the-art review on vibration-assisted milling: principle, system design, and application. *Int. J. Adv. Manuf. Technol.*, 97, 5–8, 2033–2049, 2018.
10. Han, X., Zhang, D., Song, G., Review on current situation and development trend for ultrasonic vibration cutting technology. *Mater. Today Proc.*, 22, 444–455, 2020.
11. Kumar, S., Wu, C.S., Padhy, G.K., Ding, W., Application of ultrasonic vibrations in welding and metal processing: A status review. *J. Manuf. Process.*, 26, 295–322, 2017.
12. Wang, Y., Guangheng, D., Zhao, J., Dong, Y., Zhang, X., Jiang, X., Lin, B., Study on key factors influencing the surface

generation in rotary ultrasonic grinding for hard and brittle materials. *J. Manuf. Process.*, 38, 549–555, 2019.

13. Li, S., Wu, Y., Nomura, M., Effect of grinding wheel ultrasonic vibration on chip formation in surface grinding of Inconel 718. *Int. J. Adv. Manuf. Technol.*, 86, 1–4, 1113–1125, 2016.

14. Geng, D., Zhang, D., Xu, Y., He, F., Liu, D., Duan, Z., Rotary ultrasonic elliptical machining for side milling of CFRP: Tool performance and surface integrity. *Ultrasonics*, 59, 128–137, 2015.

15. Pujana, J., Rivero, A., Celaya, A., López de Lacalle, L.N., Analysis of ultrasonic-assisted drilling of Ti6Al4V. *Int. J. Mach. Tools Manuf.*, 49, 6, 500–508, 2009.

16. Kuram, E. and Ozcelik, B., Optimization of machining parameters during micro-milling of Ti6Al4V titanium alloy and Inconel 718 materials using Taguchi method. *Proc. Inst. Mech. Eng. Part B J. Eng. Manuf.*, 231, 2, 228–242, 2017.

17. Jain, A.K. and Pandey, P.M., Experimental investigations of ceramic machining using µ-grinding and µ-rotary ultrasonic machining processes: A comparative study. *Mater. Manuf. Process.*, 32, 6, 598–607, 2017.

18. Lian, H., Guo, Z., Huang, Z., Tang, Y., Song, J., Experimental research of Al6061 on ultrasonic vibration assisted micro-milling. *Procedia CIRP*, 6, 561–564, 2013.

19. Yang, Z., Zhu, L., Zhang, G., Ni, C., Lin, B., Review of ultrasonic vibration-assisted machining in advanced materials. *Int. J. Mach. Tools Manuf.*, 156, 103594, 2020.

20. Kumar, A.S., Deb, S., Paul, S., Ultrasonic-assisted abrasive micro-deburring of micromachined metallic alloys. *J. Manuf. Process.*, 66, 595–607, 2021.

21. Chern, G.L. and Lee, H.J., Using workpiece vibration cutting for micro-drilling. *Int. J. Adv. Manuf. Technol.*, 27, 7–8, 688–692, 2006.

22. Zhang, C., Guo, P., Ehmann, K.F., Li, Y., Effects of ultrasonic vibrations in micro-groove turning. *Ultrasonics*, 67, 30–40, 2016.

23. Zheng, L., Chen, W., Huo, D., Experimental investigation on burr formation in vibration-assisted micro-milling of Ti-6Al-4V. *Proc. Inst. Mech. Eng. Part C J. Mech. Eng. Sci.*, 233, 12, 4112–4119, 2019.

24. Satpute, V., Huo, D., Hedley, J., Elgendy, M., Design of a novel 2D ultrasonic transducer for 2D high-frequency vibration–assisted micro-machining. *Int. J. Adv. Manuf. Technol.*, 126, 3–4, 1035–1053, 2023.

25. Xu, L.H., Na, H.B., Han, G.C., Machinablity improvement with ultrasonic vibration–assisted micro-milling. *Adv. Mech. Eng.*, 10, 12, 1–12, 2018.

26. Gao, G., Xia, Z., Yuan, Z., Xiang, D., Zhao, B., Influence of longitudinal-torsional ultrasonic-assisted vibration on micro-hole drilling Ti-6Al-4V. *Chin. J. Aeronaut.*, 34, 9, 247–260, 2021.

27. Li, G., Li, Y.H., Liao, Q.Y., Xue, J.D., Wang, B., Mechanism of dual-direction vibration-assisted (DVA) micro-milling in surface formation considering the tool life-lengthening effect on the Ti6Al4V: design and experiment. *Int. J. Adv. Manuf. Technol.*, 123, 7–8, 2313–2330, 2022.

28. Zhang, M., Zhang, D., Geng, D., Shao, Z., Liu, Y., Jiang, X., Effects of tool vibration on surface integrity in rotary ultrasonic elliptical end milling of Ti–6Al–4V. *J. Alloys Compd.*, 821, 153266, 2020.

29. Wu, Y., Wang, Q., Li, S., Lu, D., Ultrasonic Assisted Machining of Nickel-Based Superalloy Inconel 718. *Superalloys Ind. Appl.*, 15, 60, 708, 2018.

30. Yuan, Z., Fang, B., Dong, Y., Ding, H., Zhang, Y., Study on surface texture and corrosion resistance of ultrasonic vibration-assisted micromilling Inconel718. *Int. J. Adv. Manuf. Technol.*, 121, 1–2, 601–618, 2022.

31. Yin, X., Li, X., Liu, Y., Geng, D., Zhang, D., Surface integrity and fatigue life of Inconel 718 by ultrasonic peening milling. *J.*

Mater. Res. Technol., 22, 1392–1409, 2023.

32. Fang, B., Yuan, Z., Li, D., Gao, L., Effect of ultrasonic vibration on finished quality in ultrasonic vibration assisted micromilling of Inconel718. *Chin. J. Aeronaut.*, 34, 6, 209–219, 2021.

33. Jin, X. and Xie, B., Experimental study on surface generation in vibration-assisted micromilling of glass. *Int. J. Adv. Manuf. Technol.*, 81, 1–4, 507–512, 2015.

34. Beiring, P. and Yan, J., Ultrasonic vibration-assisted microgrinding of glassy carbon. *Proc. Inst. Mech. Eng. Part C J. Mech. Eng. Sci.*, 233, 12, 4165–4175, 2019.

35. Abdo, B.M.A., El-Tamimi, A., Alkhalefah, H., Parametric Analysis and Optimization of Rotary Ultrasonic Machining of Zirconia (ZrO2) Ceramics. *IOP Conf. Ser. Mater. Sci. Eng.*, 727, 1, 012009, 2020.

36. Zhao, Q., Sun, Z., Guo, B., Material removal mechanism in ultrasonic vibration assisted polishing of micro cylindrical surface on SiC. *Int. J. Mach. Tools Manuf.*, 103, 28–39, 2016.

37. Zhang, C., Investigation on layered elliptical vibration-assisted cutting of micro groove. *Int. J. Adv. Manuf. Technol.*, 123, 9–10, 3407–3419, 2022.

38. Tesfay, H.D., Xu, Z., Li, Z.C., Ultrasonic vibration assisted grinding of bio-ceramic materials: an experimental study on edge chippings with Hertzian indentation tests. *Int. J. Adv. Manuf. Technol.*, 86, 9–12, 3483–3494, 2016.

39. Sun, J., Li, C., Zhou, Z., Liu, B., Zhang, Y., Yang, M., Gao, T., Liu, M., Cui, X., Li, B., Li, R., Dambatta, Y.S., Sharma, S., Material Removal Mechanism and Force Modeling in Ultrasonic Vibration-Assisted Micro-Grinding Biological Bone. *Chin. J. Mech. Eng. (English Ed.)*, 36, 1, 129, 2023.

40. Xu, S., Kuriyagawa, T., Shimada, K., Mizutani, M., Recent advances in ultrasonic-assisted machining for the fabrication of micro/nano-textured surfaces. *Front. Mech. Eng.*, 12, 1, 33–45, 2017.

41. Ali, S., Kurniawan, R., Xu, M., Ahmed, F., Ko, T.J., Anti-icing characteristics of hierarchical micro-dimple textured surface generated by 3D resonant vibration assisted machining. *Colloids Surf. A Physicochem. Eng. Asp.*, 675, 131967, 2023.

42. Ali, S., Kurniawan, R., Ko, T.J., Development of 3D Resonant Elliptical Vibration Transducer for Dual-Frequency Micro-Dimple Surface Texturing. *Int. J. Precis. Eng. Manuf.*, 22, 8, 1365– 1379, 2021.

43. Xing, Y., Li, C., Liu, Y., Yang, C., Xue, C., Fabrication of high-precision freeform surface on die steel by ultrasonic-assisted slow tool servo. *Opt. Express*, 29, 3, 3708, 2021.

44. Song, B., Zhang, D., Jing, X., Ren, Y., Chen, Y., Li, H., Theoretical and Experimental Investigation of Surface Textures in Vibration-Assisted Micro Milling. *Micromachines*, 15, 1, 139, 2024.

45. Zhang, H., Feng, P., Feng, F., Zhang, J., Wang, C., Wang, J., Structural coloration with two-dimensional nanostructures fabricated by elliptical vibration nanoindentation. *Precis. Eng.*, 82, 219–232, 2023.

46. Yang, Y., Pan, Y., Guo, P., Structural coloration of metallic surfaces with micro/nano-structures induced by elliptical vibration texturing. *Appl. Surf. Sci.*, 402, 400–409, 2017.

Note

**Corresponding author*: sreethuldas@vit.ac.in

25
A Significant Impact of Laser-Assisted Micromachining on Tribological Properties of High Strength Alloys

E. Venkatesaperumal, P. Jeyapandiarajan*, S. Arulvel, J. Joel and Jayakrishna Kandasamy

School of Mechanical Engineering, Vellore Institute of Technology, Vellore, Tamil Nadu, India

Abstract

In traditional micromachining, processing the high-strength alloys is a tedious process due to rapid tool wear, high cutting force, and poor tool life. To address this limitation, the laser was predominantly used to machine the high-strength alloys, including ceramic, titanium, and superalloys. Highstrength alloys have been used in various industries, such as aerospace, defense, and bio-medical. Laser produces a high heat generation in tool interaction area, leading to thermal stress. The high thermal stress causes a tool softening, wear and corrosion in the tool material. So, significant efforts were made to control the tool wear through optimizing the process parameters and tool design. This chapter precisely discusses the scientific contribution made on utilizing the laser micromachining on improving the tool wear resistance, residual stress, and surface roughness of high-strength alloys and highlights the importance of various laser sources used in the industries.

***Keywords*:** Laser power, micromachining, cutting force, tool wear, surface integrity

25.1 Introduction

Micromachining is a precise machining process that deals with processing small component diameters, cutting depths, and tolerances. There are various types of micromachining that includes micro-turning, micromilling, and microgrinding. These processes utilizes mechanical micro-cutting methods in various applications like micro molding, optical engineering, and semiconductor manufacturing [1]. Over the past 60 years, the use of lasers in materials processing has constantly increased. Lasers and related technologies provide innovative solutions for both additive and subtractive manufacturing. They are well known feasible options compared to traditional and non-traditional machining methods, especially at a microscale. And also, it provides fast and non-contact processing for wide range of materials with high accuracy and user-friendly [2]. The laser can also assist the other process like mechanical micromachining, electro-discharge machining, and electrochemical machining, which are briefly discussed in the following sections.

Laser-assisted micromachining (LAMM) is an innovative hybrid thermo-mechanical micromachining process specially designed to overcome the limitations of traditional micro-cutting techniques. Laser-assisted micromachining is a viable option for the hard materials that are difficult-to-cut. The laser source pre-heats and softens the hard material locally and increase the machinability and surface integrity [3]. Laser-assisted micromachining finds its place in various operations like drilling, threading, cutting, turning, and marking. Consequently, the LAMM has been modified and fine-tuned to improve the production processes and equipment designs, including patterns, holes, and grooves [4].

Numerous industries have employed laser cutting technology since the 1980s after the invention of the Nd-YAG solid-state laser. The overall efficiency of machining with LASER invention has evolved in a new fashion, widening the scope for machining difficult-to-cut materials, including super alloys, composites, and ceramics. Laser technology has empowered its application in various industries, especially in welding, metal cutting industries depicts ships, railways, automotive industries, and also in medical sectors. In addition, very small features are designed and manufactured through materials using lasers. The electronic, healthcare, aerospace, automobile, and other manufacturing industries rely on these small features [5].

Superalloys, such as nickel, titanium, and cobalt-based materials, are frequently employed to meet the high strength of critically engineered applications. Superalloys possess high strength and low heat conductivity, combined with additional characteristics such as deformation hardening and hard-abrasive carbides, which lead to undesirable surface roughness and rapid tool wear during machining [6]. Tool wear in machining is a crucial element that influences product superiority, energy consumption, and cost. Several wear mechanisms might occur based on cutting conditions, work piece, tool material, and tool geometry. Tool wear in high strength alloy was predominately influenced by abrasive wear, adhesion wear, and oxidation wear. The surface roughness of machined components is significant for friction, wear, corrosion, and oxidation resistance. Achieving the required surface integrity in superalloys are challenging due to high heat and mechanical loads, metallurgical changes, and induced residual stresses. Optimizing the machining parameters, tool shape and design, investigating surface texture, and using lubrication techniques are all necessary to improve surface integrity, which is more discussed in below sections [7].

25.2 Road Map of Laser-Assisted Micromachining

The roadmap outlines the evolution of laser technology and its integration into the machining process (Figure 25.1). In 1960, Kumar Patel invented the first CO_2 laser at Bell Labs and Nd:YAG laser was developed in 1964 [8]. It is utilized extensively in several sectors due to its capability to weld and cut a wide range of materials. In the late 1990s, micromachining emerged due to the growing demand for increasingly complex and tiny components [9]. Laser-assisted micromachining was employed during the year 2000 to meet the demand for cutting challenging-to-process materials. Subsequently, picosecond and nanosecond lasers were utilized for machining the high strength metals [10]. Additive manufacturing technology enables the fabrication of micro- and nano-functional devices in multiple dimensions, scales, and materials, thereby accelerating their development and applications. Micro-additive manufacturing uses various techniques, such as materials jetting, laser micro-sintering, micro-stereolithography, and materials extrusion. It has excellent potential for developing microelectromechanical systems (MEMS), and finds applications in microelectronics, circuitry, packaging, microfluidics, and structural MEMS [11].

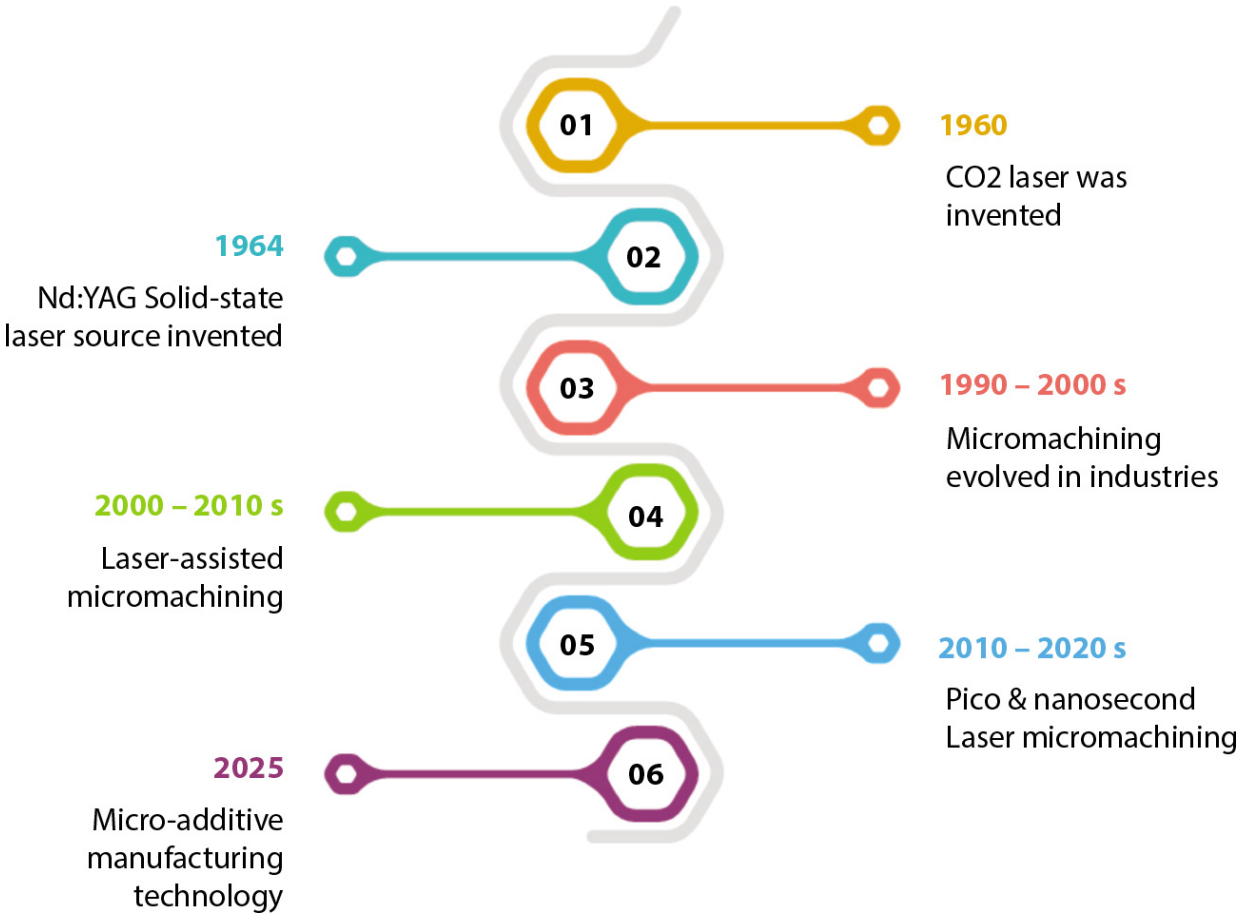


Figure 25.1 Road map of LAMM.

25.3 Micromachining

Micromanufacturing has piqued the interest of researchers in recent years because it has several benefits in the progress of miniaturization [12]. These benefits include increased portability, fewer materials and energy consumption, lighter weight, and greater sensitivity in the design. Specialized machine tools are necessary to manufacture micro-parts that have become critical components in many products.

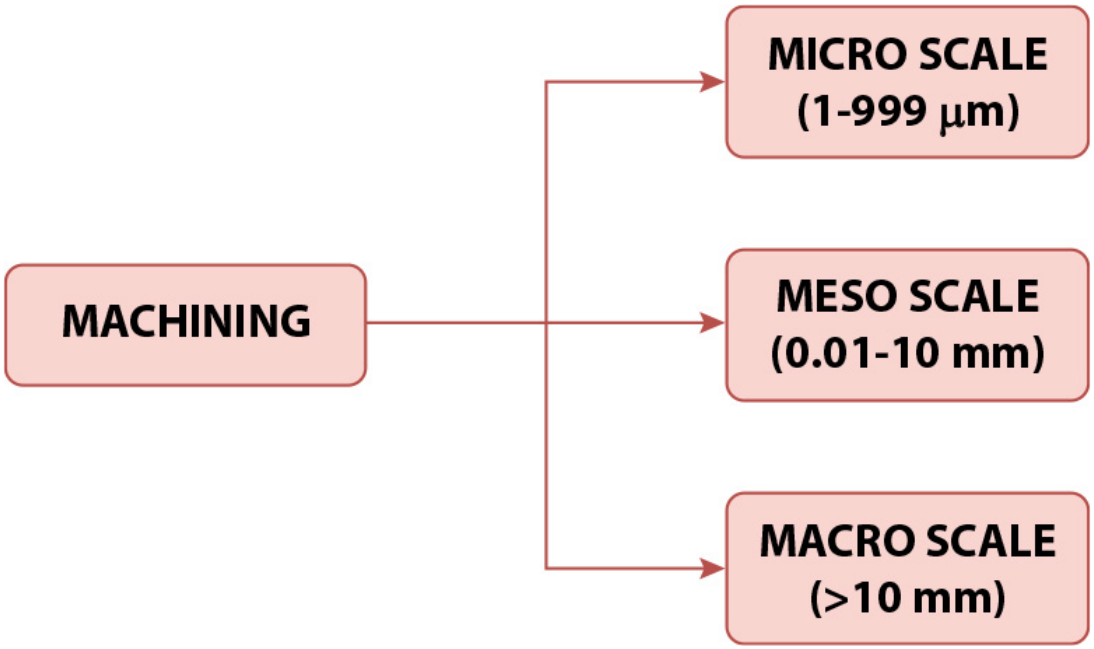


Figure 25.2 Classification based on geometry size.

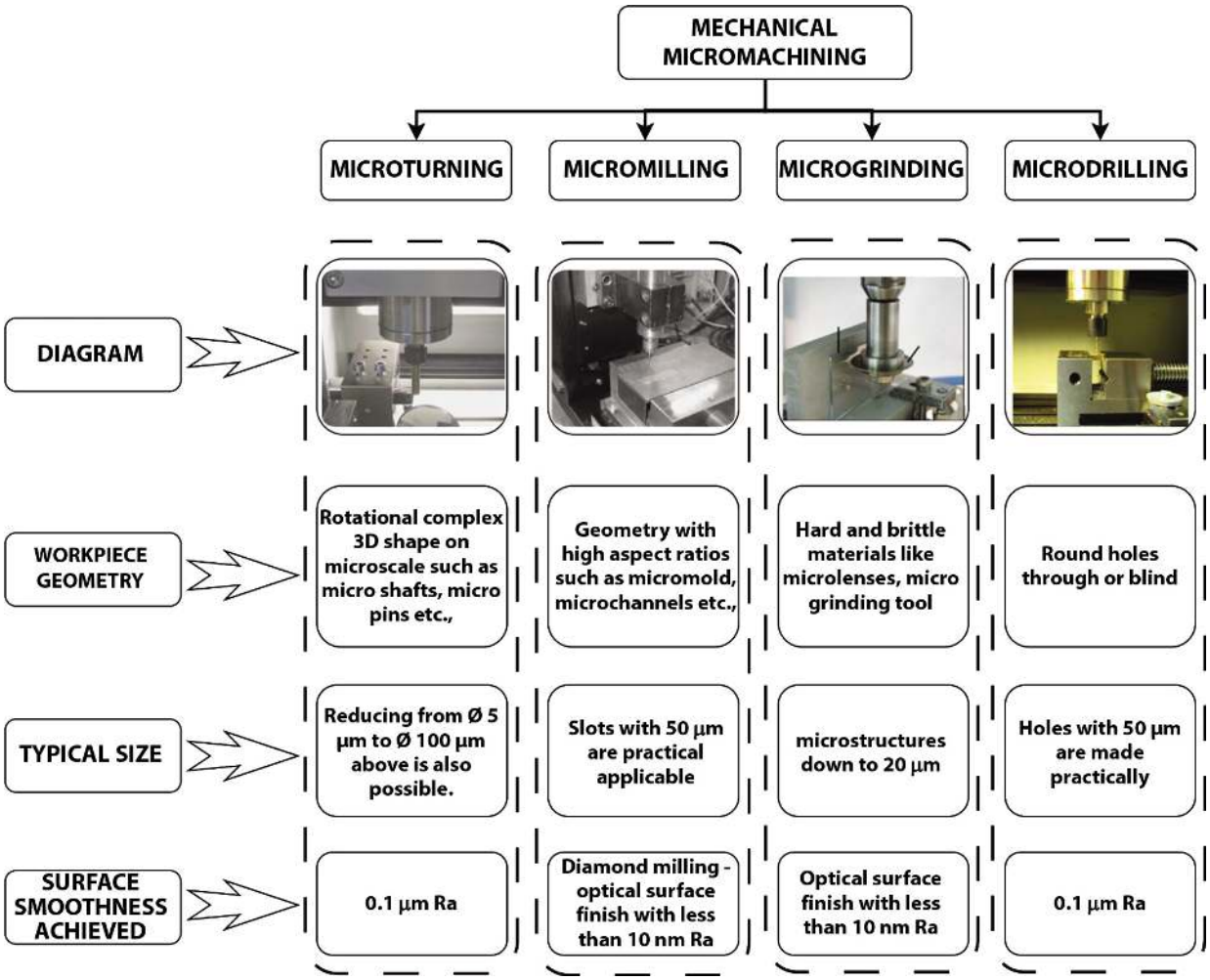


Figure 25.3 Types of mechanical micromachining.

The machining process is categorized based on scale dimensions: microscale ranges from 1 to 999 µm, mesoscale is from 0.01 to 10 mm, and macroscale is more than 10 mm (Figure 25.2). Micromanufacturing allows for the precise fabrication and development of structures at smaller scales [13]. Mechanical micromachining, geometrical shape, dimension and accuracy achieved are shown in Figure 25.3.

25.3.1 Micromilling

Micromilling is an ideal process for crafting intricate parts with complex shapes and geometries. This process involves using tiny cutters to create complex geometric shapes, facilitating the production of micro-molds, channels, and other intricate structures [14]. Micromilling of H13 hardened tool steel was studied using various cutting-edge geometries, such as chamfered and round micro end mills. Chamfered cutting edges are an excellent choice for achieving high-quality surface finishes and minimized burr formation [15]. While machining Inconel 718 using micromilling, it experiences different types of wear, including tool nose wear, diffusion, and oxidation wear. The main factors contributing to wear are the alternating contact stress, high rotating speed, and heat generation due to the material hardness [16].

25.3.2 Microgrinding

Microgrinding is a process that utilizes a small abrasive tool to shape three-dimensional (3D) microfeatures and remove excess material from high-strength alloys. To achieve excellent surface superiority, decreased cutting force, and improved tool life, it is crucial to optimize process parameters, tool modifications, and lubrication mediums [17]. Microgrinding tool wear mechanisms include abrasive wear, grain crushing, grain detachment, and electroplated bond wear. The wear rate increases with higher grinding speeds and feeds [18].

25.3.3 Microturning

Microturning is a method that focuses on producing miniature cylindrical parts, commonly used in industries such as aerospace, medical devices, and precision engineering [19]. Microturning of Ti6Al4V alloys confirms abrasion and crater wear mechanisms. The minimum surface roughness was achieved with maximum MRR [20]. The research investigates the microturning of Nimonic 90 alloy and tool wear mechanisms on the rake and flank face, which indicated wear mechanisms like abrasion, built-up edge adhesion, and edge chipping [21].

25.3.4 Microdrilling

Microdrilling is a precise technique to generate miniature holes of various shapes in a variety of materials [22]. Microdrills ranging from 50 to 300 µm in diameter are mostly used in printed circuit board (PCB) drilling production, and a hole diameter proportion of up to 15 has been attained [23]. Tool wear in microdrilling of nickel alloys is primarily caused by adhesion, diffusion, and chipping. While wet drilling shows slow tool wear and dulling of the cutting edge, dry drilling results in sudden tool failure [24].

25.4 Lasers in Micromachining

There are various lasers like CO_2, excimer, Nd: YAG, high-power diode, and fiber are utilized in recent years to process the micromachining. CO_2 laser (wavelength of 10.6 µm, and output laser power of 20 KW) is used for numerous micromachining applications, such as microlenses on optical fibers, engraving surfaces, and microfluidic devices in polymers [25]. Excimer lasers (output power of 300 W with a wavelength range from 0.12–0.35 µm) are beneficial for patterning, cutting, and shaping different materials like ceramics, glasses, and polymers [26]. Nd:YAG laser is a solid-state laser that emits power of 16 KW with wavelength 1.06 µm and has a strong optical absorption and high ablation efficiency, making them suited for diversified micromachining applications. They are widely used in ophthalmology, microfluidics, microengineering, and other industrial and medical applications [27]. High-power diode lasers are often used in industrial applications, including surface treatment, welding, and laser cutting. They have a power output of 16 KW and wavelength range of 0.65–0.94 µm [28]. Fiber lasers provide a higher laser output range from 10 to 30 KW with excellent process stability, great energy efficiency, and outstanding beam quality, making them appropriate for wide-ranging micromachining applications [29]. The process parameters and application of different laser technologies used in the machining process are displayed in Figure 25.4.

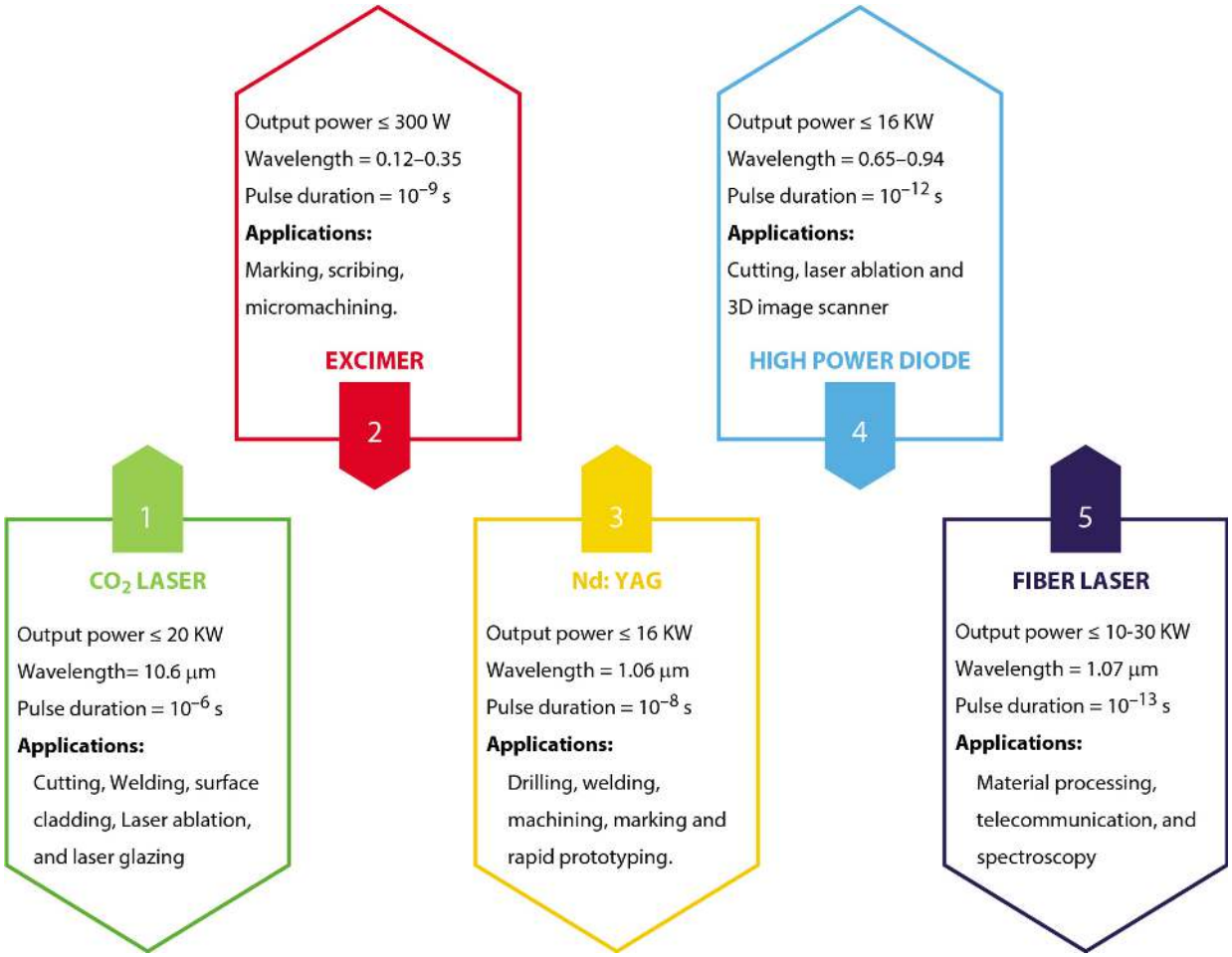


Figure 25.4 Lasers in machining.

25.5 Methodology of Laser-Assisted Micromachining

When the machining process begins, the machine parameters like spindle speed, feed rate and depth of cut are programmed using M code in the computer numerical control (CNC) machine and the laser is ON to configure laser power and wavelength. So that the heat source will be focused over the working surface and the cutting tool travelled along the laser-focus area to process the material. At the same moment, both the machine and laser sequence were controlled simultaneously. Finally, the machining process is completed. Figure 25.5 illustrates the step-by-step approach to perform LAMM.

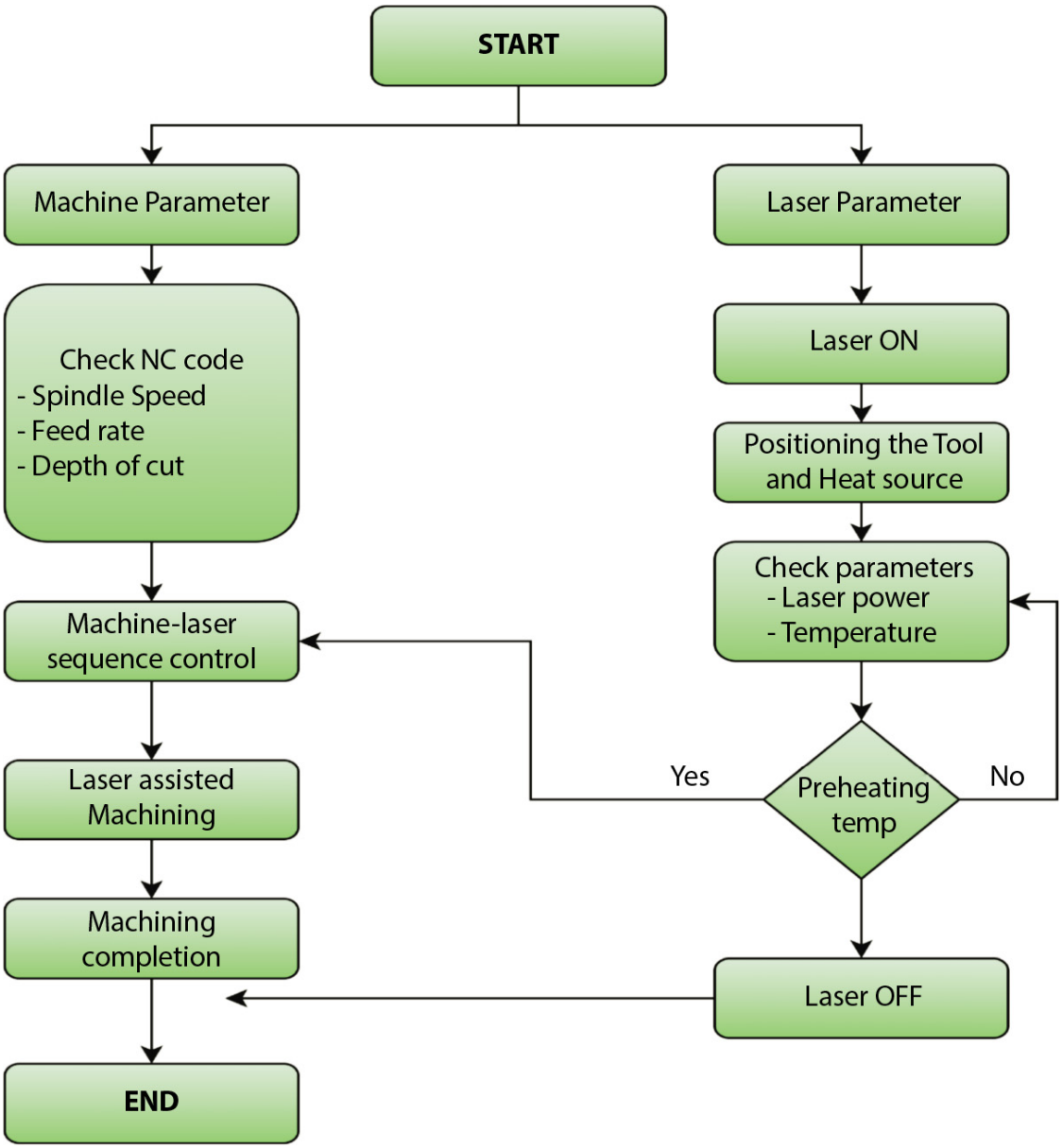


Figure 25.5 Process flow of laser-assisted micromachining.

25.6 Laser-Assisted Micromachining

Laser-assisted micromachining offers a better surface finish and reduced cutting forces as compared to the outcomes obtained using conventional micromachining. The strength and low thermal conductivity of high-strength materials require extremely high cutting forces and are challenging to machine [30]. Thermal-assisted machining involves heating hard-to-machine materials to make them easier to machine. The material resistance to deformation decreases with temperature due to thermal softening. The characteristics of the laser system could be adjusted to obtain desired outcomes; standard parameters include wavelength, repetition rate, laser power, pulse duration, and beam quality. The laser parameters are modified based on the application; these modifications may impact the process accuracy, effectiveness,

and safety [31]. Laser-assisted micromachining is a promising method to increase the material removal rate (MRR) and productivity of materials that are hard to cut. A concentrated laser beam point before the tool softens the material, reducing cutting force and low tool wear. Micromilling allows for the high accuracy and tolerance manufacturing of complicated micro-parts [32]. Table 25.1 provides a comprehensive overview of the process parameters and tribological properties for different laser-assisted micromachining processes.

Table 25.1 Overview of laser-assisted micromachining in tribological properties.

Author and year	Category	Workpiece/tool material	Laser parameter	Machine parameter	Tribological properties
Mukund Kumar and Shreyes N. Melkote [34]	Laser-assisted micromilling	A2 tool steel TiAlN-coated tungsten carbide square end mill	Power (P) wavelength (λ) spot size (d) P = 18 W λ = 1.06 µm	Cutting velocity (Vc) Depth of cut (ap) Feed (f) a_p = 16–32 µm f = 2.2, 6.6 µm/flute	The MRR is six times higher in the laser-assisted condition. Cutting force and tool wear are also substantially decreased.
Zhang *et al.* (2023) [35]		Inconel 718 Cemented carbide end mill	P = 10–30 W d = 0.6–1.4 mm	a_p = 0.08–0.16 mm f = 0.08–0.36 µm/z	The cutting force reduced 40.5%, which improves the tool life.
Hojati *et al.* (2022) [36]		Titanium alloy (Ti6Al4V) Three flute carbide PVD-TiAlN	Yb:YAG P = 50 W VL=200 mm/s frequency = 400 KHz	a_p = 1 mm Vc = 35 m/min	Improved MRR with decreased cutting force.
Kandivar *et al.* (2019) [37]		Austentic stainless steel X5CrNi18-10	Yb:YAG P = 7.5 and 10 W VL= 100 mm/s	a_p = 500 µm Vc = 50, 150 m/min f = 1-6 µm	The optimum laser beam source of 10 KW and the pattern space of 250 µm. The cutting force and temperature were lowered by up to 70% and 50%.

Author and year	Category	Workpiece/tool material	Laser parameter	Machine parameter	Tribological properties
Ashishkumar sahu and sunil jha (2023) [43]	Laser-assisted microgrinding	Titanium (Cp-Ti) Electroplated diamond micropencil tool	Fiber laser P = 50 W	a_p = 5–10 µm Vc = 1.57–2.09 m/s	The average decrease in cutting force was 31%, the MRR was enhanced by 52%, and specific grinding energy was reduced by 58%.
Wooyon Kwon *et al.*, (2020) [44]		Al2O3 Polycrystalline diamond (PCD)	CO_2 laser P = 30 W λ = 1.06 µm	a_p = 10–40 µm f = 100–1000 µm/s	The average grinding force was lowered by 46% and 44 % in the thrust and feed direction, and surface roughness was reduced by 17%.
Jongsu kim & Bongchul kang (2018) [45]	Laser-assisted microturning	Stainless mold steel Cubic boron nitride	CW fiber laser P = 10 W λ = 1070 nm d = 15-60 µm	Vc = 30–40 m/min a_p = 10–20 µm f = 0.03–0.08 mm/rev	Effectively utilized for the micromachining of hard molds, results with decrease in cutting force and better surface finish.
Zhai *et al.* (2020) [46]		SiCp/2024 Al AlTin-coated carbide insert	P = 50 W λ = 1064 nm d = 250 µm	Vc = 30–60 m/min a_p = 0.05–0.2 µm f = 0.01–0.10 mm/rev	The surface roughness reduced by 81.73% and effectively eliminates microcracks, pits, bumps, and other flaws in the SiCp/2024 Al composite.

25.6.1 Laser-Assisted Micromilling

Laser assisted micromilling (Figure 25.6) is an effective method for machining high strength materials such as Inconel, titanium, and ceramics, which are more

challenging to machine than traditional materials.

Kumar and Melkote [34] studied the processing capacity of laser-assisted micromilling of A2 tool steel compared to conventional micromilling. The study focuses on analyzing the impact of process parameters, such as cutting force, tool wear, burr development, and surface finish. When the laser spot dimensions exceed the diameter of the tool, it was verified that the height of the burr and the surface irregularity increase with laser assist owing to increased thermal degradation of the material. Laser-assisted micromachining can reduce the resultant cutting force by up to 69% on average. Laser-assisted micromilling significantly reduces the tool wear rate, resulting in a six-time increase in tool life compared to conventional methods. Zhang *et al.* [35] investigated Inconel 718 utilizing a laser-assisted micromilling technique involving both conventional and LAMM. The process parameters resulting in the best results, including spindle rotation, depth, feed and laser power, were determined. The cutting force is mainly influenced by the parameter Fz and is least impacted by the spot diameter. The surface roughness greatly influences on the depth of cut, whereas laser power has the least impact. Laser-assisted micromilling decreases surface roughness by 52.5% compared to conventional milling, reducing cutting force by 40.5% and extending the tool's lifespan. Hojati *et al.* [36] discuss modeling laser-assisted micromilling, a potential technique for producing intricate micro-parts with precise dimensions and geometries. The research proposes a model that analyses the structure of parts in terms of how it impacts the uncut chip thickness during the machining process. The model considers numerous input parameters relating to structural, tool, and process characteristics. The results reveal that structuring titanium (Ti6Al4V) parts minimizes the uncut chip thicknesses, with structure density being the most critical element. Kadivar *et al.* [37] investigated the austenitic stainless steel X5CrNi18-10 using laser-assisted micromilling and compared it with the conventional micromilling approach. Ultrashort laser irradiation is utilized to structure the workpiece surface before the micromilling process, and different laser structures are formed with varying laser intensity and line spans. The influence of laser structure on the cutting forces and temperature is decreased by up to 70% and 50%, respectively. Rahim *et al.* [38] used finite element analysis (FEA) to predict the optimal gap between the laser spot and cutting tool for Inconel 718. Their analysis helped identify the most effective distance for cutting is 240 µm. The purpose of the study was to investigates the melting process, generation of heat-affected zones and identify the specific processing parameters for laser-assisted micromilling. Mohid *et al.* [39] examined the Ti6Al4V microgroove ball milling process with laser assistance. The study concentrates on the effect of tool orientation and laser heating parameters on the cutting force and tool wear mechanism. Thicker and softer chips produced by lower feed rates are more likely to adhere to the tool flank and rake surface, leading to adhesion issues. Thick and lengthy deformed chips can cause vibration and enhance the production of built-up edges (BUE) in deep groove cutting. Titanium alloys have low heat conductivity, leading to high temperatures at the tool-workpiece interface. Laser heating improves dry-cutting performance by reducing cutting temperature and preserving tool life and quality.

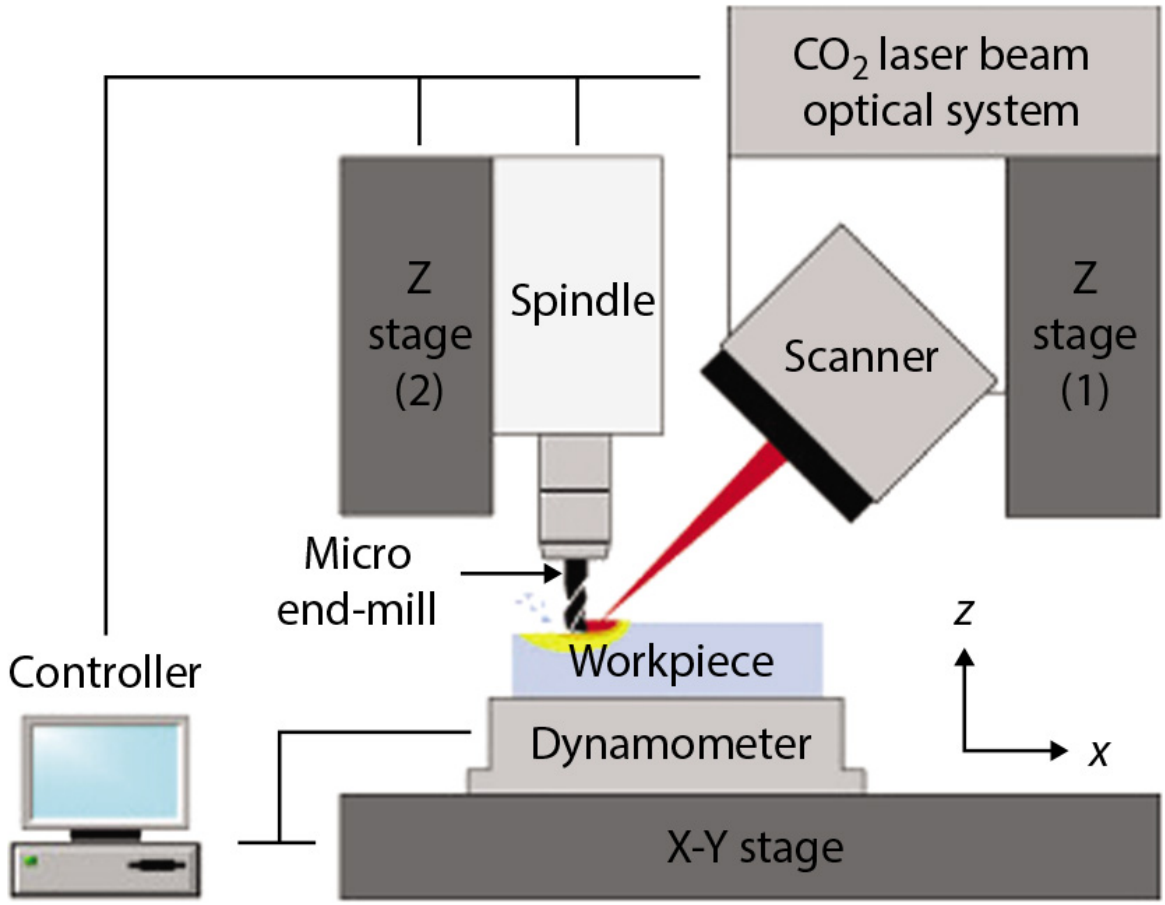


Figure 25.6 Laser-assisted micromilling [33].

25.6.1.1 Laser_Power and Its Effect on Tool Wear

In the case of Inconel 718, the degree of tool wear is significantly higher in conventional micromilling. However, this is minimized by setting the laser power (P) as 20 W. If the laser power exceeds 20 W, the tool coating is seriously damaged, and chips adhere to the tool surface, resulting in a built-up edge [35]. Carbide tools coated with titanium nitride (TiN) were employed to cut the β21s titanium alloy. The traditional cutting tool exhibits adhesion flank wear at the cutting edge, whereas laser-assisted machining tools have a small quantity of material to be bonded into the flank surface. At a power of 30 W, the laser provides an outstanding softening performance on the material, obtaining small tool wear throughout the cutting operation [40]. Figure 25.7 shows evidence that laser assistance reduces the surface roughness and cutting force during micro milling.

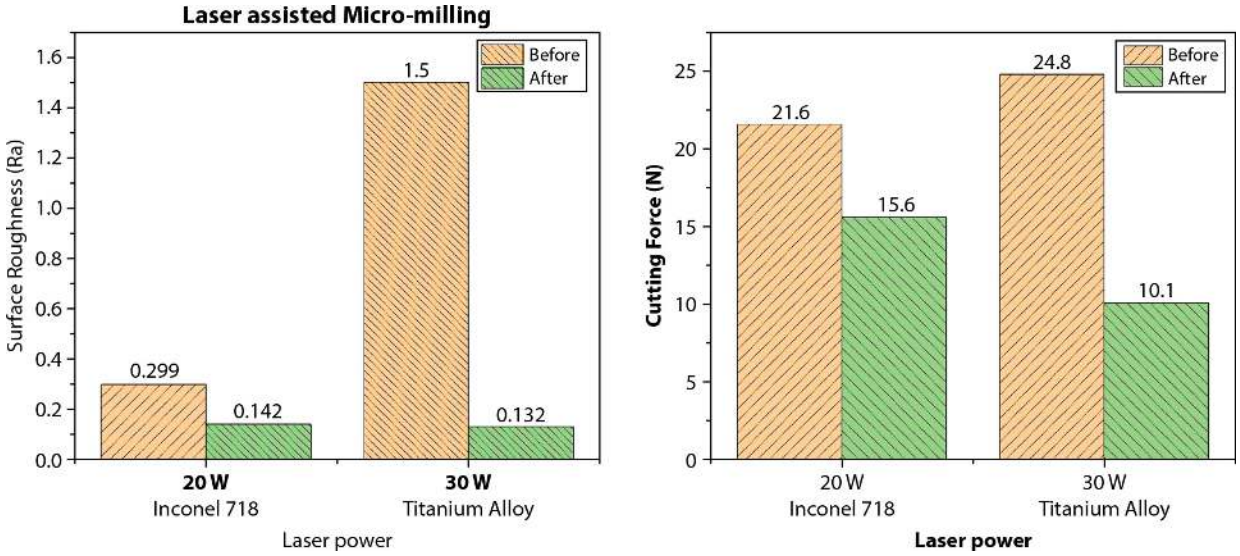


Figure 25.7 Surface roughness and cutting force in LAMM [35, 40].

25.6.1.2 Laser Assistance on Residual Stress

The residual stresses on the surface after machining impact crack propagation, surface integrity, and crack initiation. Increasing the laser power results in a 32% decrease in tensile stresses in the cutting direction and a 55% increase in compressive stresses in the thrust direction [37]. Conventional and 20 W laser power were used to determine the surface residual stress in titanium alloy. Experimental analysis reveals that the compressive residual stress range of traditional machining is –64.9 MPa to –106.1 MPa, and the compressive residual stress for LAMM range from –16.9 MPa to –73 MPa. At a laser power of 20 W, the increasing cutting speed results in an increase the surface residual stress.

25.6.1.3 Laser Assistance on Surface Irregularity

The surface of the Inconel 718 workpiece has a surface roughness of 299 nm when subjected to traditional machining. By setting the laser power to 20 W, the surface flaws decrease to 142 nm, resulting in a reduction of 52.5% compared to traditional milling. If the laser power exceeds 20 W, it results in a poor surface finish [35]. Laser treatment was applied to the β21s titanium alloy workpiece at 20, 30, and 40 W power levels, respectively. Based on the data, it can be inferred that LAMM performed best when operated at a power level of 30 W. The surface smoothness of the unprocessed material is around 1.5 µm, and the minimum roughness achieved was 0.132 µm, which represents a reduction of 61.7% [40].

25.6.2 Laser-Assisted Microgrinding

Laser-assisted microgrinding (Figure 25.8) is a recent advancement in the area of micromachining. It utilizes short and ultrashort laser pulses, which carry considerable amounts of heat energy, to produce microfeatures employing to various high-strength alloys. The method softens the workpiece material locally by laser heating. The grinding tool removes the softened material with less force and wear, reducing cutting force and enhancing tool life [41].

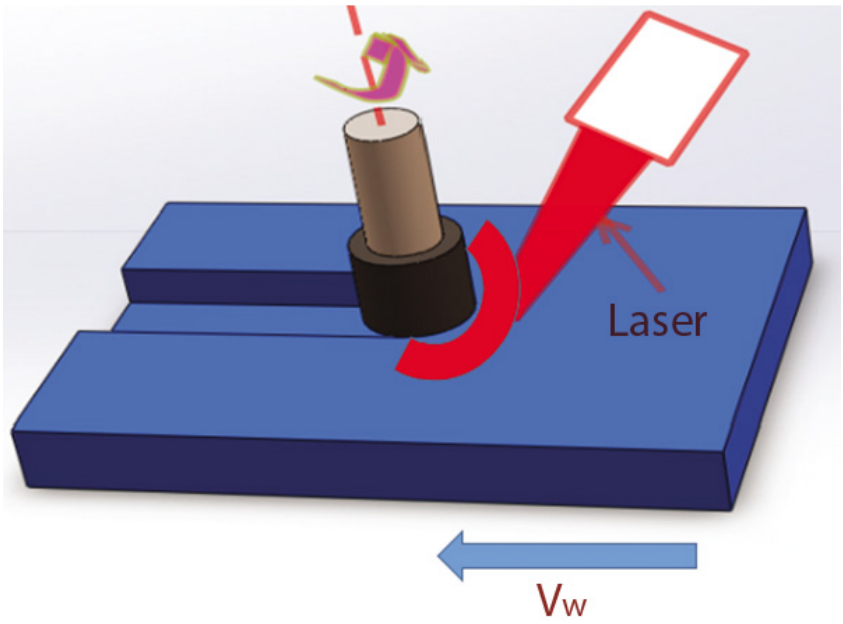


Figure 25.8 Laser-assisted microgrinding.

Kadivar *et al.* [42] investigated using laser-assisted microgrinding in machining Si_3N_4, a hard material. Microgrinding faces the challenge of producing high precision components due to tool deflection and rapid wear. An ultrashort pulse laser can structure the workpiece or tool, reducing grinding force but producing a rougher surface. Tool structuring in Si_3N_4 laser assisted micro grinding (LAMG) reduces cutting force better than workpiece structuring. A structured tool has less tool wear and a longer tool life. Ashish Kumar Sahu and Sunil Jha [43] investigated the feasibility of implementing hybrid microgrinding methods—namely, air-induced laser-assisted microgrinding and laser-assisted microgrinding to fabricate microstructures with superior quality and improve overall performance. In contrast to conventional microgrinding methods, the LAMG process substantially increases the MRR, reduces specific grinding energy (SPGE), and decreases cutting forces. Wooyong Kwon *et al.* [44] examined the characteristics of CO_2 laser-assisted microgrinding on Al_2O_3 ceramics. The research focused on investigating the impact of laser on machining variable, including laser power, cutting depth, and feed rate, on the grinding force and surface irregularity of Al_2O_3. The study found a 46% decrease in grinding force in the thrust direction and a 44% decrease in the feed direction. Increased feed rates were also found to be possible without tool fracture.

25.6.2.1 Effect of Laser on Tribological Properties

While machining Si_3N_4, the non-structured tool surface topography became flatter due to increased tool wear caused by increased cutting material volume. However, less tool wear and reduced grinding force are caused by the structured tool and surface roughness reduced by 40% roughly [42]. With laser-assisted microgrinding, the titanium (Cp-Ti) material bond is weakened by laser technology before the grinding process, which reduces the grinding force by 31%. As a result, there is a reduction in tool wear. The micrographs of titanium (Cp-Ti) show the effect of heat on the laser modified surface. The substantial temperature difference causes the material to release its residual tension as it cools, forming closer cracks on the

surface [43]. In the case of Al_2O_3 ceramics, laser power was adjusted between 9 and 11.5 W; an increase in laser beam power correlates with a reduction in tool wear and grinding force. If the laser power is less than 9 W, it appears inadequate for the workpiece pre-softening and the surface irregularity was reduced by 17% [44].

25.6.3 Laser-Assisted Microturning

Laser-assisted microturning (Figure 25.9) is a method of hybrid material removal using a focused laser during the mechanical cutting operation of hard materials, such as ceramics and superalloys. This process was used to microturn high strength steel for a micro-lens mold. Finite element modeling was employed to investigate the temperature distributions and thermal effects induced by focused laser irradiation during the laser-assisted microturning process. The study aimed to identify critical machining parameters which include cutting depth, feed, and spot size. The research findings revealed that laser-assisted microturning is an effective method for hard mold micromachining than the traditional approach. This technology shows promise for improving accuracy and efficiency in micromachining. The optimum laser-assisted microturning conditions reduce cutting force and improve surface quality [45].

Kibria *et al*. [47] experimented to investigate the microturning of alumina ceramic using Nd:YAG laser technology. The study examines the impact of laser machining process parameters, such as lamp current, pulse rate, and laser beam scanning speed, on the surface integrity and cutting depth. A greater cutting depth can be attained with higher lamp current and slower scanning speed. However, pulse rate has average effect on the cutting depth. Increasing lamp current and pulse rate can decrease surface irregularities. Zhai *et al*. [46] investigated the surface integrity during laser-assisted turning of SiCp/2024Al. The research analyzed the consequence of laser-assisted turning, which lowers surface roughness by up to 81.73% and produces higher residual compressive stress than conventional turning. The quality of a surface in laser-assisted turning depends on the cutting speed, depth and feed rate. Higher cutting speeds usually lead to rougher surfaces. In contrast to conventional turning, laser-assisted turning reduces the occurrence of micro-cracks, pits, bumps, and other imperfections, resulting in better surface quality.

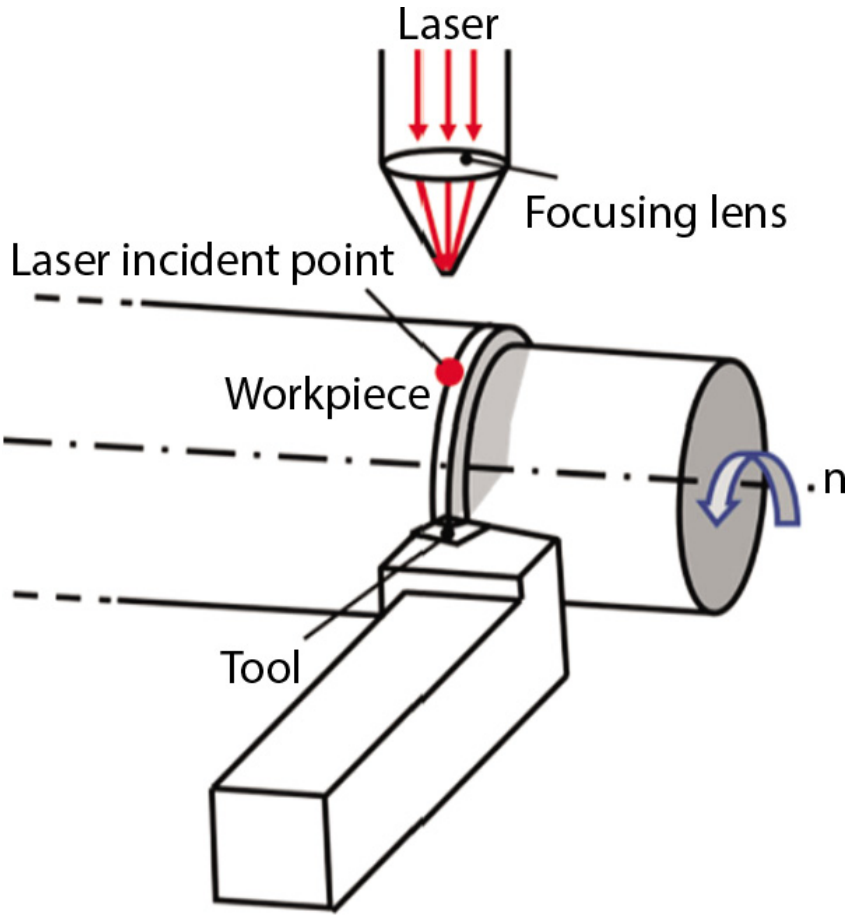


Figure 25.9 Laser-assisted microturning [46].

25.6.3.1 Laser Assistance on Tribological Properties

The optimum laser power of 8.5 W and spot size as 30 µm condition was used to execute laser assisted micro turning (LAMT), resulting in reduced cutting force of up to 46 %, leading to less tool wear and improved surface quality [45]. The surface irregularity of alumina ceramic material developed is between 9.5 µm and 10.5 µm. The findings indicate that optimizing the pulse frequency setting and decreasing the scanning speed might enhance surface quality [47]. In turning SiCp/Al composites, the tool strongly presses the material's surface and the plastic deformation on the material results in large compressive residual stress in laser-assisted turning. The laser beam of 50 W focused over the workpiece surface, which reduces the average surface roughness from 1.315 µm to 0.573 µm, a reduction of 56.4% compared to conventional turning [46].

25.7 Conclusion

Laser-assisted micromachining (LAMM) investigates the production of intricate micro shapes with dimensions in the range of a few microns, particularly high-strength alloys. This technology improves the productivity and efficiency of high-strength alloys, and it involves many factors, such as machining parameters, laser parameters, and work material properties. Therefore, it is crucial to understand and evaluate the impact of each process parameter for optimization. While machining the Inconel 718

material, the optimum laser power is 20 W and for titanium alloy, the laser power required is 30 W. When machining high-strength alloys using LAMM, the cutting force reduces by approximately 50–60%; this reduction leads to an extended tool life and also improves surface integrity. To achieve an optimized compressive residual stress on the outermost layer, it is necessary to fine-tune the laser scanning speed.

Summary

- Extensive research has been conducted on Nickel alloys, titanium alloys, and ceramics. The future of machining metal matrix composites lies in laser-assisted techniques.
- Compared to various laser sources, fiber laser has high output power with excellent stability control for machining high strength materials.
- Laser-assisted micromilling significantly lowers the cutting force and decreases surface roughness by reducing tearing defects generated by a BUE.
- Laser-assisted microgrinding allows for increased cutting depth and material removal rates by maintaining grinding forces and tool wear low.
- The laser-assisted microturning method substantially decreases the cutting force and tool wear. It is crucial to select suitable laser settings to avoid tempering effect during machining.

Scope for Future Work

- Fewer research work was done on laser-assisted microturning processes.
- Mechanical micromachining process needs to enhance the rigidity of the machine and tools to withstand increased cutting forces to avoid tool failure.
- The optimization of surface integrity involves mitigating residual stresses and distortion, which can be achieved by using multi-physics FEA.
- Adaptive control strategies need to be implemented, so that real-time changes may be made on input from sensors and monitoring systems.

References

1. Dornfeld, D., Min, S., Takeuchi, Y., Recent advances in mechanical micromachining. *CIRP Ann. - Manuf. Technol.*, 55, 2, 745–768, 2006.
2. Levy, G.N., The role and future of the Laser technology in the Additive Manufacturing environment. *Phys. Procedia*, 5, PART 1, 65–80, 2010.
3. Lee, C.M., Woo, W.S., Kim, D.H., Oh, W.J., Oh, N.S., Laser-assisted hybrid processes: A review. *Int. J. Precis. Eng. Manuf.*, 17, 2, 257–267, 2016.
4. Singh, R.K., Joseph, V.R., Melkote, S.N., A statistical approach to the optimization of a laser-assisted micromachining process. *Int. J. Adv. Manuf. Technol.*, 53, 1–4, 221–230, 2011.
5. Bharat, N. and Bose, P.S.C., An overview on machinability of hard to cut materials using laser assisted machining. *Mater. Today Proc.*, 43, 665–672, 2020.

6. Venkatesan, K., Ramanujam, R., Kuppan, P., Laser assisted machining of difficult to cut materials: Research opportunities and future directions - A comprehensive review. *Procedia Eng.*, 97, 1626–1636, 2014.

7. Sarıkaya, M., Gupta, M.K., Tomaz, I., Pimenov, D.Y., Kuntoğlu, M., Khanna, N., Yıldırım, CV., Krolczyk, G.M., A state-of-the-art review on tool wear and surface integrity characteristics in machining of superalloys. *CIRP J. Manuf. Sci. Technol.*, 35, 624–658, 2021.

8. Powell, J., CO2 Laser Cutting, in: *CO2 Laser Cut*, 1993.

9. Asad, A.B.M.A., Masaki, T., Rahman, M., Lim, H.S., Wong, Y.S., Tool-based micro-machining. *J. Mater. Process. Technol.*, 192–193, 204–211, 2007.

10. Marcinkevičius, A., Juodkazis, S., Watanabe, M., Miwa, M., Matsuo, S., Misawa, H., Nishii, J., Femtosecond laser-assisted three-dimensional microfabrication in silica. *Opt. Lett.*, 26, 5, 277, 2001.

11. Hassanin, H., Sheikholeslami, G., Sareh, P., Ishaq, R.B., Microadditive Manufacturing Technologies of 3D Microelectromechanical Systems. *Adv. Eng. Mater.*, 23, 12, 2100422, 2021.

12. Masuzawa, T., State of the art of micromachining. *CIRP Ann. - Manuf. Technol.*, 49, 2, 473–488, 2000.

13. Chavan, V. and Rajiv, B., Micromachining techniques for manufacturing high aspect ratio microelectrodes: A review. *Mater. Today Proc.*, Article In Press, 2023.

14. Leo Kumar, S.P., Jerald, J., Kumanan, S., Prabakaran, R., A review on current research aspects in tool-based micromachining processes. *Mater. Manuf. Process.*, 29, 11–12, 1291–1337, 2014.

15. Aramcharoen, A. and Mativenga, P.T., Size effect and tool geometry in micromilling of tool steel. *Precis. Eng.*, 33, 4, 402–407, 2009.

16. Lu, X., Jia, Z., Wang, H., Si, L., Liu, Y., Wu, W., Tool wear appearance and failure mechanism of coated carbide tools in micro-milling of Inconel 718 super alloy. *Ind. Lubr. Tribol.*, 68, 2, 267–277, 2016.

17. Pratap, A., Patra, K., Dyakonov, A.A., A comprehensive review of micro-grinding: emphasis on toolings, performance analysis, modeling techniques, and future research directions. *Int. J. Adv. Manuf. Technol.*, 104, 1–4, 63–102, 2019.

18. Wen, X. and Gong, Y., Modeling and prediction research on wear of electroplated diamond micro-grinding tool in soda lime glass grinding. *Int. J. Adv. Manuf. Technol.*, 91, 9–12, 3467– 3479, 2017.

19. Azizur Rahman, M., Rahman, M., Kumar, A.S., Lim, H.S., CNC microturning: An application to miniaturization. *Int. J. Mach. Tools Manuf.*, 45, 6, 631–639, 2005.

20. Aslantas, K., Danish, M., Hasçelik, A., Mia, M., Gupta, M., Ginta, T., Ijaz, H., investigations on surface roughness and toolwear characteristics in micro-turning of Ti-6Al-4V alloy. *Mater. (Basel).*, 13, 13, 1–20, 2020.

21. Airao, J., Kishore, H., Nirala, C.K., Tool Wear Behavior in l-Turning of Nimonic 90 Under Vegetable Oil-Based Cutting Fluid. *J. Micro Nano-Manuf.*, 9, 4, 041003,

2021.

22. Biermann, D., Kahleyss, F., Krebs, E., Upmeier, T., A study on micro-machining technology for the machining of NiTi: Five-axis micro-milling and micro deep-hole drilling. *J. Mater. Eng. Perform.*, 20, 4–5, 745–751, 2011.

23. Watanabe, H., Tsuzaka, H., Masuda, M., Microdrilling for printed circuit boards (PCBs)-Influence of radial run-out of microdrills on hole quality. *Precis. Eng.*, 32, 4, 329–335, 2008.

24. Imran, M., Mativenga, P.T., Gholinia, A., Withers, P.J., Comparison of tool wear mechanisms and surface integrity for dry and wet micro-drilling of nickel-base superalloys. *Int. J. Mach. Tools Manuf.*, 76, 49–60, 2014.

25. Choi, H.K., Ahsan, M.S., Yoo, D., Sohn, I.B., Noh, Y.C., Kim, J.H.T., Jung, D., Kim, J.H.T., Kang, H.M., Formation of cylindrical micro-lens array on fused silica glass surface using CO2 laser assisted reshaping technique. *Opt. Laser Technol.*, 75, 63–70, 2015.

26. Tseng, A.A., Chen, Y.T., Chao, C.L., Ma, K.J., Chen, T.P., Recent developments on microablation of glass materials using excimer lasers. *Opt. Lasers Eng.*, 45, 10, 975–992, 2007.

27. Dutta Majumdar, J. and Manna, I., Laser material processing. *Int. Mater. Rev.*, 56, 5–6, 341–388, 2011.

28. Bachmann, F., Industrial applications of high power diode lasers in materials processing. *Appl. Surf. Sci.*, 208–209, 1, 125–136, 2003.

29. Sen, A., Doloi, B., Bhattacharyya, B., *Fiber Laser Micro-machining of Engineering Materials*, pp. 227–252, Springer, Cham, 2017.

30. Kunar, S., Singh, A.K., Raviteja, D., Kibria, G., Chatterjee, P., Perveen, A., Talib, N., Overview of Hybrid Micromachining and Microfabrication Techniques. *Hybrid Micromach. Microfabr. Technol. Princ. Var. Appl.*, 1, 1–15, 2023.

31. Sun, S., Brandt, M., Dargusch, M.S., Thermally enhanced machining of hard-to-machine materialsA review. *Int. J. Mach. Tools Manuf.*, 50, 8, 663–680, 2010.

32. Hojati, F., Azarhoushang, B., Daneshi, A., Biermann, D., Laser pre-structure-assisted micro-milling of Ti6Al4V titanium alloy. *Int. J. Adv. Manuf. Technol.*, 120, 3–4, 1765–1776, 2022.

33. Kim, T., Kwon, K.K., Chu, C.N., Song, K.Y., Experimental investigation on CO2 laser-assisted micro-slot milling characteristics of borosilicate glass. *Precis. Eng.*, 63, 137–147, 2020.

34. Kumar, M. and Melkote, S.N., Process capability study of laser assisted micro milling of a hard-to-machine material. *J. Manuf. Process.*, 14, 1, 41–51, 2012.

35. Zhang, H., Chen, F., Li, Z., Hu, W., Sun, T., Zhang, J., Investigation of Laser-Assisted Micro-Milling Process of Inconel 718. *J. Manuf. Mater. Process.*, 7, 4, 149, 2023.

36. Hojati, F., Azarhoushang, B., Daneshi, A., Biermann, D., Modeling of laser-assisted micromilling. *CIRP J. Manuf. Sci. Technol.*, 40, 29–43, 2023.

37. Kadivar, M., Azrhoushang, B., Zahedi, A., Müller, C., Laser-assisted micro-milling of austenitic stainless steel X5CrNi18-10. *J. Manuf. Process.*, 48, 174–184, 2019.

38. Rahim, E.A., Warap, N.M., Mohid, Z., Ibrahim, M.R., Ismail, M.I.S., A prediction of laser spot-to-cutting tool distance in laser assisted micro milling Inconel 718. *Adv. Mater. Process. Technol.*, 1, 3–4, 529–541, 2015.

39. Mohid, Z., Warap, N.M., Ibrahim, R., Rhim, E.A., Laser assisted micro-groove ball milling of Ti6Al4V. *Appl. Mech. Mater.*, 660, 55–59, 2014.

40. Xu, J., Nie, X., Zhai, C., Ren, W., Lian, Z., Tian, J., Yu, H., The study on surface quality and tool wear on laser-assisted micromachining of β21s titanium alloy. *Int. J. Adv. Manuf. Technol.*, 110, 9–10, 2283–2293, 2020.

41. You, K., Yan, G., Luo, X., Gilchrist, M.D., Fang, F., Advances in laser assisted machining of hard and brittle materials. *J. Manuf. Process.*, 58, 677–692, 2020.

42. Kadivar, M., Shamray, S., Soltani, B., Daneshi, A., Azarhoushang, B., Laser-assisted microgrinding of Si3N4. *Precis. Eng.*, 60, 394–404, 2019.

43. Sahu, A.K. and Jha, S., Comparative investigation of laser assisted hybrid microgrinding methods. *Mater. Lett.*, 330, 133239, 2023.

44. Kwon, W., Kim, T., Song, K.Y., Experimental Investigation on CO2 Laser-Assisted Micro-Grinding Characteristics of Al2O3. *Int. J. Precis. Eng. Manuf.*, 22, 1, 51–62, 2021.

45. Kim, J. and Kang, B., Machining characteristics of micro lens mold in laser-assisted microturning. *J. Mech. Sci. Technol.*, 32, 4, 1769–1774, 2018.

46. Zhai, C., Xu, J., Li, Y., Hou, Y., Yuan, S., Liu, Q., Wang, X., The study on surface integrity on laser-assisted turning of SiCp/2024Al. *Int. J. Optomechatronics*, 14, 1, 29–43, 2020.

47. Kibria, G., Doloi, B., Bhattacharyya, B., Experimental analysis on Nd:YAG laser micro-turning of alumina ceramic. *Int. J. Adv. Manuf. Technol.*, 50, 5–8, 643–650, 2010.

Note

*Corresponding author: jeyapandiarajan.p@vit.ac.in

26
Abrasive Flow Finishing

Sandip Kunar[1]*, Jagadeesha T.[2], Gurudas Mandal[3] and Norfazillah Talib[4]

[1]*Department of Mechanical Engineering, Aditya University, Surampalem, India*

[2]*Department of Mechanical Engineering, National Institute of Technology, Kozhikode, India*

[3]*Department of Metallurgical Engineering, Kazi Nazrul University, Asansol, India*

[4]*Department of Manufacturing Engineering, Universiti Tun Hussein Onn Malaysia, Johor, Malaysia*

Abstract

The modern industry has come to recognize the importance of this non-traditional metal finishing method, known as abrasive flow finishing (AFF). Applications for the method can be found in many different industries, including the aerospace, defense, surgical, and tool production sectors. Surface finish characteristics are primarily controlled by machining parameters such as workpiece configuration, grit size, flow volume, number of cycles, and medium. The AFF method has been combined with other unconventional processes to produce hybrid processes, which has been popular recently. This has created new opportunities for completing hard-to-machine materials with intricate shapes that were previously unattainable. The fundamental technological foundation for micro-, nano-, precision-, and mesoscale engineering is emerging from these methods. To choose the ideal machining parameter settings for the smoothening of a variety of jobs in practice, this study offers a perception into the elementary and useful research

in this field and improves comprehension of this finishing process.

***Keywords*:** Abrasive flow finishing, input parameters

26.1 Introduction

Finishing operations have been historically the most laborious and unpredictable phases of production in the fabrication of précised components. A suitable finishing process is required to meet the industry's constant demand for cost-competitive and higher quality products with intricate designs and superior materials. Developed in the 1960s, abrasive flow finishing (AFF) procedure is a non-traditional finishing method. This technique is defined as an extrusion-based honing technique [1]. By applying a semi-solid putty that is loaded with abrasives, known as the media, to the surface that must be completed, a little amount of material is removed in this procedure. The AFF method is more adaptable than other finishing techniques and is appropriate for automation because of its media, which allows it to finish hard-to-reach regions, follow intricate shapes, and work on many edges and surfaces at once. For a variety of industrial components, the AFF process yields near geometric tolerances and a high degree of surface finish at a manageable pace of surface production. This procedure is used to successfully micromachine a variety of materials, comprising carbides, ceramics, and hard nickel alloys as well as soft aluminium [2]. Abrasive flow finishing (AFF) produces repeatable, predictable, and consistent outcomes across a wide range of finishing procedures. The wire electrical discharge machining (WEDM) method's microchannels and slits [5–7], the welding nozzles, extrusion dies, and aerofoil surfaces of impellers [3], spring collects [4], and diesel

injector nozzles [8, 9], have all been successfully smoothened using the AFF method.

Abrasive flow finishing (AFF) involves passing abrasive-filled compound and a semisolid, known as the AFF media across the surfaces of the job to be completed to remove a tiny amount of material. Abrasive particles are uniformly suspended in a flexible polymer carrier to produce the media. Poly-borosilixane, also referred to as silly putty, is a polymer that resembles rubber combined with lubricating gel to form the carrier. Different viscosity media can be produced by adjusting the polymer-to-gel ratio. Because the media evenly and softly abrades the surfaces, the machining action is comparable to lapping or grinding. Abrasive particles that protrude from the media operate as multiple point cutting tools, transforming it into a self-deforming abrasive stone. In a two-way flow, two vertically opposed cylinders normally extrude media forth and back across gaps made by the tooling and workpiece. Material is taken away from the required surface by means of restrictions in the route produced by the tooling and workpiece combination [10]. Improved regular surface finish and finishing efficiency were achieved by increasing the tangential forces on the machined area with the use of a direct current (DC) servo motor-driven rotating apparatus installed in the AFF [11]. Experimental outcomes reveal the efficiency and effectiveness of the AFF technique in machining of the internal surface of aluminum alloys tubes AA2024, as evidenced by the notable reduction of R_a and the attainment of a maximum value of material removal. Additionally, surface morphology research reveals that an uneven surface with full of surface flaws was produced during the boring operation. On the other hand, the surface quality of tubes AA2024 has improved due to the smooth and defect-free surface produced by the AFF technique [12]. Since titanium alloy artificial knee joints

have unique qualities and features like those of actual human knee joints. Owing to the intricate surface profile, a good surface finish that provides consistency and quality cannot be achieved using the conventional abrasive flow machining approach. Therefore, to address these problems, an appropriate limited flow channel is devised in this study to perform the abrasive flow finishing of titanium alloy for prosthetic knee joint surface [13].

It is demonstrated that a hydraulic power pack powers the hydraulic cylinders that are associated to the media cylinders. Numerous control devices, including volume flow controllers, pressure regulators, cycle counters, and limit switches, are part of this setup. The three components of this system—the machine, the tools, and the media—affect the system's output, and their parameters and those of the workpiece also have an impact. The primary direct and indirect features that impact adjustable parameters, workpiece properties, process performance and product quality, component geometry, media properties, and machine tool and tooling [14]. The significant parameters are deliberated in the following section for AFF method.

26.2 Significant Process Parameters

Controlling the process and increasing productivity and efficiency while minimizing costs requires proper understanding of the AFF process factors and how affect the machining performance. The most significant factors that influence the AFF process performance will now be covered in more detail.

26.2.1 Number of Cycles

The precise number of cycles is essential to attain the required end surface polish and must be determined during the AFF process. There are anywhere from one to several

hundred process cycles in all. Abrasion is more noticeable in some of the first cycles [15] have noted, although both the enhancement in surface finish and material removal rate (MRR) stabilize after that. The material removal improves nonlinearly as the number of cycles rises [16]. The MRR decreases due to increasing the number of cycles.

26.2.2 Extrusion Pressure

The performance features of AFF method are significantly impacted by extrusion pressure. A review of earlier studies shows that, when all other factors stay constant, the actual applied pressure ranges from 0.71 to 22.5 MPa and that machining occurs more quickly at higher extrusion pressures. The internal resistance of the media causes part of the pressure to be lost during flow, with the remaining pressure being transferred to the abrasive particles that come into contact with the job surface [17]. The MRR rises with increasing extrusion pressure and medium stiffness.

26.2.3 Media Flow Volume

In the AFF process, one of the key process parameters that governs the quantity of surface finish and abrasion at a given flowing components is the media flow volume. More medium volume will result in greater abrasion while maintaining all other input parameters constant. The media flow volume determines the slug length of flow, which in turn determines the amount of stock removal that occurs. The relationship between the media flow volume and the restricting passage’s cross-sectional area can be used to calculate the slug length of flow. Thus, if two passageways with dissimilar cross-sectional areas provide an equivalent volume of media flow, the bigger channel will have undergone less erosion than the smaller passage since it has enfolded out a reduced slug length of flow.

26.2.4 Media Flowrate

One of the crucial factors influencing the creation of an edge radius and the consistency of material removal is the media flowrate. The media flowrate is determined by the viscosity of the media, the width of the route, and the applied pressure. A wider edge radius is produced by high media flowrates, but slow media flowrates are optimal for uniform material removal. When it comes to brass, modest flow rates have comparatively little effect on material removal.

26.2.5 Media Viscosity

One of the most significant attributes is the media's viscosity since it influences both the degree of surface roughness and MRR. When all other factors remain unchanged, increased viscosity enhances surface finish and MRR. If the passage length is less than twice as long as it was initially, the greater viscosity media must be applied [18]. In contrast, if the passage length is more than twice as long as the passage size, a smaller viscosity must be chosen. Abrasive particle size and concentration have an impact on the media's viscosity as well. A temperature increases results in a noticeable drop in media viscosity. This might lead to particle settling, which affects the flow characteristics and abrasion method. Furthermore, it is shown that abrasive fragments are less probable to stay suspended in the media when the viscosity of the medium drops below 30 Pa. Particles have a propensity to gravitationally sink to the bottom of the media cylinder, which could lead to media failure.

26.2.6 Abrasive Particle Size and Concentration

Abrasive particle sizes for roughing applications should be between 8 mesh (grit) and 500 mesh (for minor hole

applications) using the AFF method. While larger ones can cut more quickly, smaller abrasive grain sizes produce a superior surface quality and can fit through intricate and small spaces. When the work surface's initial roughness is modest, finer abrasives should be utilized. Furthermore, the flexible medium is pressed up against the job surface, even rough grains can manufacture a very excellent surface quality. Both the MRR and surface finish decrease as the mesh size rises. The drop in both the width and depth of penetration is caused by an increase in mesh size, which also results in a fall in MRR. Nevertheless, this effect was only noticeable up to a specific abrasive concentration percentage, after which it becomes negligible.

26.2.7 Rheology of the Media

Rheology encompasses plasticity, viscosity, and elasticity. It is described as the exploration of changes in the flow and form of matter. Special rheological properties are present in the abrasive-laden material utilized in the AFF process. This medium is made up of a unique hydrocarbon gel and an organic polymer. To follow intricate route features, the abrasive-laden material needs to be capable to flow at ambient temperature. It must also possess sufficient stiffness to enable the application of the required force to the coarse particles during machining. For regular geometries of a media flow path, the shear rate and wall shear stress near a constraint were evaluated [19] employing the rough-laden media as a time-dependent rheotropic fluid.

26.2.8 Initial Surface Condition

In the AFF approach, the MRR is controlled by the job's surface finish. An element that is handled by WEDM is more sensitive to the AFF method if it has a recast layer on its surface [20]. It was found that this recast layer was

relatively weak because the surface of the parent metal had been impregnated with copper atoms from the wire. Consequently, a greater amount of material was removed from the surface treated by WEDM. The final surface roughness of ground components was nearly identical to that of the other parts; however, the AFF process did not fully finish the rough-turned and milled surfaces because the deep grooves on the surface were not eliminated by the abrasive flow. The workpiece hardness and initial surface finish of AFF method control the MRR. Comparing softer with harder materials, the former has a greater MRR and a more enhanced surface finish (R_a). The AFF cutting forces were examined in reference to the related effects of abrasive concentration, mesh size and extrusion pressure [21]. It was discovered that the decrease in surface finish (R_a) was linearly proportional to the force ratio.

The most crucial input parameter is the percentage of abrasive in the medium. The dimensions of the number of cycles, media flow rate, and abrasive mesh come next. Burrs and loose debris vanish from abrasive-flow-finished surfaces, although tool markings remain visible. As the number of cycles grows, the quantity of tool marks decreases, and abrasive marks become noticeable only at very high magnification.

26.3 Classification of AFF Method

One-way AFF, two-way AFF, and orbital AFF are the three types of AFF method. These types of AFF processes are described in the subsequent section.

26.3.1 One-Way AFF Method

As illustrated in Figure 26.1, the apparatus for the one-way AFF approach is equipped with a reciprocating piston that

is operated by hydraulic force and a medium chamber that can receive and extrude the medium in one direction across the interior surfaces of a job that has internal channels produced in it. As the medium extrudes out of the internal paths, a medium collector gathers it, and a fixture guides the medium’s flow into the job’s internal passageways from the extrusion medium chamber. An access port is included in the extrusion medium chamber to allow medium from the collector to be periodically added. The medium in the extrusion medium chamber is collected by the hydraulically operated piston periodically withdrawing from its extruding position and opening the access port. Resuming operations occurs when the working medium is charged into the extrusion medium chamber.

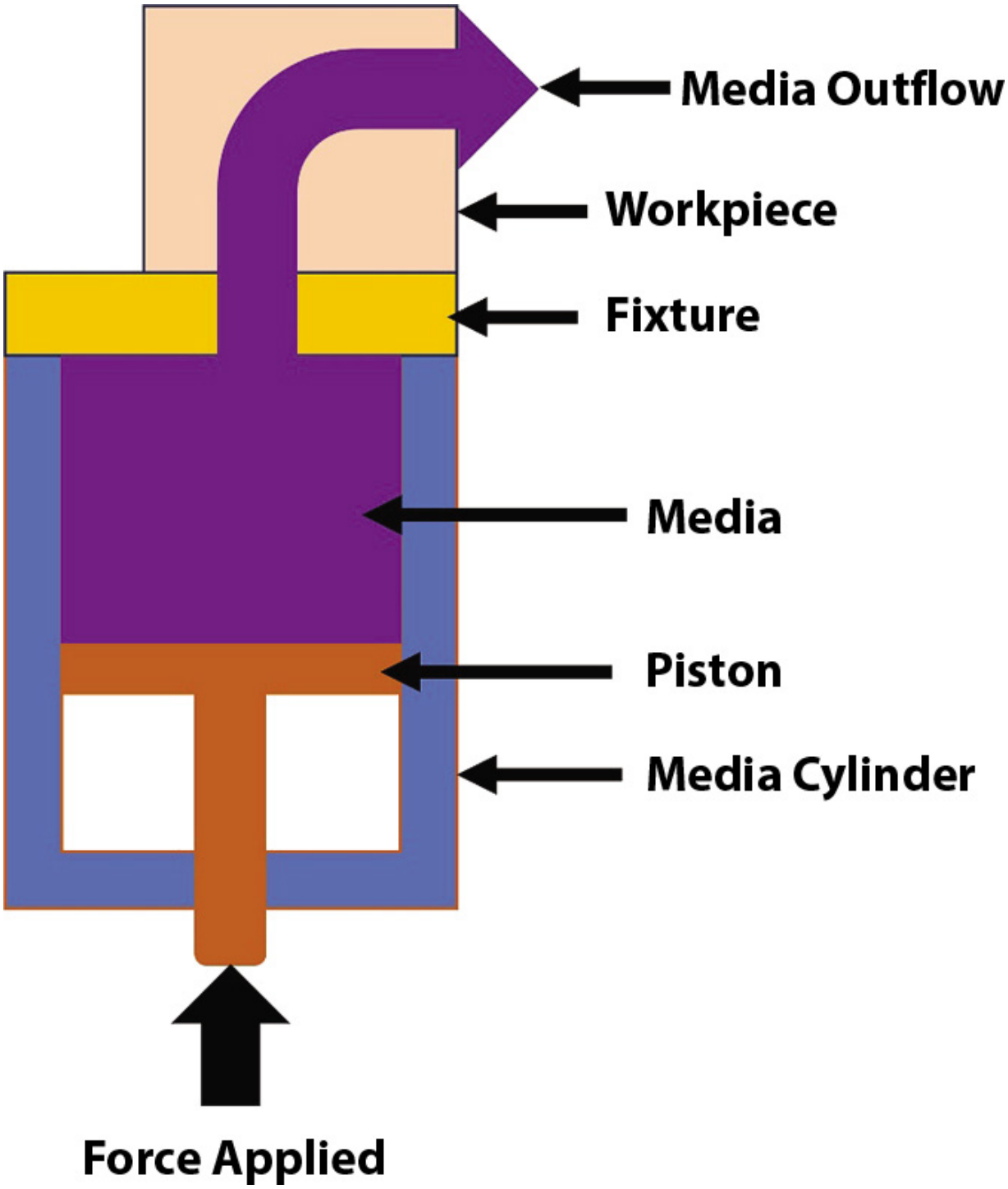


Figure 26.1 Unidirectional AFF process.

26.3.2 Two-Way AFF Method

Two medium cylinders and two hydraulic cylinders make up the two-way AFF machine. The workpiece surface to be

abraded is passed through or past the restricted passageway, which allows the medium to be extruded, either mechanically or hydraulically, from the filled chamber to the empty chamber, as shown in Figure 26.2. The medium is usually extruded for the required predetermined number of cycles, forth and back between the chambers. Restrictors and mandrels are useful tools for guiding the flow of the medium along surfaces that need to be finished, such as counter bores, recessed sections, and even blind cavities.

26.3.3 Orbital AFF Method

In orbital AFF, a slow-flowing “pad” medium surrounds the accurately oscillating workpiece in two or three dimensions. Surface and edge finishing in orbital AFF is accomplished by quick, and low-amplitude vibrations of the job in relation to an elastic plastic finishing tool that self-forms and becomes abrasive. The tool is an elastic plastic medium pad or layer that is loaded with abrasives; it is comparable to the material employed in two-way AAF, but it is usually more elastic and viscous. The workpiece will experience translational motion to the orbital AFF principle. When the job with intricate shapes turns, it moves compressively and slides peripherally through a layer of visco-elastic abrasive medium.

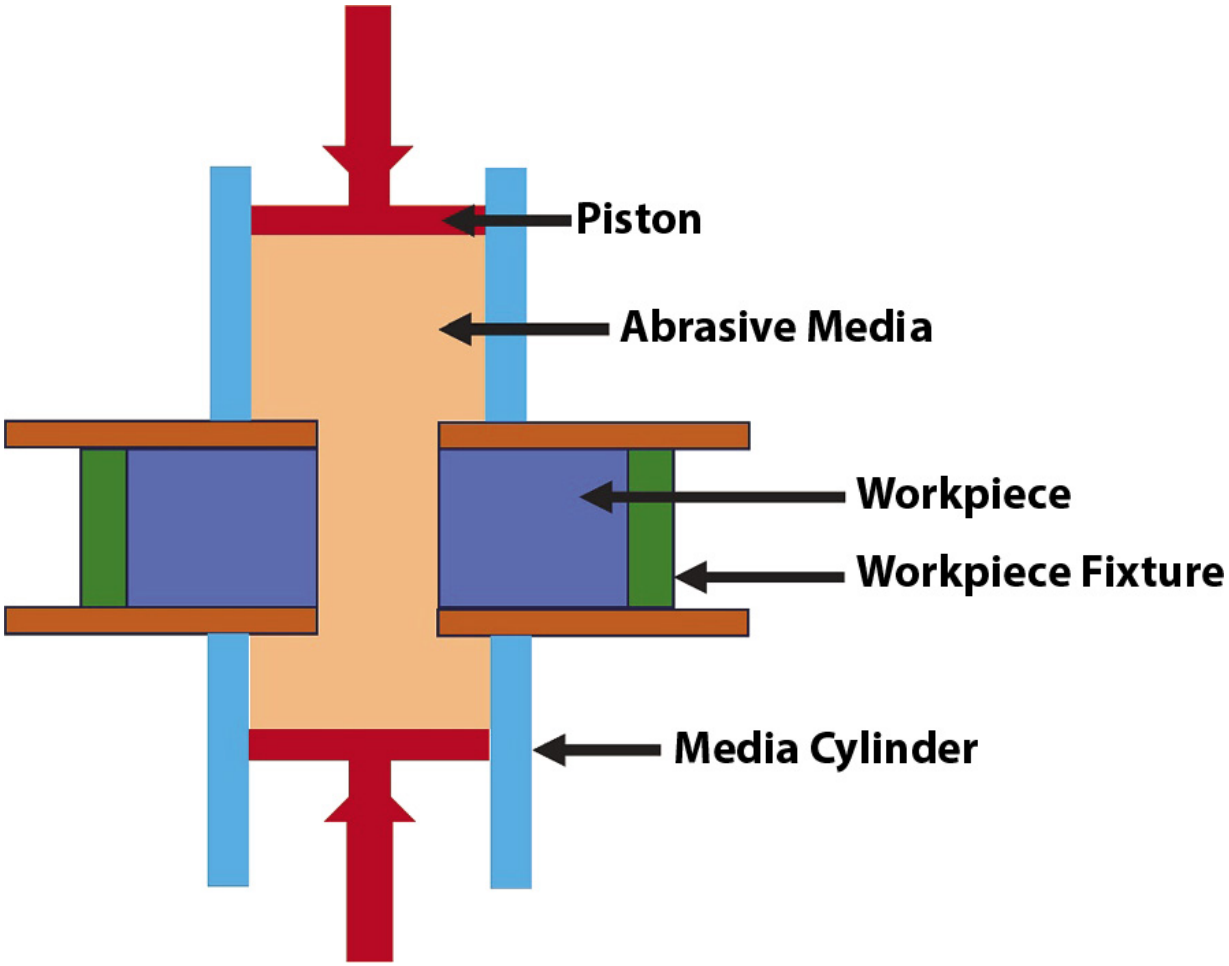


Figure 26.2 Two-way AFF process.

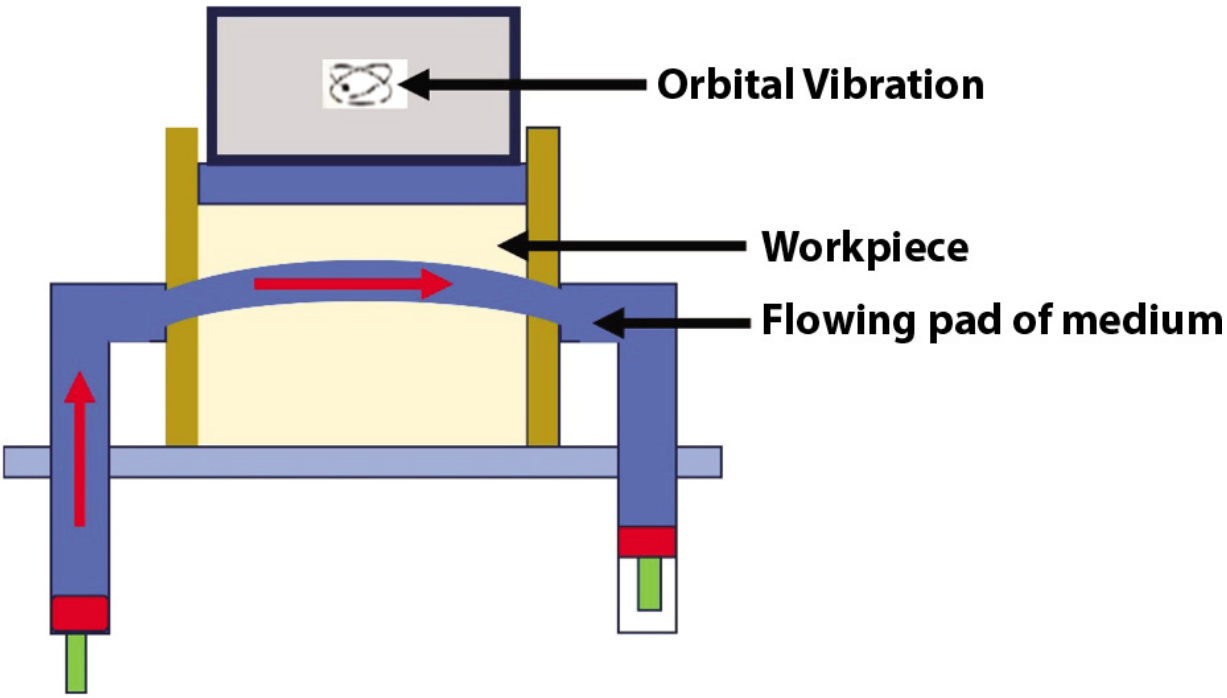


Figure 26.3 Orbital AFF method.

When the workpiece experiences circular eccentric planar oscillation with a tiny orbital oscillation applied to it, a part of its surface will always collide with the medium pad. As a result, the medium compresses between 5% and 20% and slides over the workpiece while following the direction of its orbital oscillation. The work piece slides over the medium in different places as the circular eccentric oscillation continues. Eventually, the entire circular vibration engages all surface area. The AFF media enables the practice of a straightforward setup for feeding and removing the abrasive medium pad in finishing applications, resulting in consistent outcomes. Overly filled areas of the medium pad tend to be pushed aside and shaped by the vibration of job. Overworked regions of the medium in the gap warm up because of deformation heating, becoming less elastic and more plastic as a result, and eventually being forced out of the work gap. Cast aluminum wheels and precise ground aerospace components are just two examples of many workpieces

from many sectors that can benefit from the application of orbital AFF. After just seven minutes of orbital AFF processing, coining dies utilized to create proof coins is finished from 0.51 µm before surface to an astounding 0.011 µm after finish. Using orbital AFF, prosthetic device complicated geometries can be finished to incredibly fine standards while crucial dimensional constraints are upheld. The orbital AFF technique is used to finish beverage container blow molds, which significantly lowers polishing expenses while simultaneously enhancing consistency, raising production rates, and lowering the demand for specialized manpower. The setup of orbital AFF is revealed in Figure 26.3.

26.4 Equipment

Typically, an abrasive flow machine consists of two medium chambers with hydraulic rams, a workpiece fixture, and a clamping mechanism to securely fasten all the parts together. The majority of machines have the ability to load several abrasive medium types and can also be configured to change the pressure at which the medium is extruded through the job. These can be run physically or automatically with a CNC. Accessories like unloading and reloading stations, part-cleaning stations, and media refeed devices, may be installed in machines built to handle high output volumes.

26.5 Process

Abrasive flow machining works by allowing the abrasive fluid to pass through the job, hence causing erosion. Raised features on the job’s surface are removed by abrasive particles in the fluid contact. A hydraulic ram forces the fluid through the workpiece, where it takes on the

properties of a flexible file or slug and perfectly conforms to its shape. According to Bernoulli's principle, the fluid's flow pressure and speed fall in locations where the flow is restricted, allowing for greater MRR. In these areas, the greatest amount of material removal takes place. Another reason for the extremely consistent finish is the pressure that the fluid applies to all interacting surfaces. Abrasive flow finishing can be carried out repeatedly as a two-way flow method or just once as a one-way flow procedure. A medium reservoir is present at each end of the workpiece in the two-way flow approach, and the medium alternately moves through the workpiece from reservoir to reservoir.

26.6 Application of Special Techniques

Researchers have utilized various methodologies to enhance the machining properties of the AFF method. Figure 26.4 depicts some of the methods [22–24] utilized to investigate the AFF process.

The contour of finished surfaces is unpredictable and unidirectional. The researchers developed models using a data-dependent system (DOS) and found that surface profiles produced by abrasive flow machined with two different wavelengths: a tiny wavelength linked to the cutting edges and a big wavelength corresponding to the abrasive's primary path. An acoustic emission (AE) system is used to monitor the AFF process online. This technique studies the elastic stress waves that are produced as a material's internal structure rearranges, causing a rapid release of strain energy. It was found that employing the AE method to the observing of AFF method was essential to forecasting the flow resistance characteristics because flow resistance depends on the size of the passage and the surface condition of job. Size of the abrasive mesh is an

important factor. More MRR and a stronger AE signal are obtained with bigger mesh sizes; however, it is indistinct why the mesh size substantially impacted the AE signal but not the MRR. Abrasive grain contact with the workpiece resulted in a profile of the final surface and MRR that was analyzed and simulated [25–27]. The AFF parameters affected the produced surface profile and MRR. The percentage concentration of abrasives and reduction ratio raises the number of active abrasive grains per unit volume of media flow, which in turn raises the surface quality and MRR.

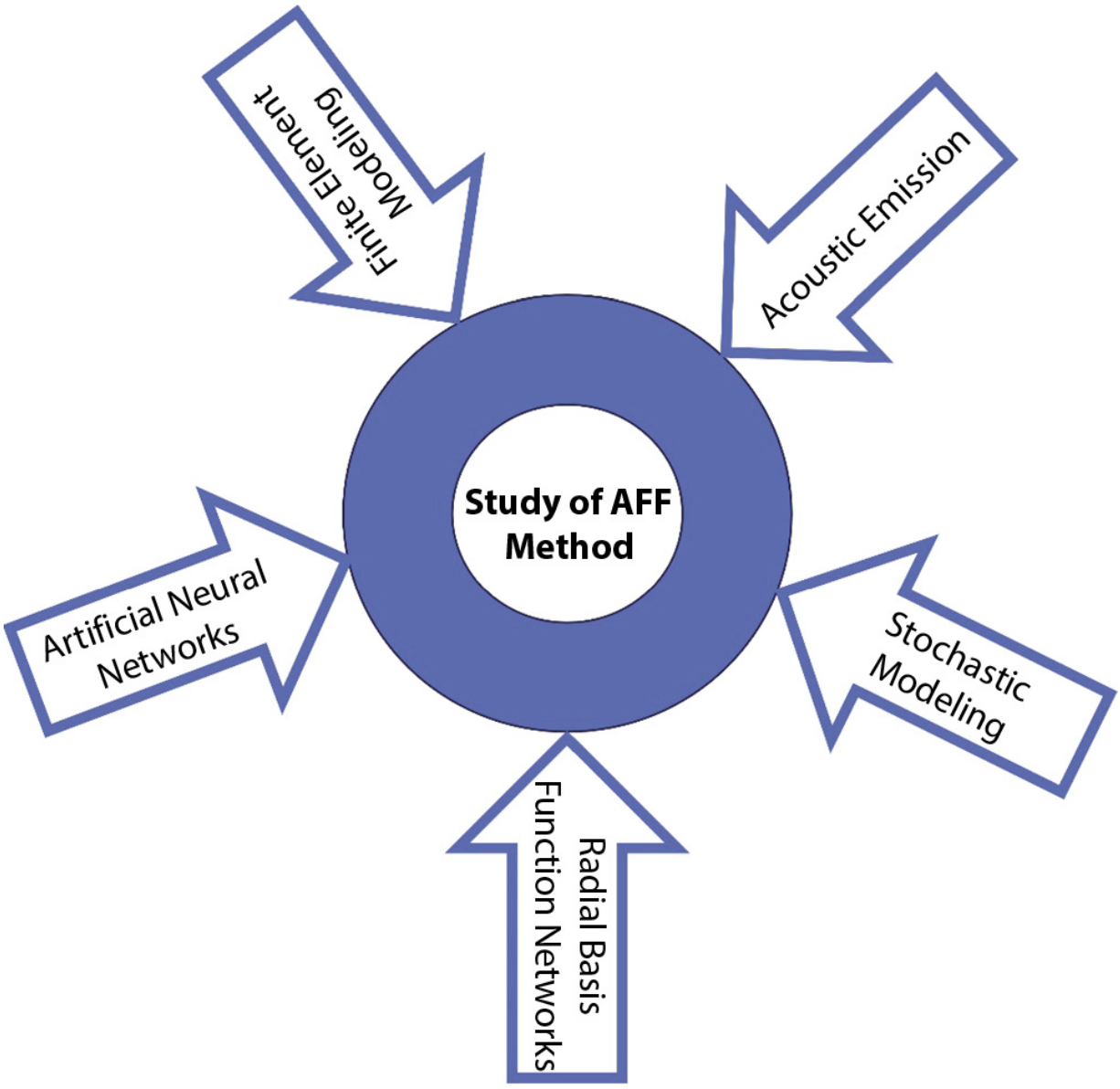


Figure 26.4 Techniques applied for study of AFF method.

The hardness and grain size of the job have an impact on how deeply a grain indentations itself into the material. A theory that explains the forces that particles in a suspension in motion exert on the surface that surrounds the flow [28]. The AFF process's specific energy range (10–110 J/mm^3) coincides with the grinding process's range (5–60 J/mm^3), and it offers a mechanism for figuring out the definite energy and tangential forces in the AFF method [29]. This supports the researchers' conclusion that AFF

machining is like grinding. Additionally, the specific energy increases with increasing workpiece material hardness, it stays nearly constant when the abrasive mesh size changes. In the AFF method, ploughing was also observed the rubbing method of material deformation [30].

A finite element method was used to develop a model for the flow of the elasto-visco-plastic material in AFF to calculate the stresses induced during the flow. To estimate the surface quality and MRR, these were then applied to an AFF set of machining parameters. Their results show that extrusion pressure and normal stresses increase linearly with piston velocity, with a stronger relationship observed for larger tooling angles. The strains normal to the workpiece surface likewise climb as the reduction ratio does, which is calculated by dividing the difference between the cross-sectional areas of the media cylinder and the extrusion channel by the media cylinder cross-sectional area.

When the extrusion pressure and the percentage of abrasive concentration in the medium increase, so does the MRR. The best AFF process parameter selection was achieved with the use of a neural network technique [31]. Back-propagation analysis was used to examine the impact of input parameter choices during offline model training. As noted by the authors, online process monitoring could be a useful application of this technology. An offline controller and neural-net-based process monitor may be utilized for the AFF of an automotive engine intake manifold [32, 33]. Additionally, for a given set of manifold attributes and a set of machine parameters, this method will estimate when the AFF method will attain the necessary air flow standards for the engine intake channels. Genetic algorithms are used to explain the process parameter optimization of complex mechanical machining processes [34]. The radial basis function

networks (RBFN) are specifically created for the AFF method, and the best networks were created by combining a genetic algorithm (GA) with a back-propagation (BP) method [35]. The RBFN trained by GA outperformed the RBFN taught by BP. This may be because there is a greater chance that the solutions of an algorithm trained with BP will become stuck in local minima. However, the type of deviation function may have an impact on how well these two algorithms perform.

26.7 Hybrid AFF Processes

Abrasive flow finishing has a low MRR, like most non-conventional machining methods. Efforts have been required to address this issue by combining AFF with other approaches to create hybrid systems. Utilizing combined or mutually improved advantages to prevent or otherwise lessen some of the negative finishing impacts is another motivation for building hybrid AFF methods. The numerous finishing techniques created using the AFF method are displayed in Figure 26.5.

With the least amount of dimensional inaccuracy or profile deterioration, the ultrasonic flow polishing (UFP) method can produce a finish of excellent quality [36]. In this procedure, the combination of flow and vibration abrades the surface of job. The UFP method is multivariable and stochastic. The centrifugal-force-assisted abrasive flow machining (CFAAFF) approach overcomes the restriction of a low MRR by advancing a spinning centrifugal force generating (CFG) rod in the workpiece path with abrasive-laden medium [37, 38]. A triangular-shaped CFG rod is better to others and can reduce machining time by as much as 80%. This procedure could raise the MRR by 37.53–42.51 mg. The stated rise in the scatter of surface roughness (R_a) value was from 0.0581 mm to 0.0619 mm.

A procedure that blends AFF and magnetic abrasive finishing (MAF), also known as magneto abrasive flow machining (MAFF) [39]. It was asserted that this method could improve the MRR because it applies a magnetic field effectively and uses magnetic abrasive particles (MAPs) instead of modest abrasive particles in the AFF method. The inner wall of the workpiece attracts the MAPs because of the magnetic field. Because of this, fewer cycles are needed to take away the same quantity of material along the wall than throughout the medium, and the effective abrasive concentration is higher there. The MRR and surface roughness value are significantly impacted by the magnetic field. It was found that the MRR rose along with the magnetic field, while the surface roughness remained same. Higher magnetic flux density and low flowrates combined to generate the greater MRR and surface finish. Medium flowrates did not appreciably impact the MRR or surface finish.

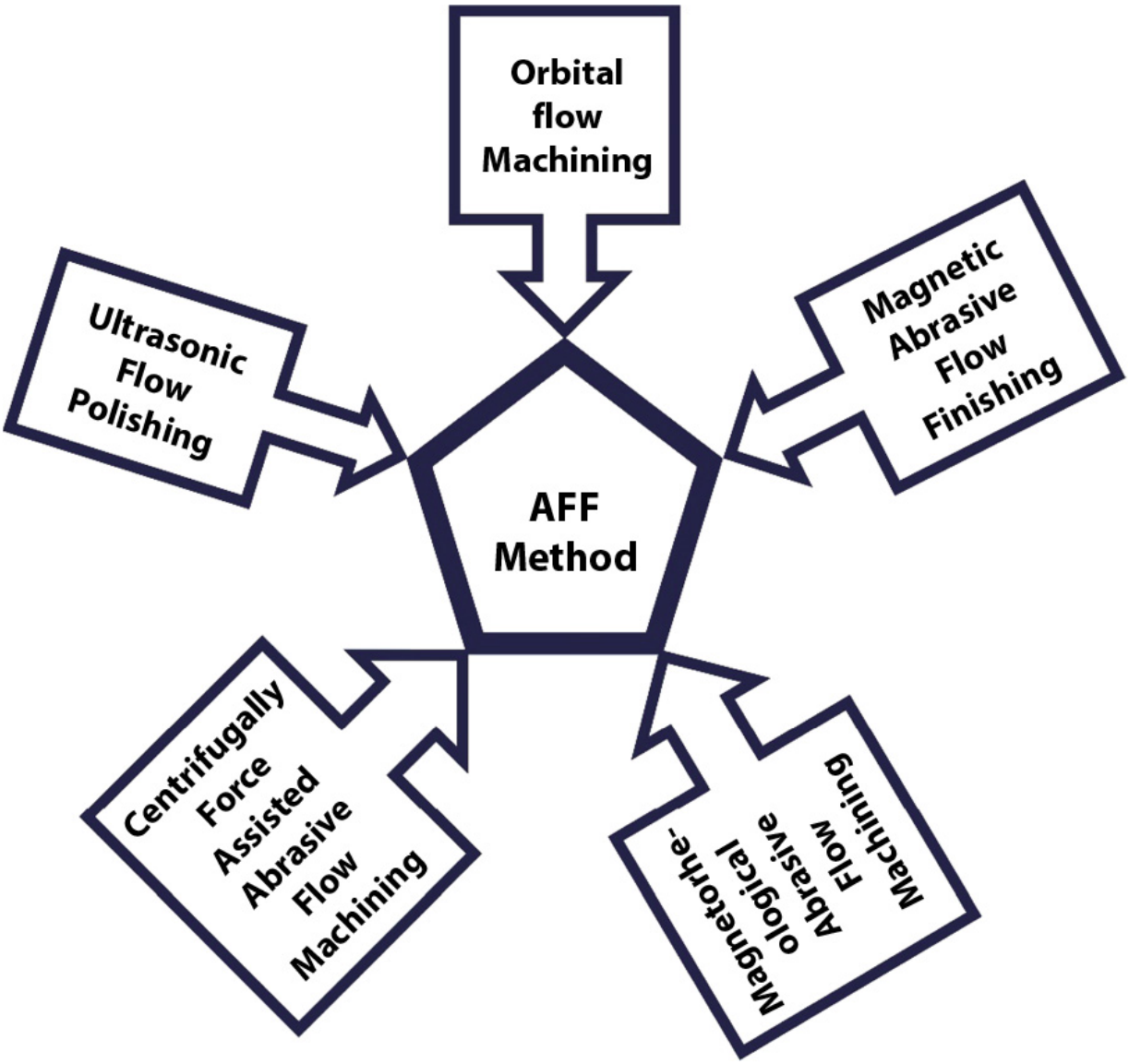


Figure 26.5 Hybrid finishing methods involving the AFF method.

By applying the simulated data and finite element approach, MAFF [40] predicts surface roughness. There is a noticeable increase in the machining pressure between the magnetic brush and the workpiece as the magnetic flux density rises. Furthermore, it was shown that although both were greatly affected by the magnetic field, the MRR was amplified by the magnetic field more quickly than the surface roughness level. The method known as magneto rheological abrasive flow finishing (MRAFF) was developed

and built [41, 42]. Their investigation indicates that this procedure provides improved control over the rheological properties of the MR finishing medium that is filled with abrasives. The presence of an external magnetic field altered the rheological behavior of the MR polishing fluid. It was composed of carbonyl iron particles (CIPs) and silicon carbide abrasives dispersed in a visco-plastic mineral oil and grease foundation. Items with complex geometries can be nano finished using this technique for engineering applications [43]. Surface finish values up to 30 nm could be attained for workpieces made of silicon nitride and stainless steel, and that the roughness steadily decreases with increased magnetic field for the same number of cycles. At specific applied pressure, the largest improvement in surface smoothness was stated [44]. The real finishing only happens after 200 cycles, at which time all the material that was lost after grinding is removed. Following that, the abrasive particle size, applied pressure limit and number of cycles, which cause the surface roughness value to progressively decrease. The amount of finishing action is determined by the tangential and radial forces acting on the abrasive particles since the CIPs are stacked in a columnar pattern in the presence of an external magnetic field. For a given magnetic flux density, it was found that the size, microstructural arrangement, and number of CIPs nearby primarily affected the finishing forces on the abrasive particles. The size of the CIPs in respect to the coarse grain size is one significant factor influencing the final surface roughness obtained in the MRAFF method. As the surface roughness value drops, the number of finishing cycles rises [45, 46]. The number of cycles required to attain the same surface polish can be significantly decreased by combining an electrochemical method with the AFF approach [47].

26.8 Monitoring of AFF Process

The acoustic emission technique is used to monitor surface roughness and material removal in real-time during the AFF process. The term “acoustic emission” refers to elastic stress waves that are created when a material’s internal structure rearranges, causing a rapid release of strain energy. The impact of AFF parameters on the output characteristics is examined in a full factorial experiment. Only grit size had a negligible impact on material removal based on the criteria. To understand the mechanism underlying AFF, the acoustic emission signals are used during grinding. The initial surface finish parameters of the job have a significant impact on the acoustic emission signal. AFF variables affect material removal, which affects the signal. The data dependent systems (DDS) is used to analyze the acoustic emission signal that was produced during AFF processing. The primary root of the signal, which had more power, and a frequency of roughly 160 kHz, whereas the secondary root had a frequency of roughly 80–90 kHz by DDS analysis. The higher frequency component is linked to the ploughing mechanism, which would be consistent with the grinding results. Furthermore, it was discovered that, when identical finishing circumstances were applied, aluminum workpieces removed more material than steel workpieces, giving stronger signals than the latter.

26.9 Advantages and Limitations of AFF

(i) Advantages of AFF

- Quicker processing of cycles.
- Simple cleanup.

- Media temperature management is not necessary.
- Able to handle bigger components.
- Easier part switching and tooling.
- Replicates the natural movement of liquids or air with accuracy.
- Does not fully capture the media’s work portion.

(ii) Limitations of AFF

- In contrast to other machining processes, the finishing rate is low.
- The ductile materials tend to become embedded with the abrasive particles.
- It can only be used in enclosed spaces.
- Tool wear is comparatively elevated.

26.10 Applications of AFF

26.10.1 Automotives

The ability of this procedure to smooth surfaces for enhanced air flow and performance is driving up demand among automakers and producers of two-wheelers. Automotive engines running at high speeds can be made to operate better using the AFF method. Turbine engine components as well as automotive and medical parts can be completed using the AFF method. A turbine engine diffuser’s internal passageways are enhanced to improve air flow to the engine’s combustion chamber.

26.10.2 Dies and Molds

Because the abrading medium in the AFF process adapts to the geometry of the channel, finishing difficult shapes is

made simple. The consistent elimination of stock by AFF allows for précised sizing of undersized precision die passageways.

26.11 Summary

Most research conducted on the AFF method, direct that when the applied pressure and the percentage of abrasives in the medium. Surface polish can achieve up to 60–70% increase regardless of the size of the grains or the viscosity of the media using a single AFF cycle. Removing stock results in 85% to 90% increase in the initial finish. This explanation states that even dull grains continue to cut the material and increase the surface finish because a higher viscosity restricts the ability of the grains to migrate and align. This is the relationship between the mean final surface finish and viscosity. Again, the smaller viscosity allows for a rapid and continuous change in either direction, it results in a higher pseudo-frequency and lower surface finish. If the passage length is noticeably less than twice the passage width, use a higher viscosity media or a lower extrusion pressure. Alternatively, if the passage length is significantly greater than twice the passage width, a smaller viscosity medium or a higher pressure is suggested. A given medium’s pass-through size range expands as processing temperature rises because the media’s viscosity decreases. Thus, in addition to the material of the workpiece, viscosity needs to be adjusted for its shape. It is noted that smoother surface finish is achieved with bigger mesh sizes.

26.12 Conclusion

This article provides a detailed review of the idea of extruding abrasive particles suspended in a self-deformable

media over a surface that needs to be accomplished. It emphasizes that this process could be a viable solution to the issue of manufacturing intricate components using automated procedures from materials that are challenging to machine. The AFF process's reaction characteristics are determined by several factors, including the setting of several process parameters, the development of hybrid strategies through integration with additional unconventional methods, machinability factors, material characteristics, and difficulty of the work. Process optimization results from the appropriate choice of factors, including the viscosity of the polymer carrier and the size, kind, and concentration of the suspended abrasive particles. An extensive, in-depth industrial research on the AFF method should be conducted to determine the best polishing conditions and to attain the necessary level of finish quality. While there has been some study on AFF and its hybrid forms, much more applied research is needed to improve the AFF process's competitiveness. There have been attempts to replace commercially available, extremely expensive AFF media with vinyl-silicone polymer-based media. It is important to steer further research on the emergence of other media. For the medium to be widely used in industry, these procedures must be affordable and environmentally sustainable.

References

1. McCarty, R.W., *Method of honing by extruding*, US Patent no. 3 521412, 1970.

2. Kalpakjian, S. and Schmid, S.R., *Manufacturing engineering and technology*, Pearson Education, Asia, 2000.

3. Benedict, G.F., *Nontraditional manufacturing processes*, Marcel Dekker, New York, 1987.

4. Kim, J.D. and Kim, K.D., De-burring of burrs in spring collets by abrasive flow machining. *Int. J. Adv. Manuf. Technol.*, 24, 469–473, 2004.

5. Tzeng, H.J., Yan, B.H., Hsu, R.T., Lin, Y.C., Self-modulating abrasive medium and its application to abrasive flow machining for finishing micro channel surfaces. *Int. J. Adv. Manuf. Technol.*, 32, 1163–1169, 2007.

6. Tzeng, H.J., Yan, B.H., Hsu, R.T., Chow, H.M., Finishing effect of abrasive flow machining on micro slit fabricated by wire-EDM. *Int. J. Adv. Manuf. Technol.*, 34, 649–656, 2007.

7. Lin, Y.C., Chow, H.M., Yan, B.H., Tzeng, H.J., Effects of finishing in abrasive fluid machining on microholes fabricated by EDM. *Int. J. Adv. Manuf. Technol.*, 33, 489–497, 2007.

8. Jung, D., Wang, W.L., Hu, S.J., Microscopic geometry changes of a direct-injection diesel injector nozzle due to abrasive flow machining and a numerical investigation of its effects on engine performance and emissions. *Proc. IMechE, Part A: J. Power Energy*, 222, A2, 241–252, 2008.

9. Jung, D., Wang, W.L., Knafl, A., Jacobs, T.J., Hu, S.J., Assanis, D.N., Experimental investigation of abrasive flow machining effects on injector nozzle geometries, engine performance and emissions in a DI diesel engine. *Int. J. Automot. Technol.*, 9, 9–15, 2008.

10. El-Hofy, H., *Fundamentals of machining processes*, Taylor & Francis, New York, 2007.

11. Cheng, K.C., Wang, A.C., Chen, K.Y., Huang, C.Y., Study of the polishing characteristics by abrasive flow machining with a rotating device. *Processes*, 10, 7, 1362, 2022.

12. Choopani, Y., Khajehzadeh, M., Razfar, M.R., An experimental study on the abrasive flow machining of aluminum alloy (AA 2024). *SN Appl. Sci.*, 5, 151, 2023.

13. Ji, R., Qi, Z., Chen, J., Zhang, L., Lin, K., Lu, S., Li, Y., Numerical and Experimental Investigation on the Abrasive Flow Machining of Artificial Knee Joint Surface. *Crystals*, 13, 3, 430, 2023.

14. Jain, V.K., *Advanced machining processes*, Allied Publishers, New Delhi, India, 2002.

15. Williams, R.E. and Rajurkar, K.P., Stochastic modelling and analysis of abrasive flow machining. *Trans. ASME, J. Eng. Ind.*, 114, 74–81, 1992.

16. Jain, V.K. and Adsul, S.G., Experimental investigations into abrasive flow machining (AFF). *Int. J. Mach. Tools Manuf.*, 40, 1003–1021, 2000.

17. Rhoades, L.J., Abrasive flow machining: a case study. *J. Mater. Process. Technol.*, 28, 107–116, 1991.

18. Kohut, T., Surface finishing with abrasive flow machining, in: *Proceedings of the Fourth International Seminar on Aluminium extrusion technology*, Washington, DC, pp. 35–42, SME Technical Paper, 1998.

19. Fletcher, A.J., Hull, J.B., Mackie, J., Trengove, S.A., Computer modeling of abrasive flow machining process, in: *Proceedings of the International Conference on Surface engineering*, Toronto, Canada, pp. 592–601, Welding Institute, Abington, Cambridge, 1990.

20. Loveless, T.R., Williams, R.E., Rajurkar, K.P., A study of the effects of abrasive flow machining on various machined surfaces. *J. Mater. Process. Technol.*, 47, 133–151, 1994.

21. Gorana, V.K., Jain, V.K., Lal, G.K., Experimental investigation into cutting forces and active grain density during abrasive flow machining. *Int. J. Mach. Tools Manuf.*, 44, 201–211, 2004.

22. Williams, R.E., Acoustic emission characteristics of abrasive flow machining. *Trans. ASME, J. Manuf. Sci. Eng.*, 120, 264–271, 1998.

23. Jain, R.K., Jain, V.K., Dixit, P.M., Modeling of material removal and surface roughness in abrasive flow machining process. *Int. J. Mach. Tools Manuf.*, 39, 1903–1923, 1999.

24. Jain, R.K. and Jain, V.K., Finite element simulation of abrasive flow machining. *Proc. IMechE, Part B: J. Eng. Manuf.*, 217, B2, 1723–1736, 2003.

25. Jain, R.K. and Jain, V.K., Simulation of surface generated in abrasive flow machining process. *Robot. Comput. Integr. Manuf.*, 15, 403–412, 1999.

26. Jain, R.K. and Jain, V.K., Stochastic simulation of active grain density in abrasive flow machining. *J. Mater. Process. Technol.*, 152, 17–22, 2004.

27. Gorana, V.K., Jain, V.K., Lal, G.K., Prediction of surface roughness during abrasive flow machining. *Int. J. Adv. Manuf. Technol.*, 31, 258–267, 2006.

28. Haan, J.J. and Steif, P.S., Abrasive wear due to the slow flow of a concentrated suspension. *Wear*, 219, 177–183, 1998.

29. Jain, R.K. and Jain, V.K., Specific energy and temperature determination in abrasive flow machining process. *Int. J. Mach. Tools Manuf.*, 4, 1689–1704, 2001.

30. Gorana, V.K., Jain, V.K., Lal, G.K., Forces pre- diction during material deformation in abrasive flow machining. *Wear*, 260, 128–139, 2006.

31. Jain, R.K. and Jain, V.K., Optimum selection of machining conditions in abrasive flow machining using neural network. *J. Mater. Process. Technol.*, 108, 66–67, 2001.

32. Sarah, S.Y.L. and Smith, A.E., Process monitoring of abrasive flow machining using a neural network predictive model, in: *Proceedings of the Sixth Conference on Industrial engineering research*, Miami, Florida, pp. 477–482.

33. Smith, A.E. and William, S.S., Neural network modeling of abrasive flow machining. *Intell. Syst. Artif. Neural Netw.*, 8, 797–802, 1998.

34. Jain, N.K., Jain, V.K., Deb, K., Optimization of process parameters of mechanical type advanced machining processes using genetic algorithms. *Int. J. Mach. Tools Manuf.*, 47, 900–919, 2007.

35. Mollah, A.A. and Pratihar, D.K., Modeling of TIG welding and abrasive flow machining processes using radial basis function networks. *Int. J. Adv. Manuf. Technol.*, 37, 937–952, 2008.

36. Jones, A.R. and Hull, J.B., Ultrasonic flow polishing. *Ultrasonics*, 36, 97–101, 1998.

37. Walia, R.S., Shan, H.S., Kumar, P., Parametric optimization of centrifugal force-assisted abrasive flow

machining (CFAAFF) by the Taguchi method. *Mater. Manuf. Process.*, 21, 375–382, 2006.

38. Walia, R.S., Shan, H.S., Kumar, P., Finite element analysis of media used in the centrifugal force assisted abrasive flow machining process. *Proc. IMechE, Part B: J. Eng. Manuf.*, 220, B11, 1775–1785, 2006.

39. Singh, S. and Shan, H.S., Development of magneto abrasive flow machining process. *Int. J. Mach. Tools Manuf.*, 42, 953–959, 2002.

40. Singh, S., Shan, H.S., Kumar, P., Wear behaviour of materials in magnetically assisted abrasive flow machining. *J. Mater. Process. Technol.*, 128, 155–161, 2002.

41. Amit, M.W., Yadava, V., Khatri, A., Simulation for the prediction of surface roughness in magnetic abrasive flow finishing (MAFF). *J. Mater. Process. Technol.*, 190, 282–290, 2007.

42. Jha, S. and Jain, V.K., Design and development of the magneto rheological abrasive flow finishing process. *Int. J. Mach. Tools Manuf.*, 44, 1019–1029, 2004.

43. Jha, S. and Jain, V.K., Modeling and simulation of surface roughness in magnetorheological abrasive flow finishing (MRAFF) process. *Wear*, 261, 856–866, 2006.

44. Jha, S. and Jain, V.K., Nano-finishing of silicon nitride workpieces using magnetorheological abrasive flow finishing. *Int. J. Nanomanuf.*, 1, 17–25, 2006.

45. Das, M., Jain, V.K., Ghoshdastidar, P.S., Analysis of magneto rheological abrasive flow finishing (MRAFF) process. *Int. J. Adv. Mf. Technol.*, 36, 5–6, 613–621, 2008.

46. Das, M., Jain, V.K., Ghoshdastidar, P.S., Fluid flow analysis of magnetorheological abrasive flow finishing (MRAFF) process. *Int. J. Mach. Tools Manuf.*, 48, 415–426, 2008.

47. Dabrowski, L., Marciniak, M., Szewczyk, T., Analysis of abrasive flow machining with an electro- chemical process aid. *Proc. IMechE, Part B: J. Eng. Manuf.*, 220, B3, 397–403, 2006.

Note

*Corresponding author: sandip.sandip.kunar@gmail.com

27
Elastic Emission Machining

Sandip Kunar[1]*, Jagadeesha T.[2], Gurudas Mandal[3] and Norfazillah Talib[4]

[1]*Department of Mechanical Engineering, Aditya University, Surampalem, India*

[2]*Department of Mechanical Engineering, National Institute of Technology, Kozhikode, India*

[3]*Department of Metallurgical Engineering, Kazi Nazrul University, Asansol, India*

[4]*Department of Manufacturing Engineering, Universiti Tun Hussein Onn Malaysia, Johor, Malaysia*

Abstract

With elastic emission machining (EMM), it is possible to easily complete a workpiece into any shape by using elastic fracture of atomic size when doing numerically controlled ultra-precision machining. Ultra-fine powder particles are used as an instrument. When water and powder particles are combined, the slurry's fluid lubrication state is used to force only the residue particles to interact with the job's surface. As so, damage-free removal of atomic sizes is accomplished. The interaction between the powder particle surfaces and metal surface is taken into consideration when analyzing the metal removal mechanism. A method that is very similar to chemical etching is proposed for the removal of the substrata's surface atoms. The principle, mechanism, advantages, and disadvantages of elastic emission machining are described in this article.

***Keywords*:** EMM, surface finish, atomic removal

27.1 Introduction

The main purpose of machining is to create the high-quality surface, and flawless machining creates an excellent surface in terms of both geometry and crystallography. Using a machining technique that operates at atomic scales can result in geometrically flawless machining. A flawless surface in terms of its physical characteristics can be achieved during machining if no physical or chemical occurrence is happening to the atoms close to the target atom. Therefore, if the physical or chemical events that follow machining are fundamentally macroscopic, performing atomic level machining just using advancements in traditional apparatus is not feasible. Which machining phenomenon is used determines how little machining is required. For example, cutting requires plastic deformation to achieve the machining, and this dislocation motion is essential. Furthermore, the quantity of machining that is required at minimum cannot exceed the dislocation's spatial volume [1].

To achieve microscopic-size machining, it is crucial to utilize or discover a novel phenomenon that contrasts with the traditional macroscopic one. A few recent instances have been created that are used for cutting novel materials for electronics and other purposes where the surface must be extremely precisely polished [2]. These techniques fall into two categories: atom removal and atom deposition. If excessive power is not used in the vicinity of the target atom during removal machining, the optimal final surface is achieved. It is believed that the most efficient technique is to create and preserve circumstances in which atoms move spontaneously and the machining proceeds in a way that minimal power is used outside of the target atom [3]. The principle, mechanism, advantages, and disadvantages of elastic emission machining are described in this article.

27.2 Principle of EEM

Many different types of interactions arise at the border between two solid phase materials made of distinct chemical components. For instance, the release of surface energy prior to contact results in the appearance of a bonding force between two contacting surfaces. Consequently, there is a chance that some of the atoms from one surface will migrate to the other when these substances are separated mechanically. This fact is used in machining, and the process known as EEM makes use of this kind of phenomena. Practically speaking, the following methods can generate EEM. Water is consistently mixed with ultra-fine powder particles, which have diameters significantly less than 1.0 µm. Particles of powder are moved and accelerated to the job surface with little normal stress by using flow of this combination. The above-mentioned mechanism is how the surface atoms are removed when they come into touch with the work surface.

Within the contacting area, the working area is restricted to be less than 10 nm^2. Removal is only feasible in this region when mutual surface atoms are ideally bound together. Moreover, the target atom can only be eliminated if the interface exhibits properties that cause the bonding energy between the atoms in the job's surface and subsequent layers to drop. To get a geometrically flawless surface, the machined area, and the depth both roughly approach atomic order. These interface properties demonstrate that atoms are being removed from the work surface in a semi-spontaneous manner. As a result, flawless surfaces are possible in terms of their physical characteristics. The following is a way to conceptualize the interface's features. To allow for the electrical polarization of this region, an interface consisting of various types of atoms was built. Moreover, local charge-up could be

created if there are different electron states in this area. In these situations, the bulk state and the surface atoms of the job are situated in quite distinct ways. This indicates that there are numerous options for helping the surface atoms to detach from the job.

27.3 Numerically Controlled Elastic Emission Machining

A revolving sphere and the work surface are lubricated by fluid, as seen in Figure 27.1**,** and this state of fluid lubrication can be used by machining apparatus to induce elastic emission machining [4]. Subsequently, to prevent damage to the work surface, the fluid film thickness needs to be kept greater than the residue particle diameter. Because the thickness is automatically maintained by the fluid's pressure and load balance, diverse powder particles will be carried without harming the job surface and the polyurethane sphere's flow rate will remain constant. The amount of stock removed per unit of time is set if the concentration and dispersion of the powder particles are kept constant during the machining operation. As a result, the residing time at that point makes it feasible to manage the stock removal at that moment. Naturally, during actual machining, the load and rotation speed should be adjusted to determine the ideal operating conditions. Polyurethane rubber was chosen for the sphere's construction because of its elasticity and water resistance. It is made via cutting, with a tolerance of less than 1.0 μm for spherical shape and a surface roughness of about 0.1μm. To keep the combined fluid in a constant state, a circulating diaphragm pump and a constant temperature unit are linked.

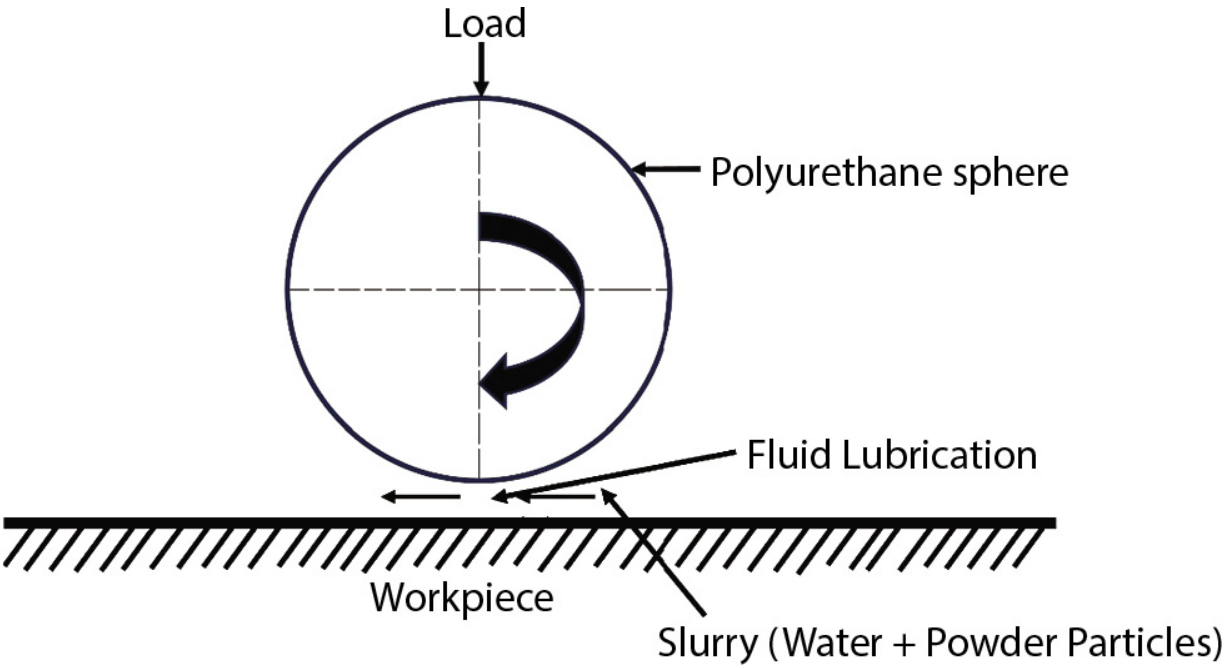


Figure 27.1 Schematic view for transporting and accelerating powder particles mixed with water in EMM.

27.4 Conclusion

Using the phenomenon of semi-spontaneous removal of atomic-sized material, ideal machining can be achieved. Both a geometrically and crystallographically perfect surface can be achieved because to this phenomena. From these perspectives, one of the best machining techniques is EEM. According to the EEM concept, the machining characteristics of EEM are said to be reliant on the interface at the work contact and powder particle. Moreover, numerically controlled EEM is particularly characterized in terms of the finished surface's precision. Lastly, it should be noted that achieving the necessary surface profile requires the creation of a sufficiently accurate profile measuring method.

References

1. Mori, Y., Yamauchi, K., Endo, K., Mechanism of atomic removal in elastic emission machining. *Precis. Eng.*, 10, 24–28, 1988.

2. Mori, Y., Yamauchi, K., Endo, K., Elastic emission machining. *Precis. Eng.*, 9, 123–128, 1987.

3. Kanaoka, M., Takino, H., Nomura, K., Mori, Y., Mimura, H., Yamauchi, K., Removal properties of low-thermal-expansion materials with rotating-sphere elastic emission machining. *Sci. Technol. Adv. Mater.*, 8, 170–172, 2007.

4. Su, Y.T., Wang, S.Y., Chao, P.Y., Hwang, Y.D., Hsiau, J.S., Investigation of elastic emission machining process: lubrication effects. *Precis. Eng.*, 17, 164–172, 1995.

Note

*Corresponding author: sandip.sandip.kunar@gmail.com

28
Magnetic Abrasive Finishing Process

Sandip Kunar[1]*, Jagadeesha T.[2], Gurudas Mandal[3] and Norfazillah Talib[4]

[1]*Department of Mechanical Engineering, Aditya University, Surampalem, India*

[2]*Department of Mechanical Engineering, National Institute of Technology, Kozhikode, India*

[3]*Department of Metallurgical Engineering, Kazi Nazrul University, Asansol, India*

[4]*Department of Manufacturing Engineering, Universiti Tun Hussein Onn Malaysia, Johor, Malaysia*

Abstract

As a cutting-edge nano finishing technique for producing a high-quality surface for superalloy, composite, and ceramic finishing, magnetic abrasive finishing (MAF) has acquired a lot of interest. This study offers an extensive overview of the MAF process. The need for precise and high-quality finishes, coupled with the challenge of finishing components using traditional techniques, has followed in the development of sophisticated finishing methods. Components can be finished, deburred, and precisely chamfered using the sophisticated MAF technique. Nanometer surface finishes on flat and tubular workpieces, both internally and superficially, can be affordably achieved using this technique. To achieve good surface finish, very small finishing forces are employed to the magnetic abrasive particles during the method. The primary components, different principles, working principle, process parameters, magnetic abrasive preparation, MAF tools, types of MAF process, advantages and

disadvantages, applications, and surface finish improvement are provided here. Lastly, difficulties and directions for the future are mentioned. Researchers and practitioners working in MAF-related domains will find this review useful. As a result, it helps finish brittle materials very well without causing microcracks or other flaws. Numerous scientists altered the procedure and created hybrid versions of it. Making the procedure more capable of completing microfeatures and more efficient is their main goal.

***Keywords*:** MAF, surface quality, abrasive particle, abrasive preparation, finishing tools

28.1 Introduction

Medical devices, semiconductors, and the aerospace industry are the primary industries that use high-performance parts with functional micro- and nano-surface layers and ultra-precision complex surfaces [1]. Generally, a high-quality surface is obtained by a variety of conventional methods such grinding [2], lapping [3], and honing [4]. The conventional methods are limited by the challenges in designing fixtures that accommodate varying workpiece forms and sizes; limitations in sophisticated engineering materials; low precision and efficiency [5]. These days, several unconventional nano finishing methods — such as elastic emission machining (EEM), abrasive flow machining (AFM), and ion beam machining (IBM) are suggested for the creation of précised parts to address issues with conventional polishing [6]. The terms magnetic abrasive finishing (MAF) and magnetorheological jet polishing (MJP) are used to categorize magnetic field-assisted finishing (MFAF) procedure. Utilizing unbound or bonded abrasive and magnetorheological fluids, as well as diverging finishing media, are the primary distinctions

between the techniques. The removal of molecules and atoms from the job is the basis for the operations of EEM [7] and IBM [8]. Other methods involve indenting and shearing material to create the microchips. By deterministically adjusting the applied magnetic field's finishing force, MFAF enhances the final surface finish. The MAF technique has drawn a lot of interest in high-surface integrity finishing for composites [9], superalloys [10], and ceramics [11]. The workpiece's size and shape, including its inner and outer surfaces, free-form surfaces, and intricately curved surfaces, are all negotiable with MAF. In a matter of minutes, MAF produces a nanometer-level surface that does not result in microcracks or a deteriorating layer [12]. The magnetic abrasive in MAF has remarkable properties such as controllability, self-adaptation, and self-sharpness [13].

The requirement to mechanize the manual finishing of elaborately formed manufacturing components led to the development of the MAF technique in East European countries [14]. The final step in the manufacturing cycle of a component is finishing. The functional qualities of a component, *i.e.*, friction, fatigue, and wear, are significantly influenced by surface roughness (R_a). One of the primary drawbacks of the traditional finishing techniques is the vibration of the rigid cutting tool when machining hard materials like nickel and cobalt, and the creation of cracks when machining brittle materials like ceramics and glasses. Advanced finishing technologies have been developed to cut machining costs while maintaining minimal surface flaws during machining operations, all while meeting the demand for high surface quality and good precision. These recently developed advanced finishing methods include magnetorheological finishing (MRF), and magnetorheological abrasive flow finishing (MRAFF). To create a flexible finishing tool, the MAF method combines

the machining behavior of abrasive particles (like SiC and Al_2O_3) with the magnetization behavior of ferromagnetic particles (like Fe). The MAF technique is mostly employed for the finishing of cylindrical and flat components. The MAF technique may reach a minimum R_a of 5 nm and a material removal rate (MRR) of about 1 µm/min [15]. Furthermore, the process's low magnitude finishing forces reduce the likelihood of producing flaws like microcracks when finishing fragile materials.

The workpiece is finished by forming a comparative motion with the magnetic abrasive during the finishing method. The developed MAF tool is simple to link with programmed machinery, such as milling machines and industrial robots, to offer relative motion as a separate module, in accordance with different finishing tasks [16, 17]. This work introduced a novel technique for smoothening the internal surfaces of tubes utilizing a six-axis robot equipped with a magnetic machining tool [18]. The development specifics of the plane workpiece MAF setup are described. The created configuration is fastened to a computer numerical controlled (CNC) milling trainer. Using the designed configuration, the impact of chosen input process parameters, electromagnet's rotational speed, number of abrasive meshes, and working gap are examined with respect to the improvement in surface finish for mild steel workpieces [19]. Through magnetic pole movement, a novel MAF approach for large-scale tubes allows the coupling of dynamic changes in the magnetic field with material removal effects. This method significantly enhances the surface quality of zirconium thin alloy tubes and increases the density of contact trajectories while facilitating the self-sharpening renewal of MAF [20].

To provide a more thorough understanding of the technology, a critical analysis of different MAF features is

offered based on the previously mentioned necessity for an MAF process review. The primary components, different principles, working principle, process parameters, magnetic abrasive preparation, MAF tools, types of MAF process, advantages and disadvantages, applications, and surface finish improvement are discussed here. Lastly, difficulties and directions for the future are mentioned. Researchers and practitioners working in MAF-related domains will find this review useful.

28.2 Primary Components of MAF

Among the crucial elements of the MAF configuration are:

i. **Magnets:** the magnetic field is created by electromagnet magnets. During the MAF process, the finishing forces are the magnetic lines of force produced by the magnets. In the case of electromagnets, the coil's number of turns, voltage, and current may all be adjusted to alter the strength of the magnetic field.

ii. **Ferromagnetic particles:** because of their inherent magnetism in an external magnetic field, ferromagnetic particles are necessary. Ferromagnetic particles create a flexible magnetic abrasive brush (FMAB) along the magnetic lines that run between the magnets' north and south poles during the MAF process. The particles that are ferromagnetic abrasive range in size from 50 µm to 400 µm. The magnetic field density created during the MAF technique is dependent on the size and kind of ferromagnetic particle.

iii. **Particles of abrasion:** the size of the particles is determined by the MRR requirements and typically ranges from 1 µm to 10 µm. Diamond, boron nitride,

silicon carbide (SiC), aluminum oxide (Al_2O_3), and so on are examples of abrasive particles. The hardness of the workpiece to be polished determines which abrasive particles are used. Magnetic abrasive particles (MAPs) are a combination of abrasive particles and ferromagnetic. They come in two varieties: bound and unbonded. A mechanical blending of ferromagnetic particles and abrasive makes up unbonded MAPs. While in bonded MAPs, abrasive particles are contained in a matrix of ferromagnetic particles created by sintering or any other procedure [21].

iv. **Lubricant:** a lubricant is occasionally added to the combination of magnetic abrasive particles to improve the MAF's flexibility. Abrasive gel is added to the MAF mixture by a few writers. Lubricants reduce the amount of MAF flown out of the working zone at high rotational speeds (RS) and promote MAF stability.

28.3 MAF Principles

This method is described as a material removal technique that uses comparative motion between the magnetic abrasive and workpiece while a magnetic field is present in the finishing zone to accomplish precise machining of the workpiece [22]. Flexible magnetic abrasive brushes (FMABs) are created along the direction of the magnetic force lines using magnetic abrasive, which is mainly made up of abrasive particles and ferromagnetic [23, 24]. Using the created flexible finishing tool, a variety of workpieces with internal, free-form, and cylindrical surfaces can be finished [25, 26]. Based on the traditional finishing approach, some researchers created MAF technology with various configurations. A work rotation system is used for the internal finishing of alumina ceramic components [27]. The four tiny permanent magnet poles on the circular yoke

were evenly spaced apart to create a magnetic field that attracted ferrous particles to the inner surface of the tube. The inner surface of the tube is micro-cut by the diamond abrasive present in the mixture when the tube is rotated at a high speed. Effective surface finishing resulted from the finishing media moving more quickly due to the vibration supplied to the magnetic poles. The MAF is utilized to finish a flat workpiece surface [28]. To create a gradient magnetic field, which allowed the magnetic abrasive to condense into a flexible brush in the working gap, the finishing tool is constructed from a single permanent magnet. By varying translational and rotational motion, the material is removed. To obtain a flawless and superior workpiece surface, further ultrasonic vibration is applied, in accordance with the MAF principles. The ultrasonic vibration used a piezoelectric transducer, an ultrasonic power, and a horn device in the horizontal direction of the job [29]. The transducer converted the high-frequency electrical signal produced by the ultrasonic power into a horizontal mechanical vibration. An ultrasonic vibration module is used to load ultrasonic vibration along the upright of the workpiece [30].

28.4 Working Principle of MAF

The combined actions of a magnetic field and magnetic abrasives form the basis of the MAF process. The main components of the working principle are as follows:

- An electromagnet produces a powerful magnetic field. Near one of the electromagnet’s poles is where the unfinished workpiece is located.
- The gap between the job and magnet is where the magnetic abrasives are injected. Iron particles are typically employed as magnetic abrasives.

- The iron particles get magnetized and take on the characteristics of tiny magnetic brushes when an electric current is run through the electromagnet.
- The magnetic abrasives organize themselves on the job surface while a magnetic field is generated.
- In addition, the magnetic field produces a compressive force that allows the magnetic abrasives to grind on the surface of job.
- A smooth finish is shaped by the magnetic abrasives' rubbing action on the workpiece, which removes microchips from the surface.
- There is neither physical touch nor pressure during the entire operation; it all happens in the presence of a magnetic field. This makes it possible to complete complex geometries.

28.5 Process Parameters in MAF

The following are the primary process variables that influence finishing performance:

- **Magnetic flux density:** the magnetic force acting on abrasives is persuaded by the magnetic field strength, which is represented by flux density. Finishing efficiency is increased with higher flux density.
- **Gap between job and electromagnet:** the distance between the job and electromagnet influences the strength of the magnetic field. A narrower gap means a higher quality of finish.
- **Magnetic abrasives' size and makeup:** finer abrasives yield a smoother surface. Various compositions provide a range of machining capabilities.

- **Magnetic abrasive speed and circulation:** while high speed increases finishing rate, it can also result in surface flaws. Speed optimization is crucial.
- **Finishing time:** while a longer finishing time effects in good surface quality, productivity is reduced. The ideal amount of time is needed.
- **Temperature:** abrasive magnetization is decreased by rising temperatures. Therefore, to maintain a lower temperature, cooling is required.
- **Voltage and current:** increased current flowing through the electromagnet strengthens the magnetic field. There must be control over the voltage.
- **Workpiece properties:** the workpiece's material, hardness, and starting surface roughness all have an impact on how well it finishes.

28.6 Magnetic Abrasive Preparation

Commercially available magnetic abrasive is made up of an abrasive phase (silicon carbide, alumina, or diamond) and a ferromagnetic phase (carbonyl iron particle), and it is essential to the finishing approach [31]. The primary purpose of the ferromagnetic phase is to enable the application of a magnetic field to cause the magnetic abrasive to produce a strong magnetic pressure. To direct finishing performance and magnetic pressure, the ferromagnetic phase volume fraction is essential. Because the abrasive phase's goal is to remove material from the job's surface, its hardness is higher than the workpiece's [32]. Numerous techniques for preparing magnetic abrasives have been proposed, including the gas atomization approach, the bonding method [34], the sintering method [35], and the simple mixing method [33].

To put it simply, the mixing procedure involves stirring in a specific proportion to create the ferromagnetic and abrasive phases. Low finishing efficiency results from the easy decomposition of magnetic abrasives during the finishing time, notwithstanding the simplicity of the procedure [36]. Using a binder to blend the ferromagnetic and abrasive phases, the bonding process yields magnetic abrasive following solidification, crushing, and screening. The produced magnetic abrasive is readily oxidized, despite the bonding method's low cost and relative simplicity. Magnetic abrasive is prepared using the sintering method [37]. The abrasive phases and ferromagnetic of the manufactured magnetic abrasive may be securely coupled, and it has numerous advantages such as longer working life and higher stability [38, 39]. Melted ferromagnetic and abrasive phases combined violently due to gas atomization and the fast solidification process. After cooling, solidifying, and screening procedures, magnetic abrasive is produced. A novel gas-solid two-phase double-stage atomization with quick solidification is used for further improving the preparation process [40]. Outstanding characteristics of the prepared magnetic abrasive made using this technology are its uniform composition, excellent cutting capability, and longer working life. The primary variables influencing an abrasive's characteristics are its composition and ratios of magnetic abrasive. A new magnetic abrasive included ferromagnetic particles, abrasive particles, plasticizers, and base polymer to enhance the performance of magnetic abrasive even more. With a mass ratio of 4:3:1 for the base polymer, ferromagnetic phase, and abrasive phase, the change in roughness reached a maximum of 94.85%. The mechanical stirring created an improved magnetic abrasive by blending the intelligent shear thickening fluid, silicon carbide particles and carbonyl iron particle [41]. Through finishing studies for Ti-6Al-4V workpiece, the original value of 1.17 µm is reduced to 54 nm for surface roughness.

28.7 MAF Tools

Magnetic abrasive finishing (MAF) tools have been created for smoothening a variety of workpieces with irregular shapes. The completed workpieces fall into two groups. The two workpieces are the inner and outer surface workpieces. A detailed discussion is given for various MAF finishing tools.

28.7.1 Finishing Tools for Outer Surface

Because magnetic abrasive is flexible and can conform to curved surfaces, planar tools are appropriate for smoothening workpieces with intricate curved surfaces. An MAF tool is fabricated for flat surface finishing [42]. By applying a magnetic field over the working gap between the job surface and revolving magnetic pole, the finishing process is carried out. Magnetic abrasive is pressed firmly on the workpiece's surface owing to the presence of magnetic equipotential lines and magnetic lines of force, which resulted in micro-cutting when the pole rotated. After creating an MAF tool for nickel-based superalloy GH4169, the processing efficiency had increased by 50% and that the surface morphology had smoothed down and the surface roughness value had greatly reduced. By applying a magnetic field over the working gap between the revolving magnetic pole and workpiece, the finishing process is carried out. Magnetic abrasive is pressed firmly on the workpiece's surface owing to the presence of magnetic equipotential lines and magnetic lines of force, which resulted in micro-cutting when the pole rotated. The workpiece's upper end is equipped with the magnetic field-generating instruments previously discussed. The workpiece is not penetrated by the magnetic field lines; they merely form a closed loop around the permanent magnet. The processing effect is impacted because the

resulting flexible magnetic brush is unable to press the workpiece firmly. The magnetic flux density is increased by installing a permanent magnet on the other side of the workpiece to overcome the weakness [43]. Experiments confirmed that the tool equipped with a permanent magnet had a superior finishing effect than one without one. Two permanent magnets placed on the top and bottom surfaces of the job serve as the unique tool offered to further improve magnetic flux density, with 0.3 T being the highest magnetic flux density [44].

For exterior surface finishing, multi-pole integrated MAF tools are developed. An MAF tool is created for deburring cylindrical surfaces. A couple of 180° distributed permanent magnetic poles is created. Between the workpiece's exterior and the magnetic poles, magnetic abrasive is inserted. The double-magnet is made up of two parallel shafts with neodymium ring magnets fastened to each end. A spindle motor powered one of the shafts, and spur gears connected it to the other shaft. The entire instrument is fixed onto a milling machine. The workpiece and magnetic abrasive moved relative to one another, removing material [45]. A unique finishing tool that is mostly made up of four magnetic poles [46]. The final instrument is fixed to a CNC machine center with four axes. Four magnetic poles could make a flexible brush with magnetic abrasive in the finishing area. The worktable's movement and the tool's rotation created a relative movement that allowed the magnetic brush to remove material. A spherical tray, a baffle, and 64 poles are used to study the MAF of Ti-6Al-4V [47]. The spindle is attached to the workpiece. The initial 1.195 µm of surface roughness is reduced to 0.073 µm. To investigate the formation behavior of FMAB, the scientists converted permanent magnets into electromagnets, which can modify the strength of the magnetic field in the completing area by varying the

applied voltage’s magnitude and frequency. The experimental study investigated the cylindrical workpiece’s surface finishing. In the space created by the separation of the two electromagnetic poles, a cylindrical workpiece is placed. The space between the job and electromagnetic pole is filled with magnetic abrasive. Due to the electromagnetic field’s presence, the magnetic abrasive displayed a dense brush and stuck firmly to the cylinder’s outside. By adjusting the axial vibration and rotating the workpiece, a relative friction is produced.

28.7.2 Finishing Tools for Internal Surface

The workpiece surface is finished by squeezing, sliding, and grinding. The design basis of finishing tools for the interior surface is the same as the principle for designing the outside surface: utilize magnetic field to absorb magnetic abrasive to generate FMAB. However, the location of the magnetic field generator with respect to the completed target surface is the primary distinction between the two design approaches. For the internal surface, the magnetic field generator is placed externally because non-magnetic materials are impervious to magnetic fields [48]. The development of interior surface finishing tools is responsible for finishing process [14, 49]. A stationary pole system-based MAF tool is created [50, 51]. An electromagnetic field is used to congregate magnetic abrasive at the finishing zone, creating a finishing force against the tube’s inner surface. The material is removed by the relative friction between the flexible brush and the interior surface of job, which is brought by the tube’s rapid rotation and vibration. As a result, the tube’s interior surface smoothed out. A unique finishing device is produced an alternating magnetic field by placing electromagnetic coils in a parallel circuit facing each other [52]. The alternating magnetic field that is created

controlled the magnetic abrasive inside the workpiece. A finishing configuration is proposed by applying two 90° electromagnet placement [53]. When the current is supplied, the abrasive is firmly bonded to the workpiece's inner surface. A surface cut is produced by the workpiece's relative motion, which is produced by the motor's rotation driving it and an axial vibration produced by a crank mechanism attached to the motor. In addition, DC power is supplied to mutually perpendicular electromagnetic poles as the finishing setup's magnetic field generator [54]. An eccentric, a gear box, and a motor produced the desired radial vibration of the magnetic field generator for the relative motion. The workpiece is secured on the chuck that is attached to the motor to supply turn. It is possible to transform the electromagnetic magnetic field generator indicated above into a permanent magnetic field. The system of spinning magnetic poles produced the relative motion. The optimal processing conditions were adjusted by varying the distribution of magnetic poles [55], placement angles of magnetic poles, and axial vibration to investigate magnetic field strength and higher finishing efficiency.

28.8 Types of Magnetic Abrasive Finishing Process

28.8.1 Flat Magnetic Abrasive Finishing Method

Flat magnetic abrasive finishing (FMAF) is applied to finish large-scale flat workpieces. The job is positioned between the magnet poles during the FMAF process. When the magnetic field is operated during the procedure, a tiny gap (1–3 mm) is maintained for the FMAB. Due to dipole interaction, ferromagnetic particles along the magnetic lines of force as the magnetic field are employed. Between

the ferromagnetic particles, abrasive particles become implanted, creating a finishing tool with a variety of randomly positioned cutting edges. To remove material during the FMAF process, finishing forces are transmitted from the ferromagnetic particles to the abrasive particles.

28.8.2 Cylindrical Magnetic Abrasive Finishing Method

Rollers with a cylindrical shape are finished using the cylindrical magnetic abrasive finishing (CMAF) procedure. The spindle chuck holds the workpiece (roller) between two magnets during the CMAF process. The spindle gives the workpiece rotary motion, and the oscillating magnetic poles with respect to the workpiece give the magnetic field axial vibratory motion. During the CMAF procedure, FMAB serves as a deformable multipoint finishing tool. By adding solid lubricants like zinc stearate, the FMAB's flexibility can also be enhanced. As a result, the CMAF process produces a workpiece with a beautifully polished surface.

28.8.3 Hybrid Magnetic Abrasive Finishing Method

To combine great efficiency and a high-quality surface finish, multiple researchers developed different hybrid MAF processes. Combining the benefits of the constituting procedures and getting rid of their drawbacks is their main goal. The results of the experimental investigations show that hybrid MAF processes outperformed MAF procedures.

28.8.4 Electrolytic Magnetic Abrasive Finishing Method

The efficiency of CMAF method is enriched by introducing the electrolytic magnetic abrasive finishing method (EMAF) [56]. The electrolyte supply system and the CMAF setup

are combined. Electrolyte fills the gap between the electrode and job during the finishing operation. The cathode and anode of the DC power supply are connected to the workpiece and electrode, respectively. When compared to MAF method, the simultaneous action of electrolysis and magnetic field accelerates the MRR and yields a better completed surface. The EMAF method finished the 6061 Al/Al2O3 composite [57]. The magnetic field reduces the electrolyte's electric resistance because of the Lorentz force acting on the electrolytic ions. Consequently, raising current density improves MRR. With the aid of the EMAF technique, the finishing of nickel-based superalloy was completed [10]. It is important to match the relationship between the magnetic and electric field intensities during the EMAF process. The abrasives do not totally remove the passive film if the electric field intensity is higher. The passive film is extremely thin, and the electrolysis process is not properly utilized if the magnetic field is greater. Surface imperfections like crests, pitting, and sags can erode the surface finish and are caused by an unregulated electrolyte supply during finishing.

28.8.5 Vibration-Assisted Magnetic Abrasive Finishing

To enhance the efficiency of procedure, the vibration-assisted magnetic abrasive finishing technique (VMAF) was created. Vibrations are employed to the flat job during the VMAF process. In addition to accelerating the abrasives' relative motion, vibrations also make the magnetic field behave dynamically. Because of this, the finishing forces produced by the VMAF method are larger than those produced by MAF. Only the horizontal (X direction) vibration is supplied at the MAF process' completing [58]. However, using a motorized cam mechanism to provide

vertical (Z direction) vibration, the MAF method was developed [59]. To facilitate effective workpiece finishing, a designed set-up is especially helpful for deburring operations. To achieve mixed mode vibration of the working table, horizontal and vertical vibrations were incorporated subsequently [60]. The fabricated setup is very helpful for nano finishing micro-curved component surfaces. When finishing the SS flat workpiece using the VMAF method, vibrations were further supplied in the X and Y directions, which correspond to the axis of the horizontal plane [61]. A vibration aided cylindrical– magnetic abrasive finishing (VAC–MAF) method is created to finish cylindrical workpieces. A high-speed lathe is altered to fit the VAC–MAF process configuration [62]. A vibration mechanism is used to spin the workpiece to cause the magnetic poles to shake. The slide unit has an electromagnet setup installed on it. During the finishing process, these vibrations aid in replacing the worn-out abrasive particles with fresh ones. The R_a and MRR were thereby increased by 100% and 150% during the VAC-MAF procedure, respectively, over the MAF process.

The MAF method has many benefits. So, MAF provides the following advantages over alternative finishing methods:

i. The MAF technique is cost-effective because it does not require expensive equipment or tools.
ii. The FMAB finishing tool, which is used in the MAF procedure, is self-adjusting and self-sharpening. Additionally, the tool does not need to be dressed or compensated. Consequently, productivity will rise.
iii. Glass and ceramics are fragile materials that can be properly finished using the MAF technique without developing surface flaws.

iv. It is simple to regulate the amount of finishing forces produced during MAF method.

28.9 Advantages of Magnetic Abrasive Finishing

Compared to traditional finishing techniques, it offers the following benefits:

- It can achieve surface finishes of up to 0.05 microns, which is not achievable with traditional methods.
- Broken parts and mechanical strains are less likely to occur when there is no direct contact between the job and tool.
- Because the method is non-contact, it is easy to complete complex internal surfaces and geometrics.
- Due to the lack of heat generation or chemical reactions, the process is environmentally friendly and clean.
- It is possible to complete several workpieces at once, which increases production.
- There is flexibility in the use of different magnetic abrasives for diverse purposes.
- Compared to other non-conventional processes, there is a reduction in capital investment and operating costs.
- It is also possible to perform post-processing tasks like edge radiusing and deburring efficiently.

28.10 Disadvantages of Magnetic Abrasive Finishing

It has certain drawbacks in addition to its benefits.

- The procedure is limited to materials that are ferromagnetic. This method cannot be used to mill nonmagnetic materials.
- The size and weight of the workpiece that can be treated efficiently are limited.
- To achieve consistent outcomes, process parameters must be carefully maintained.
- Operating costs are increased by the necessity for periodic cleaning and replacement of the magnetic abrasives.
- The workpiece may need to be demagnetized because residual magnetism can interfere with subsequent machining operations.
- Setting up the MAF facilities and equipment requires a significant initial capital commitment.
- It is not the best method for removing material in large quantities from surfaces.
- Maintaining process settings and running the MAF equipment require skilled workers.

28.11 Applications of Magnetic Abrasive Finishing

Magnetic abrasive finishing finds several industrial applications, such as:

- Enhancing surface polish and prolonging tool life on dies, molds, and tools made of steel, carbide, and high-speed steel (HSS).
- Deburring intricate holes and cavities on machined parts that are challenging to access using alternative techniques.

- Finishing titanium, aluminum, and Inconel aerospace components when a very fine surface finish is needed.
- Polishing the inside surfaces of cylinders and tubes consisting of brass, stainless steel, etc.
- Improving the fatigue strength of car engine parts such as engine blocks, pistons, and valves.
- Surface smoothing of prosthetic implants, such as replacement hip and knee joints.
- Completing compressor blades, nozzles, and fuel injection parts that require flow-quality finishing.
- Steel alloy microfinishing cutting tools, gauges, and punches to increase dimensional precision.

28.12 Surface Finish Improvement in MAF

The workpiece’s surface polish can be enhanced in MAF by:

- Employing micron- or sub-micron-sized magnetic abrasives, which are incredibly fine. The finishing effect improves with decreasing abrasive size.
- Boosting the magnetic field’s strength to enhance the magnetic abrasives’ machining performance.
- Decreasing the distance between the electromagnet pole and job. A smaller gap strengthens the magnetic field.
- Optimizing variables in the process, such as rotational speed, finishing time, and abrasive size and composition. As a result, the surface is uniformly cleared of debris.

- Employing appropriately hardened abrasive particles. Soft particles result in poor machining action, and very hard particles generate deeper scratches.
- Keeping the process temperature constant via cooling strategies. Strong magnetic fields are weakened by high temperatures.
- Using multiple stages of finishing, each using finer abrasives. Finish is considerably improved by multi-stage finishing.
- Utilizing workpiece holding fixtures that are appropriate and reduce undesired vibrations and motions during finishing.
- Use various magnetic pole magnetization schemes to provide consistent machining action.

28.13 Challenges and Future Directions

Despite recent significant technological advancements in the MAF process, there are still many opportunities and obstacles that need to be investigated.

- For hard materials and microtextured surface, highly controllable and efficient MAF concepts are developed. Currently, a lot of attention is being paid to materials that are challenging to finish, like composites, glasses, ceramics, high-speed steel, and titanium alloys. When it comes to finishing parts like gears, impellers, intricate molds, and other materials with the microstructured surface that are challenging to finish, MAF is still insufficient, which leads to low efficiency and poor consistency. To address the shortcoming, MAF technology needs to be further investigated.

- Research and development are required to create a low-cost and high-performance magnetic abrasive. The key element influencing finishing effectiveness and the intended enhancement in surface superiority is magnetic abrasive performance. The creation of appropriate magnetic abrasives is essential to achieving high-quality surfaces and increasing the rate of material removal. An appropriate magnetic abrasive must be prepared considering the characteristics, dispersibility, high saturation magnetization, and shear capacity. As a result, focus must be given to the weakness’s solution.
- More research is required on a programmable magnetic finishing device with online inspection, a real-time monitoring system, and feedback capability. Currently, the primary method for assessing finishing quality on processed workpieces is offline inspection. This has a limited impact on the automatic compensation accuracy, finishing efficiency, and workpiece’s surface quality. One of the difficulties and opportunities is the development of intelligent magnetic abrasive equipment with an online monitoring system, inspection, and feedback to achieve automatic finishing and the changing of finishing parameters.
- The MAF device simulates a magnetic field. Tools for creating magnetic fields were the primary focus of simulations in the scientific literature up to this point. The simulation findings show significant inaccuracy when compared to the final magnetic field environment. To find out more about the actual magnetic field intensity, magnetic field simulation is required. This includes automation equipment, magnetic field generation tools, magnetic abrasives, fixtures, and workpieces.

- Ensure that the MRR model system is correct and universal by considering the composition of the magnetic abrasive. To simplify the mathematical modeling of the MRR model, some assumptions are made regarding the complex mechanism of media creation and its interaction with the job surface. The Preston equation—which splits the pressure on the job into multiple components— is the primary foundation upon which the MRR model is built. Establishing a general mathematical model for MRR is therefore important.

28.14 Conclusions

A magnetic field is utilized to push abrasive particles against the job during the surface finishing process known as magnetic field-assisted finishing, also known as magnetic abrasive finishing. As a result, completing areas that are typically inaccessible—like the interior of a long, curving pipe—is feasible. Many applications, including as the microelectromechanical systems, production of medical components, fluid systems, optics, and mechanical components, have led to the development of magnetic field-assisted finishing (MAF) methods. It can be summed up like this:

- A nano-finishing technique is called MAF. Magnetic abrasive is utilized as a machining tool in the process of creating magnetic pole rotation and workpiece reciprocating motion, which allows for micro-cutting.
- The most common methods used to create magnetic abrasives are simple mixing, bonding, sintering, gas atomization, and quick solidification.
- Because electromagnetic coils can cause eddy current heat and magnetic field weakness, permanent magnets

are used in the design of the vast majority of MAF tools.

- Unlike previous processes, it can achieve surface finishes as fine as 0.05 microns.
- This method is employed appropriately hardened abrasive particles. Soft particles result in poor machining action, and very hard particles generate deeper scratches.

References

1. Guo, D.M., Sun, Y.W., Jia, Z.Y., Methods, and research progress of high-performance manufacturing. *J. Mech. Eng.*, 50, 11, 119–134, 2014.
2. Heo, J.S., Koo, Y., Choi, S.S., Grinding characteristics of conventional and ELID methods in difficult-to-cut and hardened brittle materials. *J. Mater. Process. Technol.*, 155-156, 1196–1200, 2004.
3. Evans, C.J., Paul, E., Dornfeld, D., Lucca, D.A., Byrne, G., Tricard, M., Klocke, F., Material removal mechanisms in lapping and polishing. *CIRP Ann.*, 52, 2, 611–633, 2003.
4. Dubey, A.K., Shan, H.S., Jain, N.K., Analysis of surface roughness and out-of-roundness in the electro-chemical honing of internal cylinders. *Int. J. Adv. Manuf. Technol.*, 38, 5-6, 491–500, 2008.
5. Houshi, M.N., A Comprehensive review on magnetic abrasive finishing process. *Adv. Eng. Forum*, 18, 1–20, 2016.
6. Kumari, C. and Chak SK, A review on magnetically assisted abrasive finishing and their critical process parameters. *Manuf. Rev.*, 5, 13, 1–16, 2018.

7. Mori, Y., Ikawa, N., Sugiyama, K., Elastic emission machining. Stress field and fracture mechanism. *Technol. Rep. Osaka Univ.*, 28, 1430-1458, 525–532, 1978.

8. Spencer, E.G. and Schmidt, P.H., Ion-Beam Techniques for Device Fabrication. *J. Vac. Sci. Technol.*, 8, 5, 52–70, 1971.

9. Kim, T.W., Kang, D.M., Kwak, J.S., Application of magnetic abrasive polishing to composite materials. *J. Mech. Sci. Technol.*, 24, 5, 1029–1034, 2010.

10. Du, Z.W., Chen, Y., Zhou, K., Li, C., Research on the electrolytic-magnetic abrasive finishing of nickel-based superalloy GH4169. *Int. J. Adv. Manuf. Technol.*, 81, 5-8, 897–903, 2015.

11. Zou, Y., Xie, H.J., Dong, C.W., Wu, J.Z., Study on complex micro surface finishing of alumina ceramic by the magnetic abrasive finishing process using alternating magnetic field. *Int. J. Adv. Manuf. Technol.*, 97, 5-8, 2193–2202, 2018.

12. Vahdati, M., Sadeghinia, E., Shokuhfar, A., Magnetic assisted abrasion, a new method for nano level surface finishing. *Diffus. Defect. Forum*, 297-301, 402–407, 2010.

13. Chang, G.W., Yan, B.H., Hsu, R.T., Study on cylindrical magnetic abrasive finishing using unbonded magnetic abrasive. *Int. J. Mach. Tools Manuf.*, 42, 5, 575–583, 2002.

14. Shinmura, T., Takazawa, K., Hatano, E., Matsunaga, M., Matsuo, T., Study on magnetic abrasive finishing. *CIRP Ann.*, 39, 1, 325–328, 1990.

15. Hou, Z.B. and Komanduri, R., Magnetic field assisted finishing of ceramics—Part III: on the thermal aspects of magnetic abrasive finishing (MAF) of ceramic rollers. *J. Tribol.*, 120, 4, 660– 667, 1998.

16. Wang, A.C., Tsai, L., Lin, Y.C., Wu, K.L., Evaluation of rheological properties of gel abrasive in magnetic abrasive finishing. *Adv. Mech. Eng.*, 1–7, 2013.

17. Niknam, S.A., Davoodi, B., Davim, P., Songmene, V., Mechanical deburring, and edge-finishing processes for aluminum parts—a review. *Int. J. Adv. Manuf. Technol.*, 95, 1101–1125, 2018.

18. Zhou, Z., Sun, X., Yang, Y., Fu, Y., A Study on Using Magnetic Abrasive Finishing with a 6-Axis Robot to Polish the Internal Surface Finishing of Curved Tubes. *Coatings*, 13, 7, 1179, 2023.

19. Kumar, R. and Komma, V.R., Development of Experimental Setup and Parametric Study of Magnetic Abrasive Finishing Process of Plane Workpieces. *Nanoworld J.*, 9, S1, S220–S224, 2023.

20. Zhang, X., Zhao, X., Cheng, B. *et al.*, Design and processing behavior of large tubes with a rotating magnetic pole core-based magnetic abrasive finishing. *Int. J. Adv. Manuf. Technol.*, 130, 1709–1721, 2024.

21. Fox, M., Agrawal, K., Shinmura, T., Komanduri, R., Magnetic abrasive finishing of rollers. *CIRP Ann.*, 43, 1, 181–184, 1994.

22. Yan, B.H., Chang, G.W., Cheng, T.J., Hsu, R.T., Electrolytic magnetic abrasive finishing. *Int. J. Mach. Tools Manuf.*, 46, 13, 1355–1366, 2003.

23. Kanish, T.C., Narayanan, S., Kuppan, P., Ashok, S.D., Investigations on the finishing forces in magnetic field assisted abrasive finishing of SS316L. *Procedia Eng.*, 174, 611–620, 2017.

24. Ganguly, V., Schmitz, T., Graziano, A., Yamaguchi, H., Force measurement and analysis for magnetic field–assisted finishing. *J. Manuf. Sci. Eng.*, 135, 4, 041016, 2023.

25. Singh, R.K., Singh, D.K., Gangwar, S., Advances in magnetic abrasive finishing for futuristic requirements - a review. *Mater. Today Proc.*, 5, 9, 20455–20463, 2018.

26. Heng, L., Kim, Y.J., Mun, S.D., Review of superfinishing by the magnetic abrasive finishing process. *High Speed Mach.*, 3, 1, 42–55, 2017.

27. Yamaguchi, H. and Shinmura, T., Internal finishing process for alumina ceramic components by a magnetic field assisted finishing process. *Precis. Eng.*, 28, 2, 135–142, 2004.

28. Barman, A. and Das, M., Simulation, and experimental investigation of finishing forces in magnetic field assisted finishing process. *Mater. Manuf. Process*, 33, 11, 1223–1232, 2018.

29. Mulik, R.S. and Pandey, P.M., Ultrasonic assisted magnetic abrasive finishing of hardened AISI 52100 steel using unbonded SiC abrasive. *Int. J. Refract. Met. Hard Mater*, 29, 1, 68–77, 2011.

30. Zhou, K., Chen, Y., Du, Z.W., Niu, F.L., Surface integrity of titanium part by ultrasonic magnetic abrasive finishing. *Int. J. Adv. Manuf. Technol.*, 80, 5-8, 997–1005, 2015.

31. Zhang, G.X., Zhao, Y.G., Zhao, D.B., Yin, F.S., Zhao, Z.D., Preparation of white alumina spherical composite magnetic abrasive by gas atomization and rapid solidification. *Scr. Mater.*, 65, 5, 416–419, 2011.

32. Li, W.H., Li, X.H., Yang, S.Q., Li, W.D., A newly developed media for magnetic abrasive finishing process: material removal behavior and finishing performance. *J. Mater. Process. Technol.*, 260, 20–29, 2018.

33. Chen, Y., Song, Q.H., Wang, X., Study on the characteristics of simply mixed the magnetic abrasive particles. *Adv. Mater. Res.*, 24-25, 133–138, 2007.

34. Ahn, B.W. and Lee, S.H., Run-to-run process control of magnetic abrasive finishing using bonded abrasive particles. *Proc. Inst. Mech. Eng. B J. Eng. Manuf*, 226, 12, 1963–1975, 2012.

35. Liao, G.B., Zhang, M.M., Li, Y.J., Liu, Z.Q., Chen, Y., Preparation of magnetic abrasive by sintering method finishing by sintering method. *Key Eng. Mater.*, 487, 273–277, 2011.

36. Chen, Y., Zhang, M.M., Liu, Z.Q., Study on sintering process of magnetic abrasive particles. *Adv. Mater. Res.*, 337, 163–167, 2011.

37. Chen, H.L., Li, W.H., Yang, S.Q., Yang, S.C., Research of magnetic abrasive prepared by hot pressing sintering process, in: *2010 5th IEEE Conference on Industrial Electronics and Applications*, Taichung, pp. 776–778, 2010.

38. Zhao, Z.D., Huang, Y.H., Zhao, Y.G., Preparation of magnetic abrasive by sintering method. *Adv. Mater. Res.*, 135, 382–387, 2010.

39. Hu, B. and Lu, Y.P., Study on preparation technology and finishing performance of magnetic abrasive grain. *Adv. Mater. Res.*, 452-453, 637–641, 2012.

40. Gao, Y.G., Zhao, Y.G., Zhang, G.G., Preparation of Al2O3 magnetic abrasive by gas-solid two-phase double-stage atomization and rapid solidification. *Mater. Lett.*, 215, 300–304, 2018.

41. Fan, Z.H., Tian, Y.B., Zhou, Q., Shi, C., Enhanced magnetic abrasive finishing of Ti–6Al–4 V using shear thickening fluids additives. *Precis. Eng.*, 64, 300–306, 2020.

42. Kanish, T.C., Narayanan, S., Kuppan, P., Denis, A.S., Investigations on wear behavior of magnetic field assisted abrasive finished SS316L material. *Mater. Today Proc.*, 5, 5, 12734–12743, 2018.

43. Kwak, J.S., Enhanced magnetic abrasive polishing of nonferrous metals utilizing a permanent magnet. *Int. J. Mach. Tools Manuf.*, 49, 7-8, 613–618, 2009.

44. Kala, P., Pandey, P.M., Verma, G.C., Sharma, V., Understanding flexible abrasive brush behavior for double diskmagnetic abrasive finishing based on force signature. *J. Manuf. Process*, 28, 3, 442–448, 2017.

45. Sato, T., Kum, C.W., Venkatesh, V.C., Rapid magnetorheological finishing of ti-6al-4v for aerospace components. *Int. J. Nanomanuf.*, 9, 5/6, 2013.

46. Fan, Z.H., Tian, Y.B., Liu, Z.Q., Shi, C., Zhao, Y.G., Investigation of a novel finishing tool in magnetic field assisted finishing for titanium alloy Ti-6Al-4 V. *J. Manuf. Process*, 43, 74–82, 2019.

47. Tian, Y.B., Shi, C., Fan, Z.H., Zhou, Q., Experimental investigations on magnetic abrasive finishing of ti-6al-4v using a multiple pole-tip finishing tool. *Int. J. Adv. Manuf. Technol.*, 106, 3071–3080, 2020.

48. Yang, S.Q. and Li, W.H., *Surface finishing theory and new technology*, Heidelberg, Berlin, 2018.

49. Yamaguchi, H. and Shinmura, T., Study on a new internal finishing process by the application of magnetic abrasive machining. *J. Jpn. Soc. Precis. Eng.*, 62, 11, 1617–1621, 1996.

50. Shinmura, T. and Yamaguchi, H., Study on a new internal finishing process by the application of magnetic abrasive machining internal finishing of stainless-steel tube and clean gas bomb. *JSME Int. J. Ser. C, Dynamics, Control, Robotics, Des. Manuf.*, 38, 4, 798–804, 1995.

51. Yamaguchi, H. and Shinmura, T., Study of the surface modification resulting from an internal magnetic abrasive finishing process. *Wear*, 225-229, 246–255, 1999.

52. Yamaguchi, H., Shinmura, T., Takenaga, M., Development of a new precision internal machining process using an alternating magnetic field. *Precis. Eng.*, 27, 1, 51–58, 2003.

53. Sato, T., Yamaguchi, H., Shinmura, T., Study of internal magnetic field assisted finishing for copper tubes with MRF (Magnetorheological Fluid)-based Slurry. *Key Eng. Mater.*, 329, 249– 254, 2007.

54. Singh, P., Samra, P.S., Singh, L., Internal finishing of cylindrical pipes using sintered magnetic abrasive. *Int. J. Eng. Sci. Technol.*, 3, 5474–5753, 2011.

55. Kang, J. and Yamaguchi, H., Internal finishing of capillary tubes by magnetic abrasive finishing using a multiple pole-tip system. *Precis. Eng.*, 36, 3, 510–516, 2012.

56. Yan, B.H., Chang, G.W., Cheng, T.J., Hsu, R.T., Electrolytic magnetic abrasive finishing. *Int. J. Mach. Tools Manuf.*, 43, 13, 1355–1366, 2003.

57. El-Taweel, T.A., Modelling and analysis of hybrid electrochemical turning-magnetic abrasive finishing of 6061 Al/Al2O3 composite. *Int. J. Adv. Manuf. Technol.*, 37, 7–8, 705–714, 2008.

58. Natsume, M., Shinmura, T., Sakaguchi, K., Study of magnetic abrasive machining by use of work vibration system (characteristics of plane finishing and application to the inside finishing of groove). *Trans. Jpn. Soc. Mech. Eng.*, 64, 4447–4452, 1998.

59. Yin, S. and Shinmura, T., Vertical vibration-assisted magnetic abrasive finishing and deburring for magnesium alloy. *Int. J. Mach. Tools Manuf.*, 44, 12–13, 1297–1303, 2004.

60. Yin, S. and Shinmura, T., A comparative study: polishing characteristics and its mechanisms of three vibration modes in vibration-assisted magnetic abrasive polishing. *Int. J. Mach. Tools Manuf.*, 44, 4, 383–390, 2004.

61. Lee, Y.H., Wu, K.L., Jhou, J.H., Tsai, Y.H., Yan, B.H., Two-dimensional vibration-assisted magnetic abrasive finishing of stainless steel SUS304. *Int. J. Adv. Manuf. Technol.*, 69, 2723–2733, 2013.

62. Judal, K.B., Yadava, V., Pathak, D., Experimental investigation of vibration assisted cylindrical– magnetic

abrasive finishing of aluminum workpiece. *Mater. Manuf. Processes*, 28, 11, 1196– 1202, 2013.

Note

*Corresponding author: sandip.sandip.kunar@gmail.com

29
Experimental Analysis of EDM Process While Machining Ti-VT20 Alloy

Pritam Pain[1]*, Goutam Kumar Bose[1], Dipankar Bose[2] and Sourav Giri[1]
[1]*Department of Mechanical Engineering, Haldia Institute of Technology, Haldia, India*
[2]*Department of Mechanical Engineering, NITTTR, Kolkata, India*

Abstract

In this experimental investigation, we primarily investigate the utilization of VT20, a titanium alloy that is frequently used in the production of aviation and automotive equipment. This material is well known for its extraordinary strength and hardness, as well as its outstanding resistance to high temperatures. Because it works well on these kinds of workpieces, electric discharge machining (EDM), a well-liked non-traditional machining technique, is used to shape this material. This study's main objective is to use an artificial neural network (ANN) to validate experimental data. The VT20 work material is machined while taking into account several control factors. These consist of flow pressure, charge time (Ton), discharge time (Toff), and current (Amp). The study also looks at several performance measures, including overcut, material removal rate, tool wear rate, and surface roughness (Ra). We use a genetic algorithm (GA) to do a multi-objective optimization because these performance metrics frequently contradict. This strategy aids in bringing the conflicting goals together. Fuzzy grey relation analysis (GRA) is then used to further improve the GA results. The output data from the GA is integrated in this stage to provide a unique, optimal parametric combination. This all-encompassing method seeks to improve the precision and efficiency of machining the VT20 titanium alloy using EDM.

***Keywords*:** EDM, Ti Alloy VT20, ANN, ANOVA, GA, fuzzy GRA

29.1 Introduction

The aerospace industry places a high value on titanium goods because of its remarkable strength-to-weight ratio, durability to high temperatures, and ability to resist corrosion. These characteristics make them perfect for producing jet engine blocks, other structural parts, and aircraft components. But titanium is very hard to machine, thus non-traditional processes like electrical discharge machining (EDM) are being used. Titanium and other high-temperature strength resistance (HTSR) materials can be machined using an EDM method. In this technique, a spark discharge takes place when both the conductive work material and an electrically conducting electrode are submerged in dielectric fluid. As the conductive tool, functioning as a cathode, and the work material, functioning as an anode, produce sparks in the tiny space between them, the material is removed. The substance is instantly melted and vaporized by the high temperatures that follow, and the dielectric fluid then washes it away. The schematic diagram of the electric discharge machining process has been shown in Figure 29.1. During the EDM process, the kind of dielectric fluid that is utilized has a significant impact on machining quality and efficiency. High dielectric strength, low tackiness, adequate wet capacity, and a high-level of flash point are characteristics of ideal dielectric fluids. They should also release no noxious gases or smells and be safe for the environment. Hydrocarbon fluids, silicon-based oils, kerosene oil, de-ionized oil, and water with glycol are examples of commonly used fluids. With the development of new technologies, there is an increasing need for materials and methods that offer particular qualities, such as enhanced specific strength, high wear resistance,

and a superior strength-to-weight ratio at an affordable price. Setting the ideal manufacturing process parameters to produce the desired product features and improving manufacturing system performance with the resources at hand provide problems for researchers. Additionally, they are working to create user-friendly, reasonably priced surface modification technologies that will enhance the machined surfaces' mechanical characteristics. The surface condition obtained from machining operations is influenced by surface modification, which arises from the thermal, mechanical, and chemical effects of manufacturing processes. Because the materials used in die and mold-making are very hard and production numbers are limited, EDM is especially well-liked in the automobile, electronics, and aerospace industries. The selection of dielectric in EDM has a major impact on tool life, productivity, production costs, and workpiece surface quality. Performance metrics including material removal rate (MRR), overcut (OC), surface roughness (Ra) and tool wear rate (TWR) can be controlled by adjusting various parameters like voltage, flow pressure (F/Press), pulse on time (Ton), and pulse off time (Toff) [1].

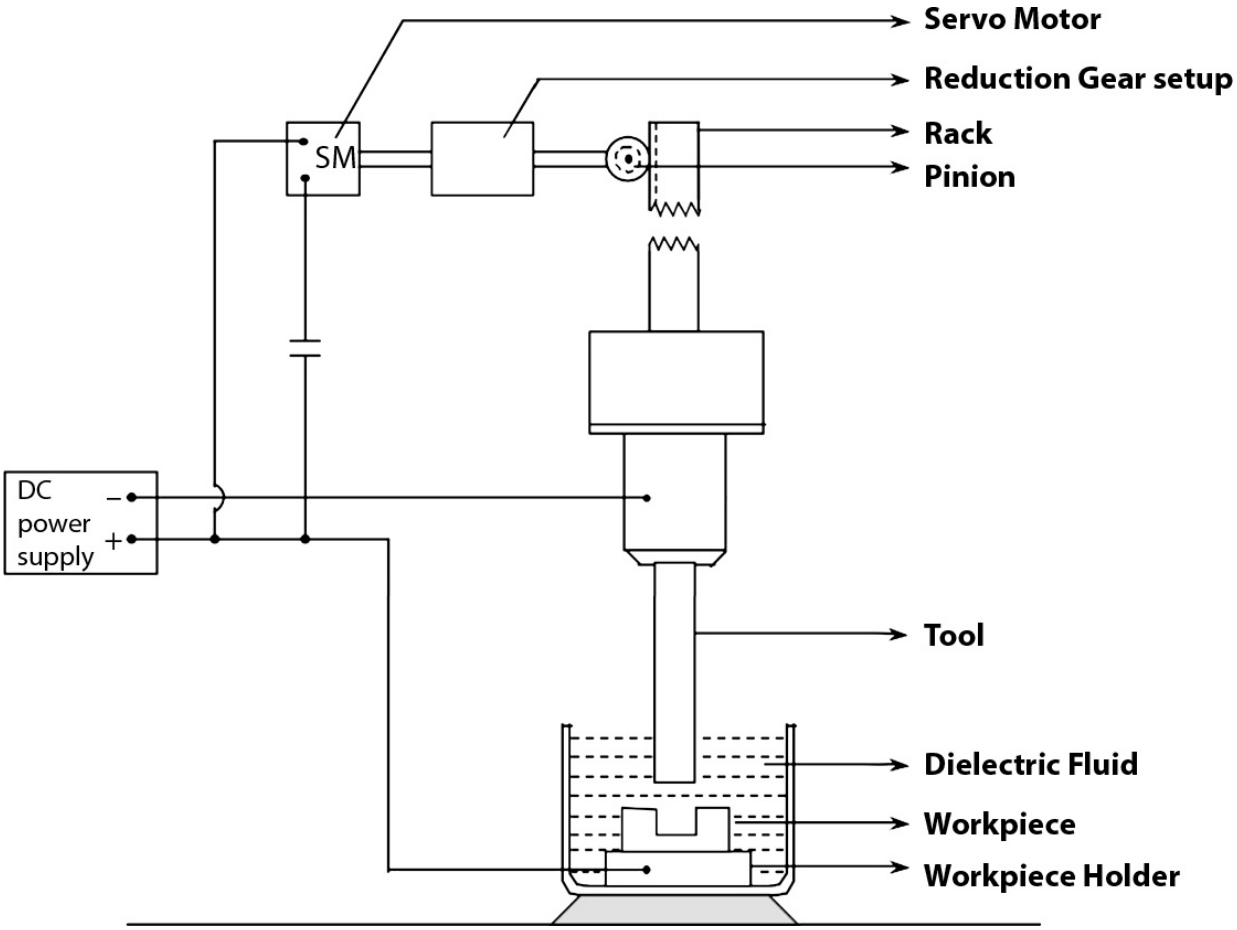


Figure 29.1 Schematic diagram of the electric discharge machining process.

A brief literature review is provided here based on the various researchers' previous research work. An electrode made of copper tungsten (CCW) is used, along with high peak currents (Ip) and pulse on time (pulse duration) to examine the effectiveness of electrical discharge machining on Inconel 718 in terms of MRR, EWR and Ra [2]. By utilizing the Taguchi technique [3] and cutting AISI D3 material with a copper electrode, die-sinking EDM variables such as charging current (Ton), discharging (Toff), ultimate current (Ip), and fluid pressure could be examined in relation to material removal rate

and electrode wear rate. While milling Ti6Al4V using an EDM method, the impacts of various control parameters, such as current, pulse on time, and pulse off time, are investigated in order to gain a better understanding of the surface roughness phenomenon [4]. The effects of using different dielectrics, such as gaseous, liquid, and additive mixed dielectrics, on the pace at which materials are removed from the workpiece and the rate at which tools wear out, are investigated [5]. To maximize MRR and reduce EWR, the copper electrode is used to manufacture stainless steel 316 as the workpiece through an EDM machine with control parameters such as current, pulse on time, pulse off time, and fluid pressure [6]. To explore the impact of control factors such as voltage, material removal time on the recast layer, micro-hardness, and subsequent effects on the chemical composition of the machined sample, the Ti6Al4V sheet is machined using a micro-EDM method [7]. Employing Inconel 718 as the workpiece and copper electrodes, the EDM control parameters current, pulse on-time, and pulse off time are selected to investigate the effects on MRR, TWR, and surface quality, respectively [8]. The most recent developments in the EDM process and modelling methodologies are described, together with current research trends [9]. In order to examine the microhardness and surface roughness of the workpiece material, Ti-6Al-4V alloy is processed by EDM using five distinct control parameters: pulse on time, pulse off time, current, and voltage [10]. The variable parameters' impacts on the MRR and TWR while machining stainless steel 410 with a copper electrode in an EDM are optimized [11]. The dying using a copper tungsten electrode and varying parameters including discharging current, charging current and electrode diameter, EDM is utilized to mill Ti-6Al-4V and investigate the effects on MRR and TWR [12]. For machining of Ti-6Al4V with a graphite electrode, the parameters are optimized using EDM to analyze the surface characteristics and improve the MRR [13]. To study copper electrode wear, an experiment was conducted using D3 steel and the EDM technique's process parameters, such as current, pulse on time, and pulse off time [14]. An experimental examination is conducted to ascertain the process outcomes, including MRR, surface roughness, and TWR, when Span 20 surfactant and graphite power are added as additives to the dielectric fluid during EDM machining on a titanium alloy material [15]. With the use of the Taguchi methodology, an experimental investigation is carried out for elevated-carbon elevated-chromium bitter job instrument for making stronger D2 [16]. For the purpose of evaluating reactions like MRR, EWR, and surface quality, optimization by grey relational analysis (GRA) is carried out when milling Ti-6Al-4V with EDM [17]. Grey relational analysis is used in titanium super alloys with copper electrodes to evaluate the multi-objective optimization of MRR and TWR using a Taguchi-based experimental design with the control parameters peak current, pulse on time, pulse off time, and tool lift time [18]. As an AISI18 workpiece is being machined with a copper tool in an EDM, research is being done to find the best parametric combination with a pulse on time, voltage, and current as well as to ascertain how the parameters affect the responses such as the MRR, TWR, and surface roughness [19]. To detect changes in the hole depth, EDM is applied to a Ti-6Al-4V workpiece using copper and graphite electrodes and variable parameters including gap voltage, peak current, pulse on time, and pulse off time [20]. Through the use of various electrode materials and performance metrics including MRR, TWR, and surface quality, the EDM process is used to determine the parametric analysis [21]. Through modelling in an artificial neural network (ANN), the impacts of input factors such as discharge current, duty cycle, voltage, pulse on time, and duty cycle on the MRR in the EDM process are evaluated [22]. Adjustments are made to input parameters like maximum current, gap voltage, discharge current, charging current, and flushing speed to see how these affect performance measures like MRR, TWR, and surface finish. The experimental data are then trained by using the backpropagation algorithm of ANN [23]. Multi-objective optimization using GRA is used to ascertain how the input parameters of the EDM process, such as current, voltage, and duty cycle, affect MRR, TWR, and surface roughness [24]. Application of the genetic algorithm (GA) and response surface

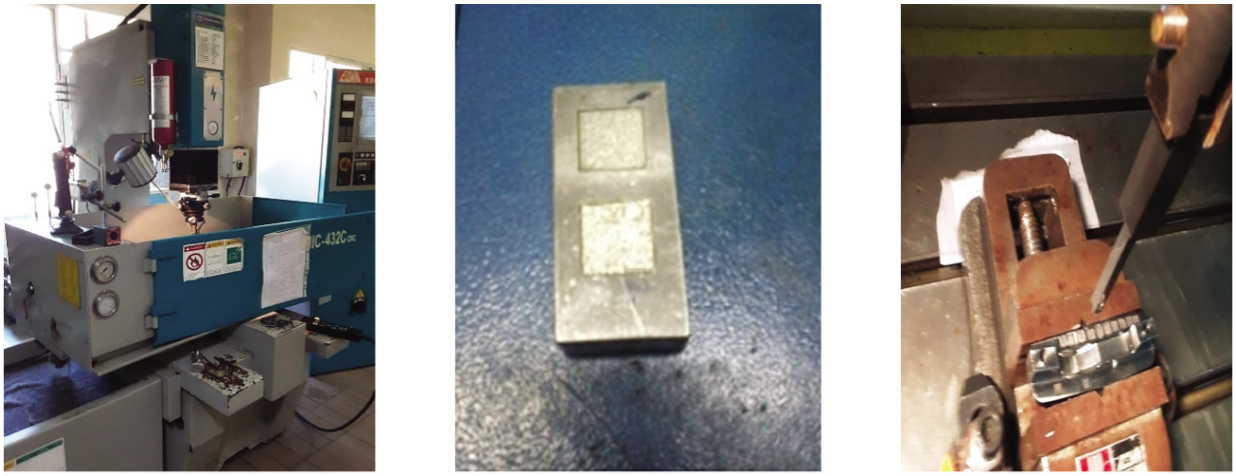
methodology against performance metrics like MRR and surface roughness allows for optimization of the various process parameters of the EDM process [25]. To analyze the impact on the responses such as MRR, TWR, OC, and SR, respectively, variable parameters are optimized by using GRA in the EDM process while milling Al-10 % [26]. With electrodes made of copper, brass, and graphite, the EDM process is used to machine the AISI P20, HE20, C45, and EN47 work materials. The input parameters discharge current, pulse on time, and pulse off time are taken into account to assess their effects on the outputs MRR and surface roughness. Multi-objective optimization is then carried out using a GA [27]. Modification of precipitation utilizing a copper tungsten electrode, hardened stainless steel is produced while taking into account various parameters such as charging current, highest current, discharging current and time to lift tool to evaluate performance metrics like MRR and Surface roughness. Optimization is then carried out using an ANN backpropagation algorithm.

This study intends to explore the unique characteristics of the Ti Alloy VT20 work material in relation to the EDM technique—a combination that has not been extensively studied previously. The study highlights the need for additional comprehensive research in this specific field of EDM by employing ANN for data validation, testing, and training.

29.2 Experimental Investigation

29.2.1 Machining Setup

The 432C computer numerical control electric discharge machining (CNC EDM) machine, made by Electronica India, is used in the current investigation. This device has a servo control system and uses electrodes with positive polarity. Commercial-grade EDM 30 oils are employed as the dielectric medium in the experiments. A copper tool is used in the machining process to enable external lateral cleansing at a pressure of 0.2 kg/cm². A machining table with a work-holding fixture, a pump, a dielectric chamber, and an operational chamber make up the machine’s configuration. It also features a servo mechanism and tool holder that are intended to control the movement of the X and Y-axis table and to keep a constant distance between the tool and the workpiece. A control panel and a generator are also included in the system. The EDM machining setup is shown in Figure 29.2(a), and the post-machined workpiece material and machining chamber are shown in Figure 29.2(b) and 29.2(c), respectively. Titanium VT20, a sturdy grade of titanium with a Brinell hardness (HB 10-1) range from 255 to 341 MPa, was chosen as the workpiece material for this investigation. Notably, the engine components of the Sukhoi-30 MK Fighter aircraft employ this material.



(a) (b) (c)

Figure 29.2 (a) EDM machining setup. (b) Workpiece material after machining. (c) Machining chamber.

29.2.2 Machining Parameters

Table 29.1 lists the control parameters for this EDM experiment: pulse time-on, discharge current (measured in amperes), flow pressure, and a constant waiting period (called pulse time-off). It is significant to note that during the experiment, constant amounts of other potential influencing parameters were maintained, including spark gap, duty cycle, flushing pressure, and tool material. Table 29.2 shows the L9 orthogonal array where the control parameters are varied simultaneously rather than one at a time.

29.2.3 Performance Measures

Surface roughness is measured in units of Ra (micrometers) using a stylus-type profilometer called the Talysurf (Taylor Hobson Surtronic 3+). The weight difference of each sample before and after machining is measured in grammes, and then divided by the machining time in minutes to determine the MRR and the TWR. The Mettler Toledo electronic scale (Model No. AG 285), which has a precision of 0.02 mg, is used for this measurement. A toolmaker's microscope is also utilized to determine the overcut (OC). With the aid of the MATLAB R2015a program, numerous graphs and computations are produced.

Table 29.1 Control parameters and their levels.

Sl. no.	Parameters	Units	Symbols	Level 1	Level 2	Level 3
1	Pulse on time	µs	Ton	100	200	300
2	Pulse off time	µs	Toff	15	30	45
3	Current	Ampere	Amp	4	8	12
4	Flow pressure	kg/cm^2	F/Press	0.1	0.2	0.3

Table 29.2 Control parameters and their levels.

Combination no	Ton	Toff	Current	F/Press
1	100	15	4	0.1
2	100	30	8	0.2
3	100	45	12	0.3
4	200	15	8	0.3
5	200	30	12	0.1
6	200	45	4	0.2
7	300	15	12	0.2
8	300	30	4	0.3
9	300	45	8	0.1

29.3 Experimental Result Analysis

29.3.1 Analysis of the Result Using ANN

MatLab R2015a is the analytical program used for the analysis of the findings. The Dividerand function is used in this method to divide the data. The mean squared error (MSE) is the performance indicator used to assess the performance following training. Figure 29.3 shows the Simulink model that takes into account four control parameters and includes responses. A total of 27 trial runs are taken into consideration for training the suggested ANN model. After the biases and weights are initialized, the network starts to be trained. It is mainly governing by these mathematical equations. The total input to each individual neuron in the buried layer is shown in Equation 29.1.

$$I_i = \sum_{i=1}^{n} W_i X_i \tag{29.1}$$

Generally, until the node's activation level surpasses a threshold value, no output will be generated. A common function used to describe a neuron's output is the sigmoid function, as illustrated in Equation 29.2.

$$O_i = f(\mathrm{I}_i) = \frac{1}{1+e^{-I_i}} \tag{29.2}$$

In neural networks, the backpropagation technique—which makes use of the backward chain rule—is used to compute the gradient and Jacobian. This method is crucial for ascertaining a network's outcomes. The MSE is commonly used by ANNs to quantify the difference between the expected and actual output of the network. The epoch method is a technique used in training that modifies the weights and biases of the training vectors (both input and/or target). The method is initially configured in every training scenario to end after a maximum of 1000 iterations. The performance of the network is optimized with the aid of this iterative method. Regression curves are frequently used to graphically depict the relationship between the targets and the network's output. Four separate graphs are usually provided in analyses utilizing this data: one for training, one for validation, one for testing, and one for the entire data. The ideal situation, in which the outputs precisely match the targets, is symbolized by the discontinuous line seen in these graphs.

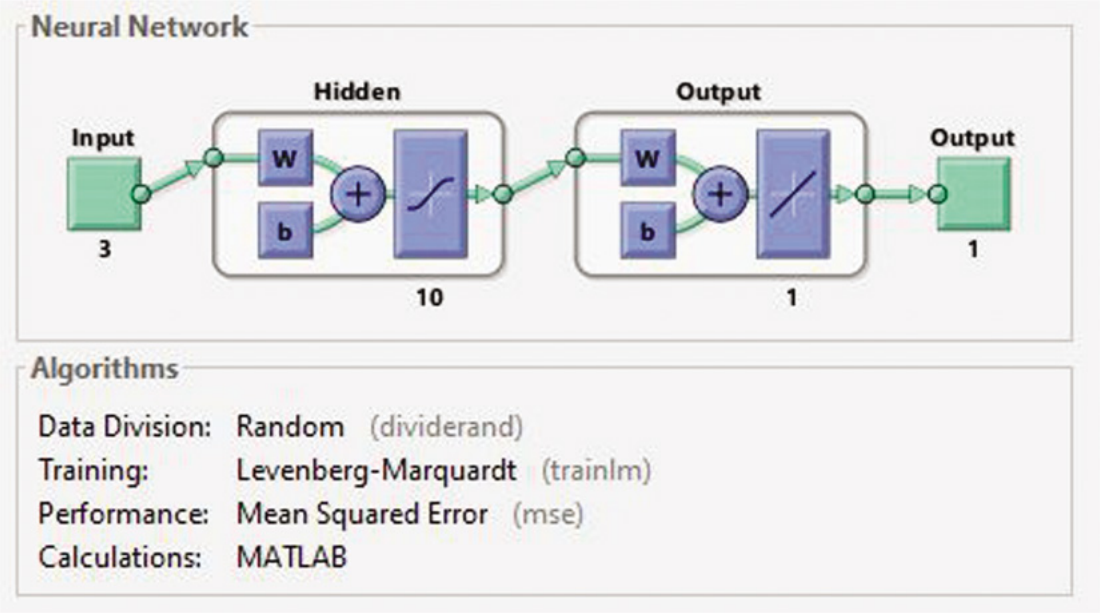


Figure 29.3 Simulink diagram.

Calculating the gradient and Jacobian makes use of the backpropagation technique. The backward chain rule is employed in this backpropagation technique to calculate the network results. The ANN model uses MSE between the desired outcome and the network output. The training (input and/or target) vectors' new weights and biases are found using the epoch method. The training for each scenario is first configured to end after a maximum of 1000 iterations. A regression curve can be used to show how the network's output and the targets interact. The training, validation, testing, and total data are represented by the four graphs. Every graph has a discontinuous line that represents the real outcome when outputs equal targets. The data is best fitted by a continuous linear regression line. The degree of correlation between the outputs and the targets is shown by the R-value. A distinct linear relationship between the targets and the outputs is evident when R equals 1 [1].

(i) Analysis to Maximize MRR

The dataset was partitioned in this computation so that 70% was set aside for training, 15% for validation, and 15% for testing. When the MSE stabilized after 141 iterations, the training procedure was stopped. After the training, the gradient was seen to reach 6.05×10^{-8}, exceeding the predetermined threshold of less than 1.00×10^{-7}. The term "number of validation checks" describes a series of iterations in which the validation performance did not increase. The default setting was for the training to end if this count reached 6. In this case, though, there were just four successive validation checks. The Mean Reciprocal Rank (MRR) performance evolution during the neural network's training is shown in Figure 29.4.

The Mean squared error (MSE) measure indicates that the best validation performance, as illustrated in Figure 29.5, occurs at epoch 137, with the lowest prediction error of 2.545×10^{-10}.

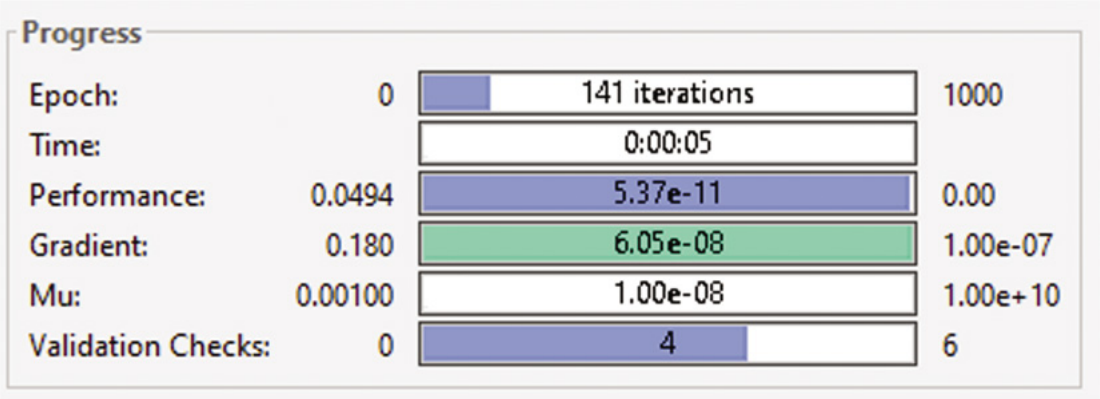


Figure 29.4 Training performance progress for MRR.

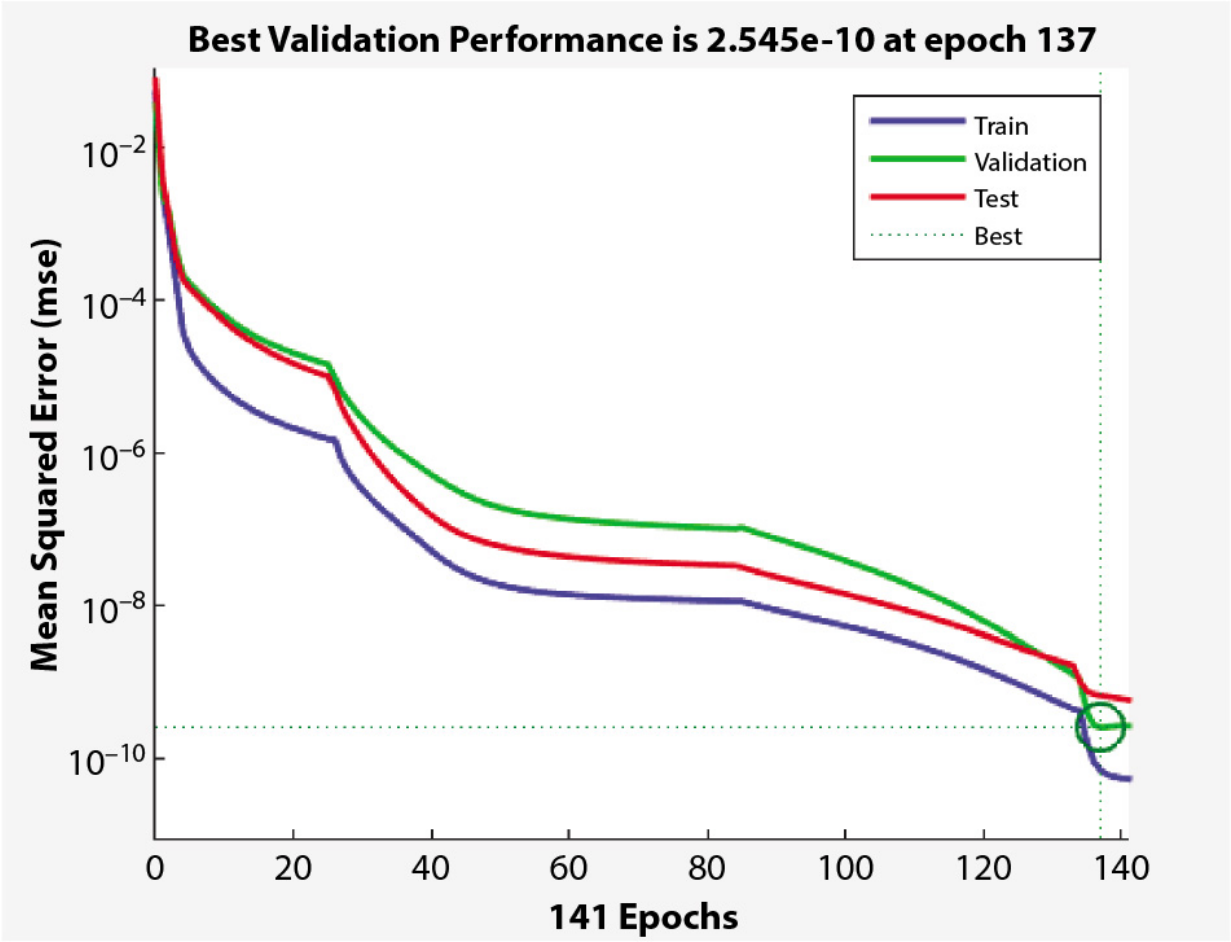


Figure 29.5 Performance plot for MRR.

Figure 29.5 displays the iteration with the lowest validation performance. There were completed 137 iterations before the training ended. This number does not point to any significant issues with the training procedure. The alignment of the test and validation curves is near.

Figure 29.6 shows that the R-value for training, validation, and testing is each 1, resulting in an overall R-value of 1. The training data indicates a good fit, as seen by the testing and validation results' R values of 1.

(ii) Analyses to Reduce TWR

Three distinct data splits were used in the computing process: 15% for validation, 15% for testing, and 70% for training. When the desired mean square error was reached after 67 iterations, the training was terminated. If the gradient's magnitude is less than $1.00x10^{-7}$, the training procedure is intended to terminate. The gradient in this instance was calculated to be $2.83x10^{-7}$. The amount of validation checks, or successive iterations where there is no progress in validation performance, is a crucial component of this procedure. The default value for this number is six, which will cause the training to end. Six times in a row, the validation checks in this case were satisfied. The training performance of the neural network for the TWR is shown in Figure 29.7.

The best validation performance was attained at epoch 61 and is 6.7703×10^{-7}, as indicated in Figure 29.8 and assessed using MSE.

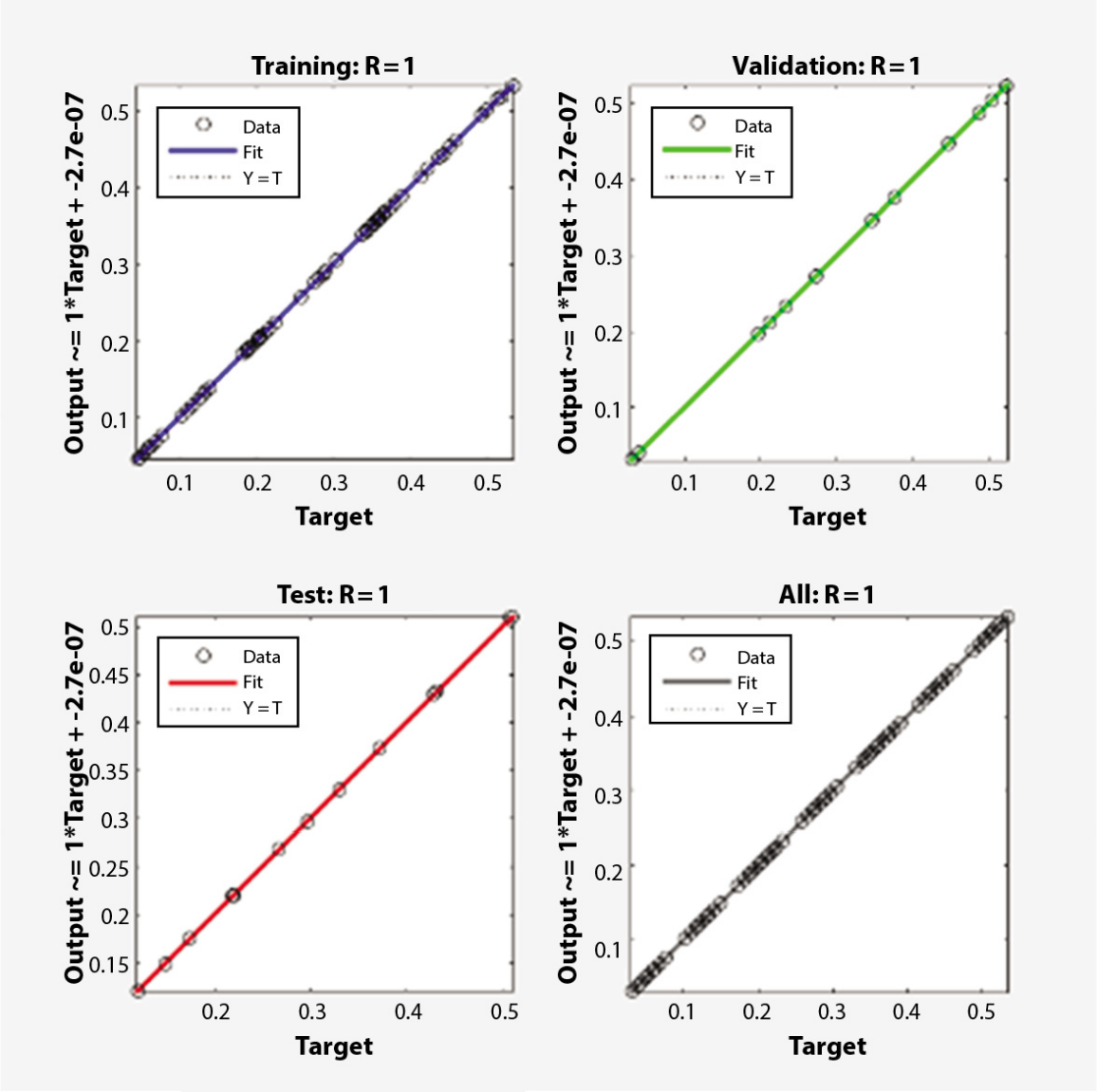


Figure 29.6 Regression plot of MRR.

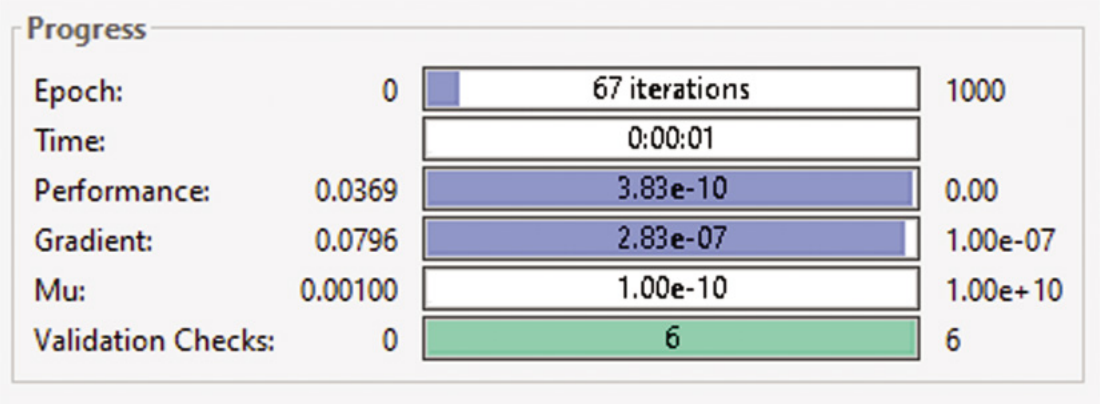


Figure 29.7 Training performance progress for TWR.

The MSE in Figure 29.8 indicates that the best validation performance was attained at

epoch 61, with a value of 6.7703×10^{-7}. Figure 29.6 displays the iteration with the lowest validation performance. After 61 cycles, the training procedure was finished, and this length of time does not suggest that there were any serious issues with the training. A consistent performance is also shown by the near alignment of the test and validation curves.

The correlation coefficients for training, validation, and testing are 1, 0.99995, and 0.99992, respectively, as illustrated in Figure 29.9. Given that the test and validation findings have R values larger than 0.9, the overall correlation coefficient (R) is high. This shows that the model's predictions and the training data have a good fit.

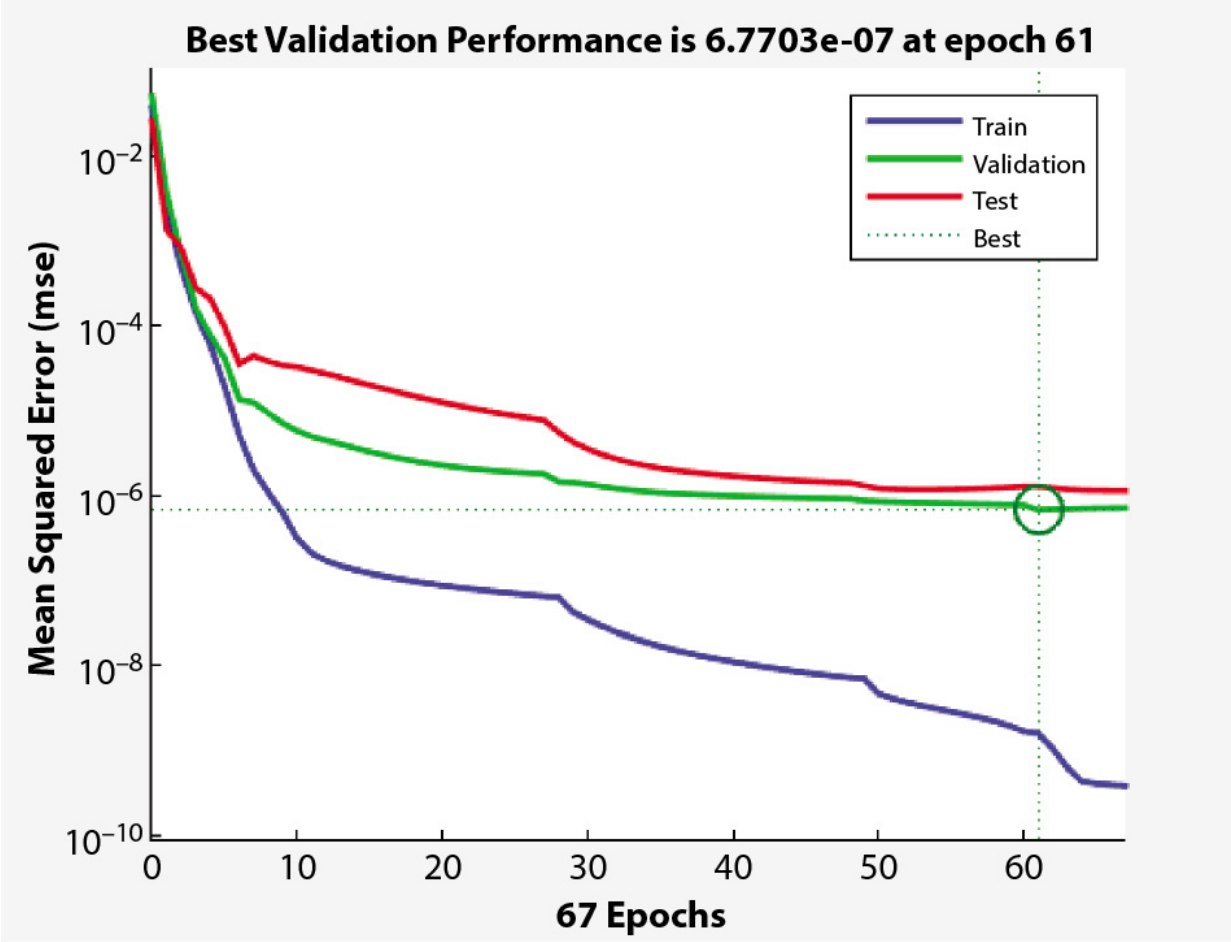


Figure 29.8 Performance plot for TWR.

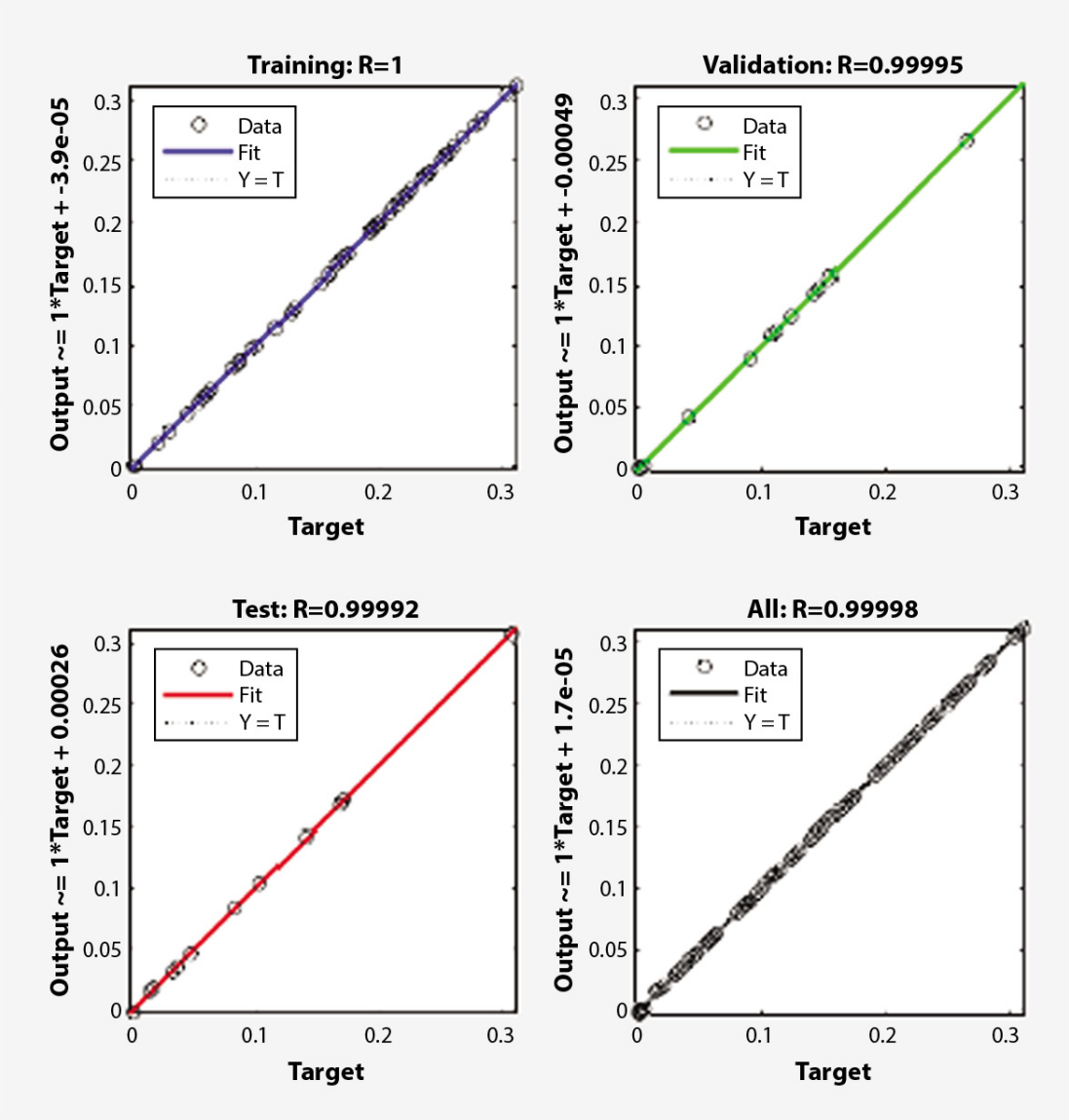


Figure 29.9 Regression plot of TWR.

(iii) Analysis to Reduce Ra

The dataset in this case is split as follows: 30% is used for calculations, 30% is used for validation, 30% is used for testing, and 70% is used for training. After 1000 cycles, the training was stopped as soon as the mean square error was reached. If the gradient magnitude drops below 1.00×10^{-7}, the training will likewise end. The observed gradient in this instance is 5.18×10^{-7}. The quantity of validation checks indicates how many iterations there have been without any increase in validation performance. If this count hits 6, which is the default option, training will end. The improvement in Ra's neural network training performance is shown in Figure 29.10.

The highest validation performance, as determined by MSE and shown in Figure 29.11, was attained at epoch 1000 and is 4.5502×10^{-9}.

The iteration that had the lowest validation performance during a training process with a total of 1000 iterations is shown in Figure 29.11. This figure, which shows which iteration

performed the worst, does not point to any significant issues with the training procedure. This figure's test and validation curves are notably well aligned.

In addition, Figure 29.12 shows that the R-value for testing, validation, and training is 1. The fact that the test and validation results both had this flawless R-value of 1 shows that the training data had an exceptionally good match across all datasets.

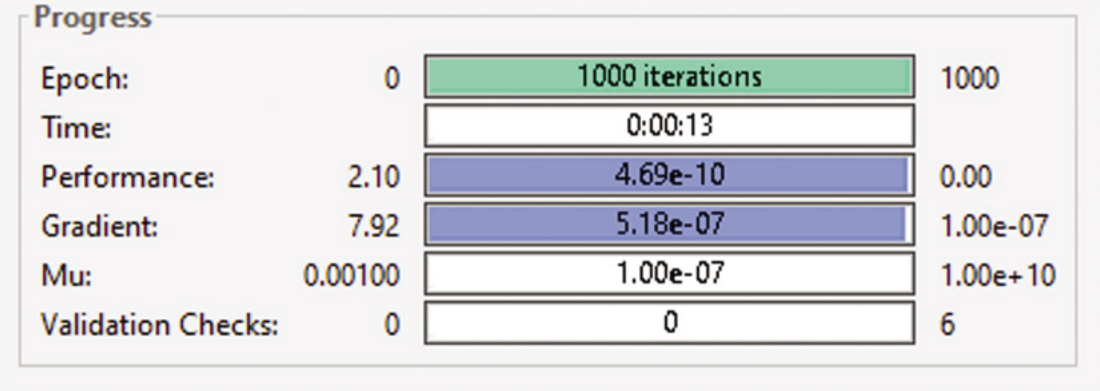


Figure 29.10 Training performance progress for Ra.

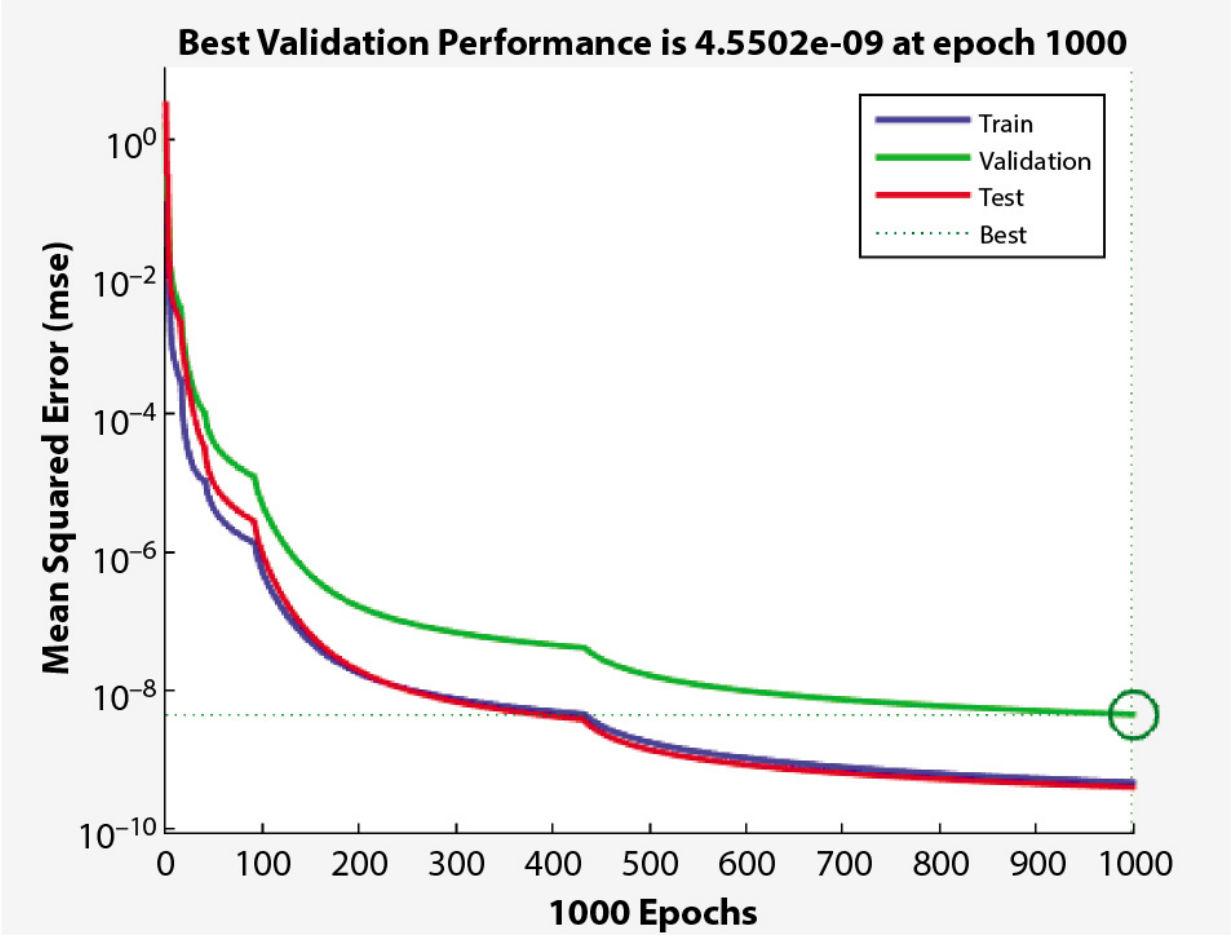


Figure 29.11 Performance plot for Ra.

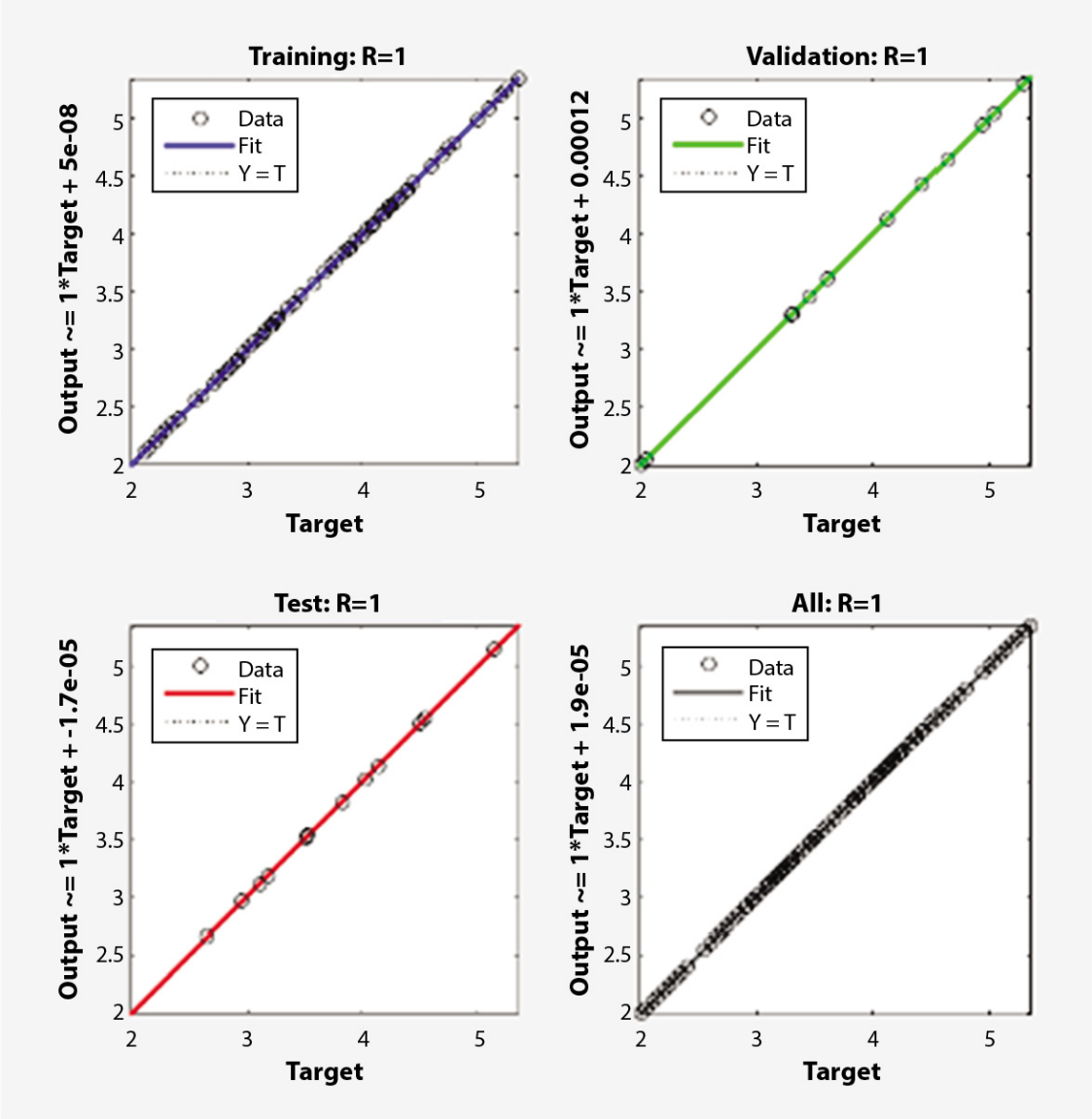


Figure 29.12 Regression plot of Ra.

(iv) Analysis to Minimize OC

In this case, 70% of the input is used for learning, 15% for validation, and 15% for testing during the computation process. After 40 iterations, the training was stopped as soon as the mean square error was reached. If the gradient's magnitude is less than 1.00×10^{-7}, the training procedure is meant to terminate. In this instance, a 9.30×10^{-8} gradient was noted. The quantity of validation checks is a reflection of the consecutive iterations in which validation performance has not improved. If this count hits 6, which is the default setting, the training will end. The training efficacy of the OC neural network is shown as a progression in Figure 29.13.

As Figure 29.14 illustrates, the best validation performance was attained at epoch 40, as evidenced by an MSE of 5.0055×10^{-9}.

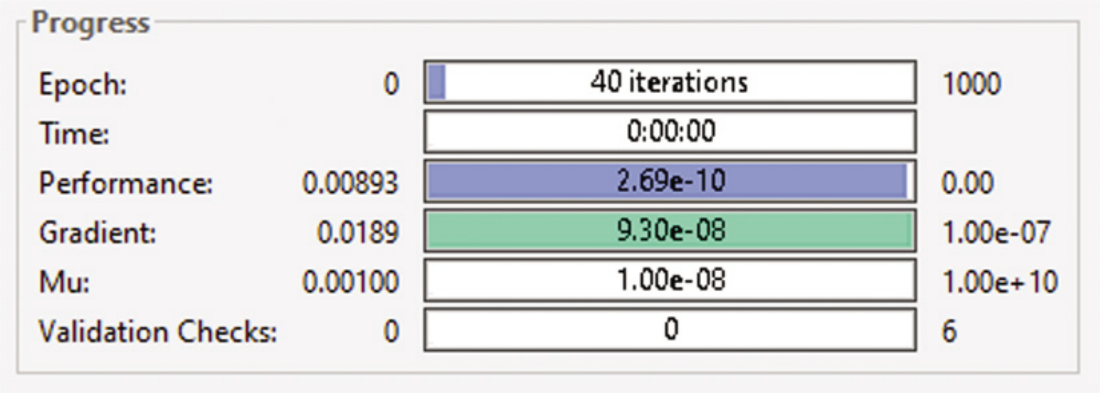


Figure 29.13 Training performance progress for OC.

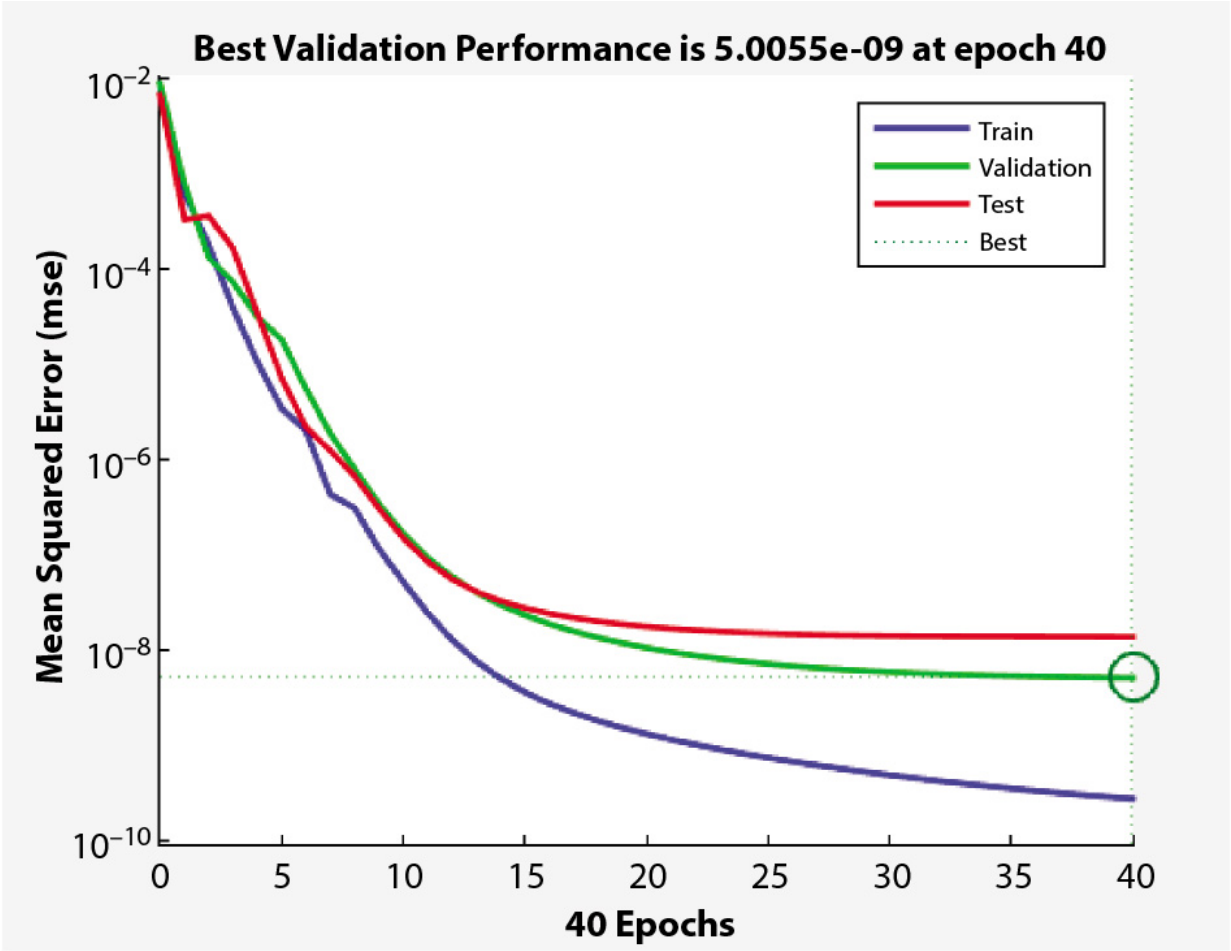


Figure 29.14 Performance plot for OC.

Out of 40 iterations, the iteration with the lowest validation performance is shown in Figure 29.14. It appears from this iteration count that there were no major problems encountered during the training process. There is a strong alignment between the test and validation curves. For training, validation, and testing, the R-value (a measure of correlation) in Figure 29.15 is equal to one, resulting in an overall R-value of 1. A strong correlation in the training data is indicated by the perfect R-value of 1 in the test and validation findings.

29.3.2 Result Analysis Using GA

The function must undergo two transformations in order to determine the best answer. The first transformation converts the initial constrained function into an unconstraint function using the penalty function, as follows [11]:

$$\text{Minimize} \quad f(\mathrm{X}) + R\sum_{i=1}^{n}\Phi\left(g_i(\mathrm{X})\right) \tag{29.3}$$

$$\text{Subjected to } x_j^{(l)} \le x_j \le x_j^{(u)},\ j = 1,2,....,n \tag{29.4}$$

Where Φ is a penalty function express as:

$$\Phi = \left(Z\right) = \left\langle Z \right\rangle^2 \tag{29.5}$$

$$\text{Where,} \quad \left\langle Z \right\rangle = \begin{cases} Z & if \quad Z > 0 \\ 0 & if \quad Z \le 0 \end{cases} \tag{29.6}$$

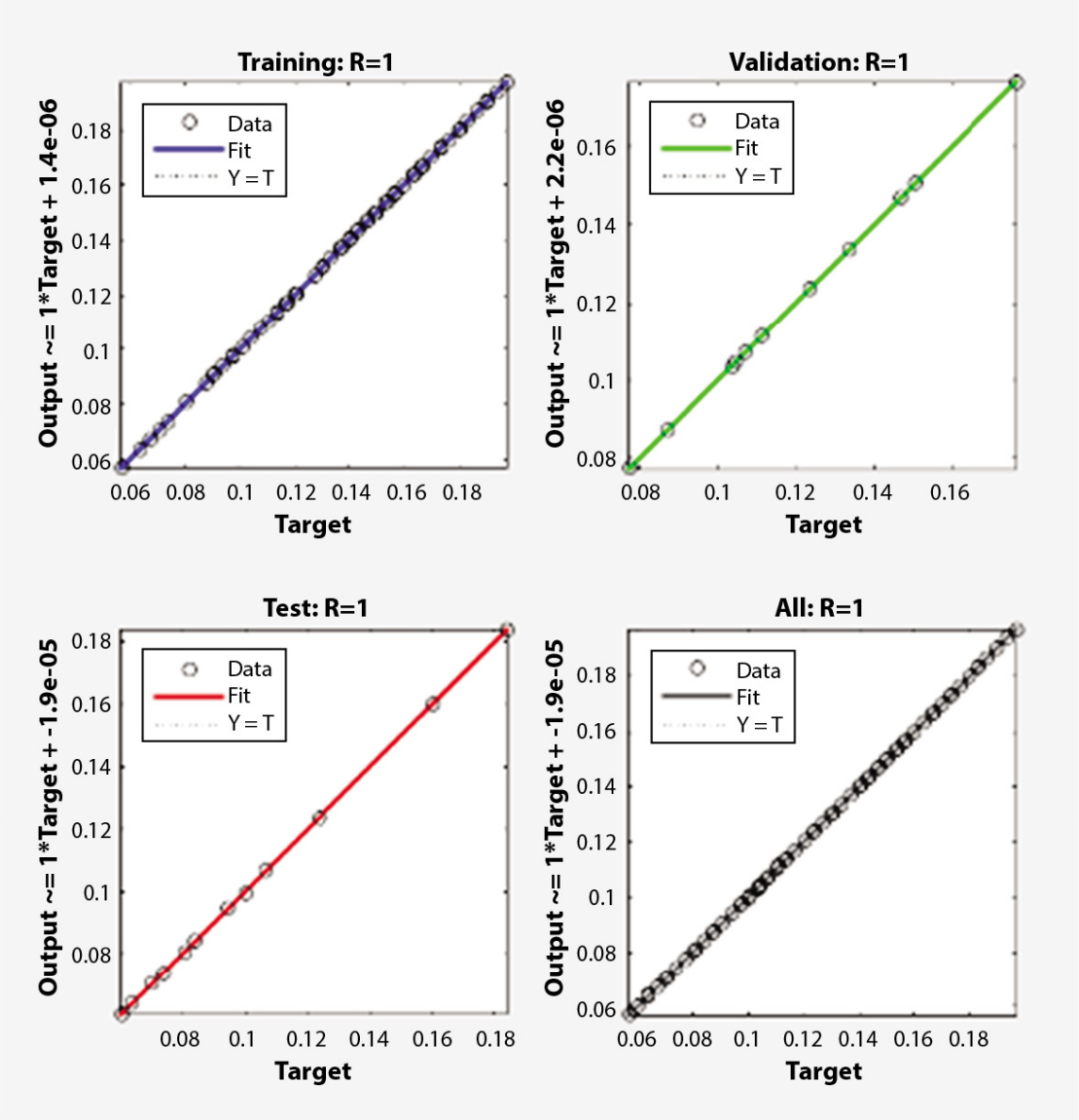


Figure 29.15 Regression plot of OC.

In this part, multi-objective optimization efficiently addresses the three competing goals of minimizing TWR, lowering overcut, enhancing surface finish, and attaining optimal material removal rate (MRR). The several plotting functions of the GA utilized in this situation are shown in Figure 29.16.

A total of 103 optimization iterations involving 49 different combinations of control parameters were carried out in this scenario. Once the desired tolerance level was reached, the optimization procedure was terminated. Since the GA's default option seeks to minimize the objective function, the sign is disregarded during this machining condition. There is no doubt in the evidence that the response parameters differ. The surface roughness (Ra) varied between 1.996 and 5.138 µm, the MRR between 0.05 and 0.51 mm^3/min, the TWR between 0.0025 and 0.3039 mm^3/min, and the overcut (OC) between 0.067 and 0.186 mm.

29.3.3 Multi-Objective Optimization Using Fuzzy Grey Relational Analysis

First, GRA converts each option's performance into a series of comparability, a procedure called "grey relational assessment." By using this technique, a standard pattern—also known as the optimal target sequence—is produced. The link between the evaluation options and the reference sequence is then measured by calculating the grey relational coefficient. The grey relational grade for each comparison sequence concerning the reference sequence is ascertained using these coefficients. The choice with the closest link to the reference sequence, as indicated by the highest grey relational grade, is considered the most favorable. Fuzzy set theory is frequently utilized in experimental research to assess the importance of controller settings.

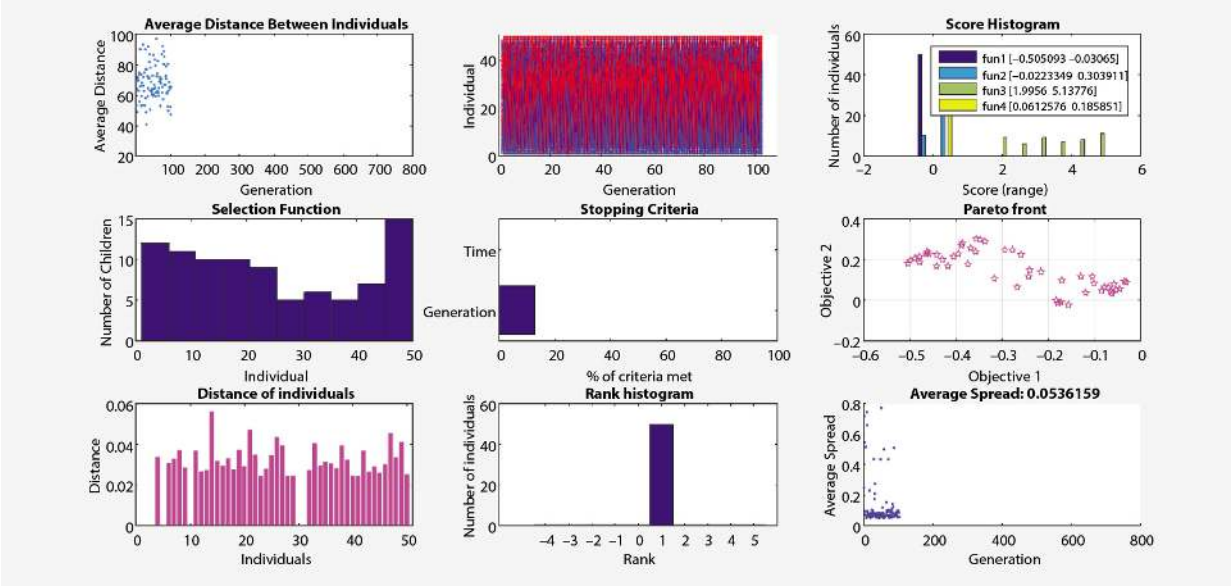


Figure 29.16 Plot functions for GA.

The equation for computing the grey relational coefficient, ξ_{ij} between the reference sequence, R, and the alternative sequence, A_i for the i-th objective function is Equation 29.7:

$$\xi_{ij} = \frac{min_k\{\mu_k(R), \mu_k(A_i)\} + \rho \cdot max_k\{\mu_k(R), \mu_k(A_i)\}}{\mu(R) + \rho \cdot \mu(A_i)} \quad (29.7)$$

where:

- $\mu_k(R)$and $\mu_k(A_i)$ are the membership grades of the k-th alternative with respect to the reference sequence and the i-th alternative sequence, respectively.
- $\mu(R)$and $\mu(A_i)$ are the average membership grades of the reference sequence and the i-th alternative sequence, respectively.
- ρ is a distinguishing coefficient.

The grey relational grade (GRG) for the i-th alternative sequence is calculated as:

$$GRG_i = \frac{1}{m}\sum_{j=1}^{m} \xi_{ij} \tag{29.8}$$

The highest GRG has been selected as the best parametric combination for the machining.

The results of the GRG and coefficient, as well as their corresponding rankings, are shown in Table 29.3. The findings demonstrate that the first experiment had the greatest GRG. This specific experiment successfully optimized several response characteristics by using a mixture of parameters such as a current of 4 amps, Ton of 101 s, Toff of 28 s, and F/Press at 0.1 kg/cm^2. The MRR, overcut, surface quality, and tool wear rate were all best achieved with this arrangement.

With these ideal settings, a GRG of 0.441 was found in a confirmation experiment. The precise measurements that were attained were a 0.061-m overcut, a 2.229-m surface finish, an MRR of 0.06 mm^3/min, and a tool wear rate of 0.0337 mm^3/min. These results confirm that choosing the optimal set of machining parameters greatly improves surface quality and lowers overcut. Table 29.4 provides a summary of the findings, which confirm the optimal machining settings.

29.4 Results and Discussion

The control parameters for die-sinking EDM of Ti Alloy VT20 were examined in a recent experimental investigation. These variables include current, flow pressure, pulse on/off time, and pulse on/off time. Initially, MATLAB R2015a was used for the data analysis, with the 'Dividerand' function being used for data segmentation. The training function was the Levenberg-Marquardt function, and the performance metric was the MSE [7].

A gradient of 6.05 x 10^{-8} was discovered in the context of optimizing the MRR by the investigation. At epoch 137, the model demonstrated its optimal validation performance, with the lowest prediction error of 2.545 x 10^{-10}. A regression model (R = 1) revealed this, indicating a strong fit throughout the testing, validation, and training stages.

The observed gradient for TWR was 2.83 x 10^{-7}. At epoch 61, the model demonstrated optimal validation performance for TWR, with a low prediction error (MSE) of 6.7703 x 10^{-7}. Once more, an acceptable model fit was indicated by R = 1.

The measured gradient for surface roughness (Ra) was 5.18 x 10^{-7}. According to MSE, epoch 1000 had the best validation performance, with a prediction error of 4.5502 x 10^{-9}. R = 1 indicates that the model fits well during training, validation, and testing.

The study found that OC had a gradient of 9.30 x 10^{-8} and that its highest validation performance occurred at epoch 40 when it displayed a low MSE of 5.0055 x 10^{-9}. A good correlation with the training data was demonstrated by the R-value of 1 in both the test and validation findings.

The range for MRR is between 0.05 and 0.51 mm^3/min, for TWR between 0.0025 and 0.3039 mm^3/min, for Ra between 1.996 and 5.138 µm, and for OC between 0.067 and 0.186 mm, according to the application of GA. An ideal parametric combination was reached by these GA-obtained values: 4 amps of current, 101 s of Ton, 28 s of Toff, and 0.1 kg/cm^2 of flow pressure. The lowest TWR, best surface finish, least amount of OC, and maximum MRR were obtained with this combination.

Table 29.3 Grey relation co-efficient and grades.

Sl. no.	Current	Ton	Toff	F/Press	MRR	TWR	RA	OC	GRG	Rank
1	4	101	28	0.1	0.06	0.0337	2.229	0.061	0.441	1
2	4	236	26	0.1	0.16	0.0223	2.965	0.085	0.397	11
3	7	163	25	0.3	0.22	0.1377	3.216	0.117	0.286	35
4	4	100	15	0.3	0.03	0.0904	1.996	0.078	0.423	6
5	4	100	26	0.2	0.06	0.078	2.198	0.074	0.394	13
6	4	100	16	0.3	0.03	0.092	2.015	0.078	0.418	8
7	5	240	35	0.1	0.18	0.0025	3.169	0.091	0.438	2
8	12	245	43	0.1	0.48	0.1858	4.953	0.166	0.350	20
9	12	107	23	0.3	0.36	0.3039	3.961	0.162	0.255	45
10	11	218	43	0.1	0.42	0.1667	4.551	0.15	0.303	31
11	10	102	25	0.3	0.28	0.2497	3.494	0.139	0.254	47
12	11	194	27	0.2	0.39	0.2272	4.313	0.163	0.278	39
13	11	107	23	0.3	0.34	0.2901	3.845	0.157	0.253	49
14	4	101	16	0.2	0.05	0.0577	2.09	0.07	0.433	3
15	8	133	27	0.2	0.24	0.1489	3.321	0.115	0.280	38
16	12	107	23	0.3	0.35	0.297	3.903	0.159	0.254	48
17	5	102	27	0.2	0.08	0.0644	2.333	0.072	0.388	15
18	10	195	24	0.1	0.37	0.1777	4.187	0.149	0.283	37
19	4	250	26	0.1	0.18	0.0156	3.112	0.092	0.406	9
20	12	262	40	0.2	0.49	0.2064	5.02	0.177	0.358	19
21	11	251	26	0.3	0.44	0.226	4.662	0.18	0.304	30
22	6	112	35	0.1	0.17	0.0987	2.92	0.089	0.316	29
23	6	103	24	0.2	0.13	0.1178	2.622	0.091	0.323	25
24	7	223	33	0.1	0.27	0.0663	3.63	0.114	0.325	23
25	11	147	28	0.3	0.37	0.2584	4.097	0.158	0.263	43
26	5	105	25	0.3	0.1	0.1144	2.476	0.089	0.337	22
27	12	154	24	0.3	0.39	0.2703	4.218	0.166	0.269	40
28	4	101	28	0.1	0.06	0.0413	2.251	0.064	0.426	5
29	12	263	45	0.1	0.51	0.1806	5.138	0.17	0.390	14
30	12	255	26	0.3	0.46	0.2387	4.788	0.186	0.319	27
31	11	125	31	0.2	0.36	0.2366	4.032	0.146	0.265	42
32	5	104	24	0.2	0.1	0.0816	2.451	0.079	0.361	18
33	4	102	27	0.2	0.07	0.0642	2.277	0.071	0.396	12
34	11	187	35	0.2	0.4	0.2153	4.399	0.157	0.284	36
35	7	193	29	0.2	0.24	0.1176	3.429	0.12	0.290	34
36	4	108	18	0.2	0.05	0.0513	2.155	0.07	0.428	4
37	11	235	30	0.2	0.43	0.2021	4.587	0.168	0.301	32
38	8	234	29	0.2	0.32	0.1054	3.917	0.132	0.299	33
39	4	236	29	0.1	0.17	0.011	3.077	0.089	0.418	7

Sl. no.	Current	Ton	Toff	F/Press	MRR	TWR	RA	OC	GRG	Rank
40	4	220	18	0.3	0.12	0.0383	2.685	0.097	0.386	16
41	11	238	41	0.1	0.44	0.1659	4.711	0.157	0.319	26
42	9	111	26	0.3	0.26	0.2245	3.395	0.133	0.259	44
43	10	105	24	0.3	0.29	0.248	3.588	0.141	0.255	46
44	12	256	34	0.2	0.48	0.2147	4.926	0.179	0.342	21
45	12	142	28	0.3	0.39	0.282	4.204	0.165	0.266	41
46	5	102	27	0.1	0.08	0.0474	2.366	0.067	0.404	10
47	12	263	45	0.2	0.5	0.1976	5.105	0.175	0.376	17
48	12	247	30	0.3	0.46	0.2291	4.809	0.181	0.323	24
49	12	239	30	0.2	0.46	0.2266	4.769	0.178	0.319	28

Table 29.4 Validation results for improvement of grey grade.

	Control parameters				Responses				Grey grade
	Current (Amp)	Ton (µs)	Toff (µs)	F/Press (kg/cm^2)	MRR (mm^3/min)	Tool wear rate (mm^3/min)	Surface finish (µm)	Overcut (µm)	
Exp 1.	4	101	28	0.1	0.06	0.0337	2.229	0.061	0.441
Validation data	4	101	28	0.1	0.05	0.0527	2.215	0.055	0.450
	Improvement of grey grade								0.009

29.5 Conclusion

In an experimental investigation, it was discovered that while cutting Titanium VT20 with the EDM process, the results vary depending on various factors: current, pulse on time, pulse off time, and flow pressure. An ANN was used in the study to confirm that the tests were carried out within a suitable experimental range. Additionally, by modifying the control settings, a GA was employed to find the best answer for the experimental design. The study also performed grey analysis, accounting for the inconsistent results of MRR, TWR, surface finish, and OC, to determine the ideal set of parameters.

The results indicate that as long as the MRR is maximized, the voltage and Ton must also be maximized. However, if the overcut is lowered, the voltage and Ton must also be reduced. But increase in the flow pressure will increase OC and reduce the surface finish in case. High current causes high TWR.

References

1. Bose, G.K. and Pain, P., Metaheuristic Approach of Multi-Objective Optimization during EDM Process. *Int. J. Math, Eng. Mang. Sci.*, 3, 3, 301–314, 2018.

2. Ahmad, S. and Lajis, M.A., An Electric Discharge Machining (EDM) of Inconel 718 using Copper Tungsten Electrode with Higher Peak Current and Pulse Duration. *Int. J. Mech. Mechs. Engg*, 15/05, 39 – 47, 2015.

3. Dixit, A.C., Kumar, A., Singh, R.K., Bajpai, R., An experimental study of material removal rate and electrode wear rate of high carbon-high chromium steel (AISI D3) in

EDM process using copper tool electrode. *Int. J. Innov. Res. Adv. Eng.*, 2, 257–262, 2015.

4. Lamba, R., Pabla, B.S., Kansal, H., Development of surface properties on Ti6Al4V by electric discharge machining. *Int. J. Res. Eng. Innov.*, 2, 555–564, 2018.
5. Singh, K., Gianender, Agarwal, A.K., Ajit, Yadav, R., Effect of Dielectric fluids used on EDM Performance: A Review. *Int. J. Em. Tech. Engg. Res.*, 5, 10–16, 2017.
6. Selvarajan, L., Raja, R., Sasikumar, R., Muralidharan, V., Effects of process parameter on performance measures in electrical discharge machining using copper and brass electrodes. *Mater. Today: Proc.*, 46, 9257–9262, 2021.
7. Kumar, P., Hussain, M., Das, A.K., Effect of process parameters on the surface integrity of micro-holes of Ti6Al4V obtained by micro-EDM. *Int. J. Mech. Prod.*, 8, 6, 2018.
8. Rajesha, S., Sharma, A.K., Kumar, P., On Electro Discharge Machining of Inconel 718 with Hollow Tool. *J. Materi. Eng. Perform.*, 21, 882–891, 2012.
9. Jamwal, A., Aggarwal, A., Gautam, N., Devarapalli, A., Electro-discharge machining: recent developments and trends. *Int. Res. J. Eng. Technol.*, 5, 433–448, 2018.
10. Singh, G., Ablyaz, T.R., Shlykov, E.S., Muratov, K.R., Bhui, A.S., Sidhu, S.S., Enhancing corrosion and wear resistance of Ti6Al4V alloy using CNTs mixed electro-discharge process. *Micromachines*, 11, 9, 850, 2020.
11. Pain, P., Bose, G.K., Bose, D., Parametric analysis and optimization of aluminium and SS 204 material using micro-EDM system. *Int. J. Interact. Des. Manuf.*, 17, 3025–3042, 2023.
12. Pala, M., Viswanath Sarma, K., Sakthivel, D., Rao, D.V., Experimental investigation of machining of Ti-6Al-4V through EDM using copper tungsten electrode and modelling of machining parameters using artificial neural network. *Int. J. Adv. Eng. Res. Sci.*, 2, 9, 2349–6495, 2015.
13. Bhui, A.S., Singh, G., Sidhu, S.S., Bains, P.S., Experimental investigation of optimal ED machining parameters for Ti-6Al-4V biomaterial. *Facta Universitatis, Series: Mech. Eng.*, 16, 3, 337– 345, 2018.
14. Bundel, B.R., Experimental Study of Electrode Wear in Die-Sinking EDM using Cylindrical Copper Electrode. *Int. J. Eng. Res. Technol.*, 3, 10, 2278–0181, 2014.
15. Philip, J.T., Mathew, J., Kuriachen, B., Transition from EDM to PMEDM–impact of suspended particulates in the dielectric on Ti6Al4V and other distinct material surfaces: a review. *J. Manuf. Processes*, 64, 1105–1142, 2021.
16. Sandeep, M. and Jamaleswara Kumar, P., Analysis of Machining Parameters on D2Tool Steel in Wire Cut EDM, in: *Advances in Lightweight Materials and Structures*, A. Praveen Kumar, T. Dirgantara, P.V. Krishna, (Eds.), p. 8, Springer Proceedings in Materials, Springer, Singapore, 2020.
17. Gaikwad, S., Teli, S., Gaikwad, L., Optimization of EDM parameters on machining Ti-6Al-4V with a core electrode using grey relational analysis. *Int. J. Res. Aeronaut. Mech. Eng.*, 2, 12, 24–31, 2014.
18. Laxman, J. and Raj, K.G., Optimization of EDM process parameters on titanium superalloys based on the grey relational analysis. *Int. J. Eng. Res.*, 3, 5, 344–348, 2014.

19. Goyal, S., Jamwal, A., Pandey, R., Optimization of process parameters in electro-discharge machining using Taguchi method. *Carbon*, 100, 0–14, 2016.

20. Tiwary, A.P., Pradhan, B.B., Bhattacharyya, B., Investigation on the effect of dielectrics during micro-electro-discharge machining of Ti-6Al-4V. *Int. J. Adv. Manuf. Technol.*, 95, 861–874, 2018.

21. Sahu, S.N., Nayak, D., Rana, H.K., ANN Performance Evaluation In Modeling of MRR In EDM Process, in: *Proc. of Int. Conf. on Emerging Trends in Engineering and Technology*, 2013.

22. Panchal, V.A., Patel, R.K., Patel, B.A., Patel, H.A., Effect of process parameters on surface quality and mrr in EDM of ss 440 c using ann. *Int. J. Recent Innovation Trends Comput. Commun.*, 2, 7, 1949–1957, 2014.

23. Kalita, K., Chakraborty, S., Ghadai, R.K., Chakraborty, S., Parametric optimization of nontraditional machining processes using multi-criteria decision-making techniques: Literature review and future directions. *Multiscale Multidiscip. Model. Exp. Des.*, 6, 1, 1–40, 2023.

24. Tzeng, C.J. and Chen, R.Y., Optimization of electric discharge machining process using the response surface methodology and genetic algorithm approach. *Int. J. Precis. Eng. Manuf.*, 14, 709–717, 2013.

25. Singh, P.N., Raghukandan, K., Pai, B.C., Optimization by Grey relational analysis of EDM parameters on machining Al–10% SiCP composites. *J. Mater. Process. Technol.*, 155, 1658–1661, 2014.

26. Aharwal, K.R. and Krishna, C.M., Optimization of material removal rate and surface roughness in EDM machining of metal matrix composite using genetic algorithm. *Mater. Today: Proc.*, 5, 2, 5391–5397, 2018.

27. Quarto, M., D'Urso, G., Giardini, C., Micro-EDM optimization through particle swarm algorithm and artificial neural network. *Precis. Eng.*, 73, 63–70, 2022.

Note

**Corresponding author*: pritam.me.dscsdec@gmail.com

30
Estimation of Machining Performance and Machining Characteristics Using Artificial Neural Network in Wire Electric Discharge Machine for Titanium & P-20 Materials

Prathik Jain S.[1]*, Sundaramahalingam A.[1], Sudhagara Rajan S.[2], Chethan K. N.[3], Rudresh Addamani[4] and Ugrasen G.[5]

[1]*Department of Aeronautical Engineering, Dayananda Sagar College of Engineering, Bengaluru, Karnataka, India*

[2]*Department of Aerospace Engineering, School of Mechanical Engineering, REVA University, Bengaluru, Karnataka, India*

[3]*Department of Aeronautical & Automobile Engineering, Manipal Institute of Technology, Manipal, Karnataka, India*

[4]*Department of Mechanical Engineering, PES College of Engineering, Mandya, Karnataka, India*

[5]*Department of Mechanical Engineering, BMS College of Engineering, Bengaluru, Karnataka, India*

Abstract

Wire electrical discharge machining offers a dynamic solution for shaping solid materials with intricate configurations. This specific machining process excels in accurately crafting components for hard materials and also for complex shapes material. The focus of the current investigation revolves around the machining of titanium grade-2 and P-20 tool steel materials employing the L_{16} orthogonal array. The study takes into account various process parameters, namely, current, bed speed, pulse on time, pulse off time, voltage and flush rate. Voltage and flush rate were kept constant during the machining operation, but the other four parameters are changed during the experiments. The electrode material employed for the present study is a 0.18-mm diameter molybdenum wire. A phenomena known as an acoustic emission occurs when localized sources within a solid quickly release stored elastic energy, creating momentary elastic waves that travel as a spherical wave. When subjected to appropriate processing and analysis, the waves which have been detected will be converted as an electric signal that can provide useful information on the source of energy releases. In order to determine the main influences on machining characteristics, such as electrode wear and surface roughness, and machining performance, such as acoustic emission signals optimization of process parameters was first carried out. Using the optimized parameters, simple functional relationship charts between the parameters were built to

acquire data on acoustic emission signals, electrode wear, and surface roughness. However, this straightforward analysis does not offer comprehensive information about the material, electrode, and signals status. Consequently, a more advanced method of analysis, namely artificial neural network was employed for predicting (estimating) the experimental values. At 70% of the training data, compared to 50% and 60% of the training data, the correlation between the predicted values of the artificial neural network and the experimental data was found to be stronger.

***Keywords*:** Wire electric discharge machining, electrode wear, surface roughness, acoustic emission, artificial neural network

30.1 Introduction

The wire-cut machine was invented with the goal of manufacturing hardened steel tools, specifically dies. Wire electric discharge machining (WEDM) uses a wire as the tool's electrode. To prevent wear and tear and damage to the wire, it is wrapped between two spools, ensuring a continuous replacement of its active section. Initially, numerical controlled (NC) machines were adapted from vertical milling machines employing punched tape technology. P-20 tool steel is a commonly utilized material in the manufacturing of zinc die casting and plastic molds [1]. Wire electrical discharge machining is capable of effectively machining materials that possess high hardness, strength, corrosion resistance, and wear resistance properties. This technology enables the machining of complex geometries that would be difficult or impossible to achieve with standard processes like grinding, milling and turning. Wire electrical discharge machining has a wide range of applications, including aircraft engine turbine blades, extrusion dies, fuel injector nozzles, and machining of harder materials including titanium, tool steel, cemented carbides and Metal matrix composites (MMCs) [2–5]. During electric-erosion cutting, there are no traditional cutting forces present. This means that conductive materials can be machined irrespective of their mechanical properties, toughness and hardness [6, 7]. The impact of WEDM parameters on machining AISI 4140 steel with brass wire was investigated, considering factors such as surface texture, micro voids, micro cracks, and surface roughness (SR). Results indicate that the pulse on duration has a more pronounced effect on the surface texture of machined parts compared to pulsed current. Machined parts with greater pulse on duration and pulsed current exhibit a lower surface finish [8].

It was observed that significant decreases in the SR values at lower discharge energy levels have been achieved during machining of Inconel 718 by WEDM with nonabrasive brass wire parameters such as current, discharge energy and pulse timing for both trim and main cuts. Conversely, when higher discharge energy levels were employed, a thick white layer

developed on the surface that exhibited non-uniformity, discontinuity, and the presence of micro voids [9]. When brass wire was used for machining 16MnCr5 steel material in WEDM, it caused the formation of craters on the surface.

The outcomes revealed a higher incidence of deep craters at lower cutting speeds, while minimal major craters were observed at higher cutting speeds. At moderate cutting speeds, micro cracks and fine surface cracks were identified [10]. When working with nickel-based super-alloys in machining processes, several notable challenges arise. These alloys possess low thermal conductivity, leading to heightened thermal effects during machining. They also frequently demonstrate significant work-hardening tendencies and exhibit high adhesion to the tool face, necessitating adjustments to cutting process parameters. Additionally, these alloys may include hard abrasive particles and carbides, which can cause tool wear to go beyond acceptable levels. This can ultimately affect the surface integrity of the finished products [11]. There are several factors that influence the material removal rate, size, and topographic and chemical characteristics of a machined surface. This shall cover the type of wire electrode, dielectric fluid used, and the condition of the machine. However, the major role in determining these results lies with the parameter setting of erosion processes [12]. The surface integrity results, including SR and fatigue strength, of Inconel 718 material were examined using both conventional machining processes (broaching and grinding) and WEDM. The surface integrity of the parts produced by WEDM and traditional methods has been shown to have different characteristics [13]. From the use of copper to the widespread use of brass wire electrodes, the development of EDM wire electrode technology has progressed, with further developments resulting in the adoption of coated wire electrodes. It has been determined that utilizing zinc-coated wire material can enhance the productivity of the WEDM process more effectively than other wire materials [14].

The increased concentration of the zinc concentration in the wire has offered higher cutting speed, higher productivity and improved surface integrity, as demonstrated by the zinc coated brass electrode [15, 16]. During the machining process of aluminium-based hybrid MMCs using brass wire in WEDM, the impact of process parameters on acoustic emission (AE) signals, kerf width, and SR was explored. The findings showed that the generation of AE signals is inconsistent and varies with the duration and feed rates. [17]. The efficiency of artificial neural network (ANN) models in comparison to response surface methodology (RSM) mathematical models has been evaluated in order to estimate average cut speed. Upon comparison, it was found that the ANN models outperform the RSM models in terms of accuracy in prediction [18]. Two distinct ANN models, namely the backpropagation neural network (BPN) and the radial basis function neural network (RBFN), are introduced for predicting SR in

die sinking EDM. Notably, the RBFN exhibits faster processing compared to the BPNs, while the BPN demonstrates a reasonably higher level of accuracy [19]. Artificial neural networks has shown to be incredibly effective in predicting both SR and AE signals. In particular, compared to subsets with 50% and 60% of the data, as indicated by the R values closer to one, the neural network trained with 70% of the data in the training set showed more favorable prediction results [20]. The ANN technique has also been used to predict the influence of taper angles on part geometry and whole area. The results have been consistent with the experimental data and demonstrate that ANN is effective in evaluating manufacturing processes [21].

30.2 Experimental Setup

The CONCORD DK7720C, a four-axis CNC WED machine, is used to conduct the experiments. The essential parts of this WED machine includes, a servo control system, a wire electrode, a dielectric supply system, a work table and power supply. Additionally, it enables the machinist to quickly select input parameters based on the material's height. This WED machine incorporates unique features, setting it apart from others in the field. Particularly, it employs reusable wire technology, implicating that the wire is not discarded after use instead; it is reutilized through re-looping wire technology. Furthermore, alterations are performed in the wire before each experiment to prevent erosion, which could lead to breakage. Figure 30.1 shows the experimental setup used to acquire the results.

A variety of stages, such as rough cutting, combined rough cutting with finishing, and a dedicated finishing stage, are generally covered by the WEDM procedure. However, a single pass is used for this WED machine. The computer controlled positioning mechanism reliably maintains a 0.02-mm gap between the wire and the work piece. In this process, an electrode made of molybdenum with a diameter of 0.18 mm has been used. Table 30.1 shows the various configurations of four process parameters used in the experiments: current (C), bed speed (BS), pulse-on time (Pon) and pulse-off time (Poff). Meanwhile, the flush rate and wire tension remained consistent throughout the entire experiment. A block with a square cross-section measuring 10 mm x 10 mm was subjected to machining. The work piece had a thickness or height of 40 mm, and the cutting angle was set to be vertical.

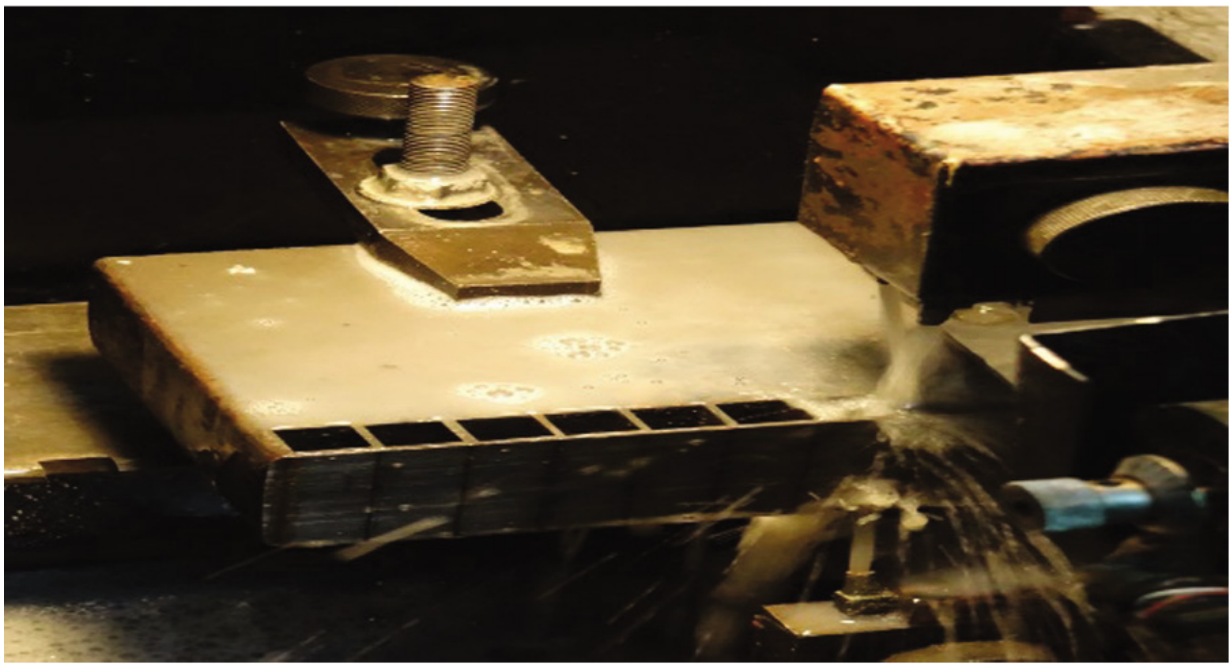


Figure 30.1 Experimental set-up during machining.

Table 30.1 The levels of different control factors.

Control factor	Level			
	I	II	III	IV
Current (amps)	3	4	5	6
Bed speed (μm/s)	20	25	30	35
Pulse-on time (μs)	16	20	24	28
Pulse-off time (μs)	4	6	8	10

Table 30.2 Chemical composition of titanium grade-2 material.

Sl. no.	Constituent	Percentage
1	Ti	99.2
2	Fe	0.3
3	O	0.25
4	C	0.1
5	H	0.015
6	N	0.03

Table 30.3 Chemical composition of P-20 tool steel material.

Sl. no.	Constituent	Percentage
1	C	0.388
2	Si	0.31
3	Mn	1.41
4	P	0.010
5	S	0.009
6	Cr	1.85
7	Ni	0.95
8	Mo	0.17

The present work employs in machining the titanium grade-2 and P-20 tool steel materials using the molybdenum wire in the above said machine. The chemical composition of the materials used for the present study has been incorporated in Tables 30.2 and 30.3.

The L_{16} cluster, comprising five elements divided into four level sections, is wellsuited for the current study. The standard L_{16} configuration with four levels is depicted in Table 30.4. Table 30.5 gives run of the mill L_{16} orthogonal array (OA) relegated with control factors.

30.2.1 Acoustic Emission (AE) Sensors

An acoustic emission is defined as a phenomenon in which the rapid release of stored elastic energy from localized sources within the solid produces momentary stress waves that travel as a spherical wave in the event of fracture, phase change and plastic deformation. By placing a very sensitive transducers, which are usually electromechanical devices, on the surface of the material, this energy can be picked up from its surface. Analyzing these signals allows extraction of data about the source causing the energy release. There are two main types of AE signals *viz.*, burst signals and continuous signals. The AE measuring system used for the present study includes peripheral components such as AE sensors, a 2-channel SP board with a 2-AE channel interconnect card (PCI), and pre-amplifiers. To identify activity within structures and materials, the AE sensors play a crucial role by “listen”, serving as essential connections between analysis instrumentation and test structures. The mechanical energy carried by the elastic waves is converted in to electrical signals by the AE sensor. The AE sensor used for the present work is shown in Figure 30.2.

Table 30.4 Standard L’16 OA.

Run	Current (amps)	Bed speed (µm/sec)	Pulse-on time (µs)	Pulse-off time (µs)
1	1	1	1	1
2	2	2	1	2
3	3	3	1	3
4	4	4	1	4
5	2	3	2	1
6	1	4	2	2
7	4	1	2	3
8	3	2	2	4
9	3	4	3	1
10	4	3	3	2
11	1	2	3	3
12	2	1	3	4
13	4	2	4	1
14	3	1	4	2
15	2	4	4	3
16	1	3	4	4

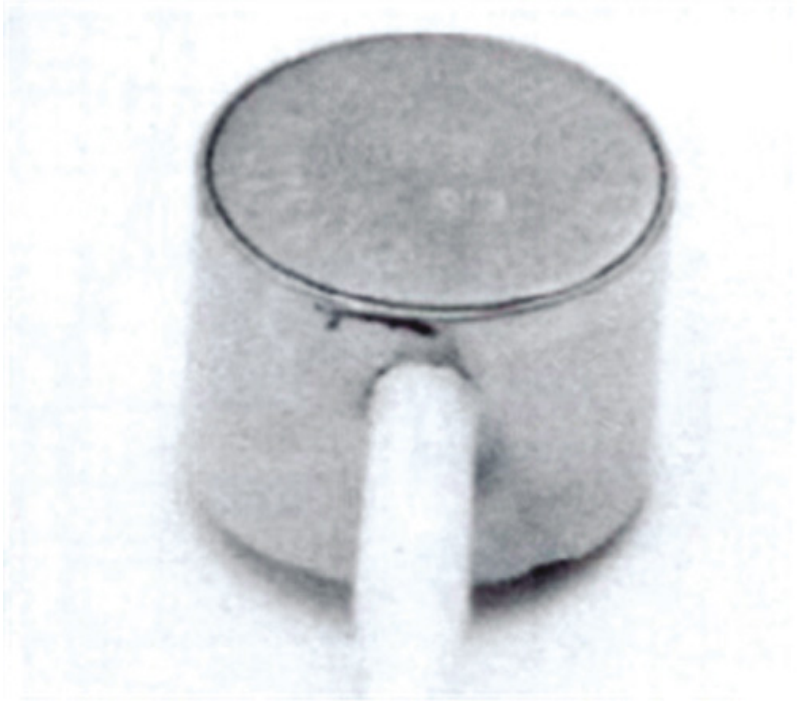


Figure 30.2 AE sensor.

30.3 Artificial Neural Network (ANN)

Due to the intricate and time-varying characteristics of the machining process, traditional identification methods face challenges in generating precise models. In contrast to conventional computational techniques, ANNs offer resilience and universal solution. Artificial neural networks learn from a dataset that is similar to the system's behavior, which creates an inherent connection between input and output. It is also known as neural networks, and is made up of interlinked artificial neurons which employ statistical or computational frameworks to interpret input, employing a connectionist approach to computation. There are typically three layers to these networks: the input layer, the hidden layer, and the output layer. A set of hidden units is connected to an array of input units, which in turn connects to a series of outputs. Through an input layer, patterns are introduced into the network and interact with one or more hidden layers. In these hidden layers, the processing takes place on a network of weighted connections. The hidden layers are then linked to the output layer. In this respect, the layer is a collection of parallel neurons which have an independent functioning. A typical ANN network is shown in Figure 30.3.

Table 30.5 L_{16} OA assigned with factors.

Run	Current (amps)	Bed speed (µm/sec)	Pulse-on time (µs)	Pulse-off time (µs)
1	3	20	16	4
2	4	25	16	6
3	5	30	16	8
4	6	35	16	10
5	4	30	20	4
6	3	35	20	6
7	6	20	20	8
8	5	25	20	10
9	5	35	24	4
10	6	30	24	6
11	3	25	24	8
12	4	20	24	10
13	6	25	28	4
14	5	20	28	6
15	4	35	28	8
16	3	30	28	10

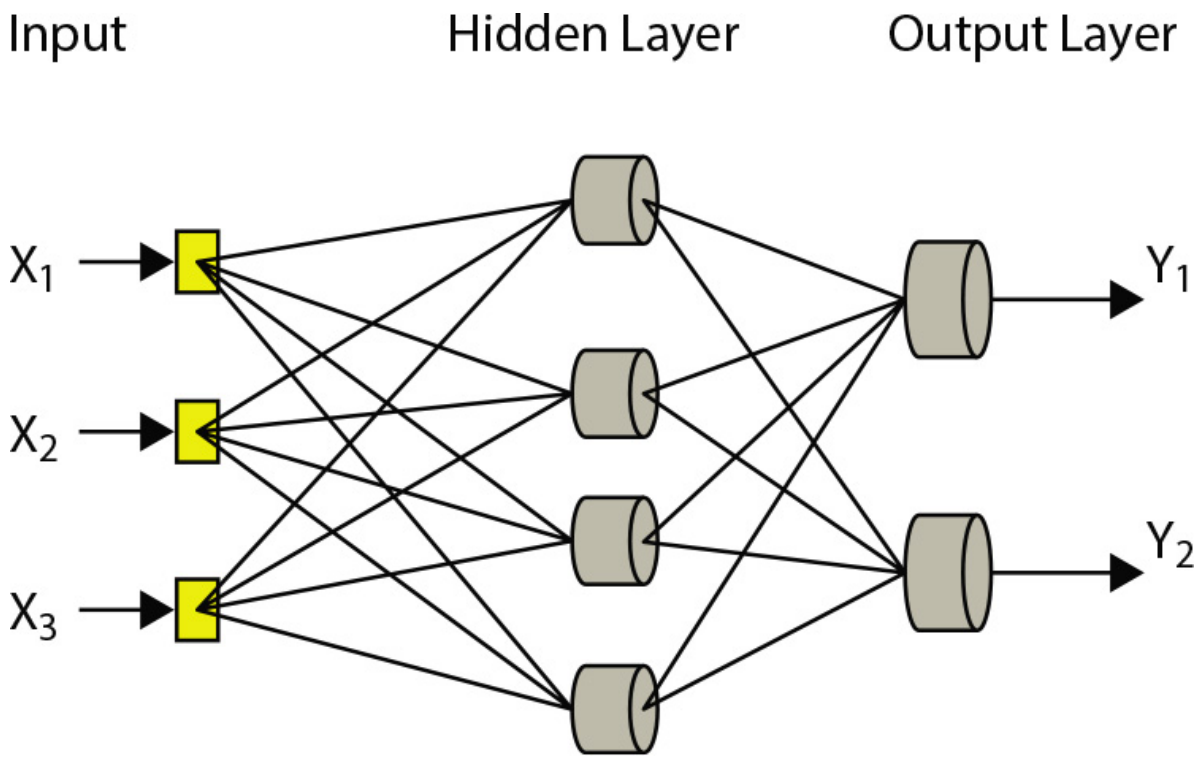


Figure 30.3 A sample ANN.

30.4 Results and Discussion

Tests were conducted using Taguchi's L_{16} OA, with Pon, Poff, C, and BS as input process parameters. Acoustic emission signals, *viz.*, signal strength (AE_{SS}) and AE_{RMS}, were acquired as indirect signals during machining, while SR and EW served as direct signals. Utilizing Taguchi's technique, a single-objective optimization was executed. Initial experiments were undertaken to understand the characteristics of the material, electrode, and performance status. The work piece condition was assessed based on its roughness, the electrode condition was evaluated in terms of wear, and performance was gauged through AE signals. Subsequently, the optimized process parameters were employed for monitoring the performance of the machining response.

30.4.1 Selection of Response Parameters: AE Signals

In order to examine whether AE signals can be used as a response parameter for measuring machining performance, an initial investigation was conducted in the form of a pilot test. The test reveals that merely AE_{SS} and AE_{RMS} amplitude directly impact the measured wear of electrode and finish in the material, indicating that as machining qualities rise, these AE signals increase as well. Consequently, AE_{SS} and AE_{RMS} have been

identified as response parameters for SR and EW, in line with the findings of Yan Wang *et al.*, (2017) [22]. Through pilot studies, A_{ESS} and A_{ERMS} exhibited a significant match to the characteristic phases of observed EW and SR. Therefore, these signals hold potential for assessing machining performance. Figure 30.4 (a) and (b) shows the variation of the SR and AE_{RMS}, respectively, for both the materials. From the figure, it is clear that the AE signal exhibits the similar characteristics with the SR. The similar variation was seen for AE_{SS} along with the machining characteristics.

30.4.2 Effects of SR, EW, and AE Signals on Titanium and P-20 Material Parameters

Figure 30.5 (a)–(d) presents the S/N ratio of the process variables on SR and EW for titanium and P-20 tool steel material. The charts reveal that Pon and C have the largest impact on both the SR and EW. Energy supply escalates as the Pon increase, resulting in a greater number of particles striking the work piece and electrode. As the energy increases, particles penetrate more deeply, leading to a thicker recast layer both on the work piece as well as on electrode. This will increase the values both SR and EW [23]. With an increase in C, a more substantial crater forms on the material's surface, resulting in higher values of roughness on the work piece [24]. When the C decreases, it decreases its density and same way the spark will also decrease and it minimize EW, hence an increase in C will increase the EW [25].

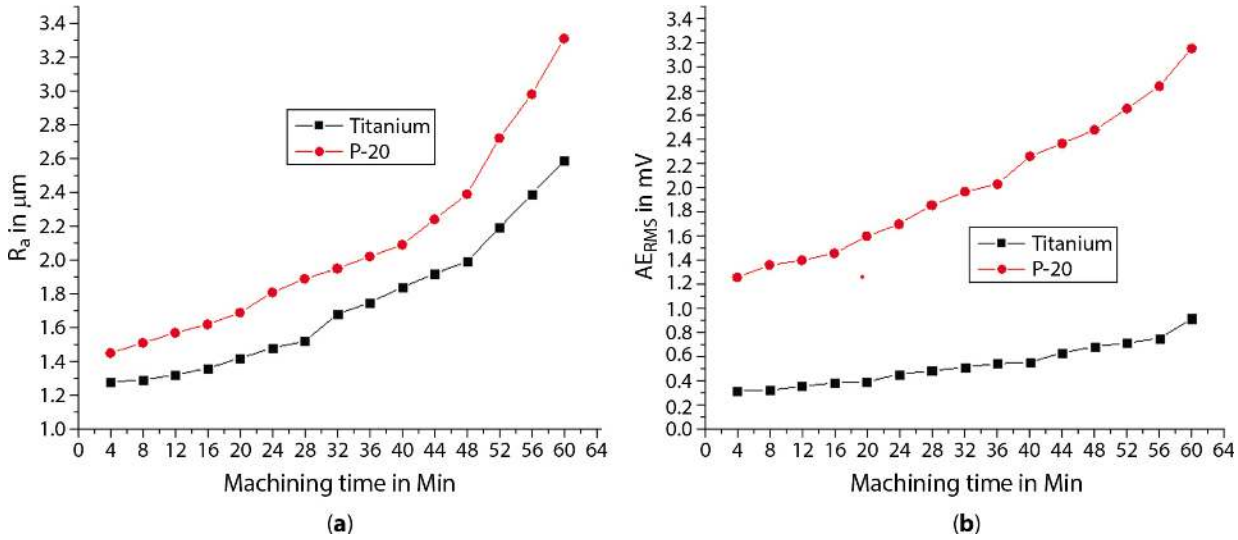
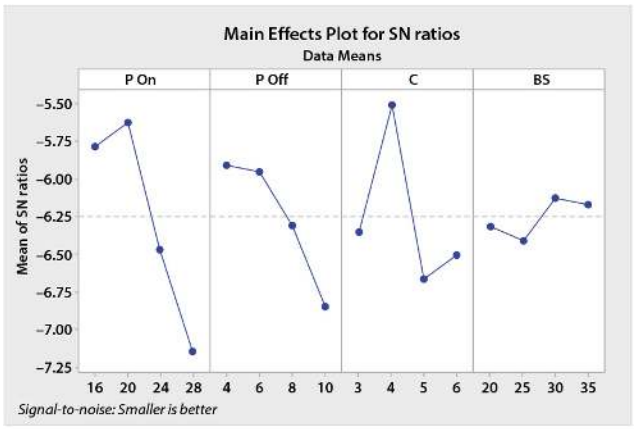
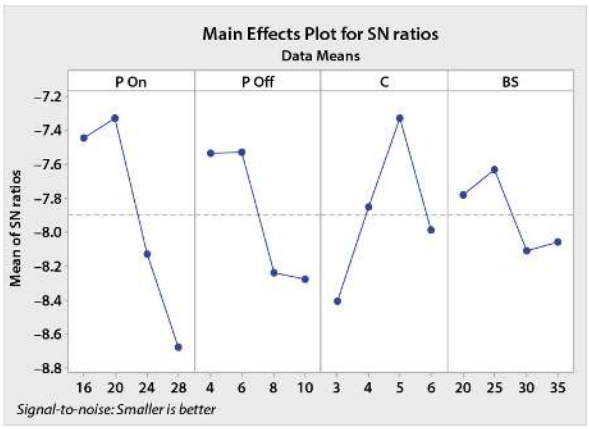


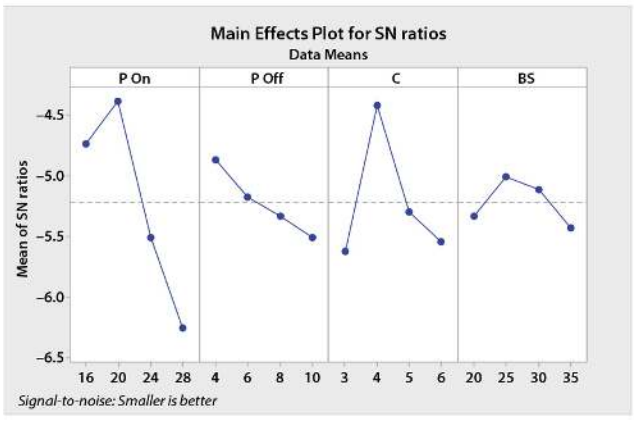
Figure 30.4 Variation of SR and AE_{RMS} with machining time for Pon (16 µs), Poff (8 µs), C (6 A), and BS (20 µm/s).



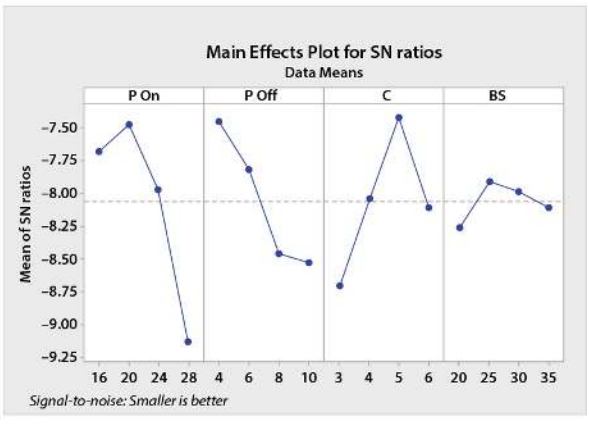
(a) Response plot on SR for Titanium grade 2 material



(b) Response plot on SR for P-20 tool steel material



(c) Response plot on EW for Titanium grade 2 material



(d) Response plot on EW for P-20 tool steel material

Figure 30.5 (a): Response plot on SR for titanium grade-2 material. (b): Response plot on SR for P-20 tool steel material. (c): Response plot on EW for Titanium grade-2 material. (d): Response plot on EW for P-20 tool steel material.

Table 30.6 Measured metrics for titanium material: F-value and R-square values.

Parameter	**SR**		**EW**		**AE_{SS}**		**AE_{RMS}**	
	Optimal value	**F-value**	**Optimal value**	**F-value**	**Optimal value**	**F-value**	**Optimal value**	**F-value**
C (amps)	4	6.27	4	9.17	5	21.48	4	5.57
BS (µm/s)	30	2.52	25	2.88	25	2.23	35	2.12
Pon (µs)	20	12.51	20	18.39	16	54.39	20	10.10
Poff (µs)	4	4.49	4	3.69	4	14.10	8	3.33
R-square value	95.91%		96.31%		99.36%		93.66%	

Table 30.7 Measured metrics for P-20 tool steel material: F-value and R-square values.

Parameter	**SR**		**EW**		**AE_{SS}**		**AE_{RMS}**	
	Optimal value	**F-value**	**Optimal value**	**F-value**	**Optimal value**	**F-value**	**Optimal value**	**F-Value**
C (amps)	5	12.51	5	8.89	3	25.89	3	5.76
BS (µm/s)	25	4.67	25	2.57	25	11.57	25	3.21
Pon (µs)	20	15.08	20	15.29	24	30.00	28	9.11
Poff (µs)	6	10.28	4	7.55	4	10.89	6	4.56
R-square value	91.34%		96.44%		95.15%		92.51%	

It should be mentioned that Pon and C were the primary influencing parameters for the AE signals. Plots also reveals that Poff and BS do not have much influence on the machining characteristics and machining performance. Tables 30.6 and 30.7 display the F- and R-Square values of the variables obtained for titanium material and P-20 tool steel material, respectively.

The tables above also highlight that a moderate Pon, minimal Poff, medium C, and medium BS contribute to improved EW conditions, as well as SR, along with corresponding AE signals for all the materials. Therefore, in the subsequent machining stages, only changes to the Pon and C are taken into

consideration, while maintaining a constant Poff and BS, specifically by considering the predominant values of 4 µs for Poff and 25 µm/s for BS.

30.4.3 Raw Data Analysis

The optimized process parameters were applied to machine of both titanium and P-20 tool steel material, with changes made to Pon and C with constant Poff and BS. At first, an attempt was made to obtain a comprehensive grasp of the machining performance (AE signals) and machining characteristics (SR and EW) of WEDM, by plotting against machining time to observe signal behavior. Progressive wear and its impact on SR were examined to evaluate their role in understanding machining characteristics. The study of AE signals was conducted to assess machining performance, and a comparison was made between EW and material status (SR), with AE signals (both AE_{SS} and AE_{RMS}) to understand their behavior.

30.4.3.1 Variation of Pon and C in Determining Titanium Grade-2 and P-20 Tool Steel Materials' Workpiece Status, Electrode Condition and Machining Performance

The SR is calculated using the arithmetic mean of surface deviation (Ra), as estimated by the stylus method. Figure 30.6 (a) and (b) illustrates the impact of SR on machining time for different Pon (16 µs, 2 µs, 24 µs, 28 µs), while maintaining a consistent Poff of 4 µs, C of 5A, and BS of 25µm/s for titanium and P-20 tool steel materials, respectively.

The plots reveal that SR rises with an increase in Pon for both the materials. This is explained by the longer Pon, which intensifies the energy discharge between the electrode and work piece. More material melts as a result, causing the work piece to develop deeper and larger craters. Therefore, resulting in increase in the roughness values of the materials [26].

Acoustic emission signals (SS and RMS) were periodically measured using AE sensors to monitor the machining performance. Figure 30.7 (a) and (b) as well as Figure 30.8 (a) and (b) illustrate the effect of AE_{SS} and AE_{RMS} on machining time for different Pon (16 µs, 20 µs, 24 µs, and 28 µs), while maintaining the Poff (4 µs), C (5 A), and BS (25 µm/s) constant for titanium and P-20 tool steel materials, respectively.

Upon observation, it is evident that AE_{SS} and AE_{RMS} exhibit a similar trend to Ra, higher gradient of AE values observed at higher Pon, as depicted in the plots. Pon directly influences EW, material removal rate, and SR. Consequently, increasing the Pon results in higher material removal rates and greater melting capacity (fracture energy) of the material, as detected by AE sensors. As the spark intensity increases, the voltage also rises, leading to higher values of AE_{SS} and AE_{RMS} at higher pulse on times.

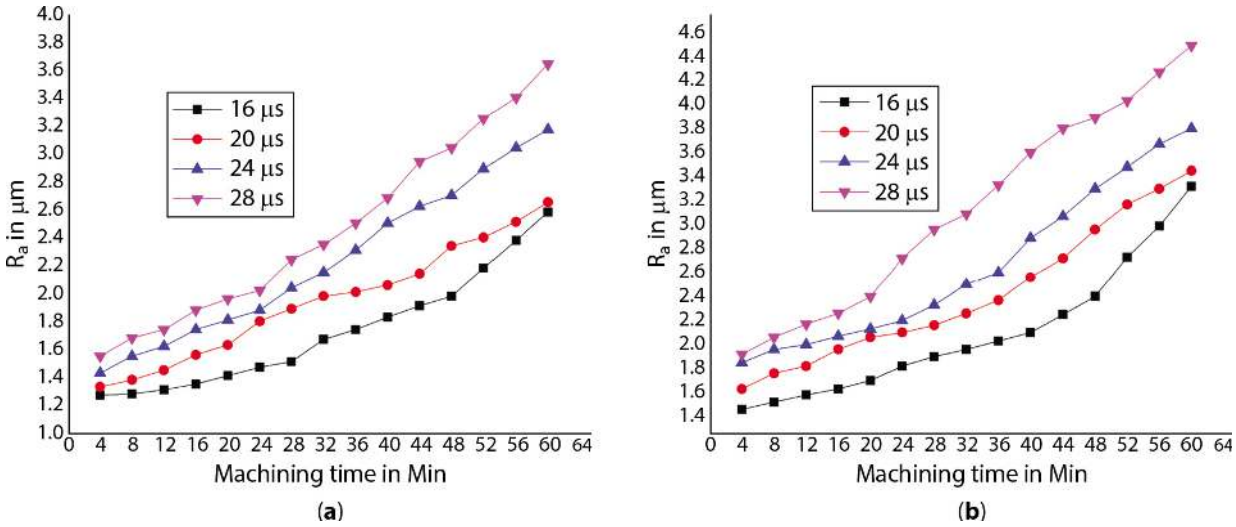


Figure 30.6 (a): Ra v/s machining time for titanium material. (b): Ra v/s machining time for P-20 tool steel material.

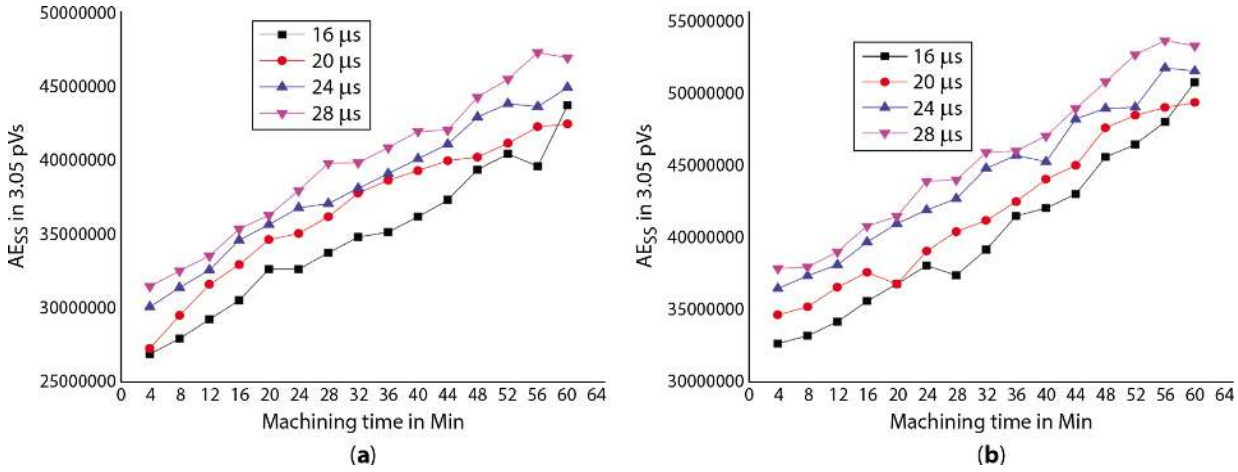


Figure 30.7 (a): AE_{SS} v/s machining time for titanium material. (b): AE_{SS} v/s machining time for P-20 tool steel material.

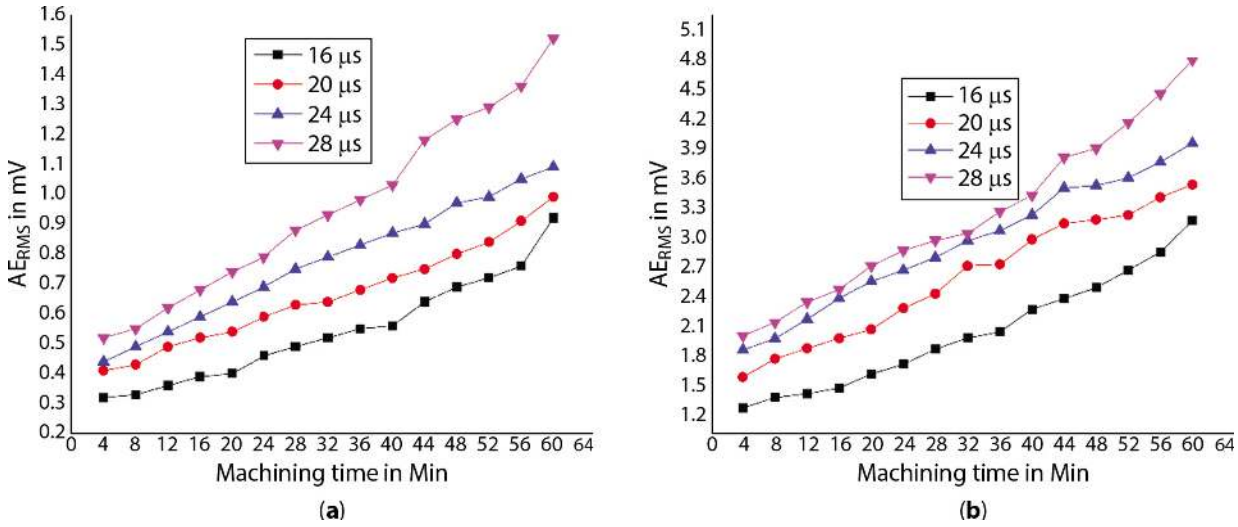


Figure 30.8 (a): AE_{RMS} v/s machining time for titanium material. (b): AE_{RMS} v/s machining time for P-20 tool steel material.

The effect of the EW versus the machining time for the variation of C (3 A, 4 A, 5 A, 6 A) at constant Pon of 20 µs, Poff of 4 µs, and BS of 25 µm/s for titanium and P-20 tool steel material are displayed in Figure 30.9 (a) and (b).

The plots also indicate that as the current increases, so does the EW. This is because a higher current leads to a more powerful discharge, generating increased heat energy. While some of this heat is absorbed by the work piece due to its size, the remaining energy is concentrated at the wire, resulting in higher wear [27].

Figure 30.10 (a) and (b) as well as Figure 30.11 (a) and (b) illustrate the impact of AE_{SS} and AE_{RMS} over machining time for different C (3 A, 4 A, 5

A, and 6 A), while maintaining constant BS (25 µm/s), Pon (20 µs), and Poff (4 µs) for titanium and P-20 tool steel materials, respectively.

Upon observation, it is evident that AE_{SS} and AE_{RMS} exhibit a similar trend to EW, *i.e.*, the plots show that a larger gradient of AE_{RMS} and AE_{SS} was seen at higher currents.

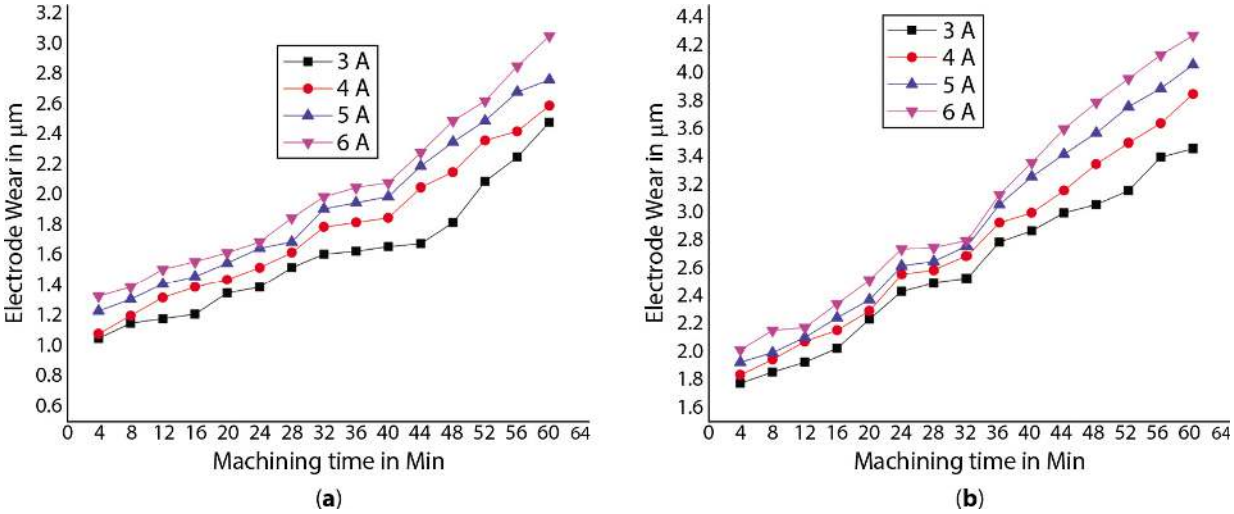


Figure 30.9 (a): EW v/s machining time for titanium material. (b): EW v/s machining time for P-20 tool steel material.

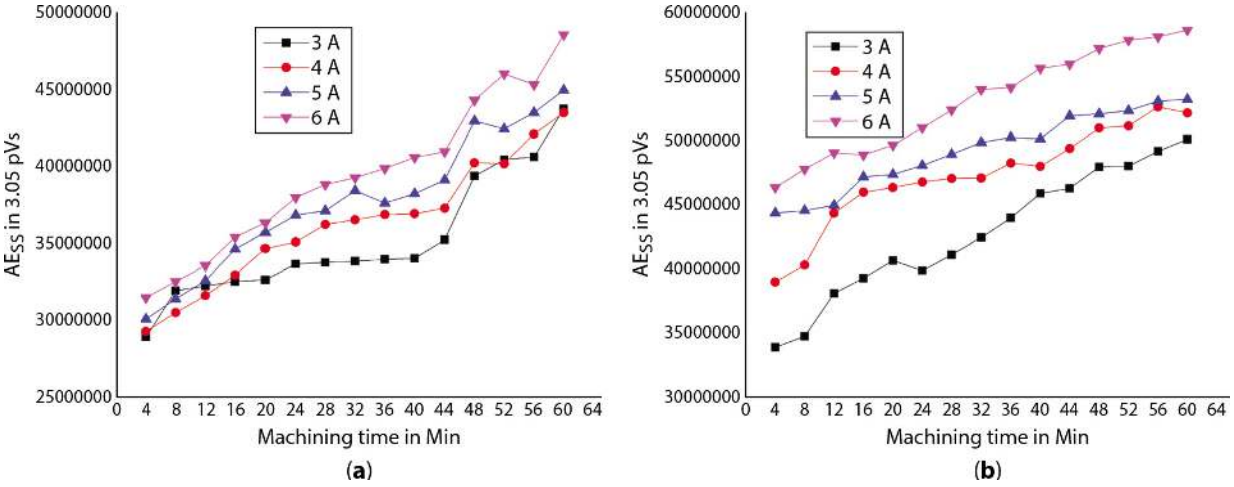


Figure 30.10 (a): AE_{SS} v/s machining time for titanium material. (b): AE_{SS} v/s machining time for P-20 tool steel material.

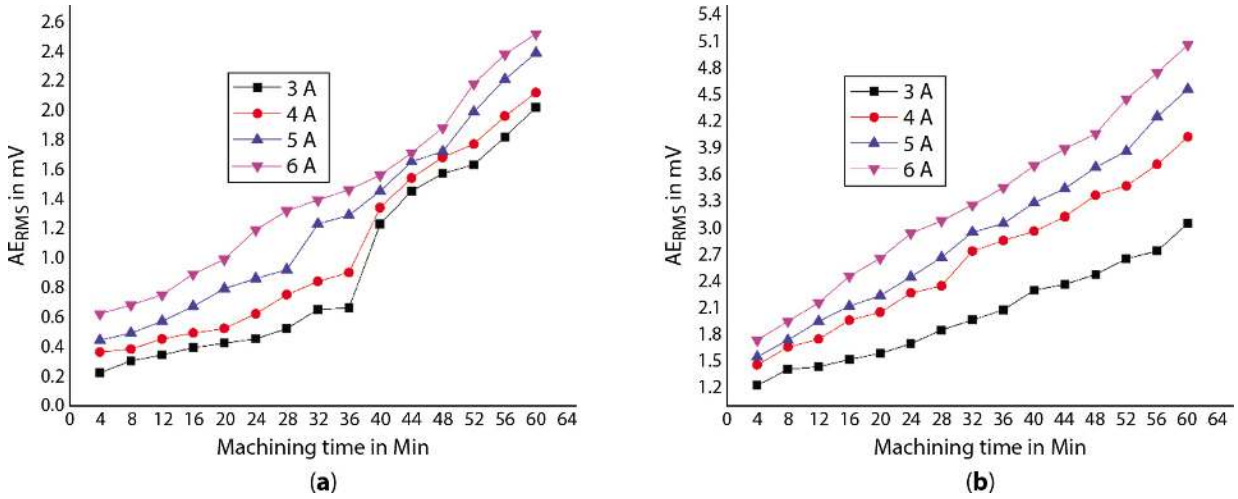


Figure 30.11 (a): AE_{RMS} v/s machining time for titanium material. (b): AE_{RMS} v/s machining time for P-20 tool steel material.

After comparing the AE signals from the plots, it was discovered that AE_{RMS} had greater correlation with EW and SR than A_{ESS} for both materials. Furthermore, compared to the median condition, larger signal variations were observed under the lowest and maximum Pon and C values. Therefore, in order to investigate machining characteristics and performance, further theoretical estimations have been conducted, especially for the minimum and maximum conditions of Pon and C.

30.4.4 Estimation of Machining Characteristics and Machining Performance Using Artificial Neural Network (ANN) for Titanium and P-20 Tool Steel Material

The plots generated from the raw data analysis lacked clarity in conveying the measured values comprehensively. A complete statement of a measured value necessitates the inclusion of an estimate of the associated level of confidence. It is possible to evaluate the experiment's quality and make insightful comparisons with other comparable values or predictions based on theory when experimental data are appropriately reported, including their uncertainties. It is impossible to evaluate whether the experimental value being measured has an ideal quality to the best of one's ability over time without an estimate of the uncertainty. Hence, ANN is used for the estimation/predication of the measured data.

In this study, ANNs are employed to estimate and validate machining characteristics and performance. The Levenberg-Marquardt algorithm (LMA) is utilized to construct the network. One kind of multi-layer perceptron (MLP) network is the BPNN, which consists of an input layer, one or more hidden layers, and an output layer. Multiple hidden layers may exist, each containing numerous neurons (nodes). Consequently, when utilizing BPNN, there is ample opportunity to examine how the network's

architecture (number of hidden layers and neurons) impacts its estimation performance. The flow of information within the network progresses sequentially starting from the input layer and culminating in the output layer. Each layer awaits information from the preceding layer before computing and transmitting its own value. The development of the back-propagation algorithm facilitates the training of network weights and biases using experimental data. Back propagation addresses this issue by propagating the prediction error backward through the network's layers, enabling comprehensive network training. One hidden layer, one output layer, and four input parameters make up the BPNN arrangement. Several configurations were tested with varying numbers of neurons in the hidden layer. The ideal number of neurons was assessed based on the regression value (R value) nearing one. Training, validation, and testing were conducted over a thousand epochs to evaluate machining performance. The network underwent training, validation, and testing phases to monitor machining performance status. The input neurons represent the parameters under investigation for estimating characteristics and performance metrics. Variables such as SR, EW, and AE_{RMS} are treated as dependent variables, while Pon, Poff, C, and BS are considered independent variables. This approach aims to ensure optimal performance across various sensory scenarios.

Figure 30.12 illustrates the SR plot for titanium material with Pon at 20 µs, Poff at 4 µs, C at 5 A, and BS at 25 µm/s, using different percentages of the data training set (50, 60, and 70%). Figure 30.13 depicts the optimal performance plot fit, which occurs when 70% of the data in the training set is utilized. As seen from the plot, a greater correlation with the measured value is established when 70% of the data is used. Better correlation of the data were seen by considering four input parameters, one hidden layer and nine neurons in the architecture, *i.e.*, by considering the one hidden layer and nine neurons, the regression coefficient 'R' raised closer to 1 and mean squared error (MSE) is closer to zero between the input and output parameters.

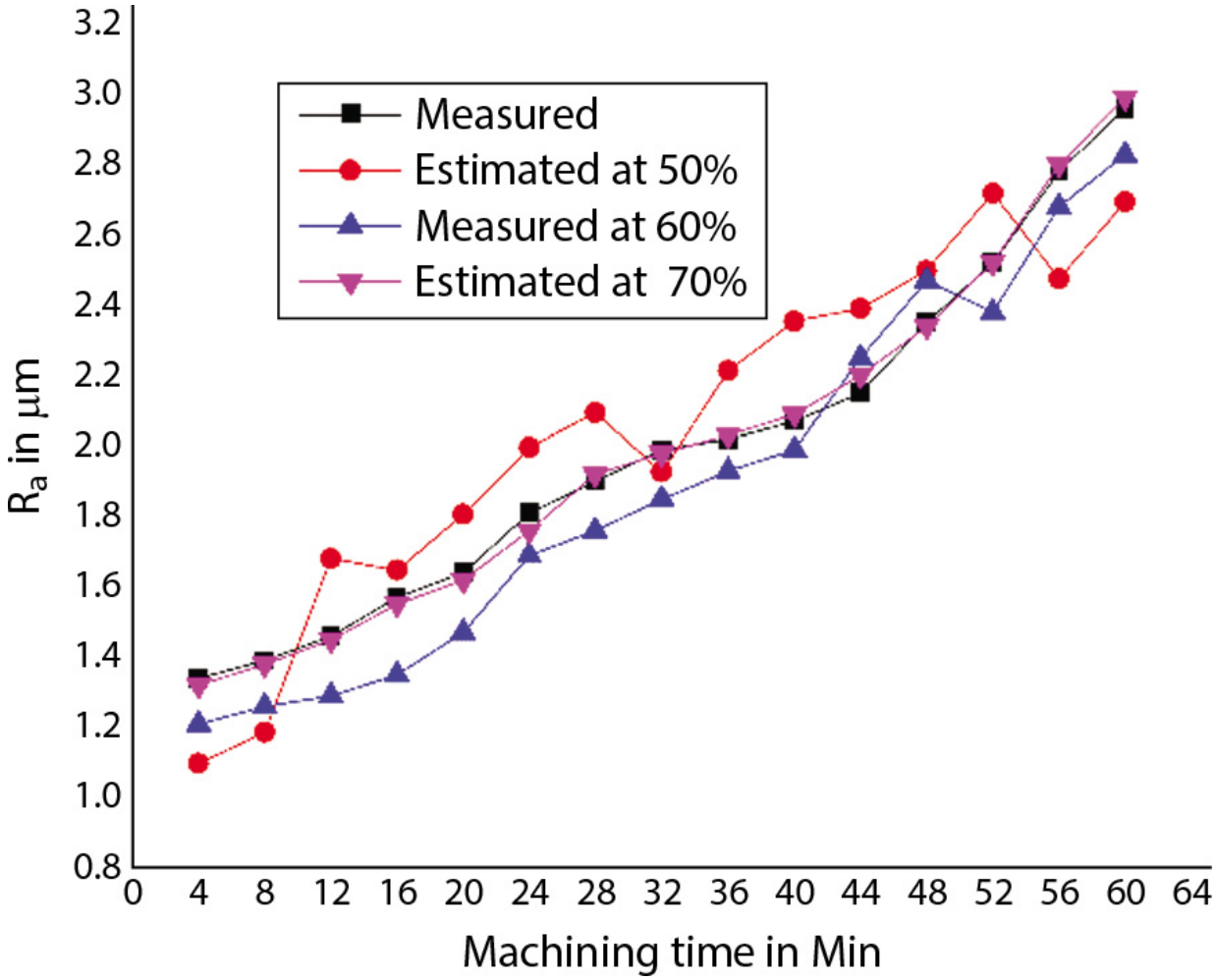


Figure 30.12 Study of percentage for titanium material.

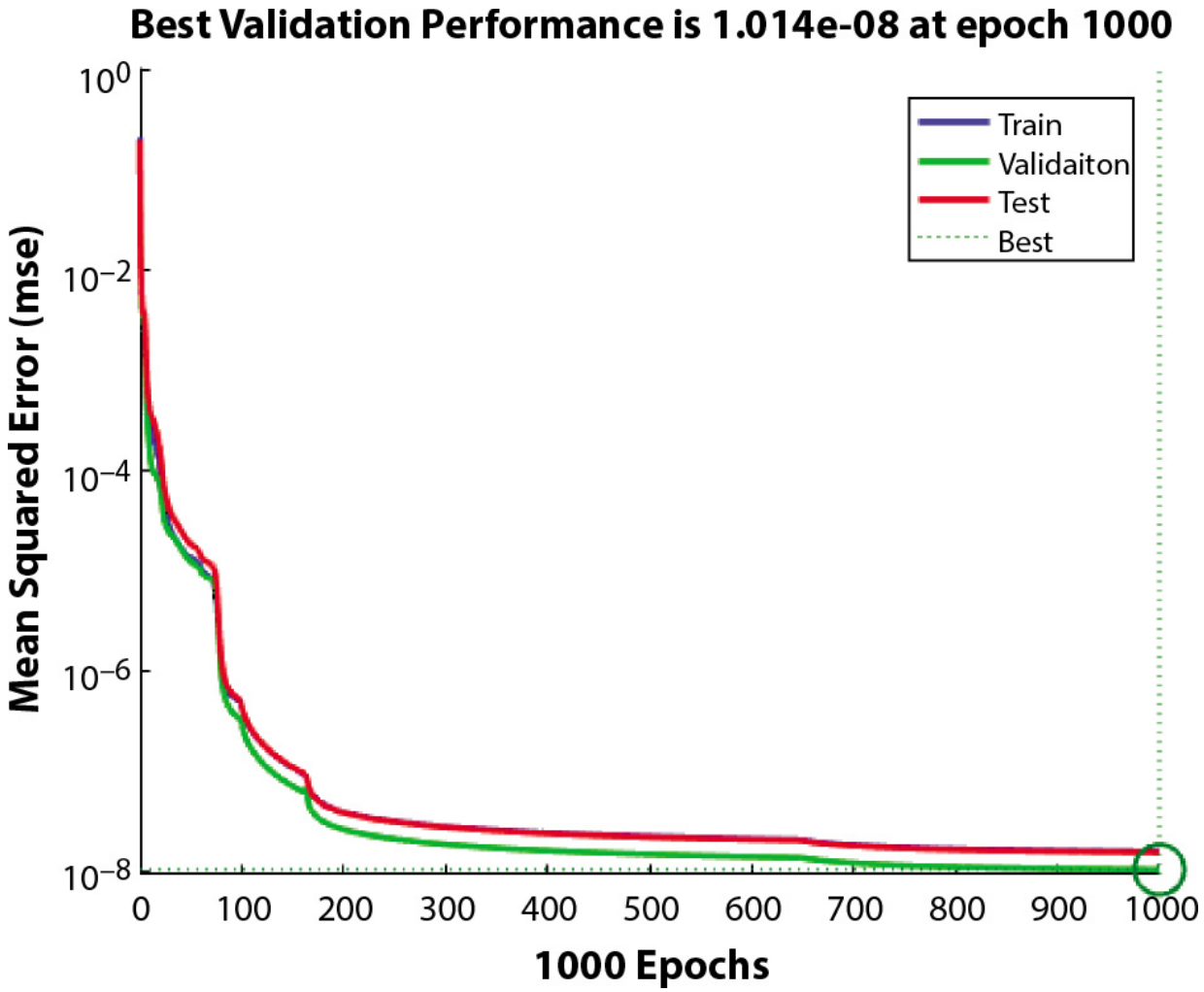


Figure 30.13 The performance plot for titanium in ANN.

30.4.4.1 Estimation of Minimum and Maximum Pulse on Time for SR and AE_{RMS} of Titanium and P-20 Tool Steel Materials

In order to analyze the relationship between SR, EW, and AE_{RMS} with independent parameters, an estimation of these parameters was conducted. Figures 30.14 and 30.15 present the results of experimental and theoretical estimations of SR for titanium and P-20 tool steel materials, respectively. The estimations were performed with varying Pon values, ranging from minimum to maximum, while keeping constant Poff at 4 µs, C at 5 A, and BS at 25 µm/s. These figures provide valuable insights into the signal characteristics.

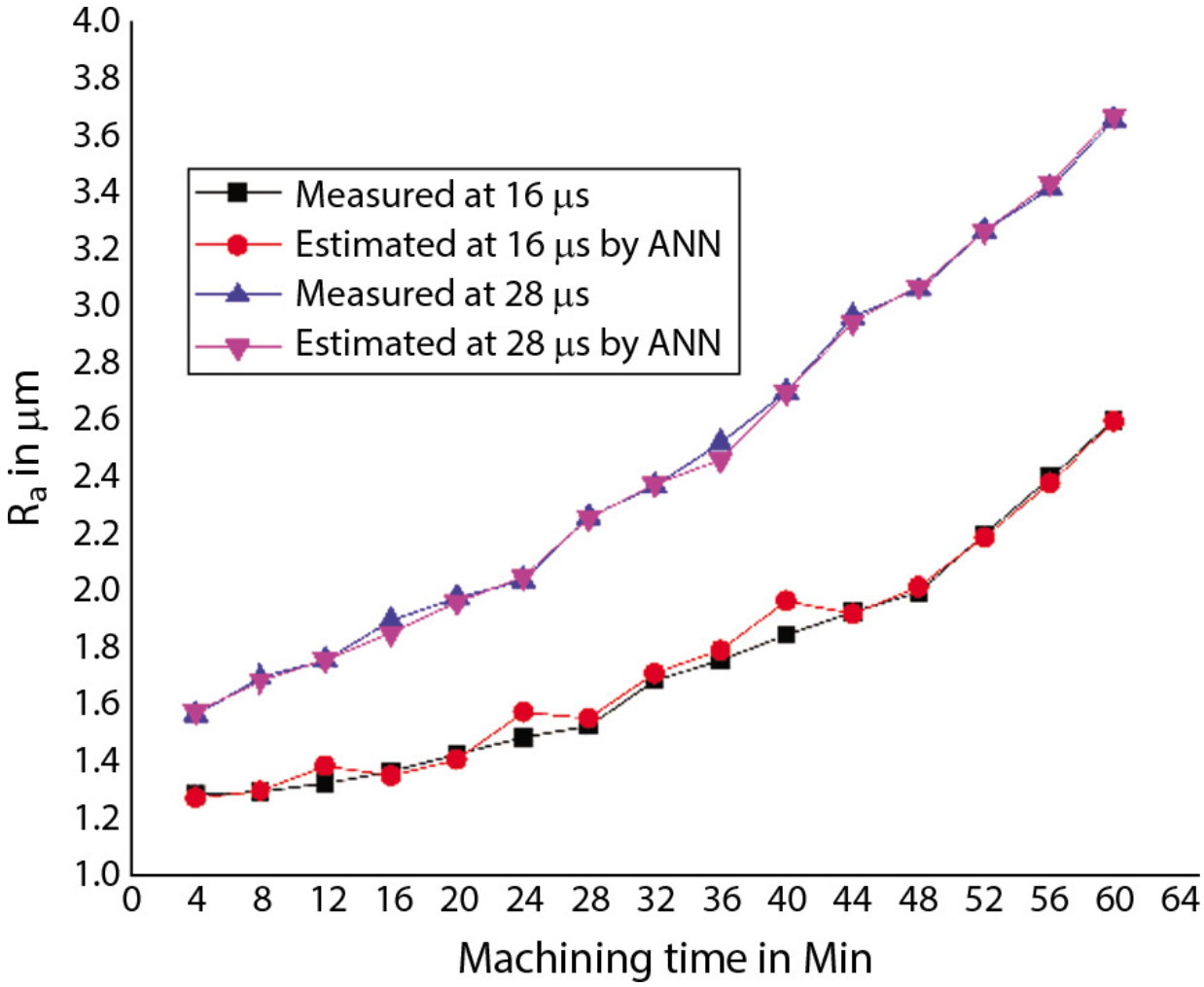


Figure 30.14 Measured and predicted by ANN for SR of titanium material.

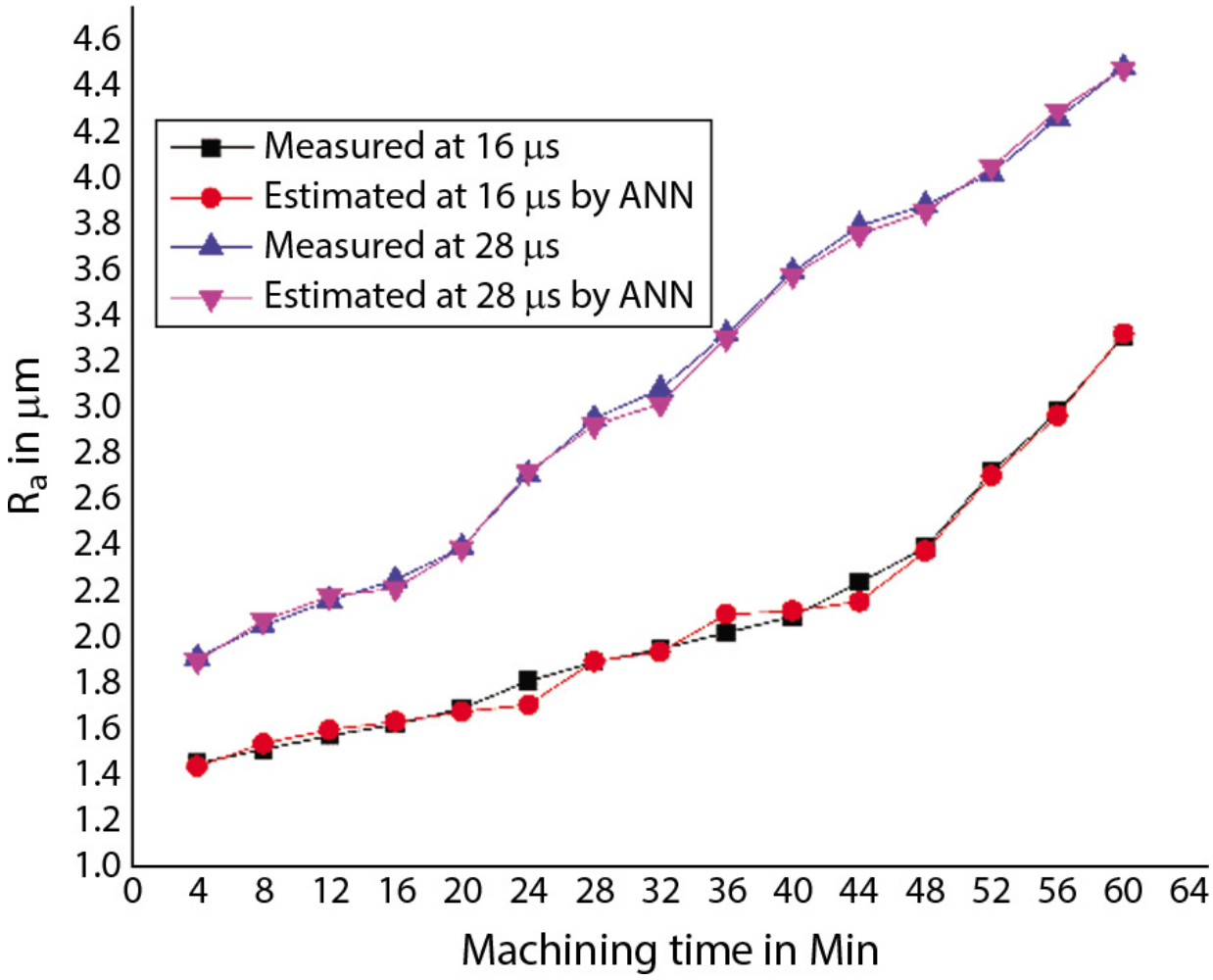


Figure 30.15 Measured and predicted by ANN for SR of P-20 tool steel material.

Moreover, it is clear that the measured and estimated values exhibit a good correlation with the lowest MSE value under the maximum Pon condition. The P-20 tool steel material was found to have the best fit.

Figures 30.16 and 30.17 illustrates the estimation of AE_{RMS} with varying Pon values, ranging from minimum to maximum for both the materials, while maintaining constant values for Poff of 4 µs, C of 5 A, and BS of 25 µm/s. This provides valuable insights into the signal characteristics.

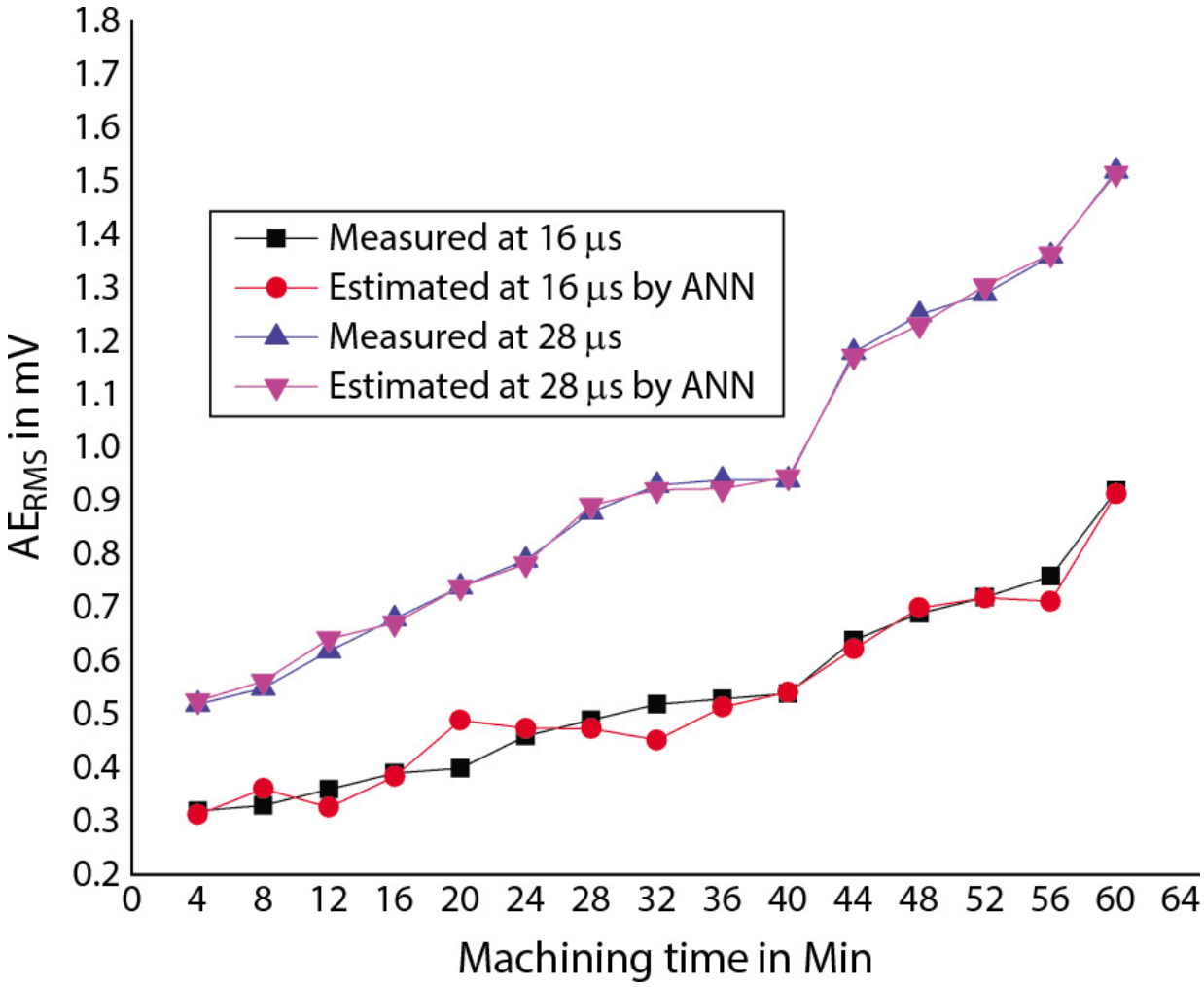


Figure 30.16 Measured and predicted by ANN for AE_{RMS} of titanium material.

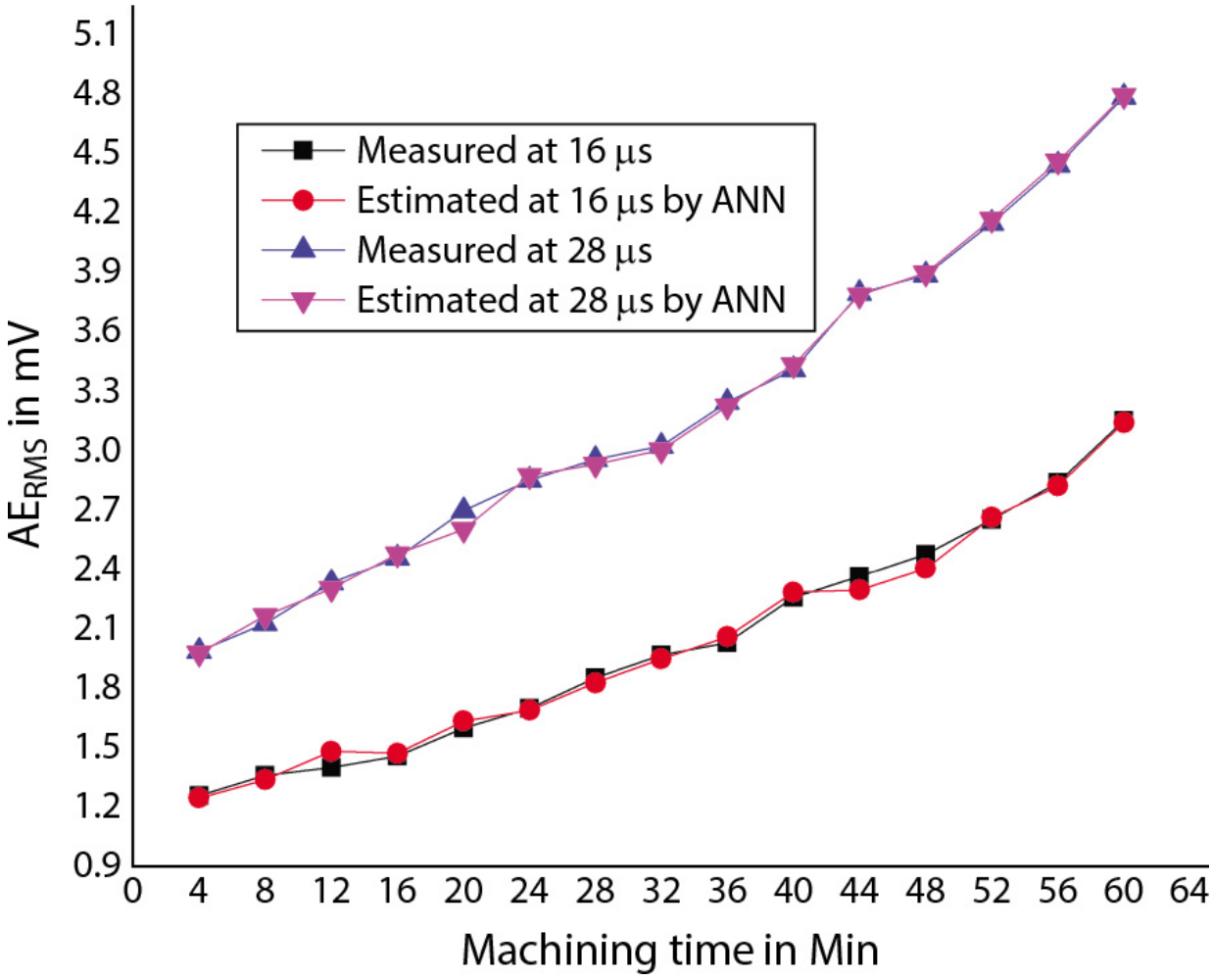


Figure 30.17 Measured and predicted by ANN for AE_{RMS} of P-20 tool steel material.

From the plots it is evident that under the maximum Pon condition, there is a strong correlation between the measured and estimated values, with the lowest MSE value followed by the minimum condition. The most optimal fit was found in the P-20 tool steel material.

The same attribute was seen for EW for both the materials, *i.e.*, best fit was found in P-20 tool steel material and best correlation with the measured values was found for maximum condition of Pon. Additionally, it was noted from the above figure that SR, EW and AE_{RMS} showed improved correlation with the measured values when using a 70% training set. This is likely because with more data considered for training, the algorithm's ability to learn and estimate improves.

30.4.4.2 Estimation of Minimum and Maximum Current for EW and AE_{RMS} of Titanium and P-20 Tool Steel Materials

Figures 30.18 and 30.19 show estimation of EW for minimum and maximum C at constant Pon of 20 µs, Poff of 4 µs, and BS of 25 µm/s, through which a clear insight can be obtained about the signal.

The plots reveal that under the minimum condition of C, there is a strong correlation between the measured and estimated values, with the lowest MSE value observed. Better correlation was observed in P-20 tool steel than in titanium material.

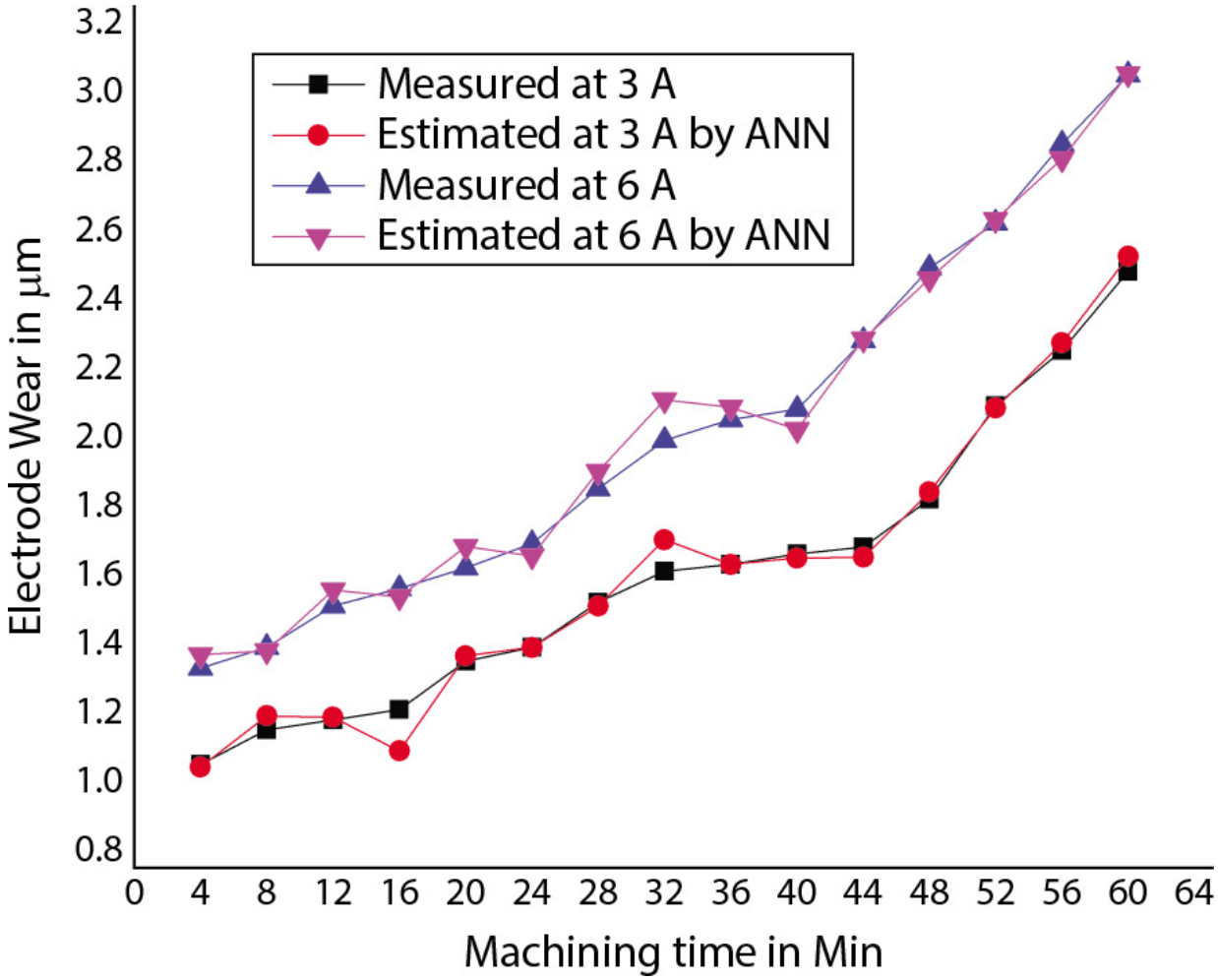


Figure 30.18 Measured and predicted by ANN for EW of titanium material.

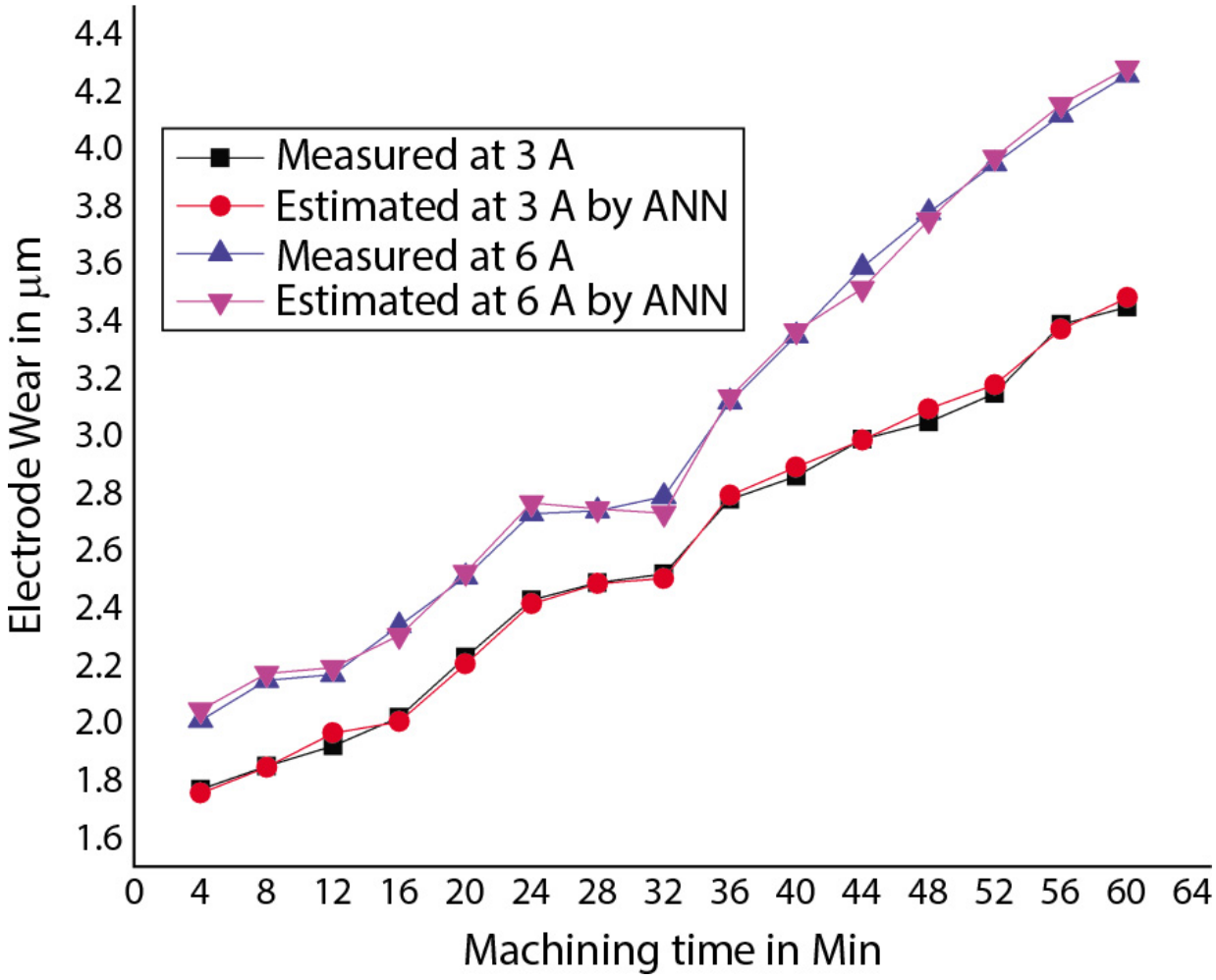


Figure 30.19 Measured and predicted by ANN for EW of P-20 tool steel material.

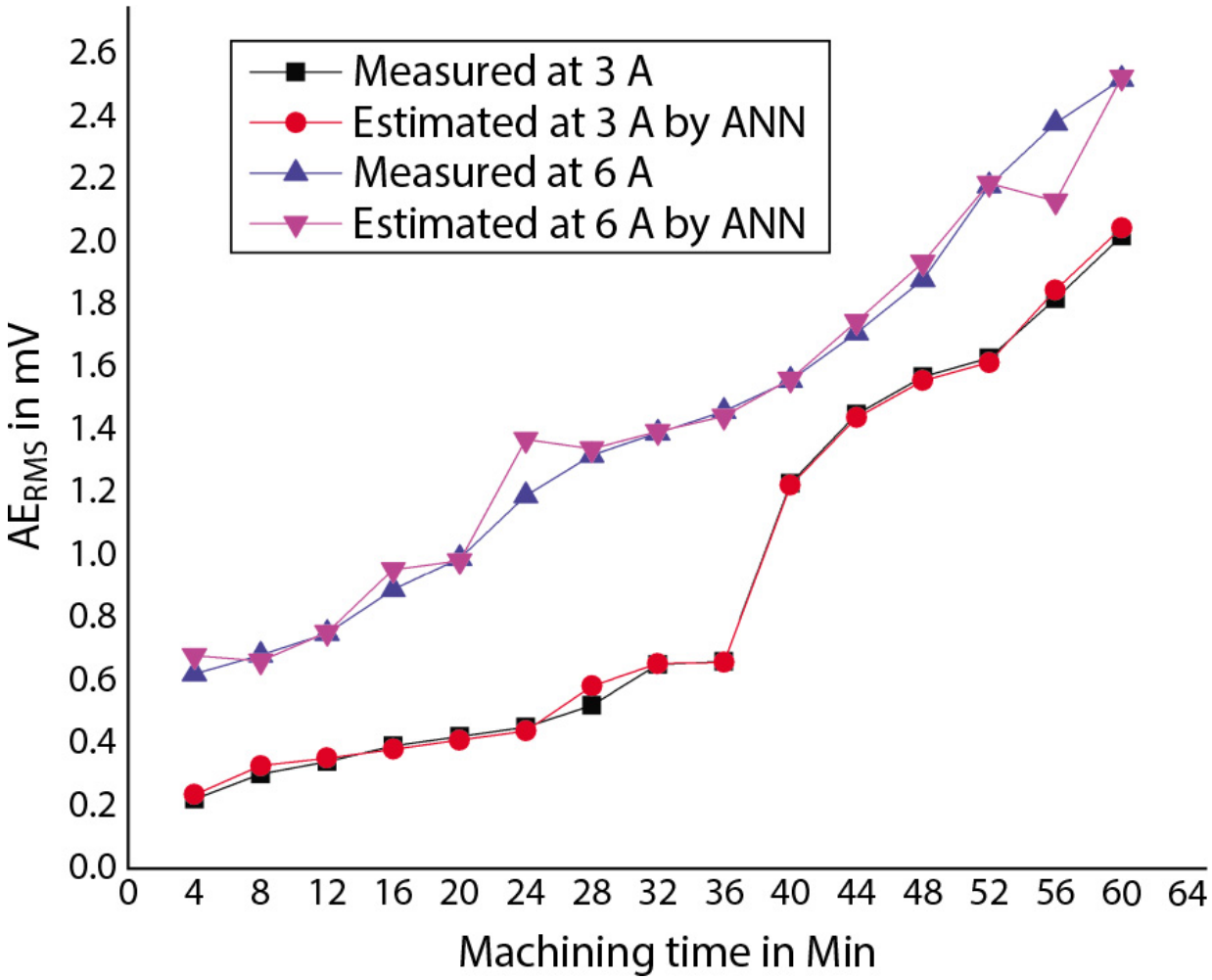


Figure 30.20 Measured and predicted by ANN for AE_{RMS} of titanium material.

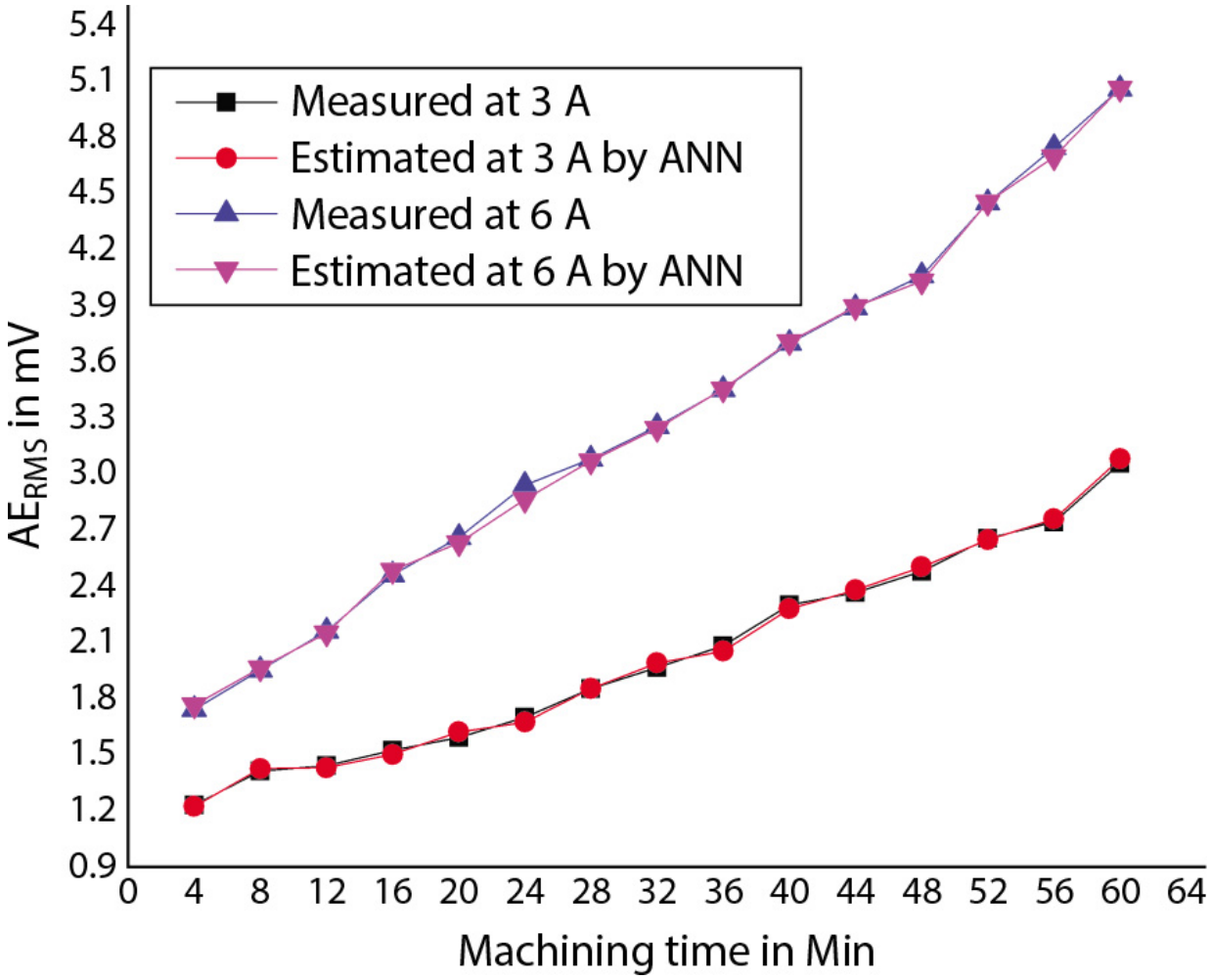


Figure 30.21 Measured and predicted by ANN for AE_{RMS} of P-20 tool steel material.

Figures 30.20 and 30.21 show estimation of AE_{RMS} for minimum and maximum C at constant Pon of 20 µs, Poff of 4 µs, and BS of 25 µm/s, through which a clear insight can be obtained about the signal.

The plots indicate that under the minimum condition of C, there is a strong correlation between the measured and estimated values, with the lowest MSE value. The P-20 tool steel material exhibited the best fit. Similar trends were observed in SR with variations in C.

30.5 Conclusion

The present investigation focused on optimizing machining characteristics and machining performance by varying process parameters during the machining of materials, *viz*., titanium grade-2 and P-20 tool steel materials using molybdenum wire. The aim was to identify the most influential process parameters. Experiments were conducted based on Taguchi's L_{16}

array design. The input process parameters included Pon, Poff, C, and BS, while the output parameters were SR, EW, and AE signals (AE_{SS} and AE_{RMS}). Single-objective optimization was carried out using Taguchi's technique. The process parameter optimization showed that Pon and C have the most significant impact on both machining characteristics and performance. The machining properties and performance, on the other hand, were shown to be unaffected by Poff and BS. In order to comprehend the machining characteristics and machining performance, raw data analysis was done to examine at the relationship between machining time and the variation of Pon and C. It was observed that higher values of SR, EW, AE_{SS}, and AE_{RMS} were associated with higher Pon (28 µs) and higher C (6A) compared to lower and medium levels of these process parameters. When comparing the variation of Pon and C, it was evident that higher values of machining characteristics and machining performance were consistently observed with the variation of C. An ANN estimating model was built utilizing different percentages of data from the training set, namely 50%, 60%, and 70%. It was shown that employing one hidden layer with nine hidden neurons produced a regression coefficient "R" that was closer to 1 and an MSE that was closer to zero after taking into account four input factors. The best fit and highest correlation with the measured values were obtained when 70% of the data were included in the ANN's training set. Prediction comparison also showed that P-20 tool steel correlated well with the estimated/predicted value than titanium grade-2 material.

References

1. Dewangan, S., Biswas, C.K., Gangopadhyay, S., Influence of Different Tool Electrode Materials on EDMed Surface Integrity of AISI P20 Tool Steel. *Mater. Manuf. Process.*, 29, 387–1394, 2014.

2. Kanlayasiri, K. and Boonmung, S., Effects of wire-EDM machining variables on surface roughness of newly developed DC 53 die steel: Design of experiments and regression model. *J. Mater. Process. Technol.*, 192-193, 459–464, 2007.

3. Saha, P., Tarafdar, D., Pal, S. *et al.*, Modeling of wire electro-discharge machining of TiC/Fe in situ metal matrix composite using normalized RBFN with enhanced kmeans clustering technique. *Int. J. Adv. Manuf. Technol.*, 43, 107–116, 2009.

4. Patil, N. and Brahmankar, P.K., Determination of material removal rate in wire electro-discharge machining of metal matrix composites using dimensional analysis. *Int. J. Adv. Manuf. Technol.*, 51, 599–610, 2010.

5. Huang, Y., Ming, W., Guo, J. *et al.*, Optimization of cutting conditions of YG15 on rough and finish cutting in WEDM based on statistical analyses. *Int. J. Adv. Manuf. Technol.*, 69, 993–1008, 2013.

6. Ho, K.H. and Newman, S.T., State of the art electrical discharge machining (EDM). *Int. J. Mach. Tools Manuf.*, 43, 13, 1287–1300, 2003.

7. Han, F., Jiang, J., Yu, D., Influence of discharge current on machined surfaces by thermo-analysis in finish cut of WEDM. *Int. J. Mach. Tools Manuf.*, 47, 7-8, 1187–1196, 2007.

8. Hassan, M.A., Mehat, N.S., Sharif, S. *et al.*, Study of the Surface Integrity of AISI 4140 Steel in Wire Electrical Discharge Machining. *Proceedings of the International Multi Conference of Engineers and Computer Scientists, IMECS*, March 18-20, 2009.

9. Li, L., Guo, Y.B., Wei, X.T. *et al.*, Surface integrity characteristics in wire-EDM of inconel 718 at different discharge energy. *Procedia CIRP*, 6, 220–225, 2013.

10. Mouralova, K., Matousek, R., Kovar, J. *et al.*, Analyzing the surface layer after WEDM depending on the parameters of a machine for the 16MnCr5 steel. *Measurement*, 94, 771–779, 2016.

11. Guo, Y.B., Li, W., Jawahir, I.S., Surface integrity characterization and prediction in machining of hardened and difficult-to-machine alloys: a state-of-art research review and analysis. *Mach. Sci. Technol.*, 13, 4, 437–470, 2009.

12. Spedding, T.A. and Wang, Z.Q., Study on modeling of wire EDM process. *J. Mater. Process. Technol.*, 69, 18–28, 1997.

13. Welling, D., Results of surface integrity and fatigue study of wire-EDM compared to broaching and grinding for demanding jet engine components made of Inconel 718. *Procedia CIRP*, 13, 339–344, 2014.

14. Ibrahem, M., Ahmed, A.D., Hamdi, D., Review of improvements in wire electrode properties for longer working time and utilization in wire EDM machining. *Int. J. Adv. Manuf. Technol.*, 76, 329–351, 2015.

15. Kapoor, J., Singh, S., Khamba., J.S., High-performance wire electrodes for wire electrical-discharge machining-a review. *Proc. Inst. Mech. Eng. Part B J. Eng. Manuf.*, 226, 11, 1757–1779, 2012.

16. Manoj Samson, R., Sridhar, A., Ranjith, R. *et al.*, Experimental Investigation of Heat-Treated Tool on Wire Electric Discharge Machining of Titanium Alloy (Ti-6Al-4V). *Adv. Mater. Sci. Eng.*, 2022, 1–11, 2022.

17. Suresh Kumar, S., Uthayakumar, M., Thirumalai Kumaran, S. *et al.*, Performance Monitoring of WEDM Using Online Acoustic Emission Technique. *Silicon*, 10, 2635–2642, 2018.

18. Shandilya, P., Jain, P.K., Jain, N.K., RSM and ANN Modeling Approaches For Predicting Average Cutting Speed During WEDM of SiCp/6061 Al MMC. *Procedia Eng.*, 64, 767–774, 2013.

19. Pradhan, M.K., Das, R., Biswas, C.K., Comparisons of neural network models on surface roughness in electrical discharge machining. *Proc. Inst. Mech. Eng. Part B J. Eng. Manuf.*, 223, 7, 801–808, 2009.

20. Prathik, J.S., Ravindra, H.V., Ugrasen, G. *et al.*, Study of Surface Roughness and AE Signals while Machining Titanium Grade-2 Material using ANN in WEDM. *Mater. Today Proc.*, 4, 9, 9557–9560, 2017.

21. Manoj, I.V., Narendranath, S., Mashinini, P.M. *et al.*, Artificial neural network-based prediction assessment of wire electric discharge machining parameters for smart manufacturing. *J. Behav. Rob.*, 14, 1, 20220118, 2023.

22. Wang, Y., He, D., Yang, L. *et al.*, Formation mechanism of surface topography in low-speed wire electrical discharge machining Inconel 718 and its on-line prediction based on acoustic emission technology. *Adv. Mech. Eng.*, 9, 4, 1–17, 2017.

23. Rajeev, K. and Amit, K., Effect of Pulse on Time on Performance Parameters of WEDM. *DAV National Congress on Science, Technology & Management*, November 7-8, 2014.

24. Brajesh, K.L. and Sanjay, A., Optimization of Machining Parameters in WEDM of AISI D3 Steel Using Taguchi Technique. *Procedia CIRP*, 14, 194–199, 2014.

25. Avinash, S., Parmar, A.J., Snehal, J., To Investigate Electrode Wear Rate on Steel Material with Different Parameters on EDM Machine. *Int. J. Adv. Eng. Res. Sci.*, 3, 6, 189–193, 2016.

26. Ashish, G., Anand, P., Pooja, S., Investigation of Surface Roughness for Inconel 625 using Wire Electric Discharge Machining. *IOP Conf. Ser. Mater. Sci. Eng.*, 377, 012109, 2018.

27. Ravindranadh, B., Madhu, V., Gogia, A.K., Modelling and analysis of material removal rate and surface roughness in wire-cut EDM of armour materials. *Eng. Sci. Technol.*, 18, 4, 664–668, 2015.

Note

*Corresponding author: prathik9@gmail.com

31
Chemical-Based Bulk Machining and Fabrication of Silicon Microstructures: An Overview

Sumanta Banerjee
Mechanical Engineering Department, Heritage Institute of Technology, Kolkata, West Bengal, India

Abstract

Over the past decades, MEMS (microelectromechanical systems)-based sensors and actuators have gained widespread popularity in cutting-edge applications. There has been rapid progress in both the technologies and fabrication methods of MEMS components. Silicon bulk micromachining, based on wet chemical-based techniques, has emerged as a widely adopted method for fabrication of microstructures. The latter are integral to MEMS devices. Significant contributions have been made by researchers, worldwide, in advancing wet chemical-based micromachining. Their efforts span from basic understanding of etching mechanisms, to applying them for intricate MEMS structures. Wet bulk micromachining offers diverse benefits, notably the capacity to produce slanted sidewalls for micromirrors and freestanding structures (diaphragms and cantilevers). This versatility positions wet bulk micromachining as a promising novel tool for fabricating structures for various applications. The present chapter underscores the significance of wet bulk micromachining in MEMS fabrication, offering a comprehensive overview from basic to advanced concepts. Starting with fundamental crystallography to comprehend wet anisotropic etching for silicon micromachining, it

progresses through silicon wafer manufacturing and microfabrication techniques employed in semiconductor industries for MEMS component fabrication.

***Keywords*:** MEMS, micromachining, silicon wafer manufacturing, microfabrication

31.1 Silicon: Material for Integrated Circuits and MEMS

Silicon, with the chemical symbol Si (atomic number 14), is a semiconductor material characterized by its diamond lattice structure. In this structure, each silicon atom forms four covalent bonds with its neighboring atoms, arranged tetrahedrally. The (Si) unit cell comprises of two face-centered cubic (FCC) cells that inter-penetrate along 25% of the body diagonal. Silicon primarily exists in compound forms and is widely distributed in various natural sources such as dust, sands, planetoids, and planets, mainly as silicon dioxide (silica) or silicates [1]. Silicon holds significant importance in technology, being extensively utilized in fabrication of ICs (integrated circuits) and microelectromechanical systems (MEMS) due to its favorable semiconductor properties [1, 2].

Silicon, as a semiconductor material, possesses an electrical conductivity level between that of a conductor and an insulator. Its suitability for integrated circuit (IC) devices is primarily attributed to its cost-effectiveness (being the second-most naturally abundant element). Additionally, its electrical conductivity can be finely adjusted across a wide range by introducing dopants [1–3].

Historically, research on silicon has primarily centered on its application in the IC industry, with most fabrication processes tailored for silicon. With the advent of microelectromechanical Systems (MEMS), silicon emerged

as the preferred material for device development. This preference stems from various factors, including the utilization of existing IC fabrication equipment, enhanced scalability, well-understood material properties, ready availability in pure form, and the ease of integrating electronic circuitry onto the same chip. These advantages position silicon as a versatile and advantageous material for the creation of MEMS-based devices [1–4].

31.2 Overview of Microelectromechanical Systems

The convergence of electrical and mechanical elements within a single silicon chip marked the advent of a novel technology known as MEMS, or microsystem technology (MST). As these MEMS structures are further miniaturized into the nano-scale, they are aptly termed nano-electromechanical systems (NEMS). The broad spectrum of applications for MEMS/ NEMS spans diverse fields, including chemical and biosensors, aerospace, radio-frequency (RF) circuits, and consumer electronics, marking it as one of the most promising technologies of our time.

The MEMS-based devices exhibit a size range from mere micrometers to millimeters, boasting the capability to sense, manipulate, and actuate on both micro- and nanoscales. This versatility positions MEMS technology to profoundly impact numerous product categories, offering the potential for comprehensive system-on-a-chip realization by seamlessly integrating mechanical and electrical components. Over the years, the evolution of MEMS has witnessed the integration of novel materials, concepts, and methodologies tailored to meet the demands of emerging applications, fostering continuous innovation and advancement in the field [3, 4].

Electronic components are typically manufactured using established IC technology. Fabrication of mechanical structures, on the other hand, whether movable or stationary, relies on specialized techniques such as micromachining, LIGA (German acronym for a microfabrication technique, which translates as “lithography, electroplating, molding”), and micro-stereolithography, among others. Specifically, micro-stereolithography finds its application in the creation of polymer-based MEMS.

Among these techniques, silicon μ-machining stands out as the predominant method for crafting mechanical components. This process leverages a range of equipment, including thermal oxidation furnaces, RF sputtering devices, thermal evaporators, chemical vapor deposition (CVD) machines, spin coaters, and more. Remarkably, much of this equipment mirrors that utilized in IC fabrication, underscoring the synergies between the two domains [4].

31.3 Silicon Wafers Fabrication: Procedural Stages

The manufacturing of silicon wafers with varying orientations and diameters comprises of several procedural stages, as briefly outlined in the subsequent sections [4–6].

31.3.1 Crystal Growth and Doping

Quartzite (or sand; SiO_2) is the raw material use for manufacturing of silicon. The furnace where sand is heated contain wood chips, coke, and coal (*i.e.*, sources of carbon). Metallurgicalgrade silicon (MGS) of fairly high purity (≈98%) is eventually produced through a sequence of reactions taking place inside the furnace. However,

elements such as iron and aluminum are still retained as contaminants in MGS. The latter is further distilled for further purification to EGS (electronic-grade silicon), which is a polycrystalline material used to fabricate devicegrade, single-crystal silicon wafers. Cylindrical ingots are grown by the float-zone (FZ) and Czochralski (CZ) techniques from EGS, and then used for the production of wafers.

An outline of the CZ method is presented here. The EGS is fragmented into small pieces and placed inside a fused-silicon (SiO_2) crucible. The crucible is heated (in inert argon ambient) to keep the EGS in molten state (above ~1414°C). Thereafter, a single-crystal seed is introduced within the molten (EGS) matrix for crystal growth. The seed orientation determines the crystal orientation, and development of large single crystals is favored through progressive freezing at the solid-liquid interface. In addition, controllable parameters such as the rotation rates of seed and crucible (crystal rotation ~1.0–3.0 rpm, crucible rotation ~2–20 rpm), temperature of EGS melt, and the pulling rate (which varies as ~50–100 mm/h) of seeded crystal also influence the rates of crystal growth. Dopants are added in the wafers at controlled rates to the melt in order to provide regulated levels of p-type or n-type doping. Desired levels of doping concentration (mostly, boron for p-type; phosphorus for n-type semiconductor material) in the grown crystal are attained by adding precisely calculated amounts of dopant to the EGS melt.

The FZ growth method is less prevalent, and is restricted to situations where carbon and oxygen impurities are desired to be minimum. In this operation, a vertically-mounted rod of EGS polysilicon, with the seed crystal at the bottom, is rotated inside a quartz envelope. An inert atmosphere of argon (Ar) is maintained within the enclosure. A high-power radio frequency (RF) provides coil localized heating. As the heat source is traversed along the length of

(polysilicon) rod, crystallization of silicon occurs due to localized melting (induced by eddy current heating). The system is stabilized by the combined effects of surface tension and RF field-induced levitation. Chance of contamination is practically negligible, as no crucible is used. Whereas a seed crystal sets the crystal orientation in the FZ process, the concentration of dopant is usually regulated by initiating the process with a doped rod; else, by a suitable dopant gas is added to an atmosphere of argon within the enclosure. In the latter procedure, the (dopant) gases commonly added to the inert gas are PH_3 (phosphine) for n-type and B_2H_6 (diborane) for p-type.

31.3.2 Ingot Trimming, Grinding, and Slicing

After a crystal is grown, the seed and tang ends are trimmed, and the ingot diameter is uniformly sized down to desired dimensions. Afterward, typically one or more flats are ground along the length of the ingot. The largest flat is called the primary flat, which can be ground according to customized requirement. In chemical-based wet bulk μ-machining method, for instance, the primary flat works as reference plane for the processing equipment. In addition, this provides reference direction for specific crystallographic alignment of the mask pattern. Most commonly, wafers with primary flat are supplied by manufacturers. A data sheet is also provided, wherein information on parameters such as conductivity-type, orientation, thickness, resistivity, taper, bow, diameter, impurity, flat location, etc. are provided. The use of secondary flat for specification of conductivity type and orientation of the wafer is less common nowadays [4–7].

Table 31.1 Standard silicon wafer size versus thickness.

Wafer size	Standard thickness
51 mm (2 in)	275 µm
76 mm (3 in)	375 µm
100 mm (4 in)	525 µm
125 mm (5 in)	625 µm
150 mm (6 in)	675 µm
200 mm (8 in)	725 µm
300 mm (12 in)	775 µm
450 mm (18 in)	925 µm

For wafers which comprise of silicon crystals with diameters ≥200 mm, a groove (made on the edge) commonly replaces a primary flat for purposes of orientation and positioning. The ingot is firstly trimmed and grinded, and then sliced into individual wafers using wire sawing or inner diameter (ID) sawing. Slicing determines four salient parameters of the wafer: surface orientation, total thickness variation (TTV), thickness, and wafer curvature (or bow). The size of a (sliced) wafer decides its thickness; the latter must be adequate to provide necessary mechanical support during fabrication of devices. The values of wafer thickness versus its diameter are cited in Table 31.1, as per standard industrial practice.

31.3.3 Polishing, Cleaning, and Packaging

To achieve submicron precision and resolution, fabrication procedures for ICs and MEMS need extremely flat and smooth surfaces. On the sliced wafers, multiple manufacturing stages are carried out to produce a surface which is smooth and highly flat.

At first, a solution of Al_2O_3, water and glycerin is used to lap the wafers on both sides. By eliminating the majority of the surface damage and bow (deviation from flatness characterized by roughly cylindrical or spherical curvature) caused by the sawing process, or undesired tapers, this step helps to improve the flatness of the wafers to approximately ±2 µm. After being lapped, the edges of the wafers are shaped by a procedure known as edge contouring. This prevents chipping, dislocation, and other flaws throughout the fabrication process of the device. The lap procedure typically damages and contaminates the wafer surface. Therefore, chemical etching is employed in hydrofluoric, nitric, and acetic acids (HNA) solution in order to remove damaged and contaminated zones, as well as microscopic fissures/cracks. The presence of acetic acid (in HNA) dilutes the mixture and controls etching rates. At first, nitric acid is employed to oxidize the silicon surface. This step is followed by dissolving the resulting oxide using hydrofluoric acid. The foregoing procedure removes the surface layer (containing small cracks or defects) by etching few tens of microns of silicon off on either side of the wafer. Multiple de-ionized (DI) water baths are then used to remove the acid solution [4, 8].

31.4 Silicon Microfabrication Processes

This section [3–9] provides a concise summary of the numerous fabrication techniques that are employed for Si-based IC/MEMS fabrications. Cleanrooms are facilities where microfabrication procedures are carried out. A cleanroom is a specially designed enclosed space that has been given environmental controls for airborne particles, temperature (≈ 20°C–23°C), humidity (≈ 40–46%), RH (40–46%), air pressure (requisite positive head, in order to blow

away dust), tailored airflow circulation and patterns, noise and vibration (within permissible ranges), allowable (threshold) limits for living µ-organisms, and lighting (intensity and luminance). According to how pure the air is, cleanrooms are categorized. “Class X” denotes that there are fewer than “X” number of particles, of size not less than 0.5 µm, present in every cubic foot of air available within the space. Classes 1, 10, 100, 1000, and 10,000 cleanrooms are the most typical categories [5, 6, 8].

To maintain a cleanroom’s cleanliness, the following safety measures must be taken: (a) wearing a cleanroom suit that completely encases the person in order to keep the (cleanroom) environment free of skin and hair; (b) using air showers before entering a cleanroom, to ensure that filtered air is blown on and around the person (in an air shower) to eliminate any surface impurities; (c) avoiding use of paper, pencils, and markers that leave lint or dust; (d) replacing gloves once they get soiled or torn; (e) using dust-free ballpoint pens and cleanroom paper; and (f) making provisions whereby the cleanroom is maintained at a net positive pressure head to blow dust out periodically, and doors open inward so that the pressure of the surrounding space closes them [9].

31.4.1 Wafer Cleaning

Wafer surfaces must be cleaned by removing particles, organics (photoresist [PR]), and any other traces of contaminating agents. Front-end and back-end processes are respectively used for the cleaning of silicon wafers before and after metallization. During cleaning, ultrasonic agitation (of frequency range $\sim 20 - 50$ kHz) significantly removes unwanted particles. Under the action of alternating tensile and compressive strains induced by the ultrasound, the sound waves generated in a suitable liquid promote the creation, expansion, as well as sudden collapse

of small vapor bubbles. For cleaning the wafers, megasonic agitation (~1 MHz) proves very effective. Organics like photoresists are eliminated in either O_2 plasma or in H_2SO_4 : H_2O_2 ::1: 1 (called the Piranha bath). Since this mixture is a powerful oxidant, it eliminates the majority of organic material. Additionally, it adds OH groups to most surfaces (called the hydroxylation process), which greatly increases their water-affinity (hydrophilicity). Piranha solutions also refer to other mixture ratios of H_2SO_4 and H_2O_2, such as 1:3, 1:4, etc. Piranha solutions need to be prepared carefully. It oxidizes quickly and is extremely corrosive. Prior to treatments by a piranha solution, it must be ensured that surfaces are somewhat clean and totally devoid of organic solvents from prior wash processes [9].

Organics, heavy metals, and alkali ions are typically removed from the wafer surface using the standard Radio Corporation of America (RCA) cleaning procedure. Conventional RCA cleaning is primarily carried out in the following three processes. Using a solution (NH_4OH: H_2O_2: DI water :: 1: 1: 5), the wafer surface is first cleaned using SC-1 (Standard Clean-1) to get rid of organic contaminants and particulates. This cleaning process is adversely affected by formation of an ultra-thin SiO_2 (silicon dioxide) layer (~1 nm) on the silicon surface, which accumulates varying degrees of metallic contaminations. The second stage consists of removing the thin oxide coating, and diluted hydrofluoric acid solution (e.g., H_2O: HF :: 50: 1) is used for this purpose. To get rid of any last bits of metallic (ionic) contamination, the process is finished with SC-2 (Standard Clean-2) solution, which comprises of HCl: H_2O_2: DI water :: 1: 1: 6. As bare silicon gets instantly contaminated when exposed to atmosphere, this treatment causes a super-clean, thin oxide layer to grow on the surface of the silicon wafer, which serves as a passivation

layer to shield the surface from further contamination. After completing all the three processes, a thorough rinse in DI water is carried out [9].

31.4.2 Thin-Film Formation

In ICs and MEMS, thin films serve as crucial building blocks. Thin films can be deposited on substrates using either chemical or physical processes. These films contain metals, semiconductors, and dielectrics. The deposited films are typically categorized as amorphous, single-crystal, or polycrystalline. The following sections address the most popular deposition methods used in MEMS and IC technology [4, 9].

31.4.2.1 Reactive Growth (or Thermal Oxidation)

The process of thermal oxidation refers to a method in which silicon dioxide is produced by exposure of silicon wafers either to oxygen directly (dry oxidation), or to water vapor at high temperatures (called the wet oxidation process, at temperatures ranging between 900°C −1200°C). The substrate and chemically-reactive species interact in this deposition technique to create a fresh thin coating. Therefore, it is also known as reactive growth. A thermal oxidation system’s fundamental construction is briefly described. The system includes a furnace (resistance-heated), a fused quartz (cylindrical) tube, gas cylinders, and a quartz water bubbler for generating water vapor. Silicon wafers are positioned vertically (within the setup) in a slotted quartz boat. The average flow velocity of gas (oxygen or water vapor) is maintained around ~1 liter/min, and the oxidation temperature typically ranges between ~900°C and 1200°C. Three categories of thermal oxidation are distinguished: pyrogenic, wet, and dry. Wet oxidation involves oxygen passing through boiled DI water. Dry oxidation involves oxygen being flown directly into the

tube that has been heated to the desired oxidation temperature [4, 10]. For pyrogenic oxidation, as in wet oxidation, an internal or external torch is employed to transform homogeneously mixed hydrogen (H_2) and oxygen (O_2) gases into pure steam (H_2O) by auto-ignition.

Dry oxidation: $Si + O_2 = SiO_2$

Wet oxidation: $Si + H_2O$ vapor $= SiO_2 + 2H_2$

Nitrogen gas (N_2) is flown during the temperature ramp-up and ramp-down sequences to generate an inert environment. For purposes of pushing and drawing into and out of the furnace, silica rods are employed. During the thermal oxidation process, the $Si - SiO_2$ interface penetrates the silicon. As reported in Reference [4], silicon of thickness 0.44x (0.44 times 'x') is used in order to grow the thickness of oxide layer by 'x'. Compressive stresses are produced in the generated oxide layer as a result of volumetric dilatations in the silicon and the oxide during the heat oxidation process. The fundamental reaction-kinetics (in the above oxidation) is constrained by two factors: (a) rate of reaction at the sample surface, and (b) diffusion of new species through the existing films. At the interface between SiO_2 and Si, a reaction occurs because oxygen diffuses through SiO_2 more quickly than Si.

A simple and popular approach to comprehend the growth-rate of SiO_2 is the Deal-Grove model. A significant volume of published literature on microfabrication contain information about this model. In this model, the stages of oxidation are depicted successively as linear and parabolic. Especially in early stages of oxide formation, when the thickness of oxide layer increases linearly over time, the linear stage (reaction-restricted) is considered appropriate. In this instance, silicon and the oxidants interact chemically

at the wafer surface; therefore, the growth is referred to as reaction-limited (or reaction-restricted). The amount of silicon atoms that are available to interact with the oxidants limits the reaction rate. The oxide increases linearly with time (t) for the first 500 Å of oxide growth, and the time-dependent thickness[x = x(t)] of the grown oxide is determined by the following simplified relation:

$$x = \frac{B}{A}(t + \tau)$$

In the above equation, the time coordinate (= τ) shift that takes into consideration the initial oxide layer is represented by t. The linear rate constant is known as $\left(\frac{B}{A}\right)$ [4].

When the oxide layer progressively thickens (greater than ≈ 1000 Å), diffusion-limited reaction rates take over. This is because, in order to react at $Si - SiO_2$ contact site, diffusion of the oxidant (through the oxide) must occur. This diffusion-limited step of oxidation is termed the "parabolic stage". In this instance, the oxide thickness (x ≡ x(t)) varies as follows:

$$x^2 = B(t + \tau)$$

In the above equation, the symbol B denotes the parabolic rate constant.

The SiO_2 layer grows far more quickly in a humid environment than it does in dry oxygen. The main cause of this is that H_2O has a substantially higher oxidant solubility in SiO_2 than O_2. As a result, the rate constants for H_2O are substantially bigger than those for O_2, both linearly (B/A) and parabolically (B). The time coordinate shift is

insignificant, owing to the wet oxidation process' rapid development rate [4, 10].

The advantages of a thermally grown oxide layer are manifold, namely (a) exceptional electrical insulation properties (energy gap ~9 eV, and resistivity exceeding $\sim 10^{20}$ ohm-cm); (b) high breakdown electric field (> 10^6 V/cm); (c) effective masking against diffusion and implantation ($D_{SiO_2} \ll D_{Si}$); (d) integral component in MOS (metal-oxide-semiconductor) structures; (e) utilization in MEMS fabrication; (f) surface passivation (typically involves depositing a thermally grown oxide layer onto the surface of the semiconductor) to enhance device performance and reliability; (g) electrical isolation between layers (enabling the integration of complex circuitry without interference); and (h) device isolation (ensuring optimal functionality) [11].

31.4.2.2 Chemical Vapor Deposition (CVD)

The CVD is a versatile method utilized for depositing nonvolatile solid films onto substrates by reacting vapor-phase chemicals. Widely employed in µ-electronics and MEMS applications, the CVD method facilitates the deposition of various materials (such as Si_3N_4, poly-Si, W, and SiC, among others), in forms ranging from monocrystalline to polycrystalline, amorphous, and epitaxial.

The process offers advantages like conformal coating with excellent step coverage and the capability to coat multiple wafers simultaneously. Typically, a CVD process unfolds through several steps:

- Introduction of gases (or reactants) into a heated reaction chamber, maintained between temperatures ranges ~100 −1000°C.

- Gas species migration towards the surface of the substrate (driven by concentration gradients).
- Adsorption of reactants onto the substrate surface.
- Occurrence of film-forming chemical reactions, encompassing decomposition, surface mitigation to attachment sites, site incorporation, and other surface reactions.
- Desorption and removal of gaseous by-products through forced convection.
- For instance, silicon nitride can be synthesized through the reaction between dichlorosilane (SiH_2Cl_2) and ammonia (NH_3).

Various forms of CVD techniques are reported in published literature, with three common types being APCVD (atmospheric pressure CVD), PECVD (plasma-enhanced CVD), and LPCVD (low-pressure CVD). However, films formed by chemical vapor deposition may exhibit significant tensile or compressive stress, posing challenges for specific applications. To mitigate this, careful control of deposition conditions is essential to reduce stress in the deposited film [10, 11].

31.4.2.3 Physical Vapor Deposition

The PVD (physical vapor deposition) techniques play a pivotal role in the realm of micro- and nanoelectronics, facilitating deposition of ultra-thin layers of conducting, semiconducting, and insulating materials. Unlike the CVD method, the PVD involves direct impingement of particles onto the substrate surface, offering distinct advantages in certain applications, particularly with its low-temperature deposition capabilities. The two primary methods of PVD are evaporation and sputtering. In evaporation, the primary

material is heated above its melting point. This heating process, which takes place within an evacuated chamber, is achieved through various means such as resistive (thermal) or focused electron beam (e-beam), and causes the material to vaporize. The resulting vaporized atoms travel at high velocities and subsequently condense onto the substrate, forming a thin film. Thermal evaporation is typically suitable for metals with relatively low melting temperatures; in contrast, the e-beam evaporation can accommodate materials with both low and high melting points. Overall, PVD techniques offer versatility and precision in depositing thin films for micro- and nanoelectronic applications, making them indispensable tools in modern semiconductor fabrication processes.

The sputtering method involves the creation of plasma through electrical discharge to propel ionized atoms from a target material onto the substrate's surface. This technique finds application in a diverse array of materials, which include insulators, semiconductors, and metals. The technique of DC sputtering is primarily utilized for depositing conducting layers, while RF sputtering is suitable for both conducting and insulating layers. Argon gas is commonly employed to generate plasma using RF (or DC) voltage. The resulting plasma typically comprises argon ions, and the pressure of the argon gas is an important parameter that influences the deposition rate, thereby affecting the quality of the film. Overall, sputtering offers a versatile and effective means of depositing thin films across various materials, making it a valuable technique in the realm of micro- and nanoelectronics fabrication [10–12].

31.4.3 Photolithography

Photolithography is a fundamental process in microfabrication. From a photomask, this process enables

to transfer geometric patterns onto a thin layer of radiation-sensitive material. The latter is known as resist, which covers the surface of a substrate (*e.g.*, a silicon wafer). A photomask, made of soda lime glass or quartz, features a computer-generated design in a thin chrome or emulsion layer.

Various lithographic methods, including optical lithography, e-beam lithography, X-ray lithography, and ion beam lithography, are employed in microfabrication processes, each with its own set of advantages and limitations. The performance of an exposure tool is typically assessed based on three parameters: resolution, registration, and throughput. Resolution refers to the minimum feature dimension that can be faithfully transferred to a resist film, while registration measures the accuracy of aligning patterns on successive masks with respect to previously defined patterns on the same wafer. Throughput denotes the number of wafers that can be exposed per unit time for a given mask level.

Optical lithography, also known as ultraviolet (UV) lithography or photolithography, is the most commonly used method due to its high throughput, good resolution, low cost, and ease of operation. However, it is not suitable for achieving deep-submicron resolution. For submicron patterning, e-beam lithography, X-ray lithography, and ion beam lithography are employed.

Optical exposure methods can be categorized into three classes: contact, proximity, and projection printing. Contact printing, the oldest technique, involves placing the mask directly in contact with the resist layer on the wafer. While it offers high resolution, it also causes damage to both the mask and resist layer due to the direct contact. Proximity printing, which maintains a small gap between the mask and wafer, reduces damage but compromises resolution

due to diffraction effects. Projection printing, commonly used in production lines, overcomes mask damage issues associated with shadow printing. In this method, the mask image is reduced by an optical system and scanned over the wafer surface, enabling the printing of features as small as ~1 µm with a throughput of approximately 25–50 wafers/h.

Photolithography (as a crucial step in microfabrication) encompasses four key stages: the PR coating, alignment, UV exposure, and development. Photoresist (PR), a photosensitive polymer akin to photographic film, facilitates the transfer of desired patterns from a mask to a substrate. Two types of PRs, positive and negative, exhibit distinct chemical reactions to UV light. Positive PRs become more soluble upon UV exposure, whereas negative PRs crosslink and become less soluble.

The lithography process is conducted in a cleanroom illuminated with yellow light, as PRs are insensitive to wavelengths exceeding ~500 nm. Initially, the substrate undergoes thorough cleaning to eliminate dust and dirt, followed by a dehydration bake to remove moisture. An adhesion promoter, typically hexamethyldisilazane (HMDS), is then spin-coated onto the substrate, followed by the application of PR using spin coating to ensure uniform thickness. This is due to the fact that the thickness of the spin-coated photoresist (T_{PR}) varies inversely as the square root of the (angular) speed of the spin coater. Prebaking the PR-coated wafer at ~90°C–100°C for 30 min (or 3–4 min on a hot plate) evaporates the solvent and enhances PR adhesion. Subsequently, the mask is aligned over the substrate, and UV light is directed over the assembly during UV exposure. Only transparent areas of the mask permit UV light to reach the substrate below. Following UV exposure, the substrate is immersed in a developing solution to remove soluble PR areas. The choice between

positive and negative PRs depends on the desired image orientation, as they provide reverse images of each other for the same mask. Postbaking the wafer at 120°C–130°C for ~30 min in an oven (or 2–3 min on a hot plate) hardens the resist and improves its etch resistance. The exposed layer is then etched using an appropriate etchant, such as buffered hydrofluoric acid (BHF) for oxide, with caution to avoid attacking the resist. Etching can be conducted via wet or dry methods. Finally, the PR is stripped away using a suitable solvent, such as acetone for positive PR, or oxygen plasma, completing the photolithography process and leaving behind the desired pattern on the substrate [4, 10–12].

31.4.4 Etching: Overview and Types

Etching serves as the process of removing material from unprotected areas, crucial in the patterning of substrates during lithography. In this process, the desired portions of the substrate surface (such as the oxide layer) are patterned using lithography and subsequent etching steps. A photoresist (PR) acts as a mask to selectively etch the oxide layer. Etching plays a pivotal role at various stages in device fabrication, and is categorized into two main types: wet and dry. These techniques are further subdivided into isotropic and anisotropic types. Wet etching entails immersing wafers in liquid etchants, where the exposed material is chemically etched. The etching process typically involves four steps: diffusion (or transport) of reactant molecules to the silicon surface, adsorption of these molecules, chemical reaction with surface atoms, and desorption of reaction products. Dry etching, on the other hand, utilizes gas-phase etchants in plasma, often referred to as plasma etching due to the involvement of plasma. Dry etching methods include ion beam- and laser beambased etching, both falling under the category of dry etching

techniques. Overall, etching processes are fundamental to microfabrication, enabling precise patterning and shaping of substrates for the fabrication of electronic devices.

In the etching process, several key parameters play crucial roles. They must be considered when selecting an etchant for experimentation:

- Mask layer: this layer safeguards regions of the surface where etching is not required. It is essential for the mask layer to exhibit high selectivity with the material intended for etching.
- Aspect ratio: the ratio of etch depth to width is known as the aspect ratio. It serves as a critical measure in determining the geometry and depth of etched features.
- Isotropy: isotropic etchants exhibit the same etch rate in all directions, implying that the lateral etch rate matches the vertical etch rate. In single crystal materials, isotropic etchants demonstrate uniform etch rates regardless of crystallographic direction.
- Anisotropy: anisotropic etchants, in contrast, do not etch at equal rates in all directions. For instance, in the etching of single crystals with wet chemical anisotropic etchants, the etch rate varies depending on crystallographic directions.
- Bias: the amount of undercutting (or lateral etching) at the mask edges.
- Overetch: overetching refers to etching beyond the required etch depth or film thickness. This often results in increased lateral etching or bias.
- Selectivity: selectivity represents the ratio of the etch rate of the material intended for etching to that of the material not meant to be etched, such as the masking

layer. A high selectivity is desirable for accurately patterning thin films without etching the underlying substrate or mask layer. For example, BHF demonstrates excellent selectivity when etching SiO_2 layers grown on Si substrates.

- Uniformity: uniformity denotes the consistency of the etch rate across the surface being etched. Maintaining uniform etching rates is crucial for achieving precise and consistent results.

In general, achieving highly anisotropic, selective, and uniform etching is essential for scaling down devices effectively. However, achieving all these characteristics simultaneously can pose significant challenges.

31.4.4.1 Silicon Wet Isotropic Etching

Isotropic etching refers to a process where the etch rates remain uniform in all directions. Such etchants dissolve the material being etched at an equal rate in all directions. For silicon, wet isotropic etching commonly employs a mixture known as “HNA”, consisting of hydrofluoric acid (HF), nitric acid (HNO_3), and acetic acid (CH_3COOH). In silicon wet isotropic etching, the nitric acid (HNO_3) facilitates the oxidation of silicon, while fluoride ions from hydrofluoric acid (HF) form the soluble silicon compound H_2SiF_6. The etch rates are influenced by the ratios of the chemicals used and the doping level of silicon. For further details on the isotropic etching of silicon, the interested reader should refer [12].

31.4.4.2 Silicon Wet Anisotropic Etching

Wet anisotropic etching is a process characterized by orientation-dependent etching of materials. Unlike isotropic etching, anisotropic etchants exhibit significantly faster

etching rates in one direction compared to others, gradually exposing the slowest-etching crystal planes over time. In silicon wet anisotropic etching, alkaline solutions containing potassium hydroxide (KOH) and tetra-methyl ammonium hydroxide (TMAH) are commonly employed. Within these solutions, certain crystal planes, such as {111}, etch at a much slower rate compared to others, such as {110} and {100}. The etch rate and resulting surface morphology are influenced by various parameters of the etchant, including concentration, temperature, agitation during etching, and additives. The slower etching rate of {111} planes, relative to other planes, results in distinctive profiles on differently oriented silicon substrates. Due to the slower etching nature of {111} planes, the final etched structure typically comprises different {111} planes on variously oriented wafers. Notably, as {111} silicon planes are inclined at a finite angle to the surface of a Si {100} wafer, wet anisotropic etching often results in the formation of V-shaped profiles. For further details on the anisotropic etching of silicon, the interested reader should refer [10–12].

31.4.4.3 Silicon Dry Etching

Dry etching involves the utilization of gas-phase etchants within a plasma environment. This method is employed to circumvent undercutting, a common issue encountered in wet etching, thereby offering superior control over the dimensions of etched patterns essential for achieving ultra-large scale integration (ULSI). Often referred to as plasma etching due to the involvement of plasma, dry etching and plasma etching are synonymous terms. Dry etching encompasses ion beam-based and laser beam-based etching techniques. Plasma etching, classified into physical and chemical categories, offers distinct advantages. Physical etching, such as sputter etching, lacks selectivity,

while pure chemical etching is selective yet isotropic. A combination of physical and chemical etching, known as reactive ion etching (RIE), strikes a balance between anisotropy and selectivity, becoming a cornerstone of etch technology in microfabrication. The RIE operation modes include the RIE mode and the plasma mode, distinguished by electrode configuration. In RIE mode, wafers are loaded onto the powered electrode, whereas in plasma mode, wafers are loaded onto the grounded electrode. Similar to wet etching, chemical dry etching occurs in five steps: generation of etchant species in the plasma, diffusion of these species to the surface, adsorption on the surface, chemical reaction with surface atoms forming volatile compounds, and desorption of volatile by-products from the surface.

An RIE system reactor comprises a vacuum chamber, pump system, power supply generator, gas flow control units, and ancillary equipment. Reactive etch gases, tailored to the material being etched, are continuously introduced into the chamber at reduced pressure (~1–100 mTorr). Sulfur hexafluoride (SF_6) is commonly used for silicon etching. Radio frequency voltage applied across two electrodes ionizes gas atoms, creating plasma. Highenergy electrons collide with neutral gas molecules, inducing various reactions. Plasma etching involves bombardment of ions and neutrals onto the substrate, comprising both physical and chemical etching components. Vertical sidewalls are achieved due to bombardment of sidewalls solely by neutrals, resulting in high anisotropy. However, achieving deep grooves/trenches with high anisotropy remains a challenge, particularly for bulk micromachining applications in MEMS component realization. To address this challenge, deep reactive ion etching (DRIE), a high-density plasma-based dry etching method, has been developed. In DRIE, an etch-resistant protective layer is

deposited on sidewalls between etching cycles, commonly known as the Bosch process. Polymerization during the etching process deposits an etch-resistant polymer layer on sidewalls, enabling the creation of high-aspect-ratio structures with vertical sidewalls. Recent advancements have improved DRIE performance, particularly with superior sidewall-protecting materials like SiO_2. For more details, the interested reader should refer [4].

31.4.5 Local Oxidation of Silicon

In microfabrication, local oxidation of silicon (LOCOS) serves as a technique for selectively growing a silicon dioxide layer on chosen areas of a silicon wafer. This method is pivotal for isolating neighboring MOS transistors, enhancing device performance and reliability. To facilitate the growth of the oxide layer on specific regions, areas not intended for oxidation must be shielded with a material impervious to oxygen diffusion at high temperatures, typically during thermal oxidation processes. Silicon nitride (Si_3N_4) emerges as the optimal masking material for this purpose.

Initially, a thin silicon dioxide layer (~20–50 nm), known as the pad oxide or buffer oxide layer, is grown on the wafer. This layer serves to mitigate the strong tensile stress induced in the subsequent silicon nitride layer during chemical vapor deposition (CVD), thereby reducing stress on the silicon substrate. Following the pad oxide deposition, a layer of silicon nitride (~100–150 nm) is applied. These deposited layers are then patterned using photolithography and etching processes to delineate the active areas for subsequent oxidation. Subsequently, thermal oxidation is conducted to grow the oxide layer exclusively on the exposed silicon regions, constituting the

primary step in the LOCOS process. Finally, the nitride layer is etched away.

The key advantage of the LOCOS process lies in the deposition of a high-quality oxide layer on selected areas, crucial for device isolation. However, it is important to note that oxygen diffusion within the silicon oxide layer is an isotropic process. As the oxide layer grows, oxidant diffusion beneath the nitride layer can cause it to deform upwards, forming a structure known as the “bird’s beak”. This phenomenon underscores a limitation of the LOCOS process, necessitating careful design considerations to mitigate its effects. For more details on the LOCOS technique, the reader should refer [4].

31.4.6 Micromachining

Micromachining encompasses the ability to fabricate mechanical components, ranging from a few microns to several millimeters in dimensions; nanoscale structures fabrication is termed “nanomachining”. It stands as a foundational technology within microfabrication, particularly favored for realizing μ-mechanical structures. This technology is broadly categorized into two main approaches: bulk micromachining and surface micromachining.

In bulk micromachining, the fabrication process involves the selective removal of bulk material from the substrate. This can be achieved through wet etch processes, dry etch processes, or a combination of both, depending on specific requirements. Wet chemical etching, utilizing chemical solutions as etchants, plays a significant role in bulk micromachining. The nature of wet etching can vary between isotropic and anisotropic, contingent upon material structure and etchant characteristics. For instance, wet etching tends to be isotropic when dealing

with amorphous or polycrystalline materials. The focus of the present chapter is on wet chemical-based silicon μ-machining for MEMS applications, covering both fundamental and advanced techniques.

On the contrary, surface micromachining involves synthesizing microstructures utilizing deposited layers on the substrate, which serve as structural and sacrificial layers. This approach offers superior dimensional control, enabling the production of smaller structures, as compared to bulk micromachining. An attractive aspect of surface micromachining lies in its seamless integration with IC components, as the same wafer is utilized for both microstructure fabrication and signal-conditioning circuit realization.

The fabrication process in surface micromachining typically begins with the deposition of a sacrificial layer onto the substrate, followed by patterning using photolithography steps. Subsequently, a structural layer of the desired thickness is deposited and patterned to form the intended mechanical structure. Finally, the sacrificial layer is removed through wet or dry etching methods, resulting in the formation of freestanding microstructures. For more details, the reader should refer [4].

31.4.7 Doping

Impurity doping plays a pivotal role in semiconductor technology by introducing controlled amounts of impurity dopants into substrates, thereby altering their electrical properties. Depending on the dopants used, semiconductors are categorized as either p-type, doped with acceptor impurities, or n-type, doped with donor impurities. In silicon, trivalent dopants like aluminum, indium, boron, and gallium are employed for p-type doping, while pentavalent dopants such as antimony, arsenic, and

phosphorus are utilized for n-type doping. During crystal growth, some dopants are added, ensuring nearly uniform doping across silicon wafers. Additionally, to define specific circuit elements, selected areas are further doped using techniques like photolithography. For instance, this process is used to create bases, emitters, and resistors in bipolar transistors, or to define the source and drain regions in field-effect transistors (FETs). In micromechanical structure fabrication for MEMS applications, heavily doped p-type silicon (P+-Si) serves as an etch stop in alkaline-based wet etching processes. Two primary methods are commonly used to introduce impurities into substrates: diffusion and implantation. Implantation is favored in largescale production due to its enhanced controllability.

Diffusion is a fundamental process in semiconductor fabrication, involving the movement of particles due to random motion from regions of higher concentration to regions of lower concentration. This diffusion process typically occurs at elevated temperatures ranging from ~800°C–1000°C. In the context of semiconductor manufacturing, diffusion is commonly employed by placing silicon wafers in a high-temperature quartz tube and introducing a gas mixture containing the desired dopant. The atoms of the dopant gas then diffuse into the silicon substrate. The maximum concentration of a dopant that can be dissolved into the silicon substrate under equilibrium conditions, without forming a separate phase, is referred to as the solid solubility. For p-type doping, boron is the preferred dopant due to its popularity and effectiveness, while phosphorus is extensively used for n-type doping.

In semiconductor manufacturing, there are three common types of dopant sources used for introducing impurities into the substrate:

- Solid source: solid sources include materials such as boron trioxide (B_2O_3) or boron discs for p-type doping, and phosphorous pentaoxide (P_2O_5) or phosphorous discs for n-type doping. These solid sources are typically placed in the quartz tube upstream from the substrate. During the diffusion process, a carrier gas transports vapor from the solid source and deposits them onto the silicon wafers or substrate. Disc-shaped solid planar sources, comprising dopant species and a binder, are often utilized to facilitate vapor transport over large-size wafers.
- Liquid source: liquid sources involve substances like boron tribromide (BBr_3) for boron doping and phosphorus oxychloride ($POCl_3$) for phosphorous doping. In this method, the liquid dopant source is typically bubbled through an inert carrier gas before being introduced into the diffusion furnace tube.
- Gas source: gas sources include compounds such as diborane (B_2H_6) for boron doping and phosphine (PH_3) for phosphorous doping. These gases are directly supplied to the diffusion furnace tube in their gaseous state.

Each type of dopant source has its advantages and applications, with solid sources being commonly used due to their ease of handling and ability to provide uniform vapor transport over large wafers.

In the diffusion process of impurity doping, different techniques are employed depending on the dopant source used. When solid discs serve as the dopant source, they are stacked with the silicon wafer. On the other hand, for diffusion using liquid sources, an inert carrier gas bubbles through the liquid before entering the furnace tube. In the case of gaseous sources, dopant species are directly

introduced into the furnace tube in their gaseous state. Typically, a two-step diffusion process is utilized. Silicon nitride and silicon oxide are commonly employed as diffusion mask materials, with thermally grown SiO_2 layers being the most widely used. To facilitate diffusion in selective regions, the oxide layer is patterned using photolithography and etching steps. Subsequently, dopants are introduced into these patterned wafers in a high-temperature (~800°C–1000°C) diffusion furnace. During the diffusion process, dopants gradually move from the high-concentration region near the surface into the substrate through diffusion. This initial step, known as pre-deposition, is followed by a drive-in diffusion (or redistribution) at high temperature (~800°C–1000°C) under constant dopant conditions to achieve the desired junction depth. The oxide layer effectively masks the dopants due to their low diffusivity in oxide, thereby controlling their distribution within the substrate. The distribution of impurities in the substrate is determined by solving diffusion equations with appropriate boundary conditions. Depending on the availability of dopant atoms at the substrate surface, different distribution profiles are obtained: a Gaussian distribution for limited sources and a complementary error function for continuous sources [8].

Advantages of the diffusion process include (a) its simplicity and (b) suitability for batch processing. However, it also has drawbacks, such as (a) being a high-temperature process, (b) exhibiting high lateral diffusion, (c) having poor doping control, and (d) being unsuitable for thin junctions [11].

Ion implantation is a technique utilized for introducing impurities, or dopants, into semiconductors like silicon at relatively low temperatures. This method offers greater flexibility compared to diffusion processes. For instance, in MOS transistors such as MOSFETs, ion implantation

enables precise adjustment of the threshold voltage. Dopant ions, including boron, phosphorus, and arsenic, are typically generated from gas sources like BF_3, AsH_3, and PH_3. However, these gases are often hazardous. In cases where the desired implant species is unavailable in gaseous form, a solid charge can be heated to produce vapor, which serves as the source for implantation. The energies of charged particles, or dopant ions, used in ion implantation range from ~1 keV to 1 MeV. As a result, ion distributions with an average depth spanning from ~10 nm to 10 µm are achieved. This range allows for precise control over the depth of dopant penetration into the semiconductor substrate, offering versatility in tailoring electrical properties and device characteristics [12].

During ion implantation, the ions needed for doping are produced by ionizing the source gas into charged ions, such as B^+ or As^+, typically through methods like heat filament or plasma discharge. These ions are then extracted using a voltage bias to a mass analyzer. The magnetic field of the analyzer is adjusted to allow only ions with the desired chargeto-mass ratio to pass through without filtering. Subsequently, the selected ions enter the acceleration tube, where they are propelled to their final implantation energy. During the acceleration phase, there may be some beam neutralization, which poses a challenge as neutral atoms cannot be electrostatically scanned or counted as ion current. This can result in an uncontrolled dose at the center of the wafer. To address this, the ion path typically undergoes electrostatic deviation just before the final implantation to trap the neutrals that continue non-deflected. The focused ion beam is then directed onto the substrate (wafer) and scanned over the surface using electrostatic deflection plates to ensure uniform doping. This process can involve either keeping the wafer stationary while moving the beam or vice versa. Upon

entering the substrate, the highly energized ions collide with the electrons and nuclei, eventually coming to rest at a certain depth within the solid. The average penetration depth is influenced by factors like the dopant, substrate materials, and acceleration energy, which can be adjusted to control the depth. The dopant dose, representing the total implanted ions per unit area, can be managed by monitoring the ion current during implantation. To target specific areas for implantation, a masking layer patterned through lithography and etching processes is utilized. A significant side effect of ion implantation is the damage caused to the semiconductor lattice due to ion collisions. This damaged crystal structure needs restoration. Additionally, if the implanted species are meant to act as dopants, they must occupy the substitutional lattice sites. However, most implanted ions are not initially located in these sites. The process of moving a large fraction of the implanted impurities onto lattice sites is known as impurity activation. To activate the implanted ions and repair lattice damage, the substrate undergoes annealing at an appropriate combination of time and temperature. This annealing step achieves both tasks simultaneously, ensuring the desired electrical properties and device functionality [4].

The main advantages and disadvantages of ion implantation are as follows:

Advantages:

- Low-temperature process: ion implantation occurs at relatively low temperatures compared to other doping methods, minimizing thermal stress on the substrate and allowing for precise control over the process.
- Less transverse straggle: ion implantation exhibits less transverse straggle, meaning there is less deviation in

the distribution of implanted ions perpendicular to their direction of motion. This results in more accurate doping profiles and improved device performance.

- Independent control of impurity depth and dose: ion implantation allows for independent control over the depth of impurity penetration into the substrate and the dose of dopants implanted, enabling precise tuning of device characteristics.
- Complex profiles achievable: ion implantation enables the creation of complex doping profiles, including multi-energy implants, which can be tailored to meet specific device requirements and achieve desired device performance characteristics.

Disadvantages:

- High cost: ion implantation equipment and processes are expensive to set up and maintain, making ion implantation a costly doping technique, particularly for small-scale fabrication.
- Substrate damage: the high-energy ions used in ion implantation can cause damage to the substrate lattice structure, potentially leading to defects that affect device performance and reliability.
- Incomplete repair by annealing: while annealing can help repair some of the damage caused by ion implantation, it may not fully restore the substrate to its original state, leading to residual defects and reduced device performance.
- Dopant redistribution during annealing: during annealing, dopants implanted by ion implantation may redistribute within the substrate, altering the intended doping profile and potentially affecting device characteristics.

- Use of toxic gas sources: some of the gases used as ion sources in ion implantation, such as arsine (AsH_3) and phosphine (PH_3), are highly toxic and pose safety risks to personnel working with the equipment. Proper handling and safety precautions are necessary to mitigate these risks.

31.4.8 Silicon Direct Wafer Bonding: Overview and Types

The DWB (direct wafer bonding) of silicon is a process that involves the direct contact between two surfaces without the use of any specific bonding agent such as glue, wax, or epoxy. This method is primarily associated with bonding silicon wafers and finds diverse applications, notably silicon-on-insulator (SOI) wafers. Additionally, silicon-to-silicon bonding can serve as a substitute for epitaxial layers in bipolar devices, where epitaxy involves depositing an overlayer onto a crystalline substrate in alignment with the substrate's lattice structure. The DWV method can also be utilized to join two silicon wafers of opposite conductivity, forming a p-n diode, among other applications. In MEMS, DWB process finds use in manufacture of various micro-mechanical structures crucial for sensor development. The DWB process involves fusing two silicon wafers together through heating, which attributes it the alternate name "fusion bonding". This technique offers a versatile approach to integrate and fabricate intricate structures for diverse µ-scaled applications [4, 8, 9].

The bonding process in direct wafer bonding relies on chemical bonds formed between two surfaces. It is possible for the two wafers to have a thin film layer of SiO_2 (or another material) covering their surfaces before bonding. Successful bonding of silicon wafers necessitates clean, flat, and ultra-smooth surfaces that are completely free of

particulate contamination. Otherwise, non-bonded areas (also known as voids or interfacial bubbles) may form. Initially, the direct bonding is initiated by the van der Waals forces of attraction between the two bonding surfaces. These forces become stronger as the distance between the surfaces decreases, and are influenced by the chemical structure of the surfaces. Consequently, bonding methods are categorized into two types: hydrophilic bonding and hydrophobic bonding.

The primary distinction between these two surface types lies in the presence of water films, consisting of just a few molecular layers, which are adsorbed on hydrophilic surfaces. The surface state of a silicon wafer can be assessed by the contact angle formed by a water droplet when placed on the wafer surface. Surfaces with contact angles greater than 90° are classified as hydrophobic, whereas those with contact angles less than 90° are considered hydrophilic. This means that a lower contact angle indicates higher hydrophilic attributes, or greater wettability, of the surface.

Silicon direct wafer bonding (DWB) typically involves three main steps:

- Surface preparation: this step includes processes such as polishing, cleaning, and surface activation to ensure that the surfaces of the wafers are flat, clean, and smooth. Surface activation methods may involve treatments to enhance surface reactivity, promoting bonding.
- Pre-bonding at room temperature: once the surfaces are prepared, the two wafers are brought into contact at room temperature. At this stage, a weak bonding is formed primarily based on physical forces such as van

der Waals forces, capillary forces, or electrostatic forces.

- Annealing at high temperature: after pre-bonding, the wafer pair undergoes annealing at high temperature, typically exceeding 600°C. During annealing, the physical forces between the wafers are converted into chemical bonds, significantly improving the bond strength.

In essence, the DWB technique starts with the initial physical contact between the wafers, followed by a thermal treatment that transforms the weak physical bonds into stronger chemical bonds. This process results in a robust bond between the two silicon wafers. Prior to bonding, it is common for the wafers to undergo cleaning, using methods such as the RCA clean method to ensure surface purity and enhance bonding quality.

31.4.8.1 Hydrophilic Bonding of Silicon

In hydrophilic bonding, an oxide layer covers the silicon wafer surface. The oxide can be deposited oxide, or thermally-grown oxide, or a thin native oxide. The surface of oxidized silicon normally contains silicon hydroxyl groups (*i.e.*, Si-OH). Due to the polarization of hydroxyl (OH) groups, the extent of hydrophilic attribute of the surface is determined by the amount of Si-OH groups on the surface. The standard clean of first category (SC-1) of the RCA clean method (1:1:5 NH_3:H_2O_2:H_2O) is mostly used to enhance the hydrophilic characteristics of the surface. The formation of H_2O and the Si-O-Si siloxane bond are triggered by the interaction of two opposite OH groups, when the two wafers are brought into contact and heated. The chemical reaction (during bonding) between the hydrophilic silicon surfaces can be described as:

$$Si-OH+HO-Si \rightarrow Si-O-Si+H_2O$$

After the pre-bonding in air (or vacuum), the bond strength is increased by annealing the bonded pair (at ~800°C–1100°C) in a special gaseous atmosphere or vacuum. Therefore, annealing furnishes a certain level of thermal energy, promoting increased interaction among silanol (Si-OH) groups. This leads to the formation of new and highly stable chemical bonds. In this reaction between the silanol groups, additional water molecules are released, which facilitates the formation of Si-O-Si bonding. The water molecules on the surfaces then permeate into the silicon dioxide. When water comes into contact with silicon, it reacts to form hydrogen and silicon dioxide:

$$Si+2H_2O \rightarrow 2H_2+SiO_2$$

Hydrogen exhibits high solubility in SiO_2. By ensuring an oxide layer thickness of over 50 nm on at least one wafer surface, the formation of hydrogen-induced voids can be prevented. Moreover, the bonding strength increases with higher annealing temperatures (owing to the fact that strong Si-O-Si covalent bonds are formed at high temperatures).

31.4.8.2 Hydrophobic Bonding of Silicon

In the process of hydrophobic bonding (or DWB), the wafers intended for bonding feature a bare silicon surface (devoid of any additional layers). This surface may be terminated with hydrogen and fluorine atoms, imparting hydrophobic (water-repelling) properties. Alternatively, the surface may exhibit unsaturated (dangling) bonds in certain instances to enhance bonding. A hydrophobic surface can be produced by removing the native oxide layer through methods such as plasma treatment or the use of etching solutions containing fluorides, such as hydrogen

fluoride (HF) or ammonium fluoride (NH_4F). Hydrofluoric acid etching, a conventional method for removal of silicon dioxide, yields a (water-repellant) surface that is terminated with hydrogen and fluorine atoms. A few hydroxyl groups (OH) also exist on the hydrophobic surface due to the water rinse. The hydrophobic surface easily attracts hydrocarbons (contaminants), necessitating swift contact with (bonded) wafers or their storage in vacuum immediately after the removal of the silicon dioxide layer. The aim is to form a crystalline grain boundary, while avoiding the native oxide at the silicon wafer surfaces. At room temperature, the bonding primarily relies on the van der Waals (attractive) forces between the fluorine and hydrogen atoms. The room temperature bonded wafers are annealed at high temperature (~600°C–1000°C) in order to achieve stronger DWB through Si-Si covalent bonds, similar to bonding of hydrophilic surfaces. Upon annealing, the (wafer) surfaces release hydrogen and fluoride, facilitating the formation of Si-Si bonds as depicted in the following reaction:

$$\mathrm{Si-H + Si-H \rightarrow H_2 + Si-Si}$$

During annealing, silicon surface-diffusion takes place, which effectively seals the µ-gaps between the surfaces. The bonding energy reaches cohesive strengths of bulk silicon. Moreover, the challenge (with the bonding process) lies in the presence of hydrogen at the bonded interface, potentially leading to the formation of voids.

31.5 State-of-Art Application Areas and Present/Futuristic Trends

Wet bulk micromachining finds extensive application in fabricating a wide array of MEMS structures, ranging from

cavities with simple geometries to intricate designs [13]. Selection of an etchant for bulk micromachining entails considering various factors such as undercutting at masked edges and corners, sidewall profile, compatibility with complementary metal-oxide-semiconductor (CMOS) processes, selectivity to mask material and its availability, etch rate, anisotropy (crystal plane selectivity), selectivity to metals, control of etch parameters, etched surface morphology, safety of reactants and products, etch-stop characteristics, and so on [14, 15]. Alkaline solutions render etching characteristics, which are primarily sensitive to two factors: (a) concentration of the etchant and (b) incorporation of additives. The relative etch rates of crystallographic planes and the etched morphology undergo significant variations if an additive is introduced into the etchant, or if the solution's concentration is altered [16, 17].

Survey of published literature shows that cavities, channels, and mesa structures (nonetched areas on semiconductor wafers) are manufactured using a one-mask process. To fabricate these types of structures, a masking layer is initially patterned onto the silicon surface through lithography and etching steps. Following the patterning of the masking layer, anisotropic etching is performed. Elaborate details of these processes can be found in References [18–21]. Wet anisotropic etching stands out as a simple and efficient technique for fabrication of high-quality diffraction gratings; the latter finds diverse applications in the infrared (IR) region. These gratings are indispensable in high-resolution IR spectrographs, monochromators, and laser tuning devices. A diffraction grating, also known as an echelle grating, comprises blazed grooves. To fabricate a diffraction grating on a silicon wafer, a mask layer on a polished surface is patterned with parallel equidistant stripes using photolithography

technique. Subsequently, anisotropic etching is conducted to create blazed grooves. The blazed angle (groove profile) of the etched diffraction grating depends on the direction of the masked edge on the wafer surface, wafer orientation, as well as the type of etchant used (pure or with surfactant additives) [22–24].

Diaphragms and cantilever beams represent two fundamental types of suspended structures extensively employed in MEMS-based sensing devices, thus regarded as the backbone of MEMS. Freestanding structures can be fabricated using either silicon or non-silicon materials. In the case of non-silicon materials, it is imperative to use a material exhibiting high etch-selectivity with silicon (*e.g.*, SiO_2, Si_3N_4, etc.). A single lithography step suffices for the fabrication of rectangular/ square freestanding diaphragms. To achieve a smooth etched surface morphology, etching should be conducted in pure or surfactant-/IPA-added high-concentration TMAH/KOH solutions. Freestanding cantilever beams on silicon wafers are formed by processing either one side of the wafer, or both sides. Fabrication steps for realizing suspended cantilever beams using both sides of the wafer have also been reported in literature [4]. Various methods have been employed to control the thickness of freestanding silicon microstructures using wet bulk micromachining [25–31].

A prominent scanning probe microscopy (SPM) technique is the atomic force microscopy (AFM), extensively utilized in surface science for mapping forces near the surface with high spatial resolution (order of fractions of a nanometer). Moreover, it has demonstrated its potential as a tool for surface modification and nanolithography, thus serving as a powerful tool for the investigation of nanoscale science and technology. This state-of-art technique has far-reaching

precision attainments in µ-manufacturing, as outlined in [32, 33].

The AFM probe is comprised of a flexible force-sensing cantilever structure. A nanometric sharp tip at the free end of the cantilever is utilized to scan the surface of specimen. The working principle of AFM is based on the detection of force between tip and surface. A force between the tip and the sample surface leads to a deflection of the cantilever beam. Several methods are employed for measuring the beam deflection. These include the technique of optical deflection (detection of a laser spot reflected from top surface of the beam by a position-sensitive detector), optical interference, tunneling current, and electrical techniques (capacitive, piezoresistive, and piezoelectric sensing) [34, 35]. The sharpness of the tip apex is of great importance. The AFM cantilevers are mostly fabricated from either silicon or Si_3N_4 (silicon nitride). Silicon bulk micromachining is predominantly exploited for the fabrication of cantilevers or sharp tips. Bulk micromachining is carried out using either wet chemical etching or dry plasma etching, or a combination of both. Etching can be isotropic or anisotropic, each having its own advantages and disadvantages. However, wet etching is an economical method and requires a very simple system. Published research reports on purely wet anisotropic etchants describe several kinds of silicon tips. Silicon is the preferred material for fabrication of cantilevers with integrated tips. This is due to its excellent mechanical properties (over amorphous silicon nitride), and also because the tip can easily be sharpened through thermal oxidation [4, 36–38].

Microfluidics involves design and development of miniature components and devices, which are engineered to control (or handle) extremely small volumes of fluids ($\sim 10^{-9}$– 10^{-18}

liters), employing channels typically spanning tens to hundreds of micrometers in dimensions. Therefore, the principal advantages of microfluidic systems are miniscule consumption of chemical and/or biological reagents, and a drastic decrease in assay times due to reduced chemical reaction time. Owing to less consumption of sample volume, they are highly suitable for expensive chemical reagents. Microfluidic systems presently find diverse applications in a wide range of technical fields, which include chemical analysis, drug delivery, molecular separation, micromixers, inkjet printers, localized cooling; the list is virtually endless! [4, 39–41].

Silicon-based microvalves and micropumps are the key components (or “heart”) of a microfluidics system, and silicon bulk micromachining offers a promising method for their fabrication. An automatic microdosing system (or drug delivery system) to dispense therapeutic agents (or medical drugs) into the human body consists of a reservoir (for drugs), a micropump (μ-pump), microchannels array, microsensors, and necessary related circuits. This kind of dosing system is very useful for patients who are suffering from serious or chronic diseases such as malignant lymphoma or diabetes, or abrupt life threats, such as cerebral stroke, heart attack, and so on. The integrated microsensors enable real-time measurements to calculate the exact amount of drug to be injected by micropump. Moreover, silicon micromachining enables integration of auxiliary components such as microsensors and microfilters within the valve [4, 42–45].

A microvalve (μ-valve) is a fundamental part of any microfluidics system. Microvalves, which are studied and fabricated, are categorized as passive and active. The passive valves (or check valves) do not include any actuation. An active μ-valve consists of a flexible diaphragm actuated by an external force. Active microvalves regulate

flow rate under specific pressure differences; passive valves adjust flow rates based on the pressure difference between the valve-inlet and its outlet. Moreover, on the basis of their initial mode, µ-valves can be termed as “normally open”, “normally closed”, and “bistable” microvalves. Both types of structures are created using wet chemical-based silicon bulk micromachining. Passive valves exhibit diode-like characteristics as they only open to forward pressure. Passive microvalves are commonly used as part of micropumps due to their simple design and easy fabrication [44]. In active microvalves, various actuation schemes such as piezoelectric, electrostatic, electromagnetic, thermopneumatic, bimetallic (or thermal bimorph), and thin-film shape memory alloy (SMA) are adopted to actuate mechanical moving parts. Each actuation technique has its own merits and limitations, especially in terms of response time (*i.e.*, transition time during “close-to-open” or “open-to-close”), power consumption, force delivered by the actuator (*i.e.*, actuator performance), etc. For more elaboration, the reader is referred to Reference [4].

Micro pumps are classified as mechanical and nonmechanical. Those with moving parts (*e.g.*, a diaphragm/actuator and a microvalve) are called mechanical micro pumps; nonmechanical micro pumps are those without moving parts. The nonmechanical micro pumps utilize kinetic energy, derived from nonmechanical (energy) forms, to drive fluids in micro-channels. On the basis of their working principle, they are named as ultrasonically driven micro pumps, electrohydrodynamic micro pumps, electro-osmosis micro pumps, surface-tension-driving micro pumps, and so on. In mechanical micro pumps, a physical actuator is needed to perform the pumping function. They are further subdivided into dynamic pumps and displacement pumps, depending on

whether mechanical energy is periodically added to enhance the velocity of (driven) fluid continuously, or increase pressure (head) to move the fluid. The displacement pumps, as classified above, typically employ a flexible diaphragm within a pressure chamber. Commonly, this diaphragm is driven by an actuator and passive valves. The actuator and the check valves determine the performance, such as the output pressure and flow rate. For a micro pump, the output pressure is proportional to the available force the actuator can deliver. Similarly, the dynamic characteristics of the actuator diaphragm determines the flow rate. Analogous to active micro valves, micropumps are equipped with various types of actuation mechanisms, such as electrostatic, piezoelectric, thermopneumatic, SMA, and bimetallic. Each technique of actuation has its own benefits and drawbacks in terms of flow rate, output pressure, and fabrication. The actuation unit comprises two silicon chips which embody both the flexible (pump) diaphragm and the rigid counter electrode, and arranged in a configuration similar to a capacitor. When (electrical) voltage difference is applied between pump diaphragm and counter electrode, (capacitive) electrostatic forces come into play, causing the diaphragm to flex towards the counter electrode. This (bending) action creates a suction effect, drawing fluid in through the inlet valve. Upon deactivation of supply voltage, the diaphragm returns to its original position, expelling fluid through the outlet valve. The (inlet to outlet) direction of fluid flow is regulated by two passive check valves. Since the electrostatic pump is driven by the electrostatic force, adjusting the applied voltage allows for precise control over the diaphragm’s deflection. Similarly, the working principle of other actuation methods can be understood. The flexibility of the diaphragm determines the volume stroke of the micropump. Therefore, it is important to design a

flexible diaphragm. Elaborate details can be found in References [4, 45–52].

It is widely recognized that wet silicon anisotropic etching faces limitations in forming arbitrarily shaped mesas, cavities, or grooves, such as circular or rectangular structures with vertical sidewalls, due to the constraints imposed by crystallographic properties. Conversely, the DRIE process offers a solution for fabricating such structures because its etching rate is largely independent of crystallographic direction. However, DRIE is not suitable for creating microstructures with slanted sidewalls or suspended structures when only one side of the silicon wafer (typically the front side) is utilized in the lithography process. A potential approach to overcome these limitations involves combining processes like LOCOS, DRIE, and wet anisotropic etching. This integration enables the realization of arbitrarily shaped mesa structures with suspended microstructures, leveraging the strengths of each process while mitigating their individual drawbacks [53, 54].

Wet bulk micromachining also emerges as a promising method for crafting mold patterns crucial for realizing polydimethylsiloxane (PDMS) stamps in soft lithography. This lithographic approach garners significant attention due to its remarkable versatility, high throughput, and potential cost-effectiveness attributed to its master and replication system. In addition, silicon is ideal for hot embossing processes due to its superior bending resistance (rigidity) as well as resistance to mechanical load (stability) [55, 56].

HAR (high-aspect-ratio) structures in MEMS are usually created by DRIE [57–59]. The etch rate of the DRIE process depends on several parameters such as power, chamber pressure, and mask dimensions. Moreover, the formation of scalloping contours (resembling periodic corrugations) on

the side walls of μ-structures is a major concern. Photoelectrochemical etching (PEC) of silicon is an alternative technique to fabricate HAR microstructures. This method is very cheap in comparison to DRIE, and can etch trenches with smooth sidewalls and uniform etch-depth, as well as produce holes with higher aspect ratios. However, there is a limitation in PEC. This technique requires sharp pits (*e.g.*, V-groove) which act as nucleation sites for deep etching. For more details, the following References [4, 60–63] must be visited.

References

1. Hopcroft, M.A., Nix, W.D., Kenny, T.W., What is the Young's modulus of silicon? *J. Microelectromech. Syst.*, 19, 229–238, 2010.

2. Schroder, D. K., *Semiconductor material and device characterization,* Wiley, Ukraine, 2006.

3. Madou, M.J., *Fundamentals o f Microfabrication: The Science of Miniaturization*, 2nd ed, CRC Press, Boca Raton, 2002.

4. Pal, P. and Sato, K. (Eds.), *Silicon Wet Bulk Micromachining for MEMS*, Jenny Stanford Publishing, Singapore, 2017.

5. Plummer, J. D., *Silicon VLSI Technology: Fundamentals, Practice and Modeling*, Dorling Kindersley, India, 2009.

6. Sze, S.M., *Semiconductor Devices: Physics and Technology*, 2nd ed, Wiley India, New Delhi, 2008.

7. Sze, S.M., *VLSI Technology*, 2nd ed, McGraw-Hill, New Delhi, 1988.

8. Streetman, B. G., Banerjee, S. K., *Solid State Electronic Devices*, 6th ed, PHI Learning, New Delhi, 2009.

9. Hsu, T.R., *MEMS & Microsystems: Design and Manufacture*, 1st ed, McGraw-Hill, New Delhi, 2003.

10. Gandhi, S.K., *VLSI Fabrication Principles: Silicon and Gallium Arsenide*, Wiley India, New Delhi, 2009.

11. Tong, Q.Y. and Gosele, U., *Semiconductor Wafer Bonding: Science and Technology*, John Wiley & Sons, New York, 1998.

12. Suni., T., *Direct Wafer Bonding for MEMS and Microelectronics*, VTT publications 609, dissertation for the degree of doctor of science in technology, Helsinki University of Technology, Finland, 2006.

13. Yagyu, H., Yamaji, T., Nishimura, M., Jpn., *J., Appl. Phys.*, 49, 096503, 2010.

14. Xu, Y.W., Michael, A., Kwok, C.Y., Formation of ultra-smooth 45° micromirror on (100) silicon with low concentration TMAH and surfactant: techniques for enlarging the truly 45° portion. *Sens. Actuators, A*, 166, 164–171, 2011.

15. Rola, K.P., Ptasinski, K., Zakrzewski, A., Zubel, I., Silicon 45° micromirrors fabricated by etching in alkaline solutions with organic additives. *Microsyst. Technol.*, 20, 221–226, 2014.

16. Fruhauf, J. and Kronert, S., Wet etching of silicon gratings with triangular profiles. *Microsyst. Technol.*, 11, 1287–1291, 2005.

17. David, C., Bruder, J., Rohbeck, T., Grunzweig, C., Kottler, C., Diaz, A., Bunk, O., Pfeiffer, F., Fabrication of

diffraction gratings for hard X-ray phase contrast imaging. *Microelectron. Eng.*, 84, 11721177, 2007.

18. Keller, L.D., Jaffe, D.T., Ershov, O.A., Benedict, T., Graf, U.U., Fabrication and testing of chemically micromachined silicon echelle gratings. *Appl. Opt.*, 39, 1094–1105, 2000.

19. Graf, U.U., Jaffe, D.T., Kim, E.J., Lacy, J.H., Ling, H., Moore, J.T., Rebeiz, G., Fabrication and evaluation of an etched infrared diffraction grating. *Appl. Opt.*, 33, 96–102, 1994.

20. Ashok, A. and Pal, P., Synthesis of anodic oxide thin films on Si{100} wafers and their characterization in TMAH for MEMS. *ECS J. Solid State Sci. Technol.*, 4, Q1–Q7, 2015.

21. Pal, P. and Sato, K., Various shapes of silicon freestanding microfluidic channels and microstructures in one step lithography. *J. Micromech. Microeng.*, 19, 055003, 2009.

22. Elwenspoek, M., Elwenspoek, M., Jansen, H. V., *Silicon Micromachining*, Cambridge University Press, United Kingdom, 2004.

23. Lang, W., Silicon microstructuring technology. *Mater. Sci. Eng.*, R17, 1–55, 1996.

24. Gad-el-Hak, M., *The MEMS Handbook*, CRC Press, Boca Raton, 2002.

25. Abedinov, N., Grabiec, P., Gotszalk, T., Ivanov, T., Voigt, J., Rangelow, I.W., Micromachined piezoresistive cantilever array with integrated resistive microheater for calorimetry and mass detection. *J. Vac. Sci. Technol., A*, 19, 2884–2888, 2001.

26. Pal, P., Kim, Y.J., Chandra, S., Front-to-back alignment techniques in microelectronics/MEMS fabrication: a review. *Sens. Lett.*, 4, 1–10, 2006.

27. Pal, P., Tuli, S., Chandra, S., A new technique of front-toback alignment for MEMS. *Sens. Lett.*, 2, 78–81, 2004.

28. Tang, B., Sato, K., Xi, S., Xie, G., Zhang, D., Cheng, Y., Process development of an all-silicon capacitive accelerometer with a highly symmetrical spring-mass structure etched in TMAH + Triton-X-100. *Sens. Actuators, A*, 217, 105–110, 2014.

29. Tatic-Lucic, S., Zhang, W.Y., Navneet, N., Etch-stop characteristics of heavily B/Ge-doped silicon epilayer in KOH and TMAH. *Sens. Actuators, A*, 123-124, 640–645, 2005.

30. Steinsland, E., Nese, M., Hanneborg, A., Bernstein, R.W., Sandmo, H., Kittilsland, G., Boron etch-stop in TMAH solutions. *Sens. Actuators, A*, 54, 728–732, 1996.

31. Chung, G.S., Study of electrochemical etch-stop for high-precision thickness control of single-crystal Si in aqueous TMAH: IPA: pyrazine solutions. *Microelectron. Eng.*, 85, 271–277, 2008.

32. Wallman, L., Bengtsson, J., Danielsen, N., Laurell, T., Electrochemical etch-stop technique for silicon membranes with pand n-type regions and its application to neural sieve electrodes. *J. Micromech. Microeng.*, 12, 265–270, 2012.

33. Ashruf, C.M.A., French, P.J., Sarro, P.M., Bressers, P.M.M.C., Kelly, J.J., Electrochemical etch stop engineering for bulk micromachining. *Mechatronics*, 8, 585–612, 1998.

34. Saya, D., Belaubre, P., Mathieu, F., Lagrange, D., Pourciel, J.B., Bergaud, C., Si-piezoresistive microcantilevers for highly integrated parallel force detection applications. *Sens. Actuators, A*, 123-124, 23–29, 2005.

35. Pruitt, B.L. and Kenny, T.W., Piezoresistive cantilevers and measurement systems for characterizing low force electrical contacts. *Sens. Actuators, A*, 104, 68–77, 2003.

36. Huang, Y., Ergun, A.S., Haeggstrom, E., Badi, M.H., Khuri-Yakub, B.T., Fabricating capacitive micromachined ultrasonic transducers with wafer-bonding technology. *J. Microelectromech. Syst.*, 12, 128–137, 2003.

37. Pal, P. and Sato, K., Suspended Si microstructures over controlled depth micromachined cavities for MEMS based sensing devices. *Sens. Lett.*, 7, 11–16, 2009.

38. Alessandrini, A. and Facci, P., AFM: a versatile tool in biophysics. *Meas. Sci. Technol.*, 16, R65– R92, 2005.

39. Kwon, J.W. and Kim, E.S., Multi-level microfluidic channel routing with protected convex corners. *Sens. Actuators, A*, 97-98, 729–733, 2002.

40. White, N.M., The origins and the future of microfluidics. *Nature*, 442, 368–373, 2006.

41. Gravesen, P., Branebjerg, J., Jensen, O.S., Microfluidics: a review. *J. Micromech. Microeng.*, 3, 168–182, 1993.

42. Bohm, S., Burger, G.J., Korthorst, M.T., Roseboom, F., A micromachined silicon valve driven by a miniature bi-stable electromagnetic actuator. *Sens. Actuators, A*, 80, 77–83, 2000.

43. Park, J.M., Evans, A.T., Rasmussen, K., Brosten, T.R., Nellis, G.F., Klein, S.A., Gianchandani, Y.B., A microvalve with integrated sensors and customizable normal state for low-temperature operation. *J. Microelectromech. Syst.*, 18, 868–877, 2009.

44. Oh, K.W. and Ahn, C.H., A review of microvalves. *J. Micromech. Microeng.*, 16, R13–R39, 2006.

45. Fazal, I., Louwerse, M.C., Jansen, H.V., Elwenspoek, M.C., Design, fabrication and characterization of a novel gas microvalve using micro- and fine-machining. *J. Micromech. Microeng.*, 16, 1207–1214, 2006.

46. Pramanick, B., Das, S., Bhattacharyya, T.K., MEMS based normally closed silicon microregulator for gas and water. *Sens. Actuators, A*, 205, 15–25, 2014.

47. Au, A.K., Lai, H., Utela, B.R., Folch, A., Microvalves and micropumps for BioMEMS. *Micromachines*, 2, 179–220, 2011.

48. Laser, D.J. and Santiago, J.G., A review of micropumps. *J. Micromech. Microeng.*, 14, 35–64, 2004.

49. Woias, P., Micropumps: past, progress and future prospects. *Sens. Actuators, B*, 105, 28–38, 2005.

50. Nisar, A., Afzulpurkar, N., Mahaisavariya, B., Tuantranont, A., MEMS-based micropumps in drug delivery and biomedical applications. *Sens. Actuators, B*, 130, 917–942, 2008.

51. Tsai, N.C. and Sue, C.Y., Review of MEMS-based drug delivery and dosing systems. *Sens. Actuators, A*, 134, 555–564, 2007.

52. Amirouche, F., Zhou, Y., Johnson, T., Current micropump technologies and their biomedical applications. *Microsyst. Technol.*, 15, 647–666, 2009.

53. Pal, P. and Chandra, S., Recessed microstructures with perfect convex corners for accelerometers. *Sens. Lett.*, 2, 226–231, 2004.

54. Venstra, W.J., Pham, N.P., Sarro, P.M., Eijk, J.V., Particle filters integrated inside a silicon wafer. *Microelectron. Eng.*, 78-79, 138–141, 2005.

55. Venstra, W.J. and Sarro, P.M., Fabrication of crystalline membranes oriented in the (111) plane in a (100) silicon wafer. *Microelectron. Eng.*, 67-68, 502–507, 2003.

56. Shikida, M., Ando, M., Ishihara, Y., Ando, T., Sato, K., Asaumi, K., Non-photolithographic pattern transfer for fabricating penshaped microneedle structures. *J. Micromech. Microeng.*, 14, 14621467, 2004.

57. Kim, G.M., Kovalgin, A.Y., Holleman, J., Brugger, J.P., Replication molds having nanometer-scale shape control fabricated by means of oxidation and etching. *J. Nanosci. Nanotechnol.*, 2, 55–59, 2002.

58. Chu, H.Y. and Fang, W., A vertical convex corner compensation and non-{111} crystal planes protection for wet anisotropic bulk micromachining process. *J. Micromech. Microeng.*, 14, 806– 813, 2004.

59. Bogdanski, N., Schulz, H., Wissen, M., Scheer, H.C., Zajadacz, J., Zimmer, K., 3D-Hot embossing of undercut structures: an approach to micro-zippers. *Microelectron. Eng.*, 73-74, 190–195, 2004.

60. Pal, P., Sato, K., Gosalvez, M.A., Tang, B., Hida, H., Shikida, M., Fabrication of novel microstructures based

on orientation dependent adsorption of surfactant molecules in TMAH solution. *J. Micromech. Microeng.*, 21, 015008, 2011.

61. Wu, B., Kumar, A., Pamarthy, S., High aspect ratio silicon etch: a review. *J. Appl. Phys.*, 108, 051101, 2010.

62. Sun, G., Zhao, X., Kim, C.J., Fabrication of very-high-aspectratio microstructures in complex patterns by photoelectrochemical etching. *J. Microelectromech. Syst.*, 21, 1504–15012, 2012.

63. Pal, P., Sato, K., Gosalvez, M.A., Etched profile control in anisotropic etching of silicon by TMAH+Triton. *J. Micromech. Microeng.*, 22, 065013, 2012.

Note

Email: sumanta.banerjee@heritageit.edu

Index

3D CFD, 258

Ablation process, 88
Abrasive assisted micromachining, 215
Abrasive blending and distribution, 401–402
Abrasive flow, 26
Abrasive flow finishing (AFF), 447–459
Abrasive jet machining (AJM), 23
Abrasive materials, 131
Abrasive particle density, 29
Abrasive particle size, 131
Abrasive particle size and concentration, 450
Abrasive particles, 26, 219, 395–399, 401–404, 409
Abrasive slurry, 130
Abrasive types, 25
Abrasive water jet machining (AWJM), 396–397, 402–412
Absorption coefficient, 334
AC (alternating current), 51
Accuracy, 111
Acid resistant material, 172
Acoustic emission (AE), 506–507, 509–510, 512–524
Adaptive control system, 68

Additive manufacturing, 274, 333
Additive manufacturing technologies, 324
Advantages, 103, 169
Advantages of AJM, 27
Advantages of EBM, 154
Advantages of EDM, 58
Advantages of IBM, 112
Advantages of USM, 133
Advantages of WJM, 44
Aerospace, 416, 420
Air compression unit, 24
Alloying, 333, 335–337, 340
Alumina, 378
Aluminum, 69
Aluminum oxide, 25
Amplification unit, 128
ANN, 483, 486, 488–496
Anode, 383
Antimicrobial, 333
Application of EBM, 153
Application of electrochemical micromachining, 318
Applications, 103, 132, 166
Applications of AJM, 27
Applications of AWJM, 395, 405–406
Applications of AWJMM, 255

Applications of EDM, 58
Applications of IBM, 111
Applications of LBM, 88
Applications of wire EDM, 71
Applications of WJM, 42
Applied voltage, 381
Arc modes, 97
Arc stability, 98
Argon laser, 81
Artificial neural network (ANN), 505–507, 510, 518–524
Atomic clean surfaces, 112
Atomic force microscopy (AFM), 338, 547
Auxiliary electrode, 383
AWJM, 4, 9, 11
Axial force, 131

Basic requirements of EDM process, 49
Beam current, 152
Beam deflection, 152
Beam parameters, 86, 144
Benefits of AJM, 27
Bioactivity, 333, 337, 339
Biocompatibility, 333–335, 337, 339, 340, 342
Biomechanical, 338
Bio-MEMS, 378
Bio-samples, 378

Bonding, 339
Bonding (silicon wafer)
  hydrophilic bonding, 545
  hydrophobic bonding, 545–546
Borosilicate glass, 378
Brass, 69
Brinell hardness, 487
Brittle materials, 30
Burr, 104
Burr formation, 417, 424, 425
Burr-free machining, 169

Calculations, 150
Carbon dioxide (CO_2) as carrier gas, 25
Carbon dioxide laser, 83
Carbon nanofibers, 290, 291
Cardiovascular, 333, 336
Carrier gas, 25
Cascade effect, 80
Cathode, 100, 383–384
Cavitation bubbles, 291
Cavitation effects, 131
Cavity machining, 55
Cell adhesion, 336–337
Cell culturing applications, 379
Center line average (CLA), 26

Challenges of EBM, 155
Characteristics, 99
Characteristics of AJM, 28
Characteristics of electron beams, 145
Charge transfer, 301, 303
Chemical blanking, 165
Chemical engraving, 172
Chemical erosion, 379
Chemical etching, 379, 383, 531, 538–540, 547, 549
Chemical machining, 159
Chemical milling, 168
Chemical vapor deposition (CVD)
  atmospheric pressure CVD (APCVD), 534
  low-pressure CVD (LPCVD), 534
  plasma-enhanced CVD (PECVD), 534
Chip formation, 421, 424
Cladding, 333, 335–336
Class x, 531
Cleaning, 160
Cleanroom, 531, 536
Clinical, 333–334, 336, 342
CNC integration, 140
Combined ion beam process, 349, 365
Complex iterations, 232
Composition, 338–339, 341

Computer numerical control (CNC), 434
Conduction laser welding, 88
Configuration parameters, 102
Contouring using USM, 140
Contours, 171
Controlled fracture, 89
Conventional machining, 416, 420, 425
Cooling system, 96
Coordinate measuring machine (CMM), 266
Cracks, 338
Crystal growth, 529, 540
Crystallographic, 339
Current, 177, 178, 181–187, 189, 192, 193, 196, 201
Current (effect of increasing), 56
Current carrying capacity, 69
Current density distribution, 295, 306
Cut and peel maskant, 162
Cutting capabilities, 41
Cutting capacity, 26
Cutting force, 429, 433–436
Cutting parameters, 102
Cutting speed, 69
Cutting tool design, 129
Czochralski (CZ) technique, 529

Data points and variability, 235

Deal-grove model, 533
Degree of freedom, 381
De-ionized (DI) water bath, 531, 532
Demasking, 169
Dental, 333, 335–338
Depth of cut, 132, 170
Description of process, 24
Design aspects, 99
Design of experiments, 380, 384
Developed ion beam process, 349, 364
Deviation sequence, 388–389
Dielectric circulation system, 281
Dielectric fluid, 52, 66, 275, 276, 277, 278, 281, 283, 290
Dielectric strength, 68
Dielectric system, 49, 67
Diffusion, 533–534, 537–540, 541–542, 546
Direct current (DC), 381
Direct electron excitation, 81
Direct wafer bonding (DWB), 544–546
Directivity, 77
Disadvantages, 104, 169
Disadvantages of EBM, 155
Disadvantages of IBM, 113
Disadvantages of USM, 134
Discharge energy, 278, 279, 282

Dopants, 528–529, 540–543
Doping, 529, 538, 540–543
Double-layer capacitance, 301–304, 319
Drawbacks of AJM, 28
Drilling, 421
Drilling capabilities, 132
Driving innovation, 245
Drug delivery, 337–338
Drug-eluting coatings, 338
Dry and wet etching, 378
Dry oxidation process, 532–533
Ductile materials, 30
Duty cycle, 177, 180, 184
Duty factor, 380–381, 389
Dynamic forces, 135

EDM 30, 486
EDM equipment, 49
EDM tool design, 54
Elastic emission machining (EMM), 463, 464, 465
Electric arc, 98
Electric discharge machining (EDM), 378
Electrical connection, 98
Electrical discharge micromachining, 10
Electrochemical discharge machining (ECDM), 377
Electrochemical disintegration, 182

Electrochemical grinding (ECG), 177–179, 181, 184–202

Electrochemical machining (ECM), 6, 115–124, 177–179, 187, 191, 199, 201, 202, 378

Electrochemical micromachining, 312, 314, 318, 319

Electrochemical reactions, 298

Electrode holder, 51

Electrode manufacture, 50

Electrode material, 50

Electrode temperature, 177, 180, 181

Electrode wear (EW), 50, 505–506, 512–519, 522, 524

Electrode wear ratio (EWR), 284

Electrolyte, 116–119

Electrolyte concentration, 177–181, 188, 379, 380, 381, 383, 390

Electrolyte resistance, 295, 301, 319

Electrolytes, 312, 319

Electrolytic-plasma machining, 117

Electron beam generation by electron gun, 145

Electron beam machining (EBM), 90, 143

Electronic-grade silicon (EGS), 529

Emission, 80

Environmental sustainability, 44

Equipment, 66, 95, 145

Equipment considerations, 44

Equipment description, 24, 128

Erosion mechanisms, 30

Erosion patterns, 223
Etch rate, 110
Etchant composition, 164
Etchant medium, 164
Etchant resistant material, 162
Etching
  dry etching, 537–538, 539, 540
  wet anisotropic etching, 538, 546–547, 549
  wet isotropic etching, 538
Etching depth, 162
Etching time, 164
Evolution of shape, 305–306
Extrusion pressure, 449

Fabrication of micro tool, 314–315
Feed, 102
Feed mechanisms, 130
Fiber laser, 82
Figure descriptions, 24, 25
Filtration system, 49
Fine drilling applications, 27
Finishing operation, 50
Float-zone technique, 529
Flow rate, 25
Fluence, 334, 340
Fluid flow feed mechanism, 130

Fluid properties, 39
Flushing system, 70
Focused ion beam (FIB) deposition, 350, 360
Focused ion beam (FIB) etching, 350, 359
Focused ion beam (FIB) fabrication, 350, 359
Focused ion beam (FIB) machining, 349, 350, 357, 358
Focused ion beam (FIB) milling, 350–356
Focusing units, 146
Frequency (effect on MRR), 56
Frequency of vibration, 131
Friction, 336
Fumes, 104
Functional surface, 341–342

Gas flow rate, 29
Gas laser, 82
Gas supply, 96
Generating plasma, 94
Generators, 51
Genetic algorithm (GA), 483, 486, 495–498, 503
Glass, 377
Glass beads as abrasives, 25
Glass engraving applications, 27
Gold nanoparticles, 378
Grain direction, 170
Grain sizes, 339

Gravity feeding unit, 130
Grey relational analysis (GRA), 380–381, 386
Grey relational coefficient (GRC), 386
Grey relational grade (GRG), 381, 387

Hard to process materials, 73
HASJM, 259
Heat affected zone (HAZ), 104, 340–341, 380
Heat generation, 149
Helium neon laser, 84
High focused power density, 77
High strength alloys
  ceramics, 440–442
  inconel, 432, 438, 439
  titanium, 429, 430, 437, 438
High voltage applications, 144
High-aspect-ratio fins, 258
High-frequency waves, 128
High-pressure water jet, 35
High-speed machining (HSM), 4
High-temperature plasma, 94
High-temperature strength resistance, 483
High-velocity jet, 24
Hybrid AFF processes, 456
Hybrid approaches in ECM, 121–122

Hybrid type of electrical discharge micromachining, 289
simultaneous micro-EDM and micro-ECM (SEDCM), 289
ultrasonic cavitation-assisted micro-EDM, 290
Hydraulic coal mining, 42
Hydraulic valve burr removal, 27
Hydro pump systems, 397
Hydrogen embrittlement, 170
Hydrogen gas, 379
Hydrophilic; hydrophilicity, 532, 544–546

Identification coefficient, 387
Image placement, 172
Impact forces, 135
Impact of abrasive flow rate, 28
Implant, 333–342
In vivo, 334
Inconel, 420, 422
Ingot, 529–530
In-situ monitoring, 216–217
Inspection techniques, 132
Integrated circuits, 112, 527–528
Intergranular and transgranular brittle fracture, 23
Internal consistency, 237
Introduction, 23, 93, 143
Ion beam deposition, 363
Ion beam etching, 349, 362, 363

Ion beam figuring, 349, 363, 364
Ion beam machining, 107, 349, 360–362
Ion beam micromachining, 14
Ion bombardment, 108
Ion etching, 111
Ion source, 109
Ionization, 94

Kerf width, 402–404, 408
Kinetic energy, 396, 399, 402, 404
KOH, 378

L9 orthogonal array, 381
Lab-on-chip, 378
Larger is better, 381, 388
Laser ablation, 333–337, 340, 378
Laser assisted
  micro grinding, 439, 440
  micro milling, 438
  micro turning, 441, 442
Laser beam machining (LBM), 7, 77
Laser beams, 334
Laser mirrors, 111
Laser power, 438–440, 442
Laser processing, 339–341
Laser pulse, 334
Laser surface modification, 333–342

Laser-assisted micromachining, 430, 435
Lasing action, 79
LIGA, 528
Liquid media, 131
Local oxidation of silicon (LOCOS), 539, 549
Logistics of EBM, 155

Machine learning and data driven approaches, 243
Machining characteristics, 56
Machining of composite materials, 407–408
Machining of plastics, 42
Machining time, 55
Magnetic abrasive, 471
Magnetic abrasive finishing (MAF), 467–479
Main effects, 389
Masking material, 166
Material compatibility, 324
Material microstructure, 227
Material properties, 40
Material removal, 88
Material removal mechanisms, 135
Material removal rate (MRR), 30, 39, 56, 103, 110, 177, 179–181, 183, 184, 190, 193, 196–198, 201, 281, 284, 379
Material variability, 234
Materials in ECM, 119–120
Mathematics of electron beam machining, 148

Mean squared error (MSE), 489–495
Measurement of microfeatures, 317
Mechanical properties, 334–335, 337–339
Mechanical stresses, 89
Mechanics of cutting in AJM, 30
Mechanics of EBM, 149
Mechanics of material removal in EBM, 146
Mechanism of material removal, 135
Media flow volume, 449
Media flowrate, 449
Media viscosity, 450
MEMS, 2, 10, 11–15, 527–528, 530–532, 534, 539–540, 544, 546–547, 549
Metal removal mechanism, 300
Metal removal rate (MRR), 170
Metallurgical grade silicon (MGS), 529
Micro (μ)-machining, 528, 530, 540
Micro pump, 548–549
Microchannels, 335, 423, 425
Microcracking and surface degradation, 225
Microdrilling, 433
Micro-EDM, 1–3, 18
Microelectromechanical systems (MEMS), 121, 377
Microfluidic channels, 377
Microfluidic systems, 547–548
Microgrinding, 433, 440

Micro-holes, 378
Micromachining, 111, 112
Micromachining applications, 132, 153
Micromachining precision, 118–122
Micromilling, 432, 438
Micromilling metals, 257
Micro-mixers, 379
Microneedles, 216
Micro-pumps, 379
Microreactors, 377
Micro-sensors, 379
Microstructures, 338
Microturning, 433
Micro-USM, 331
Micro-valves, 379
Mixed electrolyte, 377
Mixed tube design, 222
Mixing ratio, 29
Modes of operation, 97
Motor-controlled feed mechanism, 130
MRR equation, 301
Multi response performance index (MRPI), 379, 381
Multiple tool passes, 377
Multi-response optimization, 381

NaCl, 379

$NaNO_3$, 379–380
Nano-ECM, 122–123
NaOH, 378
Nd:YAG, 335
Noise considerations, 128
Non resonant, 418
Non-transferred arc, 98
Normalization, 381, 386
Nozzle, 25
Nozzle design, 39
Nozzle geometry, 226, 400
Nozzle pressure, 29
Nylon and teflon burr removal, 27
One-way AFF method, 451
Operating aspects, 99
Operational parameters, 177
Operator safety, 128
Optical pumping, 81
Optical surfaces, 111
Opto-fluidic detection devices, 379
Orbital AFF method, 452
Orthopedic, 333, 335–338
Osseointegration, 333–338
Osteoblast, 337
Overcut, 70, 380

Overview, 295, 298
Oxide layer, 337
Oxygen-injected torch, 97

Parameter exploration, 240
Parameters, 97
Particle filters, 379
Particle velocity distribution, 220
Patterning, 333, 335–338
PCM parametric effect, 210
PEO, 262
Photo chemical blanking, 173
Photochemical machining (PCM), 9, 203–212
Photochemical machining of brass, 212
Photochemical machining of inconel 718, 212
Photolithography
  e-beam lithography, 535–536
  ion beam lithography, 535–536
  optical lithography, 535
  x-ray lithography, 535–536
Photoresist maskant, 162
Physical vapor deposition (PVD), 535
Physics informed models, 243
Physiological, 338
Piranha solution, 532
Plasma, 94, 275, 277, 280

Plasma arc machining (PAM), 7, 93
Plasma electrolytic polishing (PeP), 117
Plasma etching, 378
Polishing, 111
Polyetheretherketone, 337
Polyethylene, 337
Polymer matrix composites, 378
Polymers, 335, 341
Population inversion, 79
Pores, 338
Porous networks, 378
Power density, 88
Power supply, 49, 96, 310
Precision, 107
Precision in prediction, 231
Precision machining, 324
Precision machining techniques, 155
Precision welding, 89
Predictive modeling, 241
Preheating, 95
Preparation of workpiece, 160
Pressure amplifiers, 398
Pressure ranges in AJM, 25
Process capabilities, 26
Process capability, 41, 86, 132

Process capability of wire EDM, 72
Process characteristics, 170
Process description, 128
Process mechanisms, 30
Process monitoring techniques, 324
Process optimization, 340
Process parameters, 25, 39, 57, 131, 170, 381
Process parameters of electron beam machining, 151
Process parameters of wire EDM, 71
Properties of dielectric fluid, 53
Properties of maskant, 166
Pulse duration, 152
Punch and die, 72

Quartz, 378
Quartzite, 529

RCA cleaning, 532
Real-time predictive models, 244
Recent developments in USM, 140
References, 33
Refractory materials, 89
Removal rate, 132
Repair, 103
Research and development in USM, 331
Residual stress, 429, 439, 442
Residual stresses, 339–340

Resolution, 338
Resonant, 417, 418
Rheology of media, 450
Rock excavation techniques, 35
Role of inter-electrode gap, 312
Rotary ultrasonic machining (RUM), 423
Rotary USM, 140
Rotating mask apparatus (RMA), 264
Ruby laser, 82
Rust removal applications, 27

Safety considerations, 44
Safety measures, 48
Safety measures in EBM, 155
Safety precautions, 104
Safety procedures, 90
Scanning electron microscopy, 338–339
Schematic diagram of EDM, 48
Scribing, 169
SEM image, 385
Semiconductor, 527–529, 532, 534–535, 540–542, 546
  n-type, 529, 540–541
  p-type, 529, 540–541
Semiconductor applications, 153
Servo control system, 280
Shielding gas, 96

SiC, 378
Signal-to-noise ratios (S/N ratios), 380
Significance of tool wear, 241
Silicon wafers, 377, 529, 531–532, 540–541, 544–545, 547
Silicon μ-machining, 528, 540
Slit expansion, 379
Slurry concentration, 131
Smaller is better, 381, 388
Soda lime glass, 380
Sodium bicarbonate as abrasive, 25
Soil erosion models, 229
Solidification, 334–336
Spark discharge, 49
Spark-assisted chemical engraving (SACE), 378
Spectral purity, 77
Spot diameter, 152
Spring-driven feeding unit, 130
Sputter deposition, 112
Sputtering, 108
Sputtering yield, 109
Stability, 99
Stainless-steel, 381
Standard clean-2 (SC-2) solution, 532
Standoff distance (SOD), 29, 39
Standoff length, 404

Stimulated emission, 80
Surface chemistry, 336–337, 339
Surface finish, 54, 120–121, 171
Surface finish prediction, 240
Surface finish quality, 132
Surface melting, 333, 335–337
Surface microtexturing, 119
Surface morphology, 334, 338–339
Surface pre-treatment, 341
Surface profilometry, 238
Surface roughness, 276, 284
Surface roughness (SR), 337–338, 399, 402–403, 505–507, 512–515, 518–521, 523–524
Surface roughness, surface finish, 429, 430, 433, 438–441
Surface roughness, surface irregularity, 420, 422, 423, 425
Surface skewness, 339
Surface texture, 423
Surface finish enhancement, 242
Surgical needle burr removal, 27
Sustainability, 425

Taguchi’s methodology, 380
Taper effects, 28
Temperature, 435, 438, 440, 441
Temperature and pH control, 119
Temperature considerations in AJM, 27

Texturing, 335–336
Theory of EBM, 144
Thermal conductivity, 334, 435
Thermal energy, 98
Thermal micromachining, 11
Thin film, 532, 535, 537, 544
Threshold, 334
Through mask EMM, 308
Thrust force, 421, 422
Tissue adhesion, 335
Tissue integration, 333–337, 341
Tolerances, 172
Tool design, 129
Tool electrode design, 117
Tool feed rate, 180
Tool feeding control, 130
Tool holding units, 128
Tool wear, 134, 435–441
Topographies, 336, 341
Torch design, 97
Transducer, 418, 421
Transverse speed, 404–405
Traverse velocity, 404
Tribological, 336
Two-way AFF method, 452

Types of generators, 52
Types of lasers, 82

Ultrasonic assisted micromachining (UVAMM), 422
Ultrasonic drilling, 378
Ultrasonic lapping, 230
Ultrasonic machining (USM), 5, 127
Ultrasonic micromachining (USM), 324
Ultrasonic tool vibrations, 128
Under sizing and length of electrode, 55
Undercutting, 166

Vacuum chamber, 108
Vacuum system, 146
Vaporize, 335
Vibration assisted machining, 424
Vibration frequency effects, 135
Viscosity, 379
Visual comparison, 239
Voltage, 177–181, 183, 187, 188, 191, 194, 196, 198
Voltage (open circuit and working), 57
Voltage and current control, 118–119

Warburg impedance, 301–302
Water flow rate and pressure, 402
Water jet machining (WJM), 35
Water velocity, 222

Water-injection torch, 97

Wavelength, 86, 334–335

Wear rate of nozzle, 41

Wear rate of tools, 134

Wear types in EDM, 50

Wet bulk micromachining, 546–547, 549

Wet oxidation process, 532–533

Wettability, 336–339

Wire drive system, 68

Wire electrical discharge machining (WEDM), 6, 65, 505–508, 514

Wire electrochemical discharge machining (WECDM), 379

Wire electrode, 69

Wire tension, 69

Working gap, 57

Working of EBM, 146

Workpiece material, 70, 132

X-ray diffraction, 338–339

X-ray photoelectron spectroscopy, 338–339

Yield efficiency, 88

Yield stress considerations, 131

Zirconia, 378

WILEY END USER LICENSE AGREEMENT

Go to www.wiley.com/go/eula to access Wiley's ebook EULA.